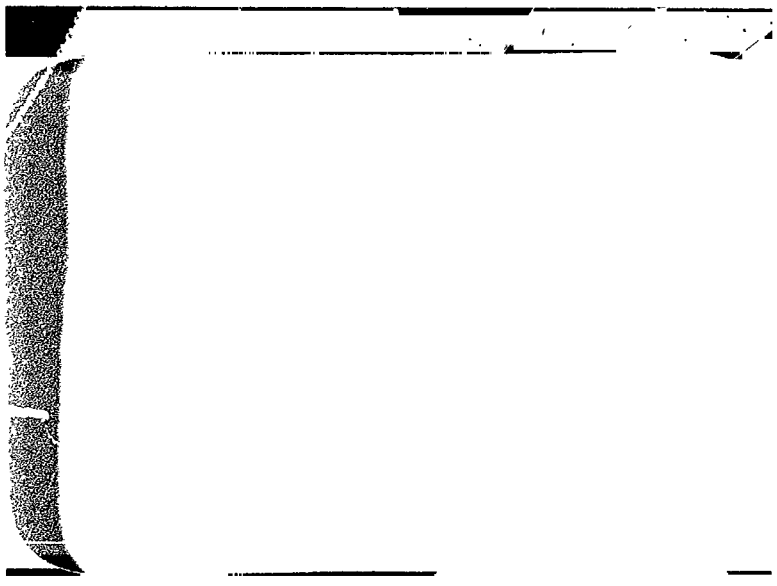

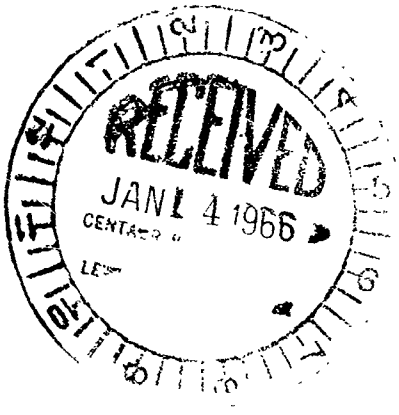

GENERAL DYNAMICS

Convair Division

A2136-1 (REV. 5-65)

GPO PRICE $ _____

CFSTI PRICE(S) $ _____

Hard copy (HC) 8.54

Microfiche (MF) 2.50

ff 653 July 65

EXTERNAL DESIGN LOADS - OPERATIONAL

CENTAUR VEHICLES (AC-6 THROUGH AC-15)

Report Number GD/C-BTD65-017
1 May 1965

Contract Number NAS3-3232

Checked by _____
H.J. Hogan
Senior Structures
Engineer

Approved by A. C. Ward
A.C. Ward
Stress Group Engineer -
Centaur

Approved by _____
R.S. Wentink
Assistant Chief Engineer -
Design Analysis - Centaur

GENERAL DYNAMICS
CONVAIR DIVISION
San Diego, California

The following Stress Group personnel prepared the information in this report. It is published with their concurrence. Any question pertaining to this report should be directed to these people at General Dynamics/Convair (GD/C), Department 966-4, extension 3754.

Prepared by F. Puhn
F. Puhn - Structures Engineer

Prepared by J. O'Husky
J. O'Husky - Senior Structures Engineer

The Centaur Aeroballistics, Structural Dynamics, and Thermodynamics groups were instrumental in assisting the above personnel in the preparation of this document.

Approved by
Aeroballistics, Dept. 966-5

Approved by
Structural Dynamics, Dept. 585-1

Approved by
Thermodynamics, Dept. 966-3

Additional copies of this document may be obtained by contacting Centaur Resources Control and Technical Reports, Department 954-4, Building 26, Kearny Mesa Plant, San Diego, California.

FOREWORD

This report has been prepared and published for the National Aeronautics and Space Administration (NASA) in compliance with the design loads requirements provisions outlined in Item 24b of the Centaur Documentation Requirements Plan, General Dynamics/Convair Report Number 55-00207E, 11 January 1965.

SUMMARY

This external design loads report for the operational Centaur vehicles (AC-6 through AC-15) presents all design loads, parameters and environments necessary to ensure operational vehicle structural integrity, maximize reliability and to provide the design department, analysis department and configuration (design) review teams with primary structure analytical supporting data within one report.

This report is conveniently divided into ten sections as follows:

I Introduction
II Nose Fairing
III Liquid Hydrogen Tank Insulation Panels
IV Interstage Adapter
V Payload Adapter (Surveyor Type)
VI Propellant Tanks
VII Liquid Hydrogen Tank Bolt-ons and Weldments
VIII Liquid Oxygen Tank Bolt-ons and Weldments
IX Atlas Booster Vehicle
X Bibliography.

TABLE OF CONTENTS

TABLE OF CONTENTS (Continued)

TABLE OF CONTENTS (Continued)

TABLE OF CONTENTS (Continued)

TABLE OF CONTENTS (Continued)

TABLE OF CONTENTS (Continued)

TABLE OF CONTENTS (Continued)

TABLE OF CONTENTS (Continued)

TABLE OF CONTENTS (Contunued)

TABLE OF CONTENTS (Continued)

TABLE OF CONTENTS (Continued)

TABLE OF CONTENTS (Continued)

TABLE OF CONTENTS (Continued)

TABLE OF CONTENTS (Continued)

TABLE OF CONTENTS (Continued)

TABLE OF CONTENTS (Continued)

TABLE OF CONTENTS (Continued)

TABLE OF CONTENTS (Continued)

LIST OF ILLUSTRATIONS

LIST OF ILLUSTRATIONS (Continued)

LIST OF ILLUSTRATIONS (Continued)

LIST OF ILLUSTRATIONS (Continued)

LIST OF ILLUSTRATIONS (Continued)

LIST OF ILLUSTRATIONS (Continued)

LIST OF ILLUSTRATIONS (Continued)

LIST OF ILLUSTRATIONS (Continued)

LIST OF ILLUSTRATIONS (Continued)

LIST OF ILLUSTRATIONS (Continued)

LIST OF ILLUSTRATIONS (Continued)

LIST OF ILLUSTRATIONS (Continued)

LIST OF ILLUSTRATIONS (Continued)

LIST OF TABLES

LIST OF TABLES (Continued)

LIST OF TABLES (Continued)

LIST OF TABLES (Continued)

LIST OF TABLES (Continued)

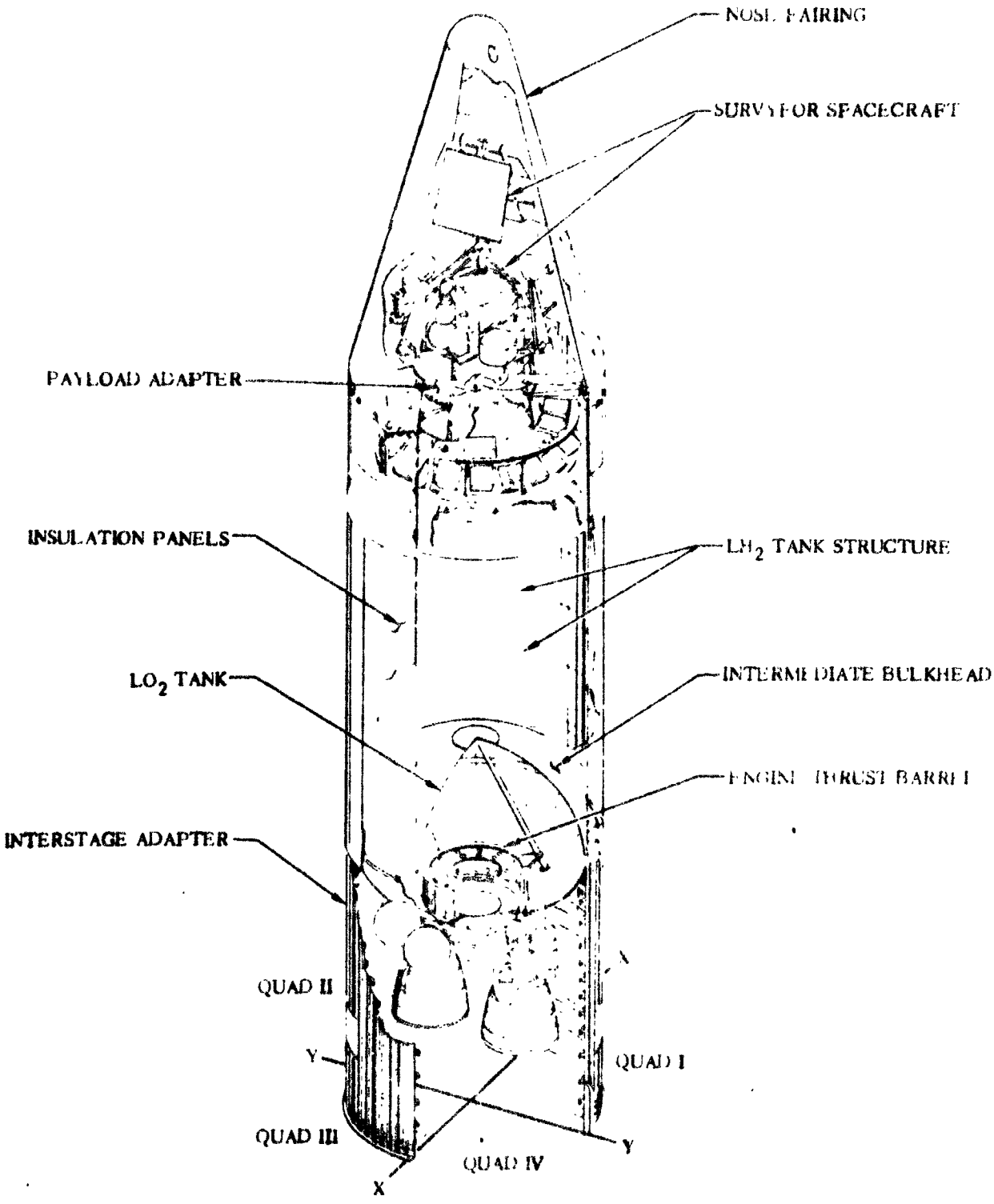
NOSE FAIRING
SURVEYOR SPACECRAFT
PAYLOAD ADAPTER
INSULATION PANELS
LH_2 TANK STRUCTURE
LO_2 TANK
INTERMEDIATE BULKHEAD
ENGINE THRUST BARREL
INTERSTAGE ADAPTER
QUAD II
QUAD I
QUAD III
QUAD IV
Y
Y
X
X

SECTION I

INTRODUCTION

1.1 PURPOSE AND SCOPE

This report presents data upon which all analytical strength evaluations and structural test requirements are based in order to assure structural integrity and ensure mission accomplishment. The external design loads and associated loading parameters presented herein, when used in conjunction with the applicable structural design criteria (Reference 1-1), shall provide the official source for all structural design criteria and design loads for Centaur Vehicles AC-6 through AC-15.

1.2 APPLICATION AND REVISIONS

This report is intended to apply to the operational Centaur vehicle configuration and necessarily reflects the most severe environment expected on Atlas/Centaur - Surveyor Flights AC-6 through AC-15. However, when significant changes in specific vehicle configuration or performance occur (e.g., addition or modification of two-burn peculiar hardware), suitable revisions and/or addenda will be established to effect agreement with current project thinking. Each revision will be identified by change letter suffix (i.e., GD/C-BTD65-017-X).

1.3 GENERAL

The residuum of Section I contains structural load parameters (of a general nature) which affect the total vehicle (i.e., mission design trajectories, propulsion system thrust histories, vehicle stiffness, inertia versus time data, etc.).

Sections II through IX present specific loads and loading parameters as related to individual structural components and/or systems. Section X presents a bibliography of Centaur Project, referenceable internal memoranda relating to a given structural component and/or system.

1.3.1 FACTORS OF SAFETY. All loads and load factors contained in this report are given as limit, consistent with the definition within Reference 1-1.

1.3.2 MISSION OBJECTIVES. Adequate vehicle strength shall support mission objectives for all operational Atlas/Centaur flights. Mission objectives are presented in the Centaur Unified Test Plan (Reference 1-2) for each operational vehicle.

1.3.3 MISSION DESIGN TRAJECTORIES. The data presented in Figures 1.3-1 and 1.3-2 present the most extreme conditions expected during the first 200 seconds of flight. The vehicle external design loads and temperatures are predicated upon these

trajectories and are consistent with vehicle design trajectory data (Reference 1-3). Three-sigma (3σ) dispersions about nominal performance parameters on drag, axial acceleration, and alpha-q are accounted for in loads data contained in other sections of this report. Figure 1.3-1 presents the low-limit (-3σ) trajectory parameters, and Figure 1.3-2 presents the high-limit ($+3\sigma$) values.

During Centaur firing, air loads are considered to be negligible, and the only significant trajectory parameter affecting loads is vehicle axial acceleration. The maximum ($+3\sigma$) and minimum (-3σ) values of axial acceleration during Centaur firing are presented in Figure 1.3-3. It should be noted that the referenced time $t = 0$ corresponds to the time of Centaur main engine start (MES).

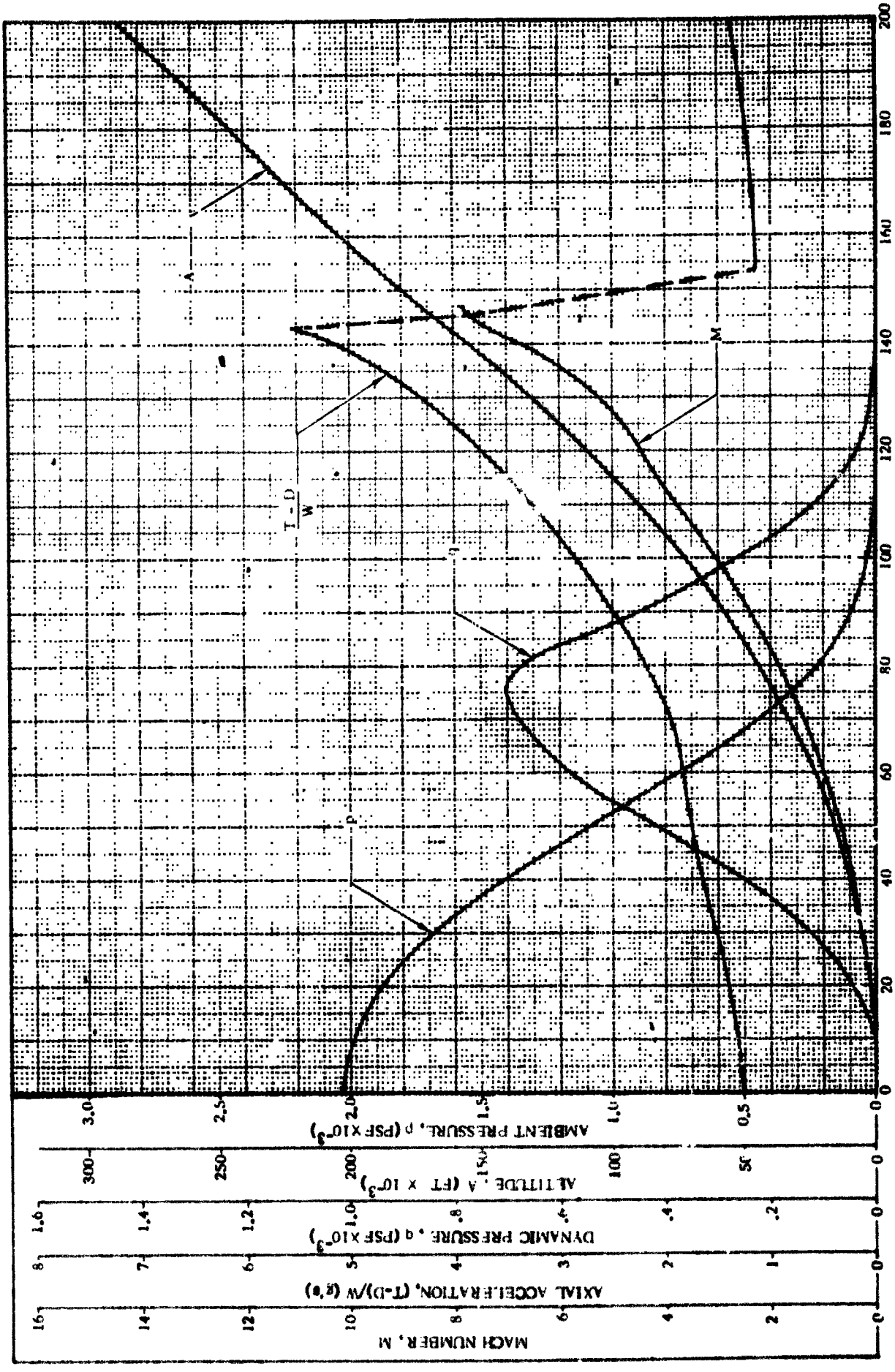

Figure 1.3-1. Operational Vehicle Trajectory Parameters (-3σ Dispersions)

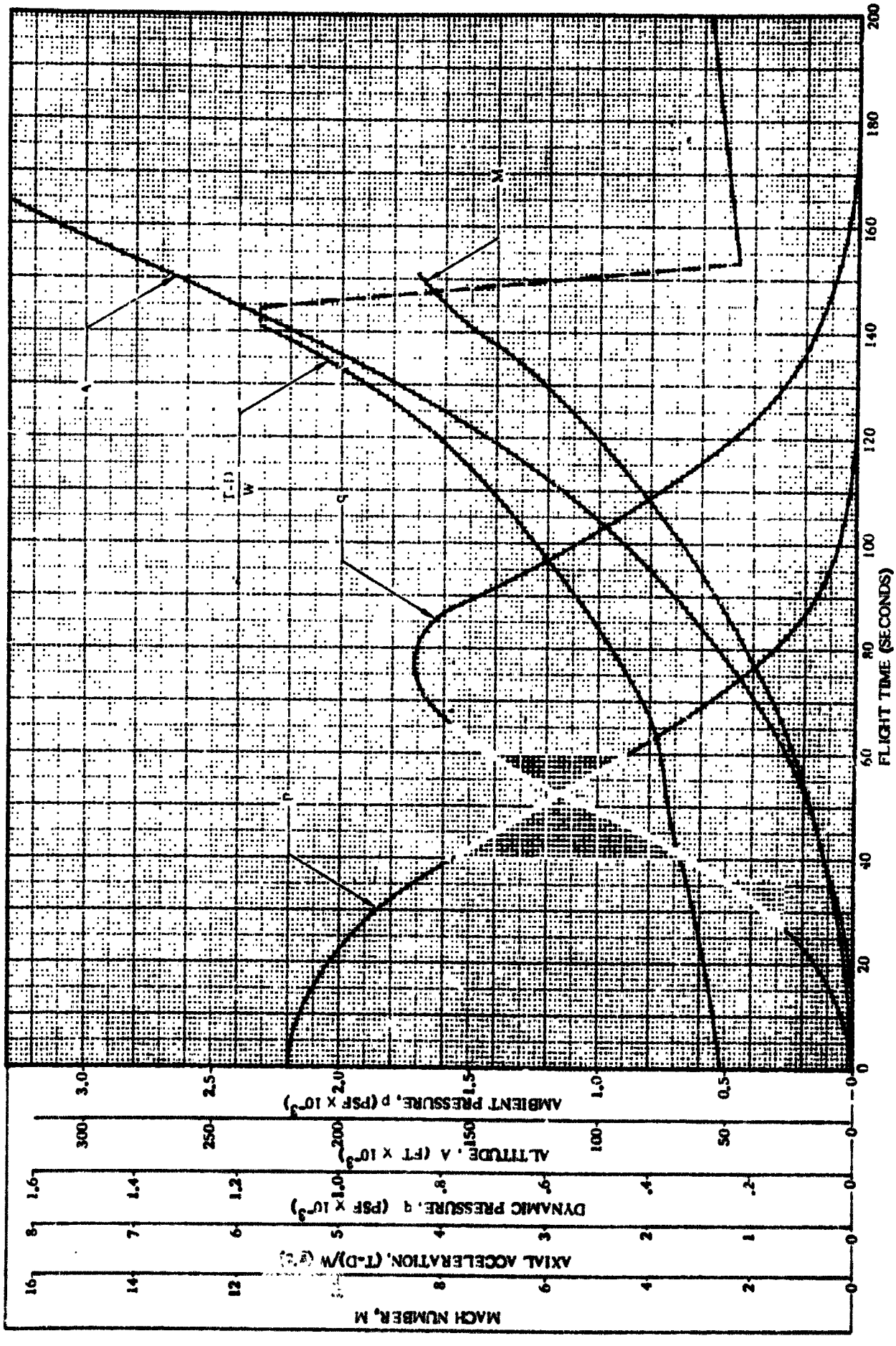

Figure 1.3-2. Operational Vehicle Trajectory Parameters (+3σ Dispersions)

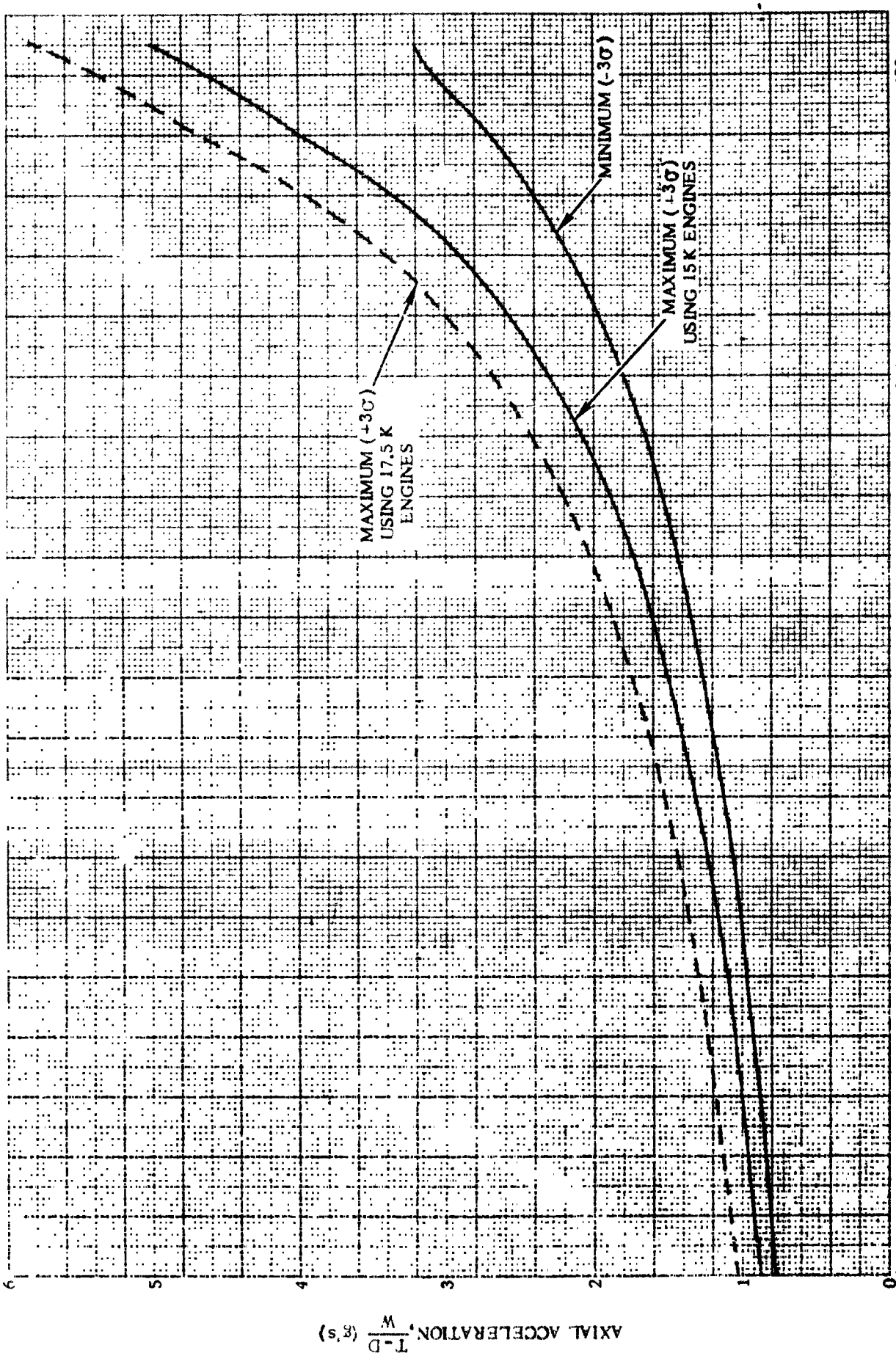

Figure 1.3-3. Axial Acceleration During Centaur Stage Firing

1.3.4 PROPULSION SYSTEM DATA. All components of the Centaur structure are subjected to thrust loads imposed by the Centaur main engine system, the Centaur attitude control system, and the Atlas vehicle engine systems. The thrust loads and parameters of each are given below.

1.3.4.1 Main Engine System - Centaur Stage. The main engine system of the Centaur stage has two Pratt & Whitney fixed thrust, single-chamber, regeneratively cooled engines. These are gimbal-mounted to the aft bulkhead of the liquid oxygen tank and are controlled by hydraulic actuators. Each engine has its own turbopump to supply liquid propellants (oxygen and hydrogen), and each has a thrust regulating system.

After termination of the first stage of flight and Atlas vehicle separation has occurred, the thrust produced by the Centaur main engines provides the major portion of the propulsion that is required to accomplish the mission.

Three models of the Pratt & Whitney engines will be structurally considered on operational Centaur vehicles. These are designated RL10A-3CM-1, RL10A-3-1, and RL10A-3-3. Each is rated nominally at 15,000 pounds of thrust except the RL-3-3, which may be uprated to a nominal 17,500 pounds of thrust. In this report, loads data are presented for both the 15K and the 17.5K engines whenever the 17.5K engines cause critical loads on the structure. Table 1.3-1 presents the thrust loads and parameters for both engine thrust ratings consistent with Reference 1-4.

TABLE 1.3-1. CENTAUR MAIN ENGINE THRUST LOADS AND PARAMETERS

Parameter	Units	15K Engine	17.5K Engine
Sea level thrust	Pounds	7.000	8,200
Maximum thrust (altitude)	Pounds	15,000	17,500
Thrust tolerance	Percent	±2.0	±2.0
Angular thrust misalignment	Degrees	±0.5	±0.5
Linear thrust misalignment	Inches	±0.125	±0.125

1.3.4.2 Attitude Control and Ullage/Propellant Settling System - Centaur Stage. The attitude control engine system has two 3-pound thrust rockets and four 1.5-pound thrust rockets. The 3-pound and the 1.5-pound thrust rockets are used during coast periods for pitch and yaw/roll attitude control, respectively. The ullage/propellant settling system has two 2-pound thrust rockets and four 50-pound thrust rockets. The 2-pound rockets are used for ullage settling and the 50-pound rockets are used for propellant settling during the coast phase of a two-burn mission only. The control and propellant settling engines are monopropellant. The thrust loads and load parameters of the attitude control and propellant settling systems are presented in Table 1.3-2.

TABLE 1.3-2. CENTAUR ATTITUDE CONTROL AND ULLAGE AND PROPELLANT SETTLING ENGINES - THRUST LOADS AND PARAMETERS

Parameter	Unit	3-Pound Engine	1.5-Pound Engine	2-Pound Engine	50-Pound Engine
Sea level thrust	Pounds	—	—	—	—
Maximum thrust (altitude)	Pounds	3.0	1.5	2.0	50
Thrust tolerance	Percent	±3.0	±3.0	±3.0	±3.0
Angular thrust misalignment	Degrees	±4.0	±4.0	±3.0	±3.0
Linear thrust misalignment	Inches	±0.062	±0.062	±0.062	±0.062

1.3.4.3 Atlas Booster Vehicle. The Atlas booster vehicle has two booster engines, one sustainer engine, and two vernier engines producing thrust during the first phases of the Atlas/Centaur flight. The thrust loads and parameters of each type of these engines are presented in Table 1.3-3. Their thrust history profiles are presented in Figure 1.3-4 where thrust is plotted against time.

TABLE 1.3-3. ATLAS BOOSTER VEHICLE ENGINE THRUST LOADS AND PARAMETERS

Parameter	Units	Booster Engine (2)	Sustainer Engine	Vernier Engine (2)
Sea level thrust/engine	Pounds	165,000	57,000	650
Maximum thrust (altitude)	Pounds	187,900	81,900	950
Thrust tolerance	Pounds	±1,500	±940	±30
Angular thrust misalignment	Degrees	±0.5	±0.5	±2.0
Linear thrust misalignment	Inches	±0.125	±0.125	±0.125

1.3.5 VEHICLE STRUCTURAL CONFIGURATION. Two views showing the general outline of the upper stage portion of the Atlas/Centaur vehicle are presented in Figure 1.3-5. This illustration shall be used for reference only. For specific details of structure or of structural components, reference shall be made to applicable specific sections of the report.

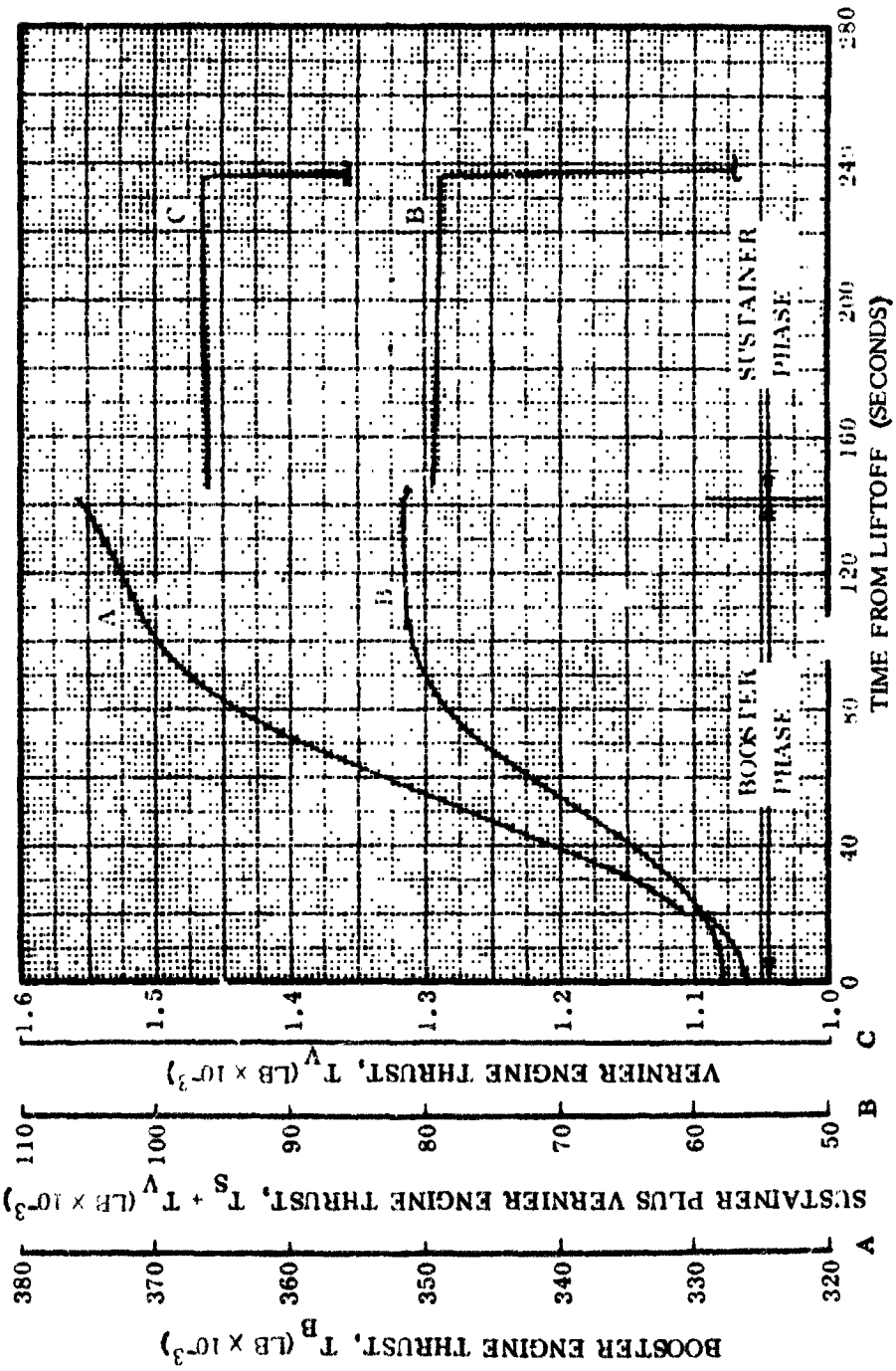

Figure 1.3-4. Atlas Stage (165K Booster) Thrust History Profiles

4B69LT

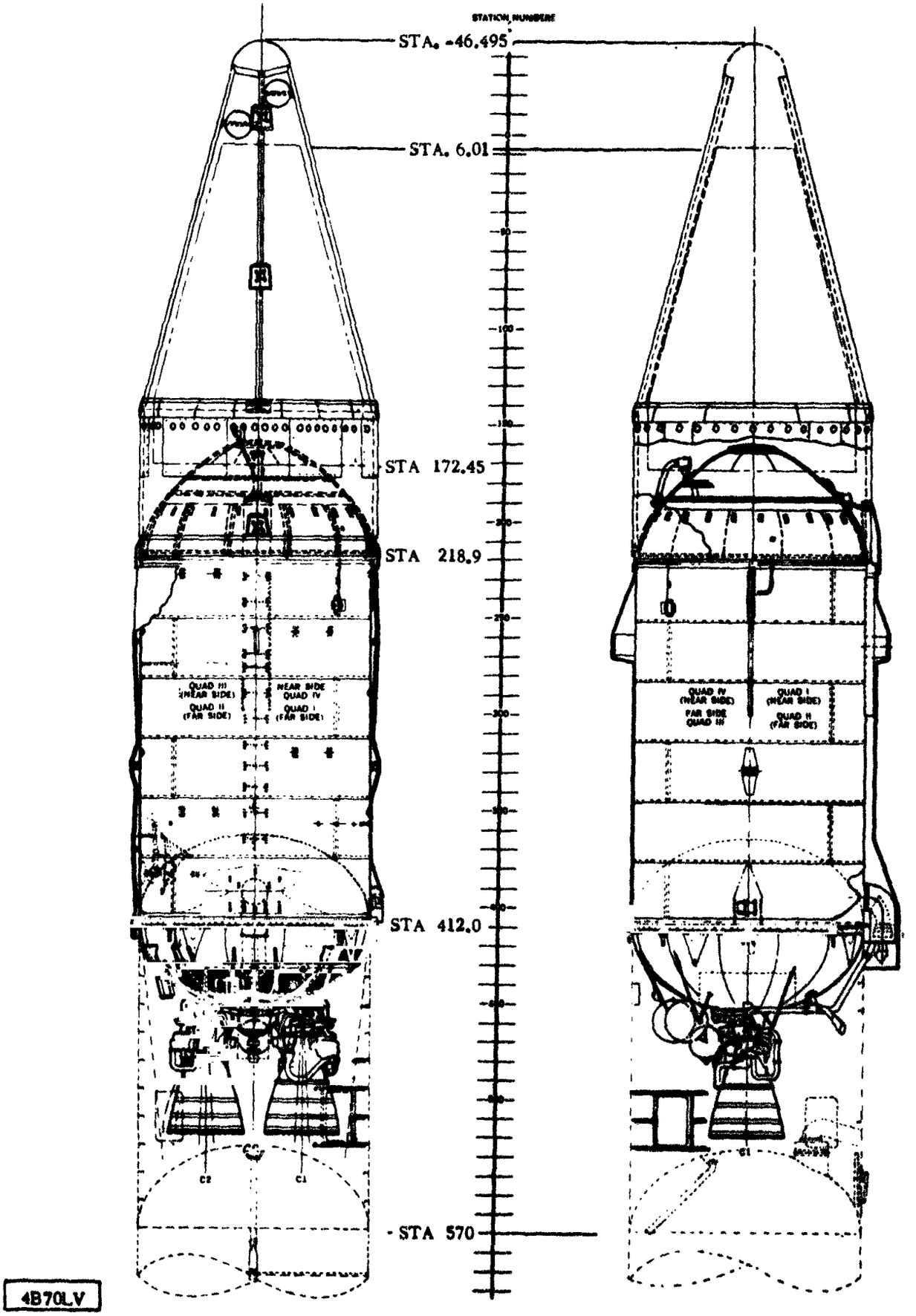

Figure 1.3-5. Centaur Operational Vehicle Configuration (Reference Only)

1.3.6 VEHICLE STIFFNESS. Figure 1.3-6 presents EI (bending stiffness) and AG (shear stiffness) plotted versus vehicle station for the operational Centaur stage and the interstage adapter. The values presented represent an analytical model with minimum stiffness assumptions. These data should not be used where maximum stiffness would be critical, without discussing their intended use with the GD/C Stress Group (Centaur).

1.3.7 STANDARD SIGN CONVENTION AND COORDINATE AXES. The standard sign convention and coordinate axes for all structural analyses are shown in Figure 1-3.7.

1.3.8 VEHICLE MASS PROPERTIES VERSUS TIME. Vehicle mass properties are presented in Table 1.3-4 (for a typical operational vehicle) based on nominal weights and C.G. data. Moments of inertia are defined as follows:

a. I_{z-z} Moment of inertia about an axis passing through the vehicle center of gravity and parallel to the Z axis (roll inertia).

b. I_{y-y} Moment of inertia about an axis passing through the vehicle center of gravity and parallel to the Y axis (yaw inertia).

c. I_{x-x} Moment of inertia about an axis passing through the vehicle center of gravity and parallel to the X axis (pitch inertia).

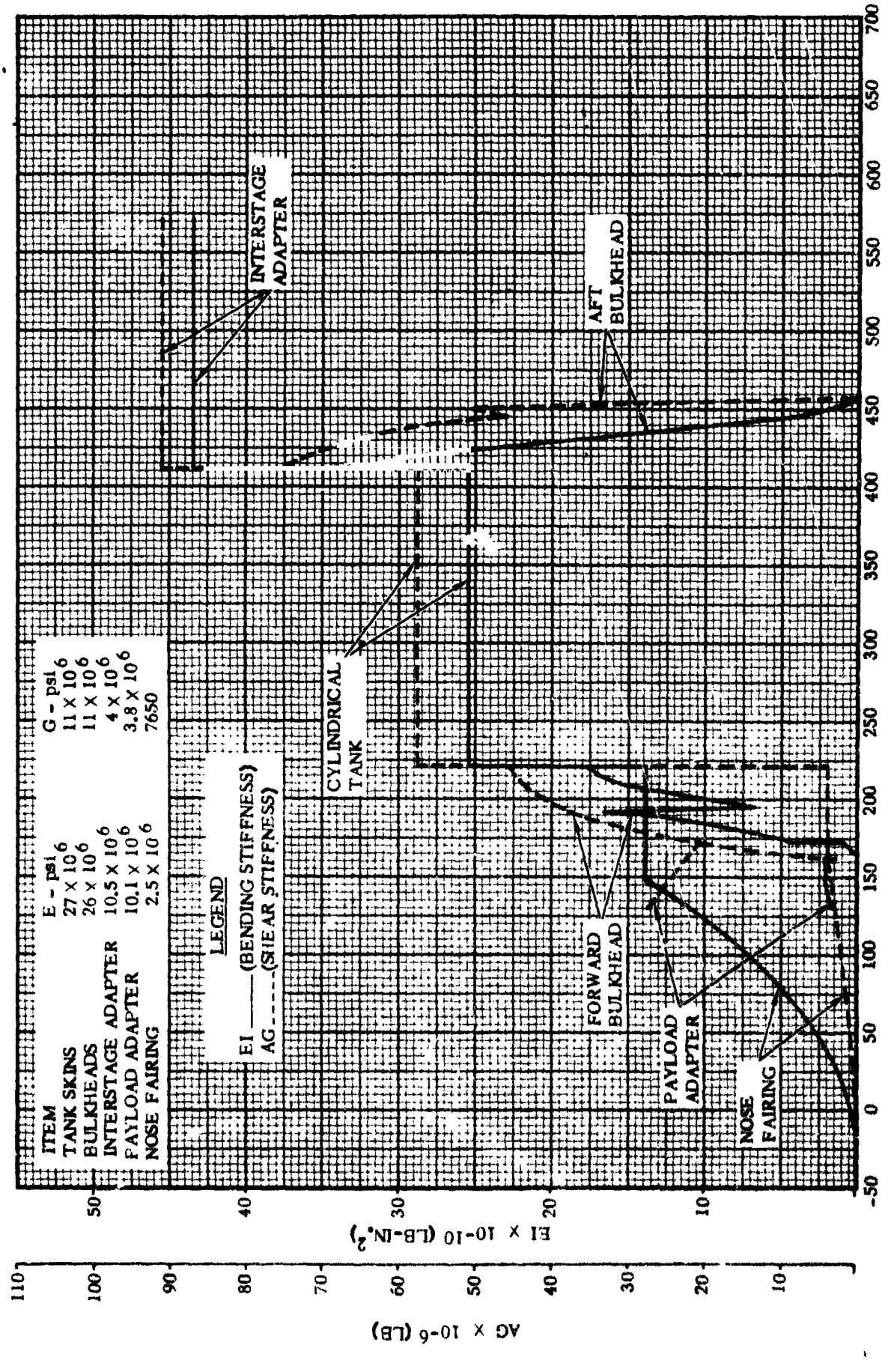

4B71LT

Figure 1.3-6. Centaur Operational Vehicle Stiffness ~ EI and AG versus Station

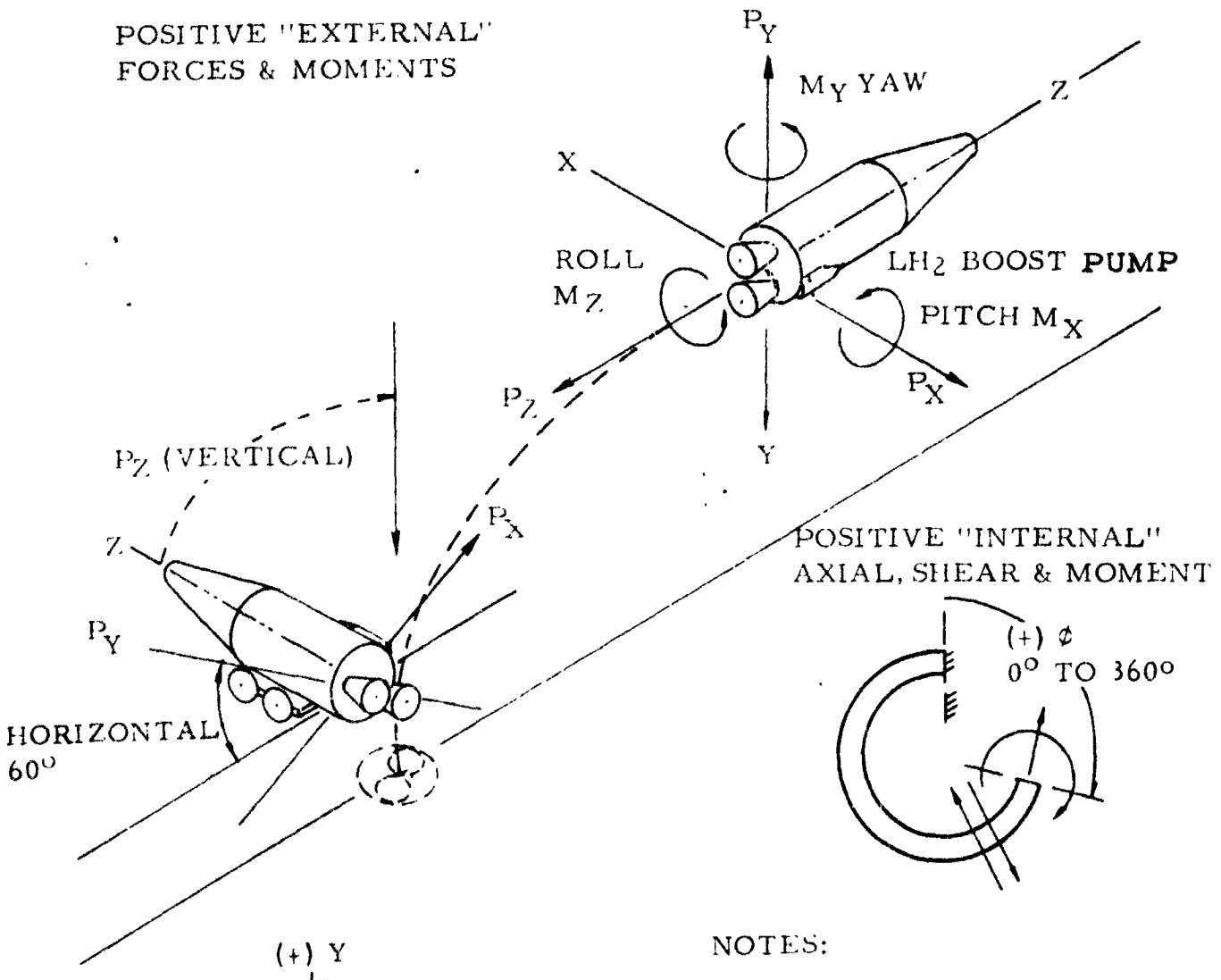

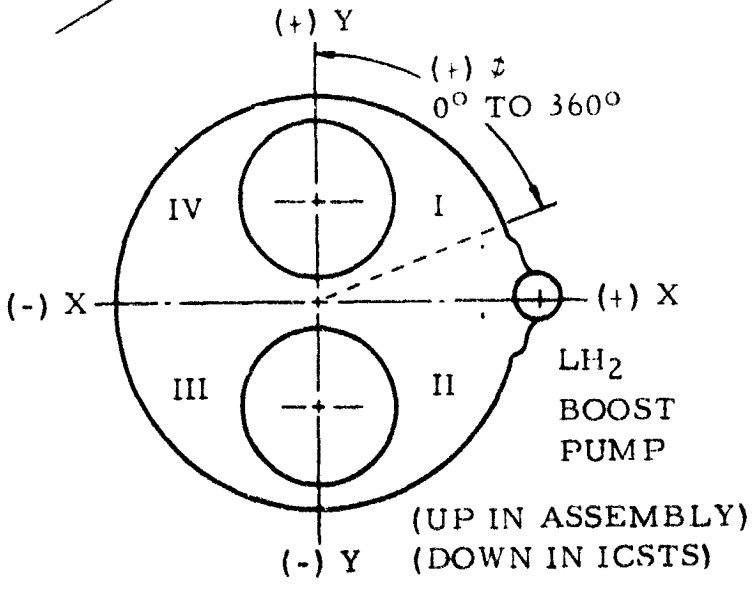

NOTES:

1. In general use right hand rule oriented as shown
2. Trailers, jigs, towers etc., securing flight vehicle take axis and sign of secured flight vehicle.
3. Ground structures unrelated to flight vehicle use same axis and sign as the vehicle in vertical position (gravity forces are +).

4B72LV

Figure 1.3-7. Centaur Standard Sign Convention and Coordinate Axes

TABLE 1.3-4. MASS PROPERTIES VERSUS TIME

CARD 1	TIME	WEIGHT	Z C.G.	Y C.G.	X C.G.	FUEL WT.	OXID WT.
2	IZZ	IXX	IYY	IZY	IZX	IXY	OXID STA
3	ALPHA ZY	ALPHA ZX	ALPHA XY	BETA ZY	BETA ZX	BETA XY	FUEL STA
4	TANK MR	INST. MR	FLOW BOT.	FUEL FLOW	OXID FLOW	FUEL DENS	OXID DENS
CARD 1	SECONDS	POUNDS	INCHES	INCHES	INCHES	POUNDS	POUNDS
2	SLUG-FT2	SLUG-FT2	SLUG-FT2	SLUG-FT2	SLUG-FT2	SLUG-FT2	INCHES
3	DEGREES	DEGREES	DEGREES	DEGREES	DEGREES	DEGREES	INCHES
4	LBS./LB.	LBS./LB.	LBS./SEC	LBS./SEC	LBS./SEC	LBS./FT3	LBS./FT3

COMPUTER OUTPUT IS REFERENCED TO A FIXED DECIMAL PRECEDING THE VALUE GIVEN. THE LAST TWO DIGITS PROVIDE THE CHARACTERISTIC OF THE ACTUAL DECIMAL LOCATION.

19334		3026450056	7869038653	40322817s0	4338226650-	7492482355	1728765056
29335	1457341755	3982533957	3980313457	7559653254	1233945655-	3243495753-	5527071353
39336	1092189950	1781745750-	8142624751	5460524549	5874834849-	4709324752-	9393408853
49337	2287936051	2307332851	1262002051-	4776070053	1092735054	5000000052	6941000052
59338							
19339	4000000051	2963686956	7892711353	4116041750	4424430550-	7301434555	1685055656
29340	1457114255	3921541e57	3919319157	7492615654	1225601755-	3236058353-	5632892353
39341	1099413350	1797323150-	8117321851	5605313749	6025283249-	4706799652-	9462241653
49342	2287936051	2307840351	1262002051-	4776080053	1092737554	5000000052	6941000052
59343							
19344	8000000051	2900923556	7915458053	4203426650	4514364550-	7110396355	1641340156
29345	1456884655	3863209357	3860984557	7428062554	1217536455-	3228524653-	5729793253
39346	1106470450	1812556150-	8092171851	5755433349	6181177049-	4704270652-	9524177053
49347	2287936051	2308375051	1262002051-	4774997553	1092460054	5000000052	6941000052
59348							
19354	1200000052	2838175756	7937316753	4294652750	4608251050-	6919396655	1597647756
29355	1456653155	3807398257	3805173457	7365886054	1209737555-	3220888853-	5625438353
39356	1113362850	1827445150-	8074031451	5911223449	6342865249-	4701736452-	9583154353
49357	2287873051	2308940851	1262002051-	4774995053	1092457554	5000000052	6941000052
59358							
19359	1600000052	2775427856	7958259653	4390003950	4706382950-	6728396855	1553949456
29360	1456419355	3754044057	3751816857	7306172454	1202213655-	3213143553-	5921313353
39361	1120102850	1841989450-	8047393451	6073017549	6510687949-	4699198252-	9641152253
49362	2287873051	2309533951	1262002051-	4763547553	1095942554	5000000052	6941000052
59363							

TABLE 1.3-4. MASS PROPERTIES VERSUS TIME (Continued)

19369	2900000052	2712586556	7978347653	4489921050	4809220350-	6537855355	1510111856	
29370	1456183155	3702975157	3700745857	7248742754	1194945055-	3205276753-	6017474653	
39371	1126694250	1856200650-	8021534151	6241512940	6685375349-	4696656052-	9698721753	
49372	2300684051	2309796951	1262002051-	4763560053	1095945054	5000000052	6941000052	
59373								
19374	2400000052	2649745056	7997383953	4594577650	4916935850-	6347312955	1466274056	
29375	1455944455	3654201857	3651972757	7194116654	1187986355-	3197283953-	6113523153	
39376	1133196550	1870118850-	8003237851	6416632349	6866827049-	4694108652-	9756324753	
49377	2300684051	2310070551	1262002051-	4755867553	1097727554	5000000052	6941000052	
59378								
19384	2800000052	2586862856	8015365653	4704392950	5029963750-	6157076955	1422364956	
29385	1455703055	3607599057	3605365357	7142298654	1181337355-	3189153953-	6209518553	
39386	1139635950	1883770650-	7968320151	6598920649	7055602949-	4691557252-	9813858653	
49387	2308141051	2310130251	1262002051-	4755865053	1097727554	5000000052	6941000052	
59388								
19389	3200000052	2523980656	8032139853	4819680150	5148623650-	5966841155	1378455856	
29390	1455458655	3563087557	3560856057	7093683154	1175039755-	3180878453-	6305522253	
39391	1146084050	1897230150-	7956129351	6788513449	7251828949-	4689001352-	9871385253	
49392	2308141051	2310193651	1262002051-	4750965053	1095355054	5000000052	6941000052	
59393								
19399	3600000052	2461212656	8047566653	4940628950	5273101950-	5776801355	1334641656	
29400	1455211355	3520633057	3518399557	7048639154	1169131555-	3172453053-	6401299253	
39401	1152604750	1910546650-	7929369851	6985360549	7455430649-	4686440752-	9928856453	
49402	2305527051	2310347151	1262002051-	4751002553	1095357554	5000000052	6941000052	
59403								
19404	4000000052	2398445056	8061594153	5067908250	5404095650-	5586761255	1290827356	
29405	1454960655	3480047457	3477811957	7007296054	1163625655-	3163859353-	6497120553	
39406	1159272050	1923817050-	7902244351	7190203349	7667175749-	4683875652-	9986329753	
49407	2305527051	2310511051	1262002051-	4744665053	1092442554	5000000052	6941000052	
59408								
19414	4400000052	2335819256	8074057753	5201712150	5541792850-	5396974755	1247129656	
29415	1454706455	3441285657	3439047857	6970078554	1158566555-	3155092753-	6592688953	
39416	1166166750	1937117850-	7873739151	7402888149	7886878149-	4681306452-	1004372354	
49417	2302463051	2310793951	1262002051-	4744672553	1092442554	5000000052	6941000052	
59418								
19419	4800000052	2277193356	8084892753	5342888850	5687077350-	5207187855	1203431956	
29420	1454448355	3404124657	3401886957	6937152854	1153970455-	3146130353-	6688267553	
39421	1173390050	1950584250-	7852811851	7624324849	8115483149-	4678732752-	1010112054	
49422	2302463051	2311097651	1262002051-	4737705053	1088550054	5000000052	6941000052	
59423								

TABLE 1.3-4. MASS PROPERTIES VERSUS TIME (Continued)

19429	5200000052	2210751056	8093892153	5491608550	5840108650-	5017679555	1159889956
29430	1454186255	3368520357	3366280457	6909055854	1149893555-	3136968053-	6783561153
39431	1181051350	1964324350-	7823751951	7854151949	8352579449-	4676153852-	1015844454
49432	2297633051	2311606251	1262002051-	4737707553	1088552554	5000000052	6941000052
59433							
19434	5600000052	2148308456	8100977553	5648974350	6002036850-	4828171255	1116347856
29435	1453919455	3334233757	3331991757	6885988254	1146355055-	3127575953-	6878864553
39436	1189273450	1978503250-	7794517951	8093531449	8599378749-	4673570952-	1021577454
49437	2297633051	2312154551	1262002051-	4730750053	1082337554	5000000052	6941000052
59438							
19444	6000000052	2086142456	8105871453	5814990950	6172841350-	4638941355	1073054356
29445	1453648255	3301208857	3298964657	6868668054	1143430655-	3117955353-	6973626653
39446	1198209850	1993283450-	7764452051	8341598649	8854933949-	4670983552-	1027299754
49447	2287875051	2313144851	1262002051-	4730750053	1082337554	5000000052	6941000052
59448							
19449	6400000052	2023976456	8108502653	5991205750	6354138350-	4449711355	1029760856
29450	1453371555	3269160857	3266916657	6857276654	1141137255-	3108063553-	7068414253
39451	1208008750	2008871550-	7741001951	8600045649	9121014349-	4668391452-	1033021454
49452	2287875051	2314219451	1262002051-	4721350053	1078887554	5000000052	6941000052
59453							
19459	6800000052	1961986056	8108634353	6178035450	6546339350-	4260857455	9866053055
29460	1453089255	3237994357	3235747957	6852424154	1139538055-	3097890853-	7162901953
39461	1218833250	2025449850-	7709677851	8868519949	9397215549-	4665794852-	1038733554
49462	2285123051	2315508851	1262002051-	4721362553	1078890054	5000000052	6941000052
59463							
19464	7200000052	1899995556	8106060853	6377056750	6751082350-	4072002955	9434497055
29465	1452800455	3207420457	3205171957	6854641154	1138687555-	3087394153-	7257348053
39466	1230910250	2043316050-	7677953751	9148315249	9684879349-	4663193552-	1044448354
49467	2285123051	2316918051	1262002051-	4711520053	1077615054	5000000052	6941000052
59468							
19474	7600000052	1838095256	8100540753	6589179450	6969294150-	3883542155	9003451055
29475	1452504655	3177291757	3175040857	6864548854	1138648955-	3076550053-	7351642553
39476	1244440050	2062708350-	7644475751	9439572649	9984119149-	4660587752-	1050150554
49477	2287193051	2318360651	1262002051-	4711527553	1077617554	5000000052	6941000052
59478							
19484	8000000052	1776194956	8091742153	6816087050	7202715250-	3695081055	8572404055
29480	1452201055	3147320857	3145067757	6883005554	1139511155-	3065313453-	7445983353
39481	1259731350	2084016050-	7610761851	9743201249	1029586350-	4657977352-	1055850554
49482	2287193051	2319950251	1262002051-	4706217553	1077285054	5000000052	6941000052
59483							

TABLE 1.3-4. MASS PROPERTIES VERSUS TIME (Continued)

19489	6400000052	1714329156	8079334953	7059259150	7452843250-	3506632355	8141490055
29490	1451888855	3117280257	3115023357	6910860954	1141361155-	3053645453-	7540399653
39491	1277081950	2107606450-	7590196951	1005963450	1062053150-	4655362352-	1061546554
49492	2289068051	2321698051	1262002051-	4706225053	1077287554	5000000052	6941000052
59493							
19494	6800000052	1652463356	8062887153	7320597750	7721700150-	3318583355	7710575055
29495	1451566955	3086863657	3084610757	6949232254	1144314055-	3041494153-	7634811453
39496	1296894650	2133975450-	7554335751	1038957550	1095882950-	4652742852-	1067242854
49497	2289068051	2323453651	1262002051-	4700457553	1079535054	5000000052	6941000052
59498							
19504	9200000052	1590530556	8041985453	7602607750	8011408650-	3130565155	7278761055
29505	1451234055	3055772357	3053517357	6999174854	1148479155-	3028794453-	7729399453
39506	1319579750	2163634850-	7516173551	1073433450	1131198950-	4650118652-	1072931354
49507	2296657051	2325063051	1262002051-	4700450053	1079532854	5000000052	6941060052
59508							
19509	9600000052	1528597856	8016019053	7907468550	8225424850-	2942547155	6846947955
29510	1450889055	3023614357	3021357057	7062297354	1154010255-	3015487853-	7823988453
39511	1345717750	2197302050-	7479343651	1109368650	1168005150-	4647489352-	1078619154
49512	2296657051	2326877951	1262002051-	4694637553	1082673654	5000000052	6941000052
59513							
19519	1000000053	1466562556	7984395253	8238650950	8666131450-	2754761655	6413878455
29520	1450530055	2990008657	2987751357	7140096654	1161091155-	3001481853-	7918875353
39521	1375918050	2235731750-	7446151551	1146950050	1206461950-	4644856052-	1084300954
49522	2306193051	2328288051	1262002051-	4694637553	1082673654	5000000052	6941000052
59523							
19524	1040000053	1404527656	7946293453	8599038650	9036934750-	2566976155	5980808955
29525	1450155455	2954429357	2952170057	7234705054	1169913355-	2986699053-	8013746753
39526	1411033050	2279977350-	7404824151	1186147250	1246542950-	4642217552-	1089983054
49527	2306193051	2329904451	1262002051-	4689197553	1086127854	5000000052	6941000052
59528							
19534	1080000053	1342376456	7900841453	8993616850	9442825450-	2379408255	5546357855
29535	1449762755	2916355257	2914093657	7348369654	1180717355-	2971010453-	8108972053
39536	1452019450	2331218050-	7360457751	1227139850	1288432150-	4639575152-	1095659754
49537	2316234051	2330982051	1262002051-	4689197553	1086127654	5000000052	6941000052
59538							
19539	1120000053	1280225056	7840912853	9426451650	9888125950-	2191840355	5111906755
29540	1449349755	2875079857	2872816857	7484001954	1193802655-	2954304553-	8204249353
39541	1500172650	2391057550-	7316518151	1269889450	1332083950-	4636927452-	1101336654
49542	2316234051	2332244151	1262002051-	4683607553	1090039354	5000000052	6941000052
59543							

TABLE 1.3-4. MASS PROPERTIES VERSUS TIME (Continued)

19549	1160000053	1217939456	7783203753	0904547850	1038001251-	2004496055	4675891055
29550	1448912655	2829839357	2827574457	7644966454	1209515455-	2936396053-	8299831553
39551	1557080550	2461449650-	7268210351	1314604250	1377711050-	4634274652-	1107006254
49552	2327350051	2332701651	1262002051-	4683622553	1090042854	5000000052	6941000052
59553							
19554	1200000053	1155653756	7708100953	1043416051	1092492251-	1817151155	4239873955
29555	1448448155	2779640557	2777374557	7835429654	1228284455-	2917118753-	8395390253
39556	1624864750	2545016050-	7219137651	1361218450	1425239250-	4631618452-	1112677654
49557	2327350051	2333253451	1262002051-	4677422553	1094665354	5000000052	6941000052
59558							
19564	1240000053	1093207956	7619591053	1102577051	1153360351-	1630054255	3802007855
29565	1447950755	2723347157	2721079457	8060[.4954	1250644855-	2896195253-	8491430053
39566	1706318150	2645187750-	7164346851	1409940350	1474921950-	4628956452-	1118340854
49567	2340317051	2332442651	1262002051-	4677430053	1094667054	5000000052	6941000052
59568							
19569	1280000053	1030762056	7515249753	1168904151	1221603651-	1442957055	3364141055
29570	1447415255	2659471257	2657201557	8326695154	1277240355-	2873367853-	8587432653
39571	1805249450	2766664950-	7104165651	1460780450	1526638750-	4626289952-	1124007054
49572	2340317051	2331421551	1262002051-	4679240053	1099236554	5000000052	6941000052
59573							
19579	1320000053	9681260455	7391743153	1244030151	1298903851-	1255787455	2924446455
29580	1446832955	2586112657	2583841757	8642367654	1308957755-	2848202453-	8683797153
39581	1927177050	2916234050-	7040860151	1513883250	1580659750-	4623618852-	1129635454
49582	2349178051	2328775151	1262002051-	4679240053	1099236854	5000000052	6941000052
59583							
19584	1360000053	9054900955	7245300153	13295495[1	1386898251-	1068617855	2484751755
29585	1446195455	2501032057	2498759557	9017335254	1346797855-	2820276553-	8780243053
39586	2079647050	3103183050-	6969815651	1569147250	1636830350-	4620942552-	1135250654
49587	2349178051	2325201551	1262002051-	4031892553	9434370053	5000000052	6941000052
59588							
19594	1400000053	8516755255	7097162753	1412991151	1472559251-	9073421254	2107376955
29595	1445570455	2416165257	2413890857	9396391954	1384989955-	2792974553-	8862518053
39596	2243705750	3303919950-	6899390551	1618246050	1686466850-	4618262252-	1140233254
49597	2339937051	2322582551	1262002051-	4031892053	9434372553	5000000052	6941000052
59598							
19599	1440000053	7978609455	6924118453	1507688751	1569775651-	7460664454	1730002055
29600	1444885755	2317977157	2315700757	9839758054	1429802255-	2762692453-	8944573753
39601	2449809650	3556172350-	6821626451	1668970850	1737698950-	4615576752-	1145445854
49602	2339937051	2318831051	1262002051-	4031898353	9434401353	5000000052	6941000052
59603							

TABLE 1.3-4. MASS PROPERTIES VERSUS TIME (Continued)

19604	1442497053	7945015755	6912375653	1514025651	1576281051-	7359987954	1706444355
29605	1444840755	2311340857	2309064957	98698[illegible]2854	1432849655-	2760664353-	8949726653
39606	2464409950	3574045450-	6818307351	1672192050	1740950750-	4615408852-	1145778054
49607	2339937051	2318542351	1262002051-	8204578652	1857085753	5000000052	6941000052
59608							
19614	1456497053	7907706855	6899050953	1520954651	1582974351-	7245123754	1680445155
29615	1444743155	2303720257	2301443957	9902409054	1435748155-	2757165653-	8955417053
39616	2480773750	3593193150-	6808823751	1675541050	1743863650-	4614467552-	1146158054
49617	2263476051	2319415351	1262002051-	8184780752	1868527453	5000000052	6941000052
59618							

BOOSTER JETTISON

19619	7356000054	1212985954	2580206551	1105464952-	5009168254	1299622555	1485411955
19620	2748339452	7422726952-	1856366550-	19715118[illegible]0	4319561250-	5724867448	
19621							
19622	1456497053	7157202155	6365600253	1409582051	5945616050-	7245109554	1680441955
29623	9265999654	1804981657	1804396557	8846109454	5443899954-	2544662553-	8955417753
39624	2823351050	1736960450-	2050872352	1408393950	5940613649-	2287001552-	1146158154
49625	2282927051	2319415551	2212002051-	8184780752	1868527453	5000000052	6941000052
59626							
19627	1480000053	7094569355	6335905553	1422065951	5998354050-	7052742654	1636525955
29628	9265671854	1787636157	1787051057	8911085254	5471379654-	2543480853-	8965033453
39629	2871834150	1762754350-	2050213452	1413547350	5962432149-	2287029152-	1146796954
49630	2282927051	2320410651	2212002051-	8184782552	1868527553	5000000052	6941000052
59631							
19632	1520000053	6987973855	6283957353	1443827051	6090283050-	6725350954	1561784855
29633	9265100554	1757291857	1756707457	9024741254	5519448154-	2541422553-	8981415653
39634	2958960150	1809107850-	2050763152	1422359250	5999738549-	2287076252-	1147914854
49635	2282927051	2322235451	2212002051-	8184786752	1868526753	5000000052	6941000052
59636							
19637	1535000053	6948000555	6264006253	1452159551	6125483650-	6602579154	1533756955
29638	9264881854	1745639657	1745055457	90683[illegible]7754	5537907254-	2540634953-	8987563953
39639	[illegible]993226750	1827338350-	2050808952	1425677350	6013786849-	2287093952-	1148340054
49640	2282927051	2322966351	2212002051-	8133[illegible]2052	1872972053	5000000052	6941000052
59641							

TABLE 1.3-4. MASS PROPERTIES VERSUS TIME (Continued)

19647	1560000053	6881395655	6230221453	1466258551	6.85044550-	639924295.	1486932655
29648	9264511954	1725938857	1725354857	9142298654	5569164154-	2539302553-	8997842653
39649	3052259650	1858740050-	2050550552	1431233750	6037310649-	2287123352-	1149049354
49650	2302800051	2323607151	2212002051-	8133457552	1872972553	5000000052	6941000052
59651							
19652	1600000053	6774827755	6174588253	1489393651	6282777950-	6073904654	1412013755
29653	9263905354	1693500057	1692916357	9263996754	5620628754-	2537117653-	9014280753
39654	3152470850	1912045050-	2050058452	1440166450	6075130649-	2287170152-	1150197554
49655	2302800051	2324721651	2212002051-	8133470052	1872970053	5000000052	6941000052
59656							
19657	1610000053	6748185755	6160368353	1495291551	6307693650-	5992569954	1393284055
29658	9263750954	1685209857	1684626357	9295102254	5633782154-	2536560853-	9018391853
39659	3178704850	1925099250-	2050233152	1442407850	6034621049-	2287182052-	1150487154
49660	2302800051	2325019251	2212002051-	8105736752	1875036753	5000000052	6941000052
59661							
19667	1640000053	6668281055	6116977453	1513263351	6383614950-	5749397854	1337032955
29668	9263279854	1659931457	1659348557	9390010454	5673916154-	2534864853-	9030741753
39669	3260345350	1969422750-	2050743752	1449157350	6113198549-	2287217352-	1151358954
49670	2313222051	2325518251	2212002051-	8105730052	1875035053	5000000052	6941000052
59671							
19672	1680000053	6561741555	6057266553	1537906551	6487719550-	5425168654	1262031555
29673	9262634654	1625150057	1624567357	9520606954	5729138854-	2532540853-	9047220853
39674	3376857150	2031391550-	2049929452	1458203650	6151500749-	2287264252-	1152535454
49675	2313222051	2326253051	2212002051-	8105735052	1875035053	5000000052	6941000052
59676							
19677	1720000053	6455201955	5995338453	1563363251	6595260550-	5100939254	1187030155
29678	9261968254	1589080357	1588498357	9656038654	5786405354-	2530141753-	9063712153
39679	3503102750	2098536850-	2050290152	1467303550	6190031049-	2287311252-	1153728254
49680	2313222051	2327081551	2212002051-	8105748652	1875040953	5000000052	6941000052
59681							
19682	1725497053	6440560755	5986648253	1566927451	6610317350-	5056381954	1176723055
29683	9261874854	1584019257	1583437257	9675043154	5794440854-	2529805953-	9065978753
39684	3521280050	2108204450-	2050101852	1468558250	6195343449-	2287317752-	1153893454
49685	2313222051	2327203651	2212002051-	8091829752	1875541353	5000000052	6941000052
59686							

TABLE 1.3-4. MASS PROPERTIES VERSUS TIME (Continued)

INSULATION PANEL JETTISON

19687	1266000054	3254000053	190[illegible]000050-	4090000151	1043600054	1542798154	1572398154
19688	3730000051	5109998352	1068000052	4280812750	5469290951	1790751652-	
19689							
19690	1725497053	6313960755	6041440053	1602155251	7562937550-	5056381954	1176723055
29691	8211128654	1561648657	1561090857	9537601454	5483957054-	2613358153-	9065978753
39692	3518861350	2022626550-	2156892652	1515154150	7152263749-	2526954652-	1153893454
49693	2317822051	2327203651	2212002051-	8091829752	1875541353	5000000052	6941000052
59694							
19695	1760000053	6222092855	5985567753	1625877251	7675018650-	4777189554	1112011255
29696	8210483754	1530119257	1529561557	9660060854	5541851354-	2610861653-	9080219353
39697	3637891650	2086321650-	2155782852	1523537850	7191934249-	2526984252-	1154974154
49698	2317822051	2327751951	2212002051-	8091837552	1875545053	5000000052	6941000052
59699							
19700	1800000053	6115588555	5918441453	1654270751	7809171350-	4453516054	1036089455
29701	8209712354	1492236057	1491679057	9807177454	5611399954-	2607874653-	9096739953
39702	3787588850	2166426750-	2155941952	1533310650	7236179349-	2527016252-	1156260154
49703	2317822051	2328473551	2212002051-	8091831452	1875542953	5000000052	6941000052
59704							
19705	1835000053	6022397355	5857534553	1679938851	7930447150-	4170301954	9713454054
29706	8209015354	1457857657	1457301057	9940655254	5674498654-	2605176253-	9111351853
39707	3930198350	2242738150-	2155488952	1541909450	7278868549-	2527048052-	1157410654
49708	2317822051	2329196851	2212002051-	8086320052	1875200053	5000000052	6941000052
59709							
19715	1840000053	6009088755	5848665753	1683669451	7948073450-	4129870254	9619694054
29716	8208914154	1452851557	1452294957	9960091054	5683686254-	2604784153-	9113449053
39717	3951530450	2254152850-	2155273852	1543141350	7284698349-	2527052352-	1157576754
49718	2318986051	2329296951	2212002051-	8086345052	1875212553	5000000052	6941000052
59719							
19720	1880000053	5902619755	5776119553	1714120151	8091945750-	3806416454	8869609054
29721	8208087754	1411900357	1411344257	1011906155	5758835454-	2601584753-	9130266353
39722	4131739650	2350583650-	2154801652	1553027550	7331480349-	2527086252-	1158023354
49723	2318986051	2330173151	2212002051-	8086351452	1875214353	5000000052	6941000052
59724							
19725	1915000053	5809459155	5710229453	1741680051	8222160150-	3523394154	8213284054
29726	8207340054	1374700657	1374145157	1026343655	5827083554-	2598690753-	9145047753
39727	4304788450	2443182250-	2154755852	1561725350	7372639949-	2527116052-	1160126854
49728	2318986051	2331071651	2212002051-	8083520052	1874800053	5000000052	6941000052
59729							

TABLE 1.3-4. MASS PROPERTIES VERSUS TIME (Continued)

19735	1920000053	5796153955	5700628853	1745688551	8241099050-	3482976554	8119544054
29736	8207231354	1369279557	1368724357	1028447255	5837027354-	2598269953-	9147163453
39737	4330794150	2457098450-	2155294452	1562971450	7378536849-	2527120052-	1160300454
49738	2319281051	2331208451	2212002051-	8083565052	1874807553	5000000052	6941000052
59739							
19740	1960000053	5689712255	5622023053	1778430751	8395798650-	3159633954	7369621054
29741	8206343654	1324875057	1324320257	1045669955	5918438154-	2594833553-	9164132053
39742	4551842650	2575381350-	2154433052	1572965250	7425824949-	2527154252-	1161781554
49743	2319281051	2332428851	2212002051-	8083577552	1874808053	5000000052	6941000052
59744							
19745	1975497053	5648474055	5590684553	1791447651	8457300150-	3034362754	7079082054
29746	8205990854	1307160157	1306605557	1052535855	5950893154-	2593467953-	9170726753
39747	4644223850	2624815750-	2154196052	1576849750	7444213249-	2527167352-	1162400754
49748	2319281051	2332971651	2212002051-	8080724852	1874279153	5000000052	6941000052
59749							

NOSE FAIRING JETTISON

19750	1965000054	1231000053	5600000050-	1740000051	1105900054	2931799754	2912699754
19751	8150000051-	4385000052	1951000052-	2557359650-	1389445551	3195929752-	
19752							
19753	1975497053	5451974055	5747816153	1876198451	9389248750-	3034362654	7079082054
29754	7094727654	1220794257	1220219857	1008340555	5499794954-	2371672353-	9170726753
39755	4761943750	2596247550-	1977479852	1692298950	8468960949-	2658522052-	1162400854
49756	2319448051	2332971751	2212002051-	8080724852	1874279153	5000000052	6941000052
59757							
19758	2000000053	5386790355	5697299253	1898956251	9503206050-	2836360654	6619827454
29759	7094091054	1194089457	1193515457	1019526855	5555828254-	2369120753-	9181174253
39760	4923110750	2681697350-	1976945652	1699311950	8504117049-	2658538352-	1163404654
49761	2319448051	2333916051	2212002051-	8080710052	1874279053	5000000052	6941000052
59762							
19763	2040000053	5280381155	5611890453	1937314551	9695280950-	2513132254	5870115854
29764	7093018754	1148930057	1148356757	1038438455	5650556854-	2364821453-	9198289553
39765	5212780450	2835277850-	1976107252	1710815950	8561788649-	2658565352-	1165108954
49766	2319448051	2335776851	2212002051-	8080717552	1874280853	5000000052	6941000052
59767							

TABLE 1.3-4. MASS PROPERTIES VERSUS TIME (Continued)

19768	2080000053	5173971855	5522503253	1977250651	9895256550-	2189903554	5120403554
29769	7091902654	1101632957	1101060357	1058229655	5749689254-	2360347753-	9220380655
39770	5541707450	3009670550-	1975162552	1722353950	8619631649-	2658591952-	1166894854
49771	2319448051	2338186851	2212002051-	8080716052	1874280453	5000000052	6941000052
59772							
19773	2105000053	5107466055	5464541953	2003055751	1002447351-	1987885654	4651833454
29774	7091181654	1070948857	1070376957	1071061955	5613965554-	2357457753-	9235327853
39775	5770699850	3131080950-	1975159852	1729591150	8655914749-	2658608852-	1168058854
49776	2319448051	2340091151	2212002051-	8076460052	1873367353	5000000052	6941000052
59777							
19783	2120000053	5067582655	5428955053	2018855951	1010359051-	1866738754	4370828354
29784	7090740454	1052082857	1051511057	1078940655	5853428454-	2355088853-	9244604753
39785	5918110950	3209236950-	1974350252	1733934850	8677690549-	2658618752-	1168863854
49786	2319541051	2341424851	2212002051-	8076455052	1873367053	5000000052	6941000052
59787							
19788	2160000053	4961226955	5330967653	2062231651	1032078951-	1543660554	3621481554
29789	7089529254	1000098857	9995277156	1100633255	5962081654-	2350834253-	9270496253
39790	6353171550	3439904350-	1973172252	1745549550	8735920249-	2658645552-	1171144254
49791	2319541051	2346004651	2212002051-	8076455052	1873367053	5000000052	6941000052
59792							
19793	2200000053	4854871255	5228253853	2107507851	1054750551-	1220622354	2872134754
29794	7088265454	9455509456	9449807056	1123370955	6075966654-	2345768853-	9298060253
39795	6861352450	3709340850-	1972256552	1757206950	8794374049-	2658672352-	1173618554
49796	2319541051	2353008551	2212002051-	8076456052	1873366453	5000000052	6941000052
59797							
19798	2225000053	4788398955	5161250953	2136826851	1069431651-	1018710954	2403793154
29799	7087447254	9098511756	9092813656	1138202255	6150252154-	2342490153-	9323836853
39800	7226866850	3903144150-	1971352952	1764450250	8830679449-	2658688952-	1175306254
49801	2319541051	2359642151	2212002051-	7812773352	1841782753	5000000052	6941000052
59802							
19808	2240000053	4749384855	5120951953	2154417851	1078240251-	9015193553	2127525754
29809	7086956354	8883635556	8877939356	1147123055	6194932954-	2340522653-	9340046453
39810	7461102350	4027341050-	1970640752	1768703450	8852004949-	2658698952-	1176477254
49811	2357401051	2359933551	2212002051-	7812769552	1841783353	5000000052	6941000052
59812							

TABLE 1.3-4. MASS PROPERTIES VERSUS TIME (Continued)

19813	2280000053	4645347255	5009701353	2202771651	1102453251-	5890085753	1390812454
29814	7065607354	8289230556	8283543056	1171748855	6318273654-	2335116553-	9391743653
39815	8172483850	4404543850-	1969539252	1780025250	8908773649-	2658725852-	1179909654
49816	2357401051	2361277051	2212002051-	7812777052	1841784853	5000000052	6941000052
59817							
19818	2320000053	4541309555	4891854453	2232124951	1102612251-	2764974953	6540985153
29819	7064174954	7654686656	7648966756	1188292155	6335761554-	2231335053-	9516332053
39820	8981115850	4786082450-	1898069052	1774255550	8764387149-	2628818652-	1184301954
49821	2357401051	2365658051	2212002051-	7812772652	1841783853	5000000052	6941000052
59822							

SUSTAINER ENGINE CUT-OFF

19823	2353936053	4453044055	4775370353	1727939651	4739537050-	1136324452	2907075652
29824	6563879254	6968815656	6962071356	9197857854	2974543054-	2929034752	1119794054
39825	7639631950	2468730750-	2482113551-	1351651450	3707428749-	1533833752-	1189604754
49826	2357401051	2558314951	2212002051-	5888045851	1506347152	5000000052	6941000052
59827							
19833	2360000053	4451907755	4773603553	1719574251	4636206450-	7792733351	1993626752
29834	6540488754	6957185656	6950421856	9146373454	2910740254-	3340066652	1122498254
39835	7609645150	2419826950-	2820206451-	1344783350	3625725349-	1508894052-	1189715054
49836	2558315051	2558315151	2212002051-	5887528951	1506215452	5000000052	6941000052
59837							
19838	2373236053	4449427655	4769724553	1701301651	4410501350-		
29839	6522164654	6931540756	6924742556	9033145154	2770431854-	4237731252	1128400054
39840	7543405450	2311727850-	3553260251-	1329789350	3447388449-	1453357052-	1189958154
49841	2558315051		2212002051-	2007244251	2329982351	5000000052	6941000052
59842							

SUSTAINER JETTISON

19843	6233000054	9498682553	9410848[illegible]	2982977051-	4408352554	1251301856	1257953756
19844	1213904054	2148386853-	6530753152	5760532650	1014053950-	5554560551-	
19845							
19846	2373236053	3614900055	3685304453	4551520149-	1341570750	5099246054	2503867555
29847	1969918754	7192000955	7202095255	9900838952-	4866410052	1990830252	3760644353
39848	8098021749-	3986050249	1076328952	3069132949-	9046331049	7125956952-	1860424953
49849	1160714351	4910270151	1030000050	2007244251	2329982351	4218000051	6878000052
59850							

TABLE 1.3-4. MASS PROPERTIES VERSUS TIME (Continued)

19851	2380000053	3614599655	3685368153	4551898449-	1342414750	5097888354	2503709955
29852	1969896854	7190989055	7201081155	9900612552-	4870906752	1990833152	3760735453
39853	8099006649-	3990309649	1076543552	3069618149-	9052700649	7126908152-	1861387753
49854	1160714351	4911268751	1030000050	2007250051	2330000051	4218000051	6878000052
59855							
19856	2400000053	3613711655	3685555653	4553016949-	1344910750	5093873854	2503243955
29857	1969832254	7187998055	7198083655	9899946252-	4884217652	1990842052	3761004253
39858	8101922949-	4002922149	1077178152	3071050149-	9071534969	7129715052-	1864173953
49859	1160714351	4914224451	1030000050	2007500051	2330000051	4218000051	6878000052
59860							
19861	2420000053	3612823555	3685742253	4554136149-	1347408150	5089858854	2502777955
29862	1969767654	7185040155	7195119355	9899286152-	4897526352	1990850952	3761272353
39863	8104805549-	4015524649	1077883852	3072480049-	9090377149	7132513952-	1866869553
49864	1160714351	4917185351	1030000050	2007512651	2330006651	4218000051	6878000052
59865							

CENTAUR MAIN ENGINE START

19866	2438236053	3612013755	3685912453	4555157149-	1349686250	5086197954	2502353055
29867	1969708654	7182335055	7192407755	9898682352-	4909657552	1990859052	3761516453
39868	8107445749-	4027026749	1078439452	3073784949-	9107571649	7135059052-	1869248553
49869	1160714351	4919889251	1030000050	1179242652	5799856652	4218000051	6878000052
59870							
19876	2600000053	3499961355	3692594353	4700992049-	1454196850	4897280854	2408746055
29877	1967932054	7042798955	7052696955	9874972052-	5254651952	1991229852	38058745.3
39878	8252634349-	4397734449	1095869352	3197354749-	9890646849	7208552352-	1977296153
49879	4918291051	4918537751	5219130050-	1179241052	5799850052	4218000051	6878000052
59880							
19881	2800000053	3361423355	3699509153	4894739149-	1537420050	4661432654	2292749055
29882	1967278154	6880186155	6890017355	9850433552-	5329086952	1991525152	3848651353
39883	8432126649-	4568502249	1102751452	3356683749-	1054321250	7233989952-	2076841553
49884	4918291051	4918550151	5219130050-	1179241552	5799850052	4218000051	6878000052
59885							
19886	3000000053	3222885255	3704920753	5105143149-	1627796050	4425584354	2176752055
29887	1966623054	6726693055	6736457355	9831232752-	5418193652	1991845852	3885119153
39888	8613212749-	4754025749	1109737152	3523797349-	1123576150	7258737152-	2165017853
49889	4918291051	4918564151	5219130050-	1179243052	5799860052	4218000051	6878000052
59890							

TABLE 1.3-4. MASS PROPERTIES VERSUS TIME (Continued)

19891	3200000053	3084347155	3708859253	5334448349-	1726290650	4189735754	2060754855
29892	1965966654	6581442455	6591142055	9817255452-	5522390452	1992195352	3917998053
39893	8796334149-	4955630649	1116591252	3699627749-	1197241750	7282821352-	2250468953
49894	4918291051	4918579551	5219130050-	117924155?	5799850052	4218000051	6878000052
59895							
19896	3400000053	2945809055	3711239653	5585321449-	1834049550	3953887454	1944757855
29897	1965308754	6444057555	6453692455	9808810052-	5643409252	1992577752	3948561253
39898	8981734049-	5175538749	1123540252	3884810449-	1275651550	7306267352-	2335772353
49899	4918291051	4918596851	5219130050-	117924155?	5799855052	4218000051	6878000052
59900							
19901	3600000053	2807270955	3711909353	5860955649-	1952444150	3718039154	1828760755
29902	1964649154	6313985755	6323553755	9806433352-	5783846652	1992997852	3977526153
39903	9170185049-	5417057349	1130822152	4079841649-	1359104150	7329100352-	2421100353
49904	4918291051	4918616151	5219130050-	1179242052	5799855052	4218000051	6878000052
59905							
19906	3800000053	2668732955	3710661153	6165206749-	2083130750	3482190754	1712763655
29907	1963987554	6190574755	6200075955	9810863152-	5947056252	1993461552	4005385553
39908	9362912549-	5684530649	1138202352	4285134049-	1447879550	7351341952-	2506437153
49909	4918291051	4918638151	5219130050-	1179241552	5799850052	4218000051	6878000052
59910							
19911	4000000053	2530194855	3707221853	6502776049-	2228128650	3246342454	1596766655
29912	1963323654	6072907855	6082342155	9823067652-	6137325352	1993976052	4032480353
39913	9561966149-	5983797149	1145708052	4500983049-	1542225450	7373015852-	2591783353
49914	4918291051	4918663551	5219130050-	117924155?	5799855052	4218000051	6878000052
59915							
19916	4200000053	2391656755	3701241053	6879453149-	2389924750	3010494154	1480769555
29917	1962657154	5959899355	5969268955	9844289252-	6360084552	1994550152	4059068253
39918	9770201949-	6322494249	1153092252	4727547749-	1642347850	7394141352-	2677138153
49919	4918291051	4918692651	5219130050-	1179242052	5799855052	4218000051	6878000052
59920							
19921	4400000053	2253118755	3692270453	7302451549-	2571617550	2774645754	1364772455
29922	1961987354	5850240355	5859543055	9876119352-	6622222252	1995194952	4085377953
39923	9991581949-	6710680649	1160844852	4964813749-	1748394550	7414739752-	2762501453
49924	4918291051	4918726751	5219130050-	1179242552	5799855052	4218000051	6878000052
59925							
19926	4600000053	2114580555	3679733753	7780876649-	2777118050	2538797254	1248775355
29927	1961313754	5742210155	5751446055	9920606952-	6932554852	1995924152	4111519653
39928	1023176150-	7161913549	1168724152	5212543549-	1860433350	7434829352-	2847873953
49929	4918291051	4918767451	5219130050-	1179241552	5799855052	4218000051	6878000052
59930							

TABLE 1.3-4. MASS PROPERTIES VERSUS TIME (Continued)

19931	4800000053	1976042455	3662887653	83263&5149-	3011433150	2302948954	1132778255
29932	1960635554	5633752255	5642919055	99803&3052-	7302426252	1996755552	4137598153
39933	1049837550-	7694394149	1177016152	5470242149-	1978434550	7454427952-	2933252653
49934	4918291051	4918816051	5219130050-	1179241052	5799850052	4218000051	6878000052
59935							
19936	5000000053	1837504455	3640755053	89541&0049-	3281080350	2067100754	1016781255
29937	1959951654	5522357455	5531457555	1005891853-	7746724052	1997712352	4163891653
39938	1080189150-	8333142449	1185200652	573707294&-	2102233&50	7473553852-	3018636853
49939	4918291051	4918876051	5219130050-	1179242552	5799855052	4218000051	6878000052
59940							
19941	5200000053	1698966355	3612015753	9684294549-	3594703150	1831252254	9007841054
29942	1959260654	5404714255	5413747455	10160&9853-	8285513752	1998825252	4190686153
39943	1115740850-	9113893049	1193591452	6011684149-	2231460250	7492222552-	3104029853
49944	4918291051	4918951651	5219130050-	1179241552	5799854552	4218000051	6878000052
59945							
19946	5400000053	1560428255	3574866853	1054408750-	3964014250	1595403954	7847870154
29947	1958560754	5276303355	5285265355	1029271753-	8946189252	2000136752	4218219253
39948	1158731950-	1008920650	1202701852	6292163049-	2365505250	7510450652-	3189432253
49949	4918291051	4919049151	5219130050-	1179241552	5799853552	4218000051	6878000052
59950							
19951	5600000053	1421890155	3526771953	1157142250-	4405290950	1359555654	6687899454
29952	1957849254	5130834055	5139724855	1046337853-	9767281352	2001701552	4246832653
39953	1212603450-	1133972750	1212068752	6575826949-	2503431250	7528253052-	3274843153
49954	4918291051	4919180551	5219130050-	1179242552	5799857552	4218000051	6878000052
59955							
19956	5800000053	1283352055	3464074453	1282055950-	4941839450	1123707154	5527927954
29957	1957122454	4959356555	4968178355	1068585453-	1060434153	2003605452	4276964353
39958	1282880250-	1299507050	1221471552	6859147149-	2643923550	7545644052-	3360261553
49959	4918291051	4919367251	5219130050-	1179241052	5799649052	4218000051	6878000052
59960							
19961	6000000053	1144814055	3381282553	1437202050-	5608246850	8878589153	4367958154
29962	1956374854	4748415355	4757161655	1097963553-	1214081053	2005970152	4309313453
39963	1379104650-	1527881850	1232049652	7137412149-	2785138950	7562636752-	3445688653
49964	4918291051	4919653451	5219130050-	1179241752	5799853552	4218000051	6878000052
59965							
19966	6200000053	1006275955	3269785353	1635067550-	6458148850	6520105853	3207987454
29967	1955597754	4476920955	4485591855	1137527253-	1390755553	2008985952	4345088053
39968	1519217150-	1861167550	1243116852	7404467749-	2924574450	7579245652-	3531125853
49969	4918291051	4920146251	5219130050-	1179242252	5799855552	4218000051	6878000052

TABLE 1.3-4. MASS PROPERTIES VERSUS TIME (Continued)

59970							
19971	6400000053	8677377954	3115218753	1896113150-	7579431950	4761621553	2048016354
29972	1954776954	4109313155	4117902955	1192373853-	1632285053	2012964752	4386808053
39973	1741706850-	2389494350	1255594352	7651827449-	3058677750	759548275?-	3616580453
49974	4918291051	4921197951	5219130050-	117?241752	5799854052	4218000051	6878000052
59975							
19976	6600000053	7291997154	2891624453	2256349050-	9126772050	1803138153	8880455053
29977	1953887754	3580222155	3588725455	1271714353-	1976109053	2018455352	4441586353
39978	2147222950-	3348234750	1269793052	7866685449-	3181988150	7611354952-	3707622553
49979	4918291051	4924999951	5219130050-	1179241852	5799854252	4218000051	6878000052
59980							
CENTAUR MAIN ENGINE CUT-OFF							
19981	6727229053	6410694054	2690661353	2566538050-	1045914451	3028005452	1501358553
29982	1953266154	3099885955	3108329255	1343024553-	2286951653	2023183152	4506341653
39983	2641516950-	4510902850	1280280052	7973139849-	3249177050	7621278452-	3791099153
49984	4918291051	4958242551	5219130050-	2694115152	1335807553	4218000051	6878000052
59985							
19991	6737229053	6250694054	2646648053	2632234150-	1073313051	3338904351	1655509652
29992	1953191254	2992466655	3000902855	1358642253-	2352237353	2024155352	4574395753
39993	2774539750-	4817785650	1281756352	7986636449-	3256577450	7622051952-	3813305453
49994	4958242051	4958242151	5219130050-			4218000051	6878000052
59995							
19996	6230800054	2640879053	2640638450-	1076739951	1953185954	2986471155	2978035355
19997	1360689353-	2360584553	2024276952	2793085850-	4859947250	1281876452	

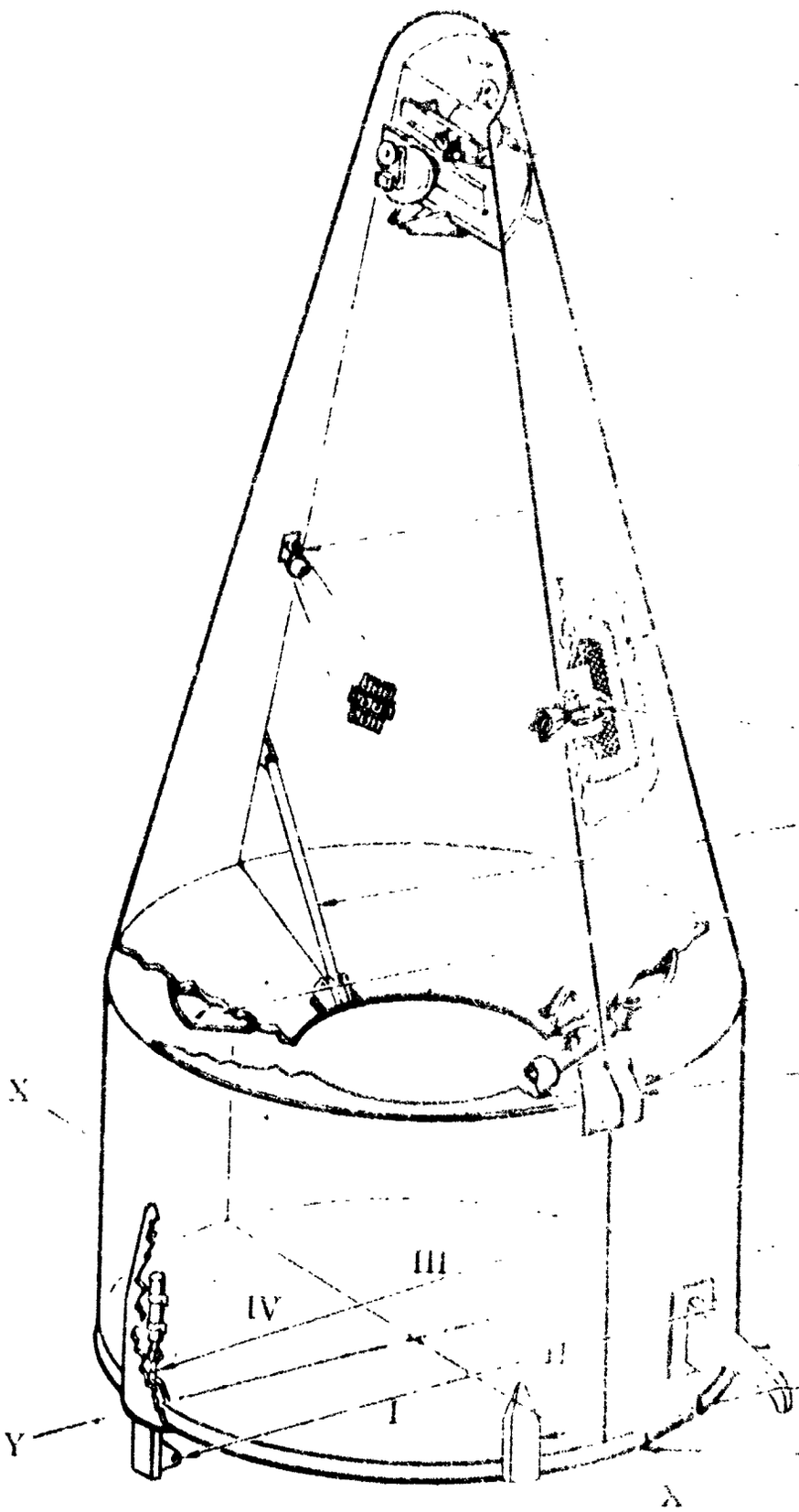

- NOSE CAP
- HEAT BUCKLES
- DIFFUSER BOTTLES
- OUTLETS FOR BUCKLED (ONLY ONE-HALF SHOWN)
- LIGHT AND CAMERA PORTS
- THERMAL BLANKET
- EXPLOSIVE CAVITY
- SUPPORT STRUTS FOR THERMAL BLANKET (FOUR)
- AIR CONDITIONING DUCT
- AIR CONDITIONING DISCONNECT
- EXPLOSIVE CAVITY FAIRING (ONLY ONE SHOWN)
- VENT ACTUATOR AND FAIRING
- BUTTOCK LINES
- VENT PIN
- DETONATOR FAIRING (ONLY ONE SHOWN)
- 218.90 AREA:
  - RING
  - SKIRT
  - ESC

SECTION II

NOSE FAIRING

2.1 INTRODUCTION

The Surveyor low drag nose fairing is a lightweight conical shroud which is attached to the front of the Centaur/Surveyor vehicle.

The primary function of the fairing is to encapsulate the payload and protect it and the electrical/electronic equipment mounted on the forward bulkhead from ambient environments prior to and during launch. In addition, the fairing reduces aerodynamic heating and loads on the vehicle, electronic equipment, and payload during ascent through the earth's atmosphere.

The fairing consists of a nose cone, a cylindrical (barrel) section, a fairing skirt, a thermal bulkhead, an environmental control and fuel venting duct assembly, and a separation system. The nose cone and cylindrical section is comprised of two halves joined during installation onto the vehicle. The base of the fairing bears on the Station 218.9 tank ring, which is attached to the liquid-hydrogen tank of the Centaur upper stage. See Figure 2.1-1 for configuration. A split line along the vehicle X-X axis allows the fairing to be jettisoned during flight. Explosive latches are provided; they carry the tension loads between the fairing halves. Hinge fittings that attach to the nose fairing and liquid-hydrogen tank are provided to permit jettisoning of the fairing.

Vent holes are located in the thermal bulkhead and around the periphery of the forward portion of the barrel section to provide for venting the environmental control gases overboard during ground operations. The vent holes (Station 154.5) also tend to equalize internal and external pressures as the vehicle ascends through the atmosphere.

The nose fairing separation system is designed to separate and jettison the fairing during flight. Separation occurs after aerodynamic loads and aerodynamic heating have diminished essentially to zero. Electrical signals from the Atlas booster activate the system.

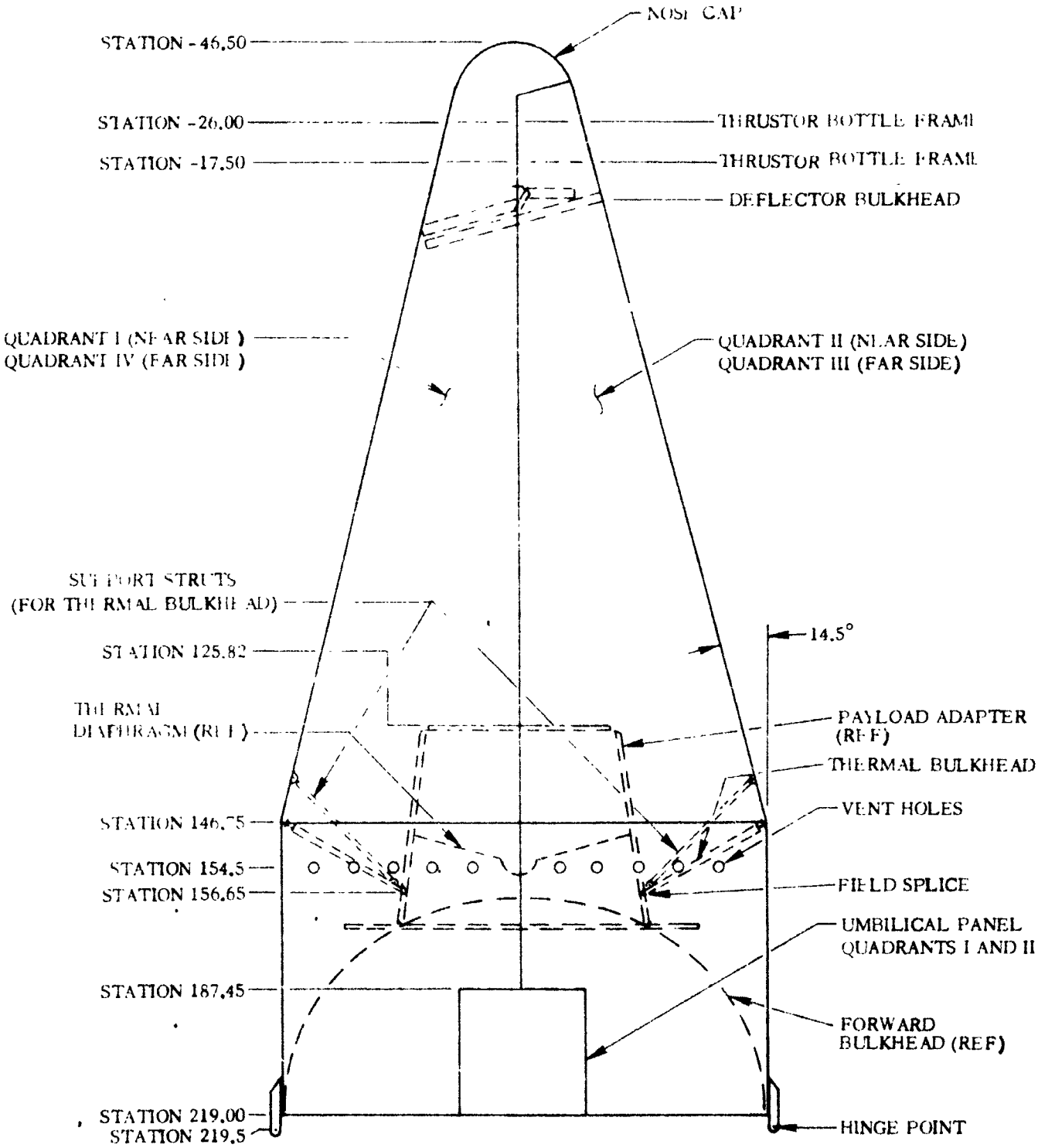

4B731.V

Figure 2.1-1. Surveyor Nose Fairing Configuration

2.2 BASIC SHELL

The basic shell structure is phenolic Fiberglas sandwich, with cloth faces bonded to a honeycomb core. Figure 2.2-1 presents basic dimensions of the Fiberglas shell structure.

2.2.1 CRITICAL CONDITIONS. Severe loads are imposed on the subject fairing at primarily three times during the course of flight. These flight times are known as transonic flight, booster engine cutoff (BECO), and fairing jettison and occur in the sequence as presented. The nose fairing may also be subjected to a critical loading condition during vehicle erection, whereby ground winds and inertia may impose servere loads on the handling fittings.

2.2.1.1 Transonic Flight. During transonic flight, the barrel section experiences fluctuating pressure aft of the shoulder or Station 146. The maximum steady-state aerodynamic loads also exist at this time; consequently these two load contributions comprise the transonic flight loads. Maximum or extreme temperature conditions do not occur at this point in flight.

2.2.1.2 Booster Engine Cutoff. At BECO, the maximum inertia loads become apparent and must be considered along with maximum temperatures which exist along the surface of the fairing. Aerodynamic loads (steady-state and fluctuating) have diminished essentially to zero at this time, therefore these should not be considered for any load contribution at BECO.

2.2.1.3 Fairing Jettison. During fairing jettison, each half of the fairing is subjected to bending caused by rapid angular acceleration. The applied loads at the thruster bottles are presented in Subsection 2.8. High temperatures exist at this time if no Thermolag is used on the fairing.

2.2.2 WEIGHT AND CENTER OF GRAVITY DATA. Since Thermolag is planned for use on the operational vehicle, two sets of data are presented for the purpose of proper design and/or analysis at a particular time during the life of the fairing or vehicle, i.e., before and after sublimation of Thermolag.

Respective of the particular analysis, the following must be taken into account:

a. Nose fairing weight should be considered with Thermolag for all ground handling conditions and flight conditions up to and including BECO (see Table 2.2-1).

b. Nose fairing weight after Thermolag sublimation should be used for loads during nose fairing jettison (see Table 2.2-2).

c. Figure 2.2-2 is presented to indicate the distribution of nose fairing weight versus station at time of jettison.

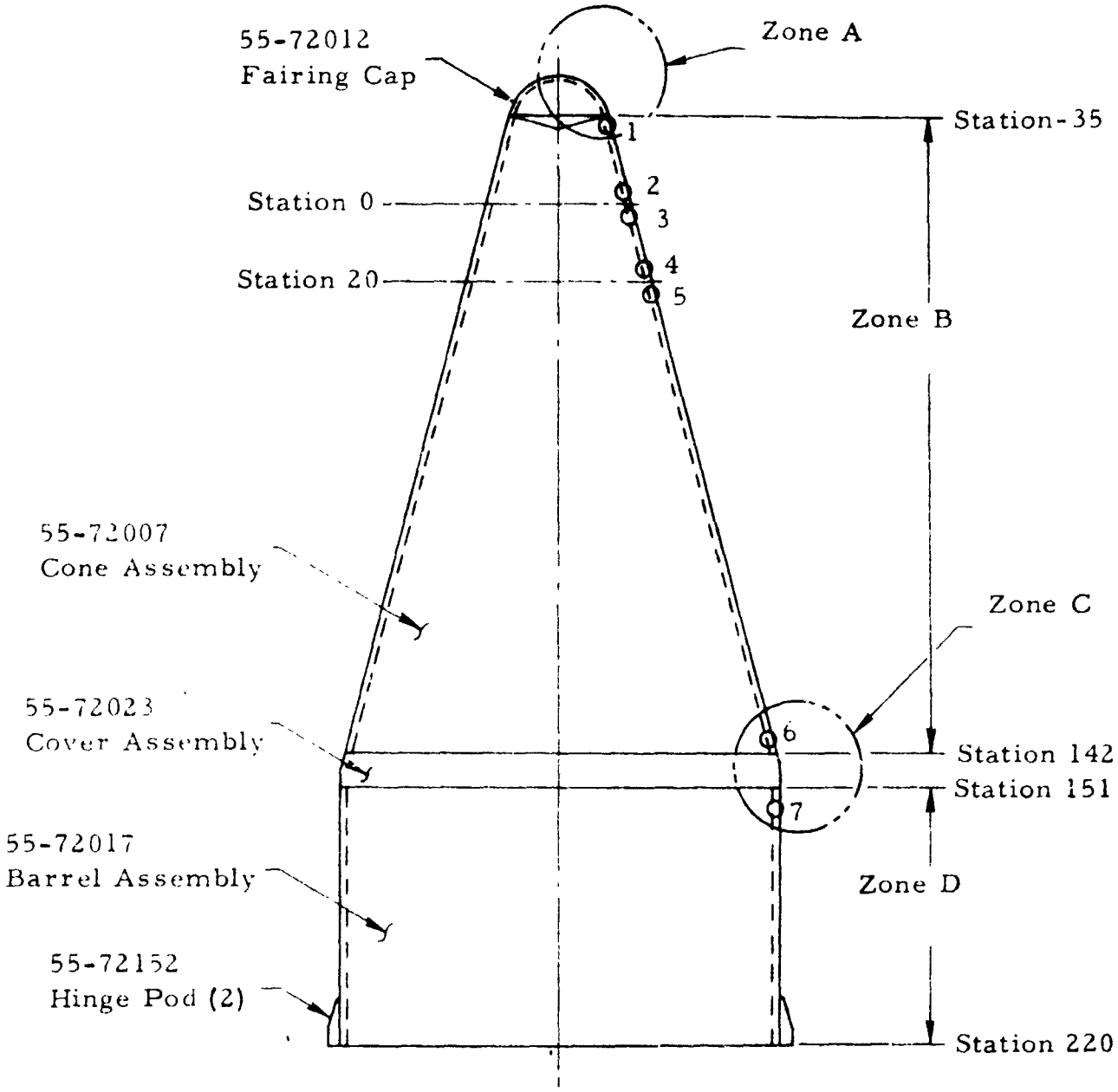

Zone	Station	Outside skin thickness (inches)	Inside skin thickness (inches)	Core thickness (inches)
A	-46 to -35	0.03	0.03	0.14 (solid)
B_1	-35	0.06	0.06	0.50
2	0	0.06	0.06	0.70
3	0	0.05	0.04	0.70
4	20	0.05	0.04	0.80
5	20	0.04	0.04	0.80
6	142	0.04	0.04	1.50
C	146	0.02	0.02	0.15
D_7	154	0.04	0.04	1.50

4B74LV

Figure 2.2-1. Surveyor Nose Fairing Shell Geometry

TABLE 2.2-1. NOSE FAIRING WEIGHTS DATA - HANDLING AND TRANSPORTING CONDITION*

Unit	Weight** (lb)
Complete Nose Fairing	1980
Heaviest Conical Half	556
Heaviest Cylindrical Half	511

NOTES:

*Also to be used for flight conditions up to and including BECO.

**A weight contingency factor of ±10% shall be considered for strength evaluation.

TABLE 2.2-2. NOSE FAIRING WEIGHTS DATA - JETTISON CONDITION*

Item	Weight** (lb)	C. G.		
		z	y	x
Complete Nose Fairing	1879	123.6	-0.2	1.9
Quadrants I & IV Combined	902	122.0	30.0	0.0
Quadrants II & III Combined	977	125.0	-29.0	3.0

Mass Moments of Inertia about C.G.

Item	I_{zz} ($in.^2$-lb)	I_{yy} ($in.^2$-lb)	I_{xx} ($in.^2$-lb)
Quadrants I & IV Combined	1,496,000	6,282,000	5,573,000
Quadrants II & III Combined	1,784,000	6,796,000	5,802,000

NOTES:

*To be used after sublimation of Thermolag.

**A weight contingency factor of ±10% shall be considered for strength evaluation.

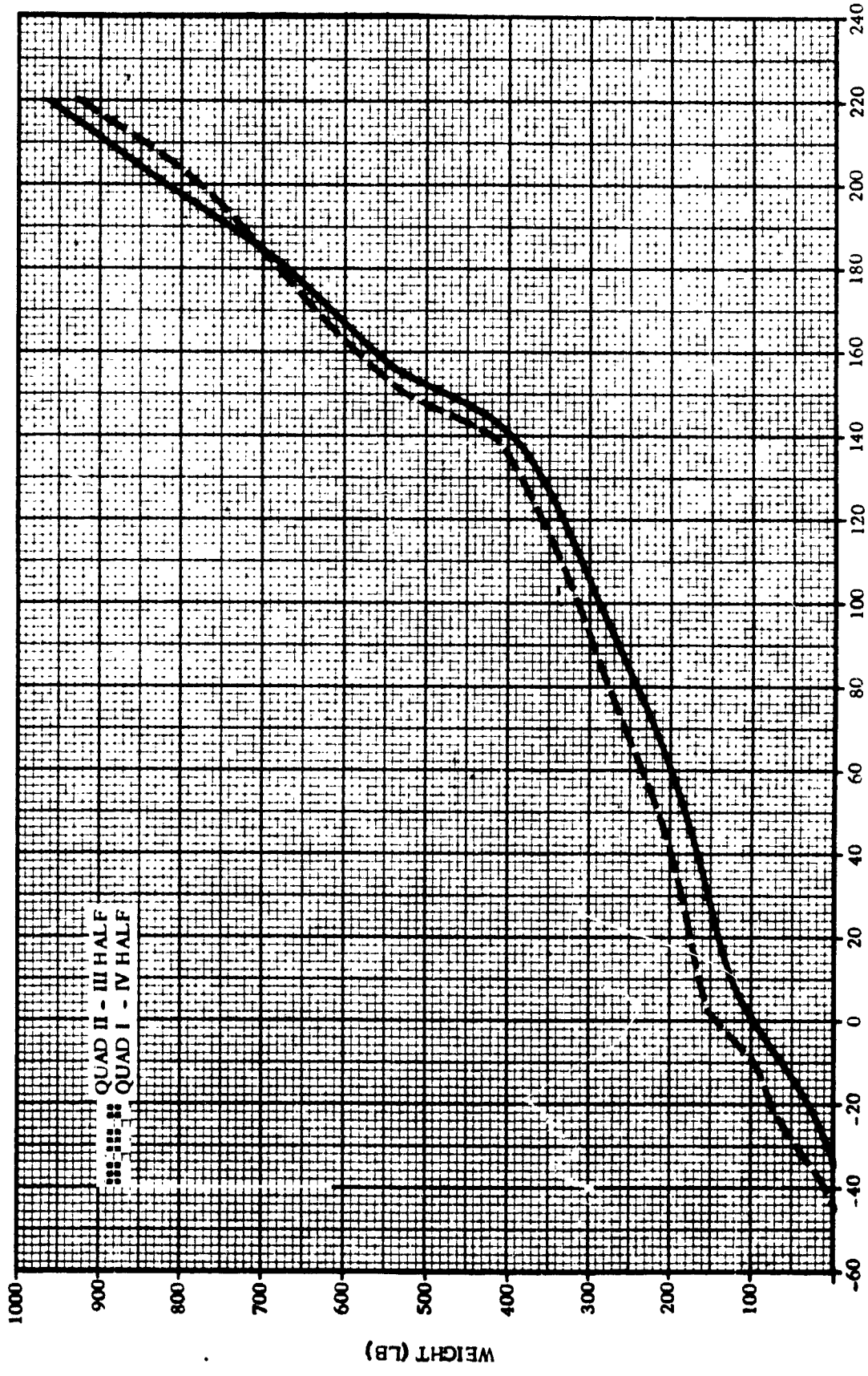

Figure 2.2-2. Nose Fairing Weight Distribution at Time of Jettison

2.2.3 THERMAL DATA. All data presented in this section assumes the maximum heating trajectory which would reflect the most severe thermal environment for any of the operational vehicles. Maximum temperatures representing each station along the fairing are given in Figures 2.2-3 and 2.2-4. A typical station (just forward of Station 146) outside bondline temperature plot is shown in Figure 2.2-5 as a function of time to correlate approximately when maximum temperatures occur. The outside bondline temperature distribution during nose fairing jettison is described in Figure 2.2-6 while the inside skin temperatures for this time will be the same as shown in Figure 2.2-4.

2.2.4 INERTIA LOADS. Steady-state inertia loads on the nose fairing are determined from the T-D/W versus time curves shown in Figures 1.3-1 and 1.3-2. Vibratory inertia loads which result from buffet response are represented as equivalent steady-state loads in Paragraph 2.2.6.

The inertia load factors which would be applicable for all ground handling conditions may be found in Reference 1-5.

2.2.5 STEADY-STATE AIR LOADS. Ground wind loads during fairing erection are found in Figure 2.2-7. With the fairing installed on the vehicle, the bending moment at Station 219 due to ground winds = 120,000 in.-lb.

During flight, maximum air loads occur at transonic velocities. Maximum axial drag, shear, and bending moment are presented in Figure 2.2-8, and maximum wall ΔP is presented in Figure 2.2-9. The above mentioned loads include the effects of an angle of attack of 4.5 degrees. The unsymmetrical circumferential pressure distribution due to angle of attack is presented in Figure 2.2-10.

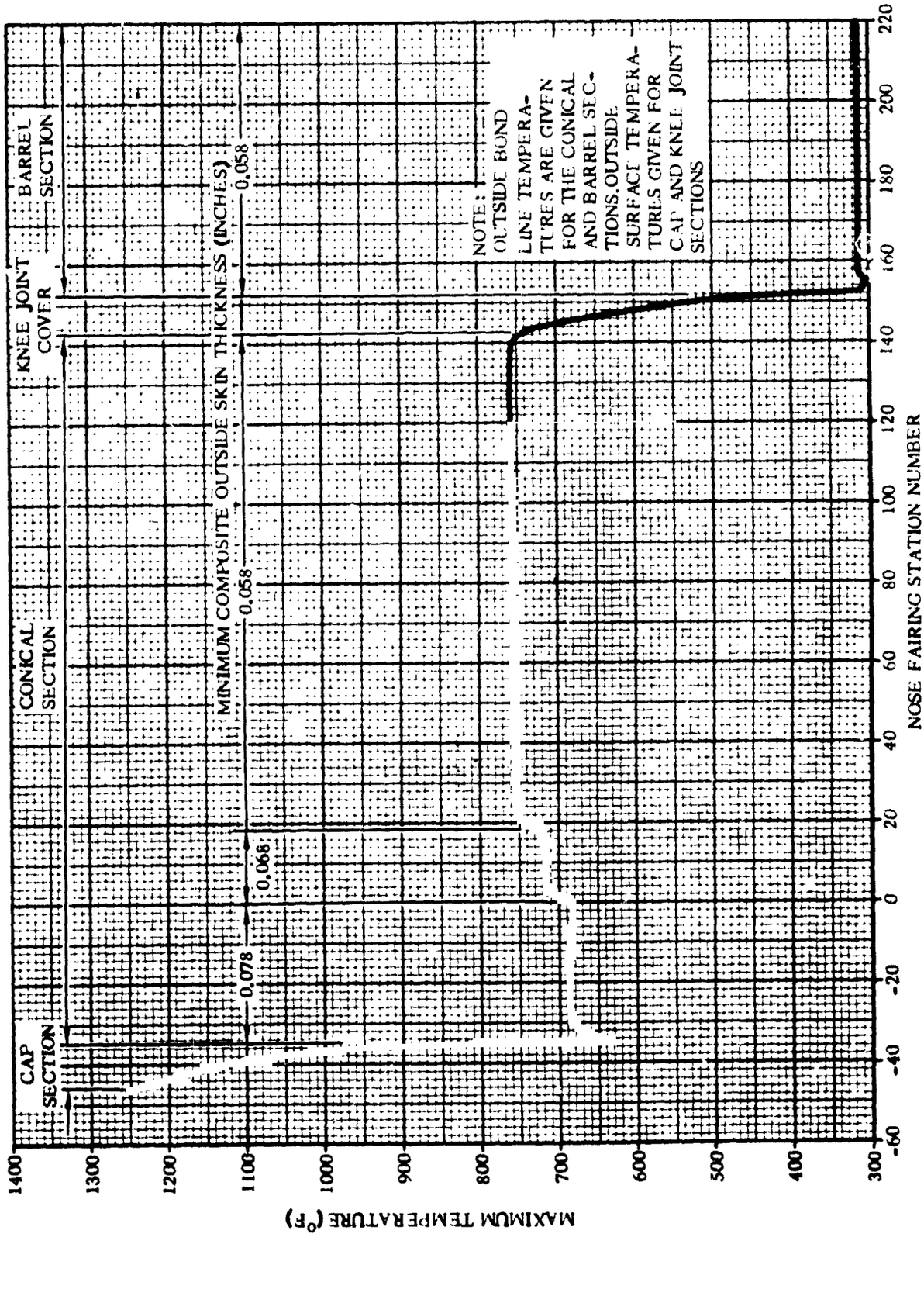

4B76LT

Figure 2.2-3. Nose Fairing Maximum Temperature Distribution

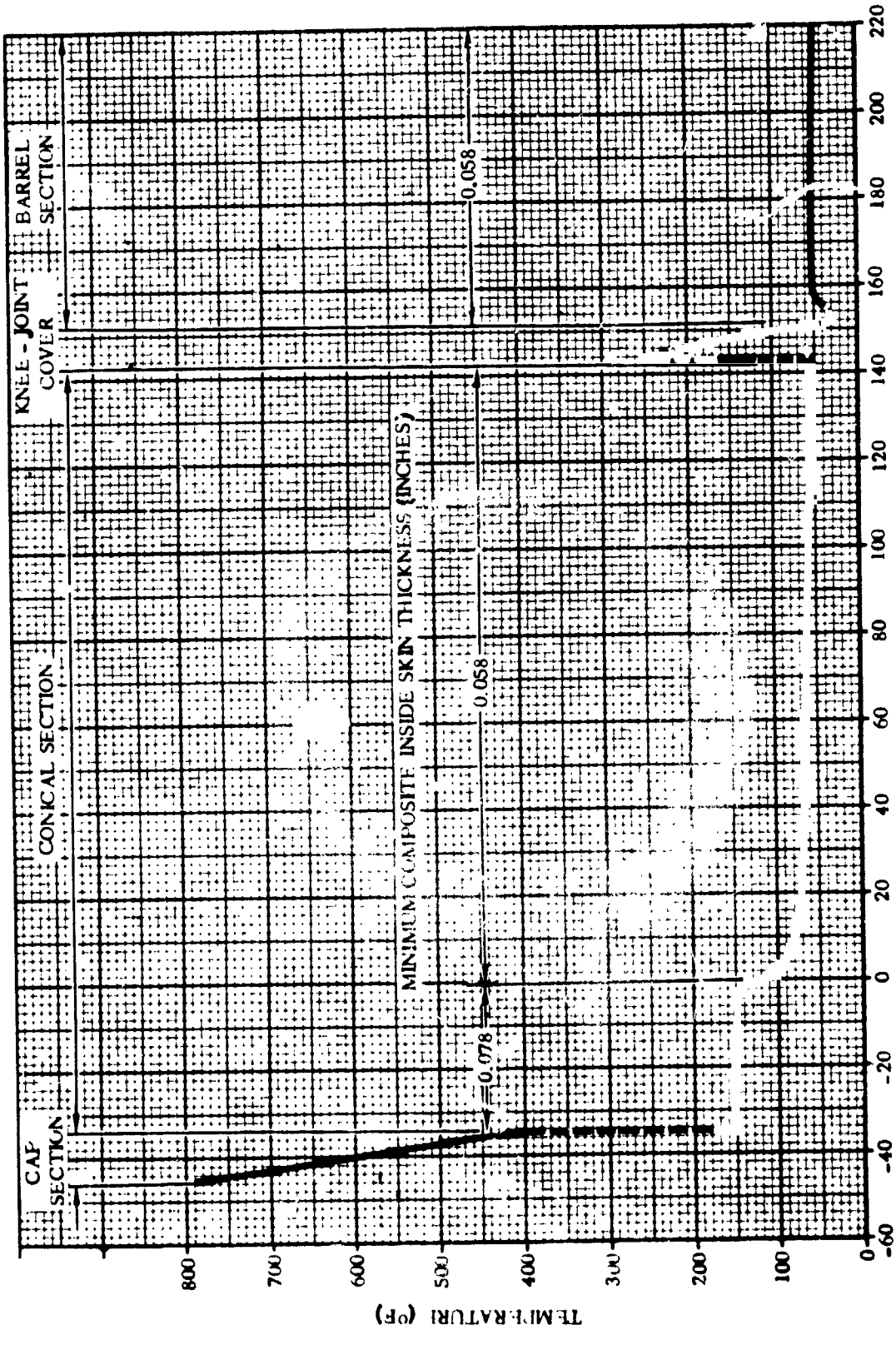

Figure 2.2-4. Nose Fairing Maximum Inside Skin Temperature Distribution

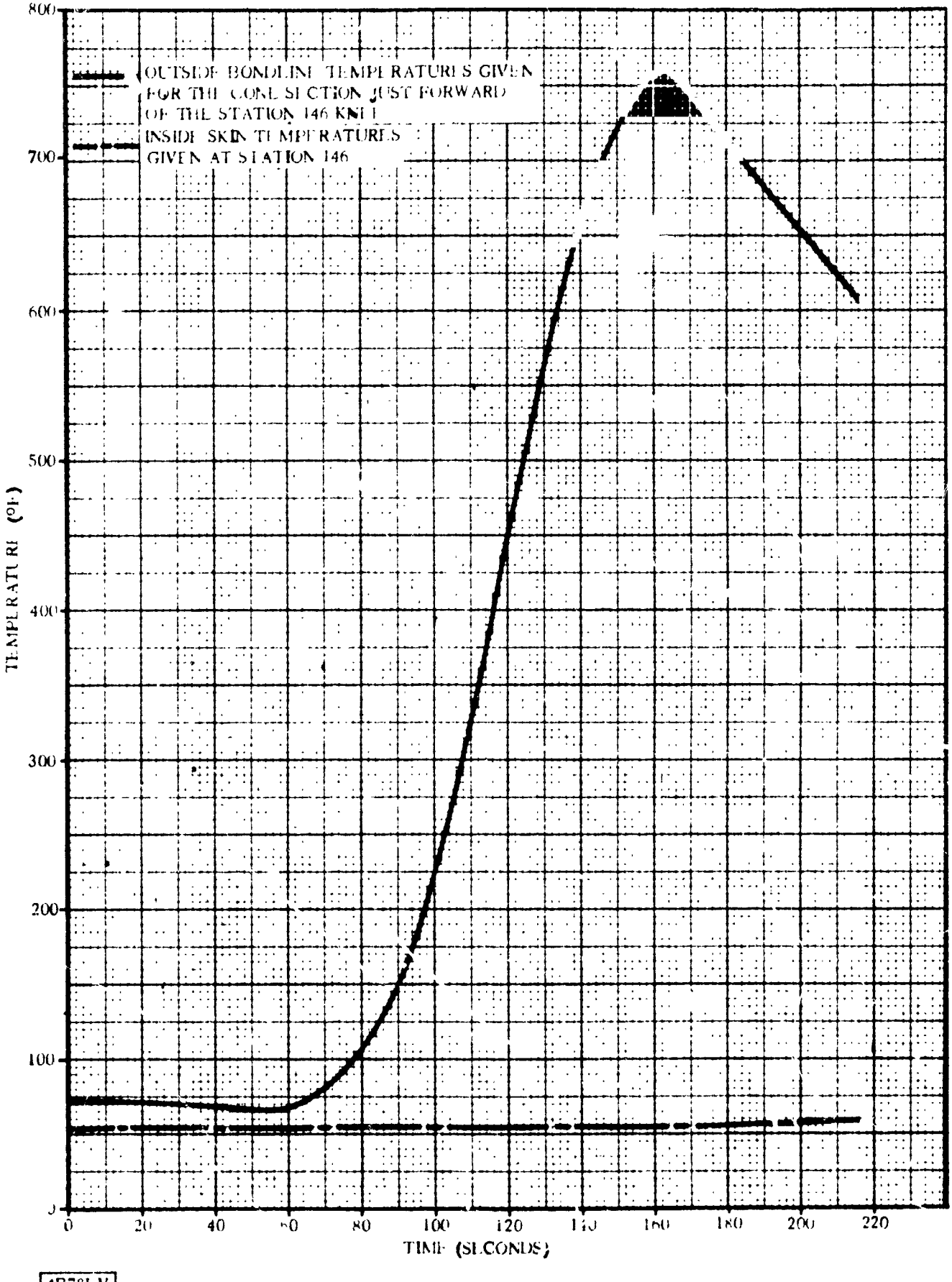

Figure 2.2-5. Nose Fairing Temperature Histories ($0 \leq t \leq 220$)

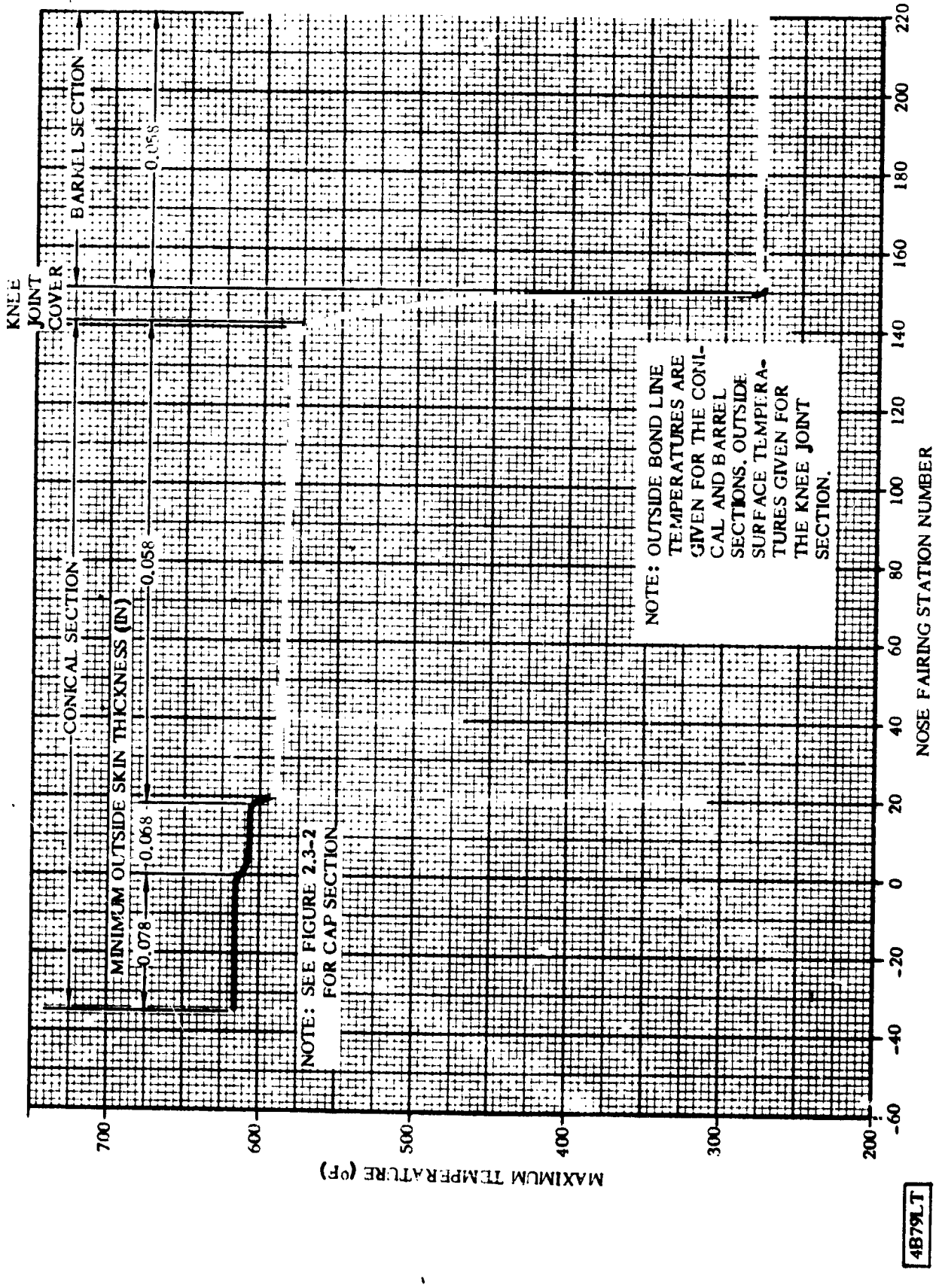

Figure 2.2-6. Nose Fairing Temperature Distribution at the Time of Jettison

NOTE :
STEADY STATE LOADS SHALL BE MULTIPLIED BY A FACTOR OF 2.0 TO ACCOUNT FOR OSCILLATORY LOADS.

THIS APPLIES TO BOTH CONE AND BARREL SECTIONS.

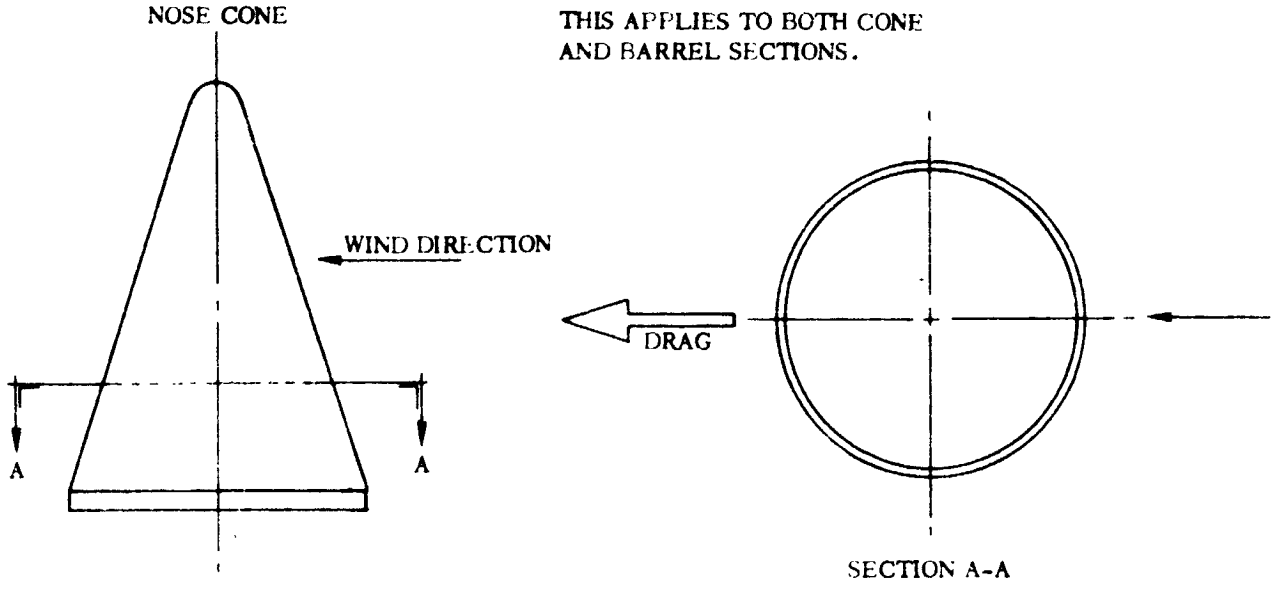

DRAG=153 LB

CYLINDRICAL (BARREL) SECTION

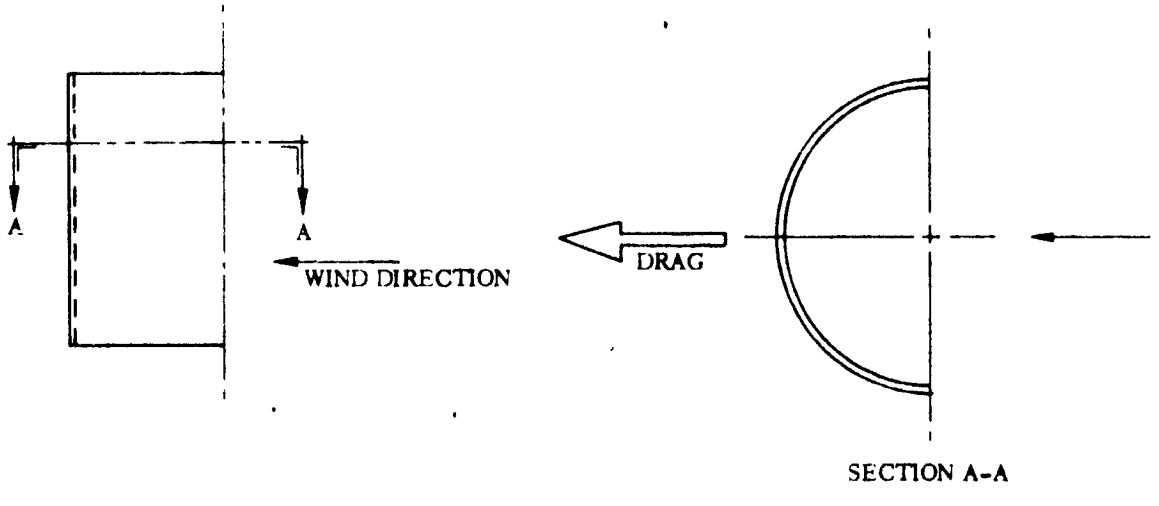

DRAG=174 LB

4B80LV

Figure 2.2-7. Nose Fairing Components Steady-State Wind Loads during Erection

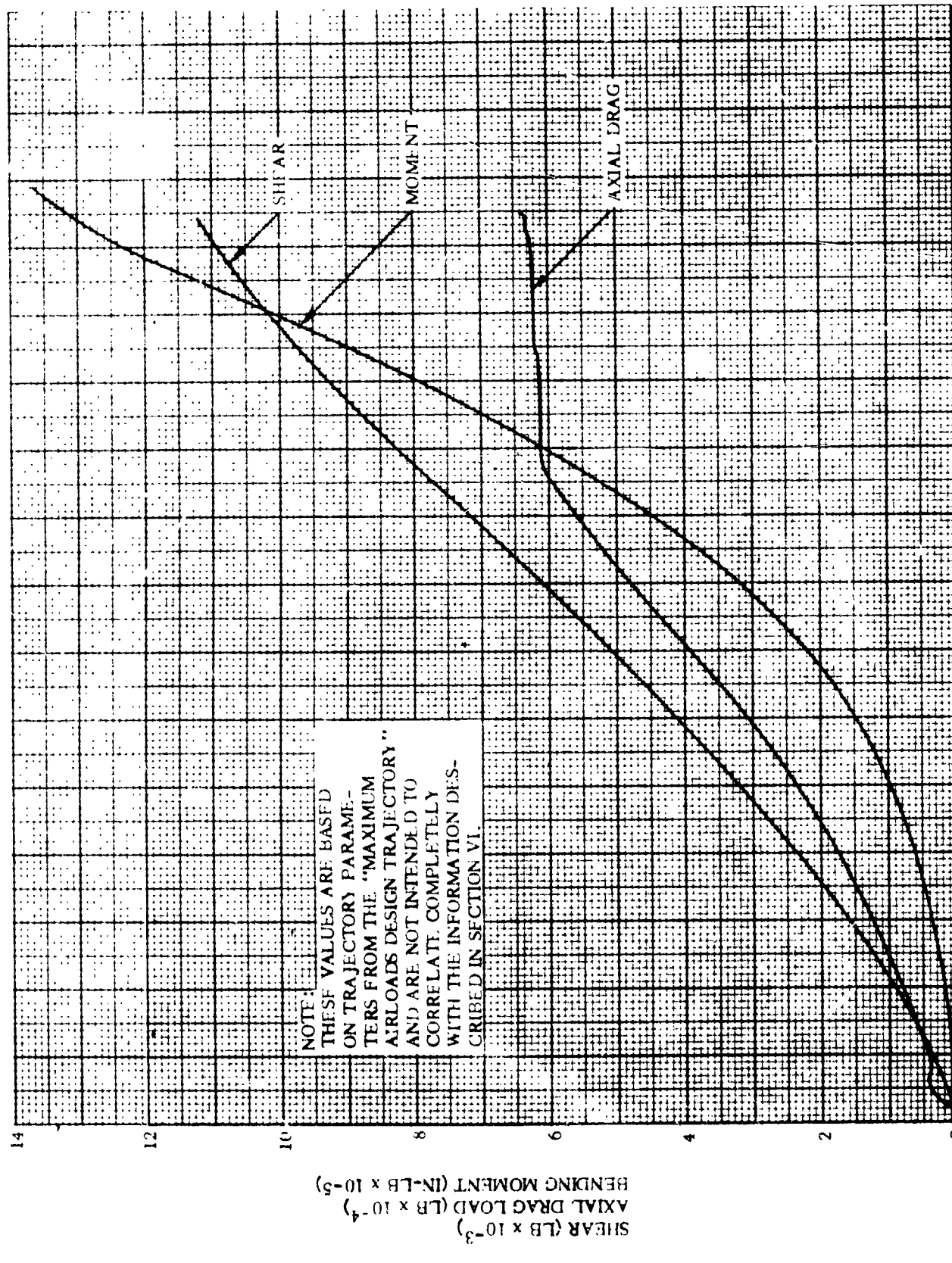

4B81LT

Figure 2.2-8. Nose Fairing Moment, Axial Drag Load, and Shear versus Surveyor Station ($\alpha = 4.5$ Degrees)

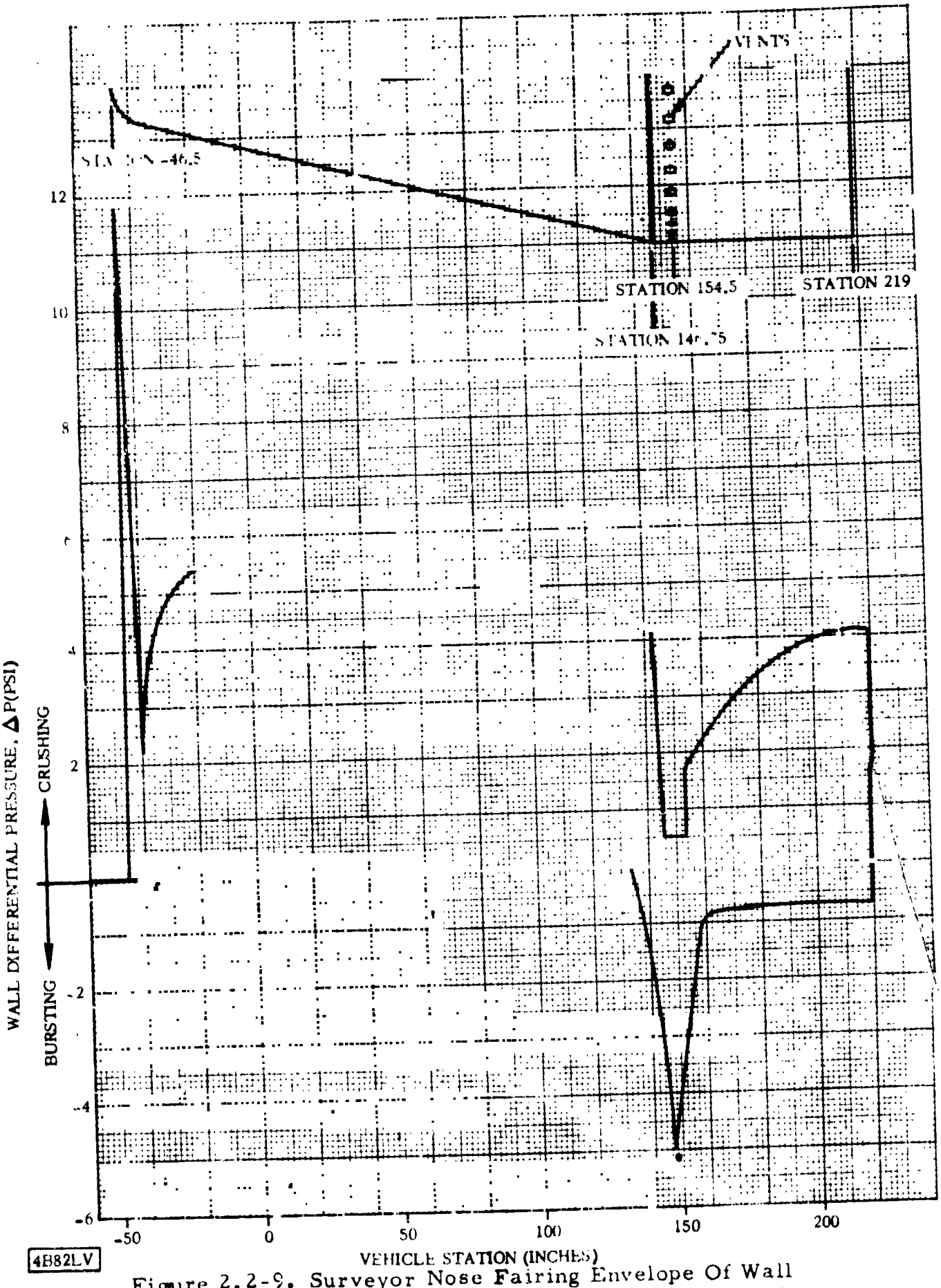

Figure 2.2-9. Surveyor Nose Fairing Envelope Of Wall Differential Pressures (α = 4.5 Degrees)

NOTE: The maximum local changes of pressure due to angle of attack are determined from the normal force distributions by assuming that the normal force at a given station is produced by a change of external pressure which is equal and opposite on the windward and lee sides and varies as the cosine of ϑ. Circumferential pressure distributions are obtained by superimposing the effect of angle of attack upon the wall differential pressure at $\alpha = 0$, i.e.,

$$\Delta P_W = \Delta P_{W(\alpha=0)} + \alpha(\Delta P_{W\alpha})\cos\theta$$

USE: $\alpha = 4.5°$

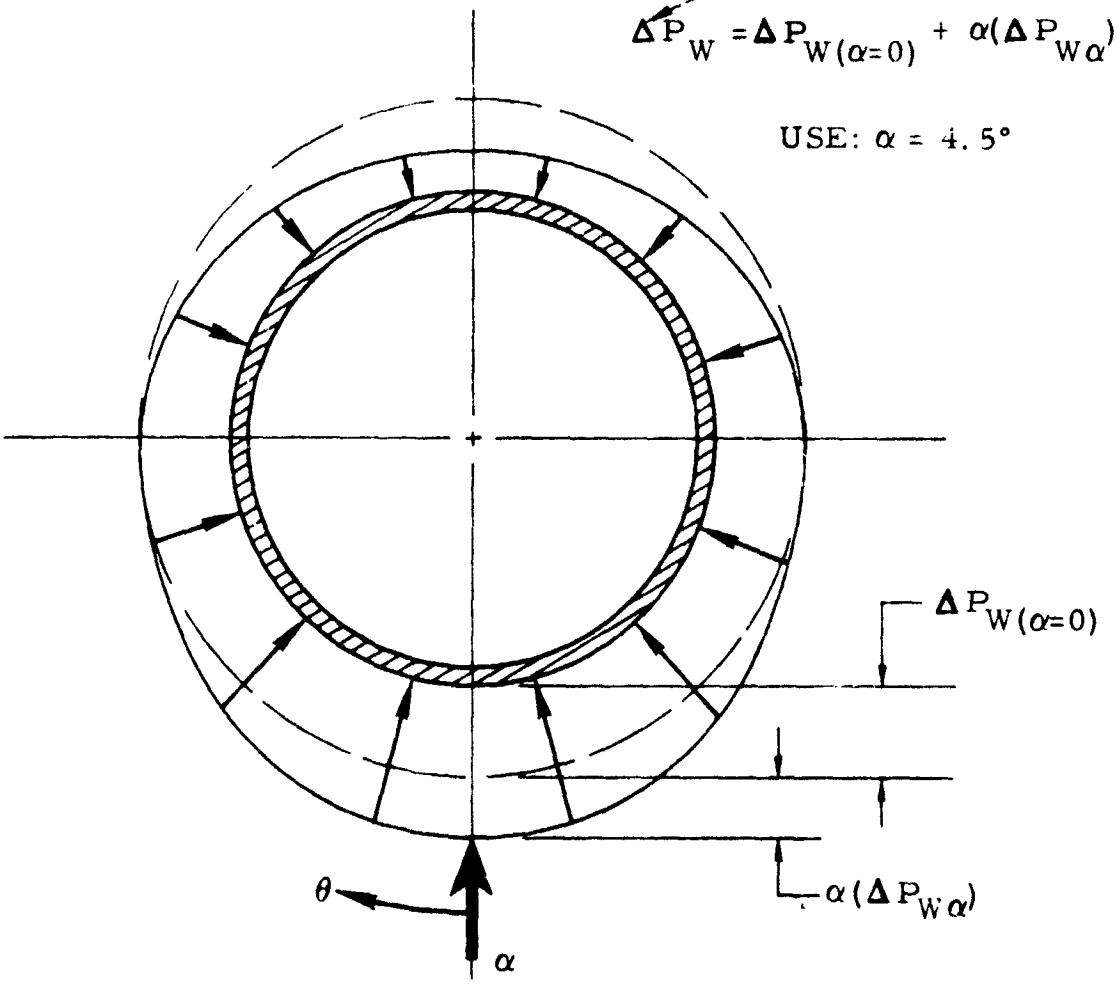

This contribution has been accounted for in the pressure envelope (Figure 2.2-9) for $\cos\theta = 0°$.

4B83LV

Figure 2.2-10. Nose Fairing Circumferential Pressure Distribution Due to Angle of Attack

2.2.6 BUFFET AND FLUTTER LOADS. During transonic flight, the barrel section is subjected to high fluctuating pressures due to oscillation of and turbulence at the normal shock. The response of the barrel section to these pressures is presented in Table 2.2-3 in terms of deflections and internal loads. Symbols and sign convention for loads and deflections are presented in Figure 2.2-11.

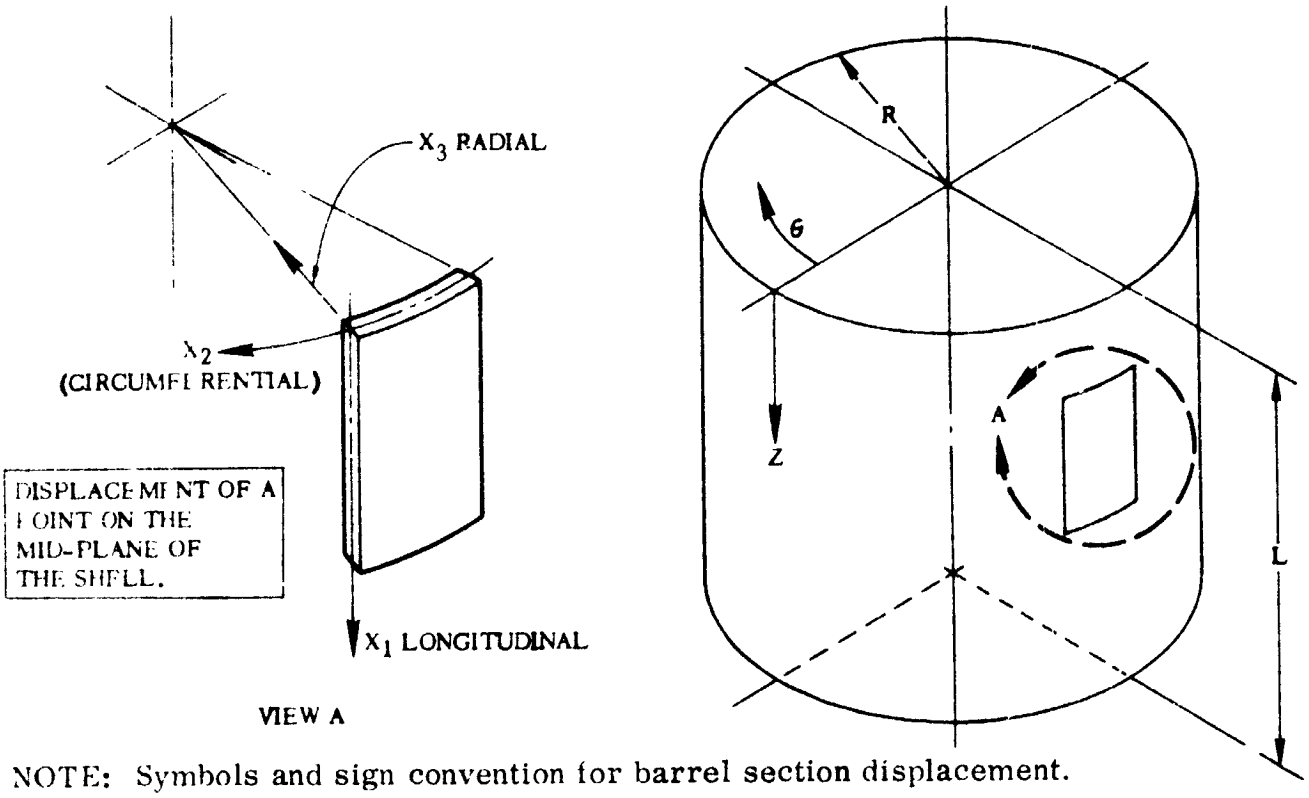

NOTE: Symbols and sign convention for barrel section displacement.

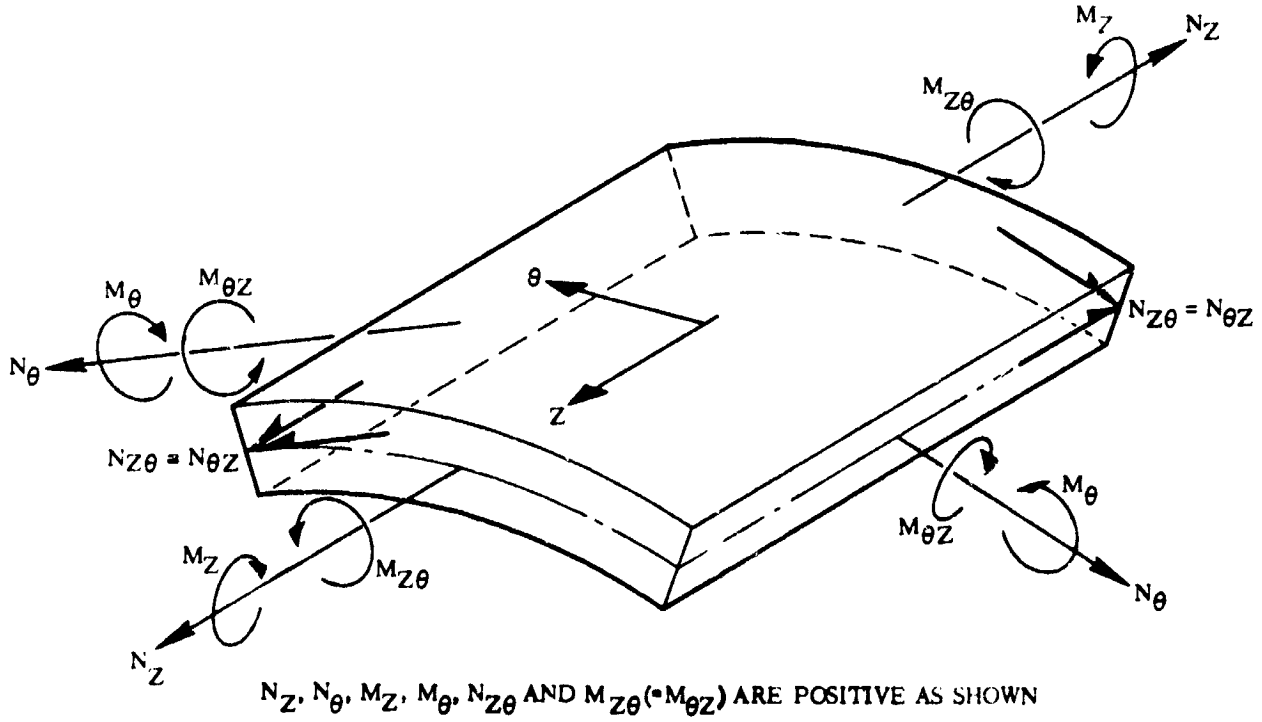

NOTE: Symbols and skin convention for internal barrel section.

4B84LV Figure 2.2-11. Nose Fairing Barrel Section Symbols and Sign Convention for Buffet Response

TABLE 2.2-3. NOSE FAIRING BARREL SECTION BUFFET RESPONSE

DISPLACEMENTS	
Mach Number 0.70-0.85	Mach Number 0.80-0.90
$x_1 = -0.0018 \sin 5\theta \cos \frac{2\pi Z}{L}$	$x_1 = -0.016 \sin 4\theta \cos \frac{\pi Z}{L}$
$x_2 = -0.0077 \cos 5\theta \sin \frac{2\pi Z}{L}$	$x_2 = -0.053 \cos 4\theta \sin \frac{\pi Z}{L}$
$x_3 = 0.050 \sin 5\theta \sin \frac{2\pi Z}{L}$	$x_3 = 0.22 \sin 4\theta \sin \frac{\pi Z}{L}$

INTERNAL LOADS		
Case / Load	Mach Number 0.70-0.85	Mach Number 0.80-0.85
N_Z, lb/in.	$+28.4 \sin \frac{2\pi Z}{L} \sin 5\theta$	$+142.4 \sin \frac{\pi Z}{L} \sin 4\theta$
N_θ, lb/in.	$-27.4 \sin \frac{2\pi Z}{L} \sin 5\theta$	$-5.33 \sin \frac{\pi Z}{L} \sin 4\theta$
M_Z, in.-lb/in.	$+48.2 \sin \frac{2\pi Z}{L} \sin 5\theta$	$+63.2 \sin \frac{\pi Z}{L} \sin 4\theta$
M_θ, in.-lb/in.	$+43.0 \sin \frac{2\pi Z}{L} \sin 5\theta$	$+113.8 \sin \frac{\pi Z}{L} \sin 4\theta$
$M_{Z\theta}$, lb/in.	$-37.5 \cos \frac{2\pi Z}{L} \cos 5\theta$	$-155.3 \cos \frac{\pi Z}{L} \cos 4\theta$
$M_{Z\theta}$, in.-lb/in.	$+35.2 \cos \frac{2\pi Z}{L} \cos 5\theta$	$+62.8 \cos \frac{\pi Z}{L} \cos 4\theta$

NOTES:

a. The N_Z, N_θ, M_Z and M_θ loads have maximum values at increments of $\theta = \frac{K\pi}{10}$ at $Z = \frac{L}{4}$ and $Z = \frac{3L}{4}$ for the first case and at increments of $\theta = \frac{K\pi}{8}$ at $Z = \frac{L}{2}$ for the second case, where K = 1, 3, 5, 7, etc. The maximum values for $N_{Z\theta}$ and $M_{Z\theta}$ are at increments of $\theta = \frac{j\pi}{5}$ at $Z = 0$, $\frac{L}{2}$ and L for the first case and at increments of $\theta = \frac{j\pi}{4}$ at $Z = 0$ and L for the second case, where j = 1, 2, 3, 4, etc. The maximum stress may occur at locations other than for the above stated maximum individual loads.

b. $N_{Z\theta} = N_{0Z}$ and $M_{Z\theta} = M_{\theta Z}$

c. Reference Figure 2.2-11 for explantion of symbols and signs.

2.2.7 MISCELLANEOUS LOAD PARAMETERS. During nose fairing jettison, each half of the fairing is subjected to bending due to thrustor bottle forces. The total jettison forces, which are imposed to each fairing half, result from three effects:

a. Thrust from the bottle.

b. Gas impingement from the opposite thrustor bottle.

c. Static pressure within the nose fairing upper cavity.

Figures 2.2-15 through 2.2-16 are to be used as input data for the basic shell bending calculation, and are all based on an initial bottle charge pressure of 2450 psi. The bending stiffness parameter (Figure 2.2-16) results from a somewhat wide range of Young's Modulus (E) which is always associated with a Fiberglas material. This data as presented, along with the respective weights and C.G.'s (reference Paragraph 2.2.2 and Figure 2.2-2), satisfies all of the load input variables which constitute the total jettison forces as defined above.

For local effects on the upper cavity basic shell walls, a burst pressure distribution as described in Figure 2.2-17 should be used as design loads for purposes of analysis. This pressure distribution includes static pressure, gas impingement, a dynamic impact factor which considers the sudden application of load as shown in Figure 2.2-12, and the response characteristics of the structure. The stagnation pressures P_2 and P_4 occur directly opposite the thrustor bottle exhaust nozzles and receive direct gas impingement. These pressures along with their respective locations vary with time as described in Figure 2.2-18. For the Quadrant I - IV fairing, the pressure along the Y-Y axis forward of the stagnation point is assumed to vary linearly from the stagnation point pressure (P_2) to the pressure labeled as P_3 at Station -22 (Reference Figure 2.2-19), while that below the stagnation point is assumed to vary linearly from the stagnation pressure (P_2) to the pressure labeled as P_1 at Station -5.0 (Reference Figure 2.2-20). Circumferentially, the pressure varies with the angle θ according to:

$$P_{(CIR.)} = P_3 + (P_2 - P_3) \cos^2 \theta \quad \text{(Reference Figure 2.2-17)}$$

For the Quadrant II - III fairing, the pressure along the Y-Y axis forward of the stagnation point is taken as that of the stagnation point (P_4), while that below the stagnation point is assumed to vary linearly from the stagnation point pressure (P_4) to the pressure labeled as P_5 at Station -22 (Reference Figure 2.2-19). Again, the pressure varies circumferentially according to:

$$P_{(CIR.)} = P_5 + (P_4 - P_5) \cos^2 \theta \quad \text{(Reference Figure 2.2-17)}$$

Figure 2.2-20 indicates the variation of pressure (P_1) with time. In this area, the pressure also varies circumferentially according to:

$$P_{(CIR.)} = P_5 + (P_1 - P_5) \cos^2 \theta \quad \text{(Reference Figure 2.2-17)}$$

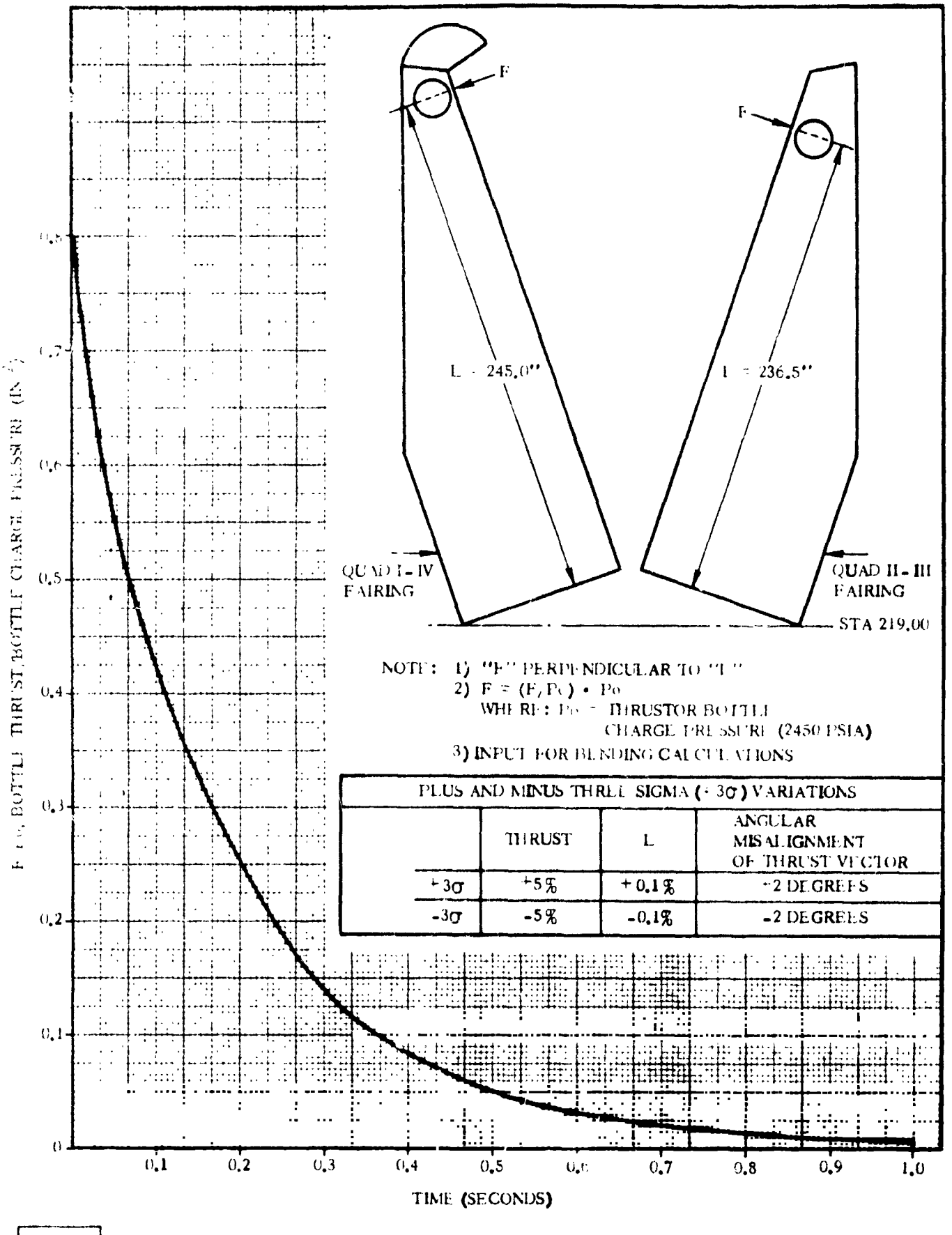

Figure 2.2-12. Thrustor Bottle - Variation of Bottle Thrust with Time

NOTES:
A. INPUT FOR BENDING CALCULATION
B. BOTTLE CHARGE PRESSURE = 2450 PSIA
C. FOR F_y AND F_z, USE LEFT SCALE; FOR Y, USE RIGHT SCALE

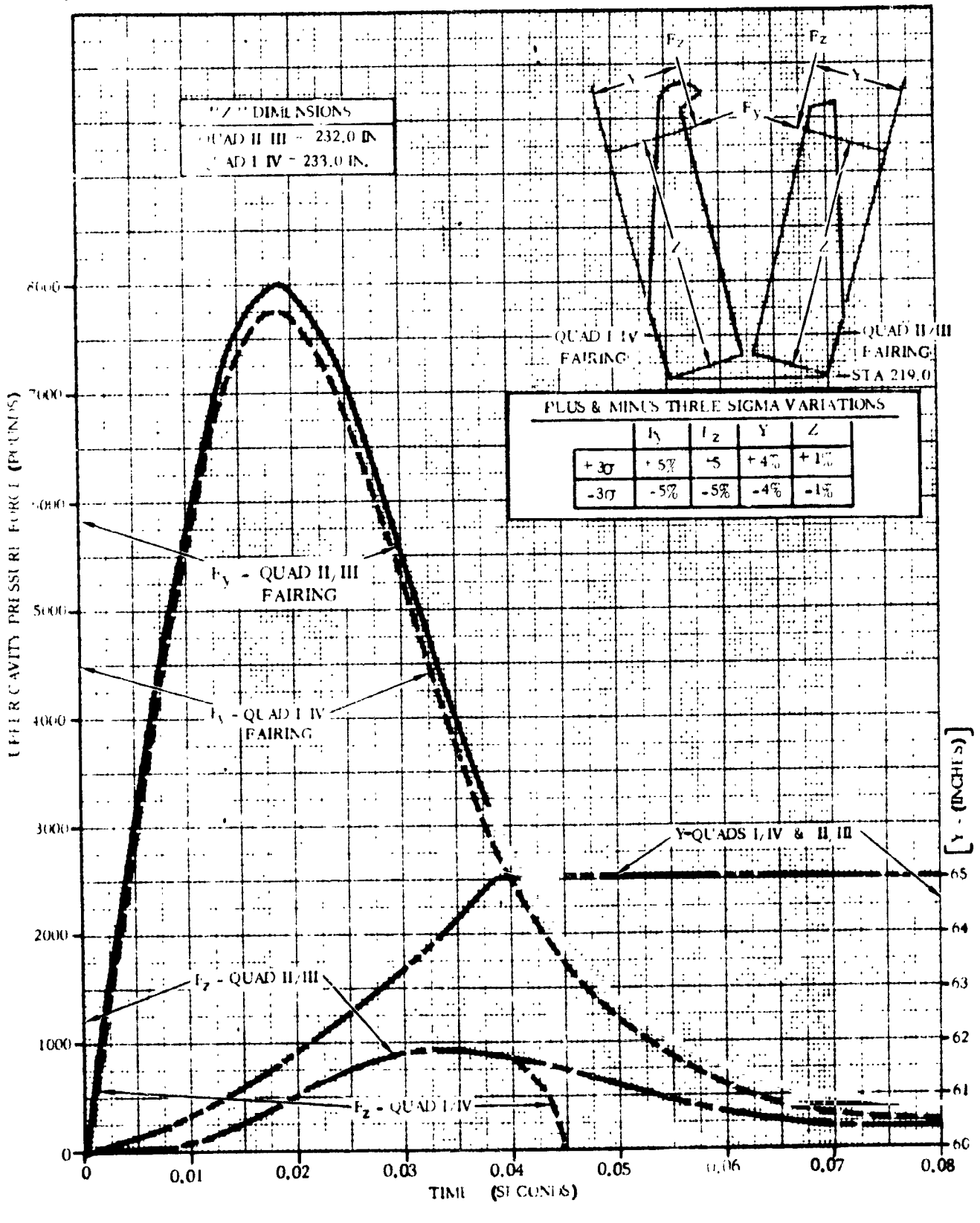

4B86LV

Figure 2.2-13. Nose Fairing Variation of Upper Cavity Pressure Force with Time

NOTES: A. INPUT FOR BENDING CALCULATION
B. BOTTLE CHARGE PRESSURE = 2450 PSIA

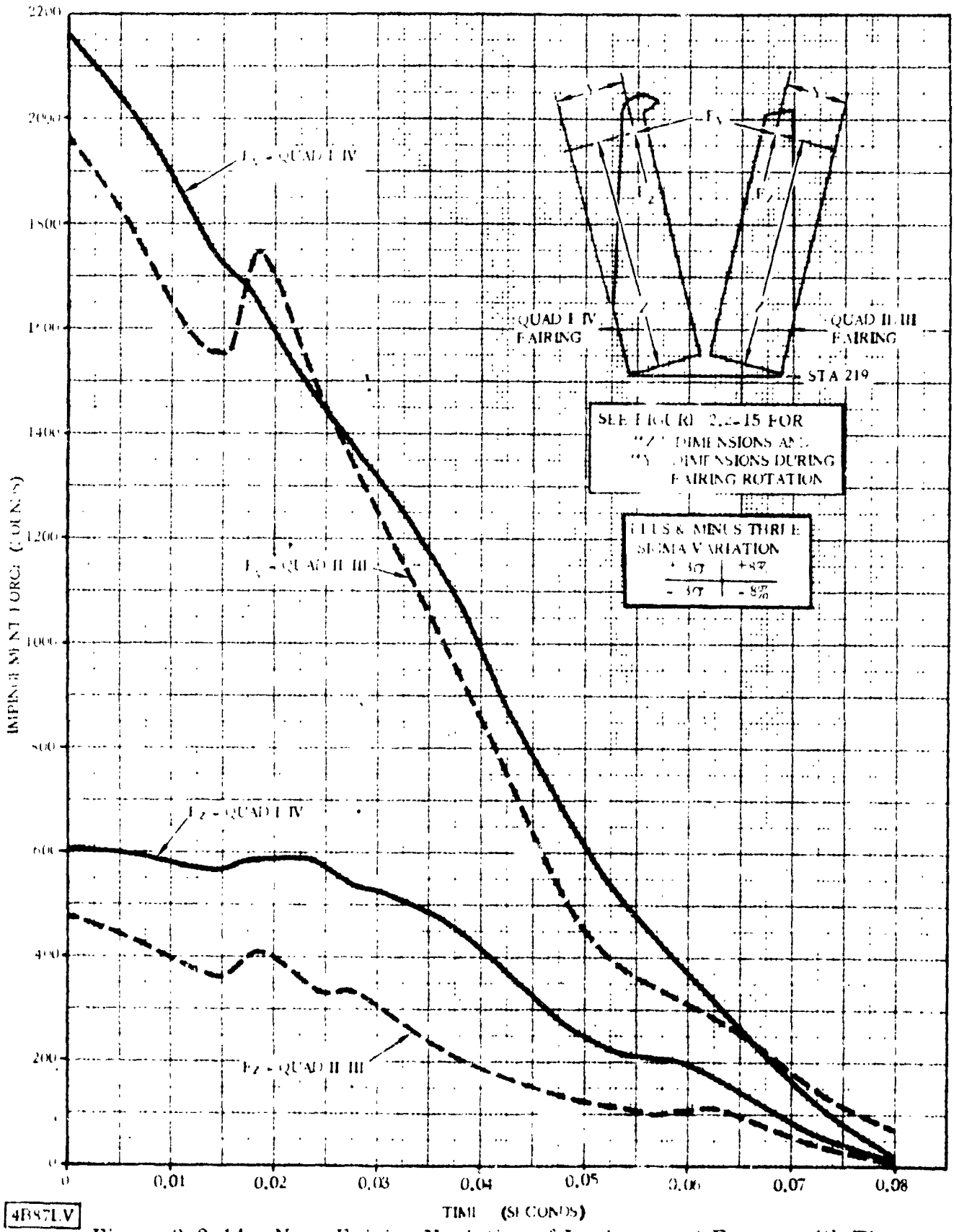

Figure 2.2-14. Nose Fairing Variation of Impingement Forces with Time

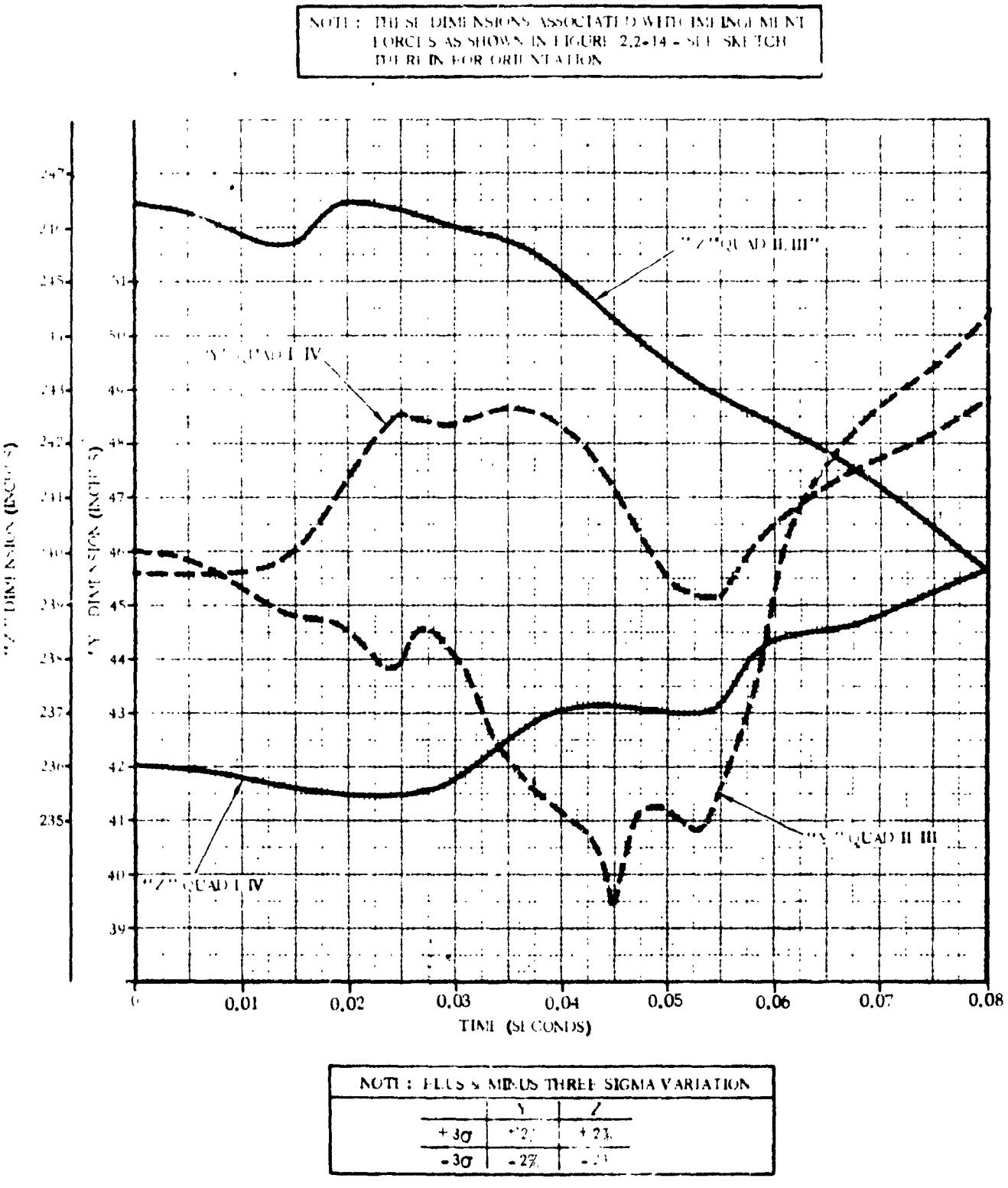

4B38LV

Figure 2.2-15. Thrustor Bottle Impingement Force - Variation of Y and Z Coordinates with Time

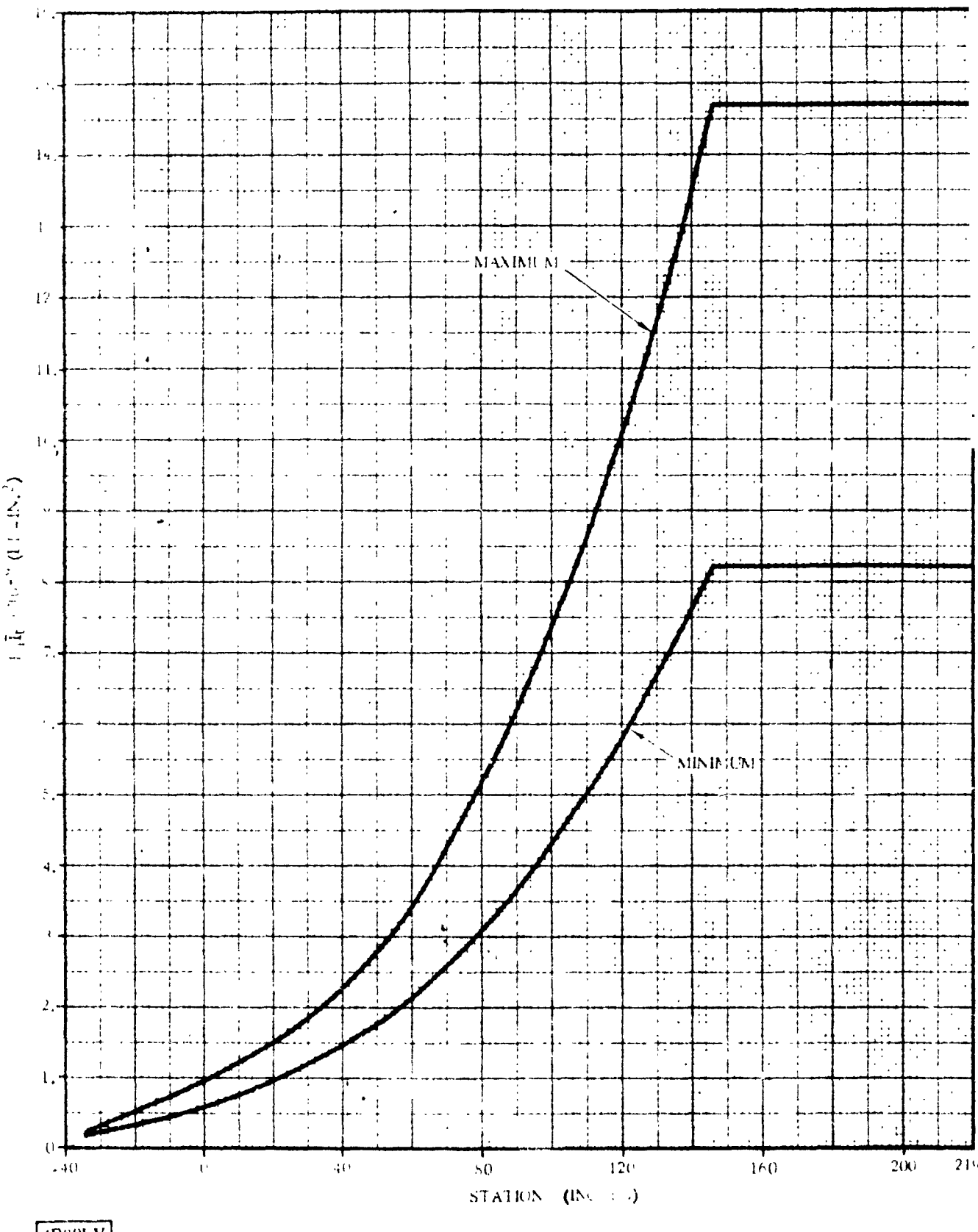

4B891 V

Figure 2.2-16. Nose Fairing, Quadrant II - III Half, Equivalent $EI(E_i \bar{I}_t)$ versus Station

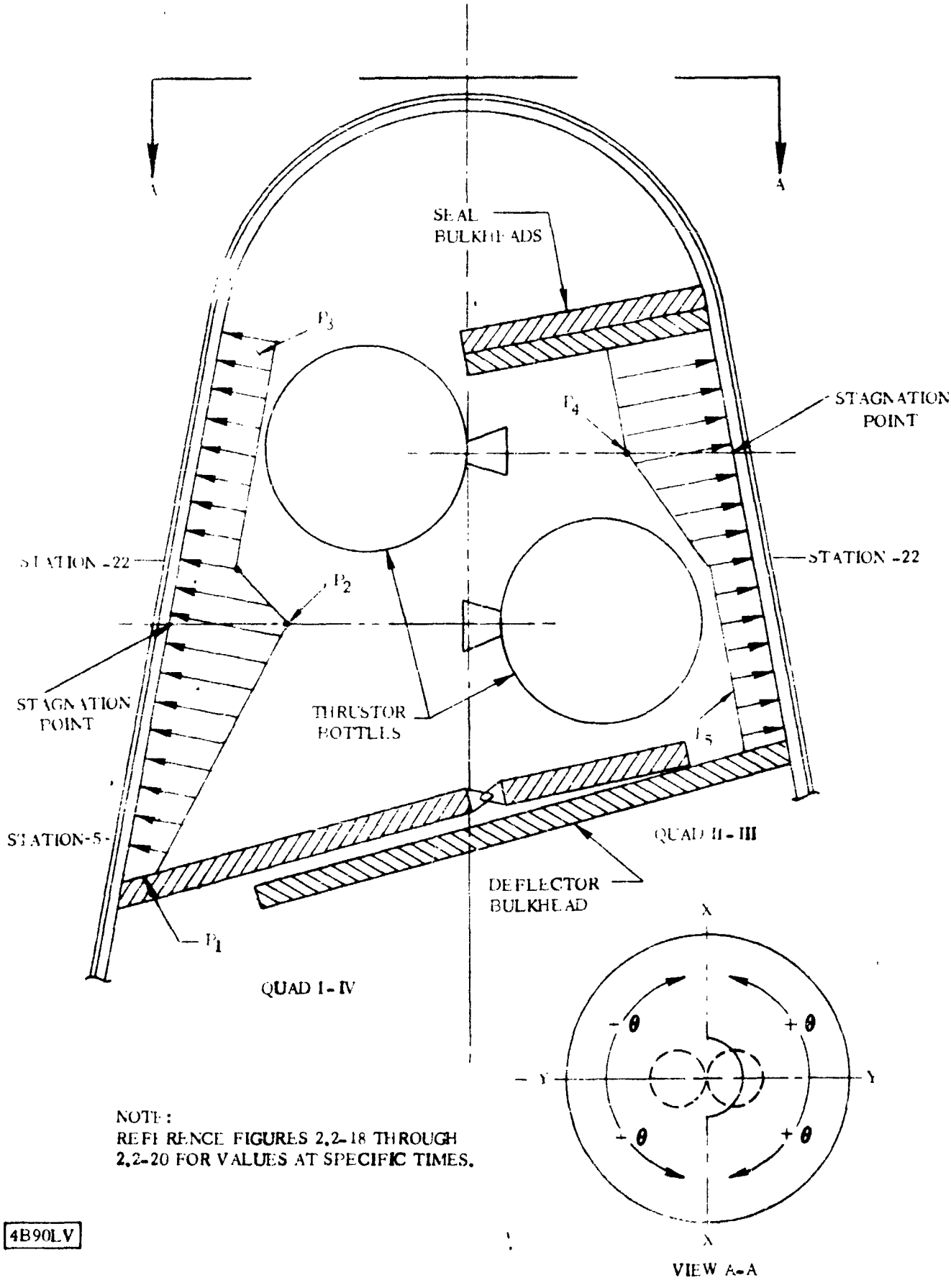

Figure 2.2-17. Nose Fairing Upper Cavity Burst Pressures During Jettison

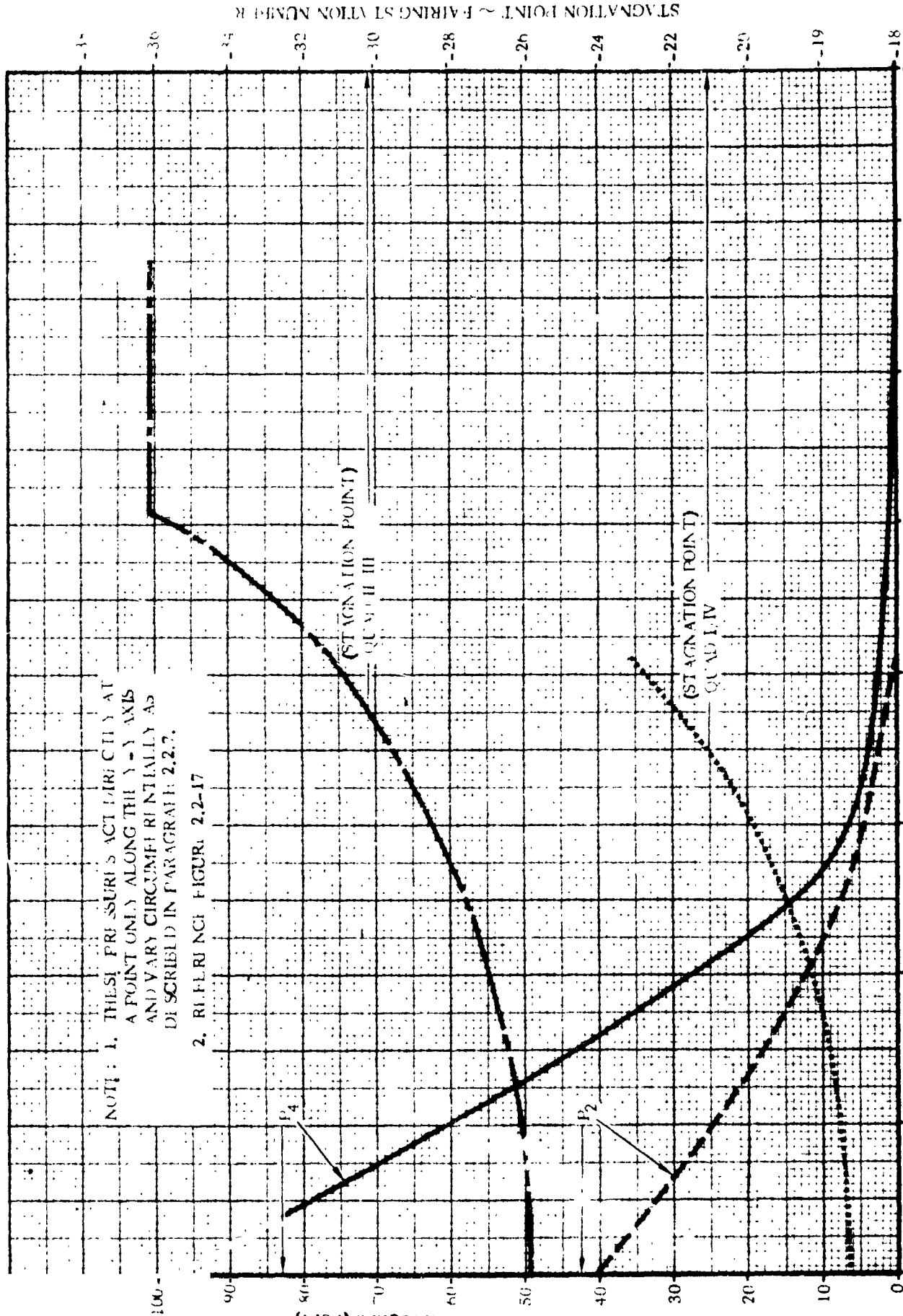

Figure 2.2-18. Nose Fairing Upper Cavity Stagnation Point Impingement Pressures (P_2 and P_4) versus Time

4B91LT

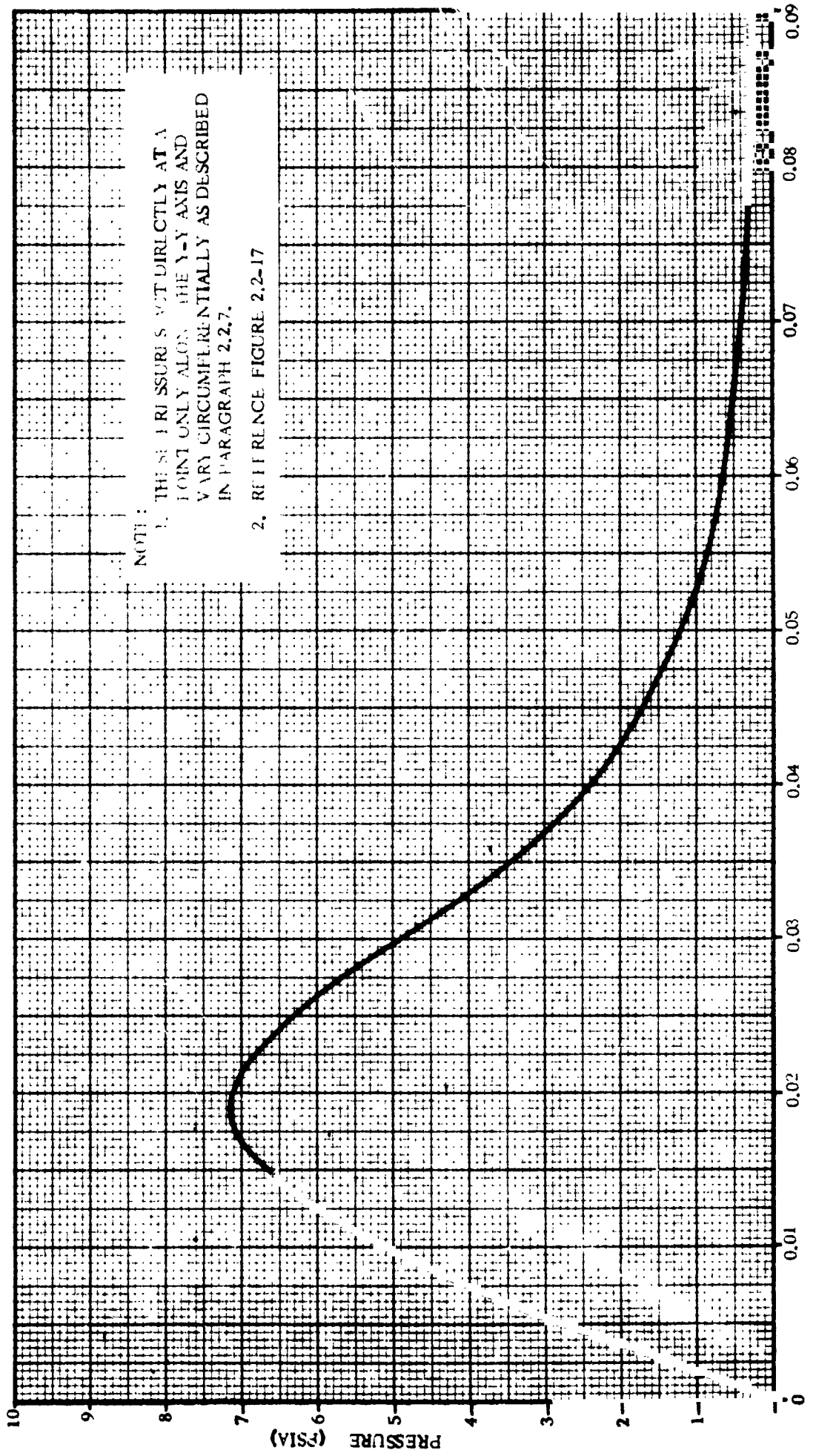

Figure 2.2-19. Nose Fairing Impingement Pressures (P_3 and P_5) versus Time

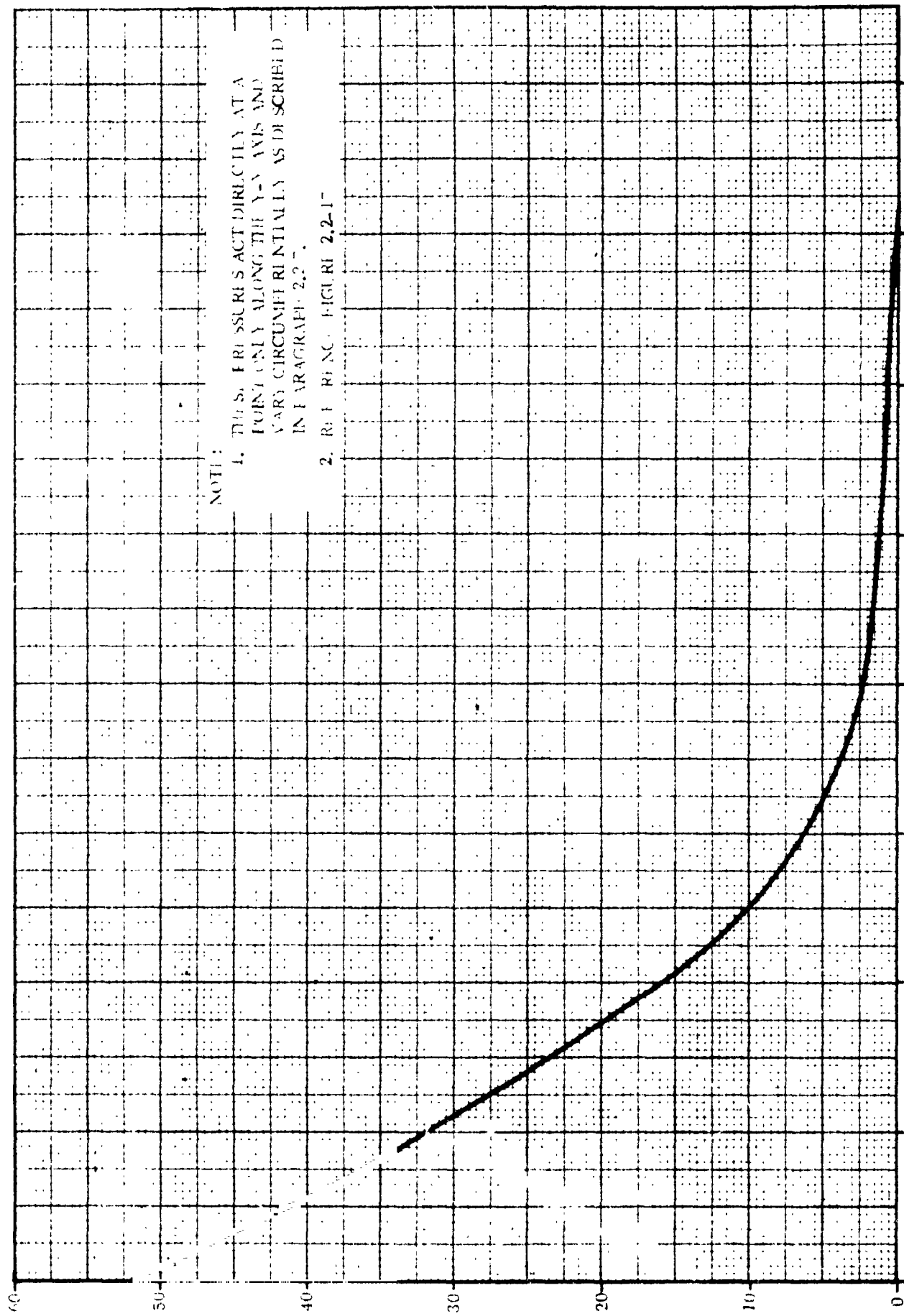

Figure 2.2-20. Nose Fairing Impingement Pressure (P_i) versus Time

THIS PAGE INTENTIONALLY LEFT BLANK.

2.3 NOSE CAP

The nose cap is a solid hemispherical shell composed of a phenolic Fiberglas interior layer covered by a high silica glass outer laminate. Figure 2.3-1 presents basic nose cap configuration.

2.3.1 CRITICAL CONDITIONS. The nose cap is subjected to high crushing pressures during the Max q portion of flight, and receives maximum temperatures at time of BECO. At nose fairing jettison, the cap receives high burst pressure and inertia loads in combination with elevated temperatures.

2.3.2 WEIGHTS AND CENTER OF GRAVITY DATA. The following weight and C. G. location shall be used for structural design and analysis.

Weight (lb)	z (in.)	y (in.)	x (in.)
18.0	-37	0	0

2.3.3 THERMAL DATA. Maximum exterior temperatures of the nose cap for various times in flight are presented in Figure 2.3-2. The temperature gradients through the laminate for maximum temperature condition and for fairing jettison are presented in Figure 2.3-3. This thermal data represents the worst expected environment for any flight.

2.3.4 INERTIA LOADS. At BECO, the cap receives a maximum axial acceleration of 5.8 g's (acting aft).

During nose fairing jettison, the angular acceleration of the nose fairing half causes additional inertia loads of magnitudes and directions as defined below.

a. Tangential inertia force = 100 g's (assumed to be concentrated at the C.G. for simplicity). This load acts perpendicular to the axis described between the C.G. of the nose cap and the center of rotation in an opposite sense to the direction of rotation (see Figure 2.3-4).

b. Radial acceleration or centrifugal inertia force = 15 g's (assumed to be concentrated at the C.G. for simplicity). This force acts along the same axis as defined above and directed away from the center of rotation (see Figure 2.3-4).

NOTE:

These loads must be applied simultaneously with the pressure loads described in Paragraph 2.3.7.

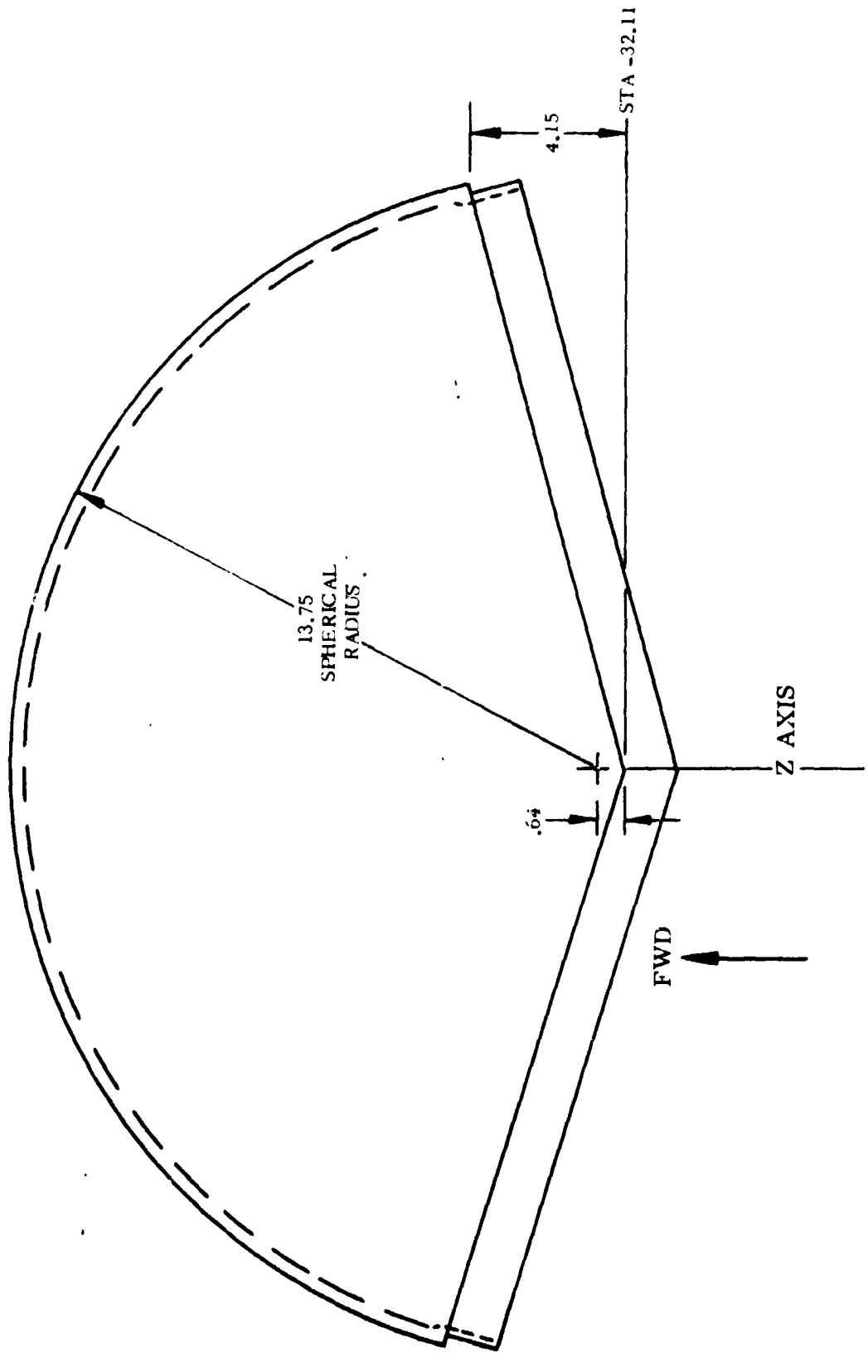

4B171LT

Figure 2.3-1. Nose Cap Configuration

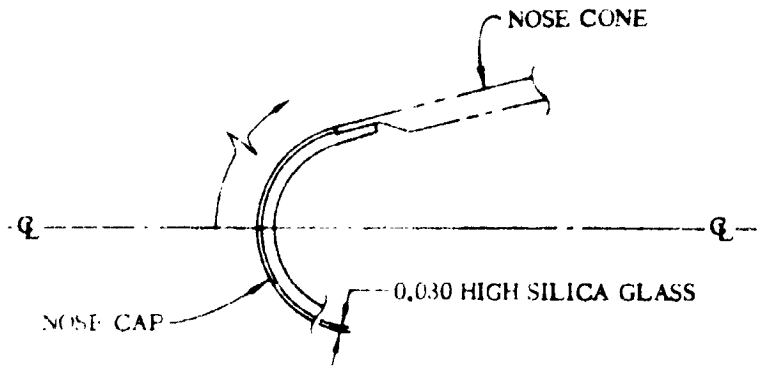

NOTE:

TEMPERATURES SHOWN ARE THOSE OF THE 0.030 INCH OUTSIDE LAYER OF HIGH SILICA GLASS

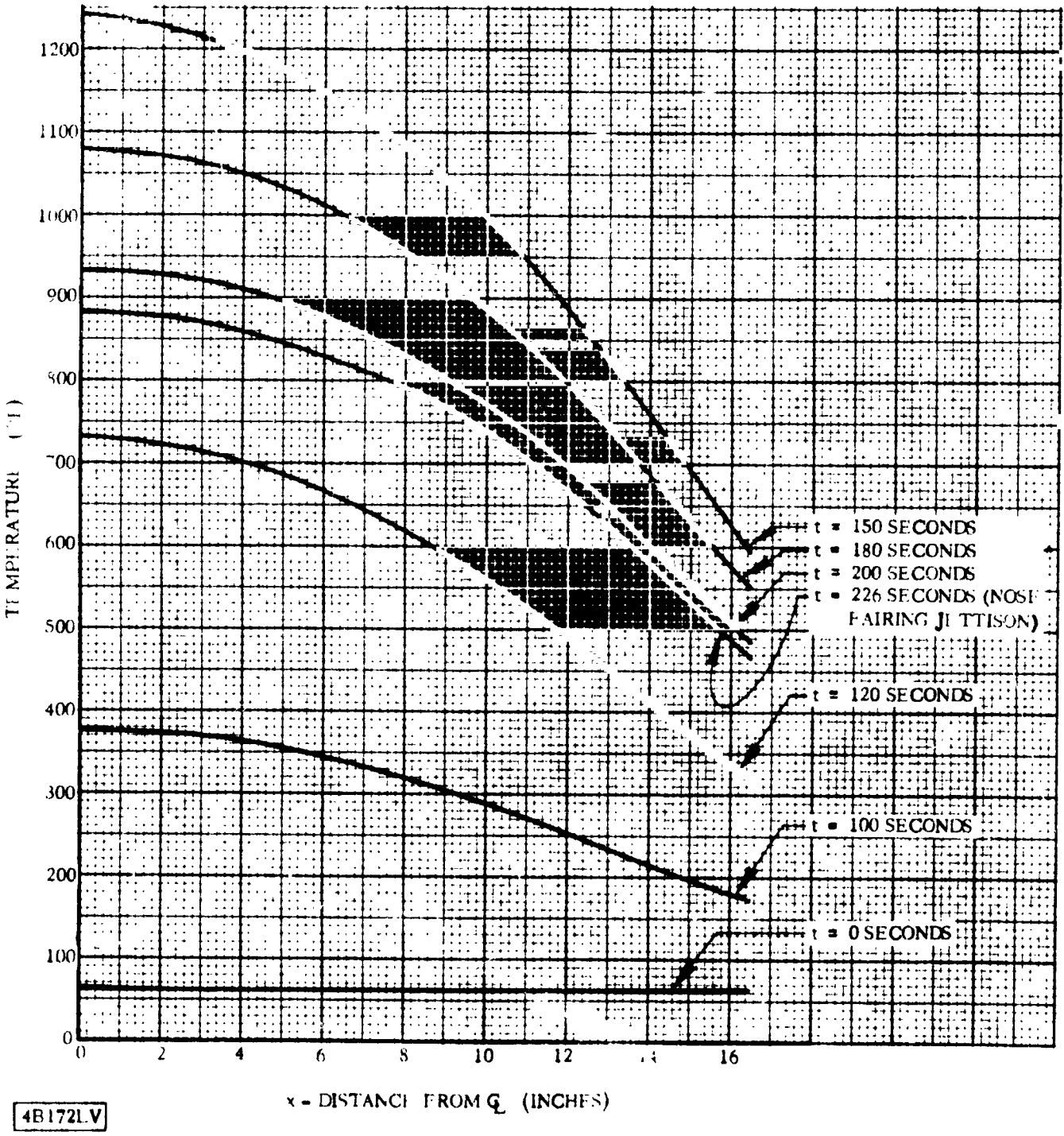

4B172LV

Figure 2.3-2. Nose Cone Cap Temperature Distribution

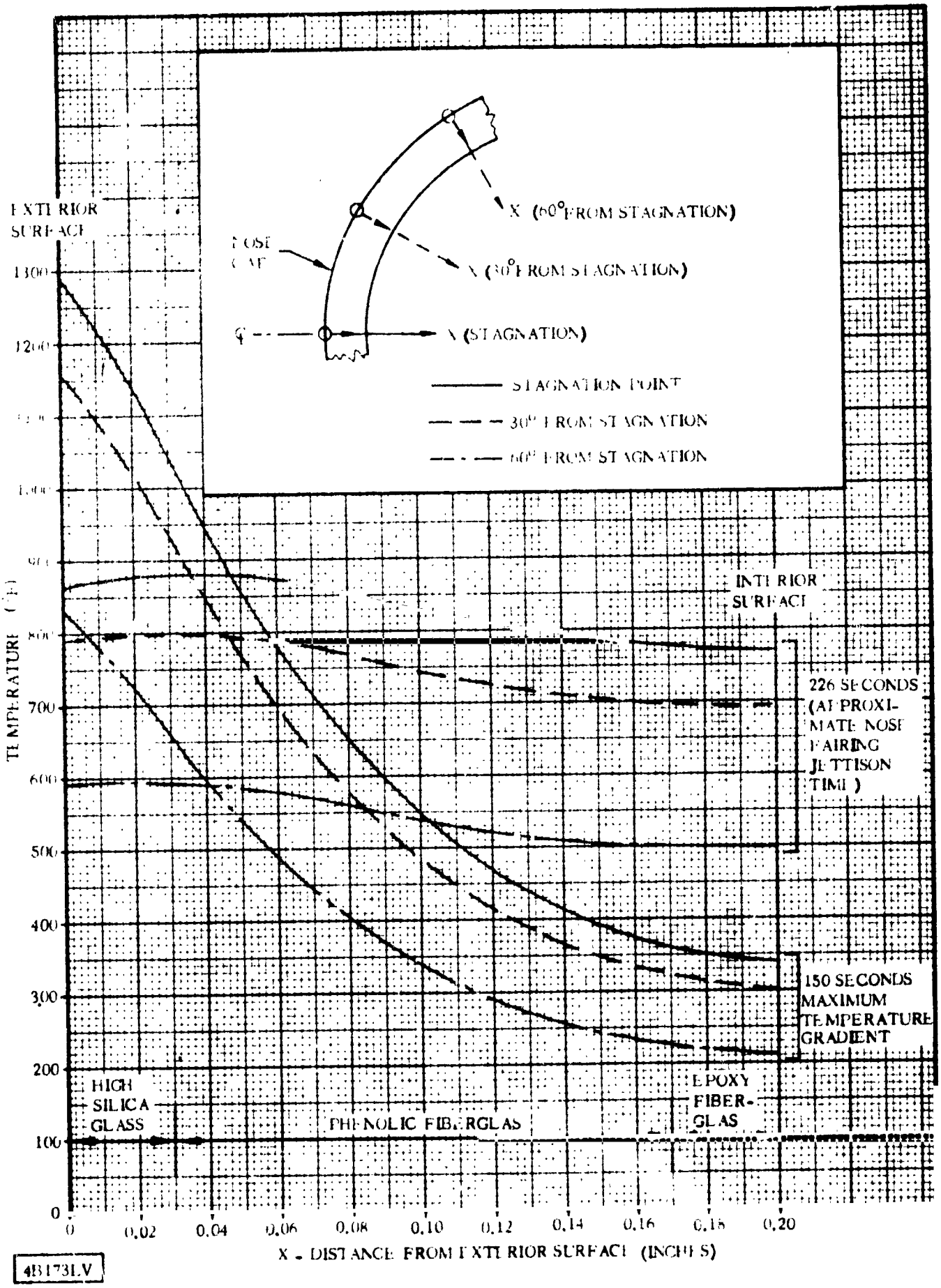

Figure 2.3-3. Nose Cap Fairing Temperature Gradients

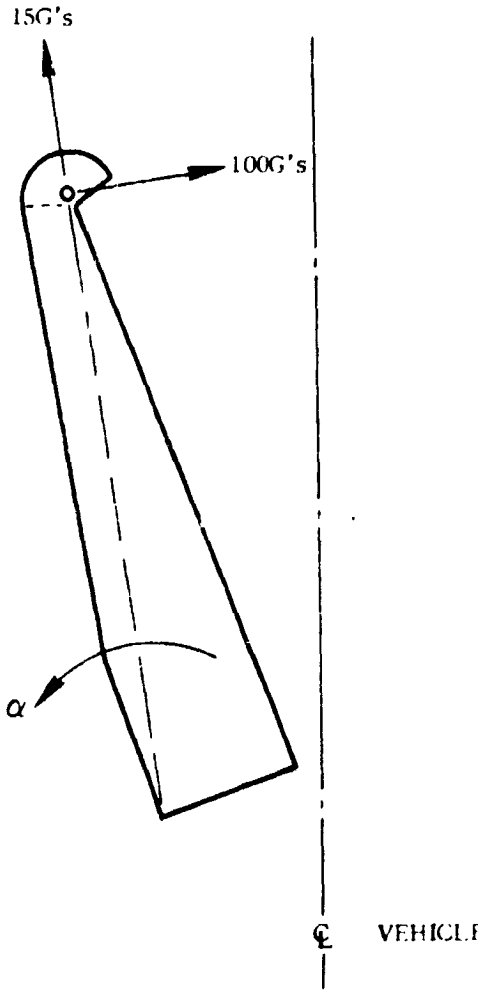

4B174LV

Figure 2.3-4. Nose Cap Acceleration Forces at Jettison

2.3.5 STEADY-STATE AIR LOADS. The wall ΔP envelope presented in Figure 2.2-9 should be used for stress analysis of the cap for maximum air loads.

2.3.6 BUFFET AND FLUTTER LOADS. Buffet loads on the nose cap are negligible.

2.3.7 MISCELLANEOUS LOAD PARAMETERS. The nose cap receives burst pressures during firing of the thrustor bottles at nose fairing jettison. This pressure is suddenly applied, which causes stresses higher than those due to gradual load application. This impact effect is included in the equivalent static pressure presented in Figure 2.3-5. The inertia loads due to fairing acceleration presented in Paragraph 2.3.4 must be combined with this pressure load.

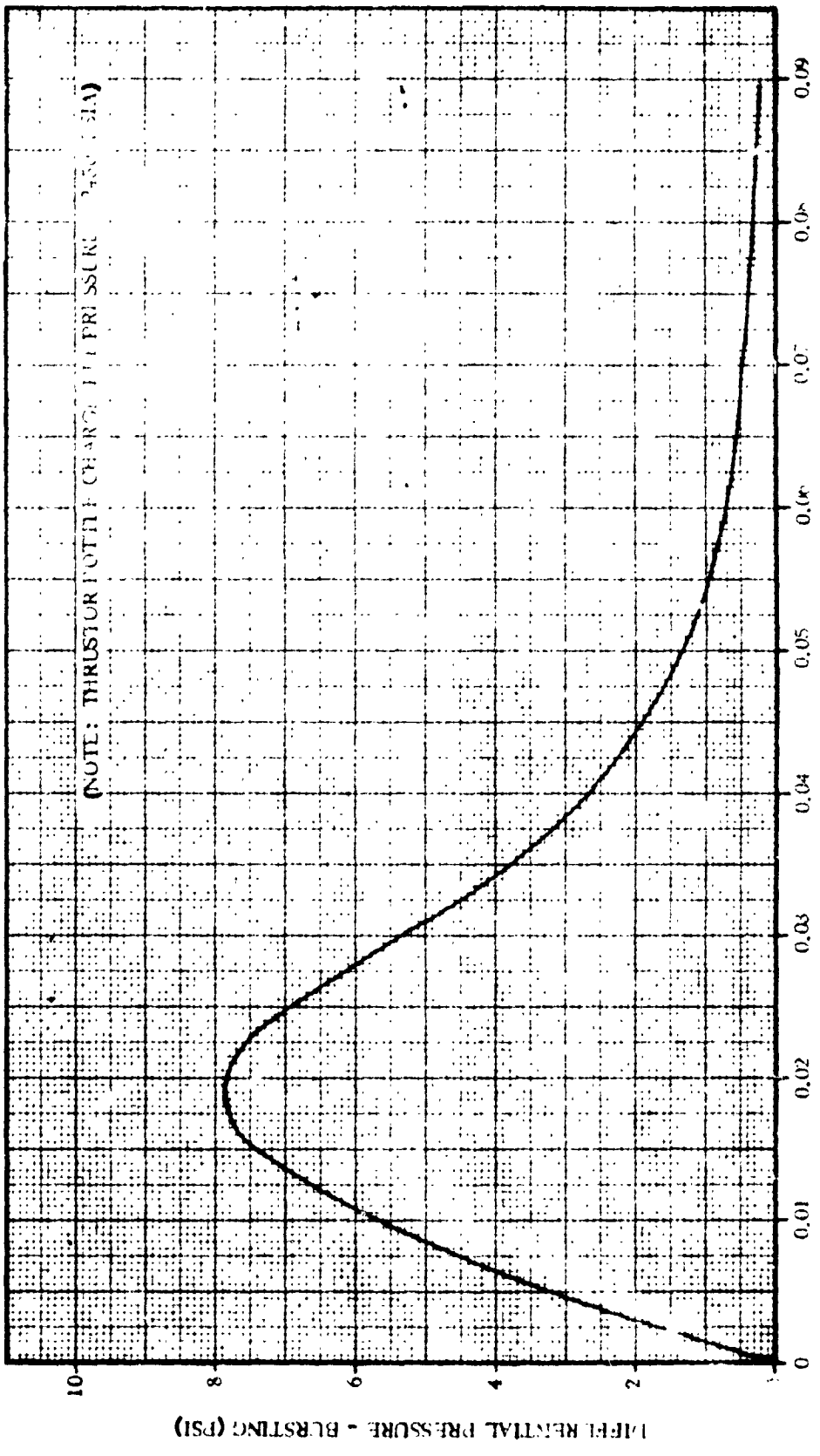

Figure 2.3-5. Nose Cap Equivalent Static Pressure during Fairing Jettison

2.4 SHOULDER COVER

The shoulder cover is a solid laminate Fiberglas fairing which provides a smoot aerodynamic surface between the nose cone and barrel section. Figure 2.4-1 presen a cross-section through the shoulder cover which illustrates the method of attachmen to the basic shell.

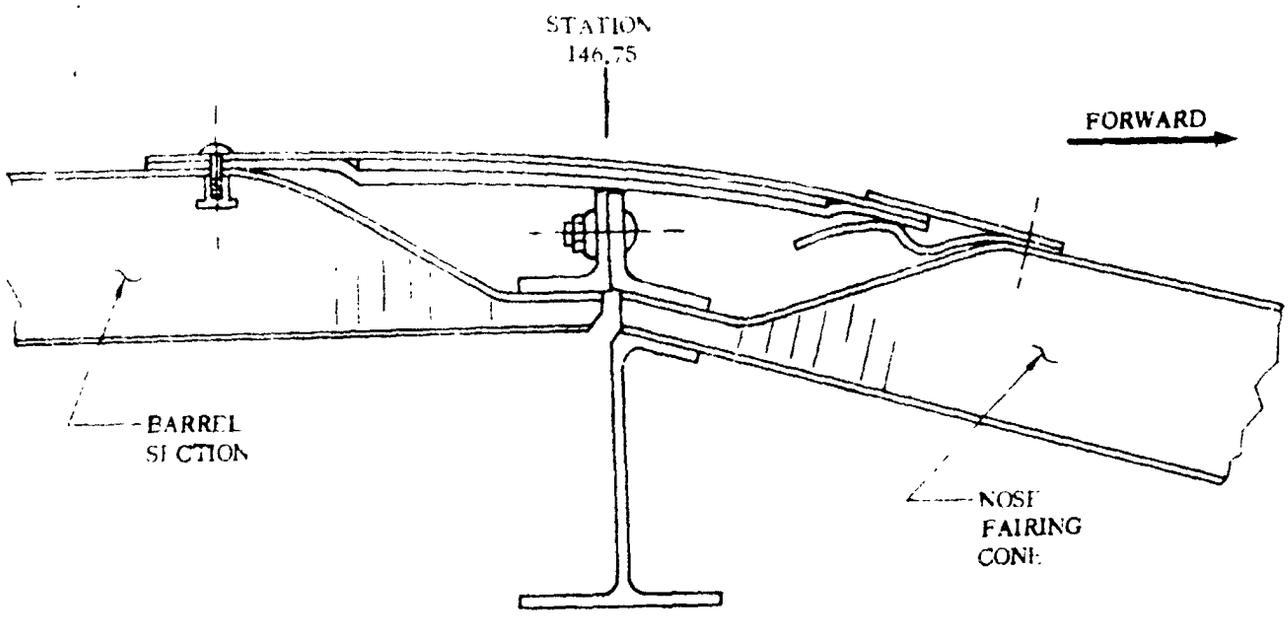

4B941V

Figure 2.4-1. Nose Fairing Shoulder Cover Configuration

2.4.1 CRITICAL CONDITIONS. The shoulder cover receives high steady-state and fluctuating aerodynamic loading during transonic flight. No elevated temperatures exist during time of maximum airloads. The maximum temperature exists at BECO, when aerodynamic loading is negligible. Due to the small mass of the shoulder cover, inertia loads are not considered critical.

2.4.2 WEIGHTS AND CENTER OF GRAVITY DATA. Loads imposed by inertia are not critical.

2.4.3 THERMAL DATA. Figure 2.4-2 presents a temperature history of three points on the shoulder cover, reflecting the most severe environment expected on any operational vehicle.

2.4.4 INERTIA LOADS. Inertia loads are not critical

2.4.5 STEADY-STATE AIR LOADS. Figure 2.4-3 presents maximum steady-state differential pressure across the shoulder cover in both bursting and crushing directions. This steady-state load shall be combined with the fluctuating pressure presented in Paragraph 2.4.6.

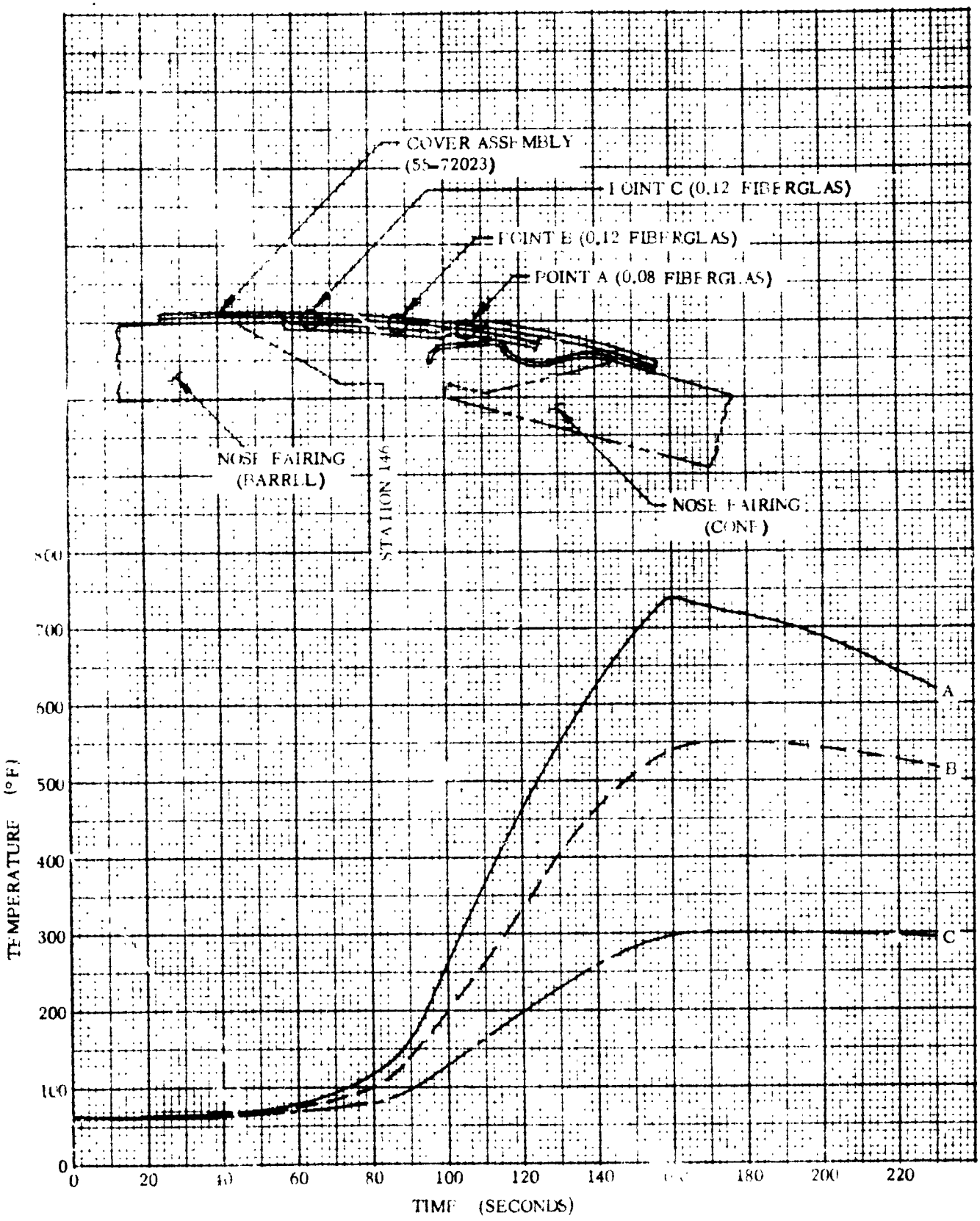

Figure 2.4-2. Nose Fairing Shoulder Cover Fairing Temperature History

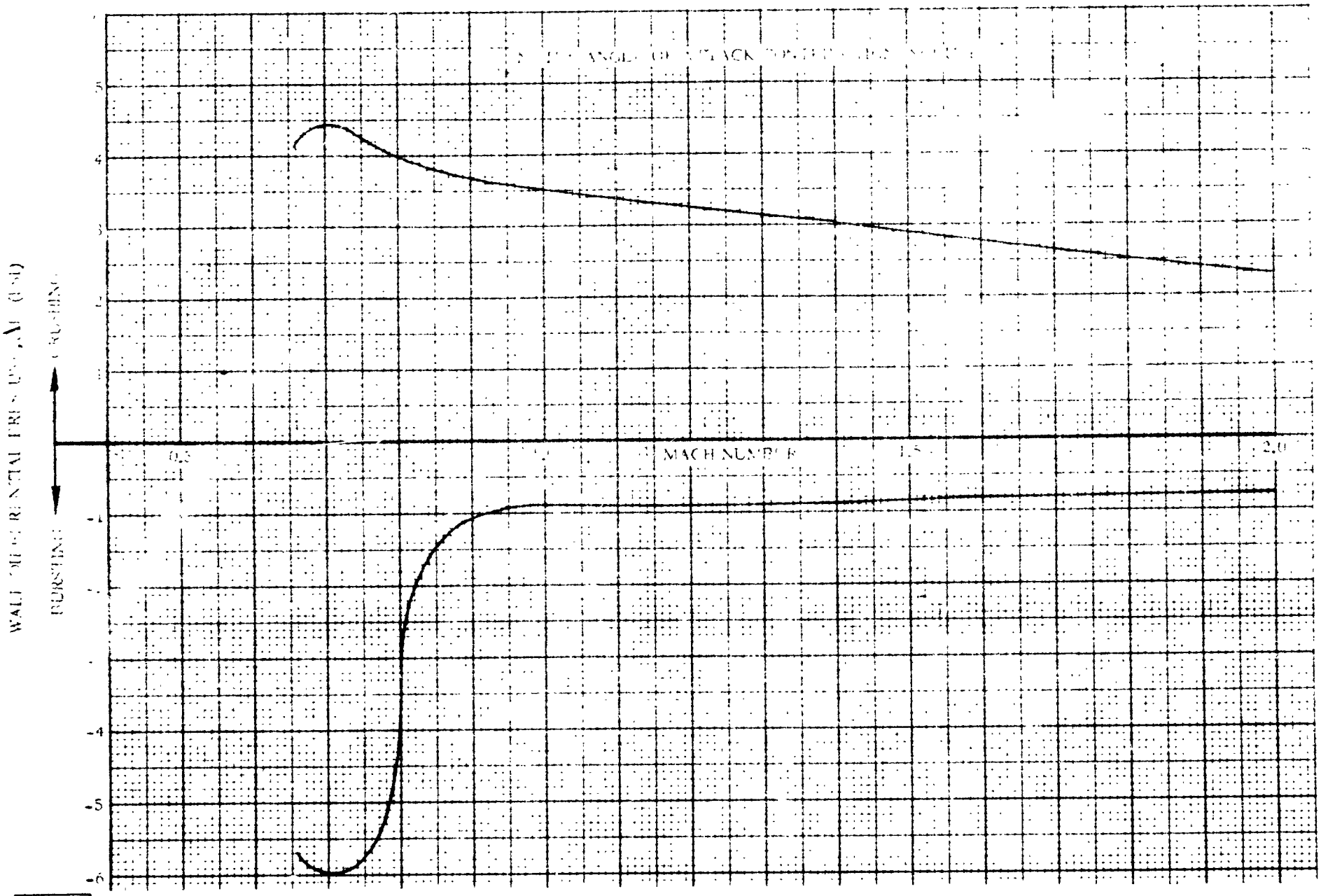

Figure 2.4-3. Nose Fairing Shoulder Cover Steady-State Differential Pressure

2.4.6 BUFFET AND FLUTTER LOADS. During transonic flight, the air flow discontinuity at the junction between the nose cone and barrel causes fluctuating pressures to act on the shoulder cover. The stresses due to response of the shoulder cover are equivalent to a static pressure as shown in Figure 2.4-4. This loading may occur at anytime between Mach numbers 0.85 and 1.30. Therefore, this condition should be considered simultaneously with the steady-state airloads presented in Paragraph 2.4.5.

2.4.7 MISCELLANEOUS LOAD PARAMETERS. No other loads are critical.

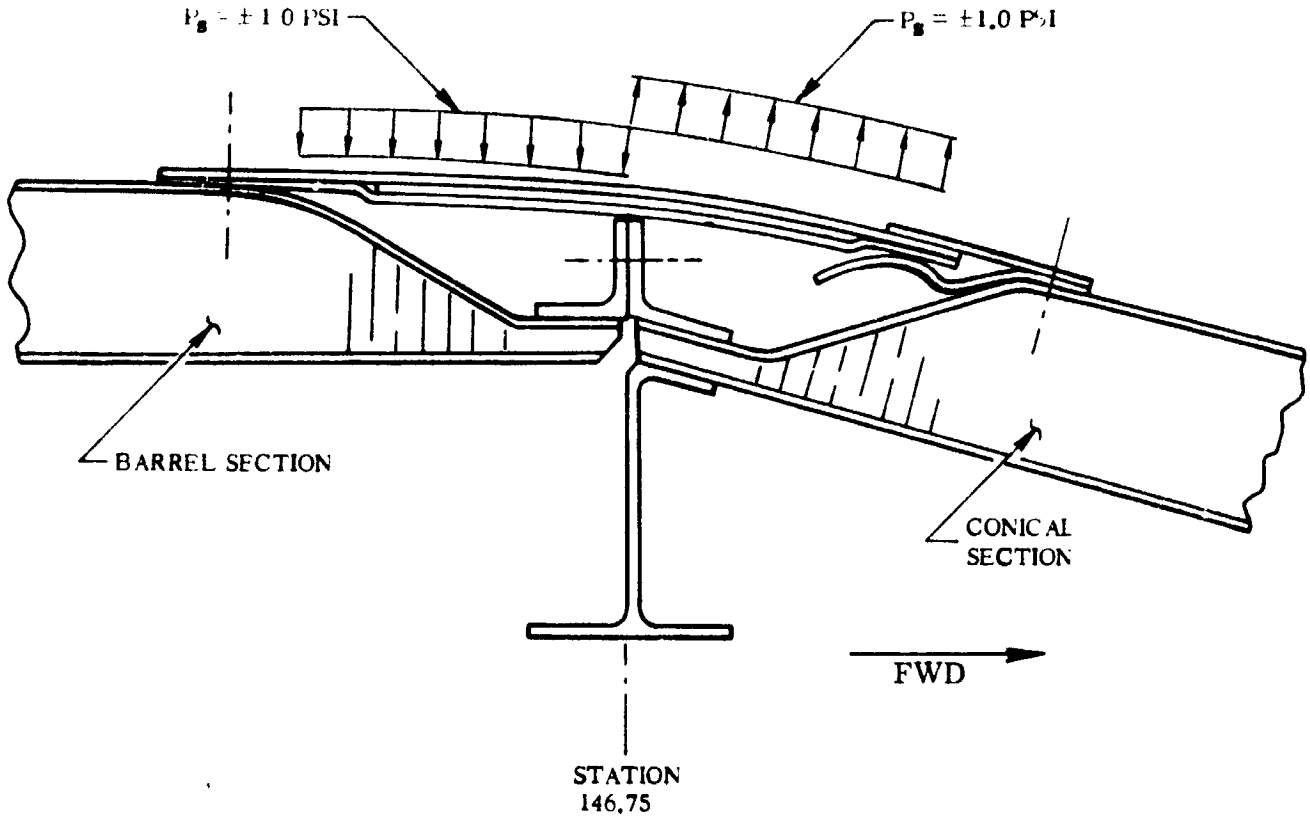

4B97LV

Figure 2.4-4. Nose Fairing Shoulder Cover Equivalent Static Pressure due to Buffet Response

2.5 NOSE FAIRING SKIRT

The nose fairing skirt provides protection to the forward edge of the insulation panels and the mating tank rings at Station 218.9 from aerodynamic heating. The skirt is jettisoned along with the nose fairing as it is attached to the aft end of the cylindrical (barrel) section. It extends aft over the mating tank rings and circumferentially around the vehicle. A flexible seal provides attachment to the insulation panels, which is severed by a shaped charge at fairing jettison. See Figure 2.5-1 for skirt configuration.

2.5.1 CRITICAL CONDITIONS. The environment considered to be most severe regarding the nose fairing skirt exists during the transonic phase of booster operation. Aerodynamic loads reach a maximum at this time since steady-state wall differential pressures and fluctuating pressure effects must be imposed simultaneously on the subject skirt. Detrimental temperature effects should not be considered at this time.

The maximum temperature condition (excessive heating of Fiberglas surfaces) occurs at a later time in flight whereby material allowables must be altered accordingly. However, during this portion of flight, the aerodynamic loads have reduced to a negligible magnitude.

2.5.2 WEIGHTS AND CENTER OF GRAVITY DATA. Due to the nature of this particular component, inertia loads are of an inconsequential magnitude compared to the aerodynamic loads discussed above, therefore, weights or C.G. data is not applicable.

2.5.3 THERMAL DATA. Thermal data on the skirt is presented in Paragraph 6.3.3.

2.5.4 INERTIA LOADS. Load contribution from inertia effects are not to be considered for this component (see Paragraph 2.5.2).

2.5.5 STEADY-STATE AIR LOADS. The static loading of the nose fairing skirt is considered to result from a differential pressure acting radially across the skirt. Figure 2.5-2 presents an envelope of wall differential pressures for the nose fairing skirt considering only a zero degree angle of attack. It is assumed that the flexible seal remains intact until insulation panel jettison, therefore venting occurs only through one hinge pod. The data at Mach number 0.94 includes an increment of 1.0 psi to account for an assumed venting lag. This analysis is valid only if the flexible seal is not ruptured in any way prior to the predetermined flight time.

Angle of attack corrections for α - 6 degrees are accounted for in Figure 2.5-3; therefore, for any smooth or clear area on the skirt installation the total ΔP would be sum of the values obtained from Figures 2.5-2 and 2.5-3.

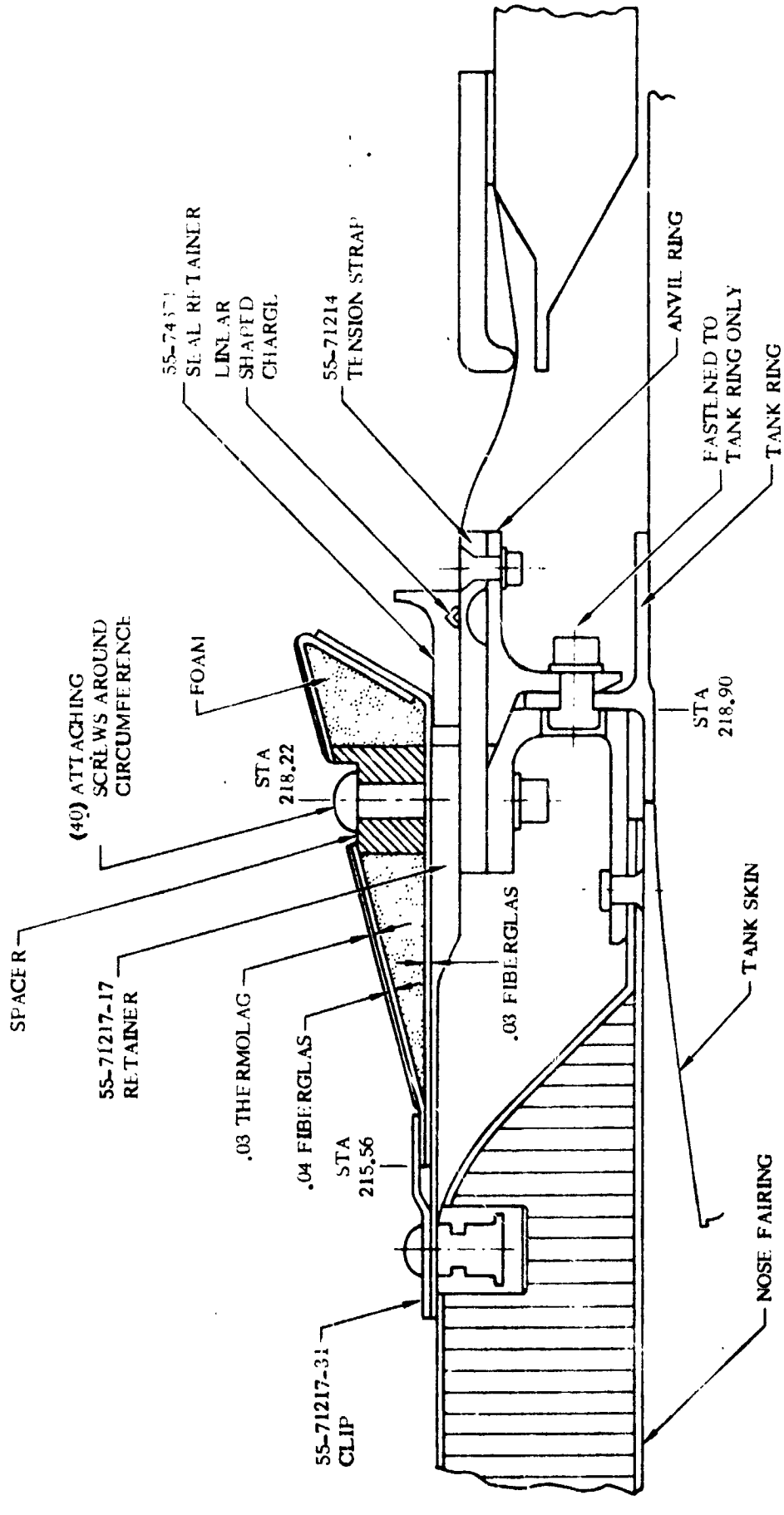

Figure 2.5-1. Nose Fairing Skirt and Station 218.9 Joint Configuration

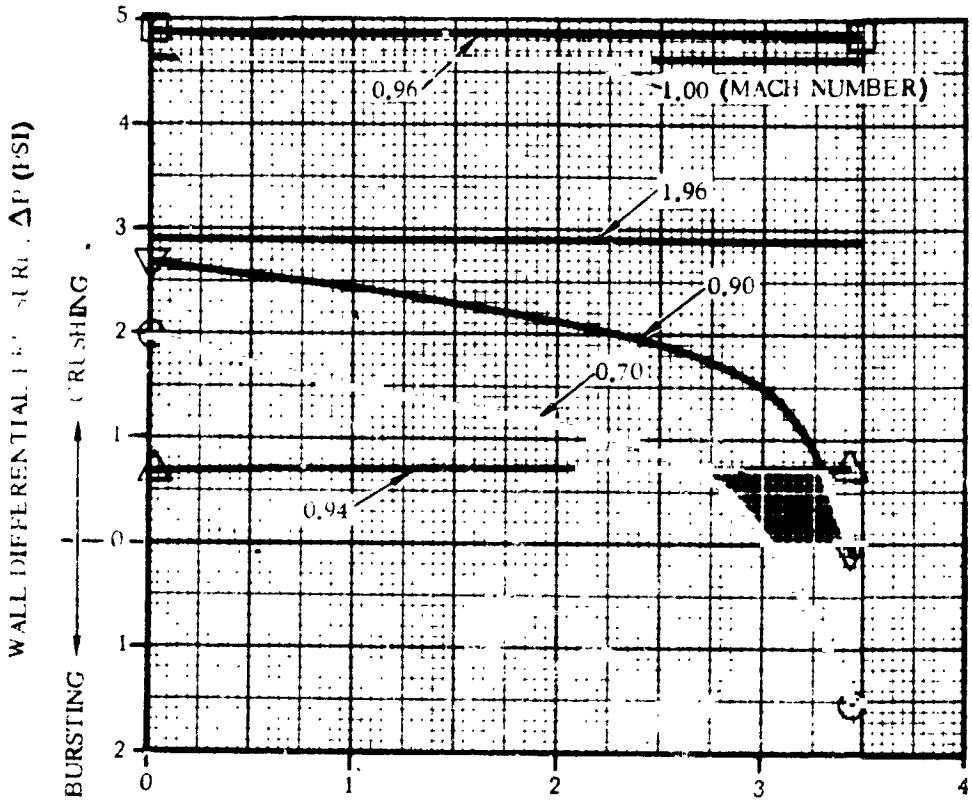

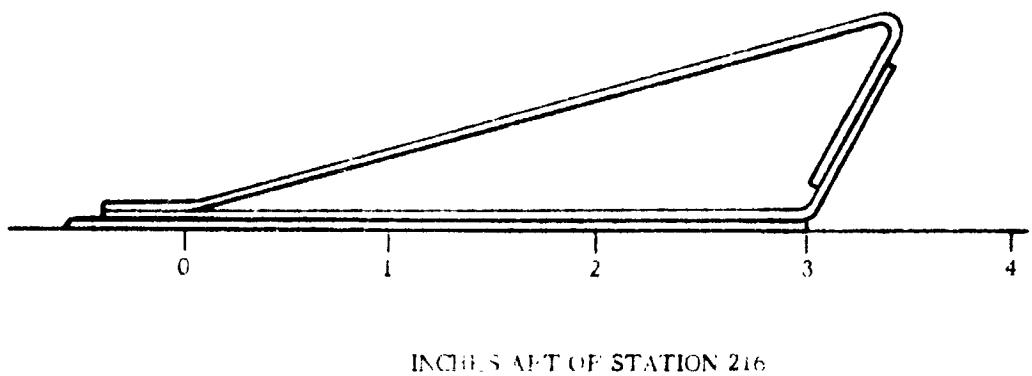

4B99LV

Figure 2.5-2. Nose Fairing Skirt (Typical Section) Steady-State Wall Differential Pressures (α = 0 Degrees)

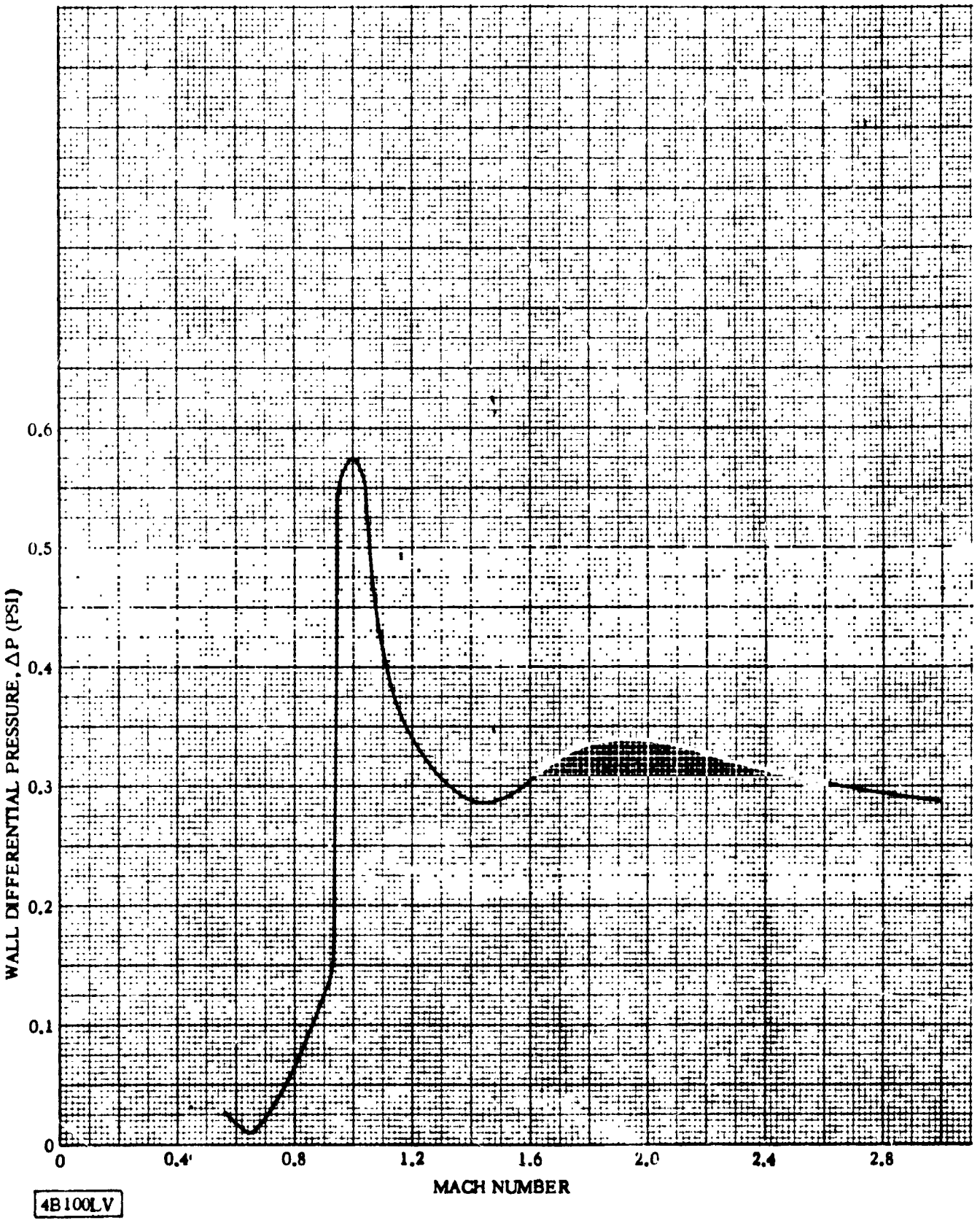

Figure 2.5-3. Nose Fairing Skirt (Typical Section) Angle of Attack Corrections for Steady-State Wall Differential Pressures (α = 6 Degrees)

The total aerodynamic drag or axial load imposed to the skirt is given in Figure 2.5-4 as a function of Mach number. This load accounts for only the smooth portion o the basic skirt. Axial loads for the protuberances are given where applicable.

In local areas near protuberances such as the hinge fairings, interference effects on the nose fairing skirt should be considered as additional contributions to differentia pressures. These increments should be applied along the full length (stationwise) of the skirt as shown in Figure 2.5-5. It should be noted that positive values indicate crushing and negative values indicate bursting.

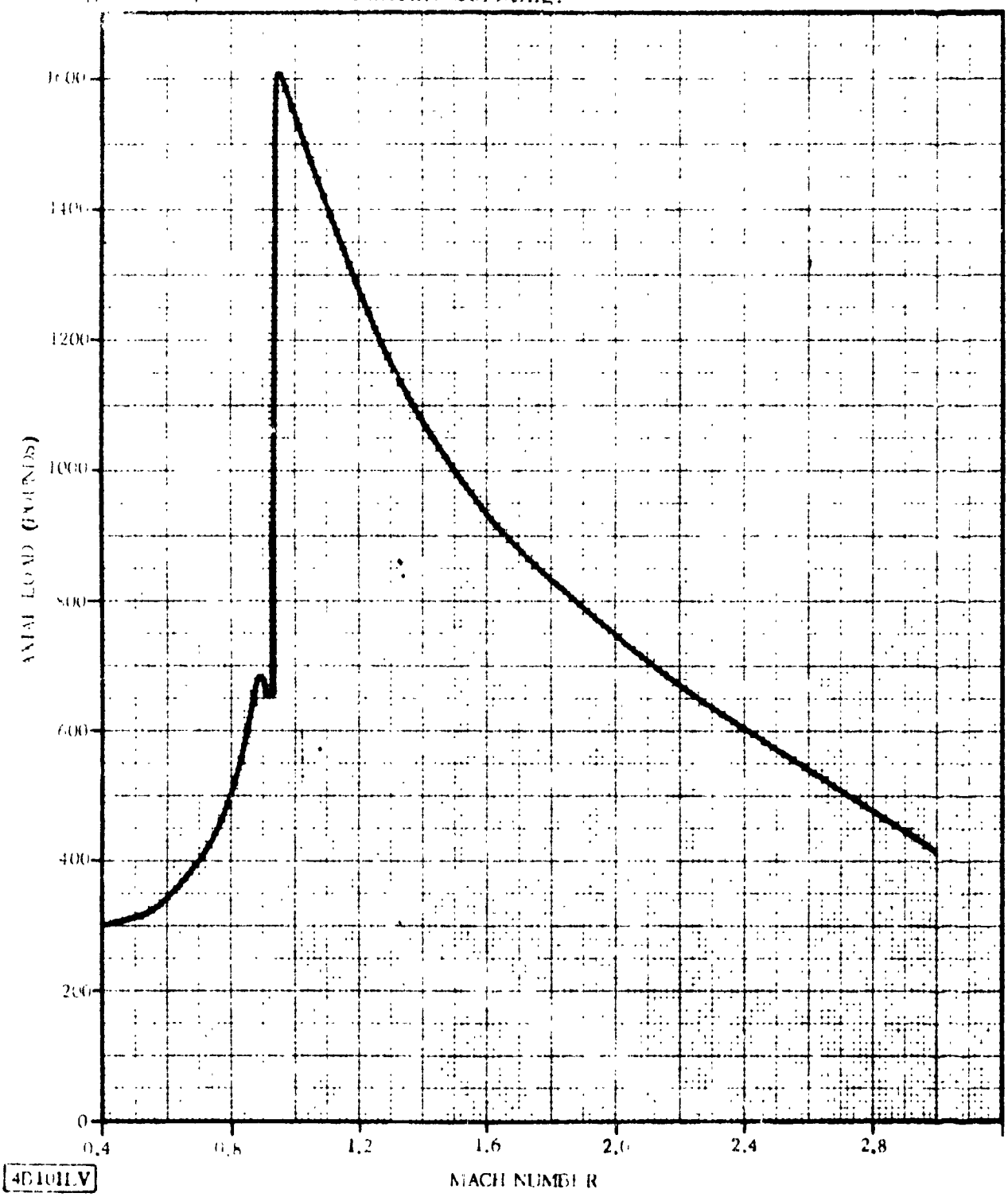

Figure 2.5-4. Nose Fairing Skirt Total Drag Load versus Mach Number

(1) ADJACENT TO ALL HINGE FAIRINGS

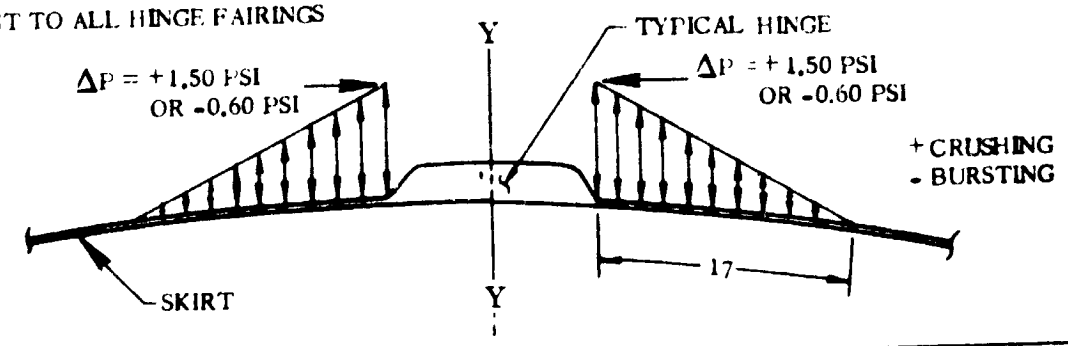

QUAD II INCLUDES HYDROGEN VENT STACK INTERFERENCE

(2) ADJACENT TO THE UMBILICAL ISLAND FAIRING

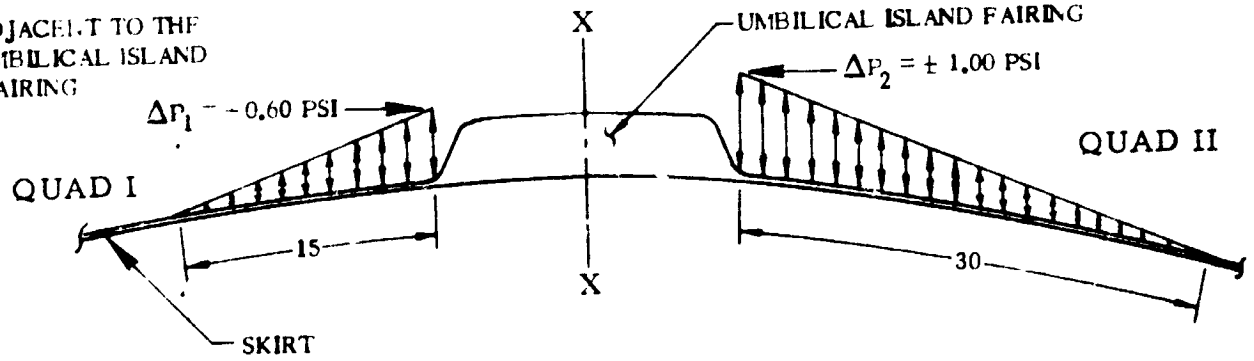

(3) ADJACENT TO DETONATOR FAIRINGS

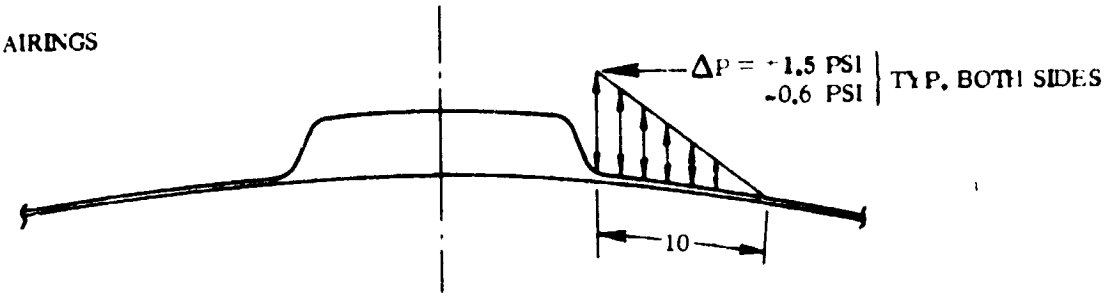

(4) ADJACENT TO INSULATION PANEL JOINT FAIRINGS

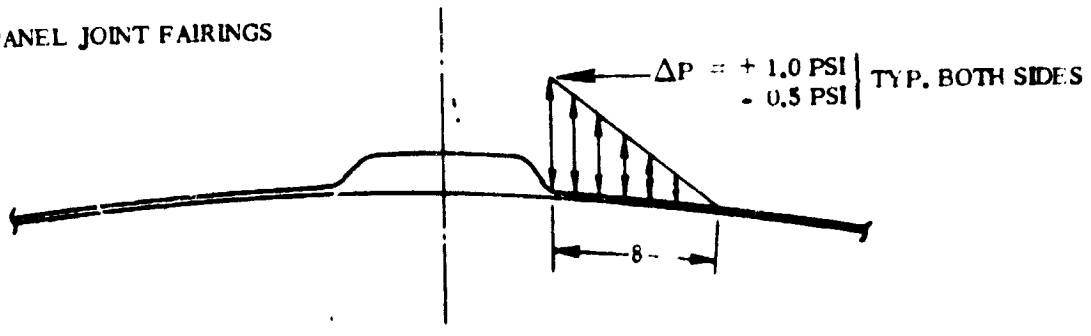

NOTE: ALL DIMENSIONS IN INCHES

ALL VIEWS LOOKING FORWARD AT STATION 218.9

4B102LV

Figure 2.5-5. Basic Skirt - Local Interference Loads from Fairings

2.5.6 BUFFET AND FLUTTER LOADS. For design of the nose fairing skirt, an equivalent static pressure can be used to represent buffet loads, which in the case of the nose fairing skirt, is ± 0.50 psi. The so-called transonic buffet effect can occur at any time between Mach 0.85 and 1.30, therefore this condition must be considered simultaneously with the steady-state conditions in Paragraph 2.5.5. Assume this pressure to act as indicated in Figure 2.5-6

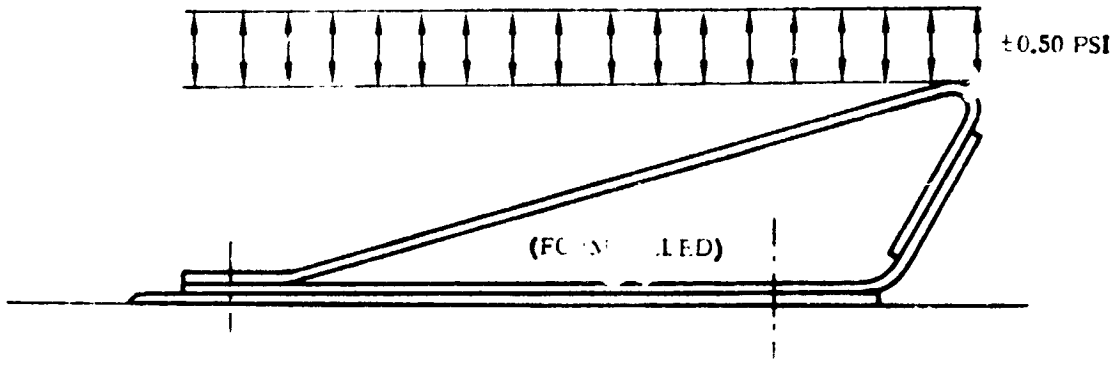

4B103LV

Figure 2.5-6. Nose Fairing Skirt Transonic Buffet Loads

2.5.7 MISCELLANEOUS LOAD PARAMETERS. No other loads should be considered for this component.

THIS PAGE INTENTIONALLY LEFT BLANK.

2.6 STATION 219 SEAL

A flexible seal made of lightweight plastic provides attachment between the insulation panels and the nose fairing skirt arrangement as shown in Figure 2.6-1. This seal, while remaining intact, also establishes the proper venting conditions for the insulation panel - LH_2 tank cavity during ascent through the atmosphere. This seal is then severed by a linear shaped charge at the proper time to accomodate insulation panel and nose fairing jettisons.

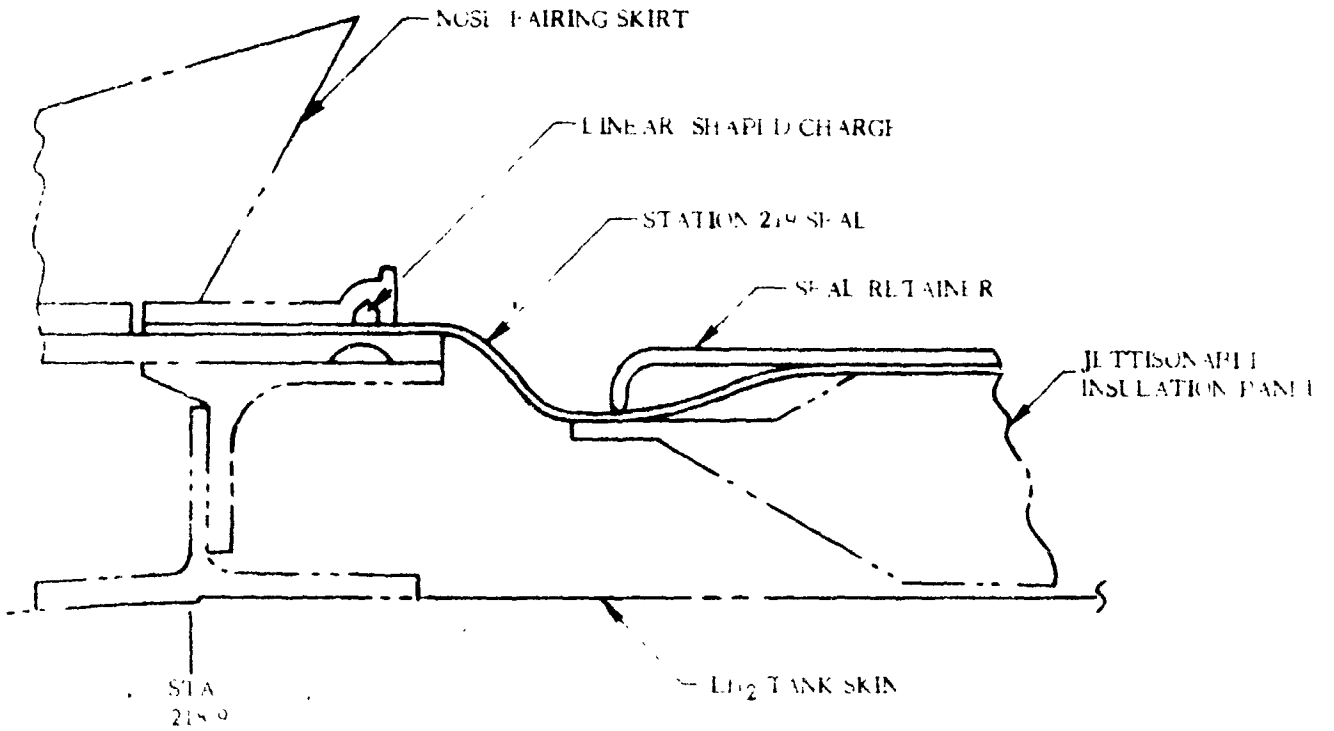

41-1041 V

Figure 2.6-1. Station 219 Seal Configuration

2.6.1 CRITICAL CONDITIONS. The critical loading condition for the Station 219 seal occurs during the transonic period of flight. At this time, the steady-state air loads must be combined with the buffet type air loads due to dynamic response of the component. The maximum heating condition need only be investigated from a thermal standpoint since the aerodynamic loads have essentially diminished to zero.

2.6.2 WEIGHTS AND CENTER OF GRAVITY DATA. The seal weight is of an inconsequential magnitude; therefore, weights and C.G. data are not applicable.

2.6.3 THERMAL DATA. The temperature history of the subject seal is presented in Figure 2.6-2, which represents the most severe thermal environment for any of the operational vehicles.

2.6.4 INERTIA LOADS. The seal weight is so small that inertia loads are negligible (see Paragraph 2.6.2).

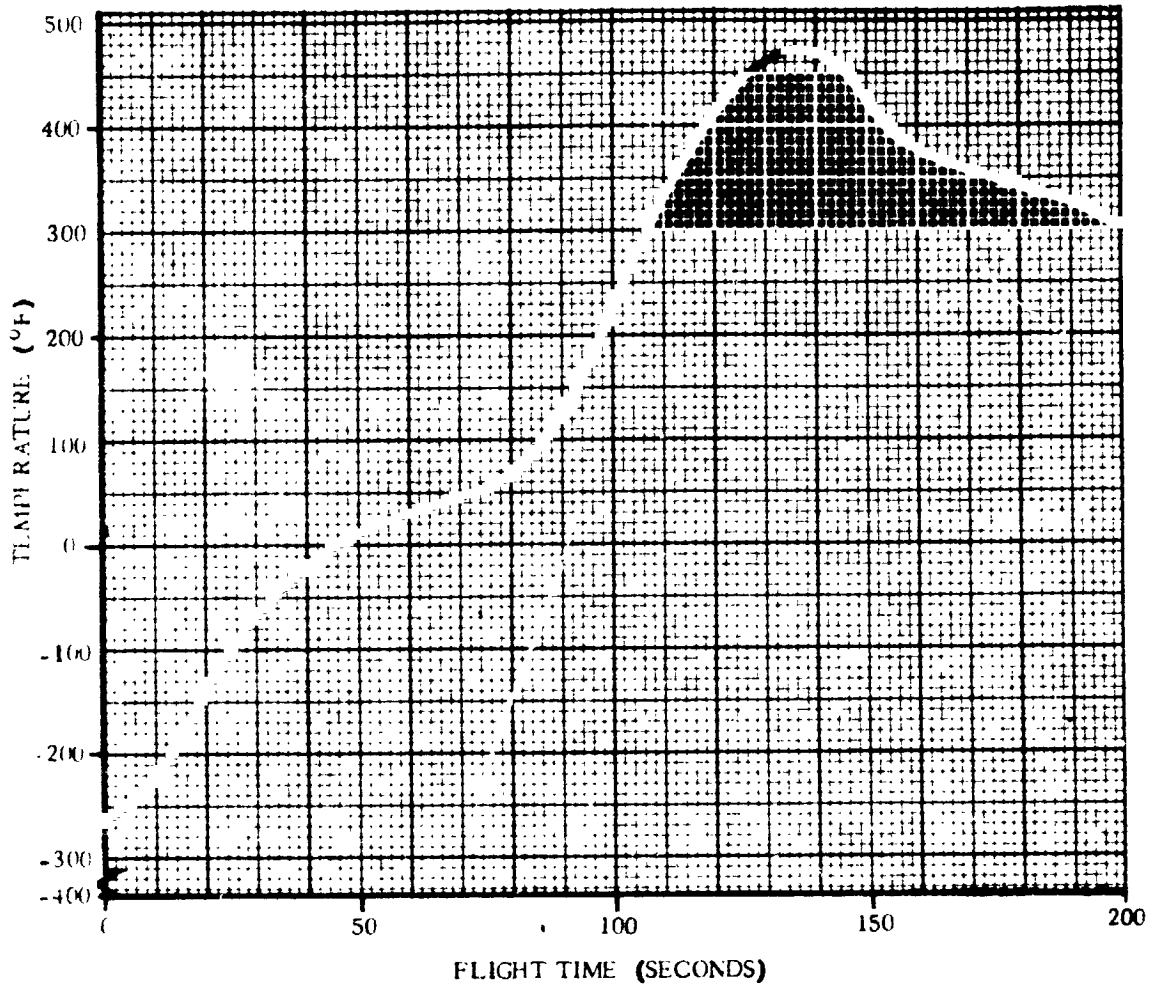

4B105LV

Figure 2.6-2. Station 219 Seal Temperature History

2.6.5 STEADY-STATE AIR LOADS. Steady-State air loads are given as differential pressures across the Station 219 membrane. For purposes of analysis, the following maximum differential pressures should be considered as determined from experimental wind tunnel data.

$$\Delta P = \begin{cases} +3.3 \text{ psi (Crushing)} \\ -2.5 \text{ psi (Bursting)} \end{cases}$$

These loads occur during the transonic range of flight.

2.6.6 BUFFET AND FLUTTER LOADS. As the Atlas/Centaur vehicle flies through transonic speeds (Mach numbers from 0.85 to 1.30), an additional ΔP can result from the effects of buffeting (alternate boundary layer separation and attachment). Due to the dynamic response of the membrane to this effect, an equivalent steady-state ΔP of ± 0.50 psi should be superimposed with the steady-state loads described in Paragraph 2.6.5, thus accounting for fluctuating pressure.

2.6.7 MISCELLANEOUS LOAD PARAMETERS. No other loads should be considered for this component.

2.7 DETONATOR FAIRINGS

These items are simply protective Fiberglas fairings used to isolate the detonator installation which in turn activates the linear shaped charge at the Station 219 joint area. Two fairings are used to protect the pyrotechnics from the severe environmental conditions which exist during the vehicle's ascent through the atmosphere. Both fairings are positioned 20 degrees from the X axis in Quadrants I and III respectively. See Figure 2.7-1 for the fairing configuration.

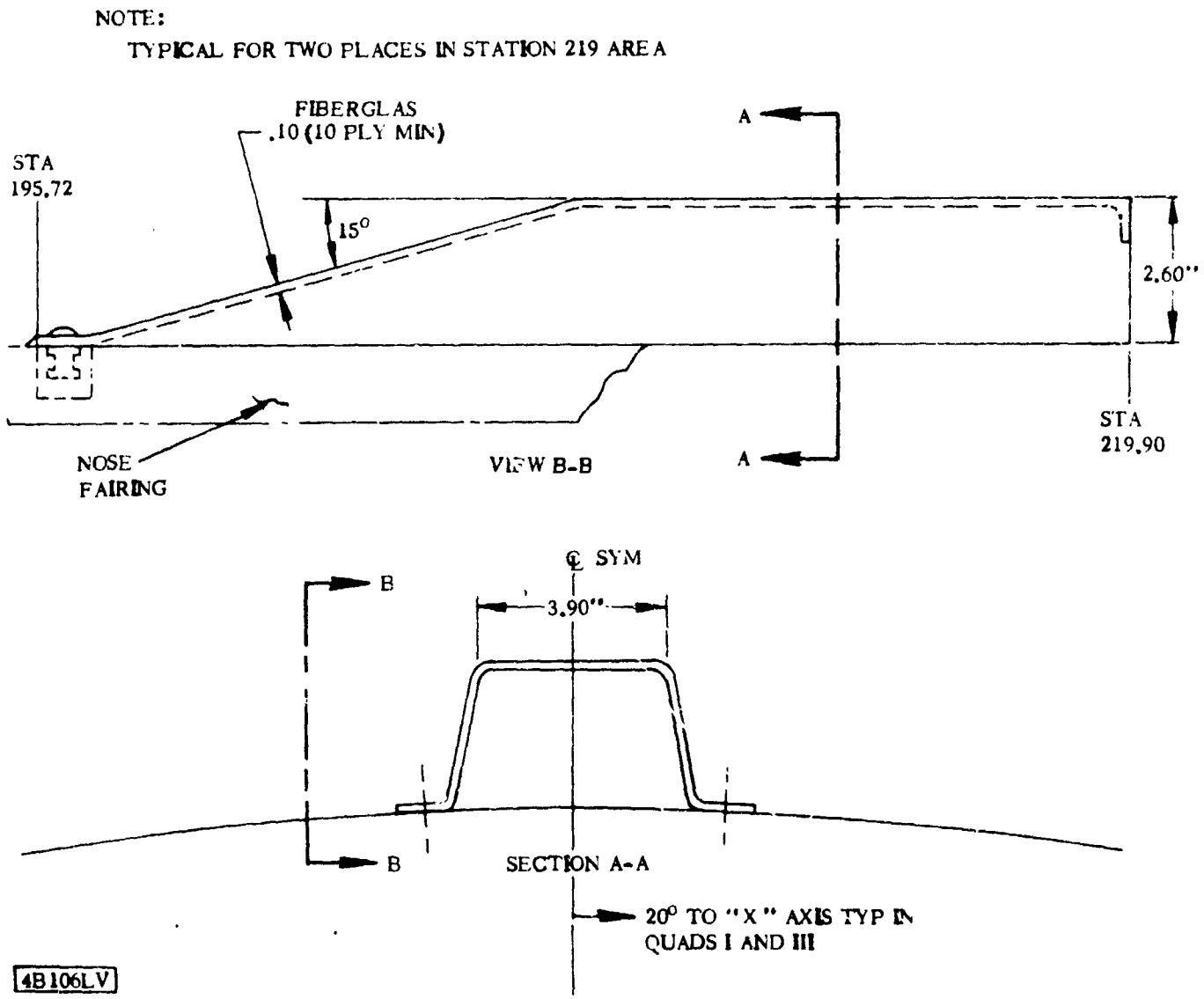

Figure 2.7-1. Detonator Fairing Configuration

2.7.1 CRITICAL CONDITIONS. The critical loading conditions for the detonator fairings occur during transonic flight when both steady-state and fluctuating air loads are at a maximum and are also acting simultaneously. Additional considerations should be made when surface temperatures attain their maximum values and immediately prior to nose fairing jettison when the linear shaped charge is activated to sever the 219 seal.

2.7.2 WEIGHTS AND CENTER OF GRAVITY DATA. Due to the nature of this component, inertia loads are of an inconsequential magnitude; therefore, weights and C.G. data are not applicable.

2.7.3 THERMAL DATA. The data presented herein represents the maximum temperatures expected for any of the follow-on vehicles. Temperature histories are given in Figure 2.7-2 for two typical points along the surface; namely, a point on the 10 degree ramp area and a point on the surface parallel to the vehicle longitudinal axis. These temperatures are assumed to be applicable for the entire surface length within the respective areas described.

2.7.4 INERTIA LOADS. Load contribution from inertia effects are not to be considered for this component (see Paragraph 2.7.2).

2.7.5 STEADY-STATE AIR LOADS. Steady-state differential pressures at zero angle of attack are presented in Figure 2.7-3. A uniform distribution over the respective area shall be assumed for purposes of analysis. The data for Mach number 0.94 includes an increment of 0.5 psi to account for an assumed venting lag. Venting occurs through the aft end of the fairings. An additional ±0.6 psi should be considered as a load contribution to be superimposed with the values from Figure 2.7-3 due to a 6 degree angle of attack.

Total axial drag and side loads for each fairing are given in Figure 2.7-4. The drag and side loads shall be assumed to act through the centroid of the projected frontal and side areas respectively. These loads represent only the external pressure effects on each pod, whereas, the wall ΔP also considers internal pressure. Consequently, the loads should be used accordingly in the analysis of the structure.

2.7.6 BUFFET AND FLUTTER LOADS. Fluctuating aerodynamic pressures are imposed on the detonator fairings during transonic flight (Mach No. 0.85 to 1.36). For design of this hardware, an equivalent static pressure of ±2.90 psi can be used to represent buffet loads which results from the dynamic response of the structure. Consider this pressure to act on the subject fairing as described in Figure 2.7-5.

These loads occur simultaneously with the steady-state air loads given in Paragraph 2.7.5.

2.7.7 MISCELLANEOUS LOAD PARAMETERS. Immediately prior to nose fairing jettison, the charges underneath the detonator fairings are activated which in turn imposes a pressure shock load to the respective fairings. Due to the extremely short duration of this load, its effect on the structure is not entirely defined, therefore the structural integrity of the subject fairings will be proven by test.

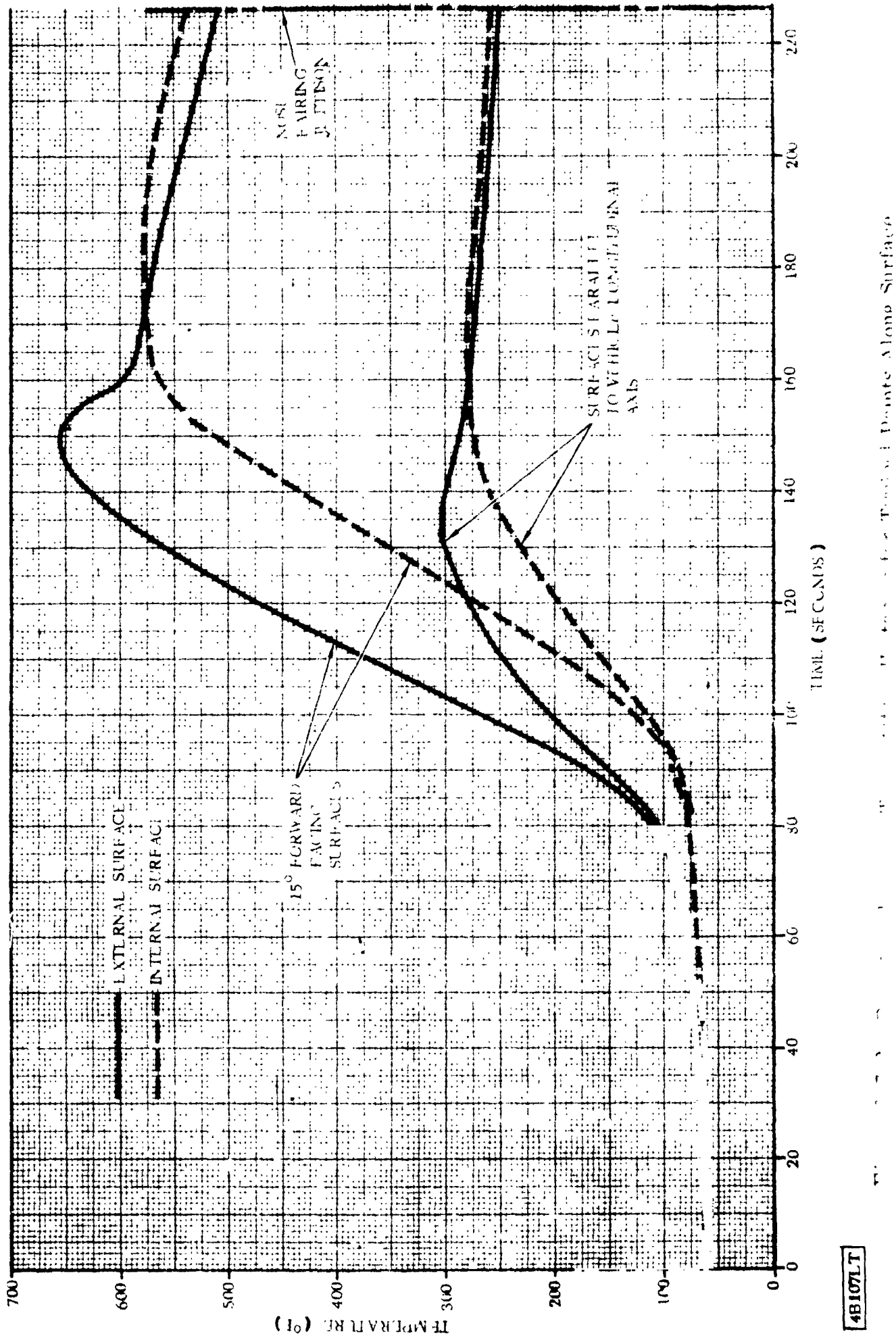

4B107LT

Figure 2-51. Temperature Time Histories at Points Along Surface

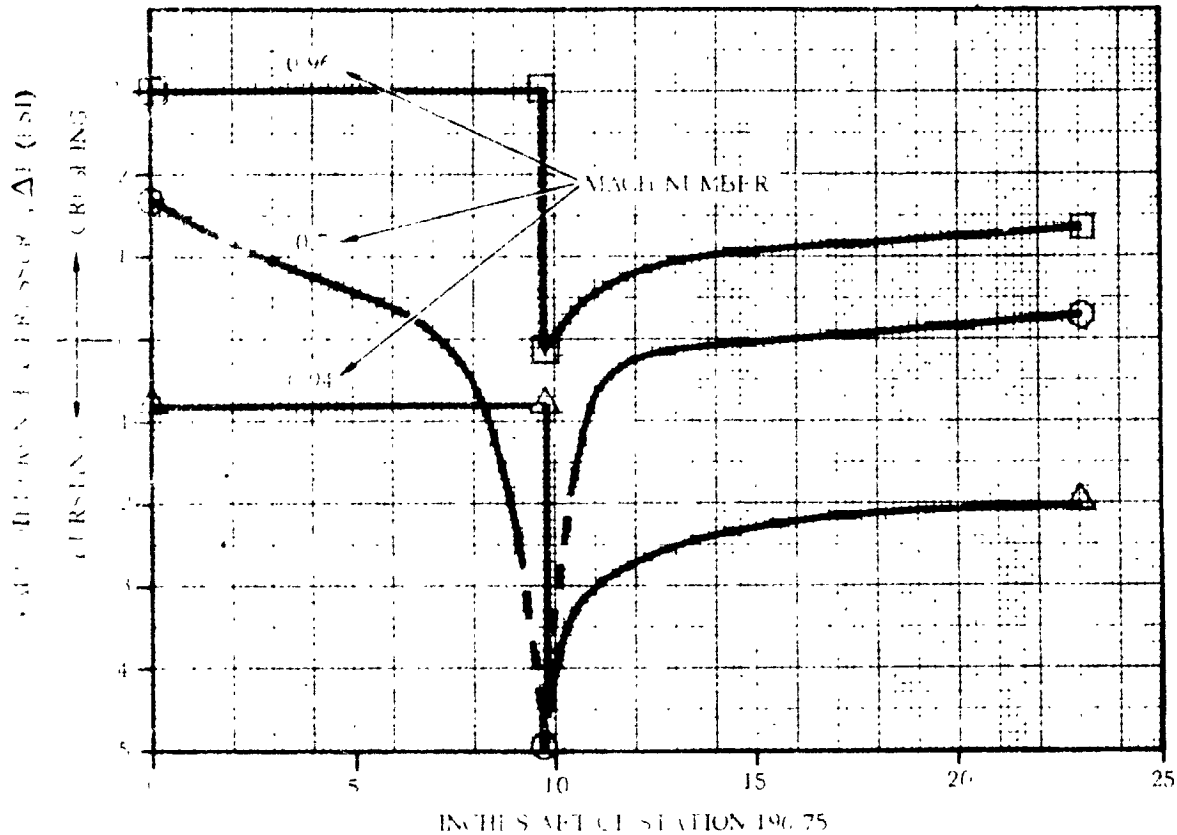

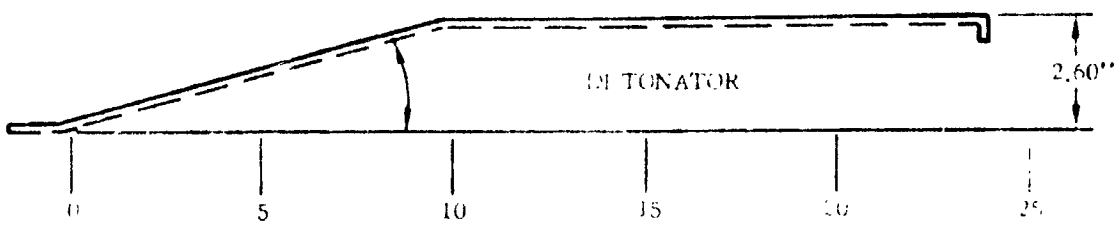

4B108LV

Figure 2.7-3. Detonator Fairings Steady-State Wall Differential Pressure (α = 0 Degrees)

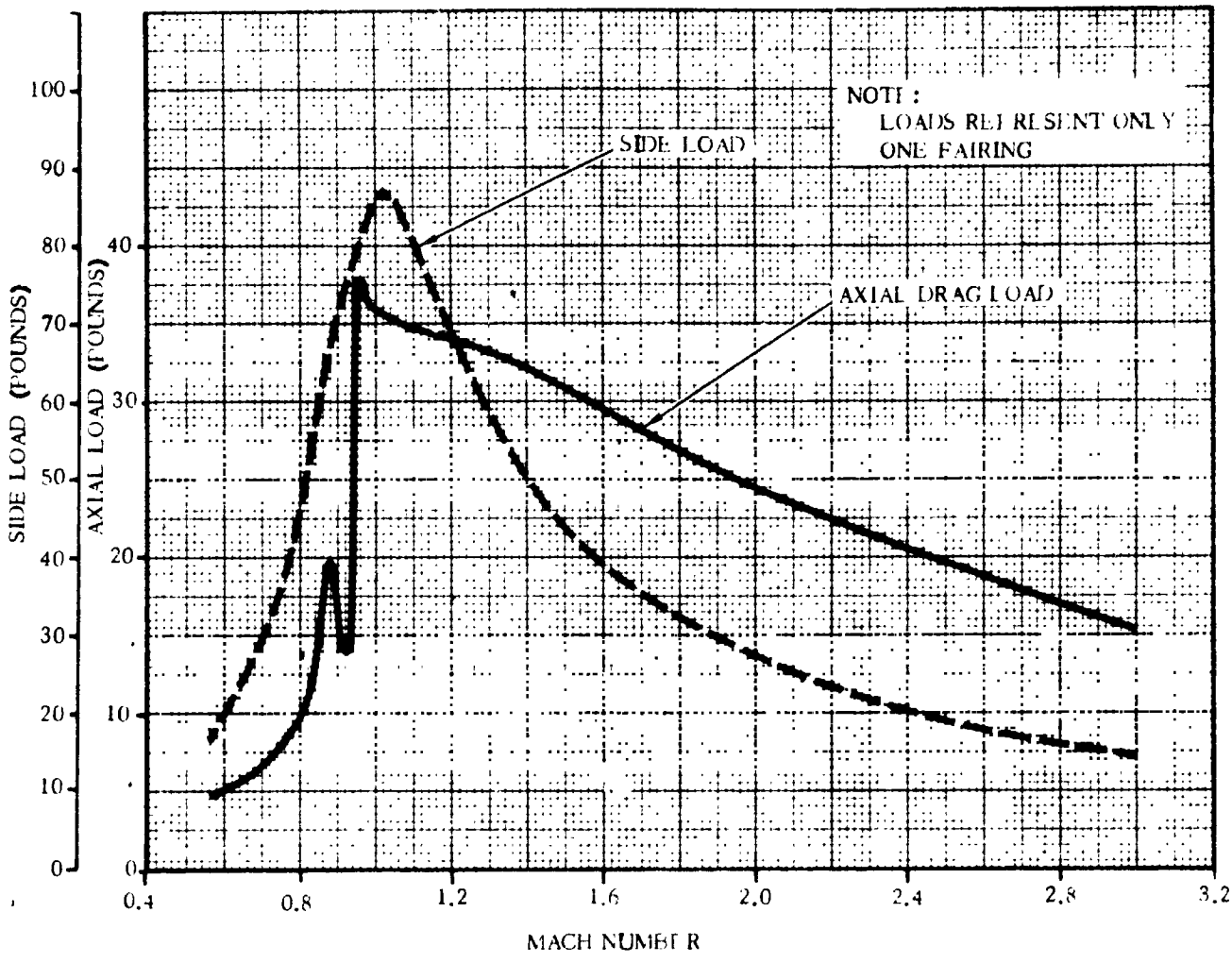

4B109LV

Figure 2.7-4. Detonator Fairings Total Drag and Side Load versus Mach Number

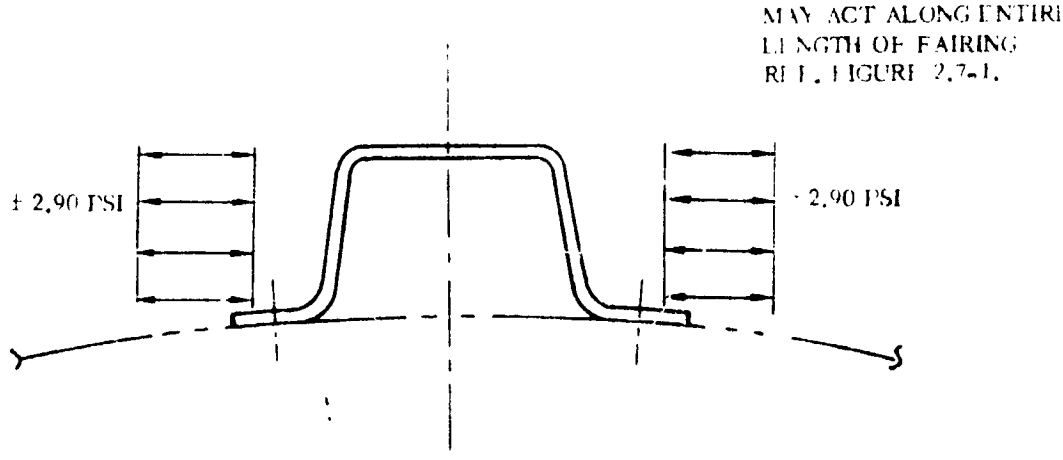

4B110LV

Figure 2.7-5. Detonator Fairings Transonic Buffet Loads

THIS PAGE INTENTIONALLY LEFT BLANK.

2.8 INSULATION PANEL JOINT FAIRINGS

The insulation panel joint fairings (four in number) are located in the Station 219 area, circumferentially aligned with the longitudinal splices of the insulation panels. They actually form that portion of nose fairing skirt at these points and provide a protective shield over the panel splice angles. See Figure 2.8-1 for the fairing configuration and locations.

2.8.1 CRITICAL CONDITIONS. The critical loading conditions for these fairings occur during transonic flight when steady-state and fluctuating air loads are at a maximum and are also acting simultaneously. Further consideration should be made at the time of maximum surface temperature even though the air loads have essentially diminished to zero.

2.8.2 WEIGHTS AND CENTER OF GRAVITY DATA. Due to the nature of these items, inertia loads are of an inconsequential magnitude; therefore, weights and C.G. data are not applicable.

2.8.3 THERMAL DATA. A temperature history for the insulation panel joint fairings is presented in Figure 2.8-2. This data reflects the maximum temperatures expected for any of the operational vehicles. The temperature, as described, is applicable to any point within the 15 degree ramp area and is assumed as representative of the entire surface length.

2.8.4 INERTIA LOADS. Load contribution from inertia effects are not to be considered for these components (see Paragraph 2.8.2).

2.8.5 STEADY-STATE AIR LOADS. Steady-state differential pressures versus Mach number at a zero angle of attack are given in Figure 2.8-3. For purposes of analysis, these pressures shall be assumed to act uniformally over the respective area of the fairing. These fairings were assumed to have a venting arrangement similar to that described in Paragraph 2.7.5, so that the ΔP at Mach number 0.94 includes 0.5 psi due to venting lag. An additional ± 0.6 psi should be used to account for a 6 degree angle of attack. Therefore ± 0.6 psi should be superimposed with the values from Figure 2.8-3.

Total axial drag and side loads for each fairing are given in Figure 2.8-4. Both the drag and side loads shall be assumed to act through the centroid of the projected frontal and side areas respectively. These loads represent only the external pressure effects on each fairing; whereas, the wall ΔP also considers internal pressure. The loads should be utilized accordingly in the analysis of the structure.

2.8.6 BUFFET AND FLUTTER LOADS. For purposes of analysis, fluctuating aerodynamic pressures which are induced to the fairings, may be represented by an equivalent static pressure. The load, in this case ± 3.30 psi, actually results from the

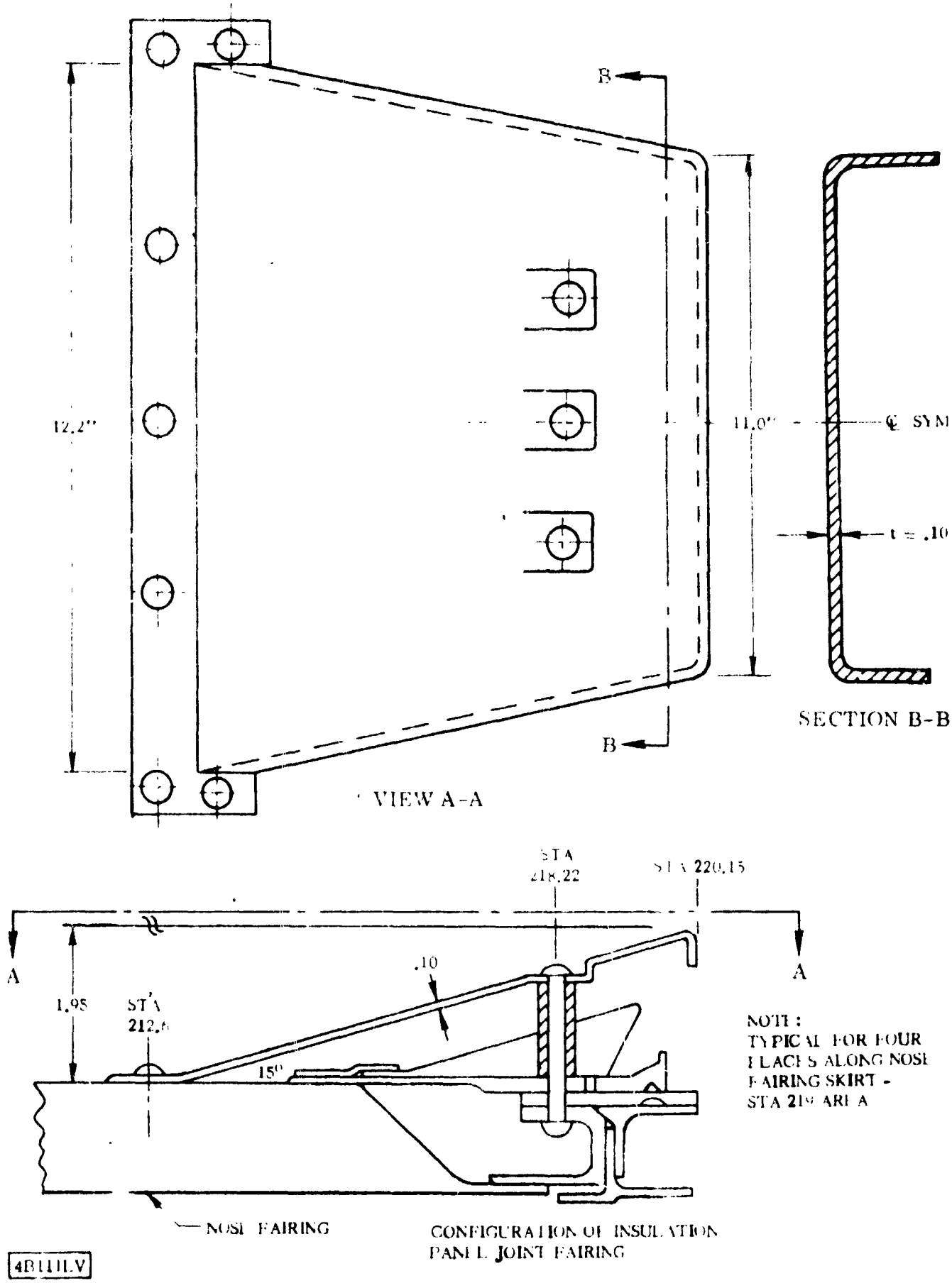

Figure 2.8-1. Insulation Panel Joint Fairing Configuration

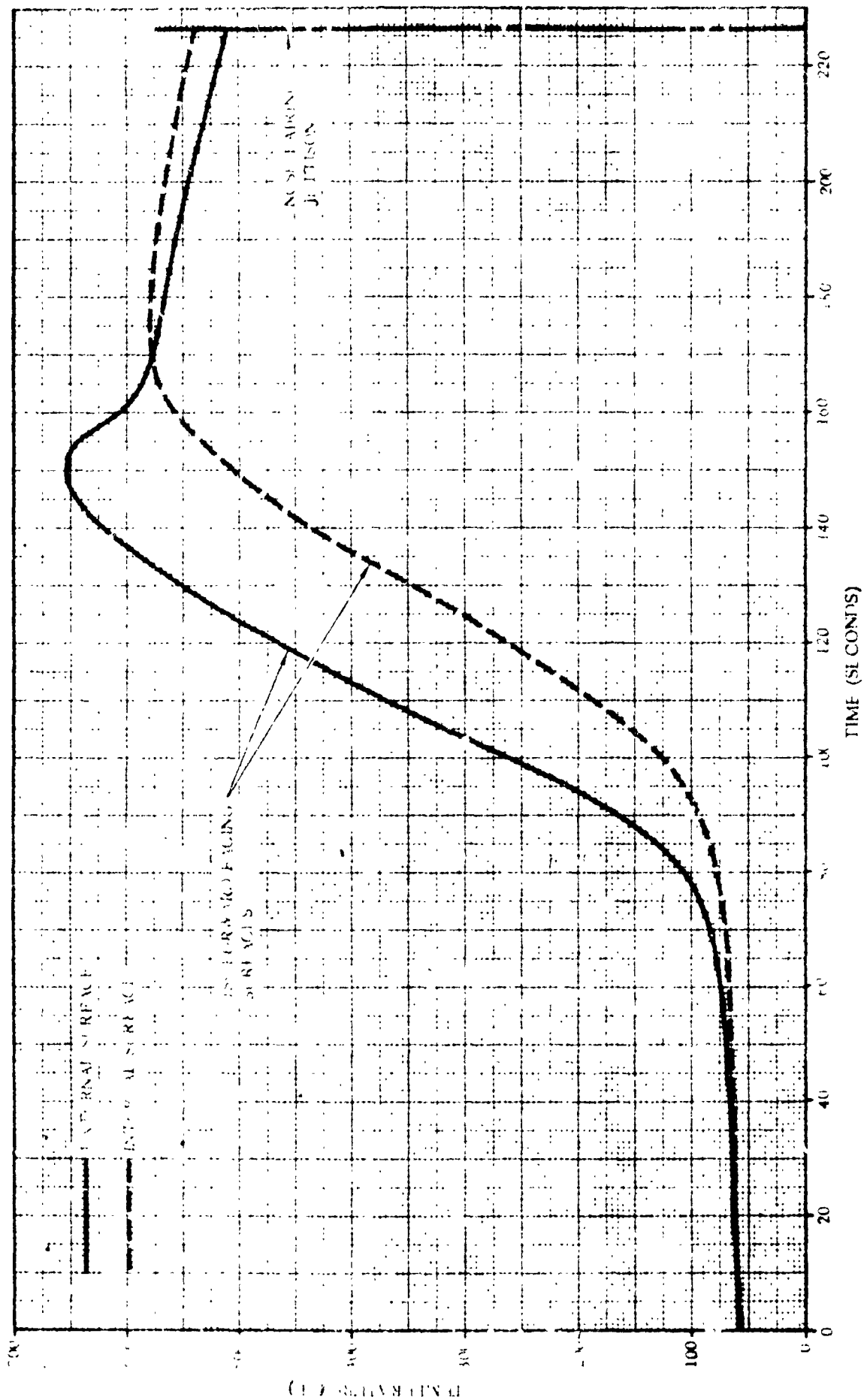

4B1127.7

Figure 2.5-2 Ablative Panel Longitudinal Joint Fairing - Temperature History for a Typical Point along the Surface

dynamic response of the structure to this phenomena. This condition can occur at any time during the transonic range of flight (Mach No. 0.85 to 1.30) therefore, consideration of these effects must be made simultaneously with the steady-state air loads given in Paragraph 2.8.5. Assume this pressure to act on the subject fairing as described in Figure 2.8-5.

2.8.7 MISCELLANEOUS LOAD PARAMETERS. No other loads should be considered for this component.

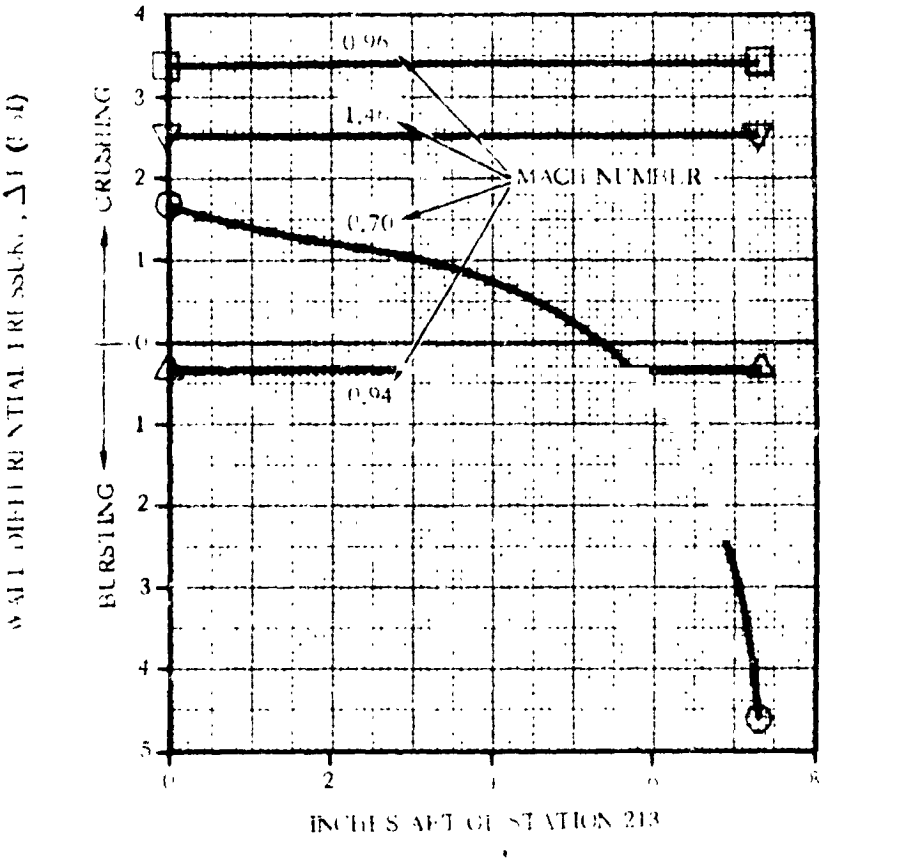

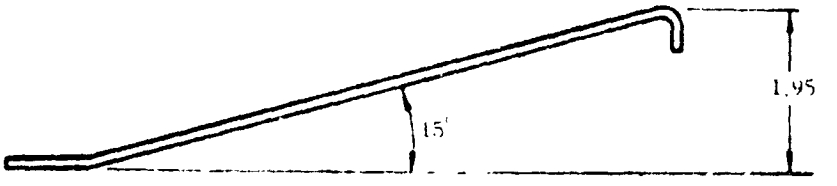

4B115LV

Figure 2.8-3. Insulation Panel Joint Fairings Steady-State Wall Differential Pressure (α = 0 Degrees)

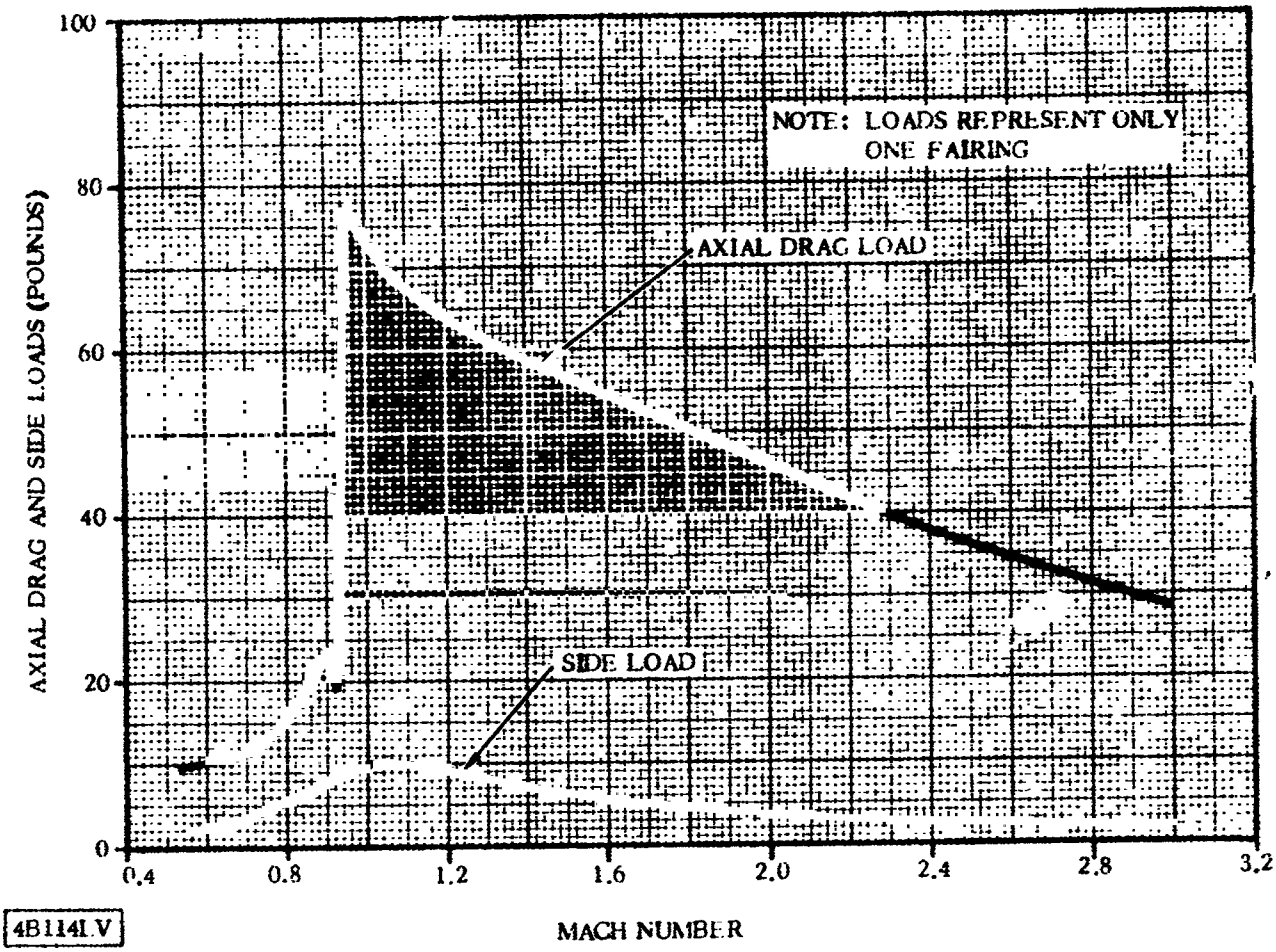

Figure 2.8-4. Insulation Panel Joint Fairings - Total Drag and Side Load versus Mach Number

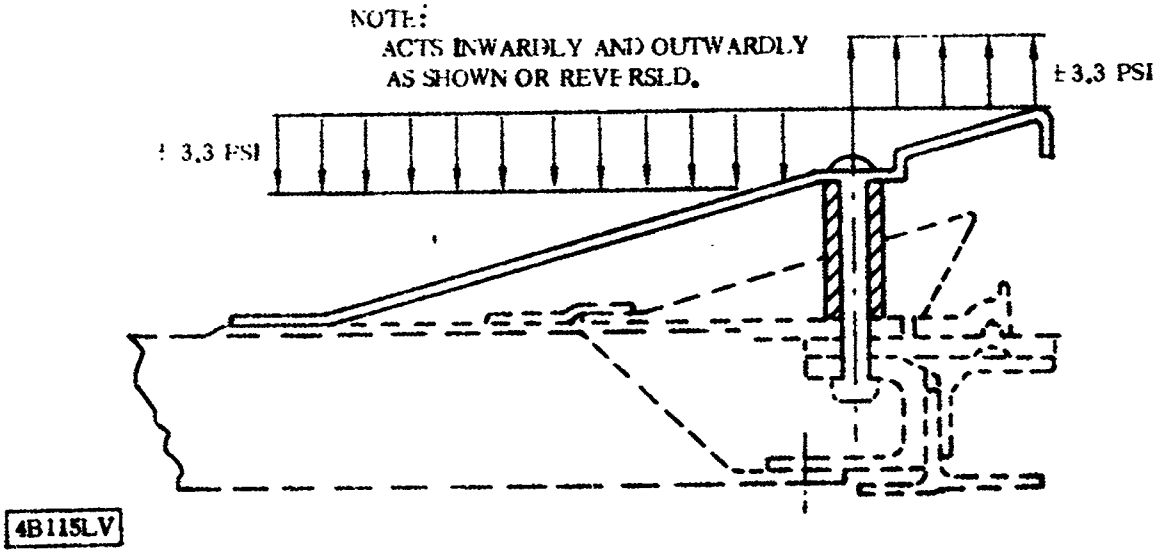

Figure 2.8-5. Insulation Panel Joint Fairings Transonic Buffet Loads

THIS PAGE INTENTIONALLY LEFT BLANK.

2.9 JETTISON HINGES

The jettison hinges (Figure 2.9-1) are part of the nose fairing separation system since they provide the pivotal point about which the nose fairing rotates during jettison. Each fairing half utilizes one hinge which is located approximately at Station 219 on the Y-Y axis of the vehicle. These components also serve as the reaction point for load transfer between the fairing and the Station 218.9 ring during this time.

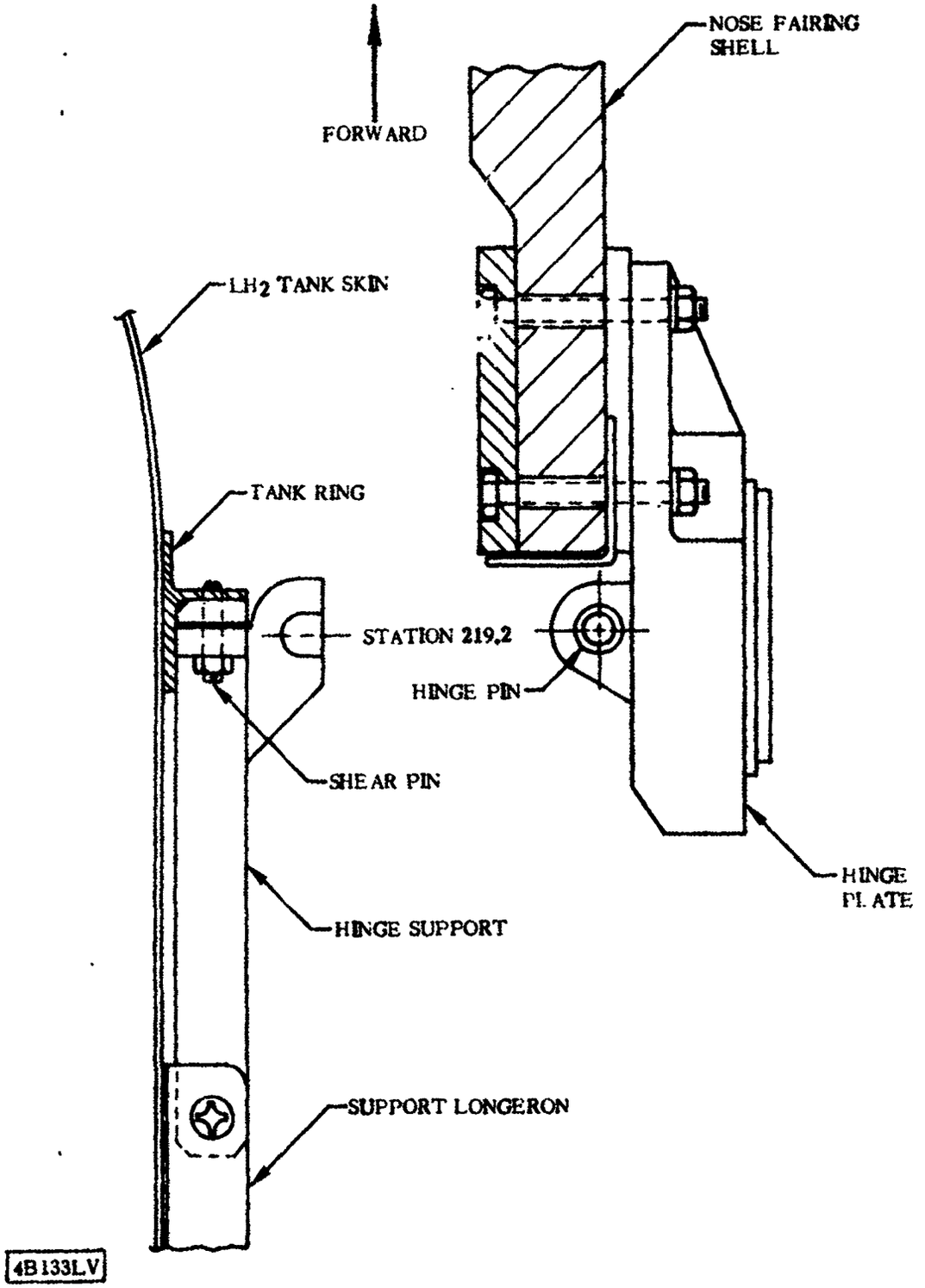

Figure 2.9-1. Nose Fairing Jettison Hinge Configuration

2.9.1 CRITICAL CONDITIONS. The nose fairing hinges are exposed to high temperatures at time of fairing jettison. A longitudinal gap is preset in each hinge before flight to prevent air loads and thermal deflections from loading up the hinges during transonic flight.

2.9.2 WEIGHTS AND CENTER OF GRAVITY DATA. See Paragraph 2.2.2 for nose fairing weights which are used to compute hinge loads during jettison.

2.9.3 THERMAL DATA. The maximum expected temperatures for various points on the nose fairing hinge assembly are presented in Figure 2.9-2 and Table 2.9-1.

Thermal deformations resulting from chilldown and subsequent flight phase (including nose fairing jettison) shall be based on these temperatures which are representative of the most severe thermal environment for any of the subsequent operational vehicles.

TABLE 2.9-1. NOSE FAIRING HINGE-HALVES AND NOSE FAIRING SECTION - TEMPERATURE TABULATION

Location (Reference Figure 2.9-2)		Flight Time (sec)			
		0	70	140	215*
A	All temperatures are given in °R	112	112	111	108
B		113	113	111	108
C		97	96	96	95
D		88	87	86	84
E		97	97	88	81
F		97	97	86	78
G		95	94	81	73
*Approximate nose fairing jettison time					

2.9.4 INERTIA LOADS. The loads on the hinges due to inertia effects at fairing jettison are included in Paragraph 2.9.7.

2.9.5 STEADY-STATE AIR LOADS. The hinges are not designed to transmit aerodynamic loads from the nose fairing. No direct air impingement loads act on the hinges since they are covered by the hinge pods.

2.9.6 BUFFET AND FLUTTER LOADS. Buffet loads on the hinges are negligible.

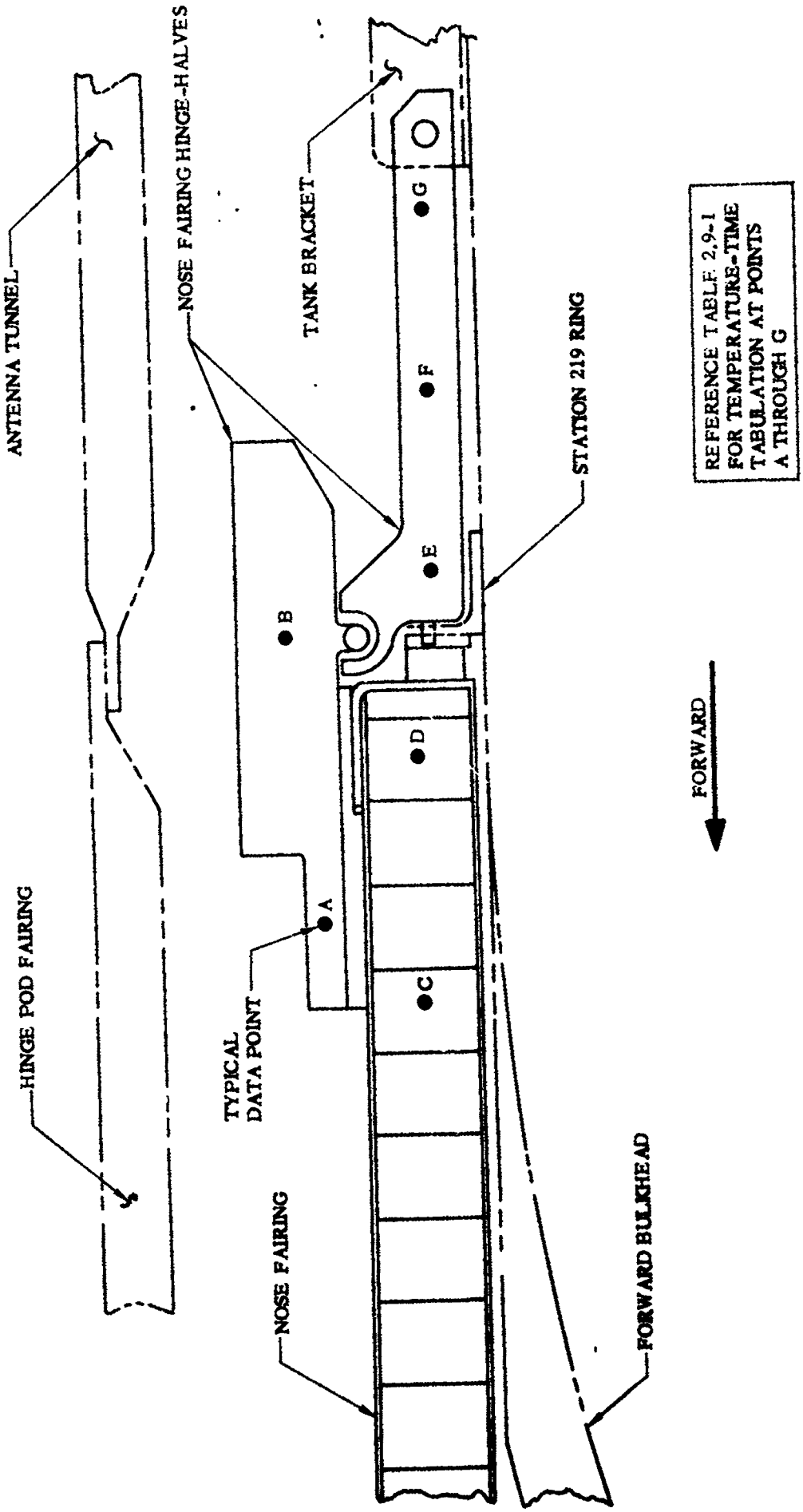

Figure 2.9-2. Nose Fairing Hinge Assembly Temperatures

2.9.7 MISCELLANEOUS LOAD PARAMETERS. The sequence of nose fairing jettison imposes the most severe loading to the jettison hinges. However, at some predetermined time prior to this condition (BECO +30 seconds for single-burn missions and BECO +50 seconds for 2-burn missions) the insulation panels are jettisoned. At this time, the shaped charge cuts the tension tie at the Station 218.9 joint. Consequently, any tension or shear loads which may occur up until nose fairing jettison must be transferred through the only remaining path, namely, the jettison hinges. The design loads for this specific condition are as follows:

Load	Units	Nominal	3σ Dispersion
Shear	lb	194	256
Axial Load	lb	2,320	2,436
Bending Moment	in.-lb	18,760	25,190

The data presented above is based on the following assumptions:

a. Aerodynamic coefficients based on Reference 2-15.

b. Nominal and 3-sigma trajectory parameters based on Reference 1-3, i.e., angle-of-attack, dynamic pressure, axial acceleration, etc.

c. Jettison times based on BECO + 30.

At nose fairing jettison, additional loads are induced to the hinges which result from jettison bottle thrust and fairing rotation. These loads act on the tank at Station 219.5 and may act either simultaneously or independently, whichever is more critical. Figure 2.9-3 is presented to correlate the fairing angle of rotation with time from initial bottle thrust. Figure 2.9-4 and 2.9-5 associate the longitudinal and radial loads, respectively, with time. In this case, an envelope of loads is employed to account for the dispersions in the many load input variables such as nose fairing weight, modal response of the fairing, dynamic characteristics of the tank, thrust buildup, thrust decay, etc.

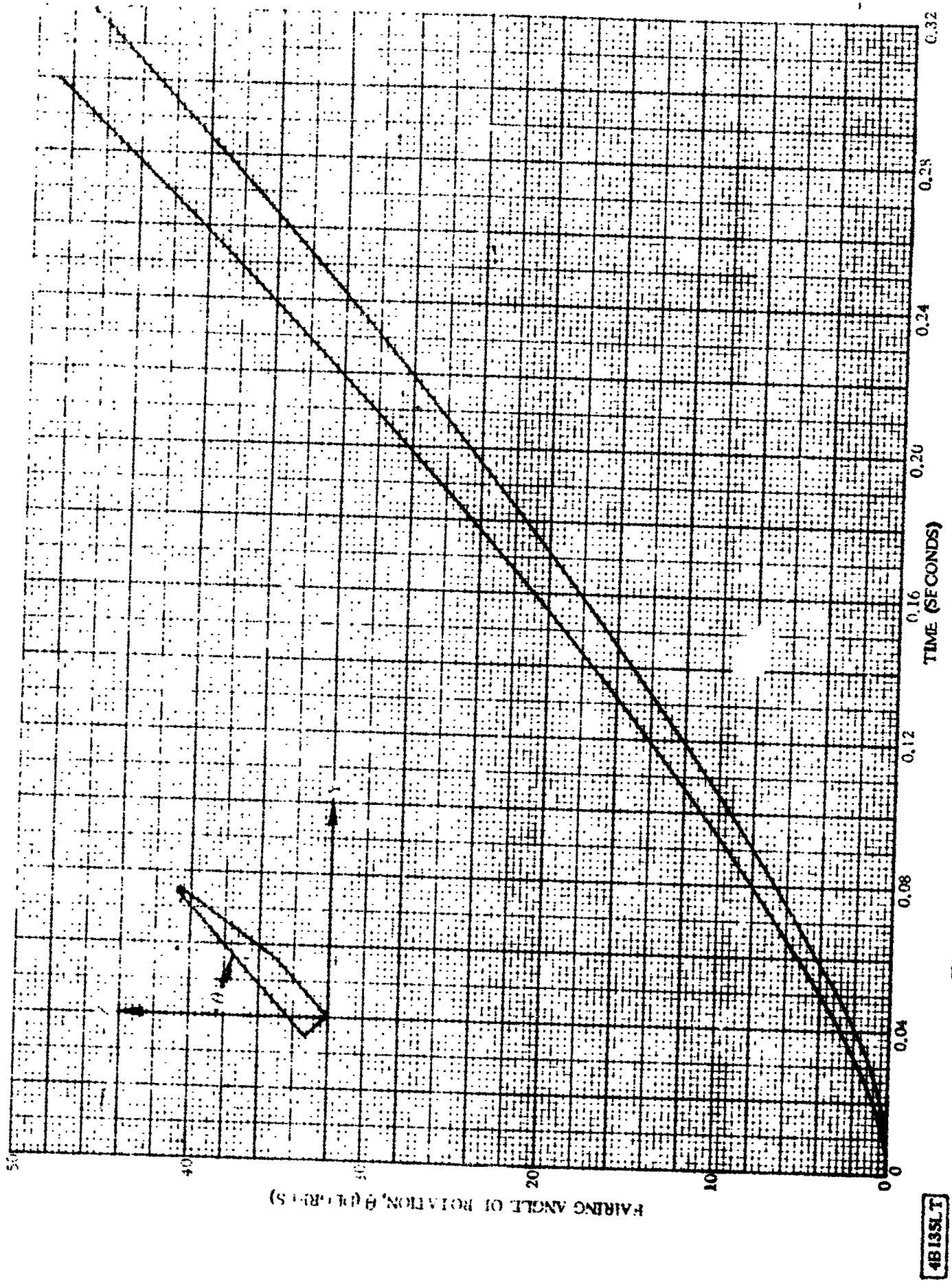

Figure 2.9-3. Nose Fairing Jettison, Angle of Rotation Limits versus Time

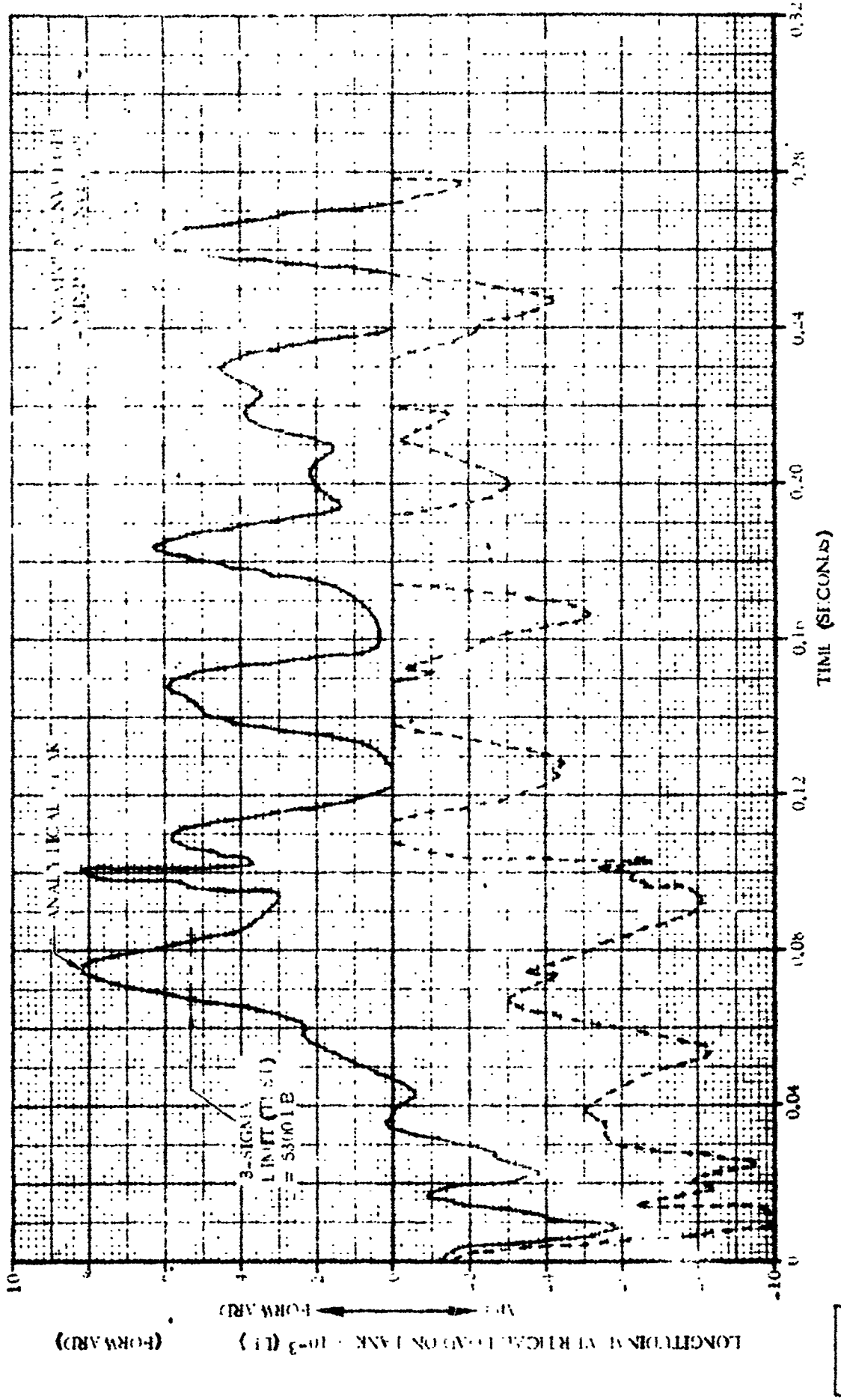

Figure 2.9-4. Nose Fairing Jettison Root-Sum-Square Longitudinal Hinge Loads versus Time

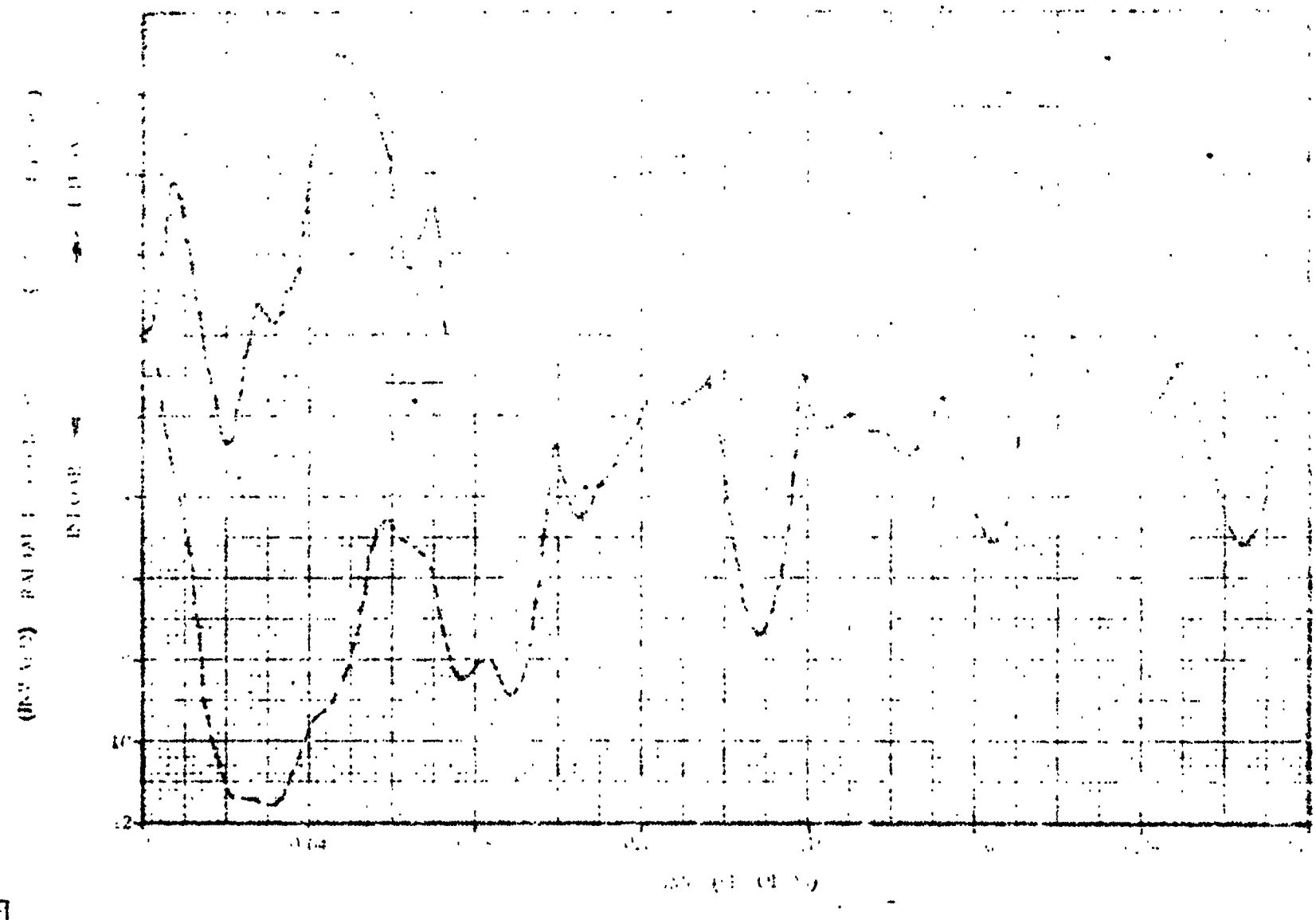

4B137LT

Figure 2.9-5. Nose Fairing, Jettison, Port Side-Separation Radial Hinge Loads versus Time

THIS PAGE INTENTIONALLY LEFT BLANK.

2.10 DEFLECTOR BULKHEAD

The deflector bulkhead is located in the nose fairing directly beneath the jettison bottles. Its purpose is to prevent the escaping jettison bottle gas from impinging on the payload. The configuration of the deflector bulkhead is shown in Figure 2.10-1.

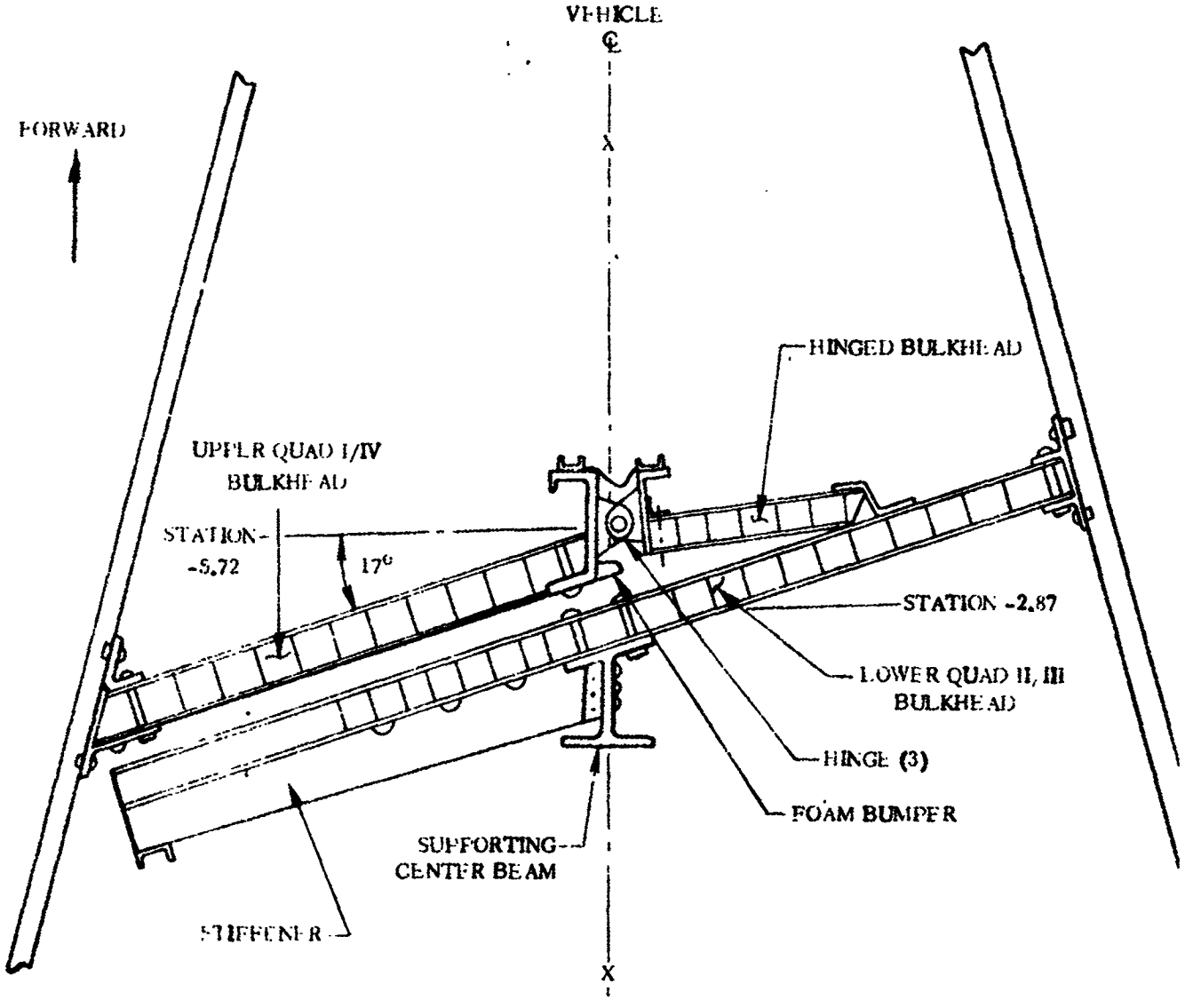

4B138LV

Figure 2.10.1. Deflector Bulkhead Configuration

2.10.1 CRITICAL CONDITIONS. The deflector bulkhead is subjected to a high differential pressure during nose fairing jettison. All other loads during flight are not critical.

2.10.2 WEIGHTS AND CENTER OF GRAVITY DATA. The weight, C.G. position, and mass moment of inertia for the hinged bulkhead are presented below.

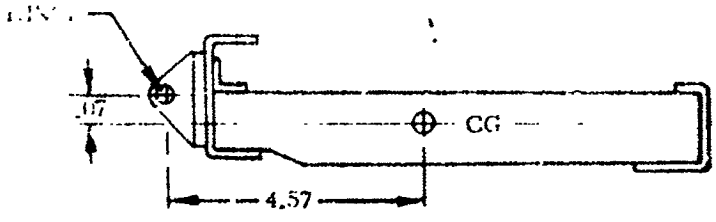

Weight = 10.4 lb
$I_{p_{I/C}}$ = 342 lb-in.^{2}

2.10.3 THERMAL DATA. Temperatures are not critical.

2.10.4 INERTIA LOADS. Inertia loads on the deflector bulkhead are not critical.

2.10.5 STEADY-STATE AIR LOADS. Since the deflector bulkhead is located within the nose fairing cavity, direct air impingement loads are not applicable.

2.10.6 BUFFET AND FLUTTER LOADS. Buffet loads are not to be considered for this component. (Not critical.)

2.10.7 MISCELLANEOUS LOAD PARAMETERS. The deflector bulkhead is subjected to maximum differential pressure loads during nose fairing jettison when thruster bottle gas is released. The effects of static pressure, direct gas impingement, and impact are included in the pressures presented in Figure 2.10-2.

Another consideration should be made regarding the design of the bulkhead when the hinged portion (see Figure 2.10-1) strikes the Stafoam bumper. This condition occurs approximately 0.09 seconds after thruster bottle command for nose fairing jettison. The resulting reaction on the hinge mechanism at this time attains a maximum magnitude of 3000 pounds as shown in Figure 2.10-3.

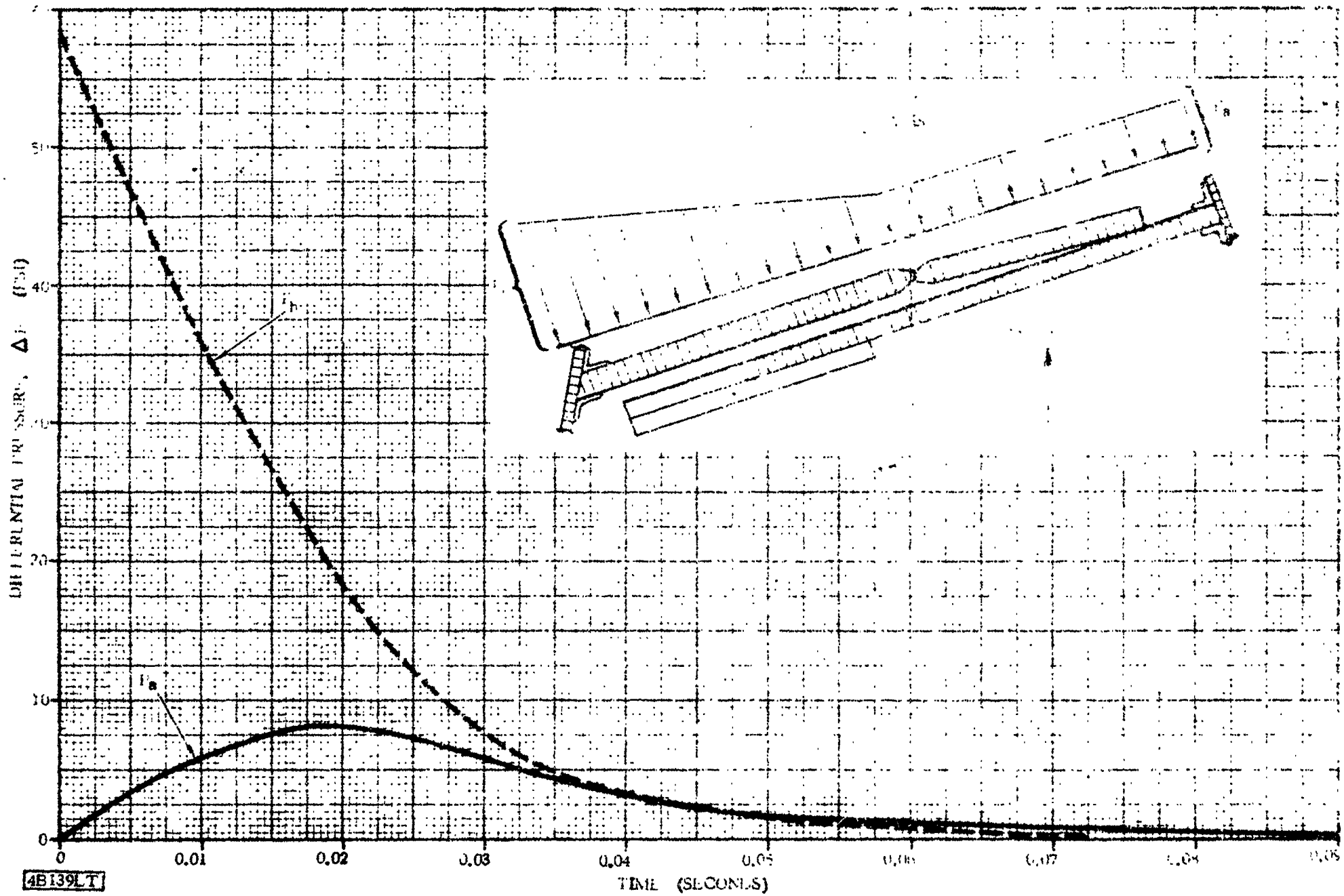

Figure 2.10-2. Deflector Bulkhead Differential Pressures at Nose Fairing Jettison

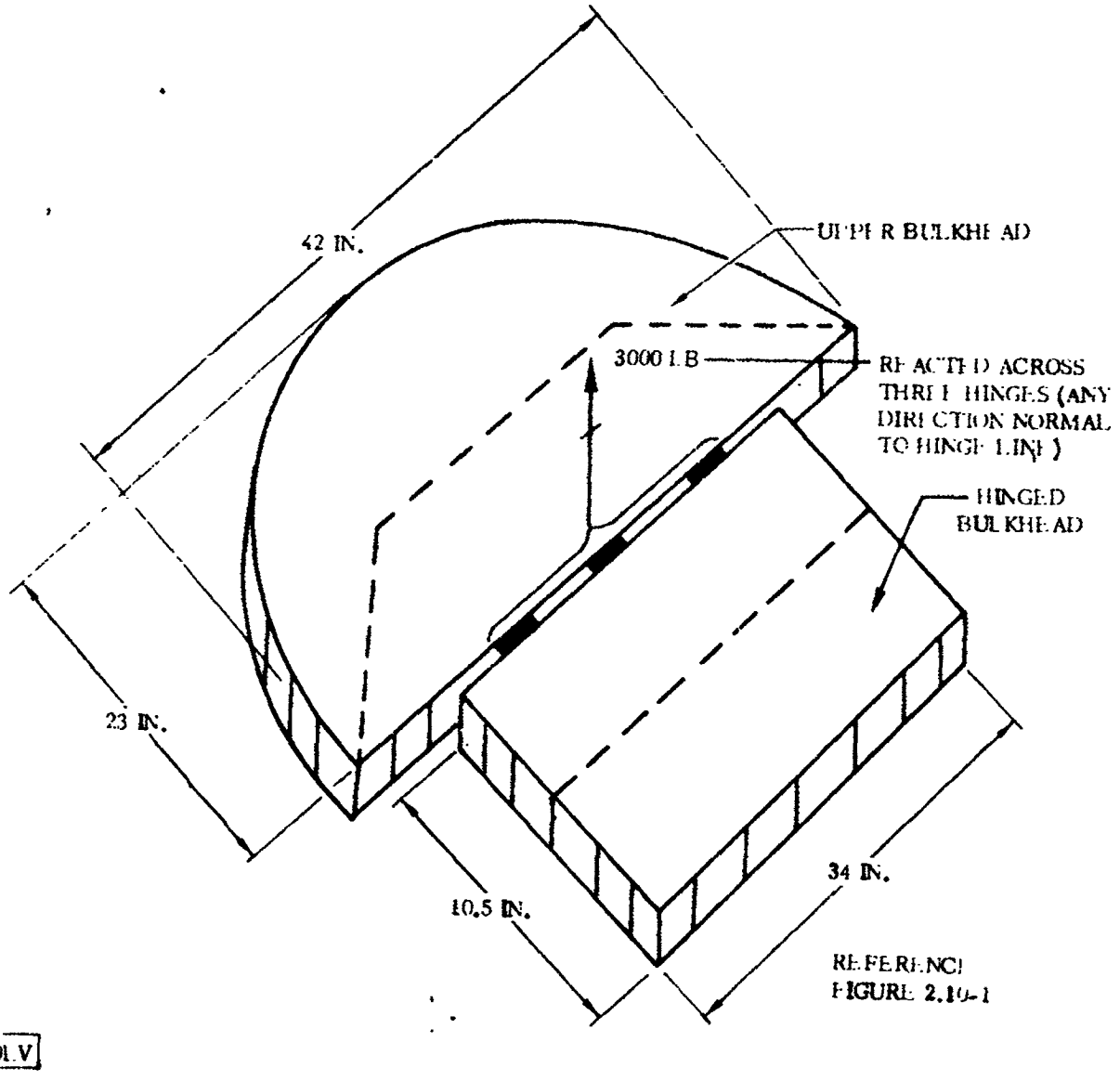

Figure 2. 10-3. Deflector Bulkhead Hinge Reaction at Jettison

2.11 THRUSTOR BOTTLES

The thrustor bottles function is to provide the jettison forces for the two nose fairing halves. The locations and configuration of the bottles are shown in Figure 2.11-1.

2.11-1. CRITICAL CONDITIONS. The thrustor bottles are subjected to high longitudinal acceleration at BECO, and are subjected to a severe combination of inertia, thrust, and gas impingement loads during nose fairing jettison. No other times in flight are critical.

2.11.2 WEIGHT AND CENTER OF GRAVITY DATA. The following weights and C.G. locations shall be used for structural design and analysis.

Item	Weight (lb)	C.G.		
		z	y	x
Upper Bottle (Full)	25.2	-26	+6	0
Lower Bottle (Full)	25.2	-17	-6	0

2.11.3 THERMAL DATA. High temperatures do not exist on the thrustor bottles. Therefore this condition is not applicable.

2.11.4 INERTIA LOADS. The thrustor bottles must withstand the following inertia loads at time of BECO:

Condition	N_z (g's)	N_{LAT} (g's)
Maximum Longitudinal Inertia	+10.0	±1.0
Maximum Lateral Inertia	+ 6.0	±6.0

During nose fairing jettison each bottle is subjected simultaneously to an inertia load caused by vehicle acceleration, a thrust load from its escaping gas, and an external force caused by impingement of gas from the opposite thrustor bottle. The longitudinal inertia load acting at the C.G. of each bottle = +1.5 ±1.0 g's (+load acts in the aft direction). Thrust loads and impingement loads are presented in Paragraph 2.11.7.

2.11.5 STEADY-STATE AIR LOADS. Since the thrustor bottles are located within the nose fairing cavity, direct air impingement loads are not applicable.

2.11.6 BUFFET AND FLUTTER LOADS. The effects of these loads are not critical.

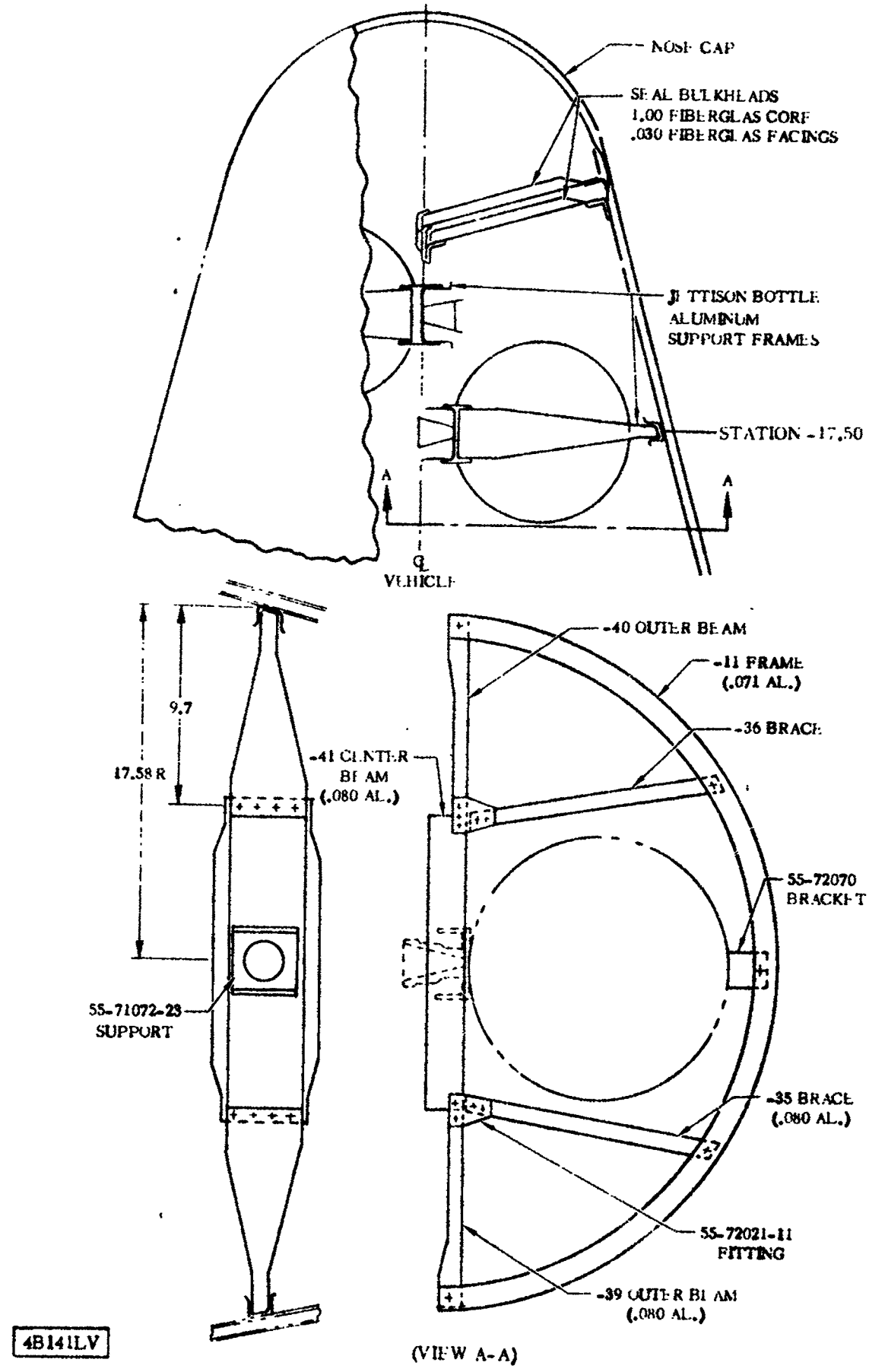

Figure 2.11.1. Thrustor Bottles and Support Structure Configuration

2.11.3.1.3 DESIGN LIMIT LOAD PARAMETERS. During nose fairing jettison, each of the [illegible] bottles experiences a combination of external loads accounting for bottle thrust, gas impingement from the adjacent bottle, and the dynamic effects of sudden engine loads.

Gas impingement effects which result from the adjacent bottle in the opposite fairing half must be considered simultaneously with a bottle thrust of 2450 pounds (maximum [illegible] load).

a. Acts along bottle centerline (see Figures 2.11-2 and 2.11-3).

b. Includes an impact factor accounting for a suddenly applied load.

c. Assume the maximum bottle thrust to remain constant throughout nose fairing jettison, then determine this load with any combination of loading conditions derived from gas impingement effects. (See Figure 2.11-2 or 2.11-3.)

As shown in Figures 2.11-2 and 2.11-3, the gas impingement forces actually vary in magnitude and position as a function of time (or rotation). Since these loads are also sudden applied, an impact factor of 1.25 must be considered in the analysis of the bottle support structure.

Bottle thrust and gas impingement forces must be considered simultaneously with the [illegible] loads described in Paragraph 2.11.4.

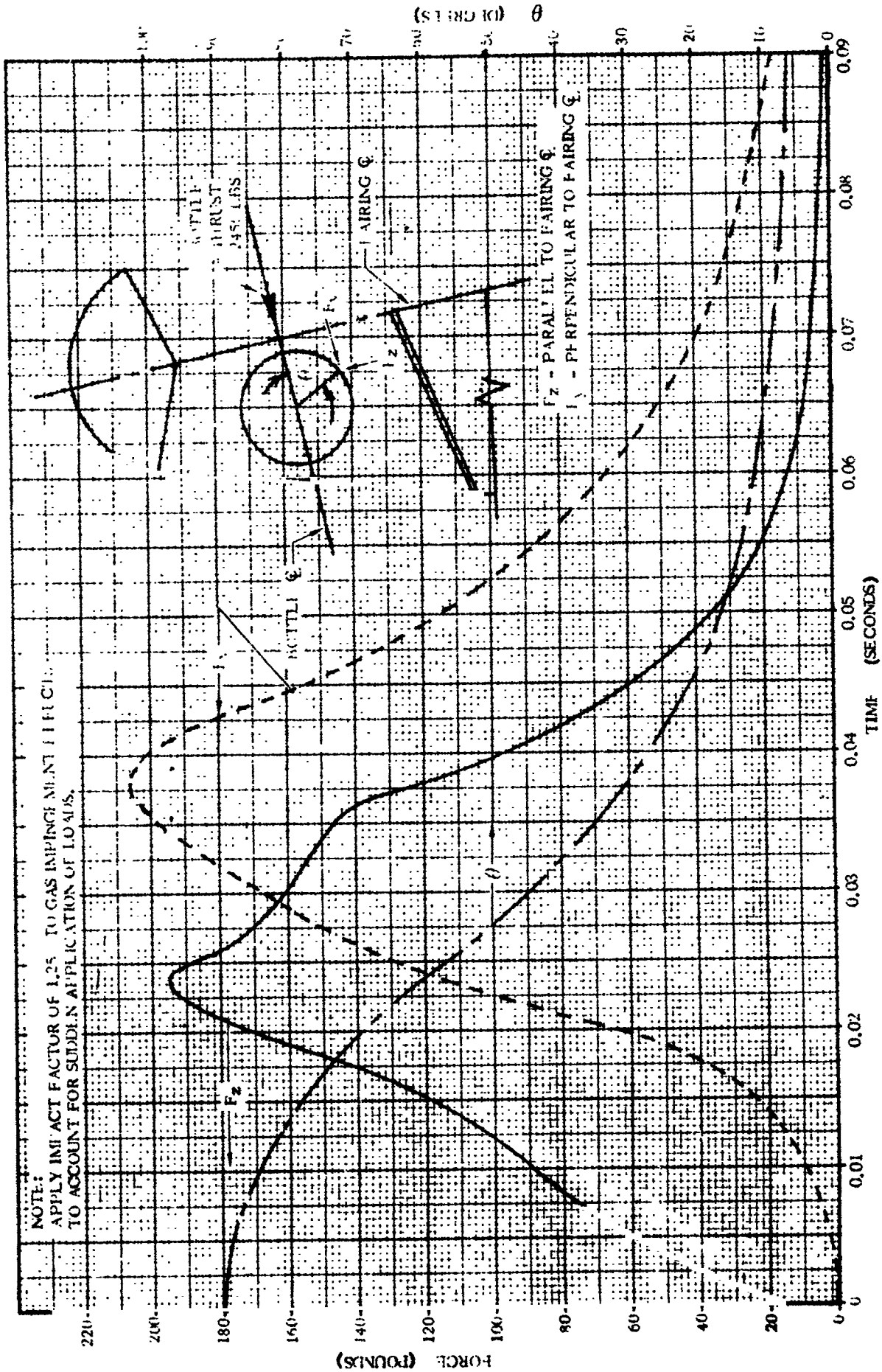

Figure 2.11-2. Nose Fairing Impingement Forces on Quadrant I - IV Thrustor Bottle from Quadrant II - III Thrustor Jet

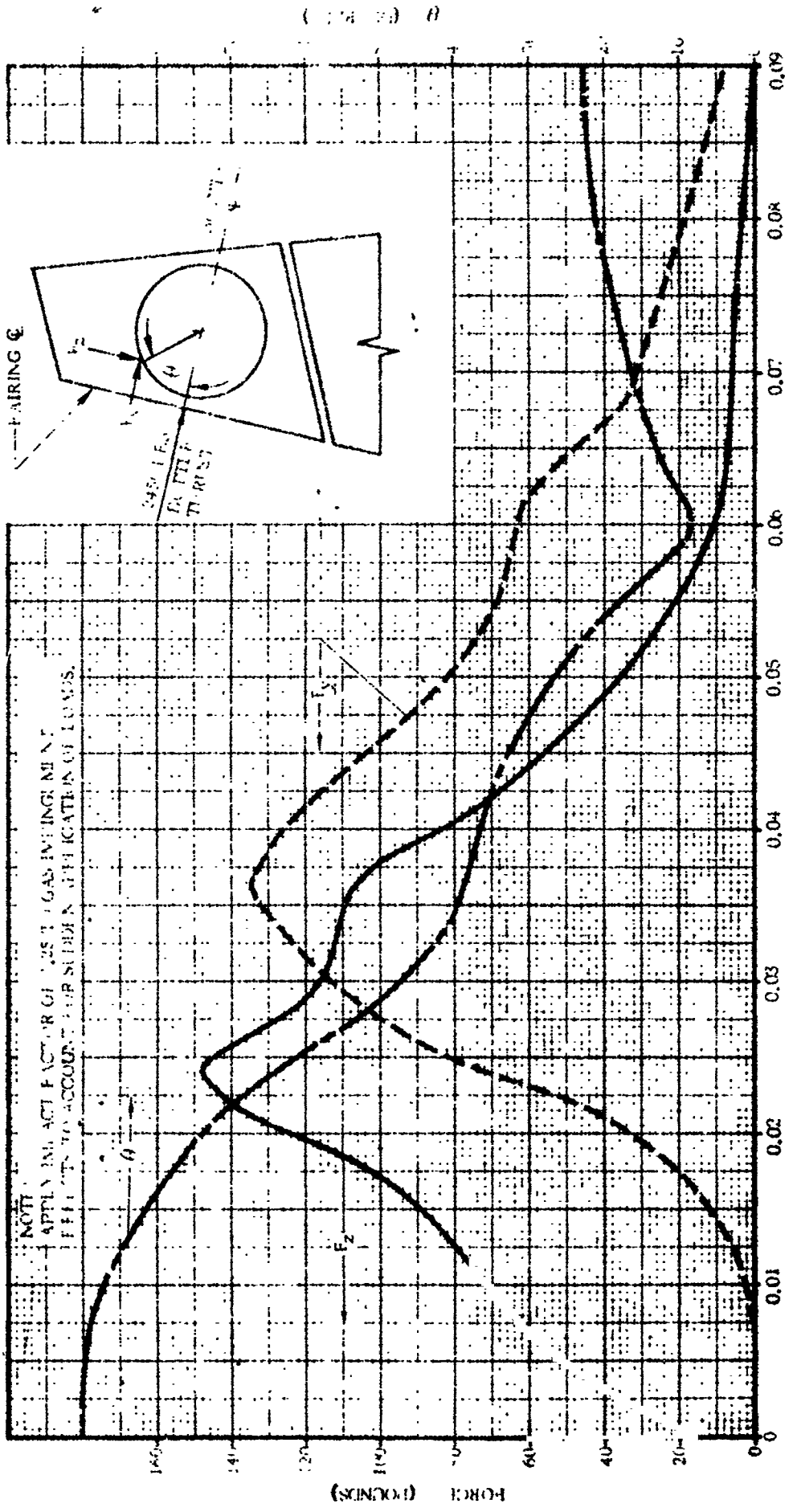

4B143LT

Figure 2.11-3. Nose Fairing Impingement Forces on Quadrant II - III Thrustor Bottle from Quadrant I - IV Thrustor Jet

THIS PAGE INTENTIONALLY LEFT BLANK.

2.12 SEAL BULKHEADS

The seal bulkheads are located between the nose cap and top of the conical shell, and serve to prevent leakage at this portion of the nose fairing split line. The configuration of the seal bulkheads is shown in Figure 2.12-1.

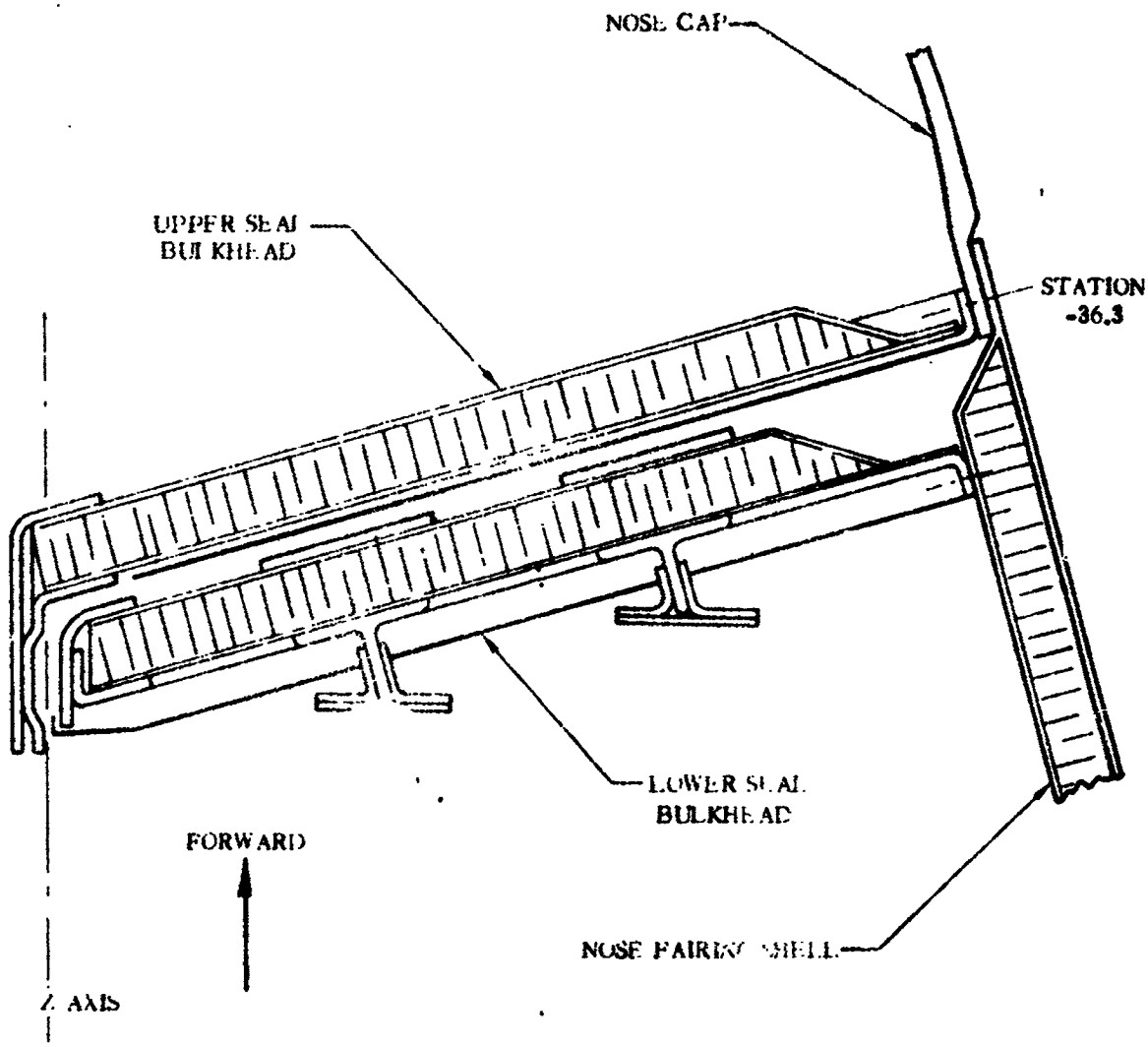

4B144LV

Figure 2.12-1. Seal Bulkhead Configuration

2.12.1 CRITICAL CONDITIONS. The seal bulkheads receive critical loads during nose fairing jettison due to gas impingement and static pressure inside the nose fairing.

2.12.2 WEIGHT AND CENTER OF GRAVITY DATA. Inertia loads are not critical.

2.12.3 THERMAL DATA. Temperatures do not become critical on the seal bulkheads.

2.12.4 INERTIA LOADS. Inertia loads are negligible in comparison to the impingement pressure loads during nose fairing jettison.

2.12.5 STEADY-STATE AIR LOADS. The steady-state air loads which may occur during transonic flight (Mach numbers from 0.85 to 1.30) are insignificant in comparison to pressure loads which occur at nose fairing jettison (reference Figure 2.2-9 and Paragraph 2.12.7). The pressures as shown in Figure 2.2-9 could result from leakage through the exterior seal.

2.12.6 BUFFET AND FLUTTER LOADS. Buffet loads are not critical.

2.12.7 MISCELLANEOUS LOAD PARAMETERS. The pressures, which occur at fairing jettison and are presented in Figure 2.12-2 for each of the seal bulkheads, include the effects of static pressure, gas impingement, and sudden application of load.

UPPER BULKHEAD

$P_{(UPPER)}$ = 7.80 PSI (MAXIMUM) UNIFORM DISTRIBUTION OVER ENTIRE SURFACE.

LOWER BULKHEAD

ALONG Y-Y AXIS: DISTRIBUTION AT A POINT ALONG THE Y-Y AXIS AS SHOWN. ASSUME A LINEAR DISTRIBUTION BETWEEN 0 AND R/2

R = 0	P = 7.80 PSI (P_{UPPER})
R = R/2	P = 108 PSI (MAXIMUM)
R = R	P = 108 PSI (MAXIMUM)

CIRCUMFERENTIAL DISTRIBUTION: THE CIRCUMFERENTIAL VARIATION IS DETERMINED THROUGH THE FOLLOWING RELATIONSHIP:

$$P_{CIR.} = P_{UPPER} + (P_{Y\text{-}Y\ LOWER} - P_{UPPER}) \cos^2\theta$$

WHERE:
$P_{Y\text{-}Y\ LOWER}$ IS DETERMINED FROM RELATIONSHIP AT A POINT ALONG THE Y-Y AXIS AS DESCRIBED ABOVE.

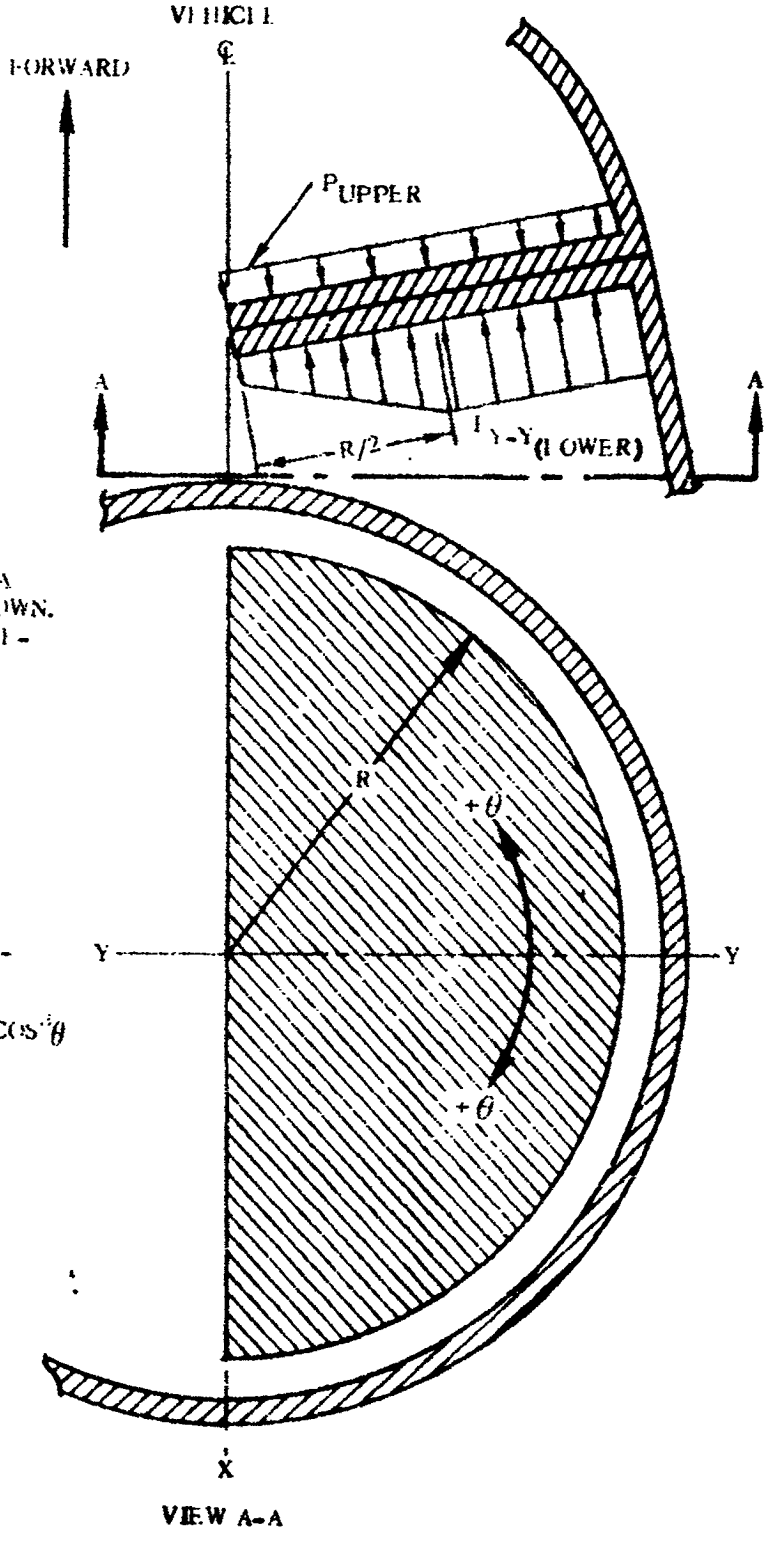

VIEW A-A

4B145LV

Figure 2.12-2. Seal Bulkheads Differential Pressures at Nose Fairing Jettison

THIS PAGE INTENTIONALLY LEFT BLANK.

2.13 THERMAL BULKHEAD

The thermal bulkhead separates the surveyor payload compartment from the Centaur equipment area. The configuration is shown in Figure 2.13-1. The purpose of the thermal bulkhead is to ensure a sterile environment for the Surveyor payload, and to prevent mixing of the Surveyor compartment and the equipment area air conditioning gases. The thermal bulkhead is composed of Fiberglas sandwich, and is supported during nose fairing jettison by struts attached to the inboard edge. The joint between the inboard edge and the payload adapter is sealed to prevent excessive leakage.

2.13.1 CRITICAL CONDITIONS. The thermal bulkhead receives its critical loads from a combination of differential pressure and inertia loads. Maximum ΔP loads occur during transonic flight, (Mach numbers from 0.85 to 1.30) when rapidly changing external pressure creates high flow rates through the vent holes. Inertia loads on the thermal bulkhead are caused by transonic buffet response of the nose fairing barrel section.

High inertia loads on the thermal bulkhead also occur during nose fairing jettison. These loads act in combination with the ΔP caused by thrustor bottle gas leaking past the deflector bulkhead and impinging on the thermal bulkhead.

2.13.2 WEIGHTS AND CENTER OF GRAVITY DATA. The following weights and C.G. locations shall be used for structural design and analysis.

Item	Weight (lb)	C.G.		
		z	y	x
Quadrants I - IV Half	55.4	150	+38	0
Quadrants II - III Half	53.7	150	-38	0

2.13.3 THERMAL DATA. The thermal bulkhead remains at or near room temperature throughout flight.

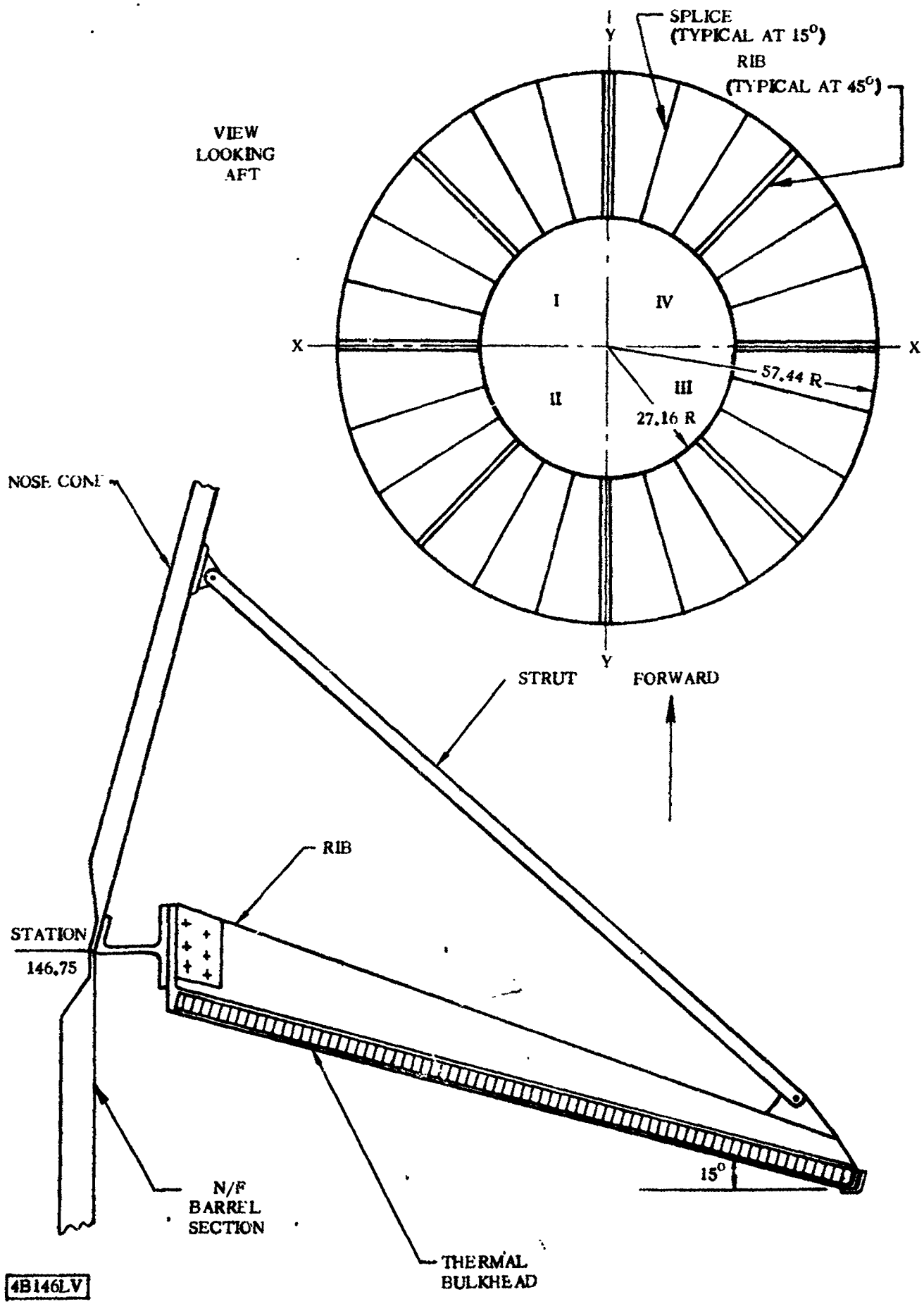

Figure 2.13-1. Thermal Bulkhead Configuration

2.13.4 INERTIA LOADS. Inertia loads on the thermal bulkhead and struts are presented below for critical conditions during flight. These inertia loads are to be combined with differential pressures presented in Paragraph 2.13.5 where applicable.

a. Loads During Launch: Vibratory Inertia.

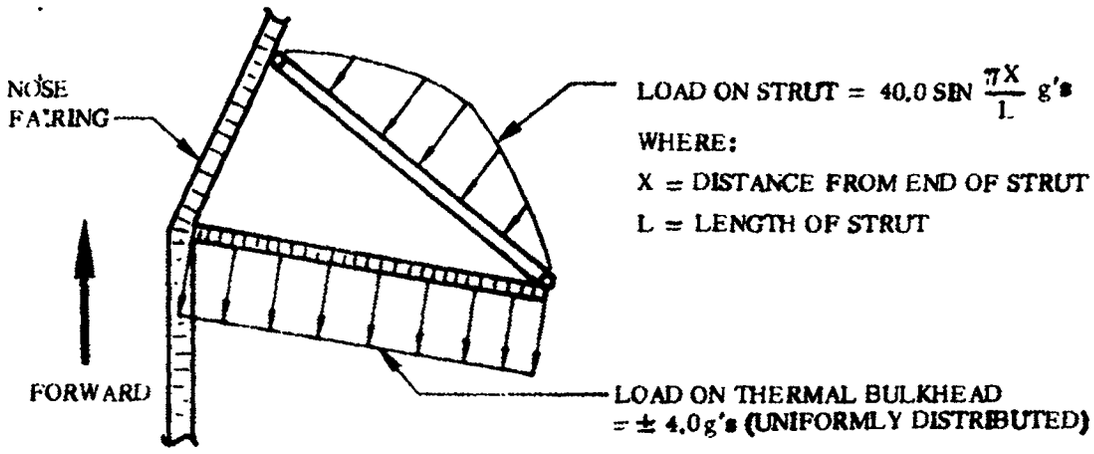

To the above loads, add a steady-state longitudinal inertia of +1.30 g's.

b. Loads at BECO: Vibratory inertia.

The vibratory inertia loads at BECO are the same as presented above, however the steady-state inertia load at BECO = +5.8 g's.

c. Loads at Jettison:

1. Maximum Tangential Acceleration.

These loads are assumed concentrated for simplicity. See Paragraph 2.13.7 for ΔP acting at this time.

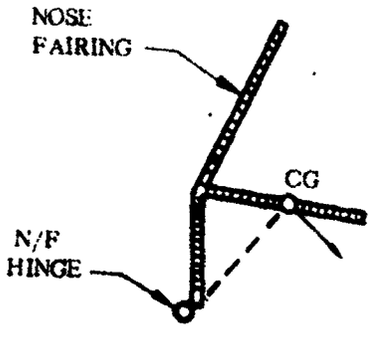

18.0 g's acting perpendicular to radius through N/F hinge

2. Maximum Radial Acceleration.

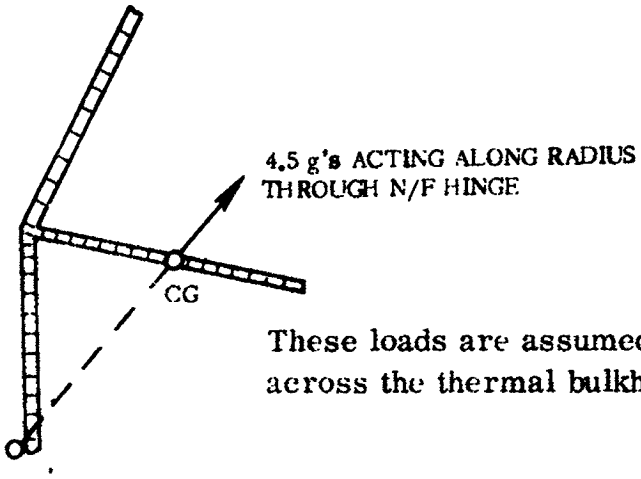

These loads are assumed concentrated for simplicity. No ΔP across the thermal bulkhead exists at this time.

2.13.5 STEADY-STATE AIR LOADS. During transonic flight, the thermal bulkhead is subjected to a differential pressure of 0.40 psi acting aft. This load acts simultaneously with buffet response loads presented in Paragraph 2.13.6.

2.13.6 BUFFET AND FLUTTER LOADS. During transonic flight (Mach numbers from 0.85 to 1.30), the thermal bulkhead is excited by the response of the barrel section to fluctuating air loads. The equivalent static pressure due to unsteady pressure acting on the thermal bulkhead = ±0.1 psi. This acts simultaneously with the steady-state ΔP presented in Paragraph 2.13.5.

2.13.7 MISCELLANEOUS LOAD PARAMETERS. Other loads acting on the thermal bulkhead are as follows.

a. Deflection Consideration:

The inboard edge of the thermal bulkhead is in proximity to the payload adapter and is attached to it by a flexible seal. This joint must be designed to prevent interference between the thermal bulkhead and payload adapter considering a relative lateral motion of ±1.0 inch.

b. Differential Pressure Condition at Nose Fairing Jettison:

The differential pressure during nose fairing jettison is 0.4 psi acting aft. This pressure reflects the effects of a suddenly applied load, static pressure, and gas impingement forces. For purposes of analysis, this pressure force should be considered simultaneously with the inertia loads described in Paragraph 2.13.4c.

2.14 HINGE FAIRINGS

The hinge fairings are Fiberglas laminated sandwich structures which protect the nose fairing hinges from aerodynamic loading. The location and configuration of the fairings is presented in Figure 2.14-1.

2.14.1 CRITICAL CONDITIONS. The critical loading conditions for the hinge fairings occur during transonic flight when steady-state and fluctuating air loads are highest, and later in flight when temperatures reach maximum values. Inertia loads are negligible due to the light weight of the pods.

2.14.2 WEIGHTS AND CENTER OF GRAVITY DATA. Loads imposed by inertia are not critical.

2.14.3 THERMAL DATA. The inner and outer skin temperatures on the hinge fairing ramp are presented in Figure 2.14-2.

2.14.4 INERTIA LOADS. Inertia loads on the hinge fairings are not critical.

2.14.5 STEADY-STATE AIR LOADS. Steady-state wall differential pressures at $\alpha = 0$ degrees, which consider the maximum bursting and crushing conditions, are presented in Figures 2.14-3 and 2.14-4. An additional pressure increment of ±0.675 psi should be considered as the contribution due to an angle of attack of 6 degrees. Consequently, the total design wall differential pressure for any area on the hinge pod would be a summation of the ΔP at $\alpha = 0$ degrees (Figures 2.14-3 and 2.14-4), the angle of attack correction, and the transonic buffet effects presented in Paragraph 2.14.6.

The total aerodynamic drag and side loads for each of the hinge fairings are presented in Figures 2.14-5, 2.14-6, and 2.14-7. The drag and side load on the fairings, represent only external pressure effects, while the wall ΔP includes fairing internal pressure. Thus, these loads are to be used for different purposes in the stress analysis of the structure.

2.14.6 BUFFET AND FLUTTER LOADS. During transonic flight (Mach numbers from 0.85 to1.30), the hinge fairings are subjected to fluctuating aerodynamic loads. The equivalent static pressure due to response of the structure is presented in Figure 2.14-8.

2.14.7 MISCELLANEOUS LOAD PARAMETERS. No other loads exist on the hinge fairings.

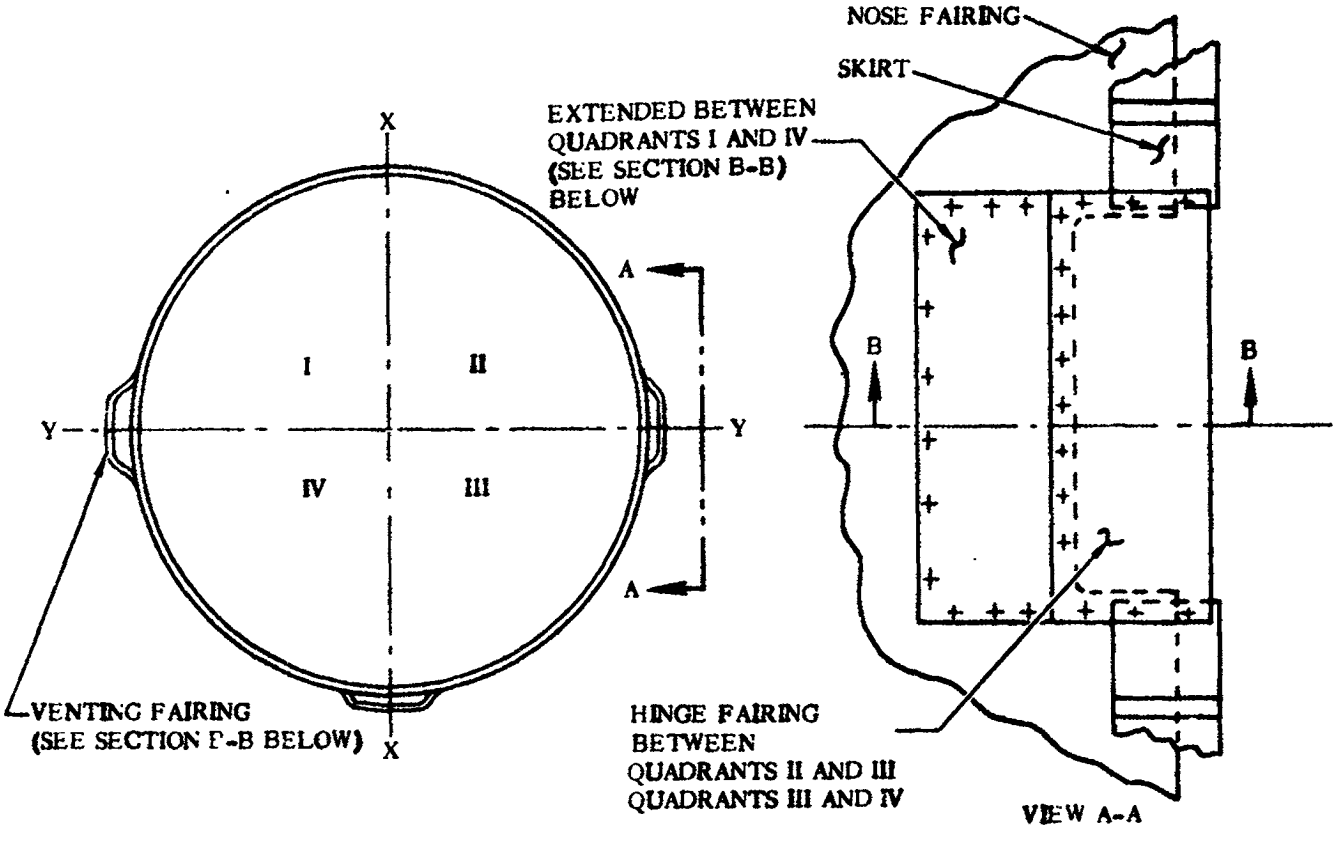

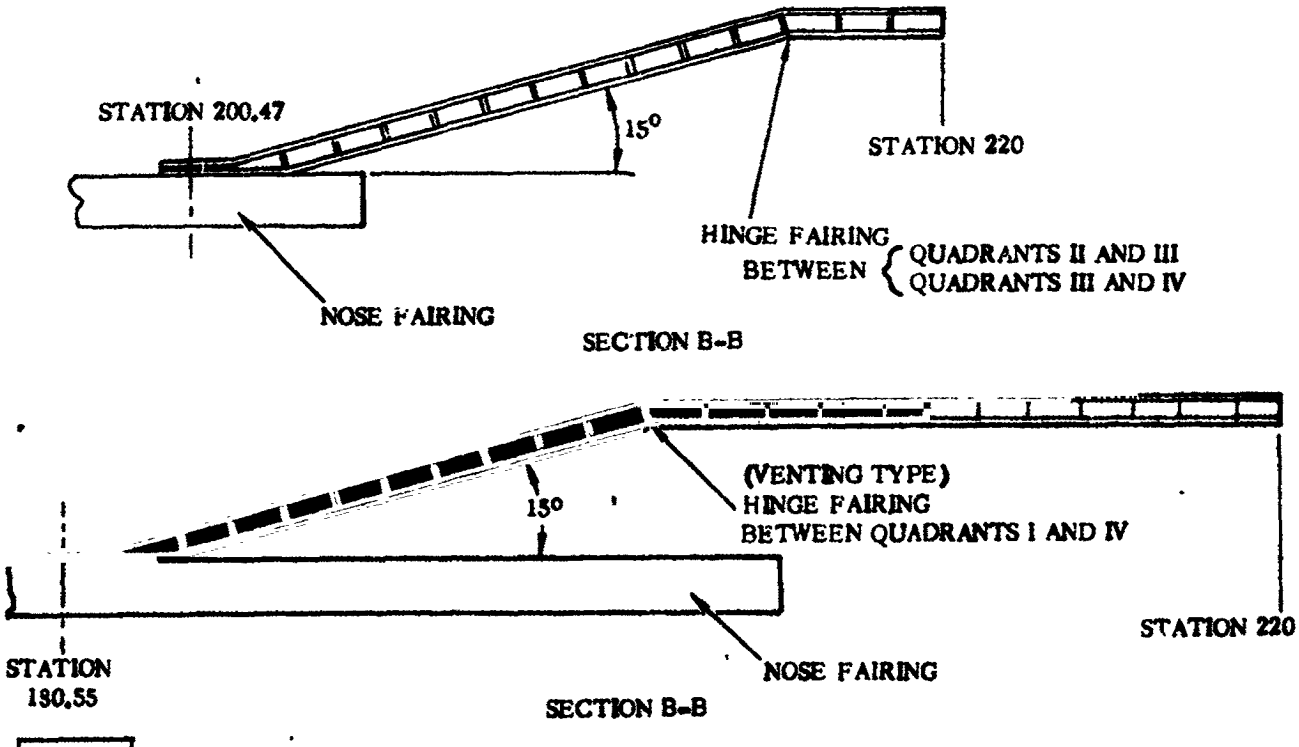

Figure 2.14-1. Nose Fairing Hinge Fairings Configuration

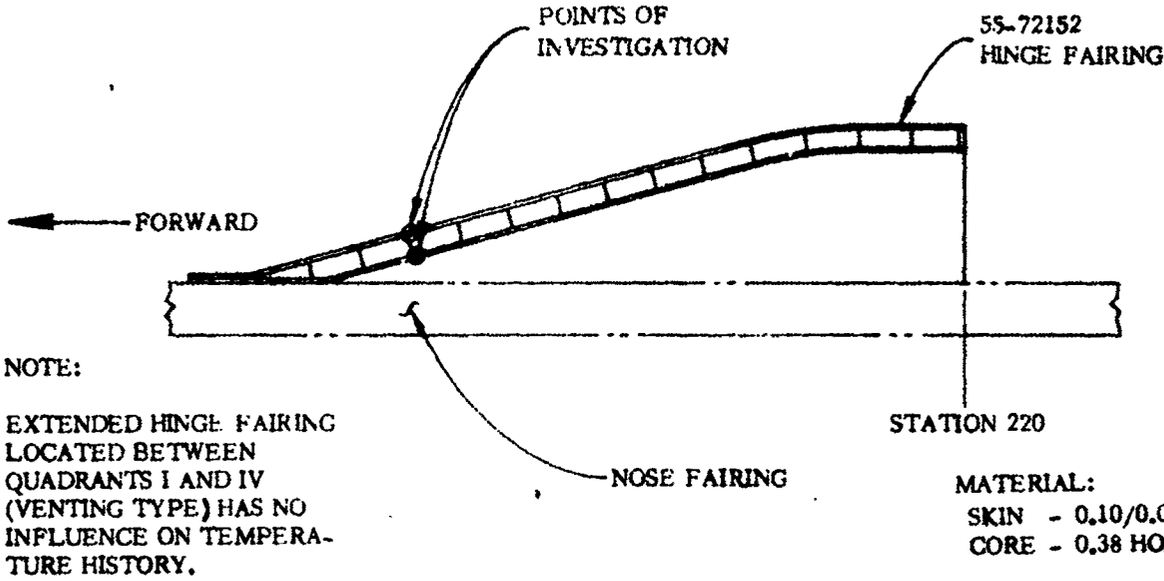

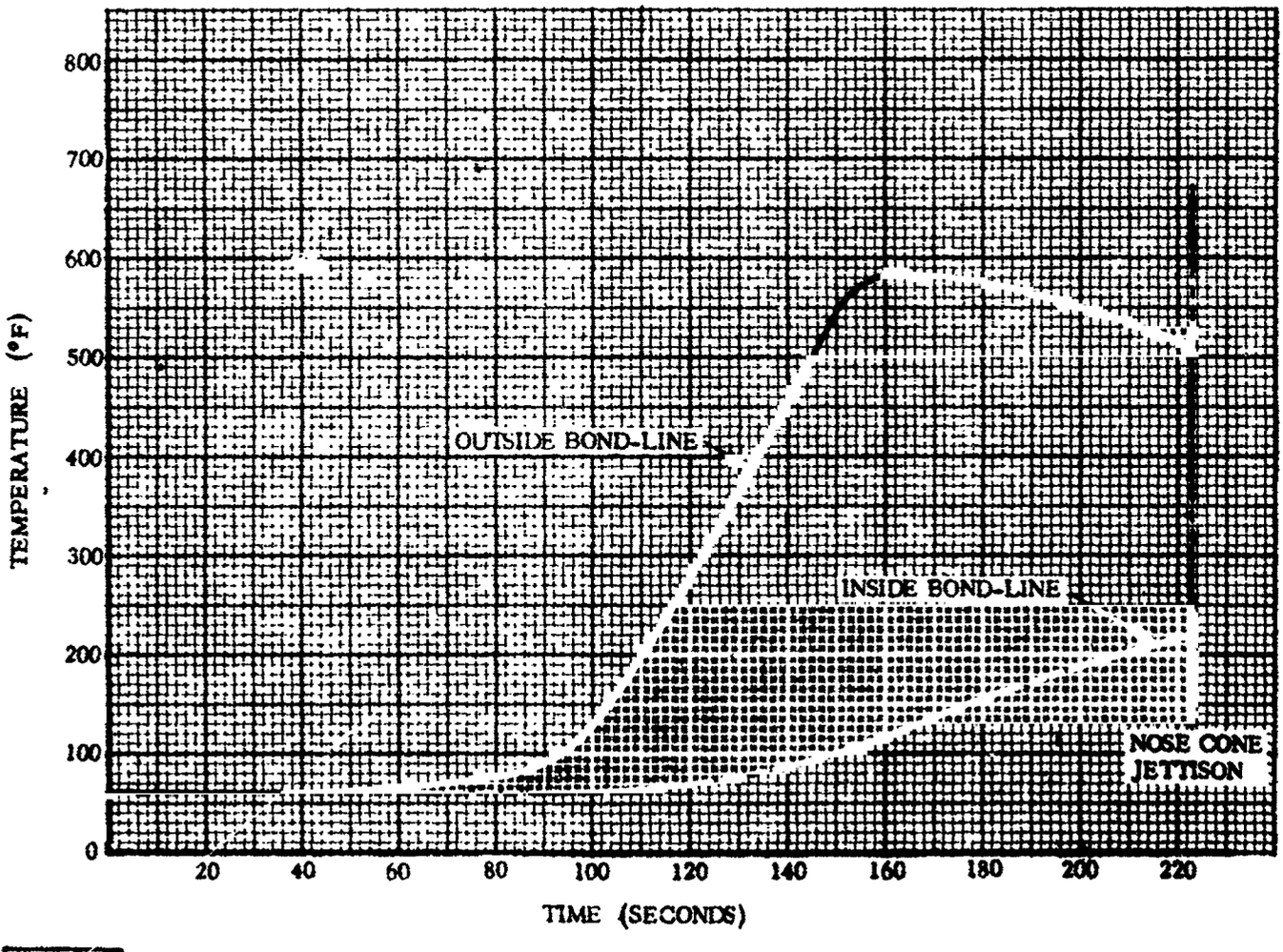

4B148LV

Figure 2.14-2. Nose Fairing Hinge Fairings Temperature History

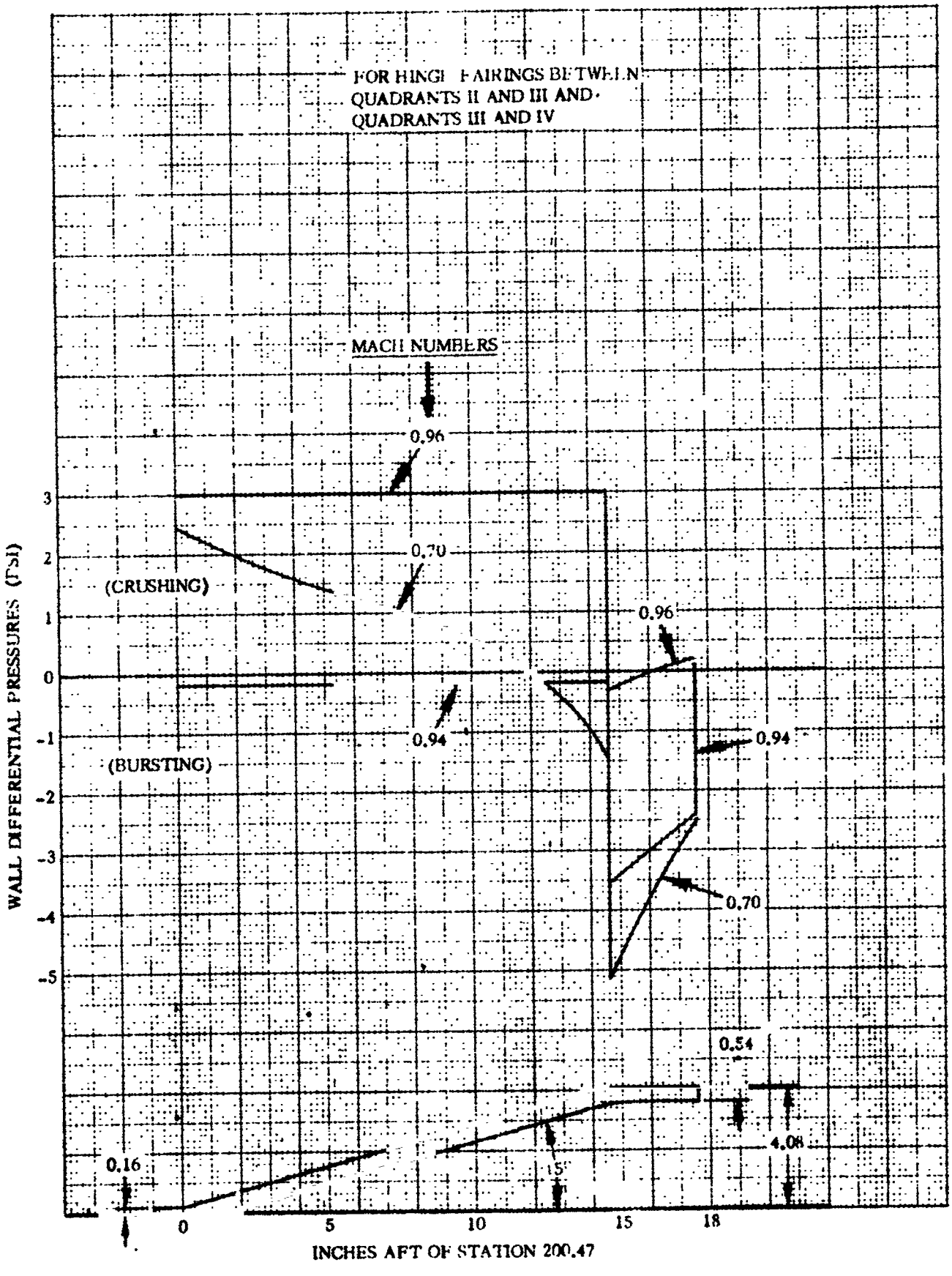

4B149LV

Figure 2.14-3. Hinge Fairing Wall Differential Pressures at Zero Angle of Attack (α = 0 degrees)

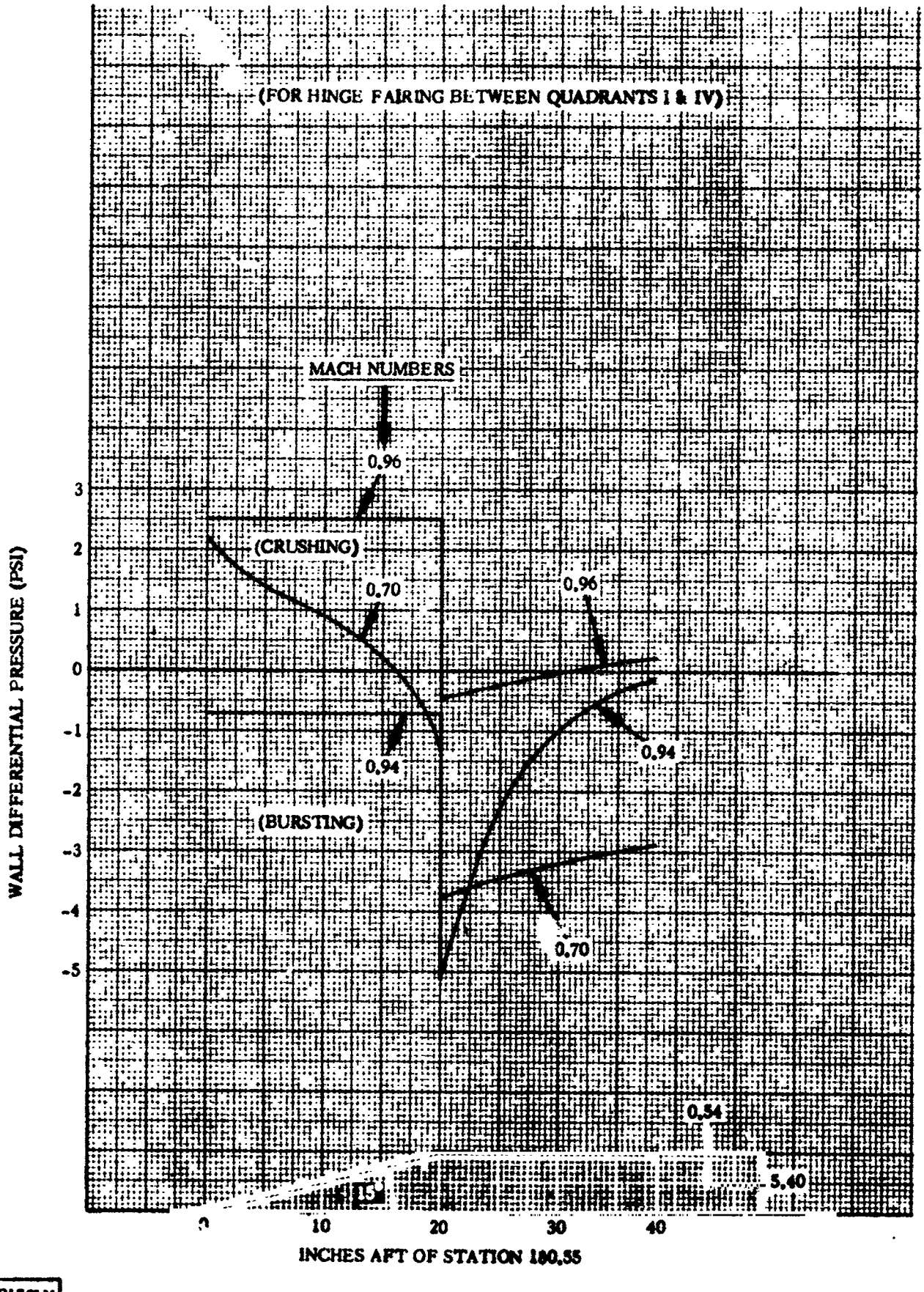

4B150LV

Figure 2.14-4. Hinge Fairing Wall Differential Pressures at Zero Angle of Attack (α = 0 degrees), for Quadrants I and IV

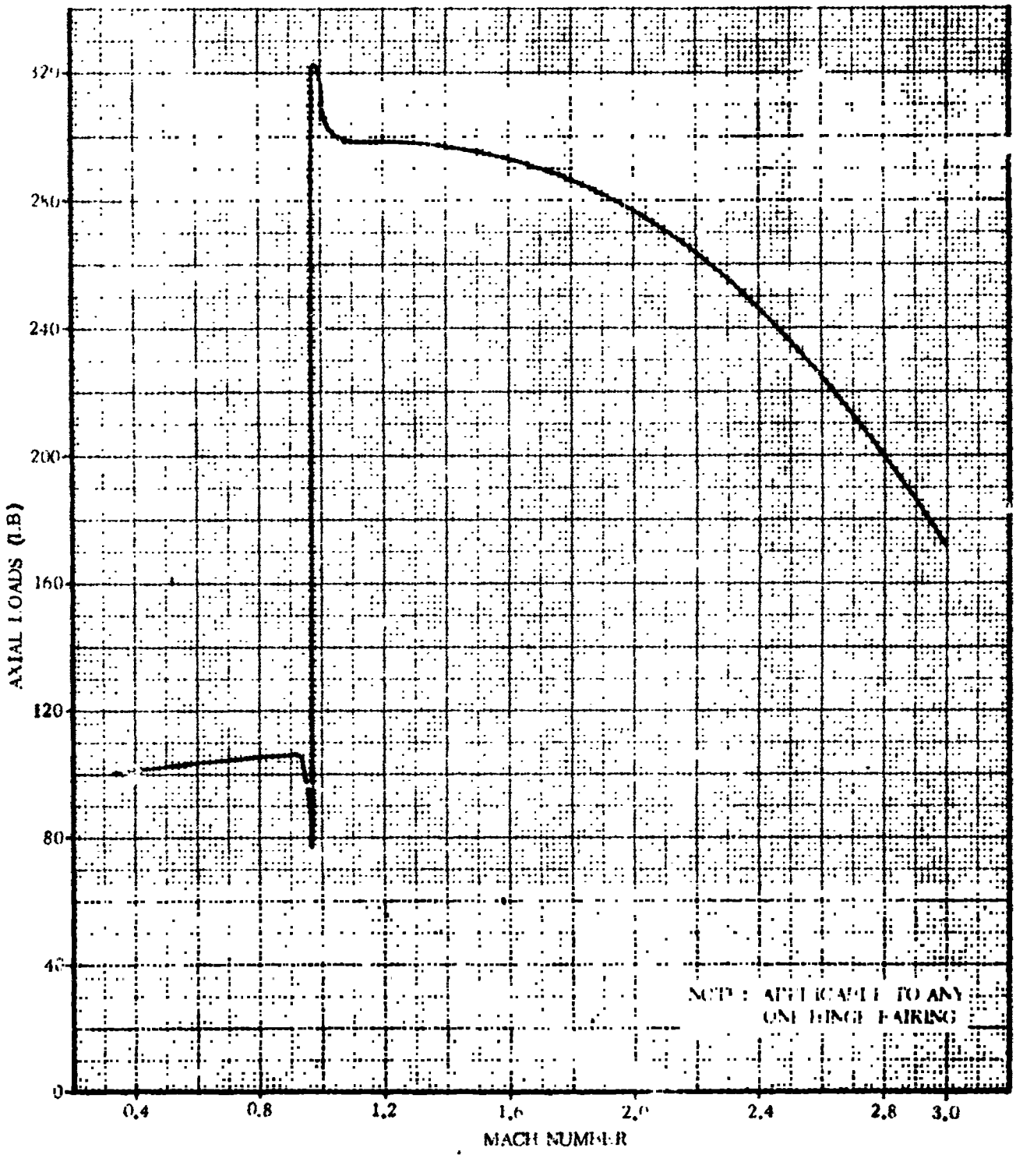

4B151LV

Figure 2.14-5. Hinge Fairing Total Drag Load versus Mach Number

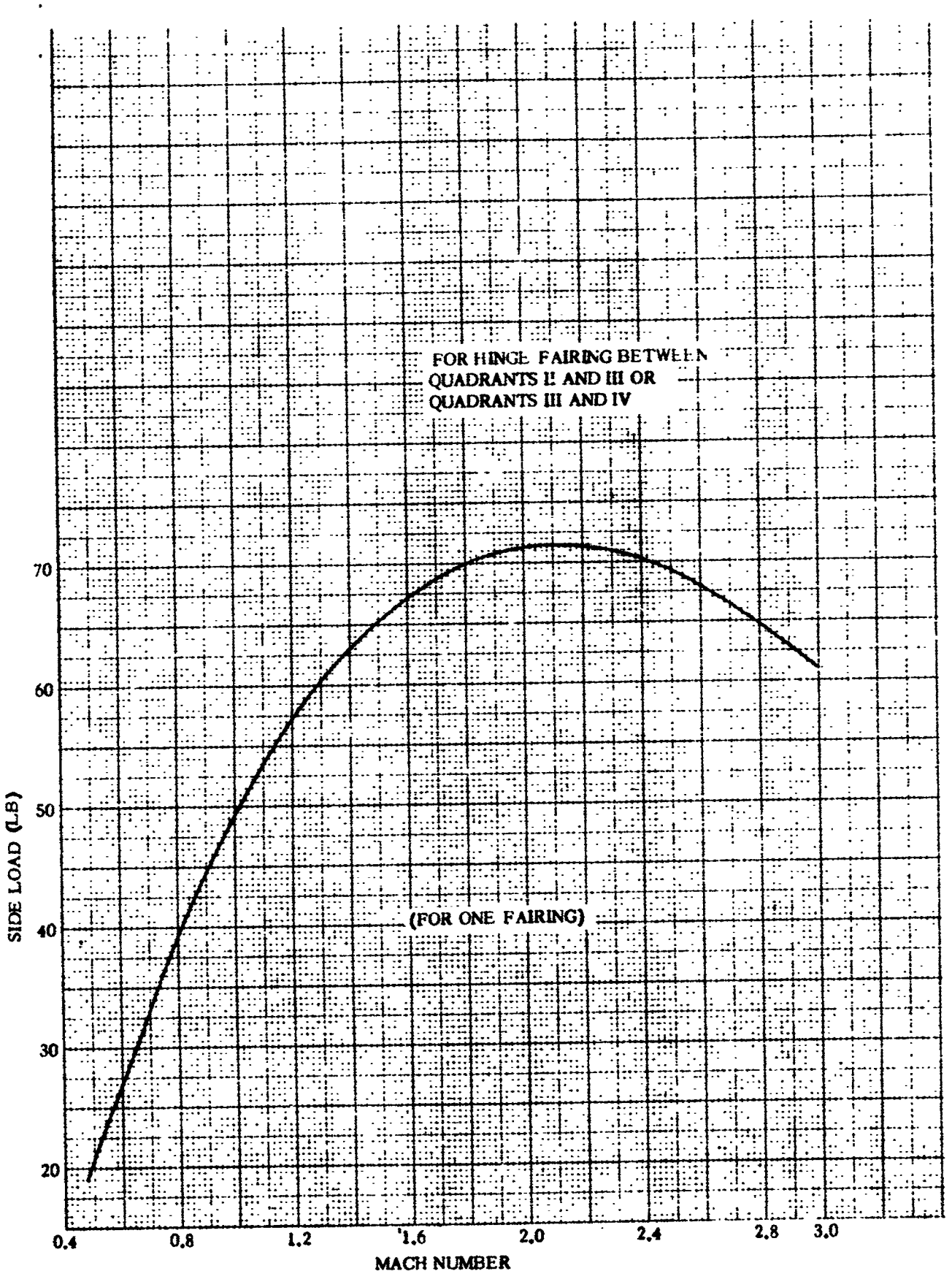

4B152LV

Figure 2.14-6. Hinge Fairing Total Side Load versus Mach Number

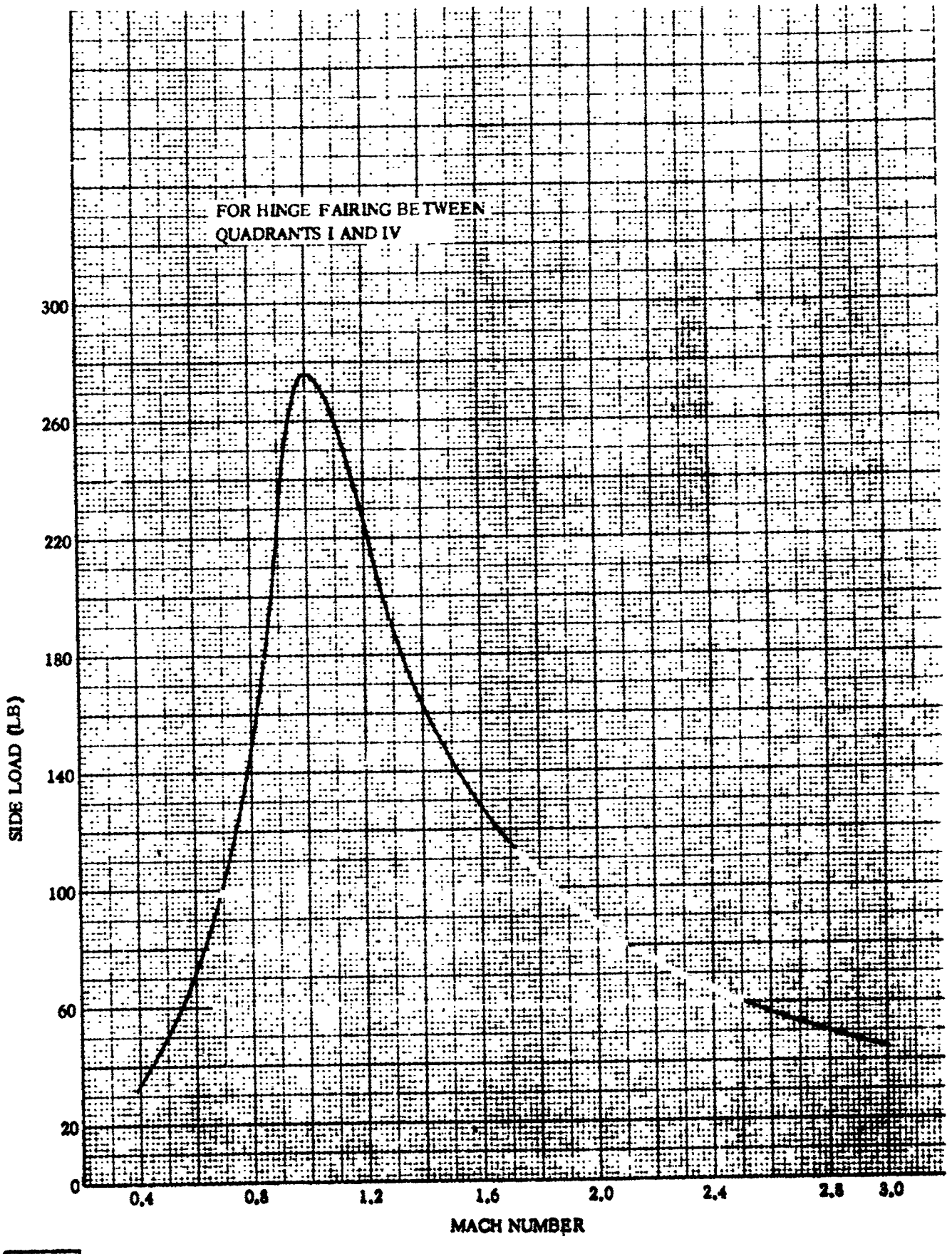

4B153LV

Figure 2.14-7. Hinge Fairing Total Side Load versus Mach Number - Quadrants I and IV

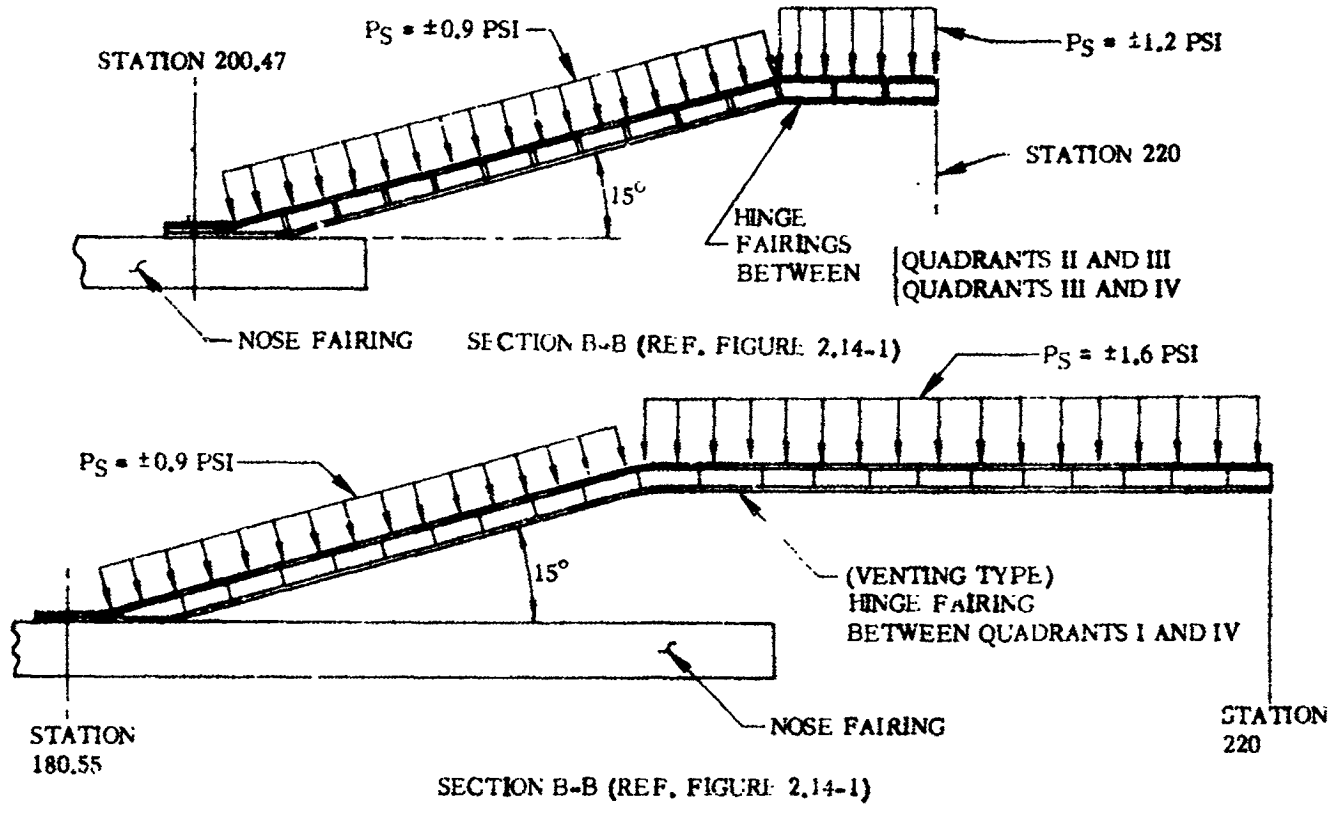

4B154LV

Figure 2.14-8. Hinge Fairings Transonic Buffet Effects

THIS PAGE INTENTIONALLY LEFT BLANK.

2.15 HYDROGEN VENT FIN

The hydrogen vent fin is designed to direct the boiled off hydrogen gas clear of the vehicle boundary layer and protuberances, so as to prevent ignition. The fin is an aerodynamically smooth, lightweight airfoil/cylindrical section extending approximately fifty inches outward from the nose fairing at Station 186.94. (See Figure 2.15-1 for configuration of vent fin.) The hydrogen vent fin is functional prior to launch, between t+69 seconds and BECO+0.1 second, and again between BECO+7 seconds and faring jettison.

2.15.1 CRITICAL CONDITIONS. The hydrogen vent fin receives critical loads at the following times in flight: launch, transonic flight, and BECO. At launch, the separation of the hydrogen vent duct from the end of the vent fin imposes concentrated loads on the fin. During transonic flight, buffet loads combine with maximum steady-state air loads. Near the time of BECO, temperatures on the fin are highest, as are steady-state inertia loads.

2.15.2 WEIGHTS AND CENTER OF GRAVITY DATA. The following weight and C.G. locations shall be used for structural design and analysis.

Weight (lb)	C.G.		
	z	y	x
38.4	199	-31	+67

2.15.3 THERMAL DATA. A temperature history of various critical points on the vent fin is presented in Figures 2.15-2 and 2.15-3.

2.15.4 INERTIA LOADS. Maximum steady-state longitudinal inertia loads versus flight time are presented in Figure 1.3-2.

2.15.5 STEADY-STATE AIR LOADS. The steady-state aerodynamic loads are presented in the form of normal loads (in the plane of the vent fin and missile centerline, also normal to the vent fin axis), and side loads (in the X-Y plane of the vehicle and normal to the vent fin radial axis). Torsional loads and loads parallel to the vent fin axis are also induced as a result of the forces denoted component B. (Reference Figures 2.15-4 through 2.15-7 for orientation of loads.) Should a design angle of attack (α_D) of less than six degrees be considered, the side load should be multiplied by the ratio $\alpha_D/6$; the normal load is assumed to be unaffected.

2.15.6 BUFFET AND FLUTTER LOADS. The dynamic loading shown in Figure 2.15-8 is considered as an equivalent static pressure which should be imposed to the vent fin to account for both mechanical vibrations and buffeting effects. This load may occur in any orientation to produce the most critical loading condition; however, it shall be considered applicable only during the transonic range of flight (Mach number range 0.85 - 1.3).

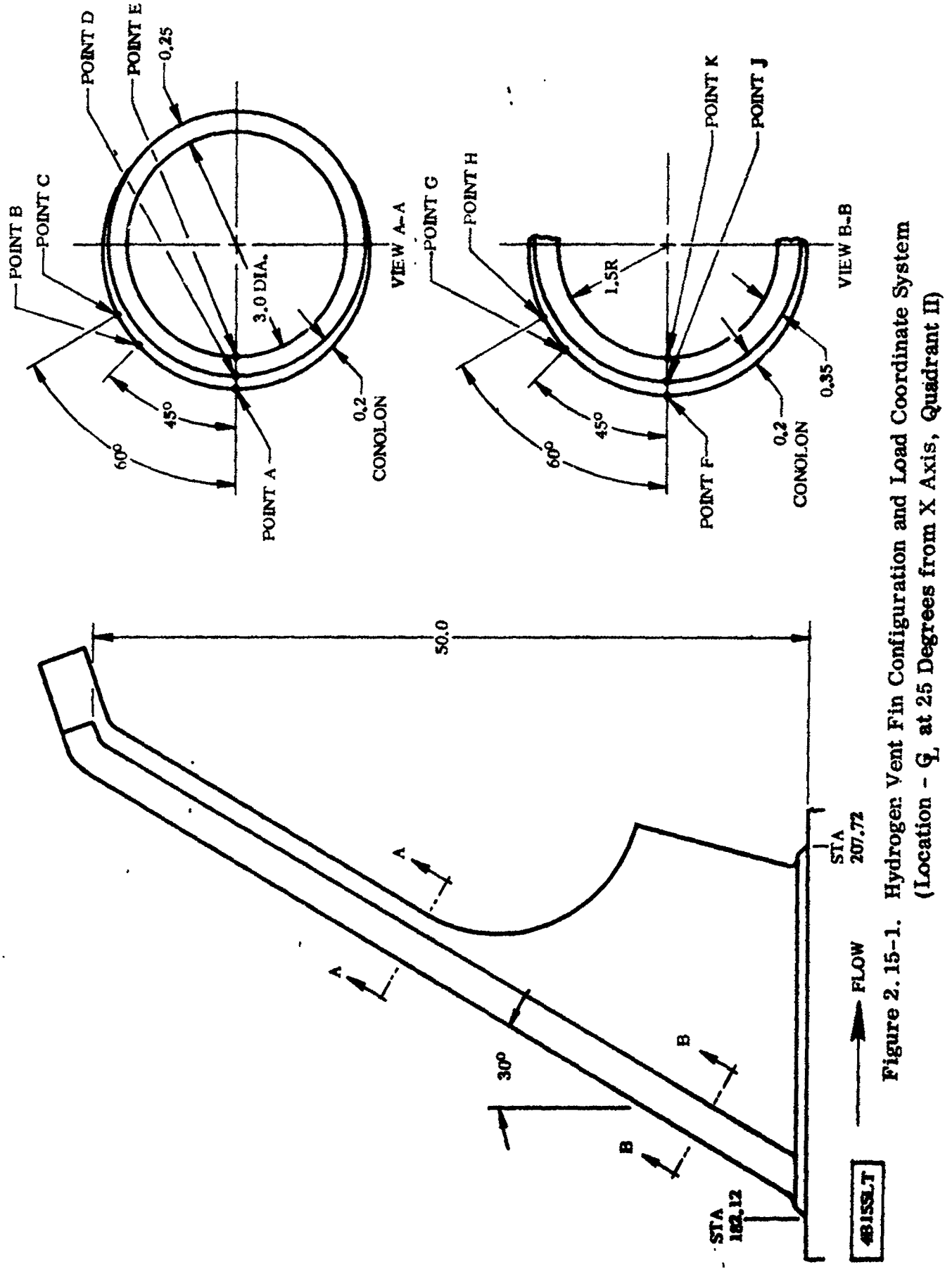

Figure 2.15-1. Hydrogen Vent Fin Configuration and Load Coordinate System (Location - ℄ at 25 Degrees from X Axis, Quadrant II)

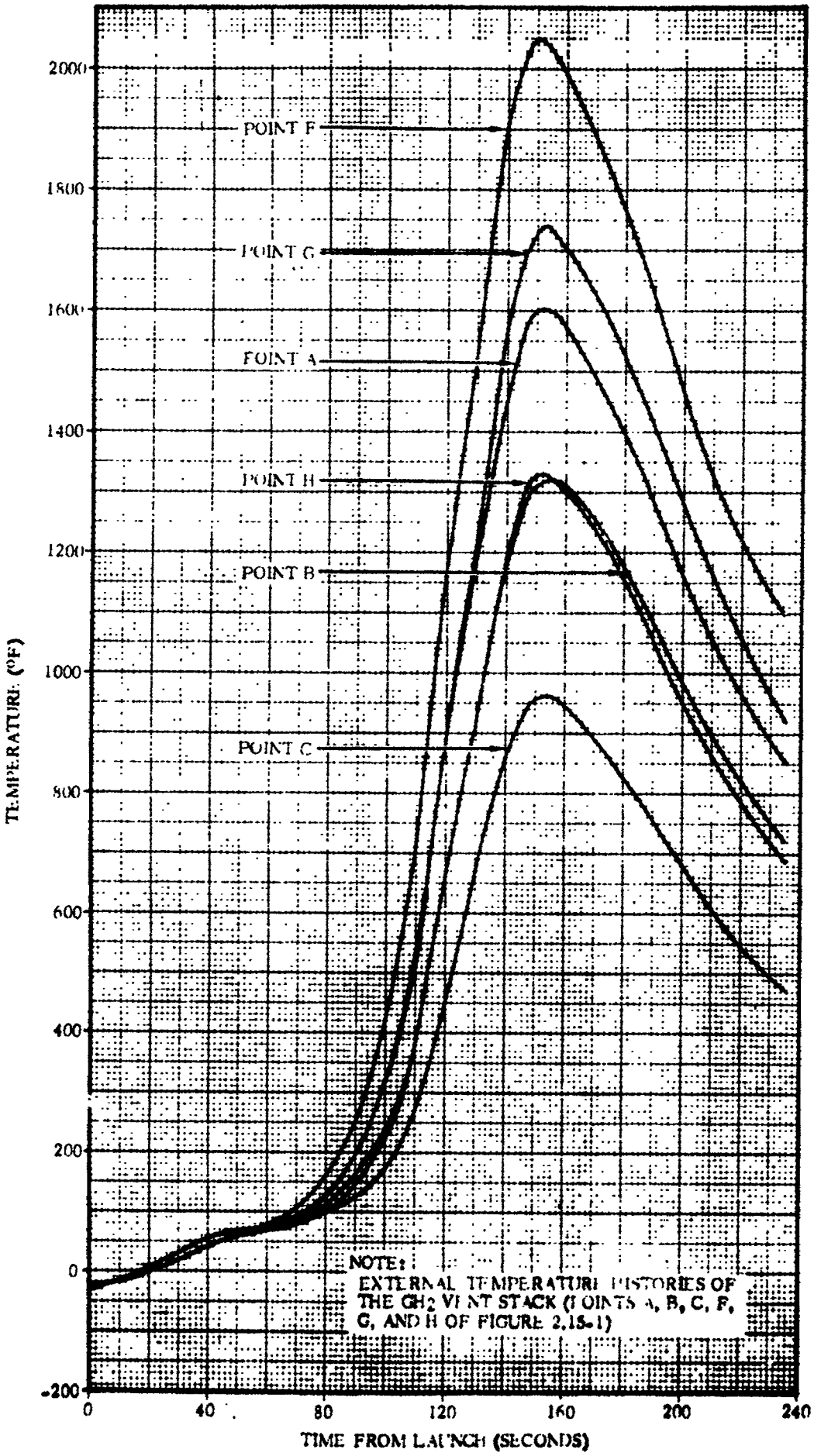

4B156LV

Figure 2.15-2. Hydrogen Vent Fin External Stagnation and Profile Temperature Histories

NOTE:
TEMPERATURE HISTORIES OF THE EXTERNAL AND INTERNAL SURFACES OF THE GH_2 VENT STACK PHENOLIC-FIBERGLAS BASIC STRUCTURE, BENEATH THE CONOLON AND BEHIND THE STAGNATION LINE (POINTS 'D', 'E', 'J', AND 'K' OF FIGURE 2.15-1) DURING A MAXIMUM HEATING DESIGN TRAJECTORY-DP35

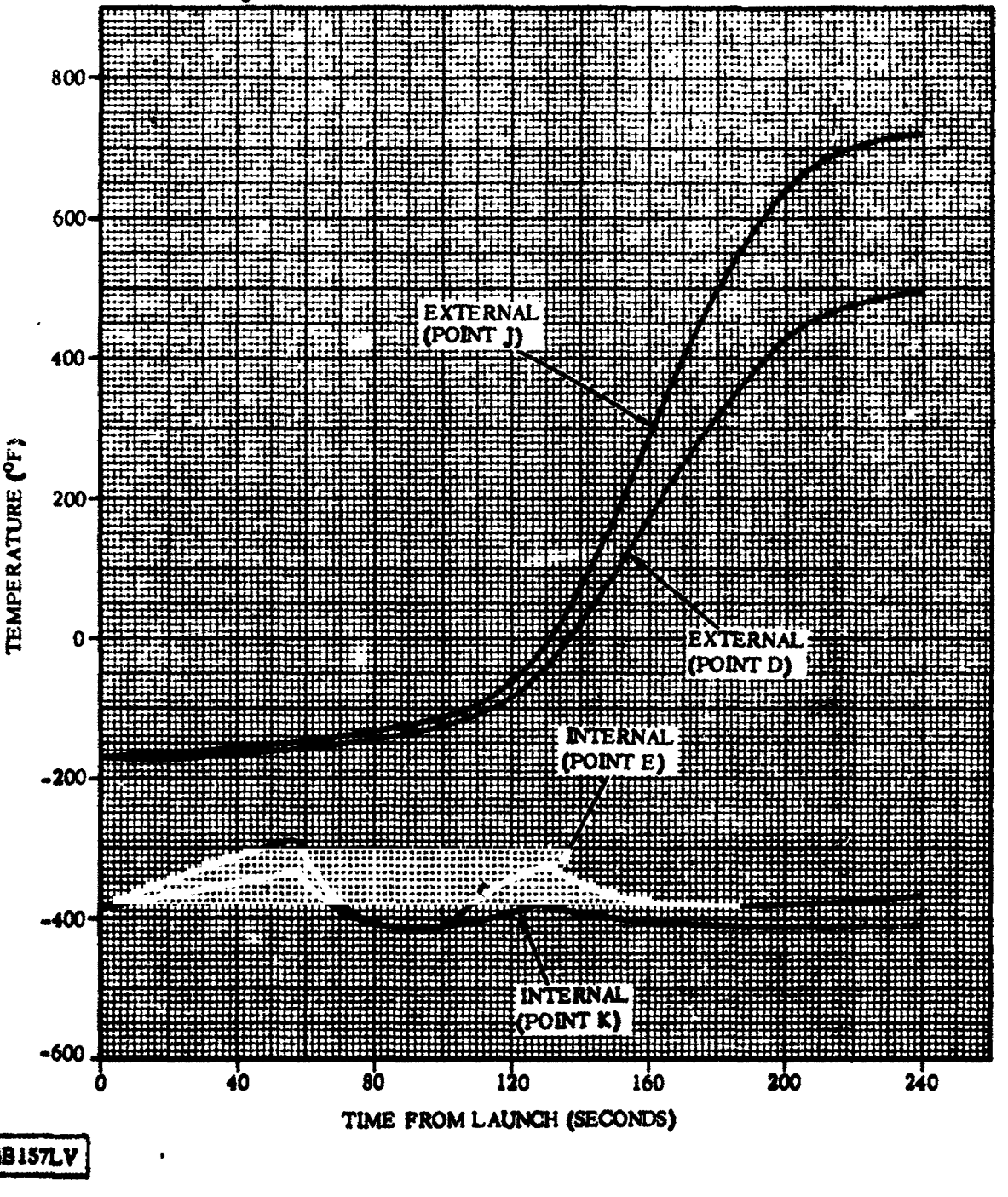

Figure 2.15-3. Hydrogen Vent Fin External and Internal Wall Temperature Histories - Maximum Temperatures

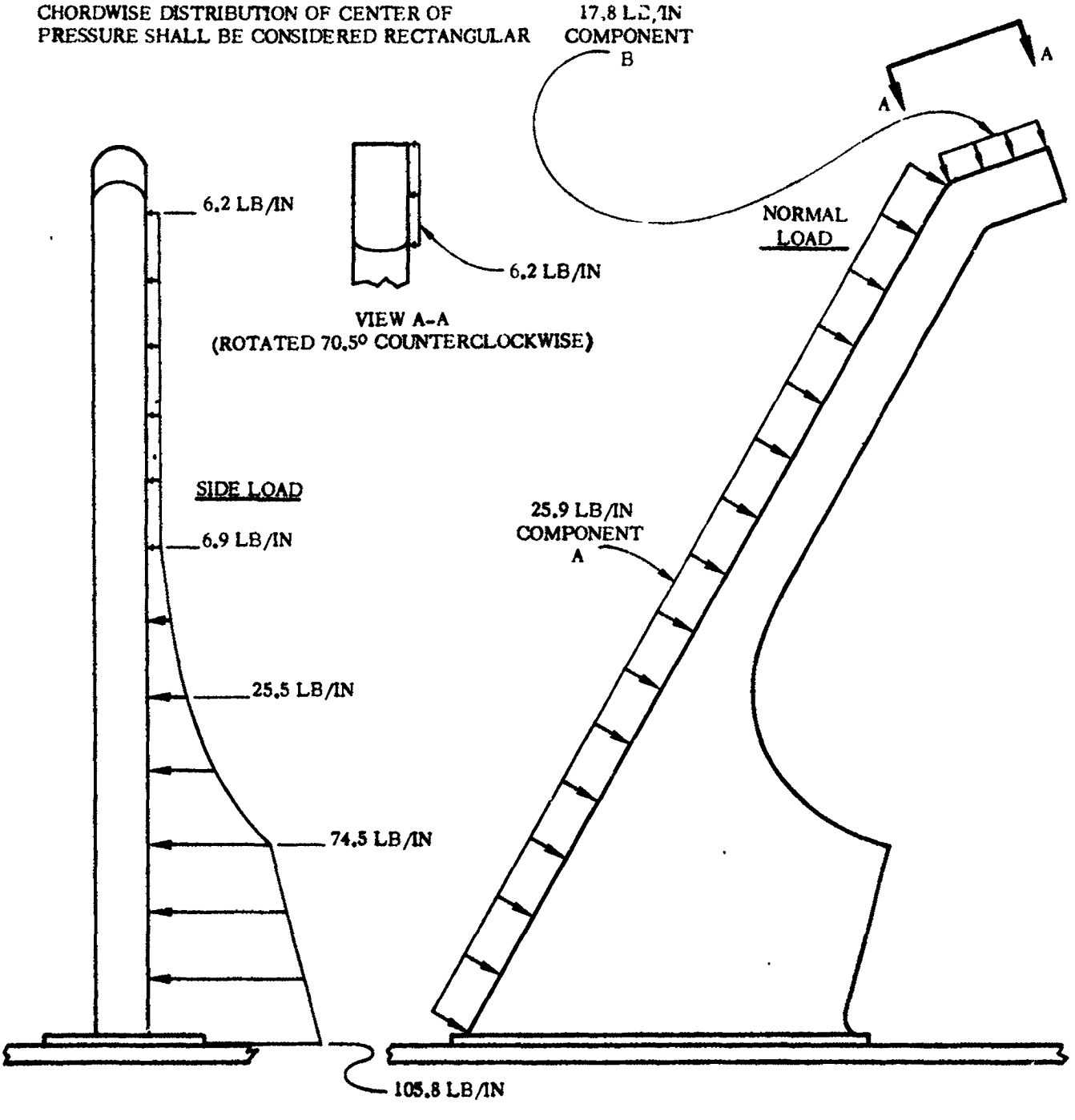

4B158LV

Figure 2.15-4. Hydrogen Vent Fin Distribution of Maximum Steady-State Aerodynamic Loading $M_\infty = 0.88$, $\alpha = 6$ Degrees

NOTE:
CONTRIBUTION DUE TO $\alpha = 6^{\circ}$ IS INCLUDED

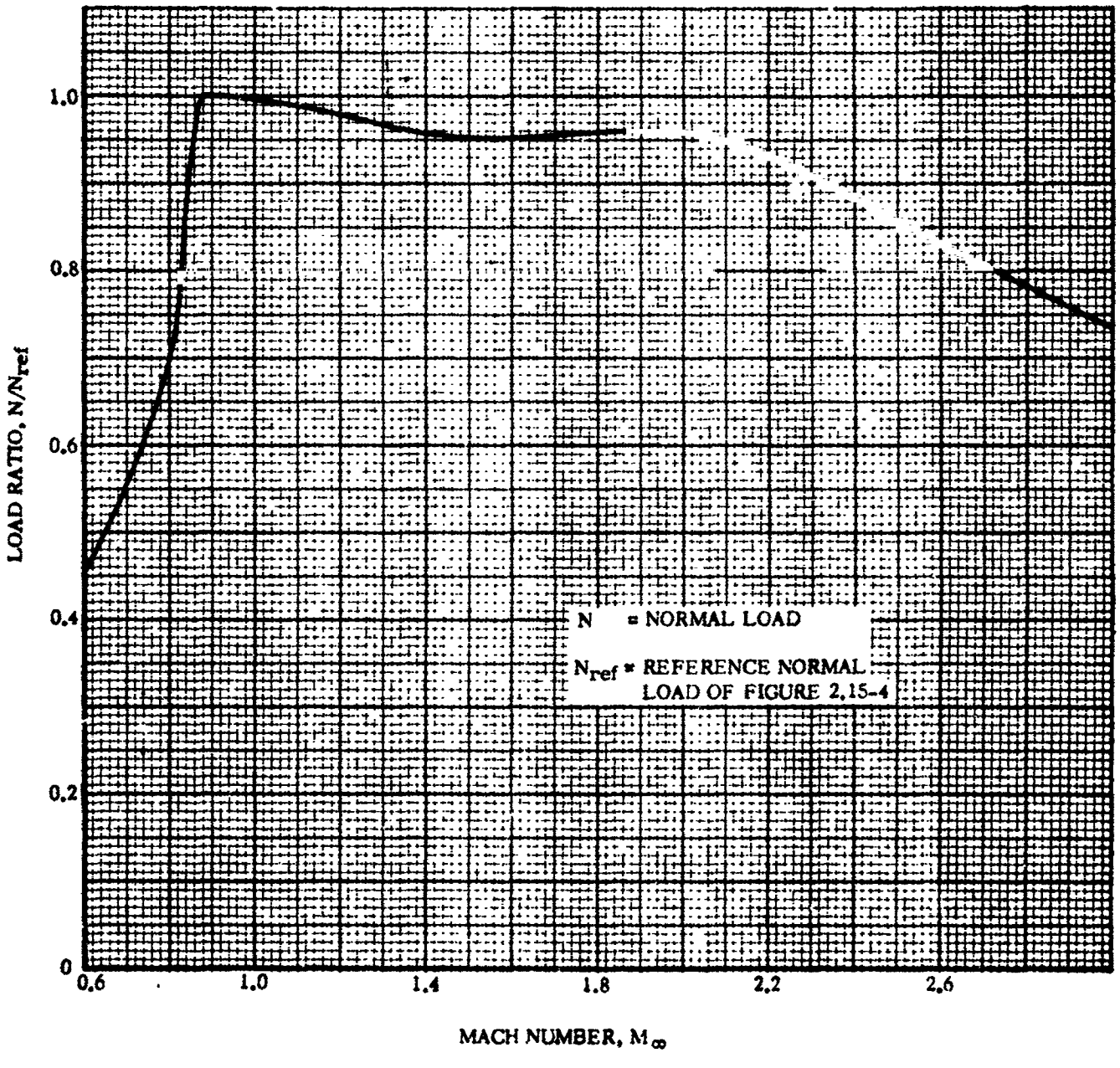

4B206LV

Figure 2.15-5. Hydrogen Vent Fin Mach Number Variation of Load Ratio, N/N_{REF} (Component "A")

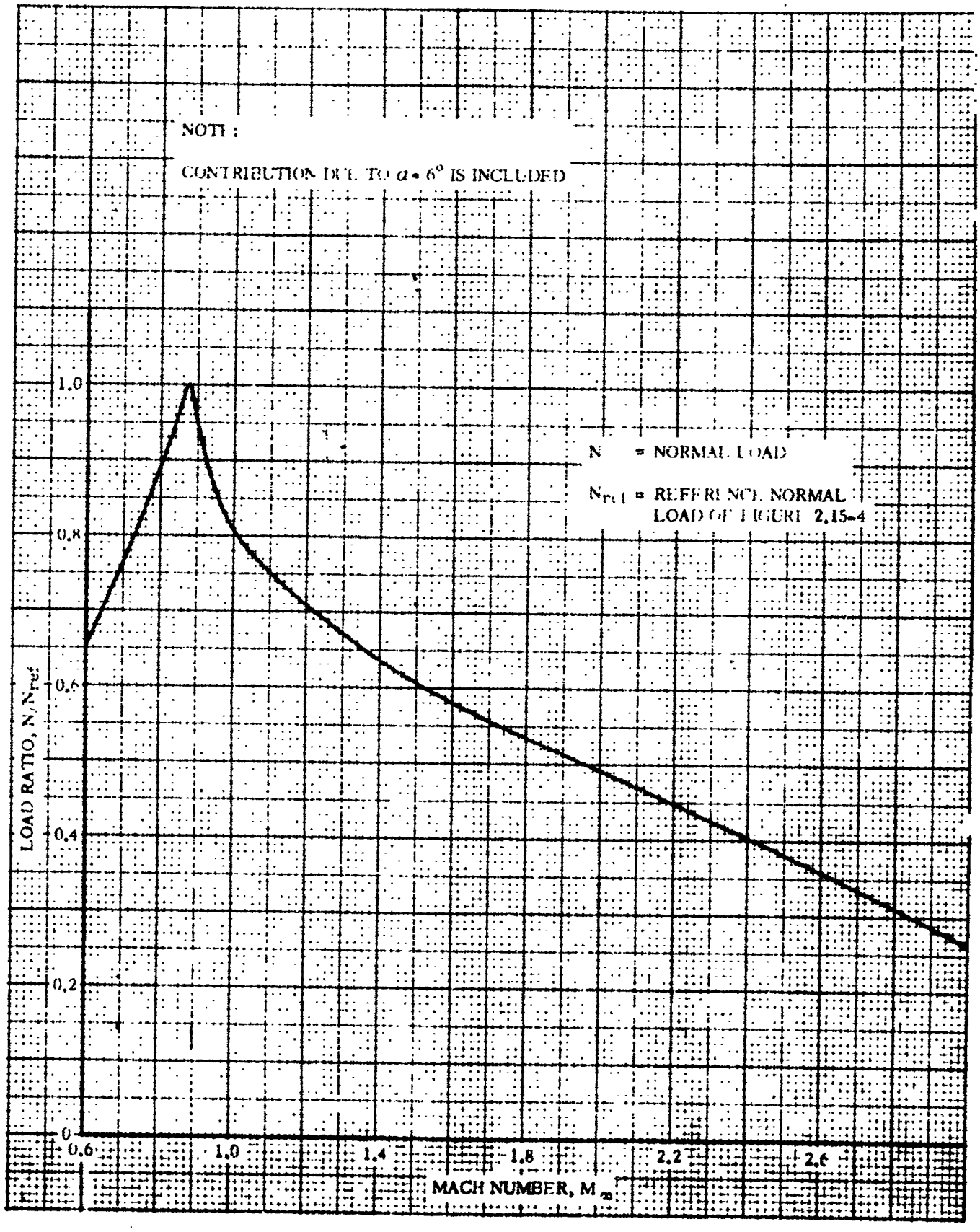

4B207LV

Figure 2.15-6. Hydrogen Vent Fin Mach Number Variation of Load Ratio, N/N_{ref} (Component "B")

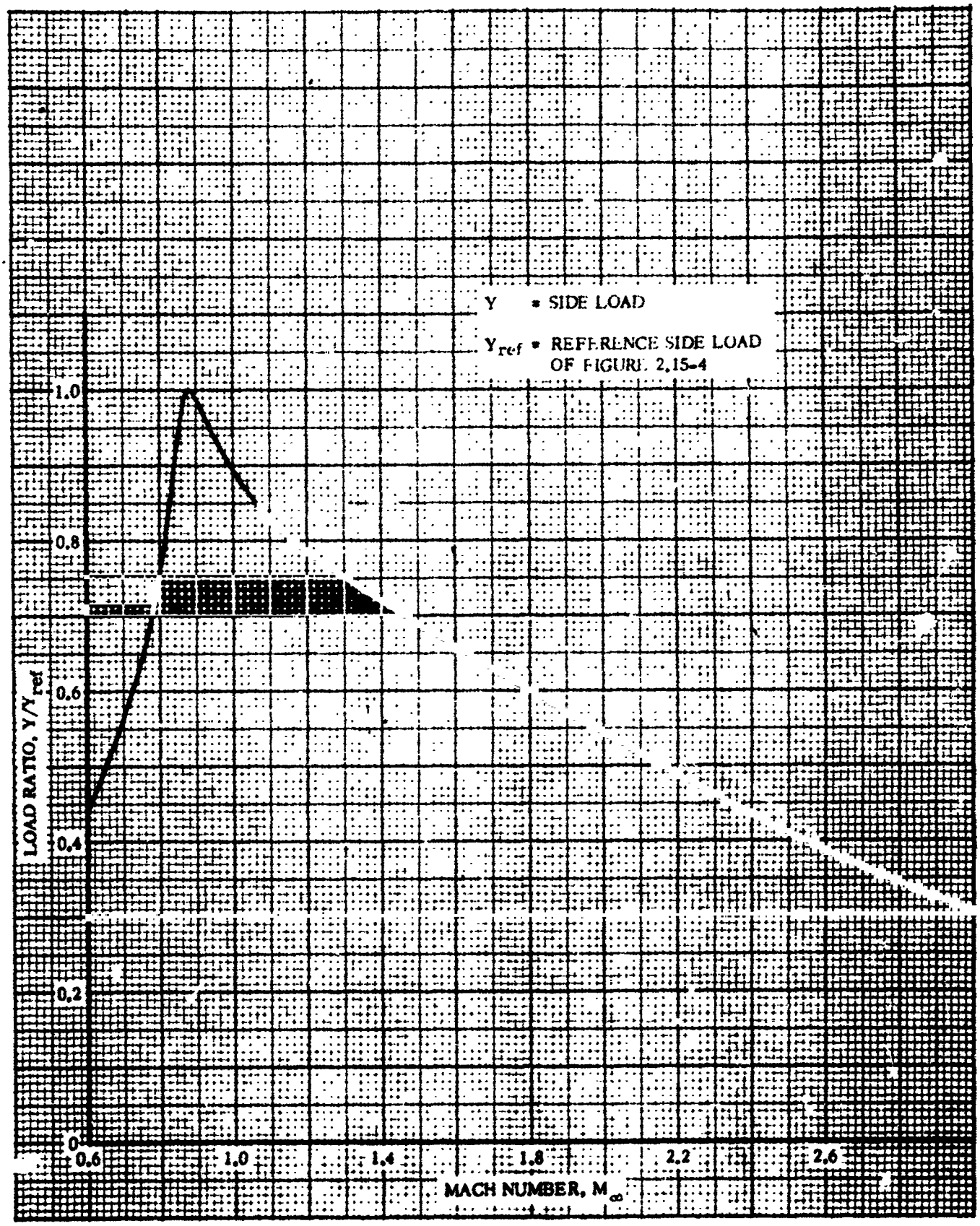

4B206LV

Figure 2.15-7. Hydrogen Vent Fin Mach Number Variation of Load Ratio, Y/Y_{ref} (Side Load)

NOTE:

DYNAMIC LOADING APPLICABLE ONLY IN TRANSONIC RANGE (MACH NUMBER 0.85 - 1.3)

CHORDWISE DISTRIBUTION OF CENTER OF PRESSURE SHALL BE CONSIDERED RECTANGULAR

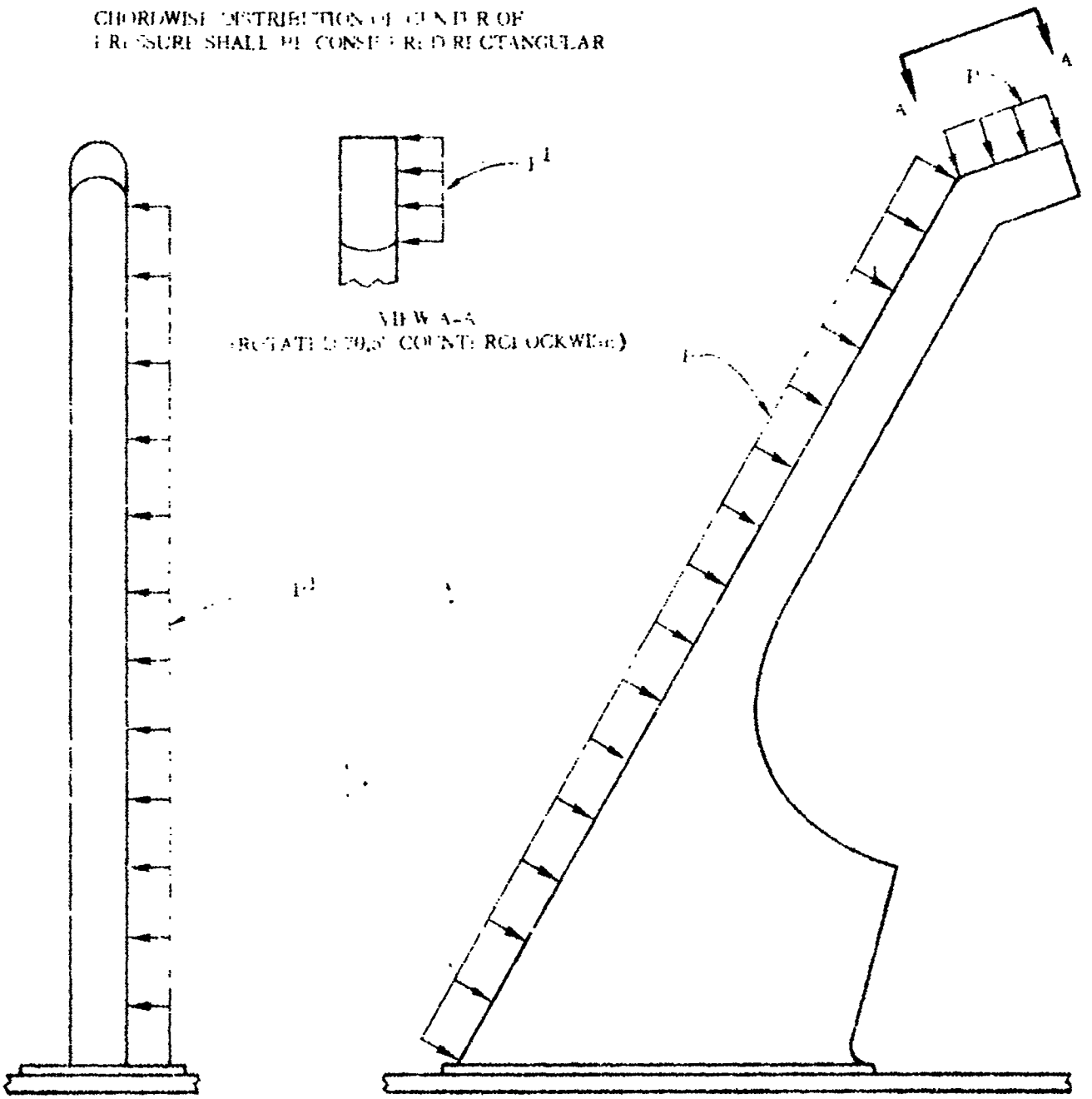

FULL VENT FIN LENGTH 50 INCHES
UNIFORM STATIC PRESSURE, P = 3.7 PSI
UNIFORM STATIC PRESSURE, p1 = 2.95 PSI

4B209LV

Figure 2.15-8. Hydrogen Vent Fin Equivalent Uniform Static Pressure for Dynamic Loading

2.15.7 MISCELLANEOUS LOAD PARAMETERS. The loading condition experienced at launch results from the vent disconnect sequence which occurs at this time. The maximum expected forces and associated moments are indicated in Figure 2.15-9.

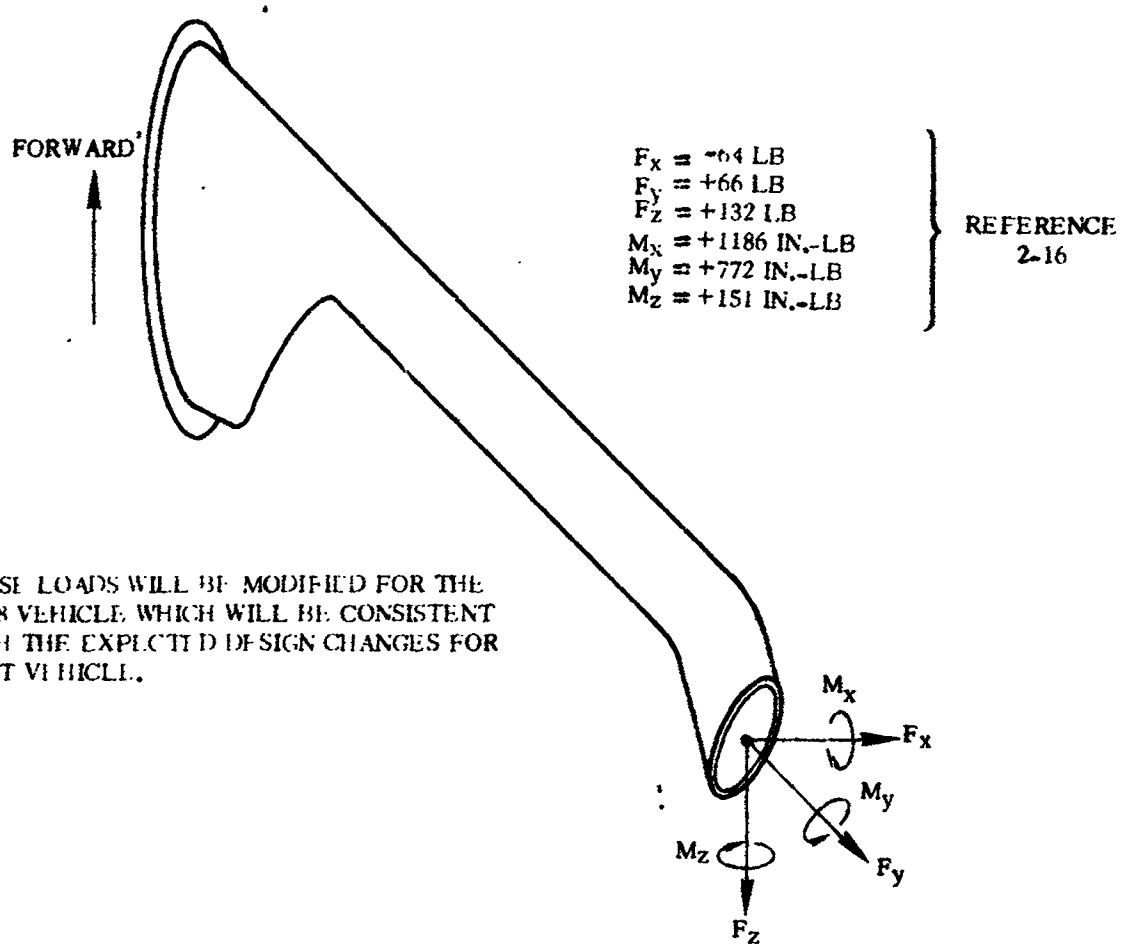

SIGN CONVENTION

F_Z = FORCE IN LONGITUDINAL DIRECTION

F_X = FORCE TANGENTIAL TO MISSILE SKIN

F_Y = FORCE IN DIRECTION OF MISSILE RADIUS

POSITIVE DIRECTION OF FORCES AND MOMENTS ARE AS SHOWN

4B159LV

Figure 2.15-9. Hydrogen Vent Fin Force and Moment at Launch (During Disconnect Sequence)

2.16 OPTICAL ALIGNMENT INSTALLATION

The optical alignment window is mounted in a tube on the nose fairing at Station 175. The tube is covered by an external door when not in use. The door is opened by an electrical signal prior to launch and is closed again prior to liftoff. See Figure 2.16-1 for configuration.

2.16.1 CRITICAL CONDITIONS. The optical alignment window and tube is subjected only to inertia loads. Aerodynamic loads are critical for the door.

2.16.2 WEIGHTS AND CENTER OF GRAVITY DATA. The following weight and C.G. location shall be used for structural design and analysis.

Weight (lb)	C.G.		
	z	y	x
8.1	175	-53	+30

2.16.3 THERMAL DATA. Temperatures are not critical for the optical alignment installation.

2.16.4 INERTIA LOADS. The maximum inertia load on the window occurs during transonic flight when the barrel section is subjected to high fluctuating pressures. The window shall be designed to withstand an inertia load of +40.0 g's in any direction. Inertia loads are not critical for the door.

2.16.5 STEADY-STATE AIR LOADS. The maximum pressure differentials existing across the door are as follows:

Maximum Burst = 0.8 psi
Maximum Crush = 3.4 psi.

These steady-state loads act in combination with fluctuating pressure loads presented in Paragraph 2.16.6.

2.16.6 BUFFET AND FLUTTER LOADS. The equivalent static pressure due to buffet response of the door = ±6.0 psi. This acts in combination with the steady-state air loads presented in Paragraph 2.16.5 since they both occur during transonic flight (Mach numbers from 0.85 to 1.30).

2.16.7 MISCELLANEOUS LOAD PARAMETERS. No other loads are critical for the optical alignment installation.

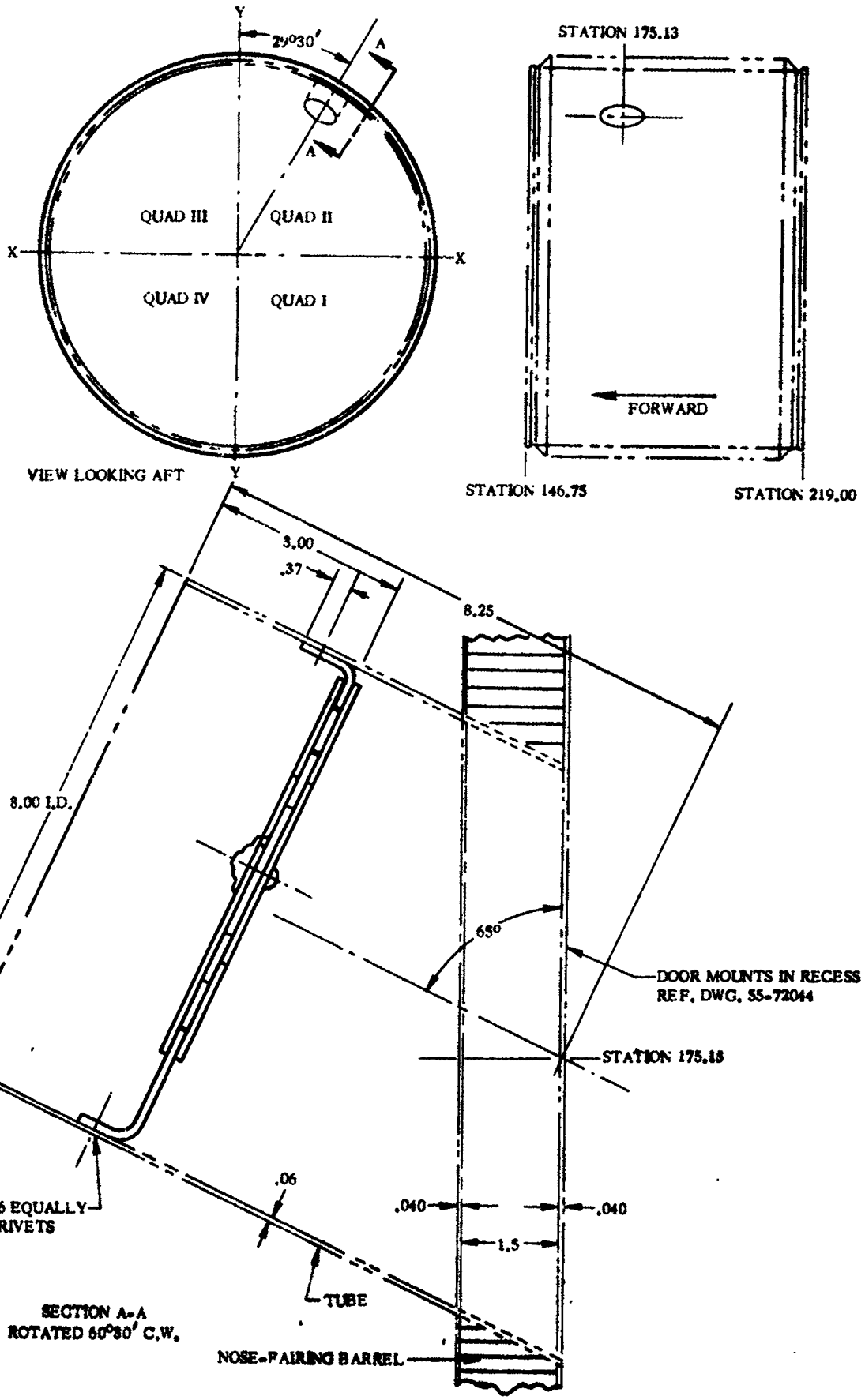

4B160LV

Figure 2. 16-1. Optical Alignment Installation Configuration

2.17 ELECTRONICS COMPARTMENT COOLING DUCT DOOR

The electronics compartment cooling duct door is located on the cylindrical (barrel) section of the nose fairing installation at Station 170.07 (Quadrant II, approximately 11.5° from the X axis). Prior to launch, this device provides access to the nose fairing cavity for a ground-stationed air conditioning unit to supply the proper environment to the payload and electrical/electronic equipment. At launch, the air conditioning duct is disconnected from the vehicle and from this point on, the door's only function is to remain closed at all times until jettison of the nose fairing. See Figure 2.17-1 for configuration of duct door and Figure 2.18-1 for duct interface.

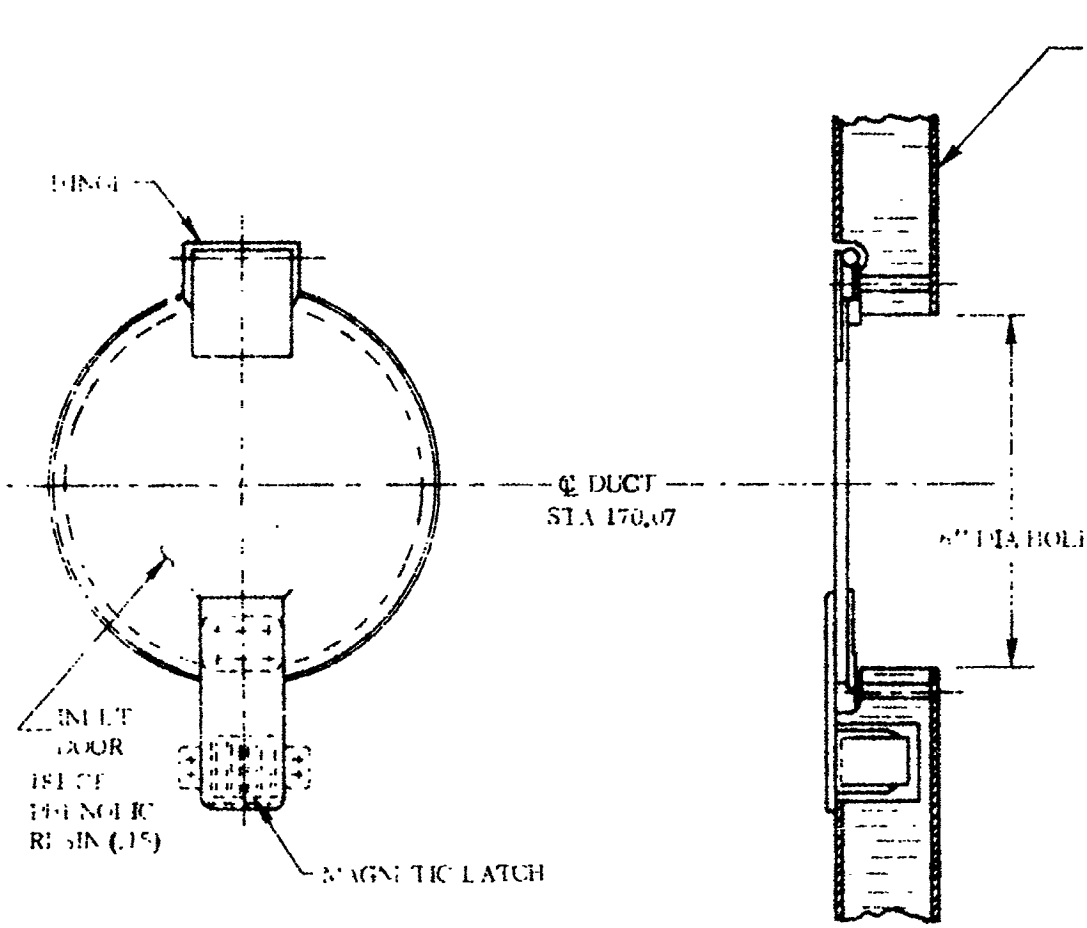

4R16LV

Figure 2.17.1 Electronics Compartment Cooling Duct Door Configuration

2.17.1 CRITICAL CONDITIONS. The duct disconnect support structure is subjected to maximum loads at vehicle liftoff during separation of the ground air conditioning duct. The door is subjected to its critical loading during transonic flight when fluctuating pressure acts simultaneously with steady-state air loads.

2.17.2 WEIGHTS AND CENTER OF GRAVITY DATA. Due to the small weight of the components, inertia loads are not critical.

2.17.4 INERTIA LOADS. Inertia loads are not critical.

2.17.5 STEADY-STATE AIR LOADS. The maximum pressure differentials existing across the door are as follows:

Maximum Burst = 0.8 psi
Maximum Crush = 2.9 psi

The steady-state loads act in combination with fluctuating pressure loads presented in Paragraph 2.17.6.

2.17.6 BUFFET AND FLUTTER LOADS. The equivalent static pressure due to buffet response of the door = ±1.65 psi. This acts in combination with the steady-state air loads presented in Paragraph 2.17.5 (occurs between Mach numbers 0.85 and 1.30).

2.17.7 MISCELLANEOUS LOAD PARAMETERS. The loads experienced at launch are due to the ground disconnect at vehicle riseoff.

The following sign convention is used for disconnect loads applied to the missile at the airborne - GSE interface.

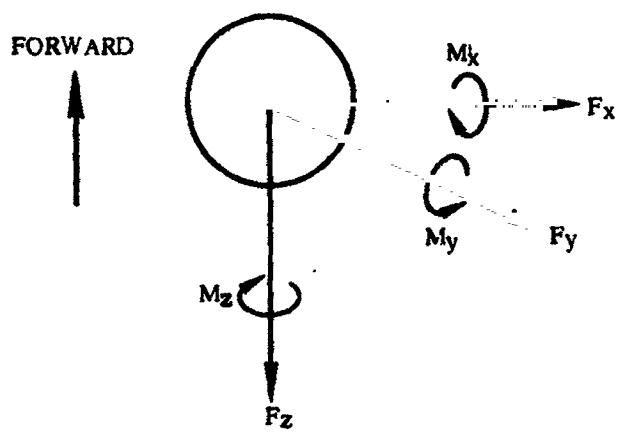

F_x = Force Tangential to Missile Skin
F_y = Force Normal to Missile Skin
F_z = Force in Longitudinal Direction
} Positive Forces and Moments are as Shown

The following loads are applied simultaneously at launch:

Condition	F_x (lb)	F_Y (lb)	F_Z (lb)	M_x (in.-lb)	M_Y (in.-lb)	M_Z (in.-lb)
Maximum Downward Load	-30	+70	+110	+830	+540	+400
Maximum Upward Load	-30	+120	+ 10	+580	+211	+630

2.18 SURVEYOR AIR CONDITIONING DUCT

The surveyor air conditioning duct is located on the cylindrical (barrel) section of the nose fairing at Station 156 in Quadrant I, 24 degrees from the X-X axis. Prior to launch, the Surveyor air conditioning duct ensures proper atmospheric environment for the spacecraft. The duct is disconnected by vehicle riseoff, and the door is shut and latched, sealing the opening in the nose fairing. See Figure 2.18-1 for duct door configuration.

The electronic equipment and payload compartment environmental control ducts are further discussed in the stress analysis report GD/C-BTD65-023, Section 1.3.10. These items are functional only during prelaunch operations in maintaining the proper environment within their respective areas. After ground disconnect sequences occur and the door shown in Figure 2.18-1 is closed, the only consideration should be to ensure that these ducts remain intact for the duration of flight. The magnitude of loads which result from use of the general structural design criteria are of such an insignificant nature, further discussion of these items will be deleted in this report.

2.18.1 CRITICAL CONDITIONS. The duct disconnect support structure is subjected to maximum loads at vehicle liftoff during separation of the ground air conditioning duct. The door is subjected to its critical loading during transonic flight when fluctuating pressure acts simultaneously with steady-state air loads.

2.18.2 WEIGHTS AND CENTER OF GRAVITY DATA. Due to the small weight of the components, inertia loads are not critical.

2.18.3 THERMAL DATA. Temperatures are not critical for the Surveyor air conditioning duct installation.

2.18.4 INERTIA LOADS. Inertia loads are not critical.

2.18.5 STEADY-STATE AIR LOADS. The maximum pressure differentials existing across the door are as follows:

Maximum Burst = 0.8 psi
Maximum Crush = 2.9 psi

Only the crushing load acts simultaneously with the fluctuating pressure presented in Paragraph 2.18.6.

2.18.6 BUFFET AND FLUTTER LOADS. The equivalent static pressure due to buffet response of the door = ±6.0 psi. This acts in combination with the crushing steady-state air load presented in Paragraph 2.18.5 (Mach number range from 0.85 to 1.30).

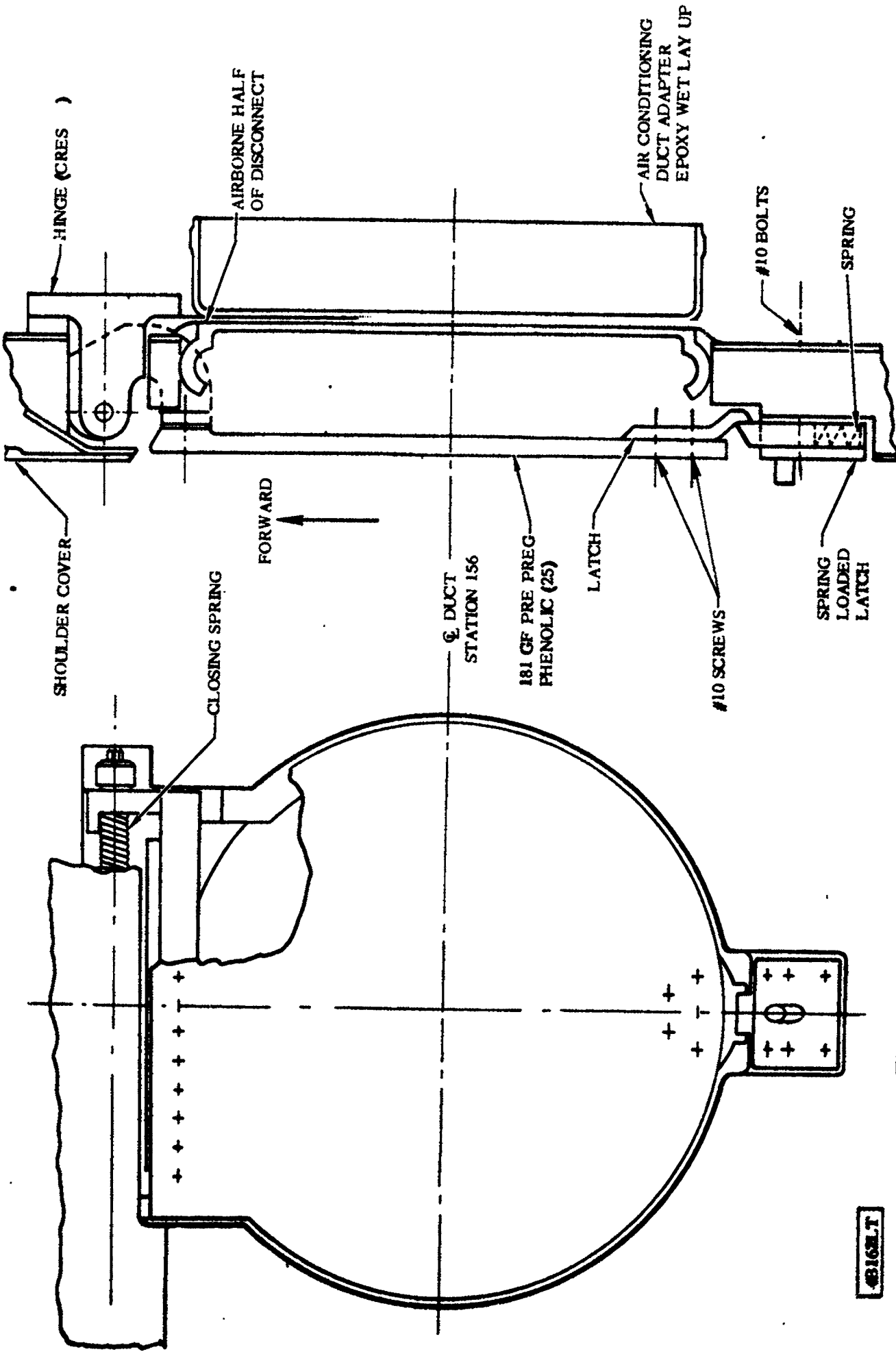

Figure 2.18-1. Surveyor Air Conditioning Duct Door Configuration

2.18.7 MISCELLANEOUS LOAD PARAMETERS. The loads experienced at launch are due to the ground air conditioning duct being disconnected by vehicle riseoff.

The following sign convention is used for disconnect loads applied to the missile at the airborne - GSE interface.

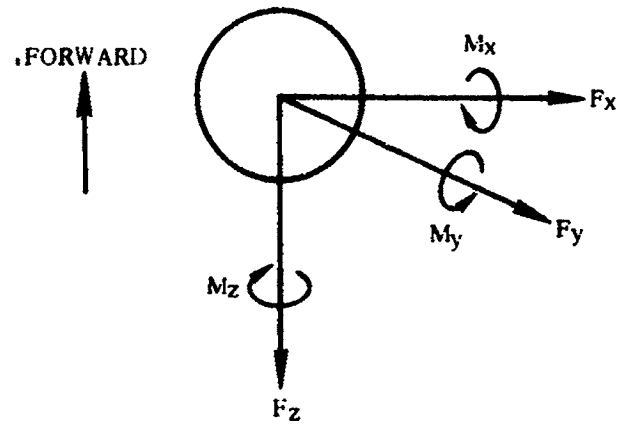

F_x = Force Tangential to Missile Skin
F_y = Force Normal to Missile Skin
F_z = Force in Longitudinal Direction
} Positive Forces and Moments are as Shown

The following loads are applied simultaneously at launch:

Condition	F_x (lb)	F_y (lb)	F_z (lb)	M_x (in.-lb)	M_y (in.-lb)	M_z (in.-lb)
Maximum Downward Load	+60	+ 80	+110	+850	-640	-740
Maximum Side Load	+110	+100	+ 35	+580	-610	-1010

THIS PAGE INTENTIONALLY LEFT BLANK.

2.19 EXPLOSIVE BOLT FAIRINGS

These Fiberglas fairings protect the nose fairing explosive bolts from aerodynamic loads during flight. There are eight fairings located on the nose fairing split line as shown in Figure 2.19-1. Also shown is the configuration of the fairing structure.

2.19.1 CRITICAL CONDITIONS. The critical loading conditions for the explosive bolt fairings occur during transonic flight when steady-state and fluctuating air loads are highest, and later in flight when temperatures reach maximum values. Inertia loads are negligible due to the light weight of the fairings.

2.19.2 WEIGHTS AND CENTER OF GRAVITY DATA. Loads imposed by inertia are not critical.

2.19.3 THERMAL DATA. Maximum temperatures on the hottest fairing (fairing A, Figure 2.19-1) are presented in Figure 2.19-2. This data is conservative for use on all fairings.

2.19.4 INERTIA LOADS. Inertia loads on the explosive bolt fairings are nct critical.

2.19.5 STEADY-STATE AIR LOADS. Steady-state differential pressures are presented in Figures 2.19-3, 2.19-4, and 2.19-5. These pressures shall be assumed to be uniformly distributed over their respective areas of the pods shown on each illustration. To the steady-state pressure, there shall be added an equivalent static pressure to account for transonic buffet effects as presented in Paragraph 2.19.6.

Total axial drag and side load on each fairing are presented in Figures 2.19-6, 2.19-7, and 2.19-8. It shall be assumed that the drag load acts through the centroid of the projected frontal area of the pod, and the side load acts through the centroid of the projected side area. The drag and side load on each pod represent only external pressure effects, while the wall ΔP includes pod internal pressure. Thus, these loads are to be used for different purposes in the stress analysis of the structure.

2.19.6 BUFFET AND FLUTTER LOADS. The equivalent static pressure due to buffet response of the explosive bolt fairings is presented below for each fairing shown in Figure 2.19-1. These loads occur at Mach numbers from 0.85 to 1.30.

Fairings A and B:	±0.5 psi
Fairings C,D, and E:	±1.8 psi

These loads act in combination with the steady-state air loads presented in Paragragh 2.19.5.

2.19.7 MISCELLANEOUS LOAD PARAMETERS. No other loads affect the explosive bolt fairings.

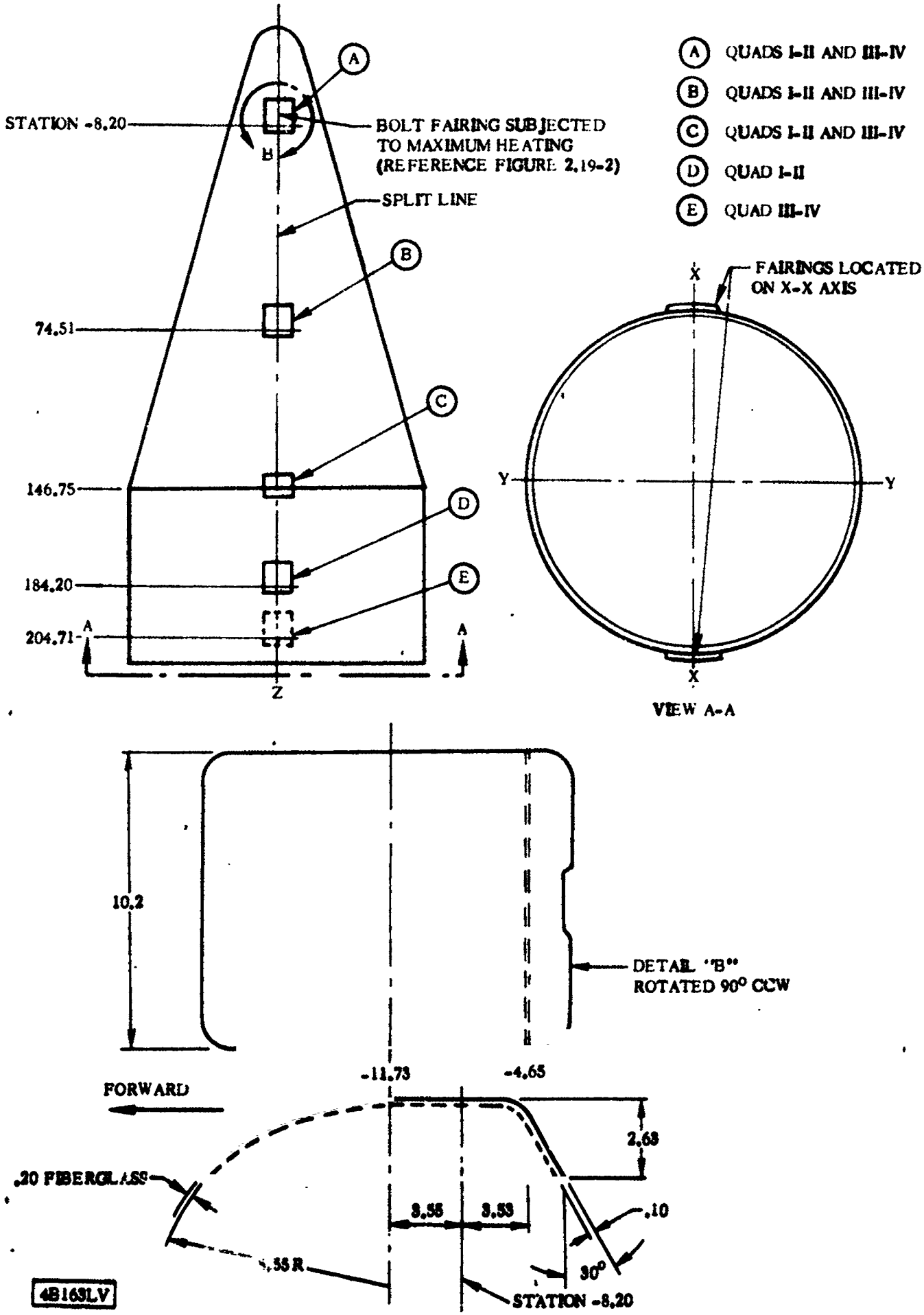

Figure 2.19-1. Explosive Bolt Fairing Configuration

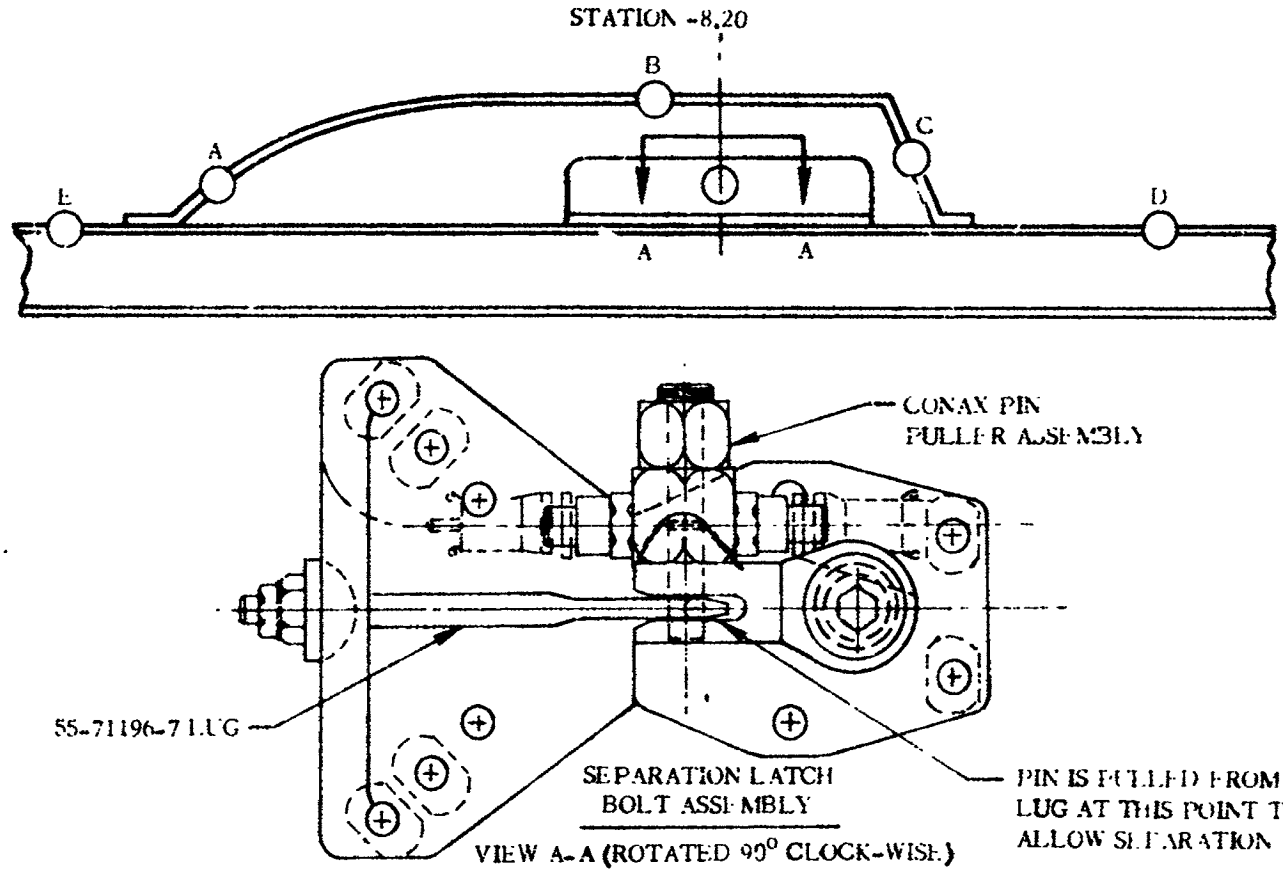

Location		Flight Time - sec			
		0	70	140	230
A_{OUT}	All temperatures are given in °F	70	92	1251	976
A		70	64	360	976
B_{OUT}		70	91	639	433
B_{IN}		70	70	141	284
C_{OUT}		70	78	358	362
C_{IN}		70	73	306	368
D		70	99	820	753
E		70	105	1070	963
(SEPARATION LATCH BOLT ASSEMBLY)		70	WILL NOT INCREASE MORE THAN APPROXIMATELY 25° DURING FLIGHT.		

4B164LV

Figure 2.19-2. Explosive Bolt Pairing and Explosive Bolt Maximum Temperatures

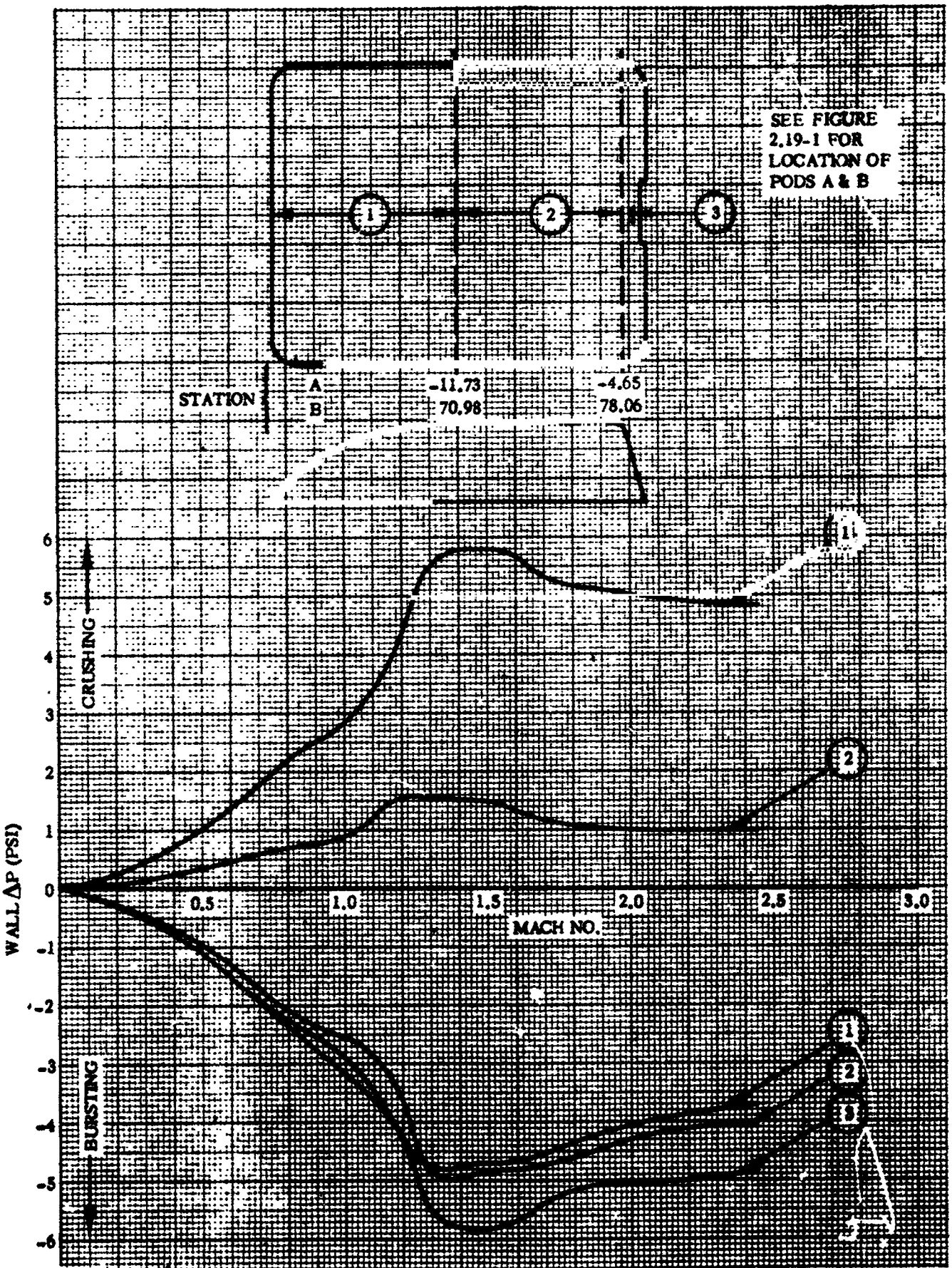

4B165LV

Figure 2.19-3. Explosive Bolt Fairings Steady-State Wall Differential Pressures (Pods A and B)

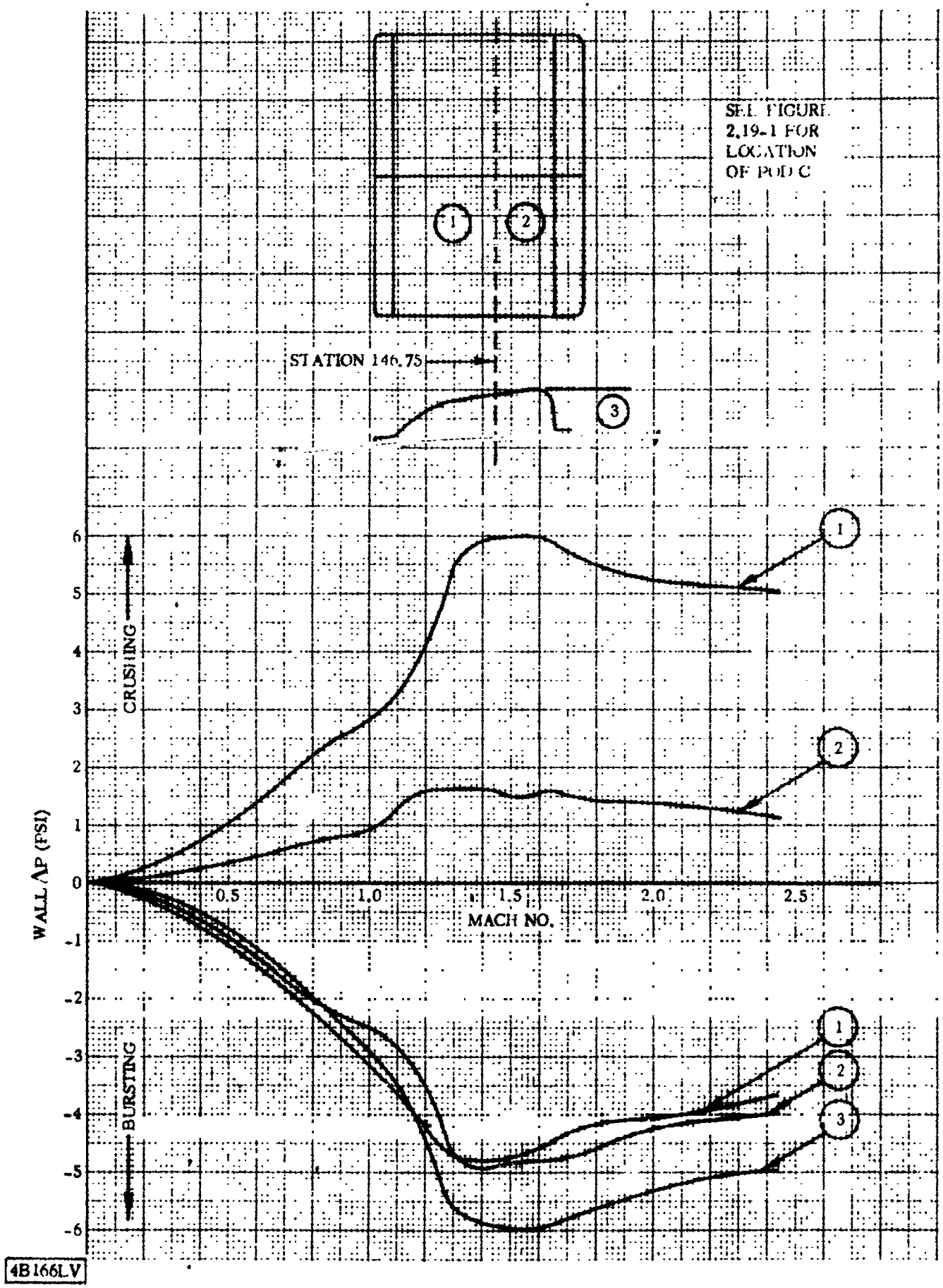

Figure 2.19-4. Explosive Bolt Fairings Steady-State Wall Differential Pressures (Pod C)

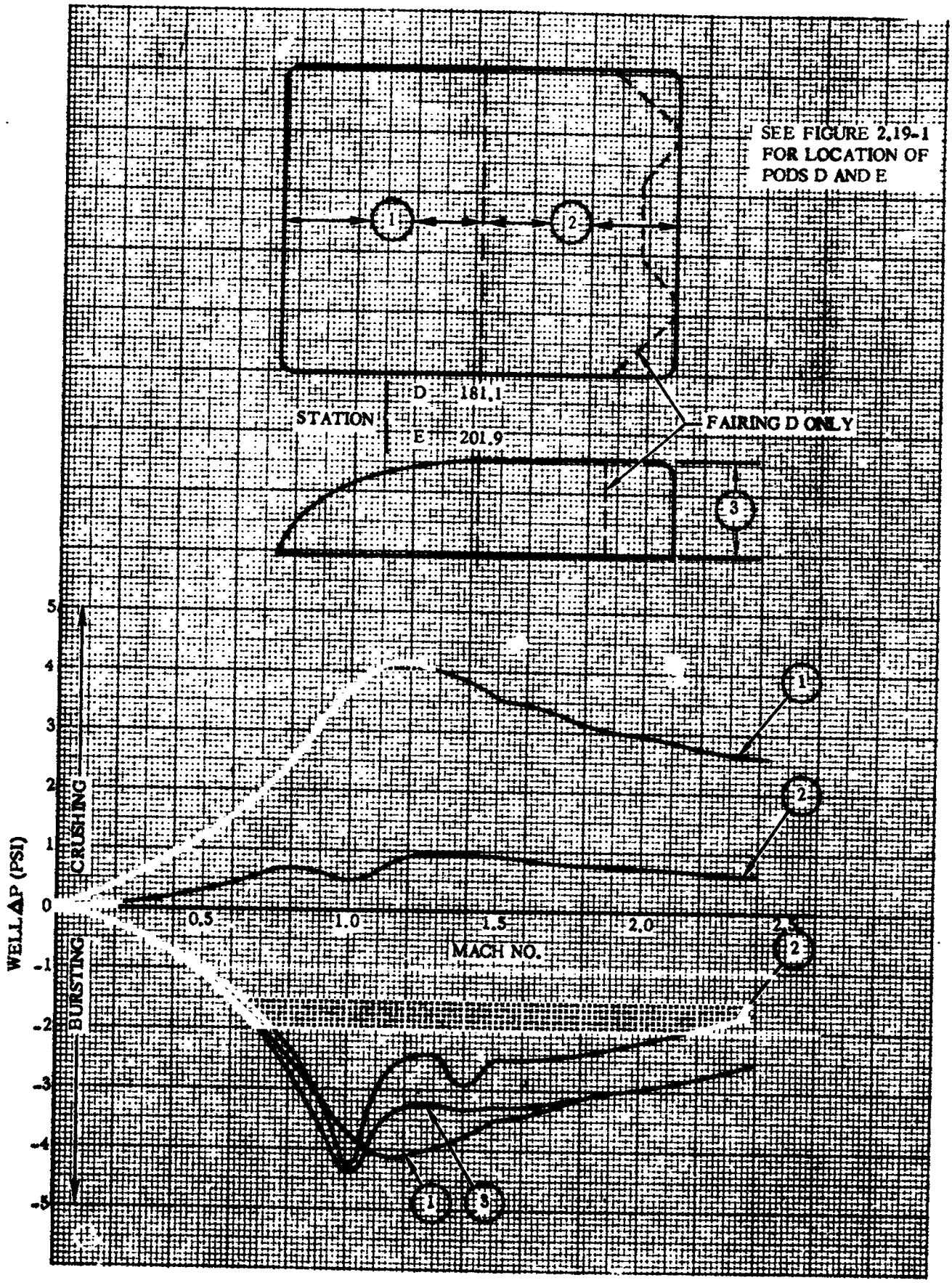

4B167LV

Figure 2.19-5. Explosive Bolt Fairings Steady-State Wall Differential Pressures (Pods D and E)

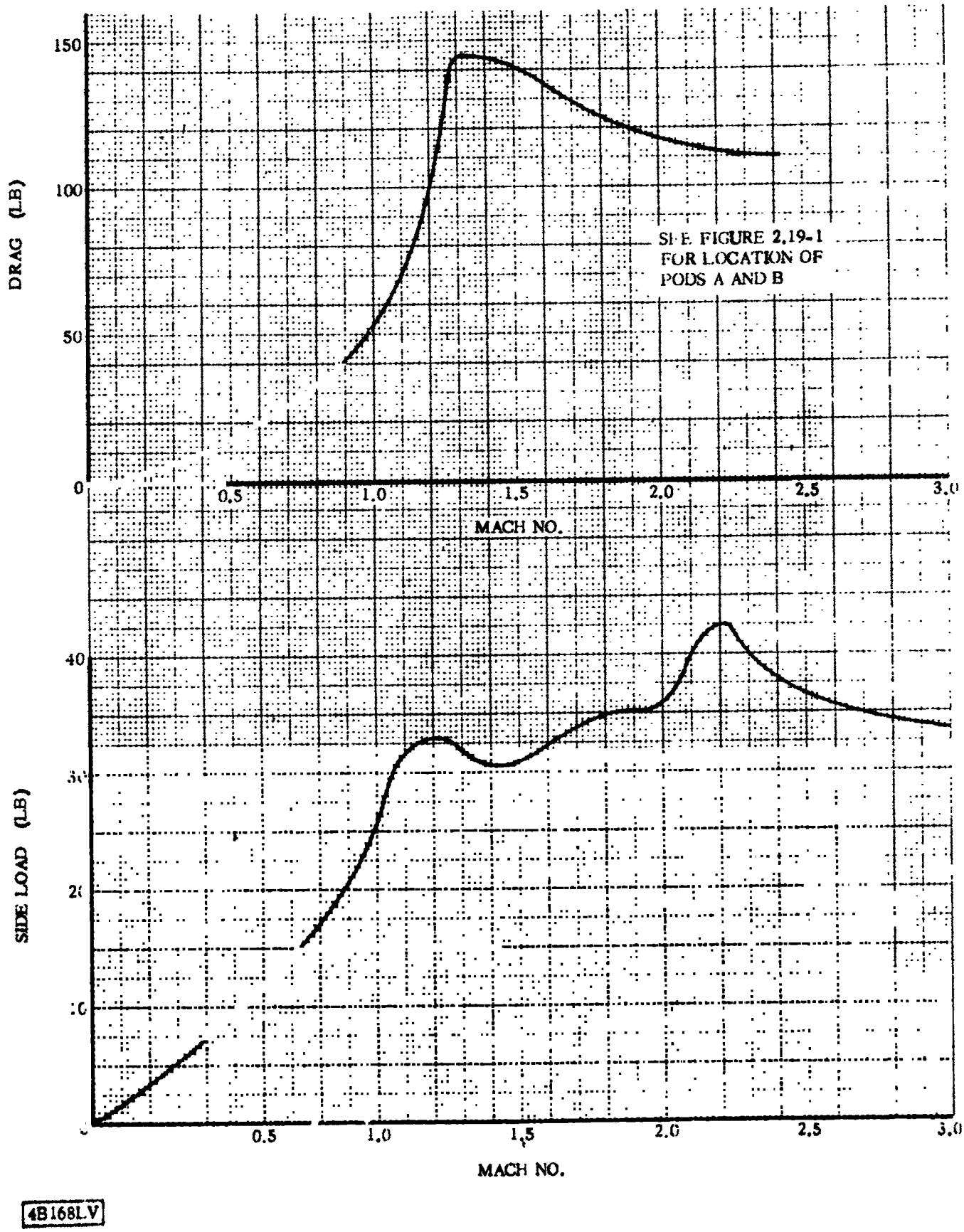

Figure 2.19-6. Explosive Bolts Fairings (Pods A and B) Drag and Side Loads

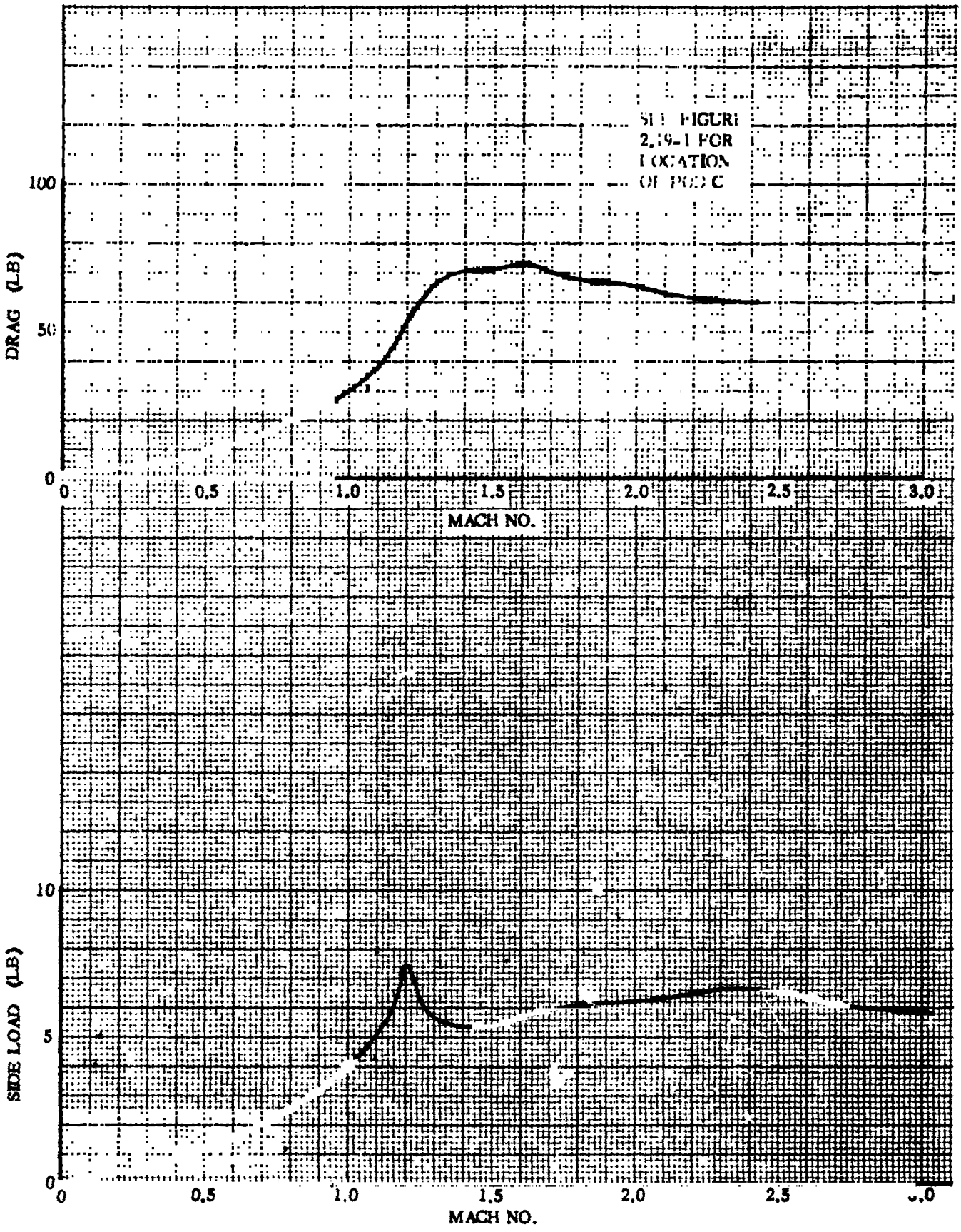

4B169LV

Figure 2.19-7. Explosive Bolt Fairings (Pod C) Drag and Side Loads

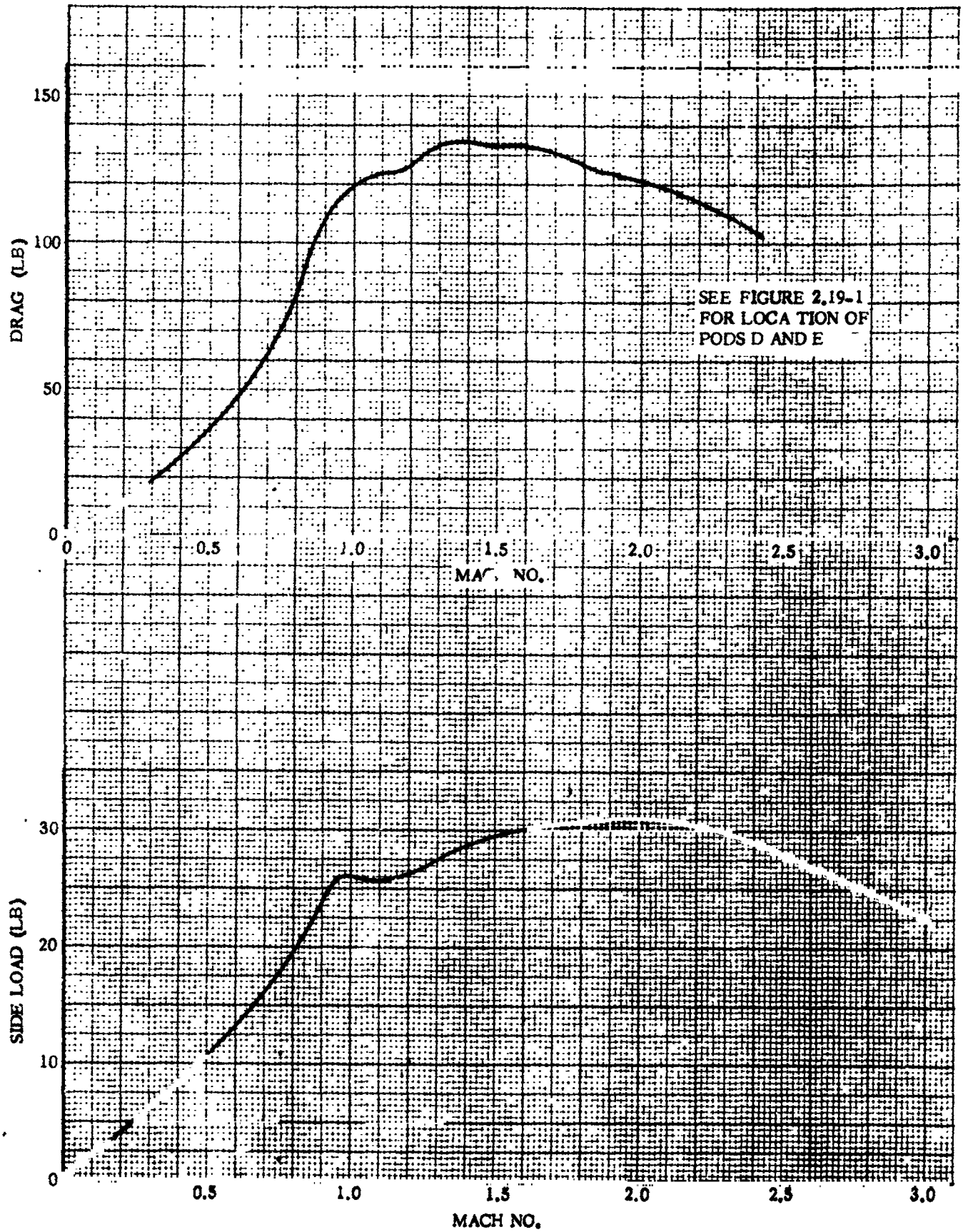

4B170LV

Figure 2.19-8. Explosive Bolt Fairings (Pods D and E) Drag and Side Loads

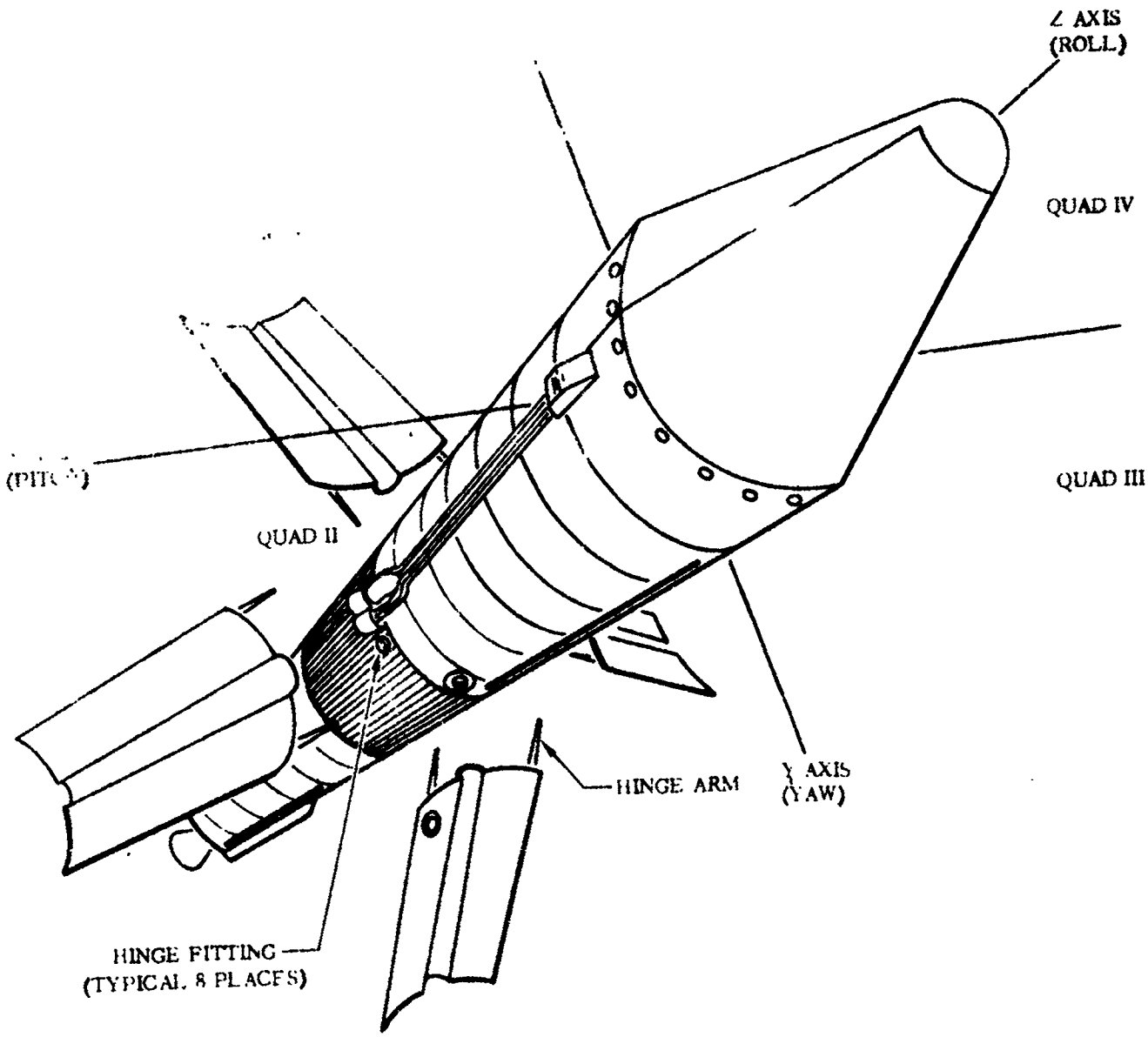
∠ AXIS
(ROLL)
QUAD IV
QUAD III
QUAD II
HINGE ARM
AXIS
(YAW)
HINGE FITTING
(TYPICAL 8 PLACES)

SECTION III

LIQUID HYDROGEN TANK INSULATION PANELS

3.1 INTRODUCTION

Liquid hydrogen (LH_2) tank insulation panels are used on the Centaur vehicle to reduce aerodynamic heating of the fuel and to protect external equipment from aerodynamic heating and loads. The insulation is cylindrical and covers the Centaur fuel tank from Station 220 to Station 412. Four 90-degree segments are bolted together along longitudinal joints to make up the insulation. Longitudinal support of the panels is provided at Station 412 where the panels are fastened to the tank ring. A sketch of the insulation panels is shown in Figure 3.1-1 and the components are listed in Table 3.1-1.

When the aerodynamic heating is reduced sufficiently, the panels are jettisoned. Shaped charges cut the panel longitudinally near the splices and circumferentially at Station 412 and at the Station 219 seal. The panels rotate (approximately 55 degrees) on hinges until they are free to fall away from the vehicle.

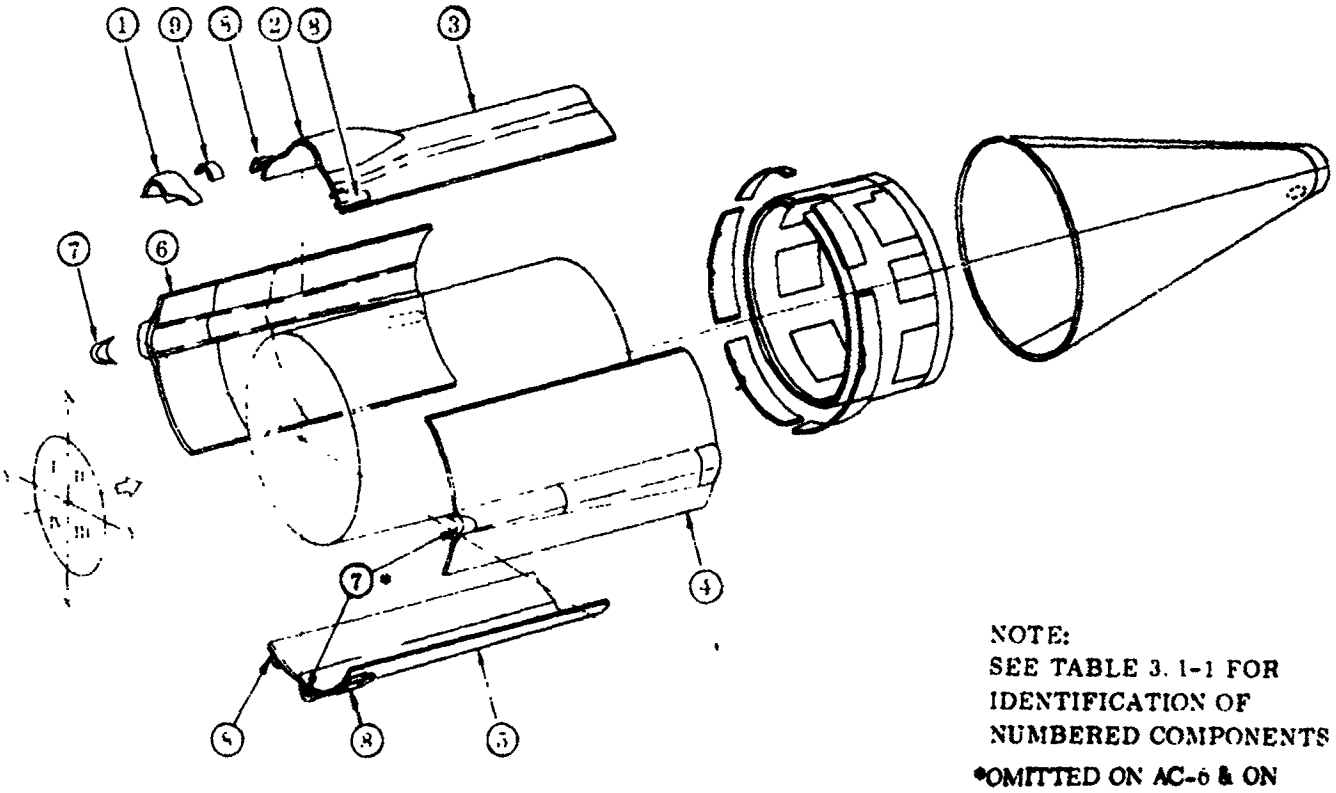

Figure 3.1-1. Liquid Hydrogen Tank Insulation Panels - Configuration

TABLE 3.1-1. LIQUID HYDROGEN INSULATION PANELS - DETAIL COMPONENTS

Item No.	Drawing No.	Nomenclature
1	55-74226	Skirt Installation - Lightweight Pod 15L
2	55-74222	Fairing Assembly - Lightweight Station 408.0 Pod 15L
3	55-74203	Panel Assembly - Jettison, Insulation Lightweight Quadrants I and II
4	55-74204	Panel Assembly - Jettison, Insulation Lightweight Quadrants II and III
5	55-74204	Panel Assembly - Jettison, Insulation Lightweight Quadrants III and IV
6	55-74206	Panel Assembly - Jettison, Insulation Lightweight Quadrants I and IV
8	55-74357	Severance System Fairings
9	55-74363	Skirt Installation - Centaur Lightweight Insulation Panel Boost Pump Pod

3.2 BASIC PANELS

Honeycomb sandwich construction is used for the insulation panels. A typical panel is shown in Figure 3.2-1. A 1.0-inch thick Fiberglas honeycomb core with a density of 3.1 pounds per cubic foot is filled with foam having a density of 2.0 pounds per cubic foot. The skins of the sandwich are 0.015 inch thick and are made of 181 glass cloth. The outer skin is impregnated with phenolic resin and the inner skin with epoxy resin. 422-J adhesive bonds the skins to the core. Local reinforcement is provided in discontinuity areas, such as joints and tunnels. Longitudinal strips of foam coated with Teflon are bonded to the inside of the panels to prevent contact of the panel skins with the tank.

The space between the panels and the tank is purged with gaseous helium during tanking, prior to launch and during early portions of flight to eliminate any air which could freeze the insulation to the tank and interfere with the jettison operation.

Contact between the insulation and the tank is maintained throughout the mission from Station 220 to Station 397.7. The combined radial deflections of the tank and panels due to pressure and temperature are such that the panels must be installed on the tank with an interference fit, thereby causing a tensile preload in the panels. The preload through transonic flight ($0.75 \leq M \leq 1.05$) is based upon the following criteria:

a. A 20-minute minimum pad chilldown time shall be assumed to allow the panel temperature to reach equilibrium.

b. The LH_2 tank shall be at a temperature of -423° F.

c. The minimum fuel tank diameter shall be based upon manufacturing tolerances.

d. The maximum panel diameter shall be based upon manufacturing tolerances.

e. The vehicle tank pressure shall be in accordance with current AC-6 and on vehicle tank pressure schedules (see Paragraph 6.2.7).

f. The panel and pod burst pressure envelope shall be as presented in Section III of this report.

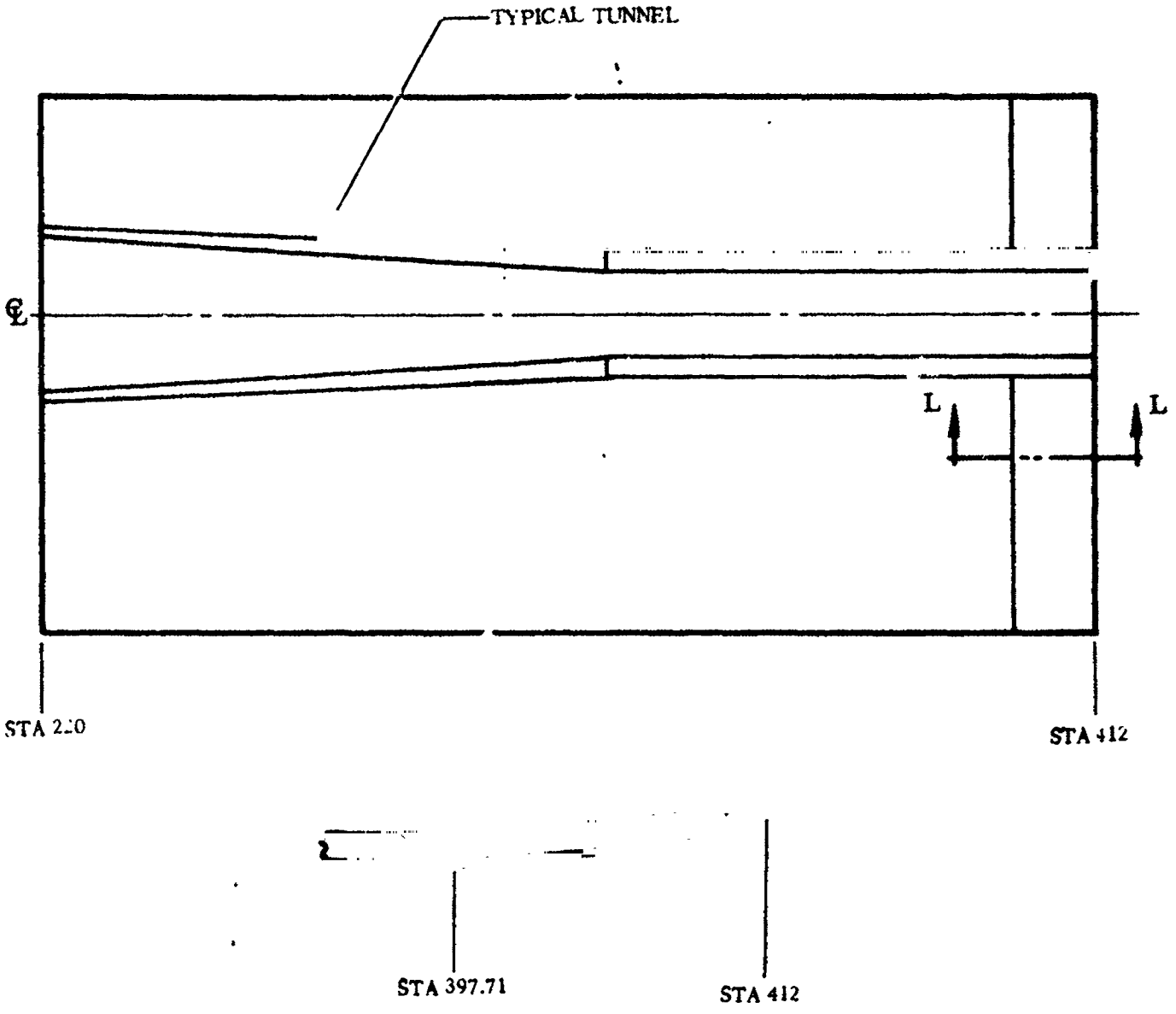

SECTION L-L
CONICAL FLARE

4B02LV

Figure 3.2-1. Insulation Panel - Typical

3.2.1 CRITICAL CONDITIONS. A variety of loading conditions are experienced by the basic insulation panels. Installation of the panels on the tank results in a preload which puts tension in the insulation and reduces the tension in the tank skins. After tanking with liquid hydrogen, the propellant tank contraction is slightly greater than the contraction of the insulation panels, thus reducing the preload in the panels somewhat. After launch of the vehicle and during flight through the atmosphere the fuel tank expands as the tank pressure increases causing additional hoop loads in the insulation panels. Aerodynamic loads cause a wide variety of pressure differentials across the panels. Local deviations from these pressures occur near pods and protuberances on the panels. The highest longitudinal loads on the panels occur just prior

to booster engine cutoff (BECO). The panel jettison hinge loads occur as the shaped charge cuts the panels during the jettison sequence.

3.2.2 WEIGHTS AND CENTER OF GRAVITY DATA. Structural design weights, C.G.'s and mass moments of inertia for the jettisonable insulation panels are listed in Table 3.2-1.

TABLE 3.2-1. LIQUID HYDROGEN INSULATION PANELS - STRUCTURAL DESIGN WEIGHTS, CENTERS OF GRAVITY, AND MASS MOMENTS OF INERTIA

Event	Item	Complete Insulation	Quad I-II Panel	Quad II-III Panel	Quad III-IV Panel	Quad I-IV Panel
Liftoff	Weight (lb)	1400				
	x-C.G. (in.)	4.1	N.A.	N.A.	N.A.	N.A.
	y-C.G. (in.)	-0.2				
	z-C.G. (in.)	325.4				
Panel Jettison	Weight (lb)		375	340	305	315
	x-C.G. (in.)		57.6	5.3	-53.4	-5.2
	y-C.G. (in.)	N.A.	7.2	-54.2	-5.7	54.1
	z-C.G. (in.)		331.7	321.4	321.5	322.3
	I_{xx} (in.^{2} lb)		1,721,600	1,406,100	1,358,700	1,189,000
	I_{yy} (in.^{2} lb)		1,493,800	1,329,100	1,137,500	1,409,700
	I_{zz} (in.^{2} lb)		285,900	258,900	253,300	246,700

NOTE: The mass moments of inertia of each insulation panel are referenced to coordinate axis passing through the C.G. of the panel and parallel to the vehicle X, Y, and Z axes.

3.2.3 THERMAL DATA. Insulation panel temperature is plotted versus flight time in Figure 3.2-2. Data is presented for the basic cylindrical skin. The temperatures do not include the effects of Thermolag which will reduce temperatures on the aft portion of the panels.

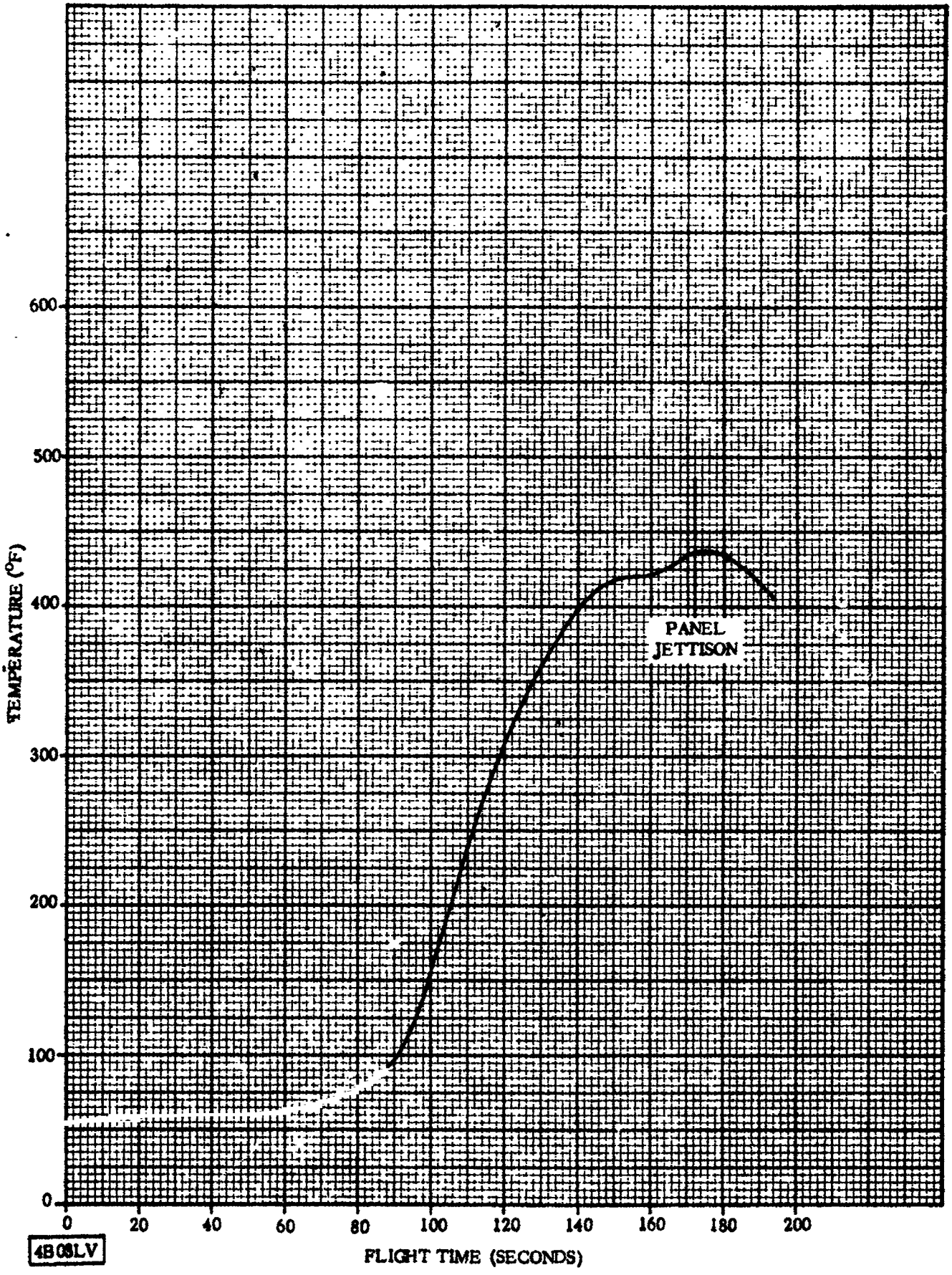

Figure 3.2-2. Basic Insulation Panels Flat Regions Temperature Histories without without Thermolag Material

Temperatures of the basic panel near the Station 412.72 joint shown in Figure 3.2-3 were established using the following assumptions:

a. All internal surfaces transfer heat by natural convection to the liquid oxygen (LO_2) tank at -284° F.

b. A contact coefficient of 300 BTU/ft²hr° F between materials.

c. The maximum heating design trajectory (DP-35) was used in the analysis.

d. External surfaces radiate to the space environment with an emissivity of 0.85.

Temperatures at several times during flight are listed in Table 3.2-2.

TABLE 3.2-2. STATION 412 LIQUID OXYGEN TANK AND INSULATION PANEL JOINT - TEMPERATURE VERSUS TIME TABULATION

Location*	Temperatures (° F) for Various Flight Times			
	0 Sec	70 Sec	150 Sec	170 Sec
A	-114	-82	-29	-20
B	-112	-81	-30	-20
C	-96	-68	-23	-15
D	-66	-48	-5	-2
E	-88	-60	-16	-10
F	-87	-51	0	4
G	20	42	164	171
H	57	65	207	214
I	59	67	210	217
J	59	68	210	217
K	59	68	210	217
L	13	33	134	156
M	-86	-86	-85	-84
N	-88	-78	-77	-75
O	-77	-77	-75	-72

*Reference Figure 3.2-3

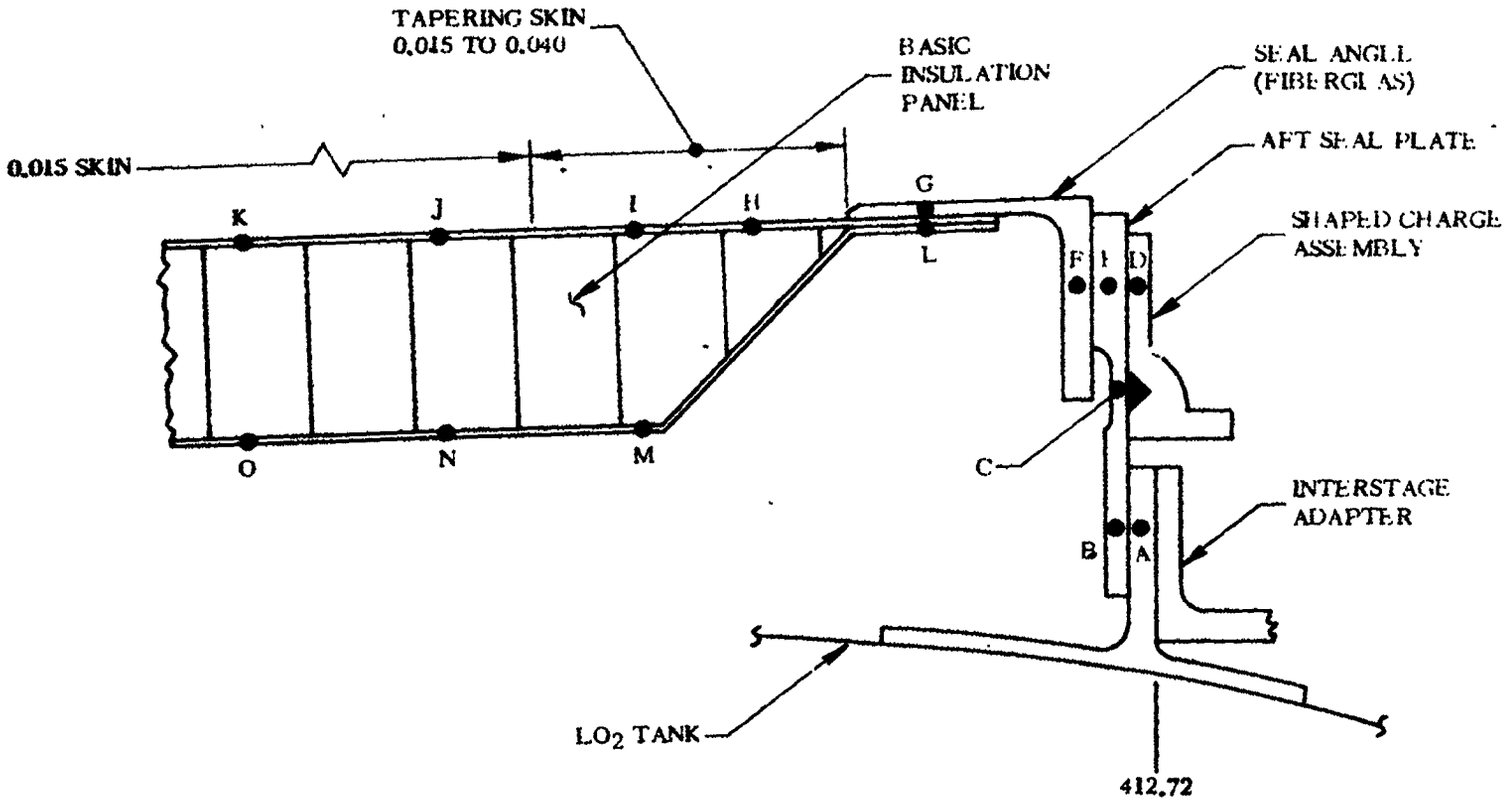

SEE TABLE 3.2-2 FOR TEMPERATURES

4804LT

Figure 3.2-3. Liquid Oxygen Tank and Insulation Panel Joint - Thermal Model

Requirements for Thermolag insulation on the aft portions of the basic insulation panels are dictated by the maximum structural temperature allowable. The assumptions used to determine the required thickness of Thermolag are:

a. The Thermolag material sublimes at a temperature of 230° F.

b. A static pressure reduction factor equivalent to expanded flow exists at all locations.

c. The maximum heating design trajectory (DP-35) was used in the analysis.

Portions of the AC-6 insulation panels, 55-74203, 55-74204, and 55-74206, require Thermolag insulation patterns as shown in Figure 3.2-4.

3.2.4 INERTIA LOADS. Steady-state inertia loads on the insulation panels are determined from the plot of (T-D)/W versus time which is presented in the mission design trajectories portion of this report (see Paragraph 1.3.3).

Inertia load factors for ground handling and transportation are given in Reference 1-5.

3.2.5 STEADY-STATE AIR LOADS. Aerodynamic loads on the insulation panels vary with Mach number. An envelope of burst and crushing pressures is presented in Figure 3.2-5. Pressures are shown for the basic panels and the tunnels which run the length of the panels along the ±X and ±Y axes. External pressures on the insulation panel were predicted from wind tunnel test data, while internal pressures were calculated using conservative assumptions of gas flow from the vent, from predicted helium purge gas pressures, and from conservative leakage assumptions.

Basic panel and antenna tunnels shall be capable of withstanding the crushing and burst pressure envelope plus the vibratory response due to buffet and flutter loads. Local deviations occur in the pressure loads near protuberances and fairings as shown in Figure 3.2-6. These pressure increments must be added to the basic panel pressures locally. The maximum drag load on each panel is also shown in Figure 3.2-6.

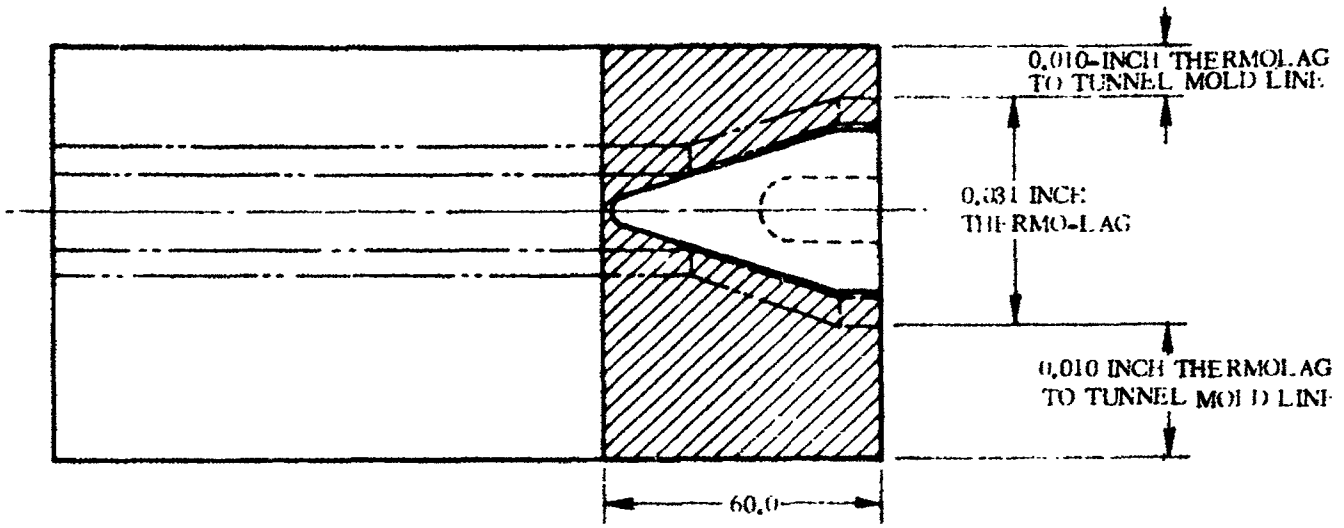

55-74203 INSULATION PANEL (QUADS I - II)

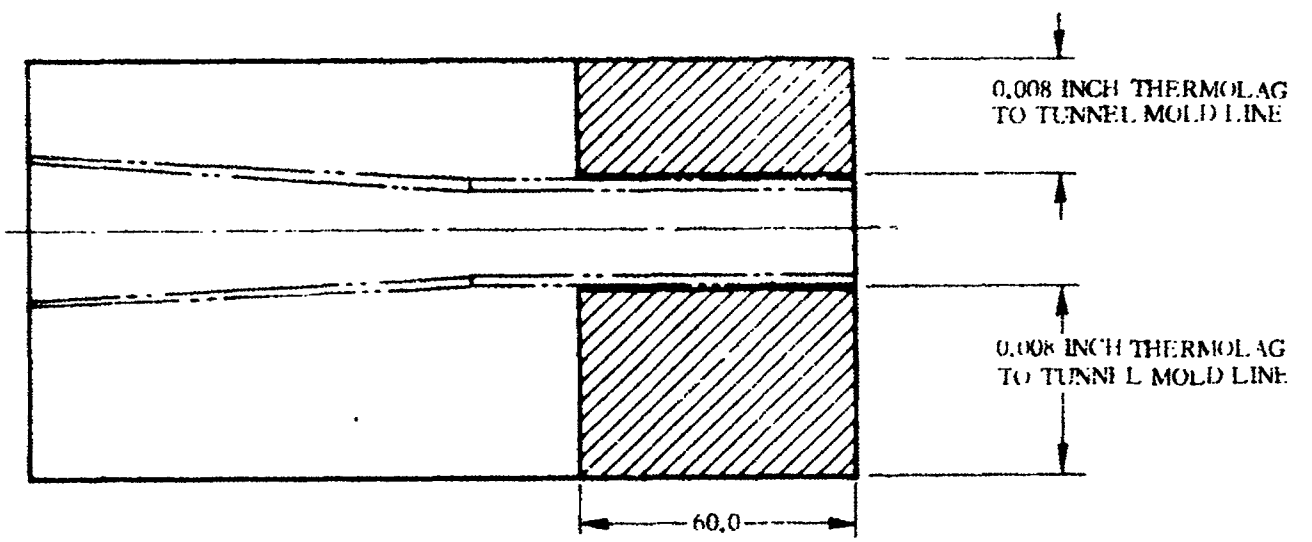

55-74204 INSULATION PANEL (QUADS II - III, III - IV)

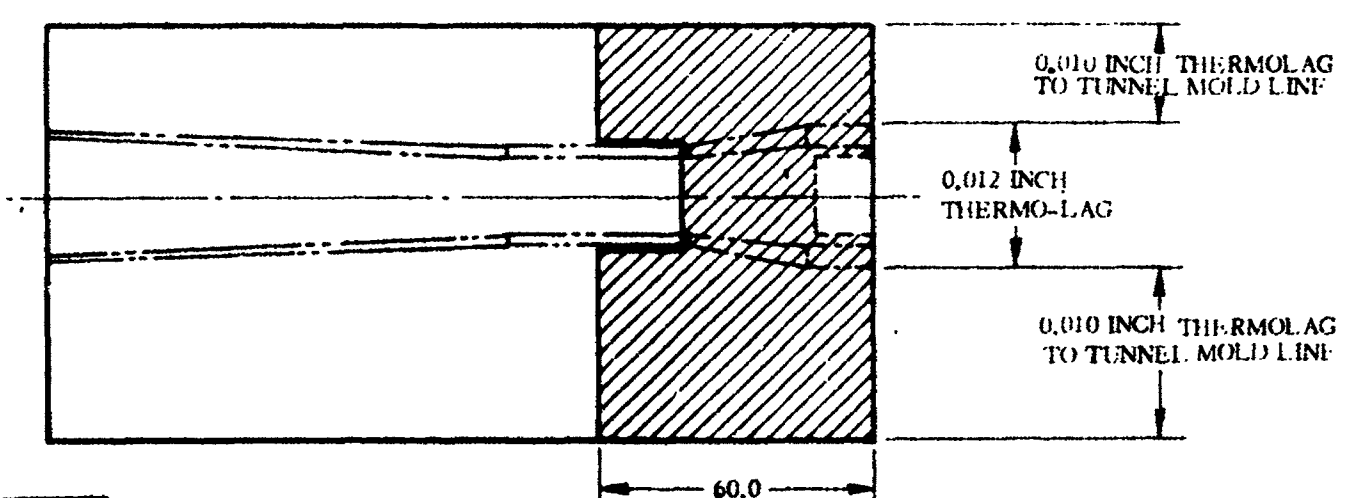

4B05LV

55-74206 INSULATION PANEL (QUADS I - IV)

Figure 3.2-4. Insulation Panels Thermolag Requirements

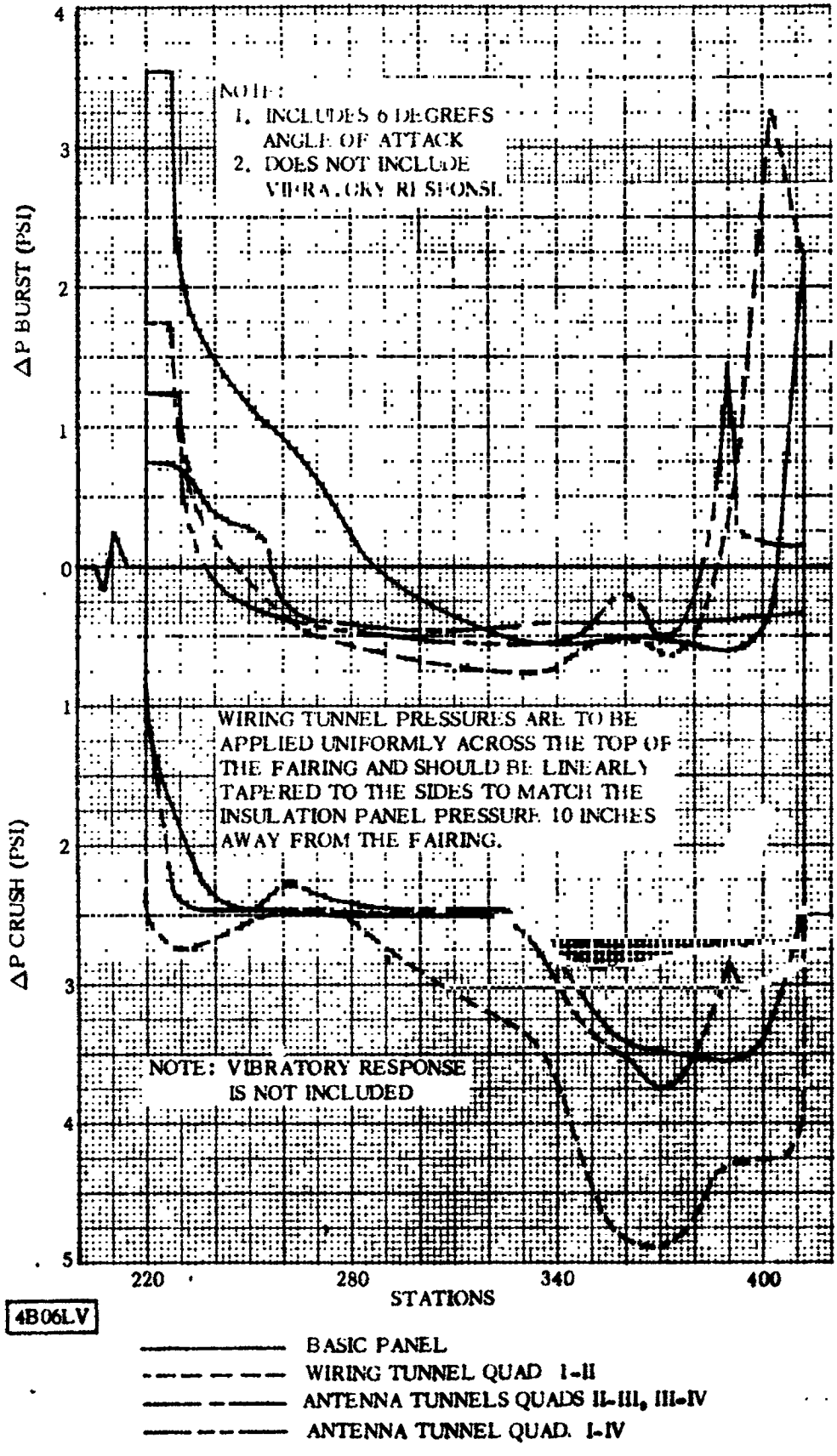

Figure 3.2-5. Liquid Hydrogen Insulation Panels - Aerodynamic Pressure Loads

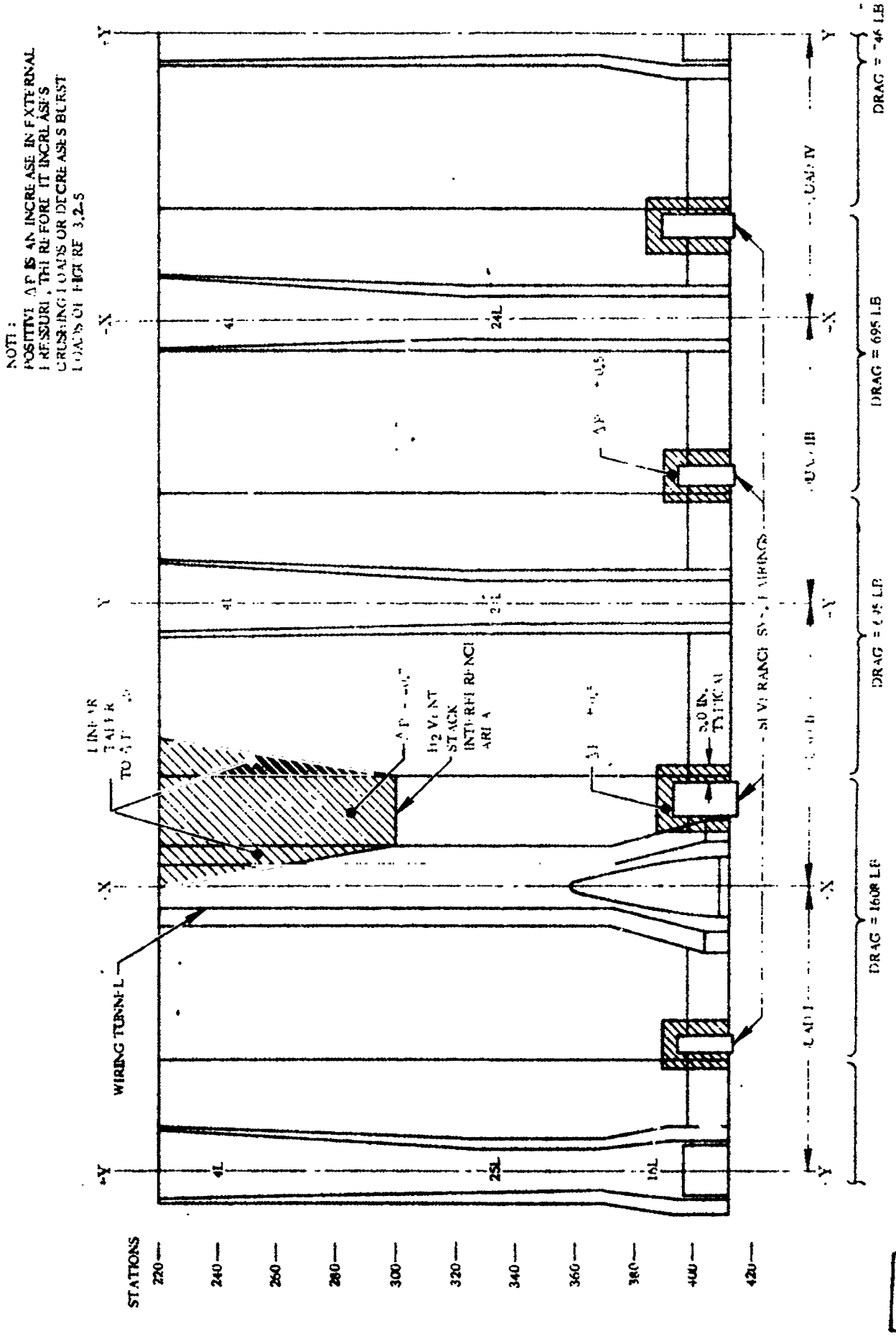

Figure 3.2-6. Liquid Hydrogen Tank Insulation Panels and Pods - Local Air Loads and Drag

Ground wind loads on the insulation panels during assembly of the vehicle are shown in Figure 3.2-7 for a 25 knot wind. The two loading condition shown are not to be superimposed but should be applied independently of each other. A factor of 2.0 shall be applied to the loads to account for dynamic effects.

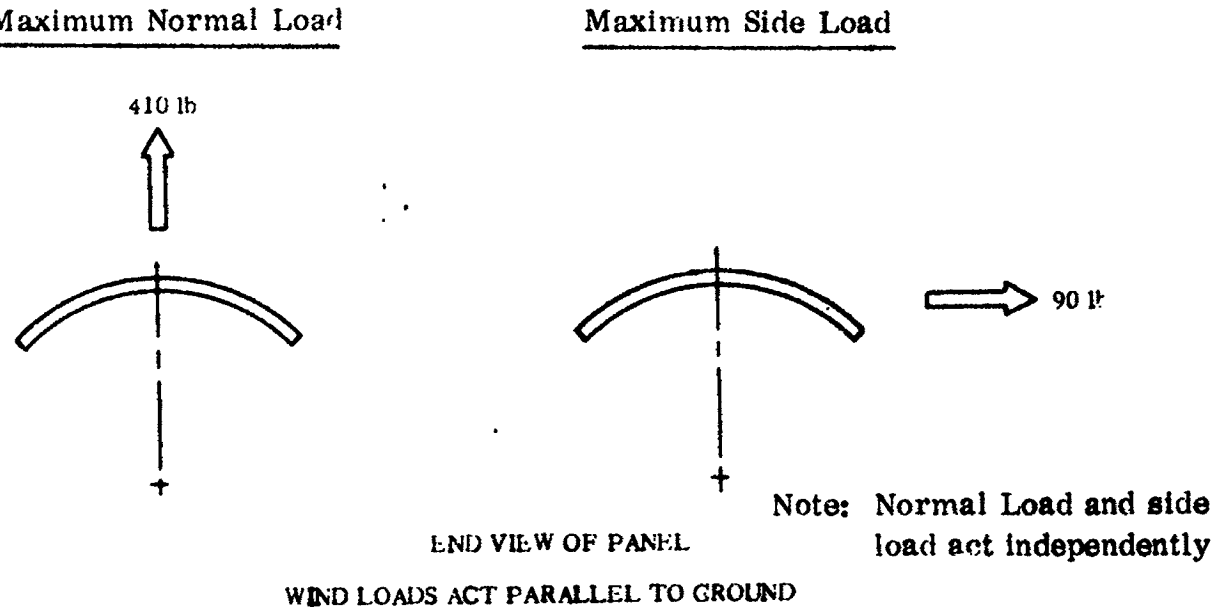

Figure 3.2-7. Insulation Panel Ground Wind Loads During Erection

Aerodynamic coefficients on the panels during jettison were obtained in terms of components normal and tangential to the panels. Nomenclature and sign conventions for these loads are shown in Figure 3.2-8. Force coefficient data for panel rotations, γ, up to 60° and vehicle angles of attack, α, up to 30° are shown in Figures 3.2-9 through 3.2-12. During normal operation the panel hinges do not separate from the vehicle until they have rotated about 55°.

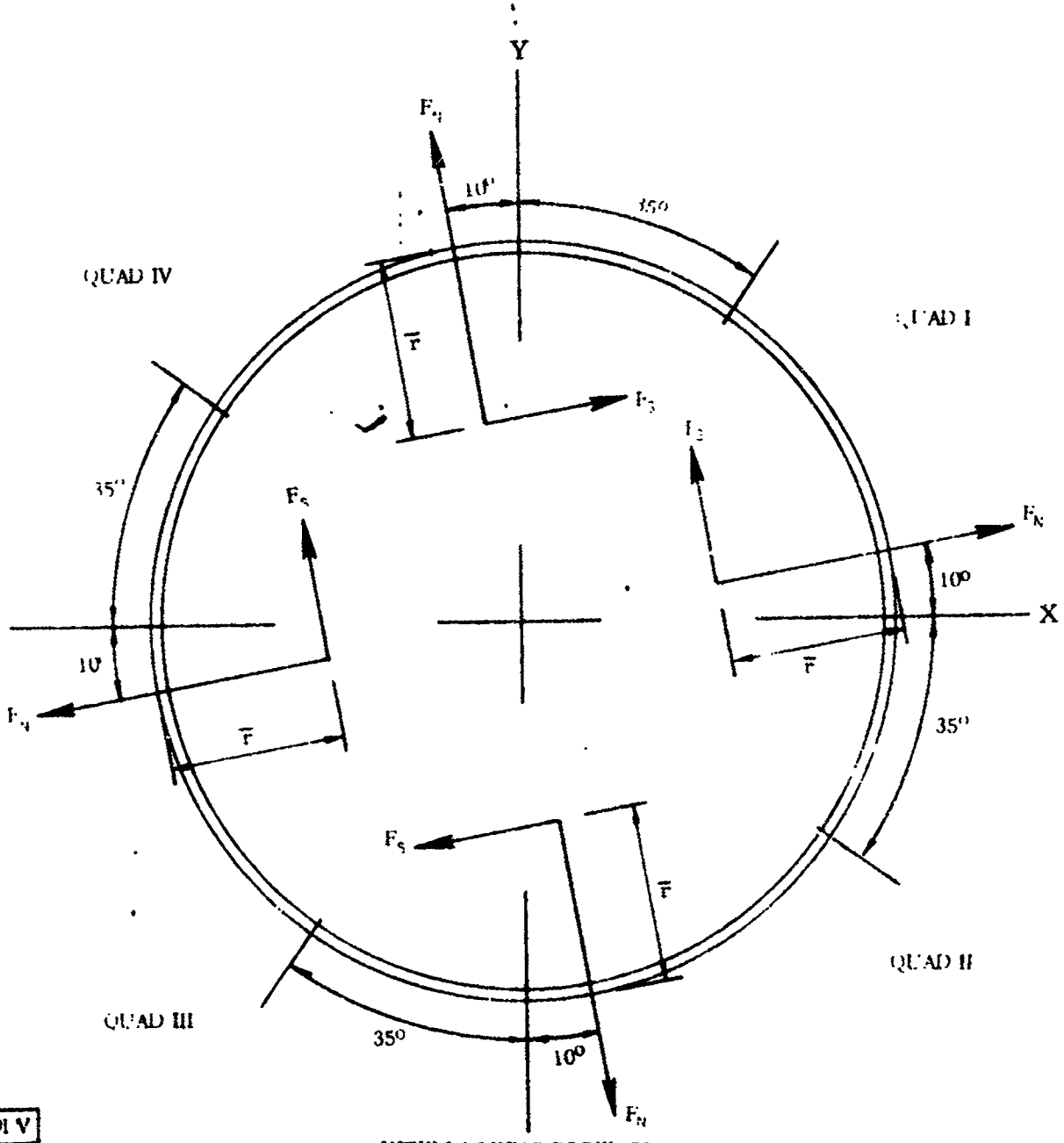

VIEW LOOKING FORWARD
(γ = 0° for all panels)

F_N = Normal force (lb)
F_S = Side force (lb)

$$C_N = \frac{F_N}{qA}$$

$$C_S = \frac{F_S}{qA}$$

q = Dynamic pressure (psf)
A = Panel projected areal normal to F_N (ft^2)

l = Panel length (ft)
$\bar{z}$ = Distance from forward end of panel to center of pressure of F_N and F_S (ft)
$\bar{r}$ = Radial offset for F_S = 5 ft

α = Vehicle angle of attack in the pitch plane (degrees)
γ = Panel rotation angle (degrees)
X,Y = Vehicle axis

Figure 3.2-8. Centaur Insulation Panel Sign Convention and Nomenclature for Aerodynamic Coefficients during Jettison

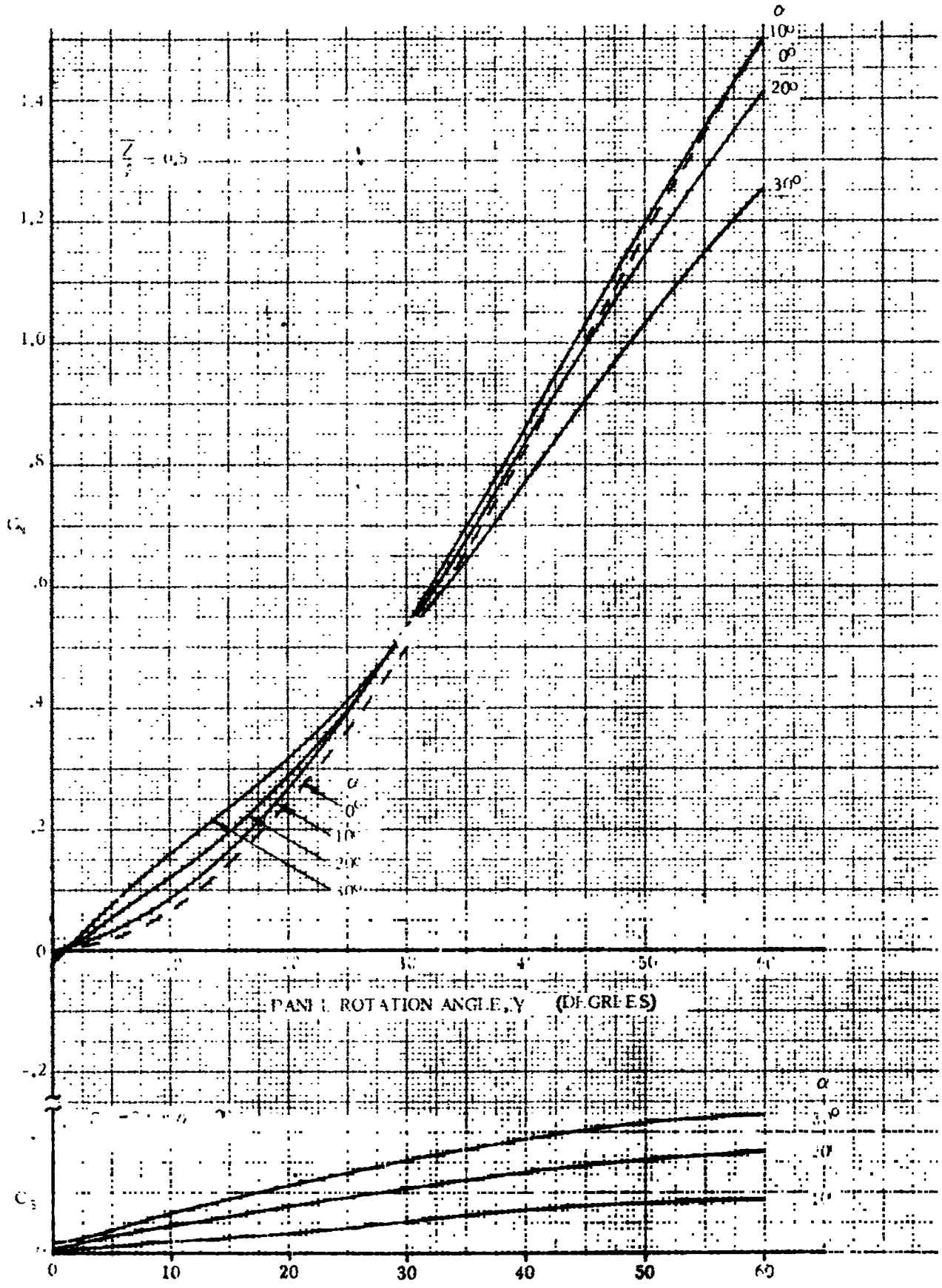

Figure 3.2-9. Centaur Insulation Panel Aerodynamic Coefficients during Jettison (Panel Attached to the Vehicle) Quad I - II Panel

4B10LV

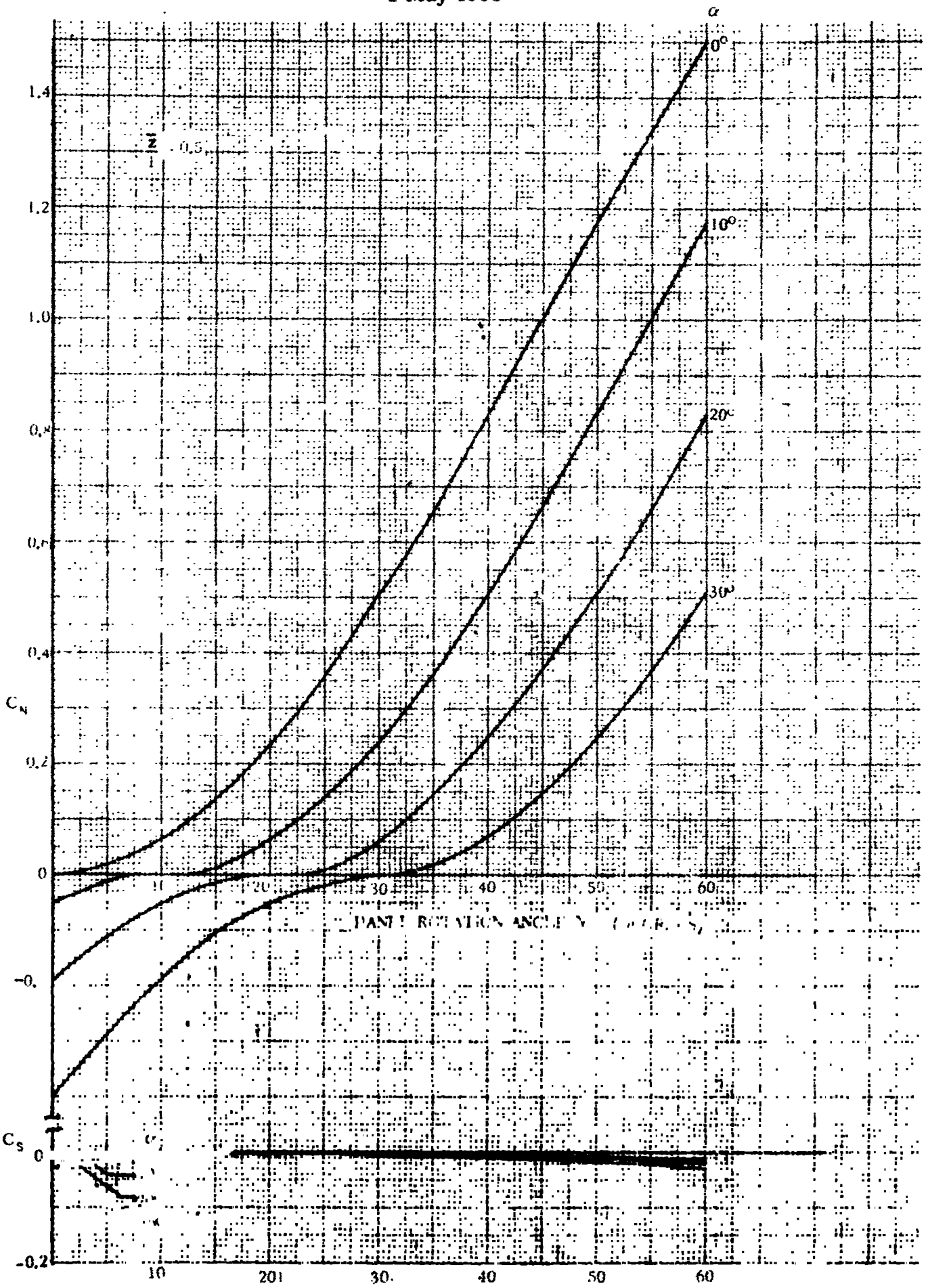

Figure 3.2-10. Centaur Insulation Panel Aerodynamic Coefficients during Jettison (Panel Attached to the Vehicle) Quadrant II - III Panel

4B11LV

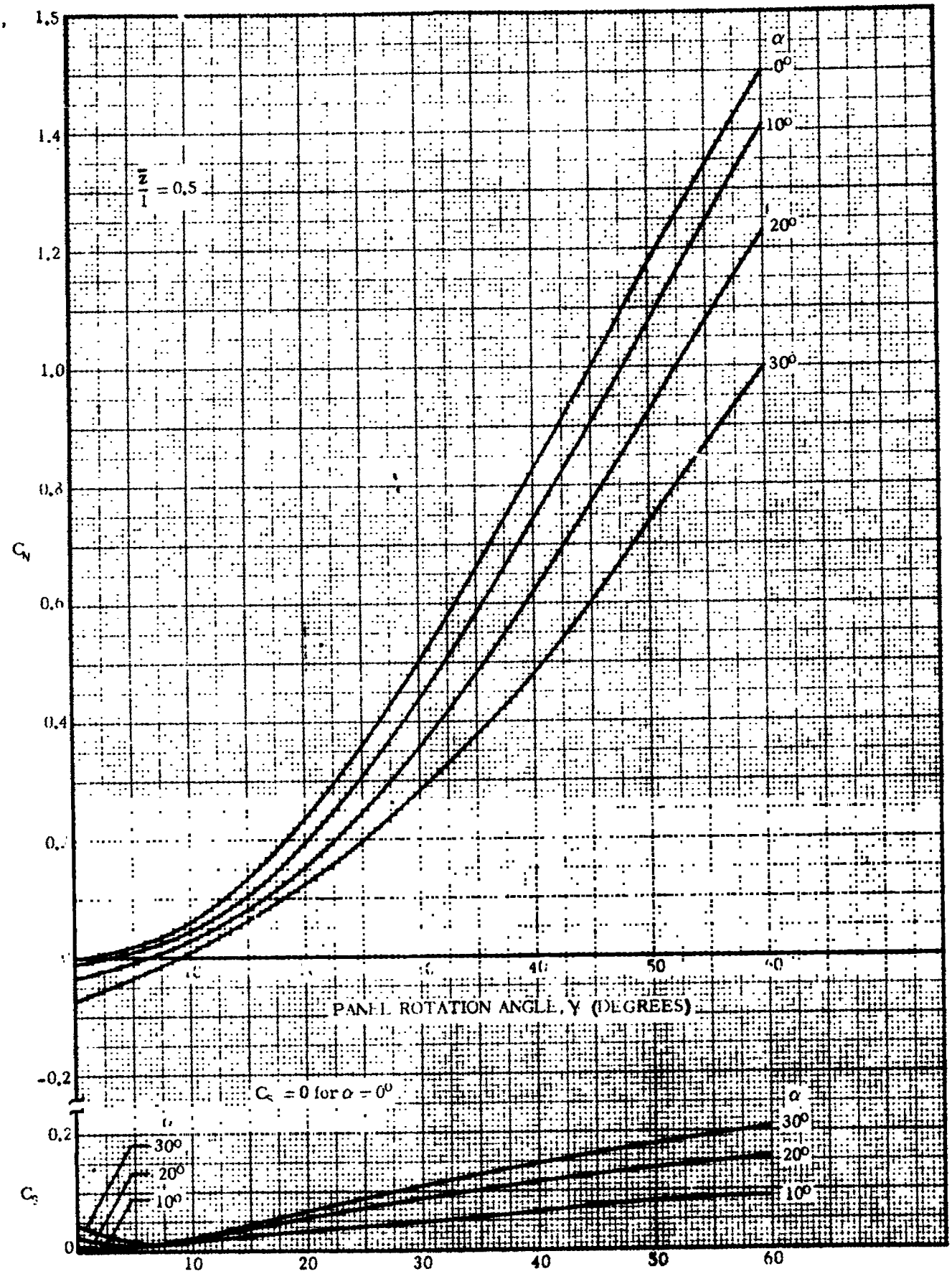

Figure 3.2-11. Centaur Insulation Panel Aerodynamic Coefficients during Jettison (Panel Attached to the Vehicle) Quadrant III - IV Panel

4B12LV

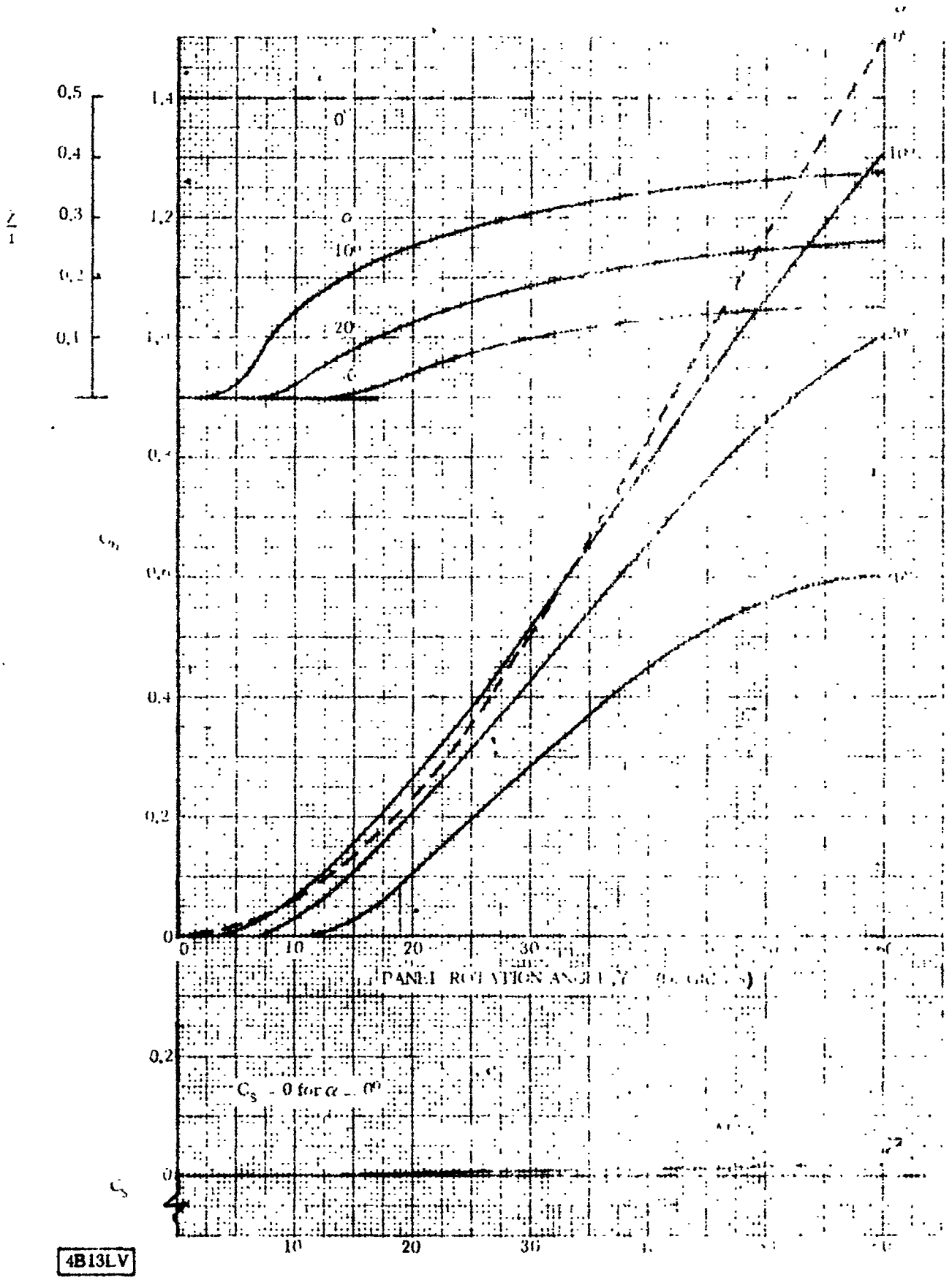

Figure 3.2-12. Centaur Insulation Panel Aerodyn[illegible] (Panel Attached to the Vehicle)

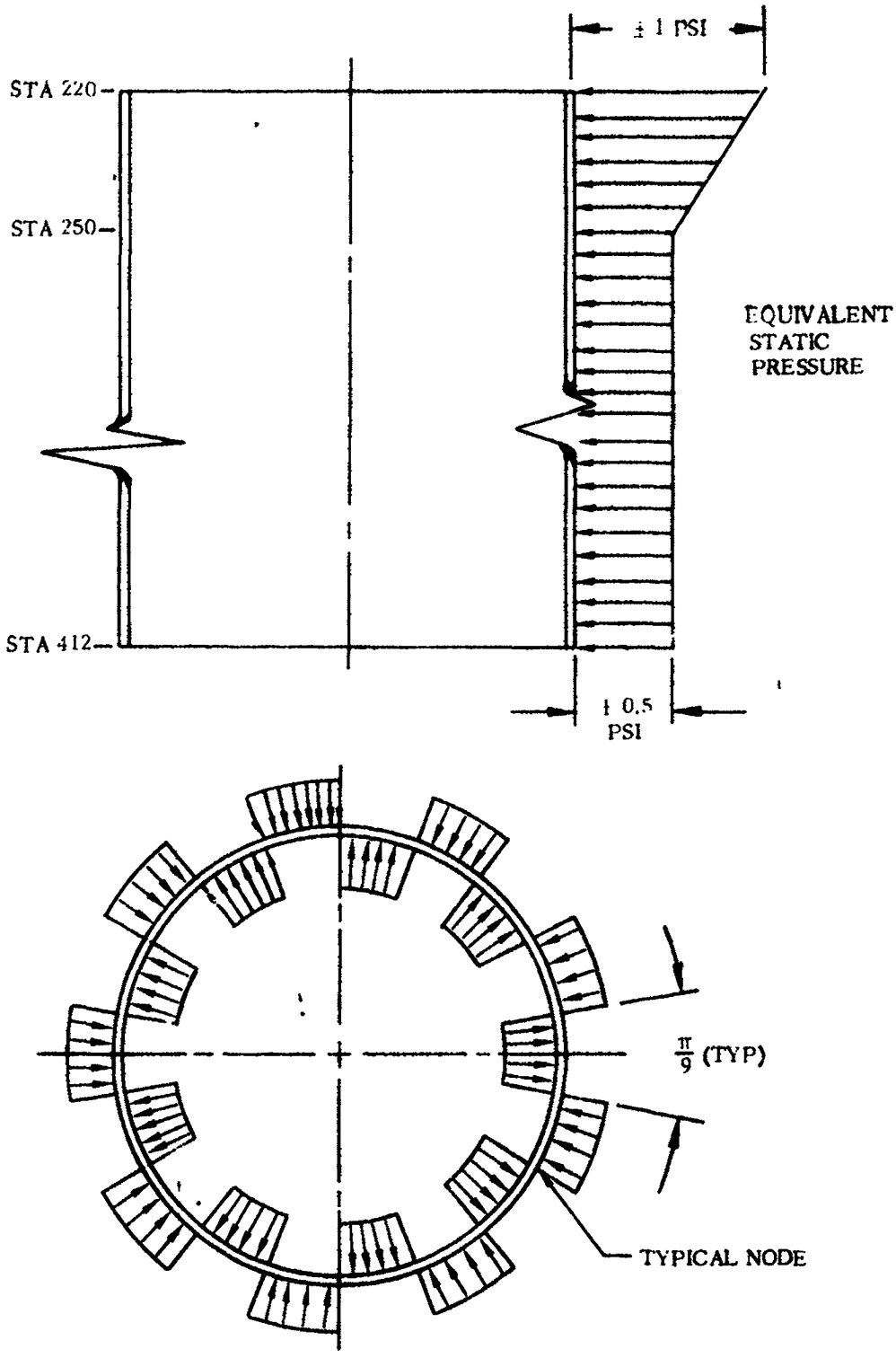

4B08LV

Figure 3.2-13. Basic Panel Vibratory Loads

3.2.6 BUFFET AND FLUTTER LOADS. Buffet loads occur on the Atlas/Centaur vehicle as it passes through the transonic speed range ($0.75 < M < 1.10$). Fluctuating pressures couple with the burst pressures, especially near Station 220 to cause vibration of the insulation panels. An equivalent static pressure distribution of the vibratory loads is shown in Figure 3.2-7. For analysis purposes it shall be assumed that the panels are cylindrical and the tunnels are neglected. This is a conservative assumption since the raised tunnels are reinforced with denser core and thicker skins.

The effect of Chevalier buffeting (alternate boundary layer separation and attachment) has been conservatively evaluated and found not to be a design contribution to the basic panel pressure envelope. Should liftoff occur forward of Station 230, the dynamic load of the vibrating panels could cause a line load of 2.77 pounds per inch on the liquid hydrogen tank for a liftoff deflection of 0.1 inch at Station 220 decreasing linearly to zero at Station 230. The panels are pretensioned to avoid liftoff, therefore, this is an emergency condition only.

3.2.7 MISCELLANEOUS LOAD PARAMETERS. No other critical loads are imposed on the basic insulation panels.

3.3 PODS 4L AND 24L (QUADRANTS II - III, III - IV)

Pods 4L and 24L form tunnels which run the length of the insulation panels along the Y-Y axis between Quadrants II and III and along the X-X axis between Quadrants III and IV. The tunnels are fabricated integral with the basic insulation panels, but have a denser honeycomb core and thicker skins. The panel containing pods 4L and 24L is shown in Figure 3.3-1. The outer skin tapers from 0.015 inches on the basic panel to 0.065 inches on the pods, while the inner skin tapers from 0.015 inches for the basic skin to 0.035 inches inside the tunnel. A 3.1 pounds per cubic foot Fiberglas honeycomb core is used in the tunnel area and in the basic panel.

REFERENCE
DRAWING NO. 55-74204

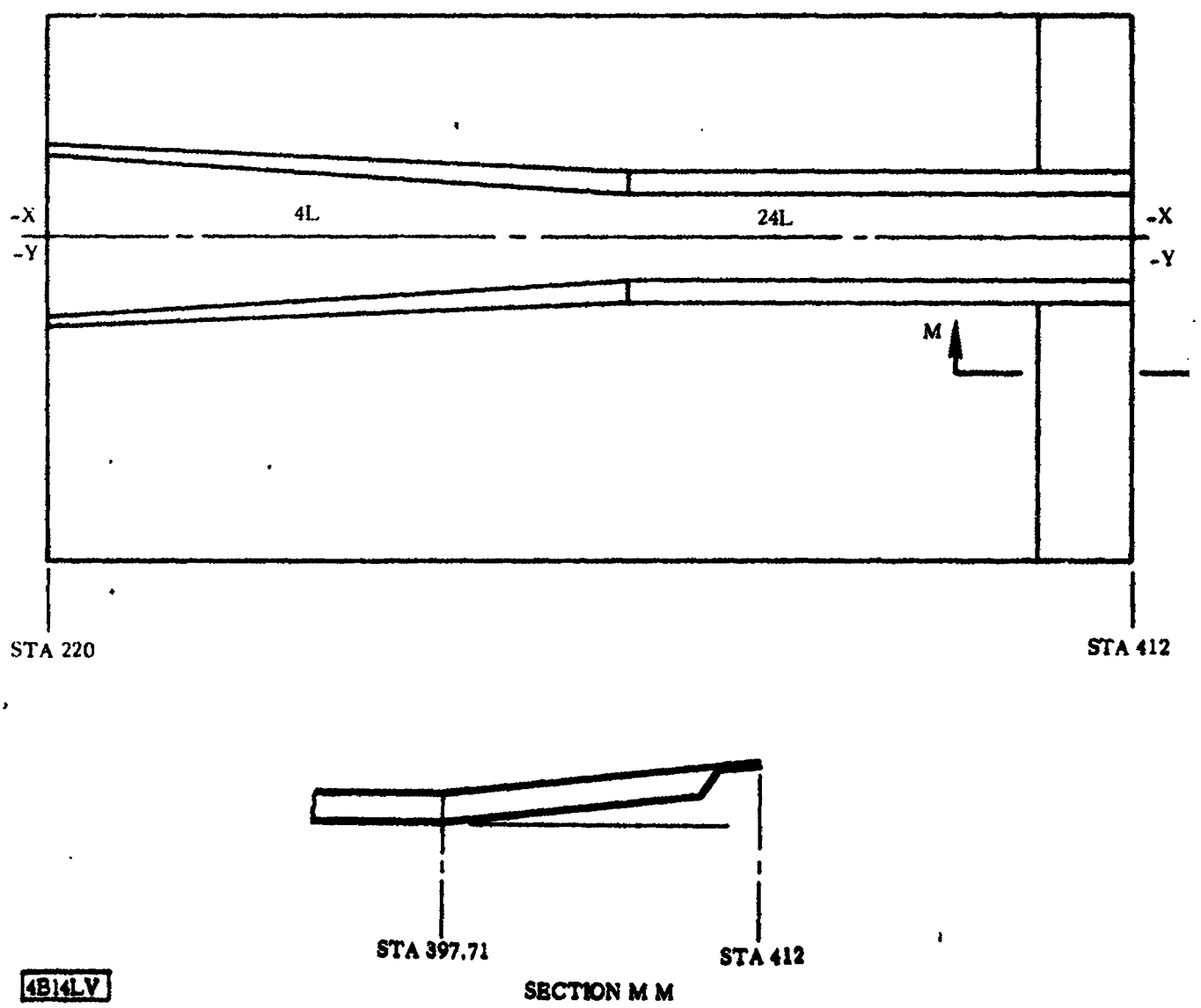

Figure 3.3-1. Liquid Hydrogen Tank Insulation Panel, Quadrants II - III and III - IV

3.3.1 CRITICAL CONDITIONS. Pods 4L and 24L experience loading conditions similar to those of the basic panels, namely, initial preload, additional tension due to tank expansion during flight, aerodynamic loads and heating, longitudinal acceleration at BECO, and jettison loads.

3.3.2 WEIGHTS AND CENTER OF GRAVITY DATA. The pod weights and C.G.'s are included in the data for the basic insulation panels because pods 4L and 24L are fabricated integral with the basic panel.

3.3.3 THERMAL DATA. Temperature maximums during flight are presented for pods 4L and 24L in Figure 3.3-2. The temperatures presented do not include the effects of any Thermolag such as described in Paragraph 3.2.3 which will lower the temperatures in the aft portion of the basic panel skins.

3.3.4 INERTIA LOADS. Inertia loads on pods 4L and 24L are the same as those of the basic panel presented in Paragraph 3.2.4.

3.3.5 STEADY-STATE AIR LOADS. A steady-state burst and crushing pressure distribution for pods 4L and 24L (antenna tunnel) is shown in Figure 3.2-5. Drag loads on the pods (4L, 24L) and side loads on the pods due to a six degree angle of attack are shown in Figure 3.3-3.

3.3.6 BUFFET AND FLUTTER LOADS. Vibratory loads on pods 4L and 24L are shown in Figure 3.3-3 in terms of an equivalent static pressure which must be added to the steady-state air loads to obtain the total burst or crushing pressure on the pods.

3.3.7 MISCELLANEOUS LOAD PARAMETERS. No other loads are critical for pods 4L and 24L.

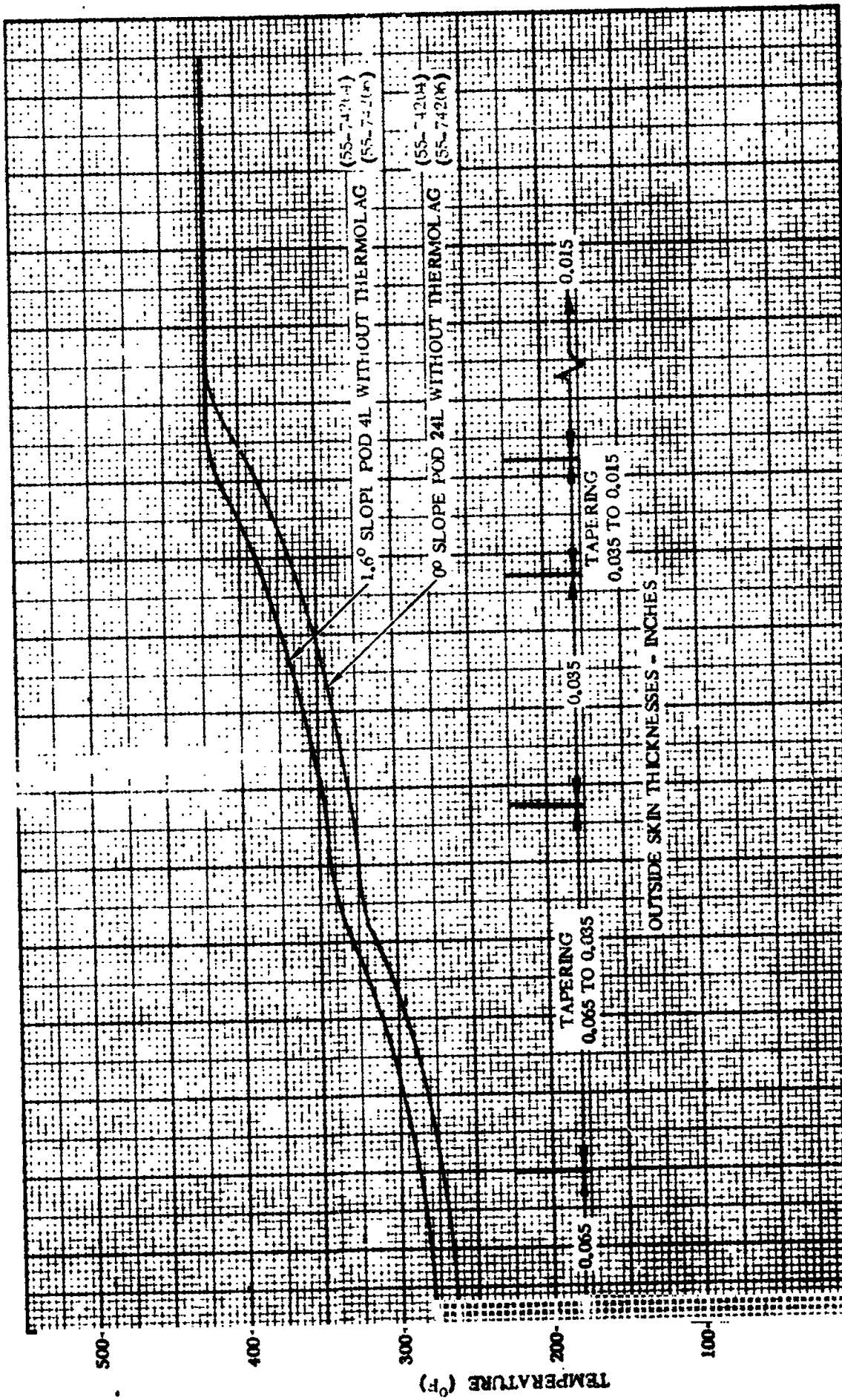

Figure 3.3-2. Insulation Panels Maximum Temperature Distribution in the Area of the Quadrants II-III and III-IV Tunnels

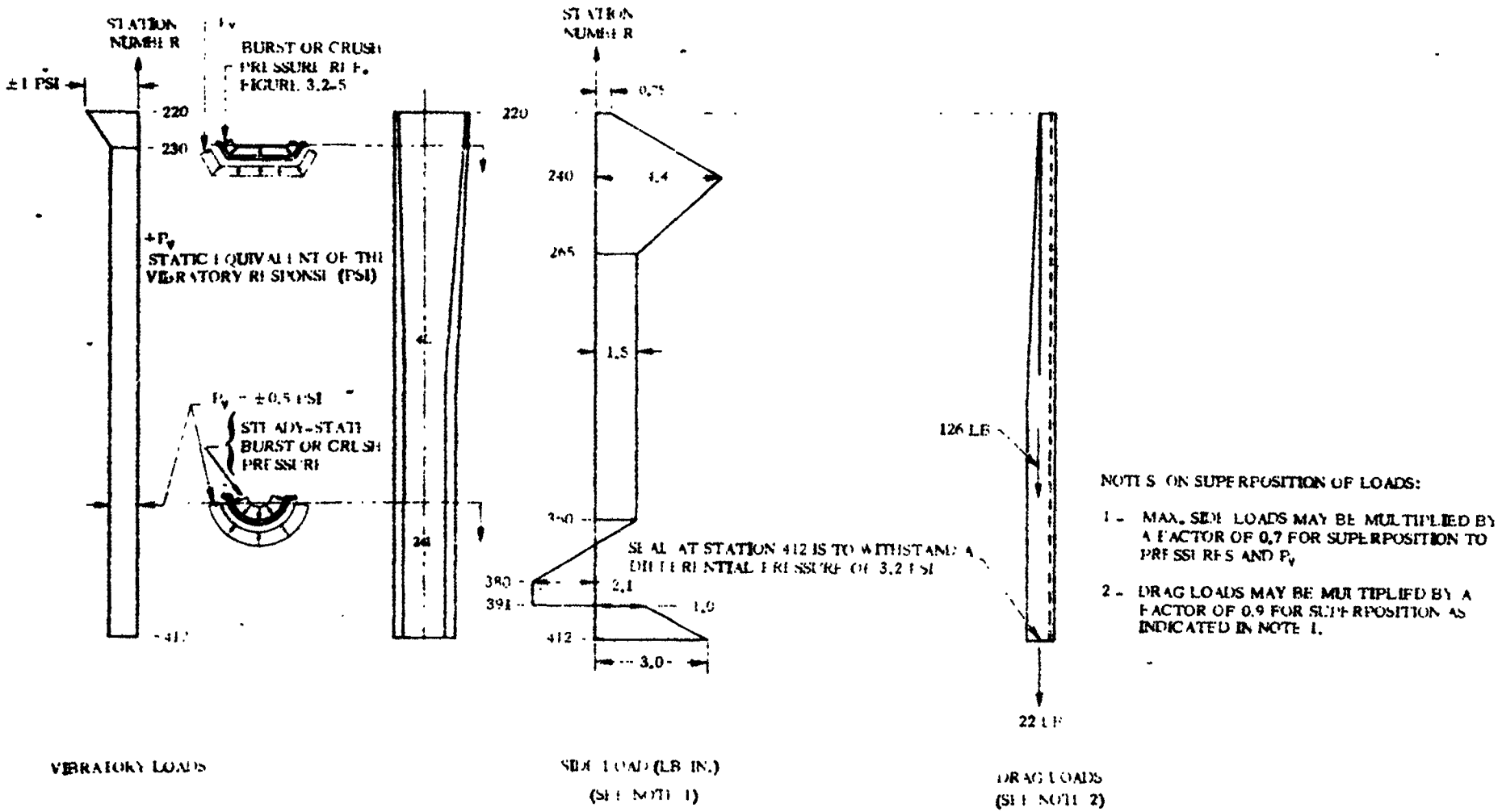

Figure 3.3-3. Pods 4L and 24L Along the Y-Y Axis, Between Quadrants II and III and Along the X-X Axis, Between Quadrants III - IV - Design Loads

3.4 PODS 4L, 25L, 16L (QUADRANTS I - IV)

Pods 4L, 25L, and 16L form a tunnel which runs the length of the insulation panel along the Y-Y axis between Quadrants I and IV. The tunnel is fabricated integral with the basic insulation panels as shown in Figure 3.4-1. The skins and core for this tunnel are the same as for pods 4L and 24L as described in Subsection 3.3.

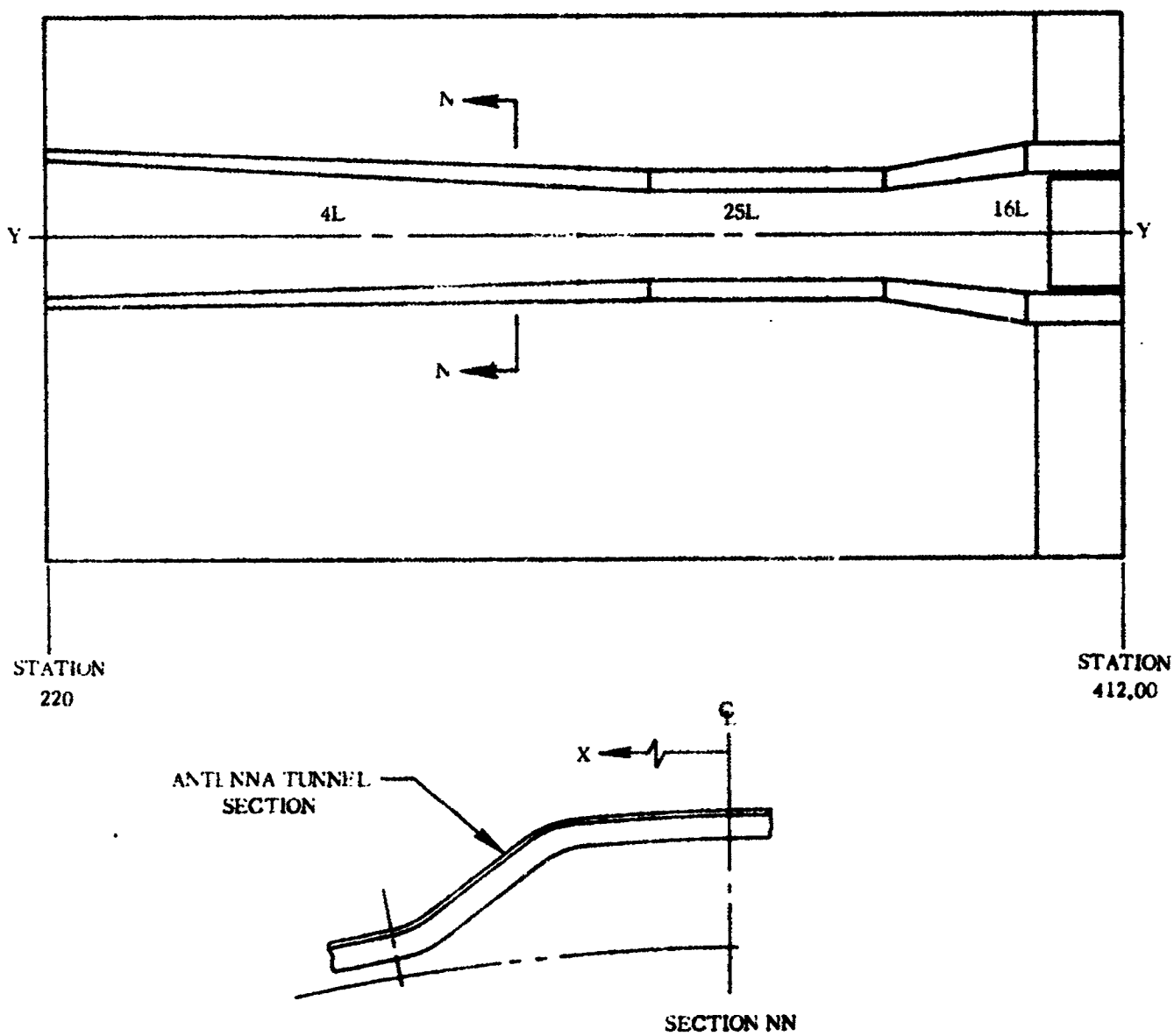

4B171.V

Figure 3.4-1. 55-74206 Insulation Panel, Quadrant I - IV

3.4.1 CRITICAL CONDITIONS. Pods 4L, 25L, and 16L experience loading conditions similar to those of the basic insulation panels and pods 4L and 24L (see Paragraph 3.3.1).

3.4.2 WEIGHTS AND CENTER OF GRAVITY DATA. The pod weights and C.G.'s are included in the data for the basic insulation panels because pods 4L, 25L, and 16L are fabricated integral with the basic panel.

3.4.3 THERMAL DATA. Temperature maximums during flight are presented for pods 4L. 25L, and 16L in Figure 3.4-2. The effects of any Thermolag such as described in Paragraph 3.2.3 will lower the temperatures in the aft portions of the basic panel skins.

3.4.4 INERTIA LOADS. Inertia loads on pods 4L, 25L, and 16L are the same as those experienced by the basic panel presented in Paragraph 3.2.4.

3.4.5 STEADY-STATE AIR LOADS. A steady-state burst and crushing pressure distribution for pods 4L, 25L, and 16L (antenna/vent tunnel) is shown in Figure 3.2-5. Drag loads on the pods (4L, 25L, 16L) and side loads on the pod due to a six degree angle of attack are shown in Figure 3.4-3.

3.4.6 BUFFET AND FLUTTER LOADS. Vibratory loads on pods 4L, 25L, and 16L are shown in Figure 3.4-3 in terms of an equivalent static pressure which must be added to the steady-state air loads to obtain the total burst or crushing pressure on the pods.

3.4.7 MISCELLANEOUS LOAD PARAMETERS. No other loads are critical for pods 4L, 25L, and 16L.

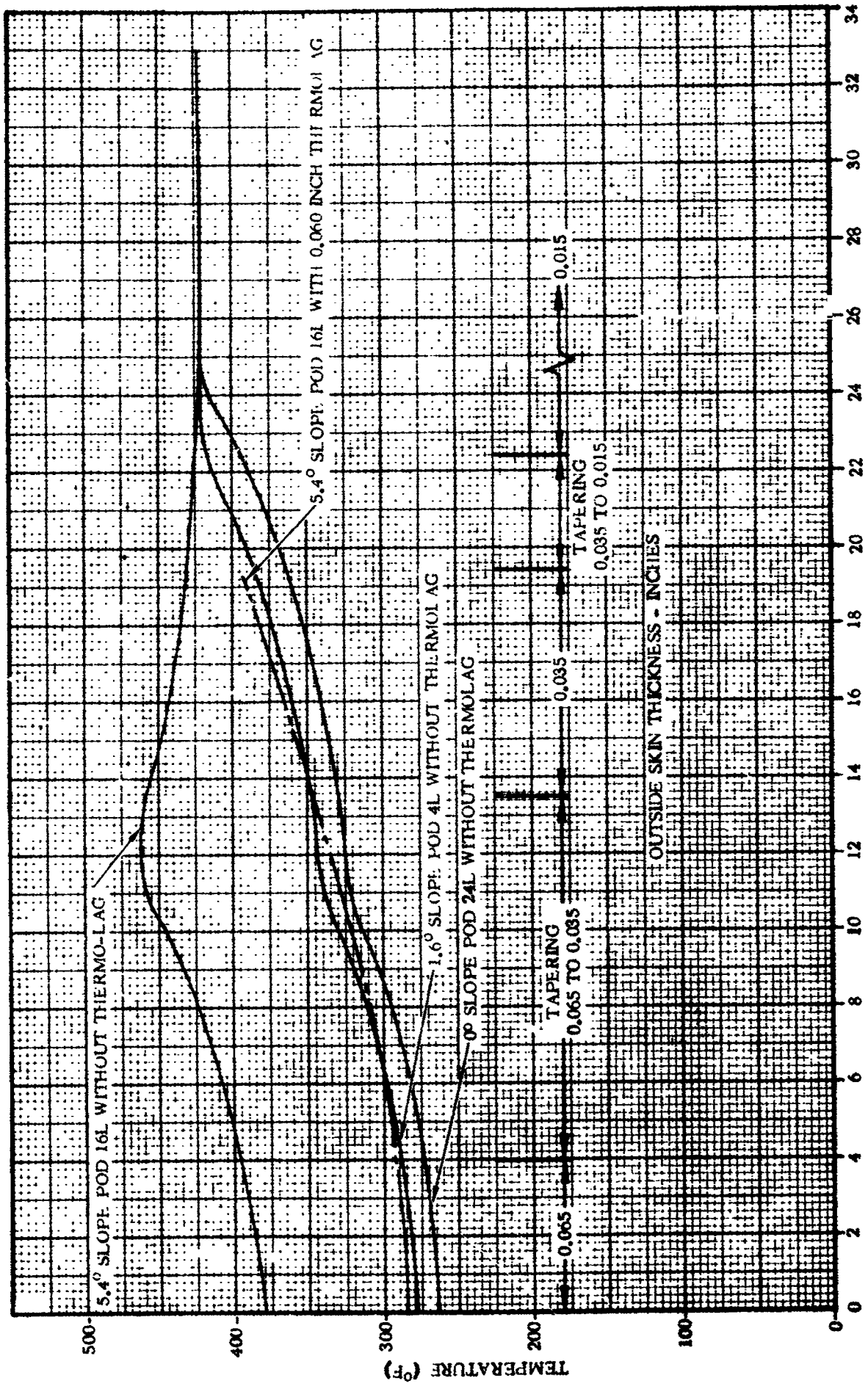

Figure 3.4-2. Insulation Panels Maximum Temperature Distribution in the Area of the Quadrant I - IV Tunnel (55-74206 Panel)

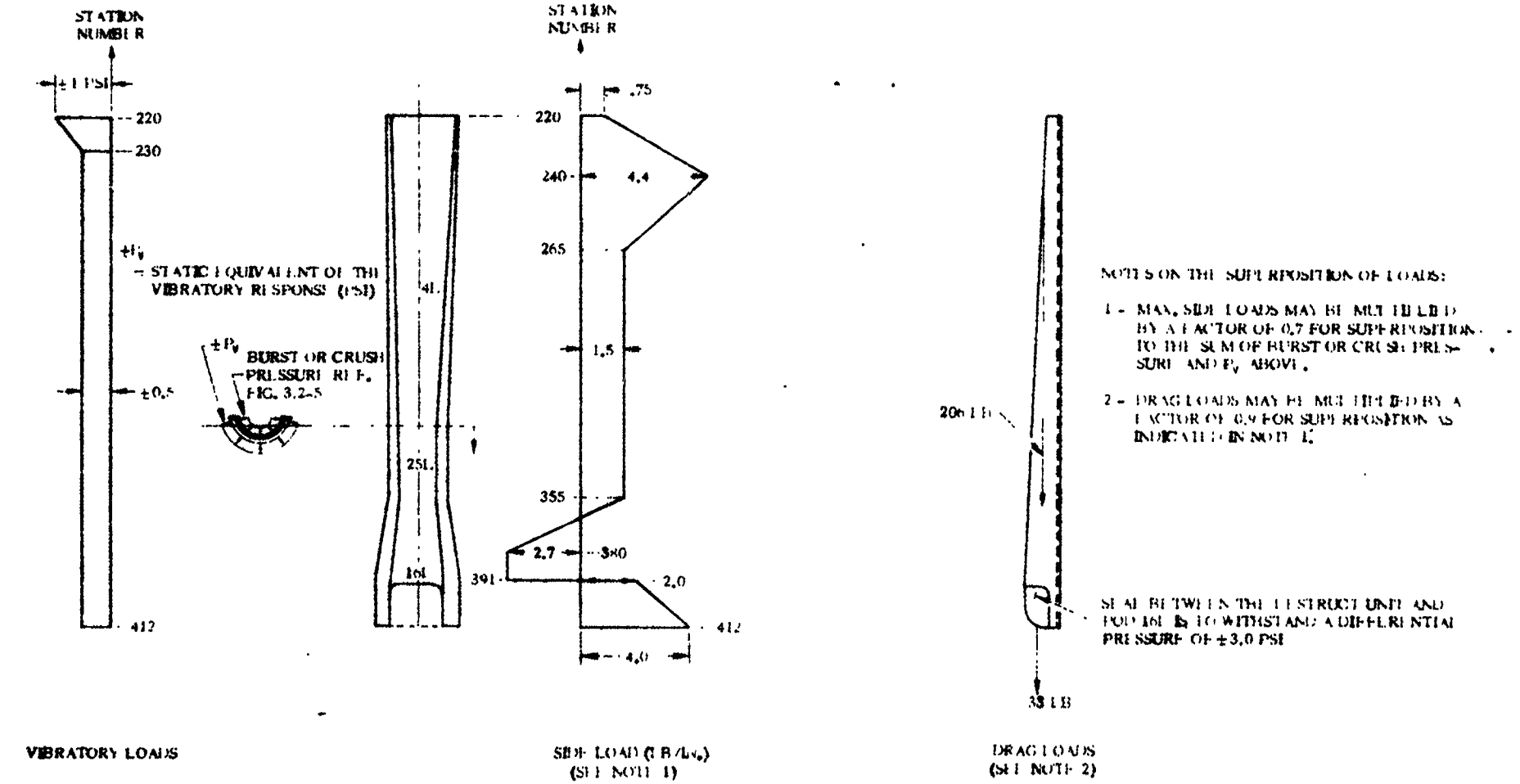

4019LT

Figure 3.4-3. Pods 4L, 25L, and 16L Along the Y-Y Axis, between Quadrants I and IV - Design Loads

3.5 WIRING TUNNEL (QUADRANTS I - II)

The wiring tunnel runs the length of the insulation panels along the X-X axis between Quadrants I and II and is fabricated integral with the basic insulation panel. The panel containing the wiring tunnel is shown in Figure 3.5-1. The outer skin tapers from 0.015 inches on the basic panel to 0.080 inches on the wiring tunnel, and the inner skin tapers from 0.015 inches to 0.045 inches inside the wiring tunnel.

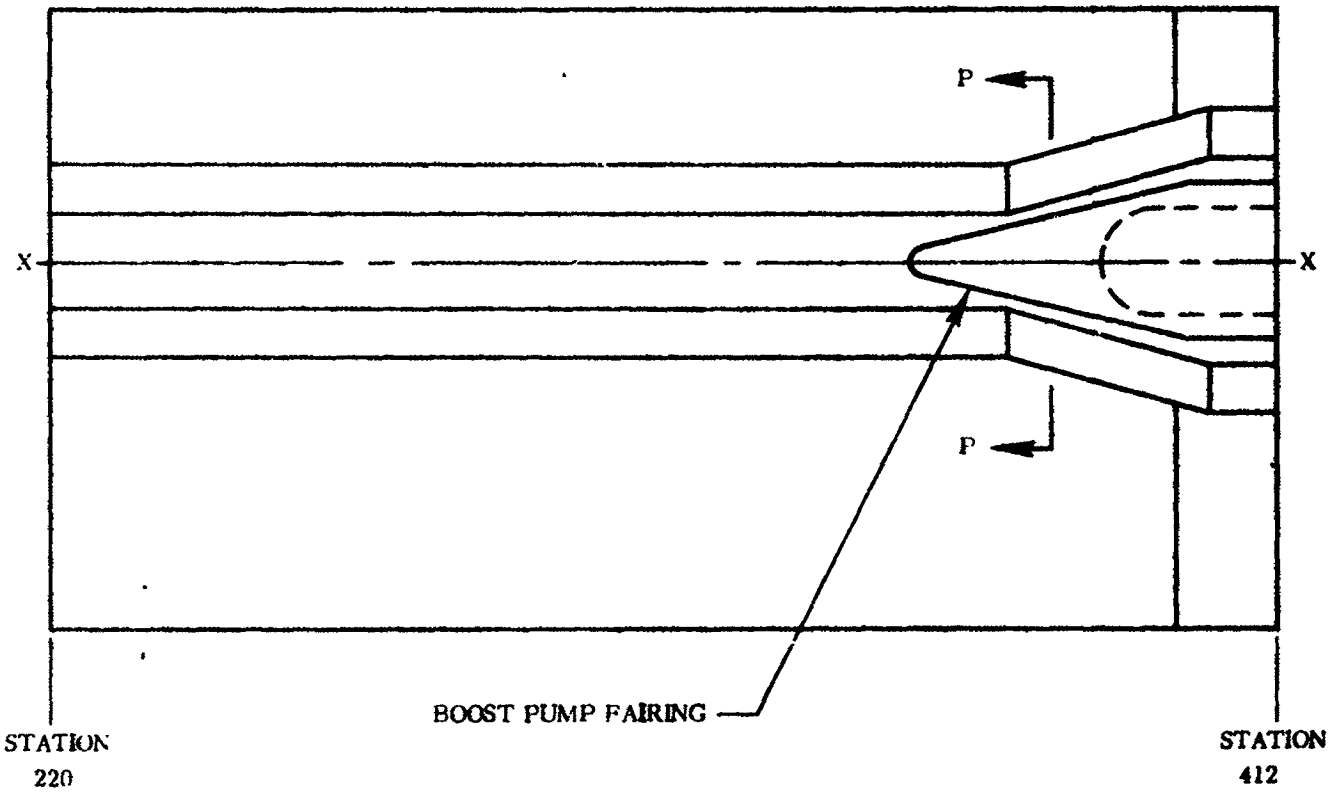

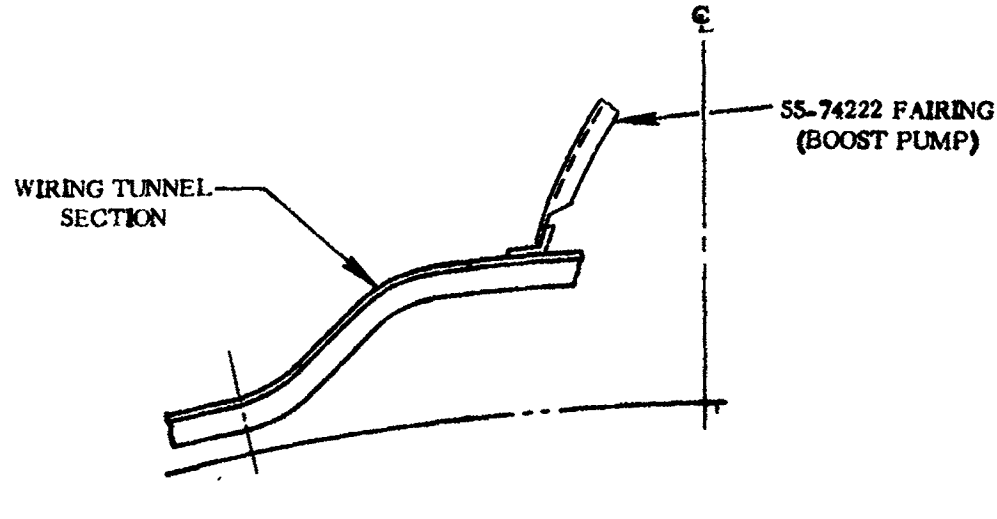

SECTION P-P

4B20LV

Figure 3.5-1. 55-74203 Insulation Panel, Quadrant I-II

3.5.1 CRITICAL CONDITIONS. The wiring tunnel experiences loading conditions similar to those of the basic panels, namely initial preload, additional tension due to tank expansion during flight, aerodynamic steady-state and buffet loads, aerodynamic heating, longitudinal acceleration at BECO, and jettison loads.

3.5.2 WEIGHTS AND CENTER OF GRAVITY DATA. The pod weights and C.G.'s are included in the data for the basic insulation panels because the wiring tunnel is fabricated integral with the basic panel (see Paragraph 3.2.2).

3.5.3 THERMAL DATA. Wiring tunnel maximum temperatures during flight are presented in Figure 3.5-2. The data does not include the effects of Thermolag which is applied to the aft portion of the tunnel to reduce the bondline temperature.

Insulation panel temperatures near the boost pump fairing are shown in Figure 3.5-3.

3.5.4 INERTIA LOADS. Inertia loads on the wiring tunnel are the same as those experienced by the basic panel presented in Paragraph 3.2.4.

3.5.5 STEADY-STATE AIR LOADS. Steady-state burst and crushing pressure distribution for the wiring tunnel is shown in Figure 3.2-5. Drag loads on the wiring tunnel and side loads due to a six degree angle of attack are shown in Figure 3.5-4. Loads on the boost pump fairing and boost pump fairing skirt are included since these protuberances are bolted to the wiring tunnel.

3.5.6 BUFFET AND FLUTTER LOADS. Vibratory loads on the wiring tunnel are shown in Figure 3.5-4 in terms of an equivalent static pressure which must be added to the steady-state air loads to obtain the total burst or crushing pressure on the pods. The loads on the boost pump fairing and boost pump fairing skirt are included since these protuberances are bolted to the wiring tunnel.

3.5.7 MISCELLANEOUS LOAD PARAMETERS. No other loads are critical for the wiring tunnel.

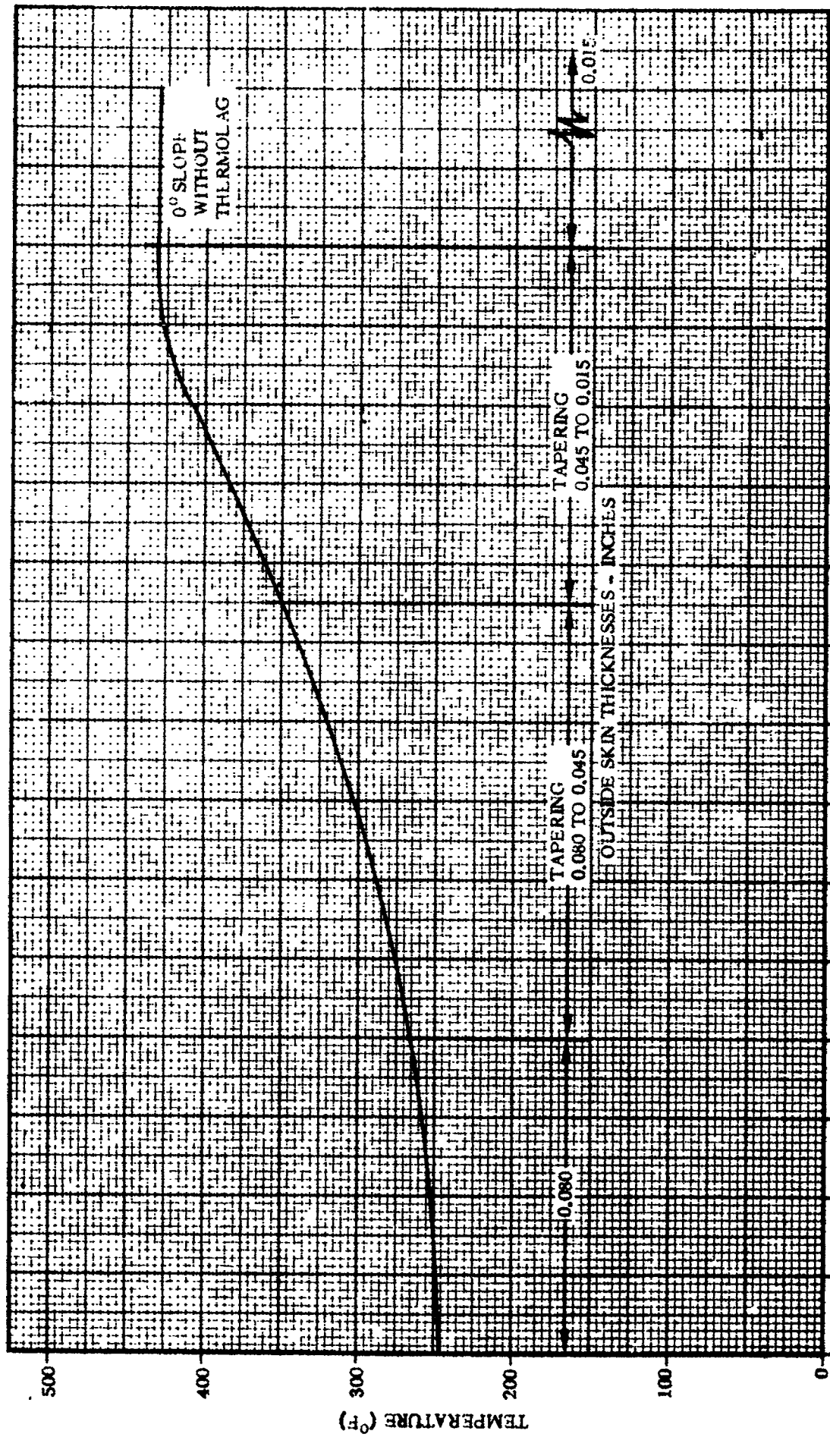

Figure 3.5-2. Insulation Panel (55-74203) Maximum Temperature Distribution Adjacent to Wiring Tunnel

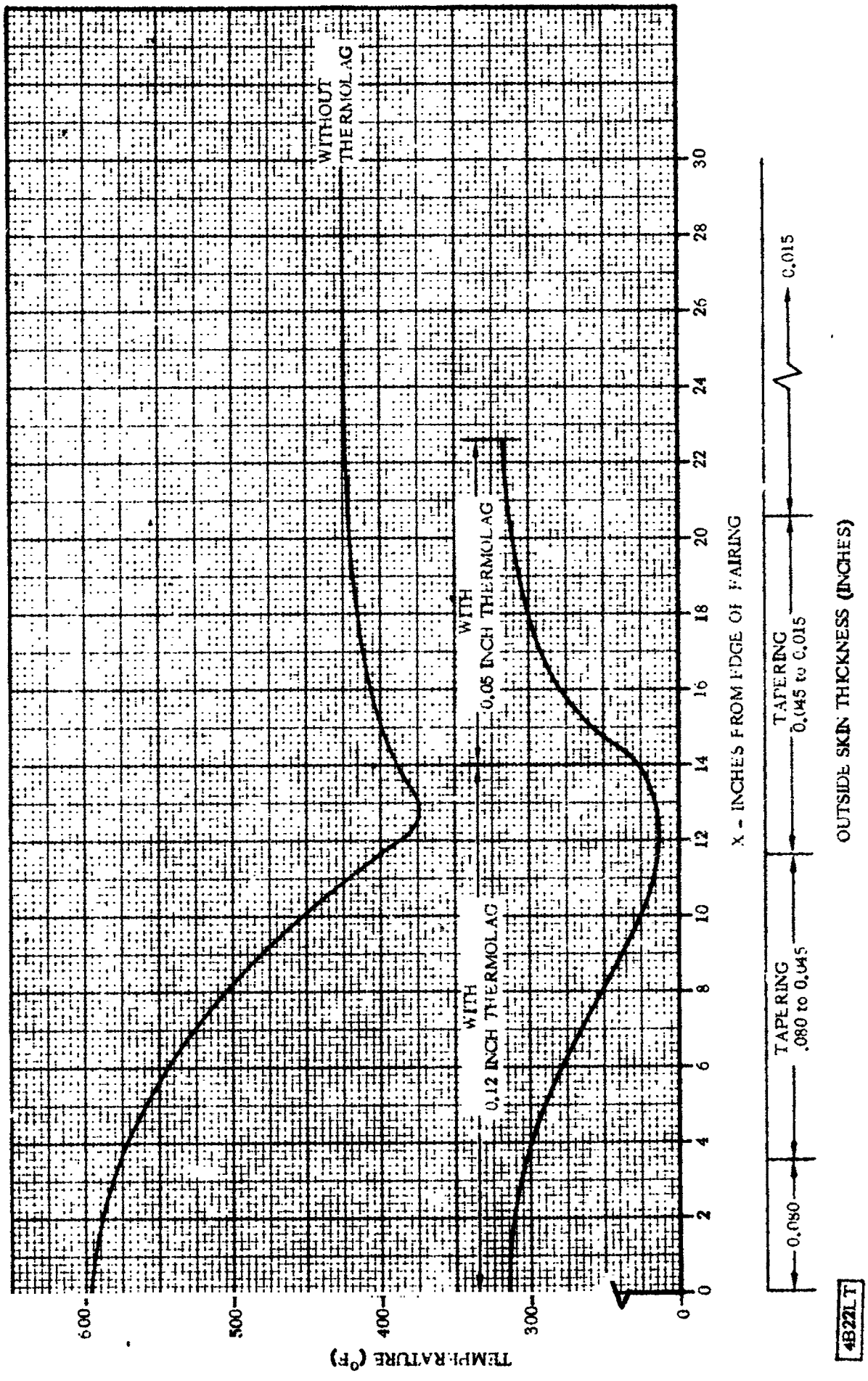

Figure 3.5-3. Insulation Panels Maximum Temperature Distribution Adjacent to Boost Pump Fairing

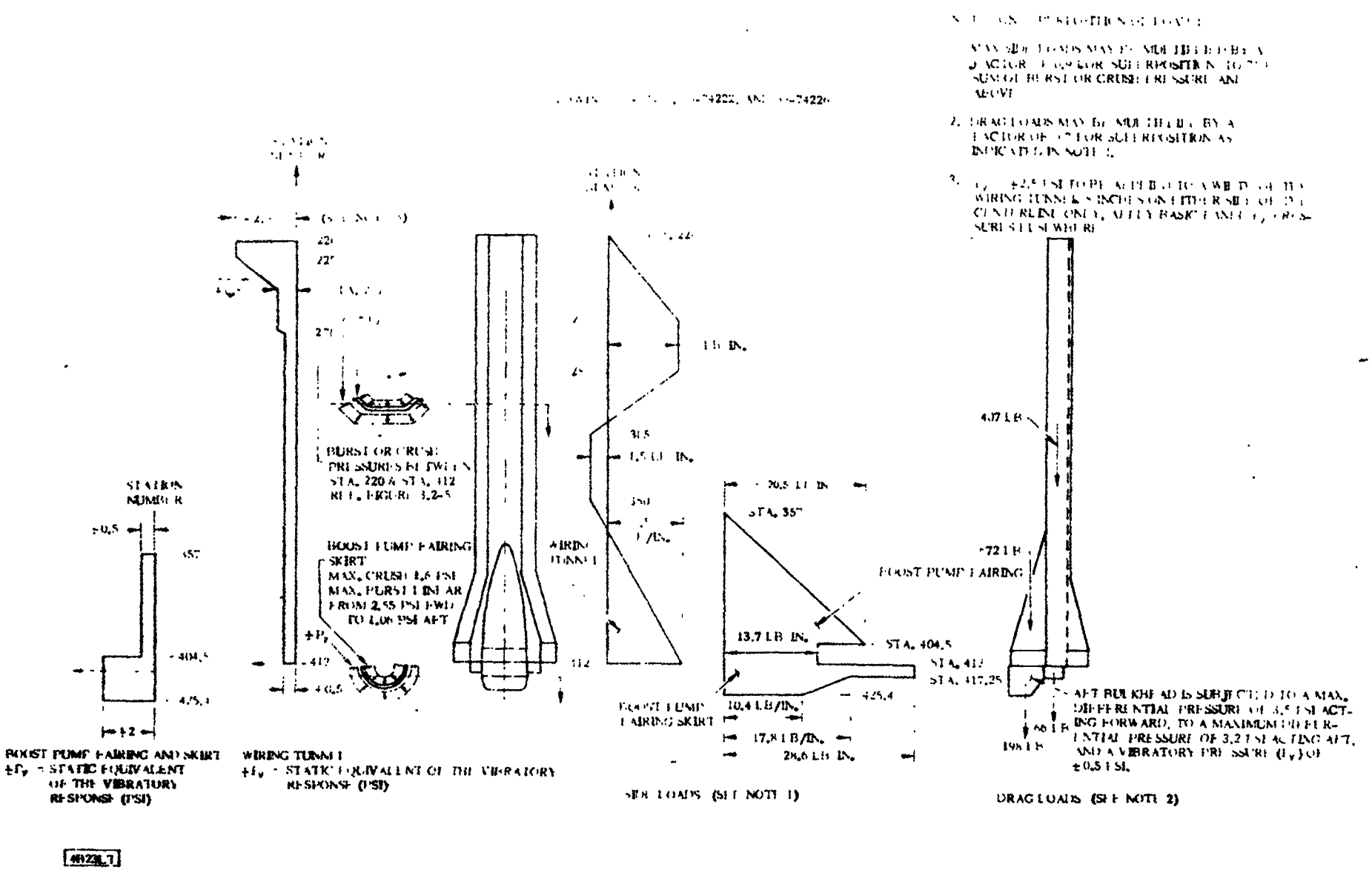

Figure 3.5-4. Wiring Tunnel and Boost Pump Fairing Along the X-X Axis, Quadrants I and II - Design Loads

THIS PAGE INTENTIONALLY LEFT BLANK.

3.6 BOOST PUMP FAIRING AND SKIRT

The boost pump fairing and skirt are mounted on the aft end of the wiring tunnel and are made of Fiberglas honeycomb sandwich and solid laminates of Fiberglas. A sketch of the boost pump fairing and skirt is shown in Figure 3.6-1.

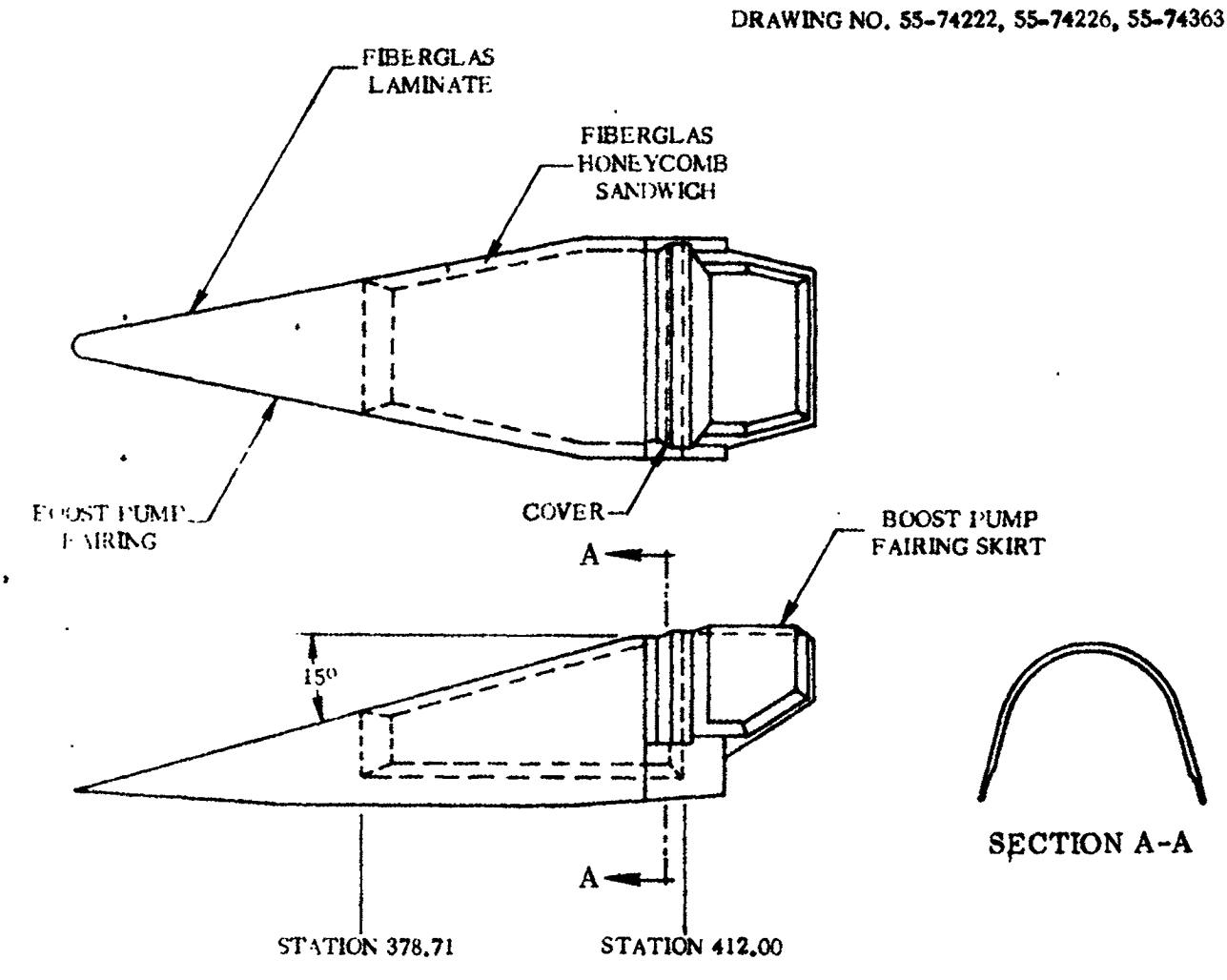

Figure 3.6-1. Boost Pump Fairing and Skirt

3.6.1 CRITICAL CONDITIONS. The boost pump fairing has two critical conditions, maximum aerodynamic load and maximum aerodynamic heating. The maximum aerodynamic load includes both steady-state and buffet loads which occur from the transonic speeds. Maximum aerodynamic heating occurs near the time of maximum longitudinal acceleration (BECO).

3.6.2 WEIGHTS AND CENTER OF GRAVITY DATA. Weight and C.G. data for the boost pump fairing and the boost pump fairing skirt are presented in Table 3.6-1.

TABLE 3.6-1. BOOST PUMP FAIRING AND SKIRT STRUCTURAL DESIGN WEIGHTS AND CENTERS OF GRAVITY DATA

Component	Weight (lb)	X - C.G. (in.)	Y - C.G. (in.)	Z - C.G. (in.)
Boost Pump Fairing	30	75	0	392
Boost Pump Fairing Skirt	11	73	0	415

3.6.3 THERMAL DATA. A temperature history of the boost pump fairing (55-74222) is shown in Figure 3.6-2. Point A is Fiberglas honeycomb sandwich construction and Points B and C are solid laminates of Fiberglas. Prior to launch Point B drops below -100° F due to the cold helium gas flowing in this region.

3.6.4 INERTIA LOADS. Steady-state inertia loads on the boost pump fairing and skirt are determined from the plot of (T-D)/W versus time presented in the mission design trajectories section (see Paragraph 1.3.3) of this report.

3.6.5 STEADY-STATE AIR LOADS. Aerodynamic loads on the boost pump fairing and boost pump fairing skirt are shown in Figure 3 5-4. The side loads are for a six degree angle of attack. Burst and crushing pressures on the boost pump fairing are included in Figure 3.2-5.

3.6.6 BUFFET AND FLUTTER LOADS. Vibratory loads on the boost pump fairing, skirt, and wiring tunnel are shown in Figure 3.5-4 in terms of an equivalent static pressure. Equivalent vibratory loads must be added to steady-state air loads to obtain the total burst or crushing pressure loads on the fairings.

3.6.7 MISCELLANEOUS LOAD PARAMETERS. No other loads are critical for the boost pump fairing and skirt.

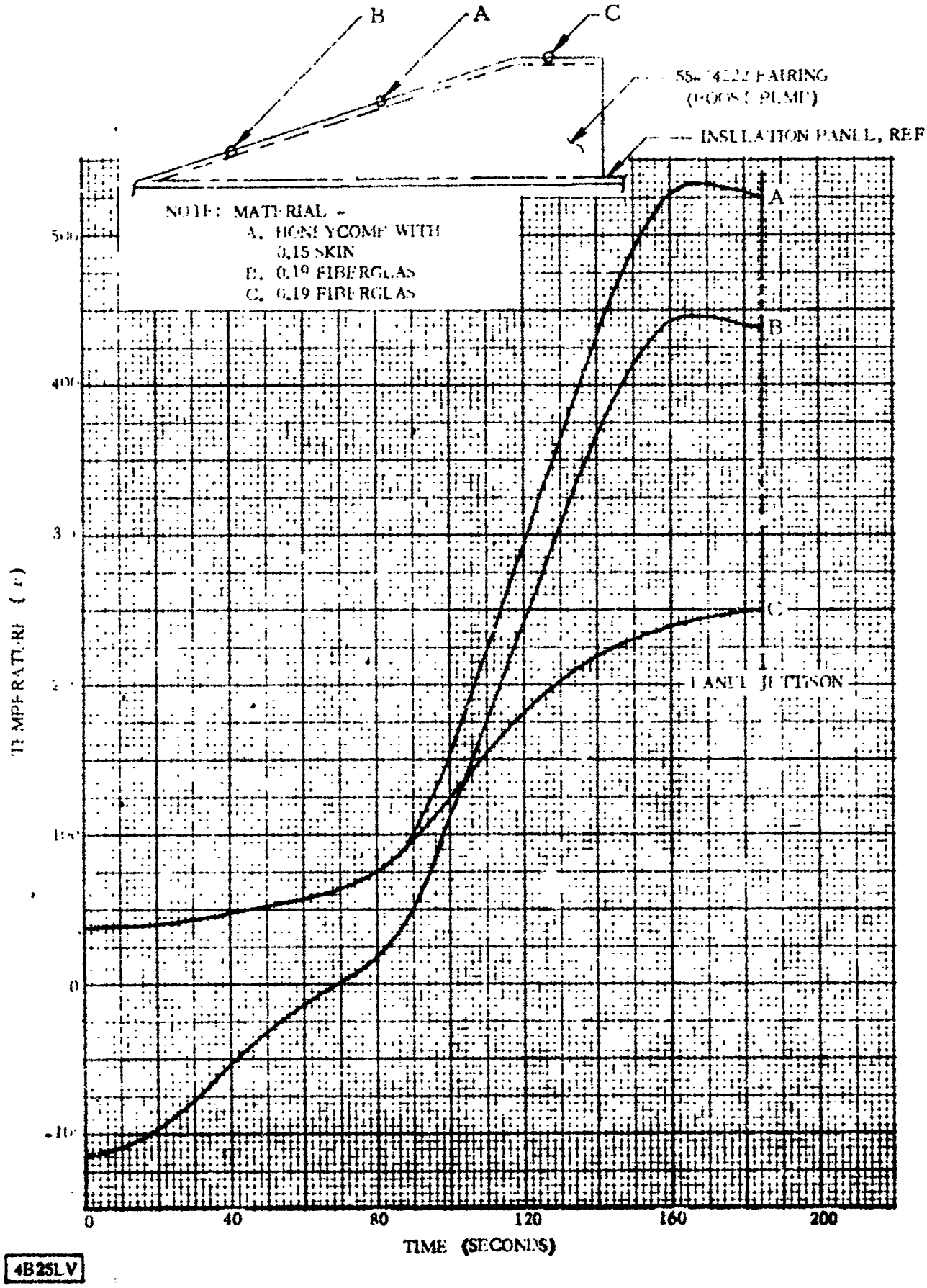

Figure 3.6-2. Boost Pump Fairing (55-74222) Temperature History

THIS PAGE INTENTIONALLY LEFT BLANK.

3.7 SEVERANCE SYSTEM FAIRINGS

The severance system fairings are located near the aft end of the insulation panels as shown in Figure 3.7-1. The fairings are made of Fiberglas laminate and are shown in Figures 3.7-2, 3.7-3, and 3.7-4.

3.7.1 CRITICAL CONDITIONS. The severance system fairings have two critical conditions, maximum aerodynamic load and maximum aerodynamic heating. Both steady-state and transient air loads are significant in flight from transonic speeds through Max α q. Maximum aerodynamic heating occurs near BECO and must not impair the structural integrity of the fairings or the severance system components which they protect.

3.7.2 WEIGHTS AND CENTER OF GRAVITY DATA. Inertia loads on the fairings are small compared to the aerodynamic loads, therefore weights and C. G. data are not given.

3.7.3 THERMAL DATA. Temperature histories of the severance system fairings are shown in Figure 3.7-5.

3.7.4 INERTIA LOADS. Inertia loads on the fairings are negligible compared to the aerodynamic loads.

3.7.5 STEADY-STATE AIR LOADS. Steady-state air loads on the fairings are summarized in Table 3.7-1. These loads shall be combined with equivalent steady-state buffet loads.

TABLE 3.7-1. SEVERANCE SYSTEM FAIRINGS STEADY-STATE AIR LOADS

Load	Units	Fairing		
		55-74357-25	55-74357-27	55-74357-29
Drag	lb	145	206	102
Side Load	lb	70	68	58
Max Crush Pressure	psi	4.6	4.6	4.6
Max Burst Pressure	psi	3.8	4.5	5.2

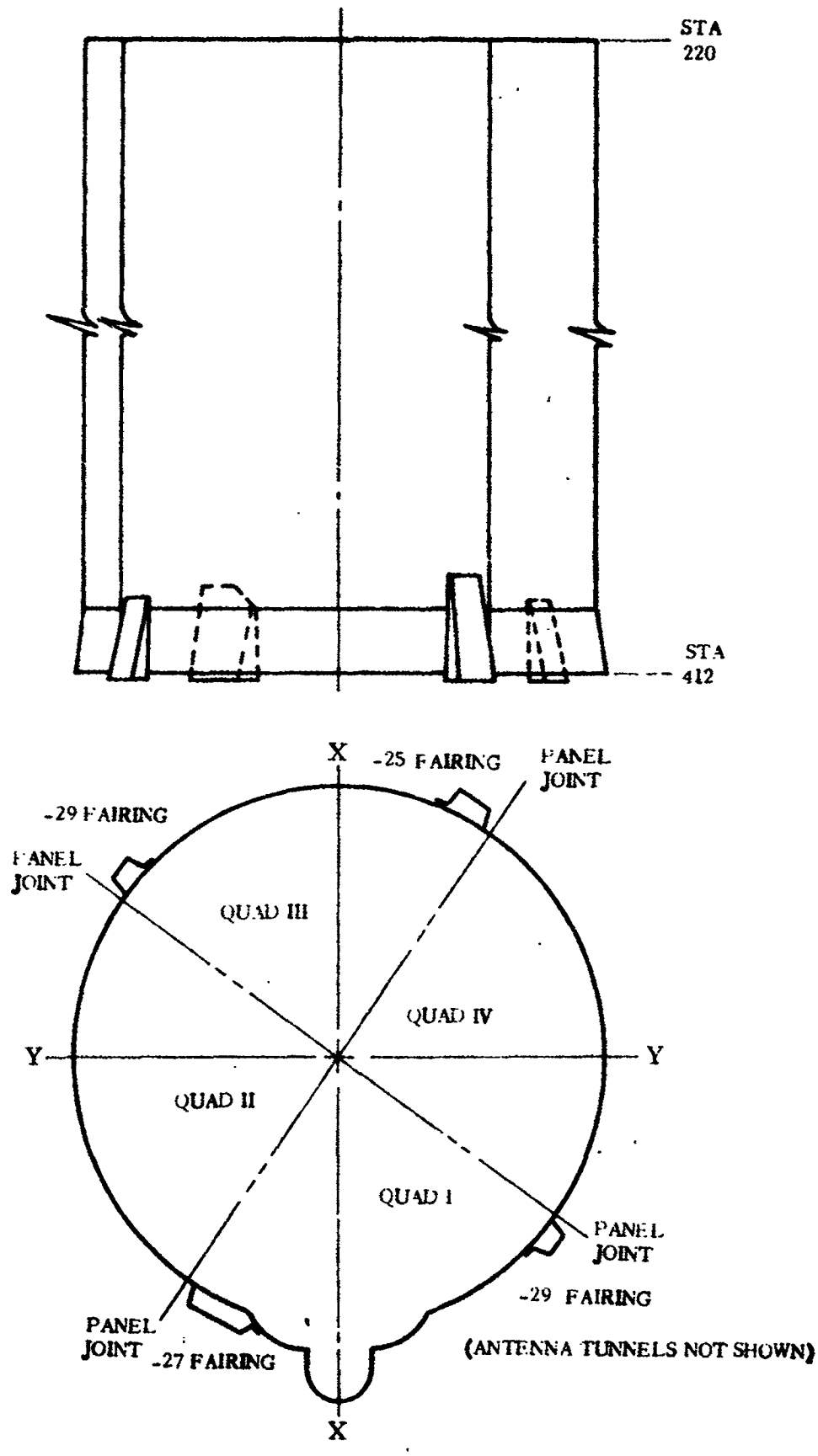

4B221LV

DRAWING NO.55-74357

Figure 3.7-1. Severance System Fairings - Location

3.7.6 BUFFET AND FLUTTER LOADS. Vibratory loads on the severance system fairings are given below as an equivalent, uniform static pressure applied over the entire area of each fairing for $0.75 \leq M < 1.0$.

Fairing	Equivalent Static Pressure, P_v (psi)
55-74357-25	± 1.9
55-74357-27	± 1.7
55-74357-29	± 2.4

These loads shall be combined with the steady-state aerodynamic loads.

3.7.7 MISCELLANEOUS LOAD PARAMETERS. During the jettison operation, the ignition of the mild detonators inside the severance system fairings causes equivalent steady-state pressures as presented below.

Fairing	Equivalent Static Pressure (psi)
55-74357-25	± 28
55-74357-27	± 20
55-74357-29	± 40

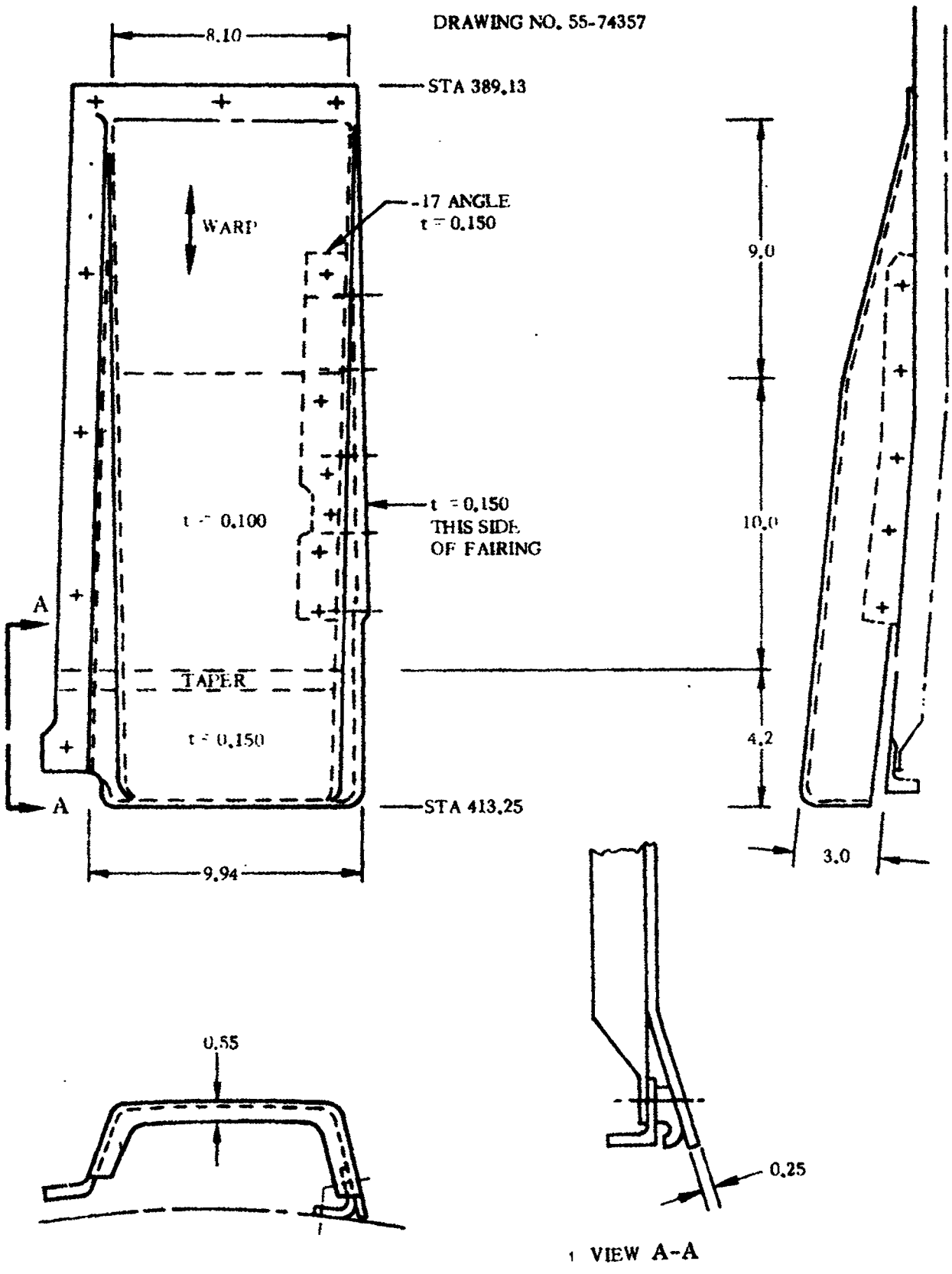

Figure 3.7-2. -25 Severance System Fairing, Quadrant IV Configuration

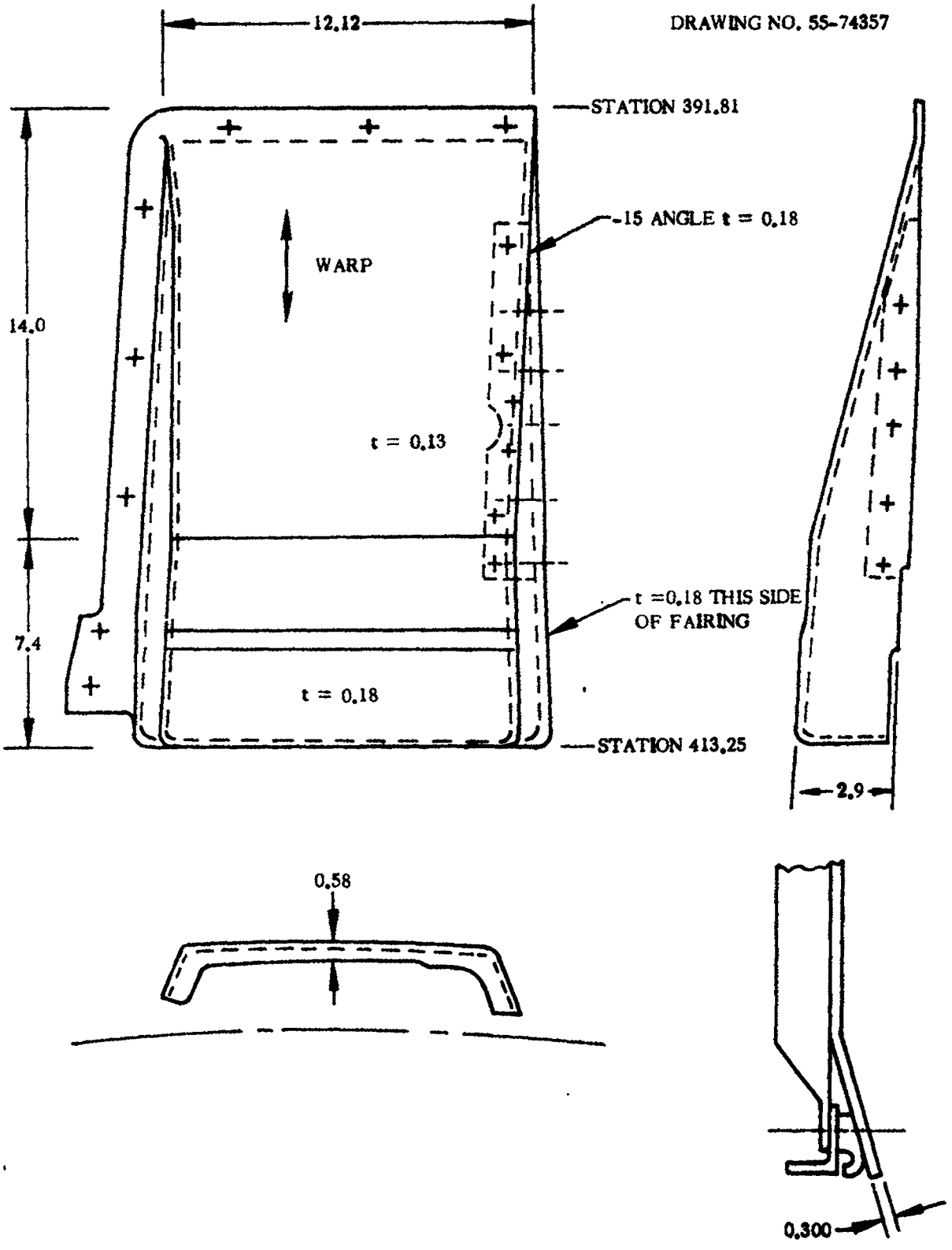

4B223LV

Figure 3.7-3. -27 Severance System Fairing, Quadrant II Configuration

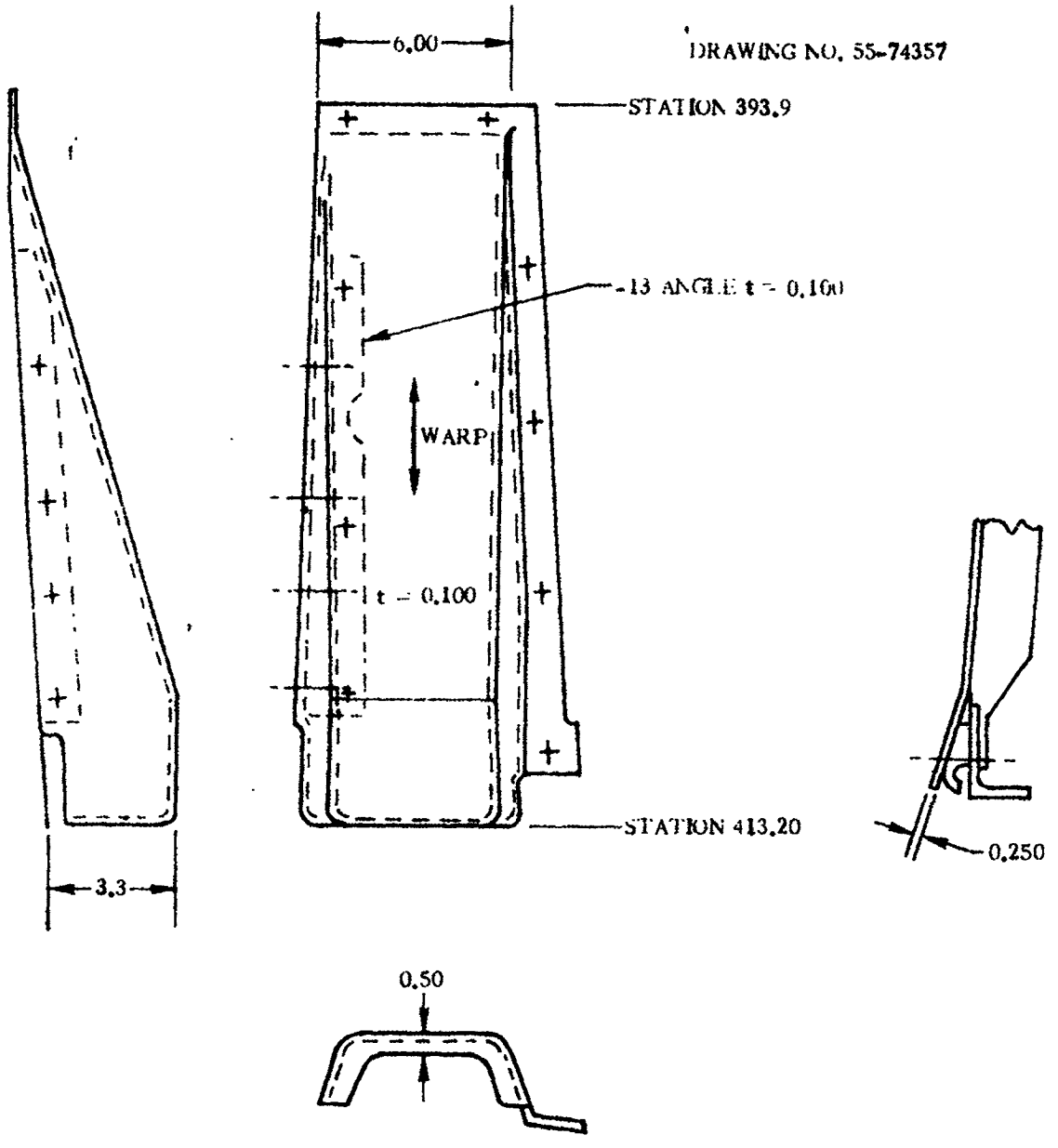

4B224LV

Figure 3.7-4. -29 Severance System Fairing, Quadrants I and III Configuration

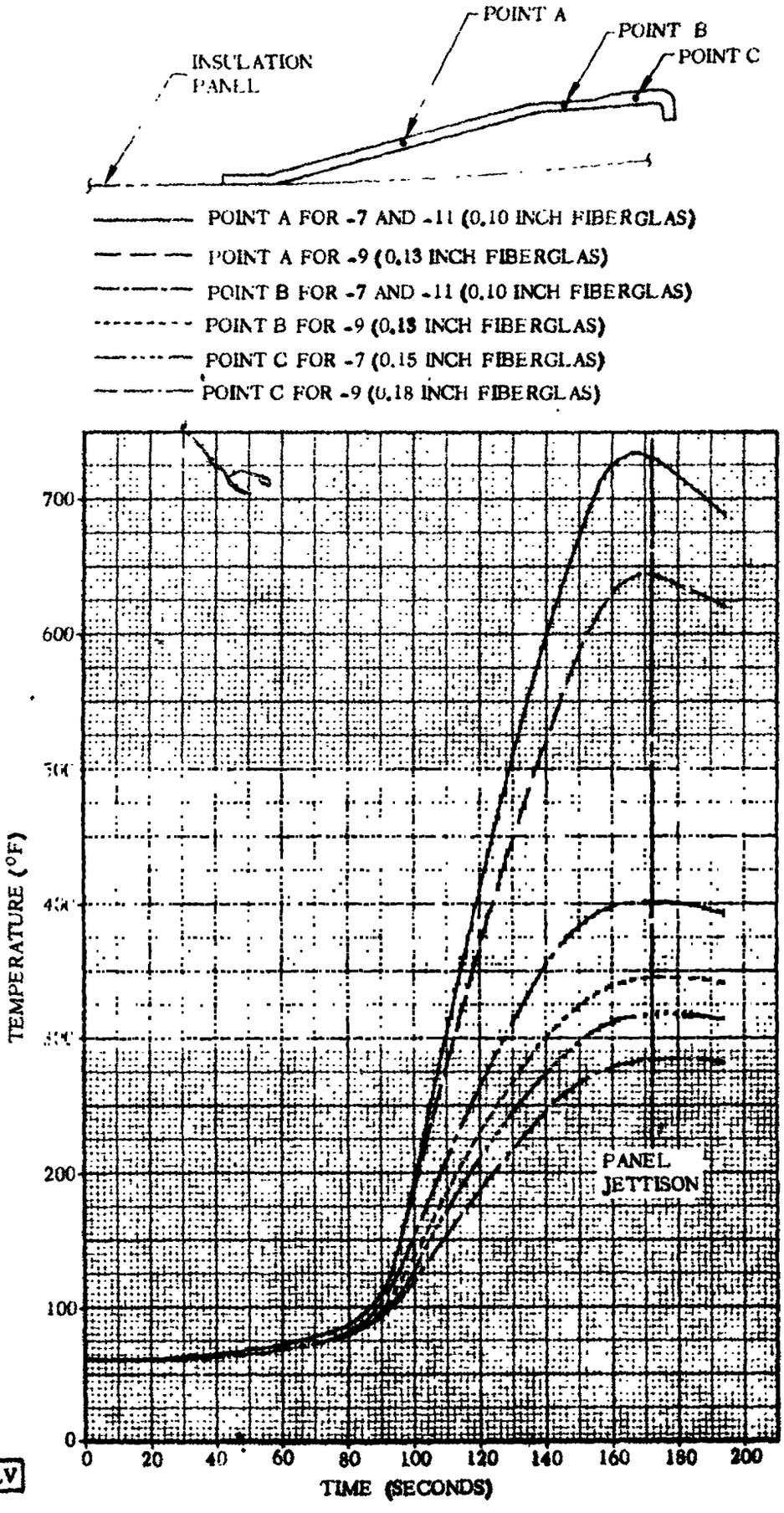

Figure 3.7-5. Severance System Fairings (55-74357) Temperature Histories

THIS PAGE INTENTIONALLY LEFT BLANK.

3.8 JETTISON HINGE ARMS

The jettison hinge arms are located at the aft end of the insulation panels as sho in Figure 3.8-1. The hinge pivot pins are located at Station 436. After the shaped charge cuts the panels, they rotate on the hinges about 55 degrees and fall free from the vehicle. A gap of about 0.08 inches is provided between the hinge arms and the hinge pins to prevent loads from building up in the hinges due to aerodynamic heatin and differential expansion between the hinge arms and the interstage adapter.

The hinges are all straight except for those in Quadrant II which are offset as shown in Figure 3.8-2 to clear the LO_2 fill and drain line. The Quadrant II hinge on the Quadrant II - III panel is only slightly offset and is treated as a straight hinge in loads analysis. The Quadrant II hinge on the Quadrant I - II panel has an appreciable offset and is treated separately for loads because of its greater flexibility.

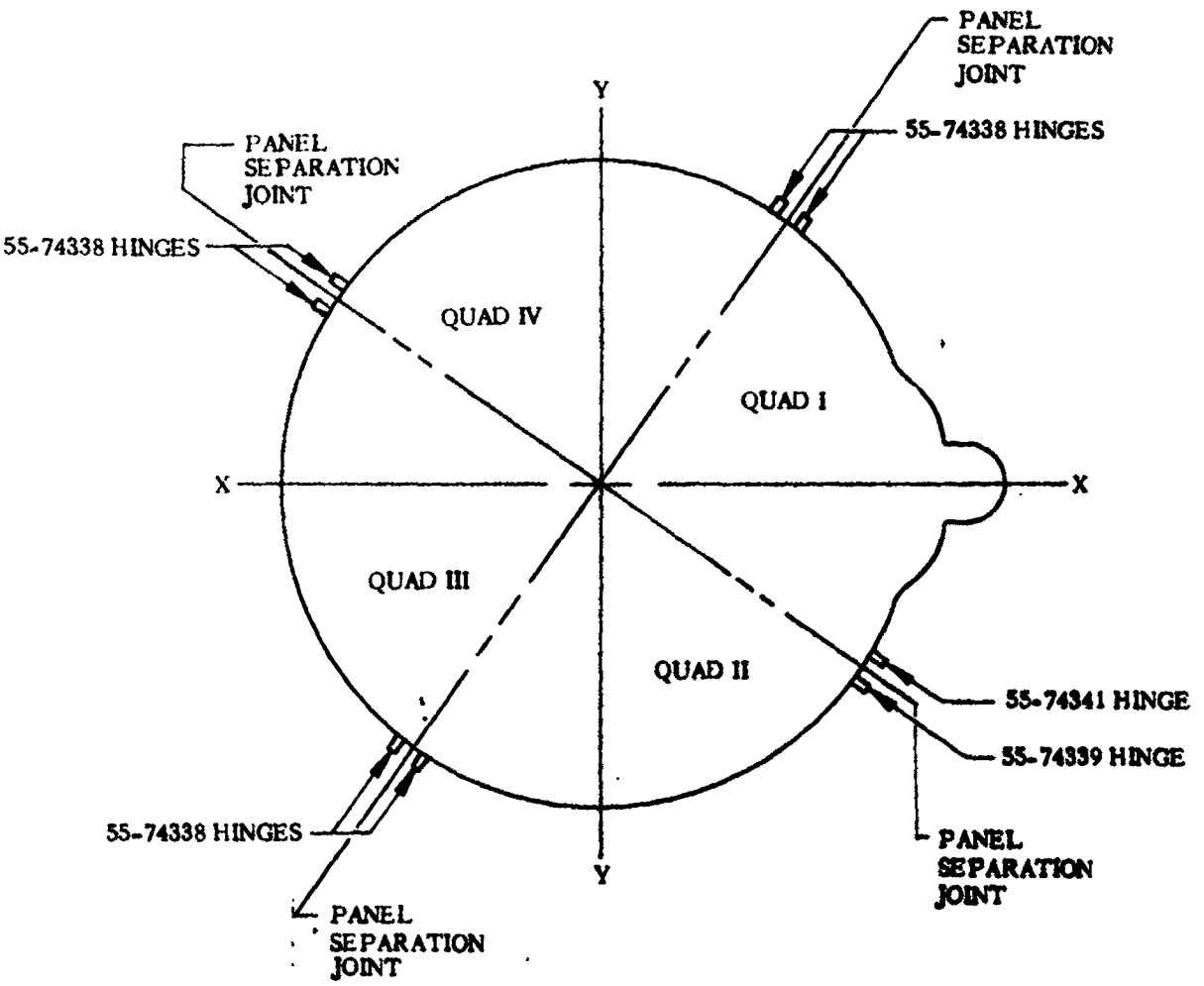

VIEW LOOKING FORWARD

4B226LV

Figure 3.8-1. Jettison Hinge Locations

3.8.1 CRITICAL CONDITIONS. The insulation panel jettison hinges,by the nature of their design. are unloaded until the shaped charge cuts the insulation. Once the shaped charge is detonated the panels move aft until the hinges bottom out on the hinge pins and the panels begin to rotate away from the vehicle.

3.8.2 WEIGHTS AND CENTER OF GRAVITY DATA. Weights, C.G.'s and mass moments of inertia data for the hinges are included in the basic panel data of Paragraph 3.2.2.

3.8.3 THERMAL DATA. Temperatures of the insulation panel hinges at the time of panel jettison (approximately 172 seconds) are shown in Figure 3.8-3. The maximum heating design trajectory (DP35) was used in the analysis.

3.8.4 INERTIA LOADS. Figure 3.8-4 denotes the force vectors for the insulation panel hinge jettison loads The load magnitudes acting on each hinge are listed in Table 3.8-1, and all act simultaneously.

3.8.5 STEADY-STATE AIR LOADS. Steady-state air loads on the insulation panel jettison hinges are negligible compared to the jettison loads.

3.8.6 BUFFET AND FLUTTER LOADS. Buffet and flutter loads on the insulation panel jettison hinges are negligible compared to the jettison loads.

3.8.7 MISCELLANEOUS LOAD PARAMETERS. No other loads are critical for these items.

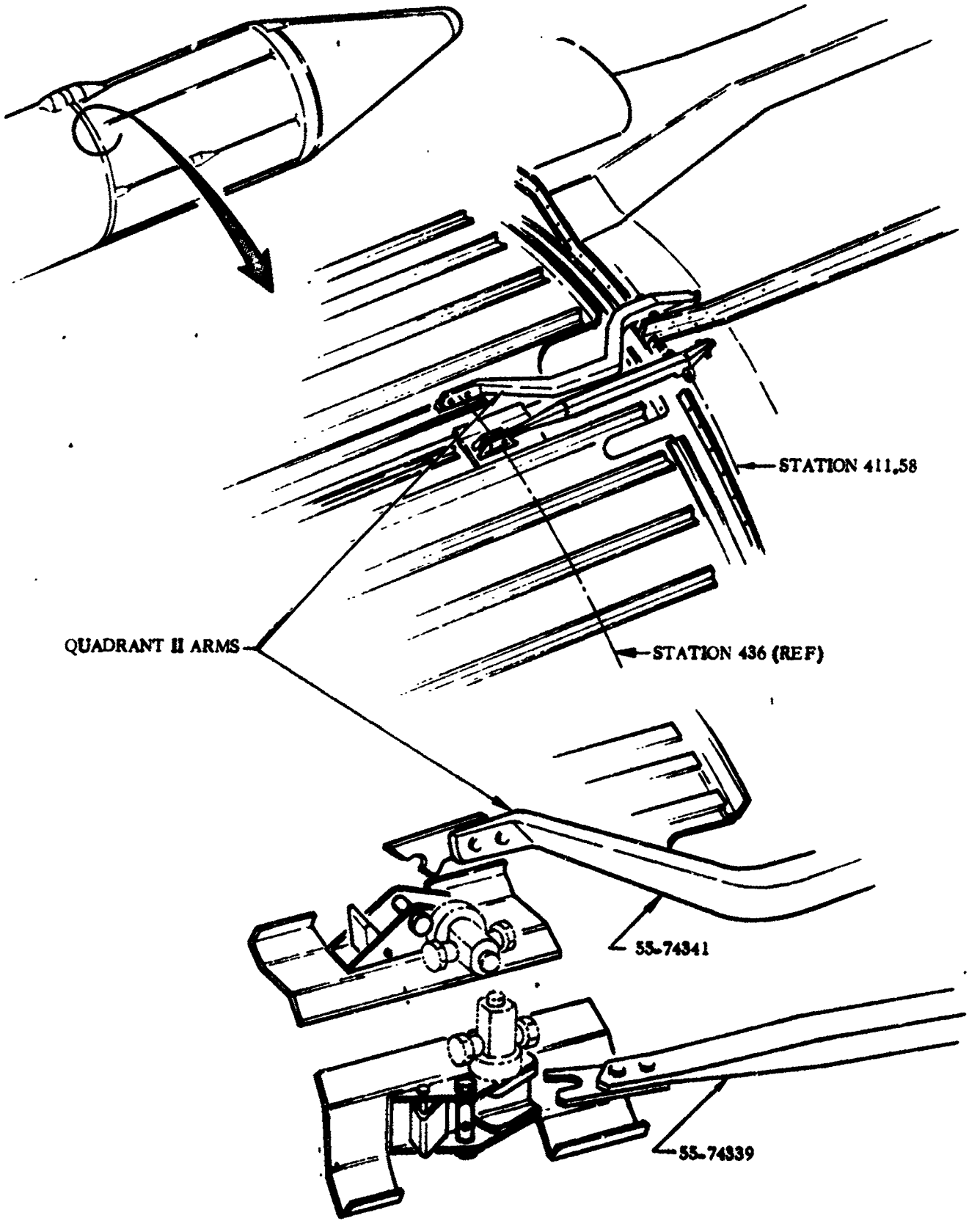

Figure 3.8-2. Insulation Panel Jettison Hinge System (Quadrant II)

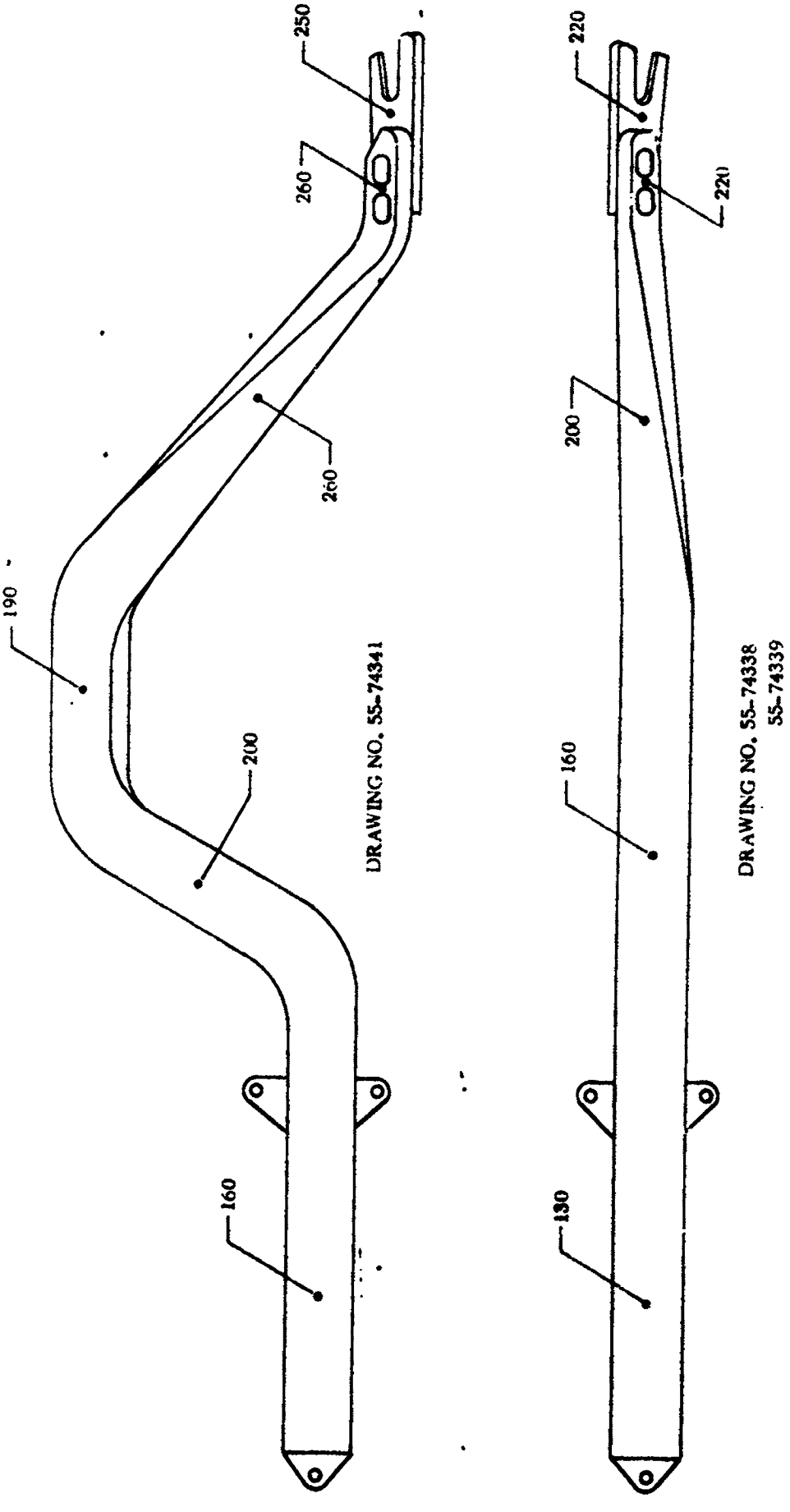

Figure 3.8-3. Insulation Panel Hinge Arms (AC-6 and On) - Maximum Temperatures at Panel Jettison (Approximately 190 Seconds)

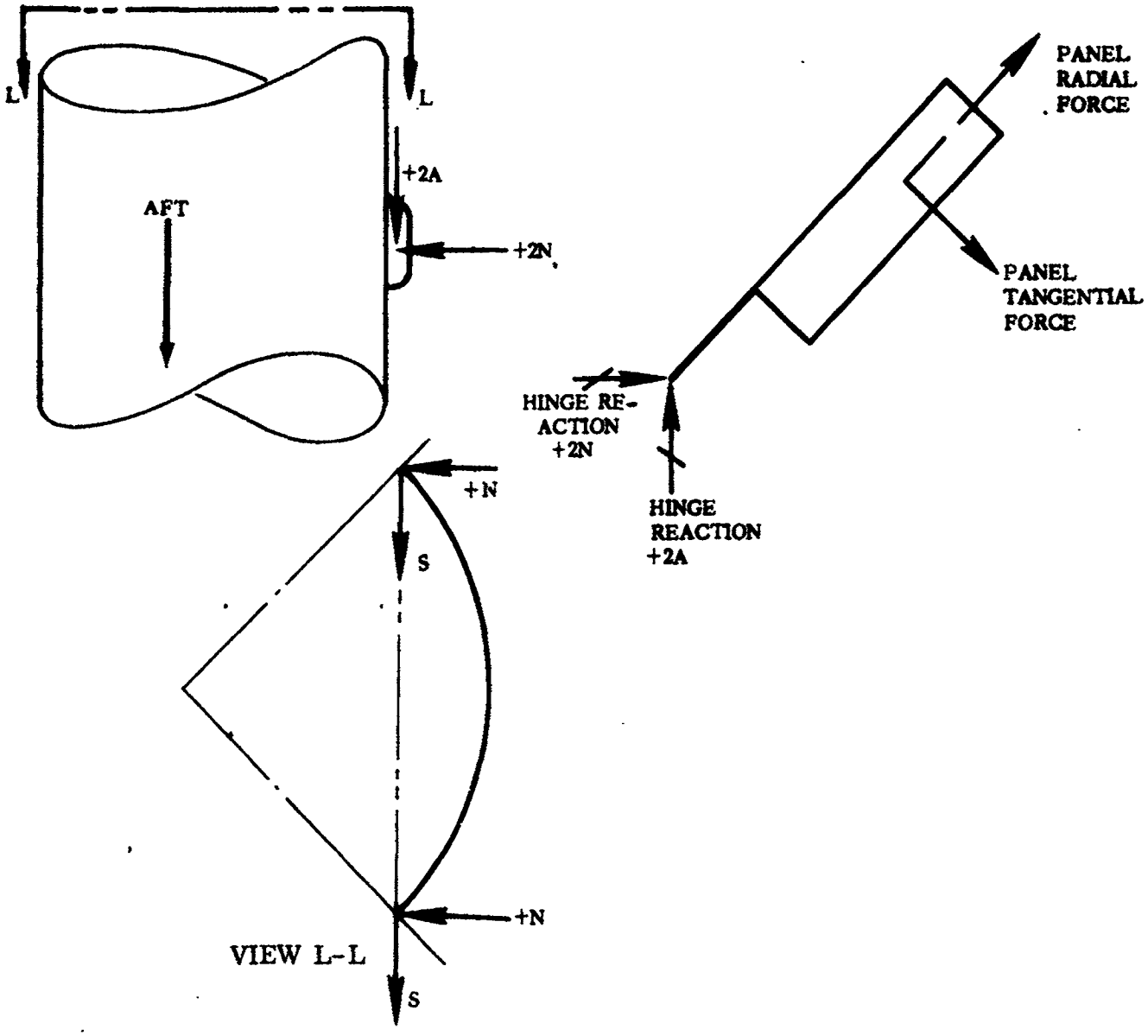

4B229LV

Figure 3.8-4. Insulation Panel Hinges - Jettison Forces

TABLE 3.8-1. INSULATION PANEL HINGE JETTISON LOADS (APPLIED SIMULTANEOUSLY)

Hinge Load	Units	Straight and Slight Offset Hinges	Offset Hinge (Only)
A. Longitudinal (Aft)	lb	2500	1420
N. Radial (perpendicular to hinge axis)	lb	±400	±400
S. Tangential (parallel to hinge axis)	lb	±100	±100

THIS PAGE INTENTIONALLY LEFT BLANK.

3.9 AFT SEAL AND ATTACHMENT AT STATION 412

The aft seal and attachment at Station 412 consists of a ring as shown in Figure 3.9-1. The ring is bolted to the Station 412 tank ring at its inner edge and to the insulation panels along its outer edge. At the X-X axis between Quadrants I and II, the wiring tunnel aft bulkhead is mounted in the space between the Station 412 tank ring and the aft seal ring. The aft seal plate provides the entire longitudinal support for the insulation panels.

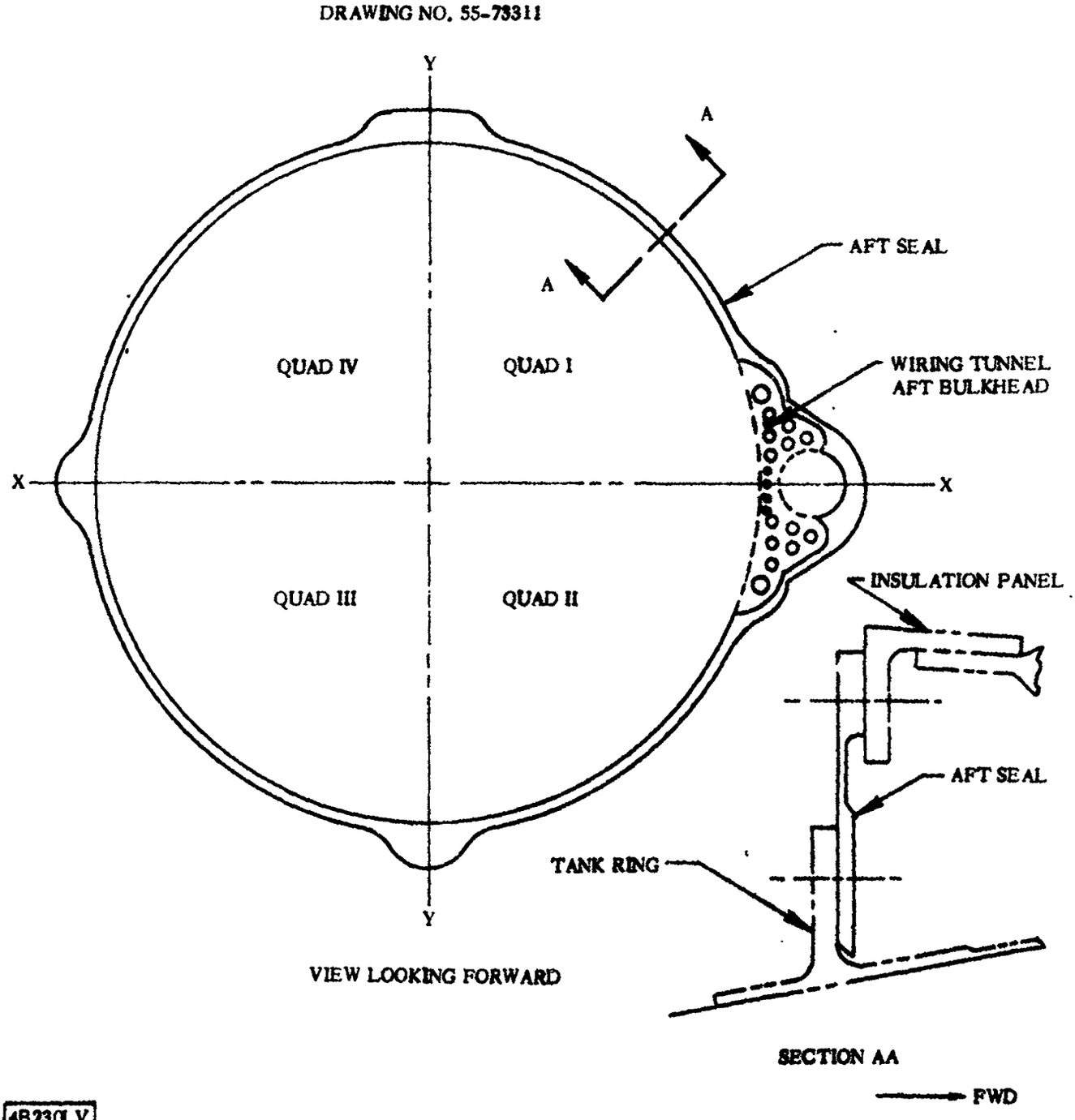

Figure 3.9-1. Aft Seal and Station 412 Attachment

3.9.1 CRITICAL CONDITIONS. Two conditions are critical for the aft seal plate. the air loads and inertia loads from the transonic regime through Max αq, and the maximum longitudinal acceleration just prior to BECO, which gives the highest inertia loads.

3.9.2 WEIGHTS AND CENTER OF GRAVITY DATA. The aft seal plate has negligible weight when compared to the weight of the insulation panels that it supports.

3.9.3 THERMAL DATA. Temperatures of the aft seal plate for several times during flight are included in Paragraph 3.2.3 of this report.

3.9.4 INERTIA LOADS. Steady-state inertia loads of the insulation panels on the aft seal plate are determined from the plot of (T-D)/W versus time which is presented in Paragraph 1.3.3 of this report and from the structural design weights of the insulation panels given in Paragraph 3.2.2 of this report.

3.9.5 STEADY-STATE AIR LOADS. Steady-state pressure differentials acting on the aft seal plate are 3.5 psi forward or 3.2 psi aft. Drag loads on the insulation panels are given in Paragraph 3.2.5.

3.9.6 BUFFET AND FLUTTER LOADS. A vibratory equivalent static differential pressure of ± 0.5 psi acts on the seal plate and must be added to the steady-state air loads.

3.9.7 MISCELLANEOUS LOAD PARAMETERS. No other loads are critical for this component.

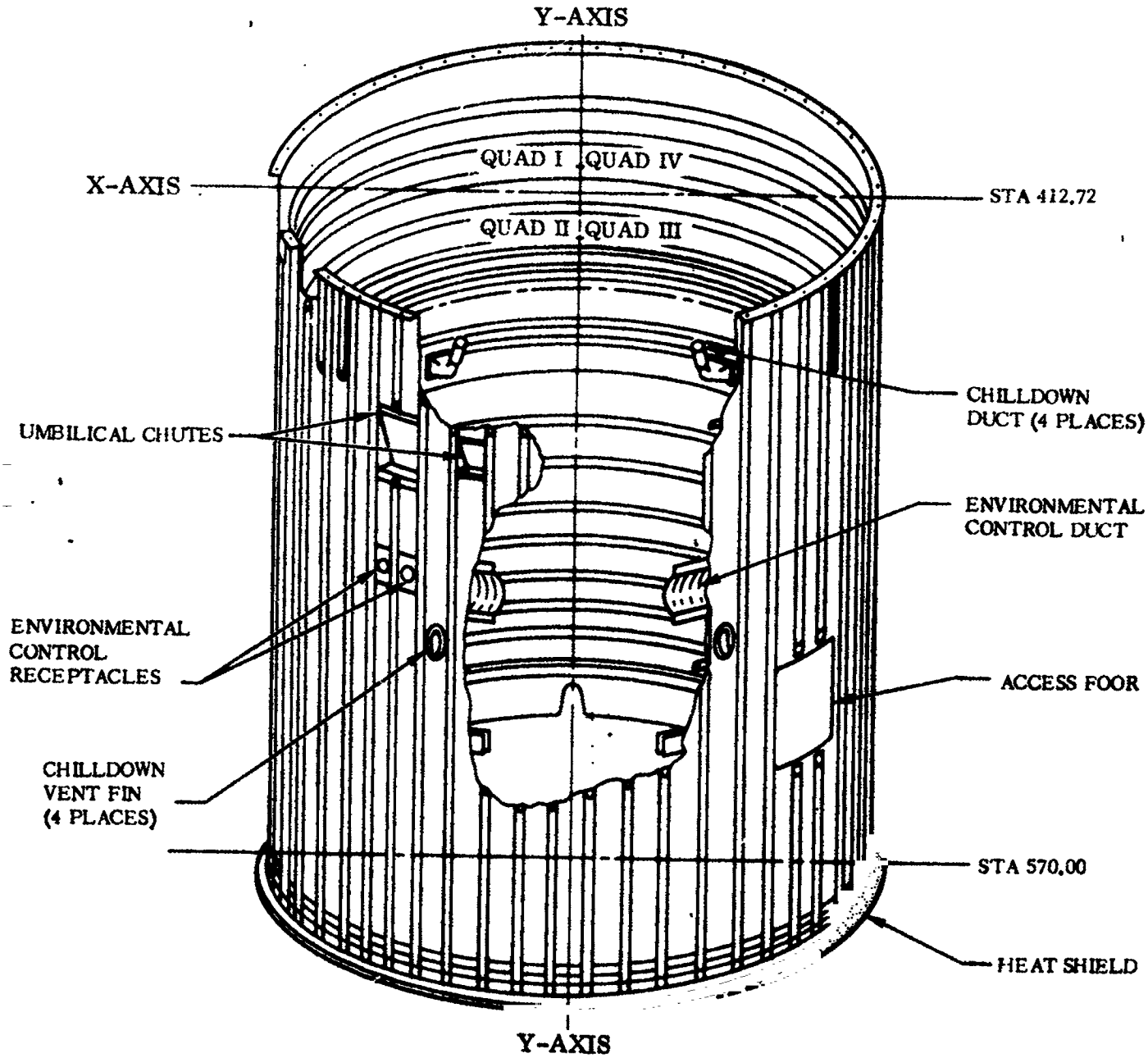
Y-AXIS
X-AXIS
QUAD I
QUAD IV
QUAD II
QUAD III
STA 412.72
CHILLDOWN DUCT (4 PLACES)
UMBILICAL CHUTES
ENVIRONMENTAL CONTROL DUCT
ENVIRONMENTAL CONTROL RECEPTACLES
ACCESS FOOR
CHILLDOWN VENT FIN (4 PLACES)
STA 570.00
HEAT SHIELD
Y-AXIS

SECTION IV

INTERSTAGE ADAPTER

4.1 INTRODUCTION

An interstage adapter supports the Centaur vehicle and provides a physical connection between the Atlas and the Centaur vehicles. The adapter is a cylindrical section approximately 13 feet long and 10 feet in diameter. It is of skin and stringer construction. For the interstage adapter general arrangement refer to Figure 4.1-1. The adapter is designed for bolt attachment to both the Atlas and Centaur vehicles.

A flexible, linear-shaped charge (FLSC) system is provided to separate the Centaur vehicle from the Atlas booster vehicle by cutting the interstage adapter near the forward end. The charge is located on the forward interstage adapter flanged ring, approximately 0.5 inch aft of the interfaces of the Centaur mating ring and the interstage adapter. Two detonators are provided with four detonation outputs. The detonators are located on opposite sides of the interstage adapter near the forward end.

A stainless steel blast shield protects the Centaur liquid oxygen tank from fragments; this shield is covered with Fiberglas matting and attached around the periphery of the tank directly in line with the shaped charge system located on the adapter. Four separation bumper guides assist in guiding the Centaur aft section out of the interstage adapter during separation.

Breakaway connections are provided for four flexible Teflon tubes that connect between the engine's helium chilldown tubing and the interstage adapter helium chilldown collector manifold.

The operation of the separation system is initiated by a signal from the Atlas programer. Physical separation of the two stages is accomplished as a result of the application of retrorocket forces which retard the forward motion of the Atlas.

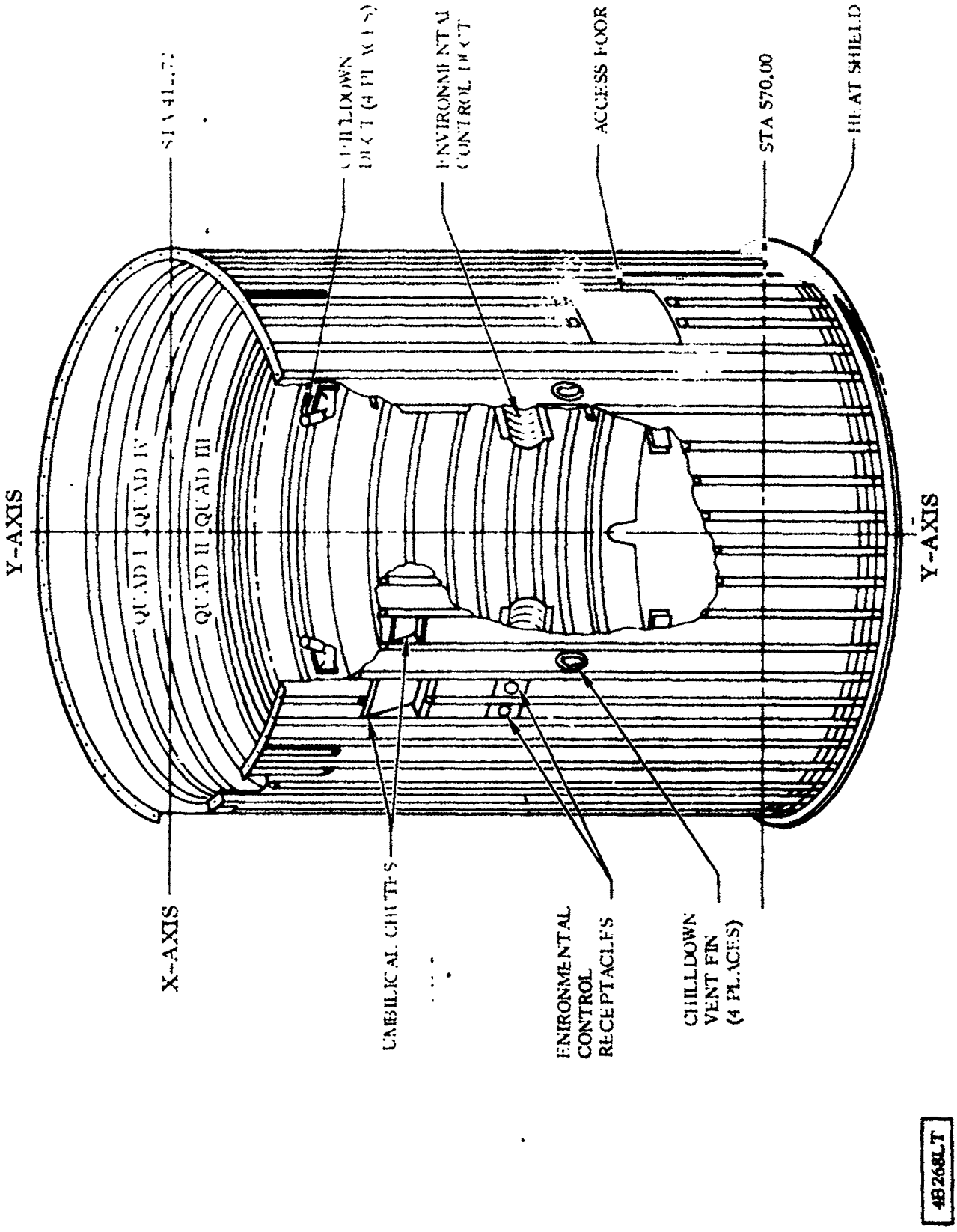

Figure 4.1-1. Interstage Adapter Configuration

4.2 BASIC STRUCTURE

The interstage adapter basic structure is essentially a thin skin cylindrical shell stiffened by internal "I section" circumferential frames and external "hat section" longitudinal stringers. Integral skin reinforcement has been incorporated where these major load carrying members attach to the basic skin. The basic structure provides a path whereby the axial, shear, and bending moment loads are transferred between the Centaur upper stage and Atlas booster vehicles. Reference Figures 4.2-1 and 4.2-2 for configuration of basic skin, frames, and stringers.

4.2.1 CRITICAL CONDITIONS. The interstage adapter basic structure experiences critical loading during prelaunch operations and essentially two flight conditions.

Combinations of ground winds and minimum propellant tanking (tower away) produce maximum preflight axial tensile stresses in the adapter as a result of moments which are conservatively based on the GD/C Ground Wind Restrictions Procedure for operational vehicles.

During transonic flight, peak bending moments are induced to the adapter through maximum steady-state and fluctuating pressures. The detailed loads will be further discussed as applicable in the subsequent pages.

The maximum booster acceleration condition, which exists at booster engine cutoff (BECO), imposes the maximum axial loads to the structure as a result of maximum inertia loading which must be considered simultaneously with the maximum temperatures at pertinent areas along the structure. Aerodynamic loads have become negligible during this time of flight, therefore they need not be considered as a load contribution at BECO.

Axial load and bending moment are negligible at the time of Atlas/Centaur separation (BECO +76.0 seconds) due to near zero aerodynamic pressure and zero acceleration. Separation is initiated by a circumferential linear-shaped charge located at Station 113.38. Adequate simulation ground tests along with AC-2, AC-3 and AC-4 flight tests, provide proof of adequate structural resistance to detonation damage to the Centaur aft bulkhead.

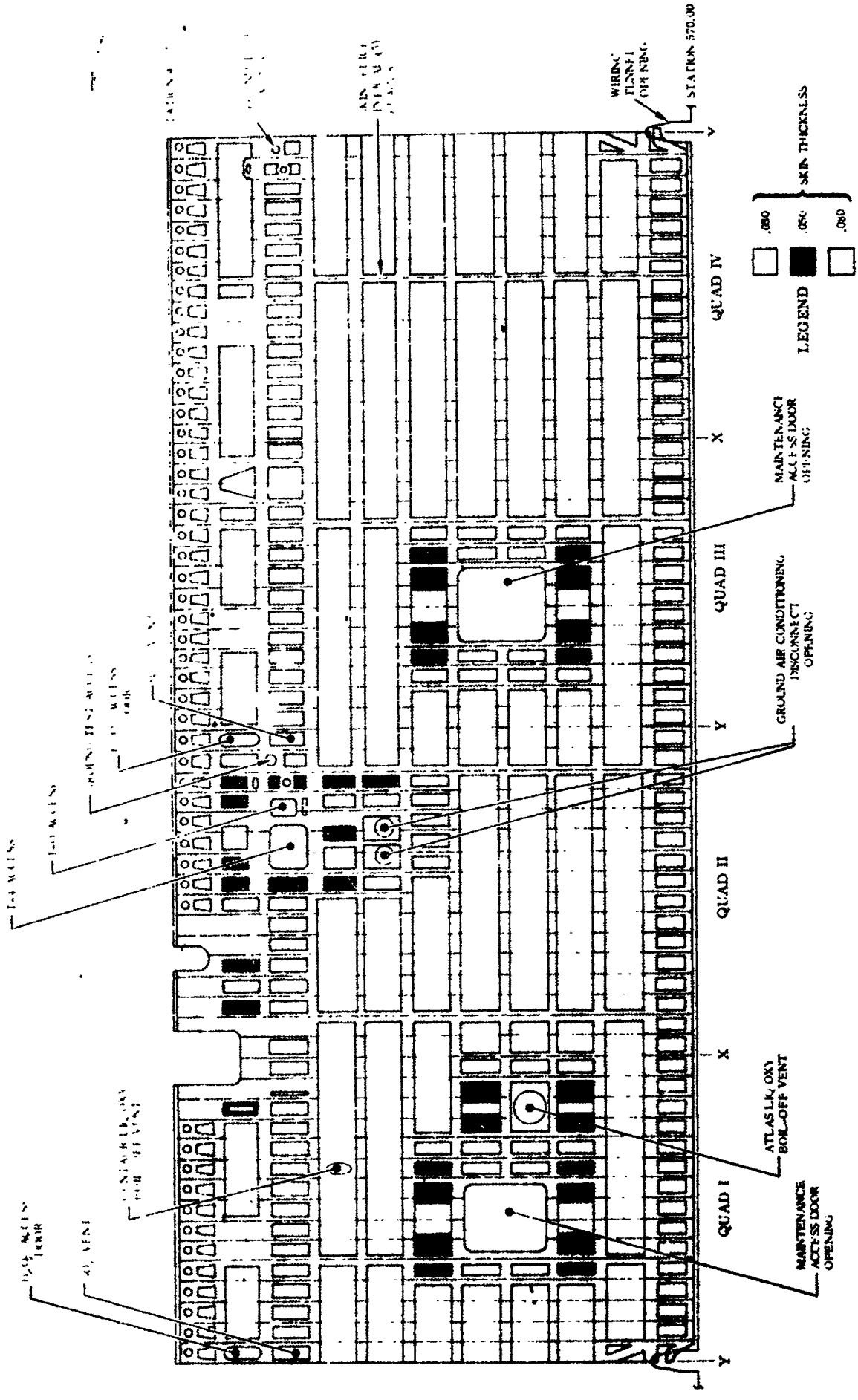

Figure 4.2-1. Adapter Integral Skin Reinforcement Configuration

TYPICAL STRINGER AND SKIN SPLICE

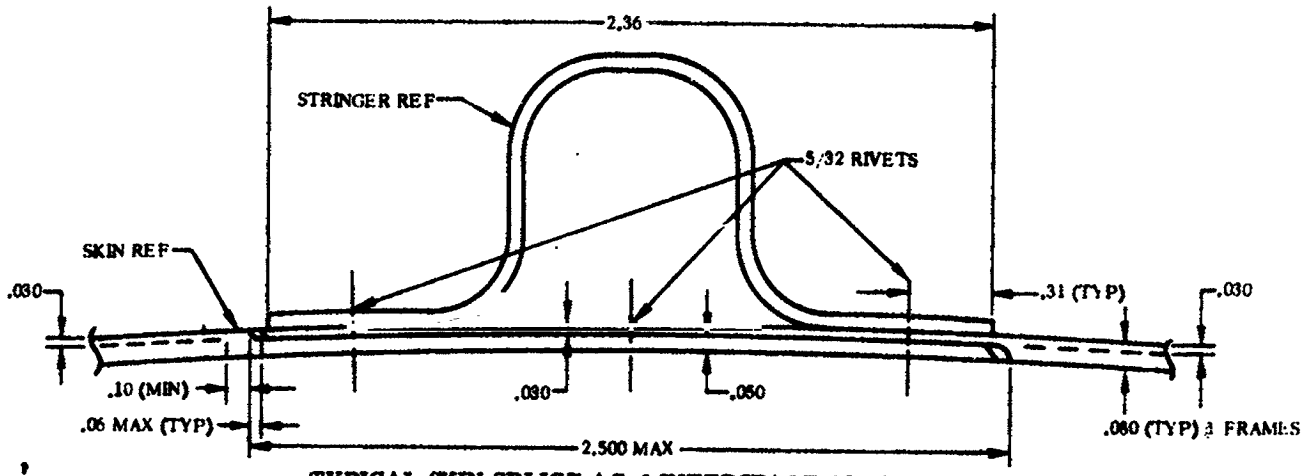

TYPICAL SKIN SPLICE AC-6 INTERSTAGE ADAPTER

VIEW LOOKING FORWARD

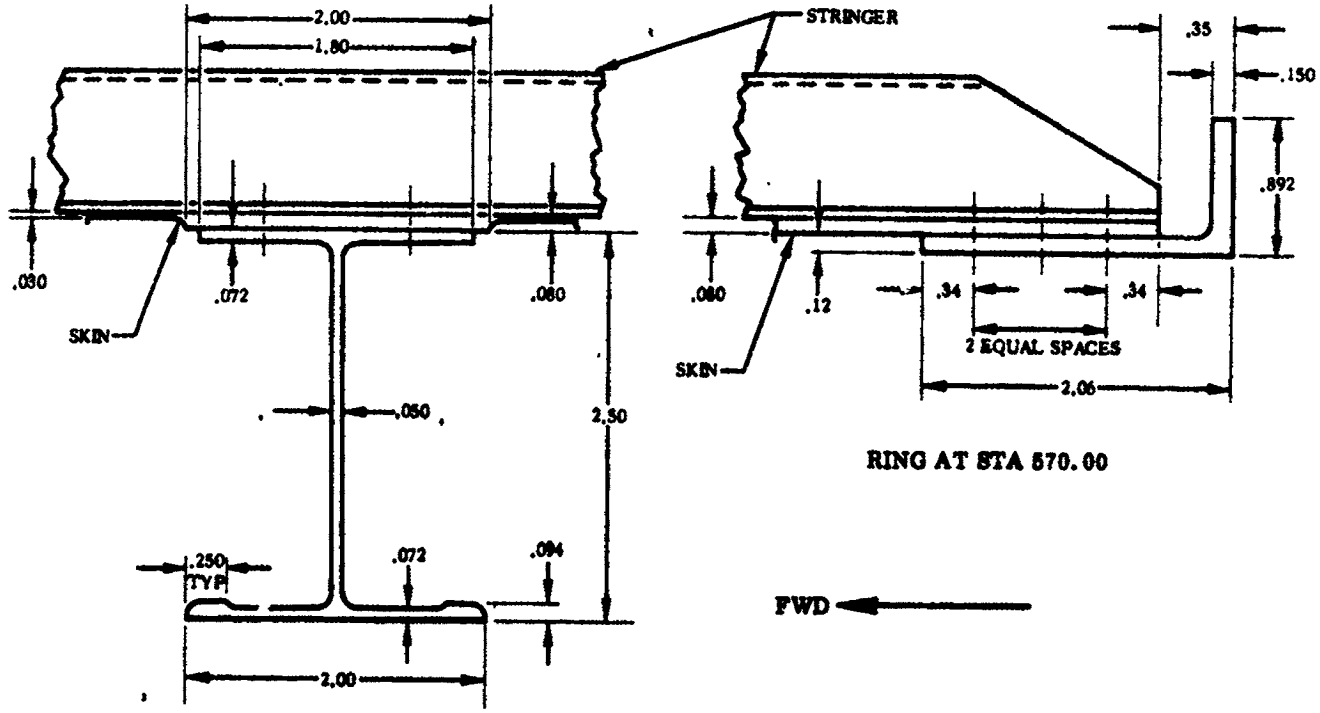

TYPICAL FRAME SECTION FOR
STA 454.77, 468.43, 482.09,
496.75, 511.41, 526.07, 540.73

RING AT STA 570.00

4B37LV

Figure 4.2-2. Typical Frames and Stringers Configuration

4.2.2 WEIGHTS AND CENTER OF GRAVITY DATA. The weights data listed in Table 4.2-1 shall be used for purposes of design and analysis.

TABLE 4.2-1. INTERSTAGE ADAPTER BASIC STRUCTURE WEIGHTS

Item	Weight (lb)
Basic Structure	
412 Ring (Jettison Half)*	14.4
570 Ring	13.2
Frames	184.7
Stringers	163.9
Doors	20.9
Skins	291.1
Doublers	4.9
Paint	4.2
Brackets, Stiffeners, and Miscellaneous	17.3
Rivets, Screws, and Other Fasteners	30.0
Total Basic Structure	744.6
Other Equipment	
Thermolag	35.0
Other Equipment	347.8
Total Jettison Weight	1127.4

*The ring weight remaining after separation is 5.8 pounds.

4.2.3 THERMAL DATA. The structural differences between the operational interstage adapter and those used on previous vehicles, as well as protuberance modifications, will result in different disturbance heating patterns and different thermal loads.

4.2.3.1 Station 412 Liquid Oxygen Tank Joint Temperatures. The interstage adapter - Centaur interface has been redesigned for the operational configuration. The wedding band between Stations 408 and 412 has been eliminated and the Centaur liquid oxygen (LO_2) tank ring has been moved aft to Station 412.72. This change alters the temperature history of the forward end of the interstage adapter.

Figure 4.2-3 shows a cross-section view of the interstage adapter just aft of the Station 412 joint. The section callouts indicate locations where thermal profiles were made. The temperature profiles at these sections are given in Tables 4.2-2 through 4.2-6. Figure 4.2-4 shows a segmented section of the Station 412.72 joint. The segment numbers versus temperature (at critical flight times) correspond to those listed in Tables 4.2-2 through 4.2-6.

The temperature histories at Section A-A of Figure 4.2-3 are expected to be the most severe (highest temperatures) of any location around the circumference, except for the regions directly beneath the insulation panel hinge arms, which may get warmer near the Station 412 ring but will not exceed 230°F due to the nearly total coverage by Thermolag T-230 (reference Figure 4.2-5). The temperature history at Section E-E, which is partially protected from aerodynamic heating by the detonator fairing, will be the least severe of any location. The adapter aft of Section F-F (taken through the boost pump) is considered thermally remote from the ring at Station 412, and being of minor structural interest, is purposely deleted from temperature tabulations of this area. No portion of the adapter between Station 434 and 446, and stringers 13 and 17 (location of shaped charge detonator) should experience temperatures outside the range of 30 to 100°F from launch to staging since the area is protected by the boost fairing (reference Figure 4.2-5 for location). Areas covered by Thermolag will never exceed 230°F.

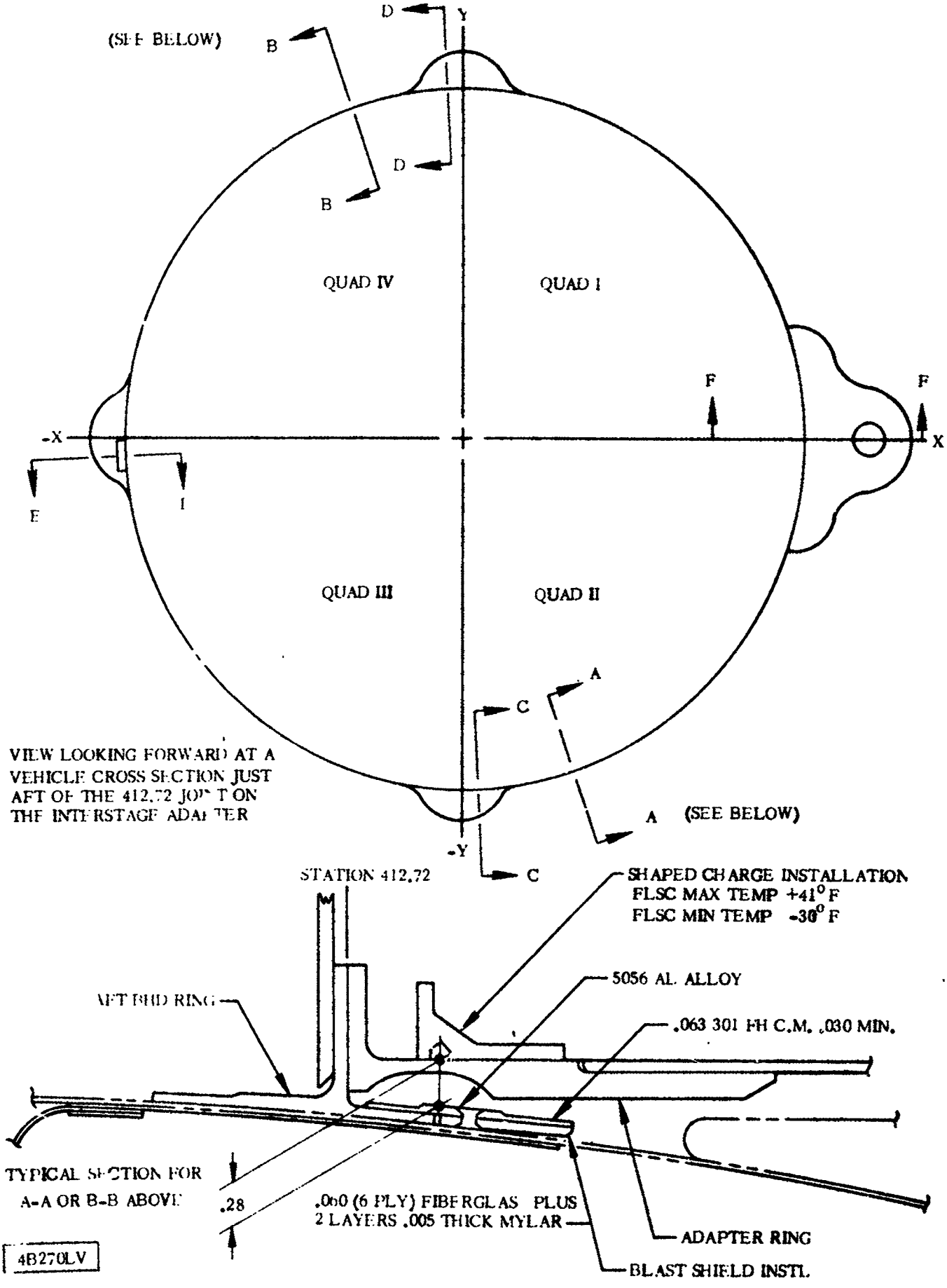

Figure 4.2-3. Station 412.72 Joint

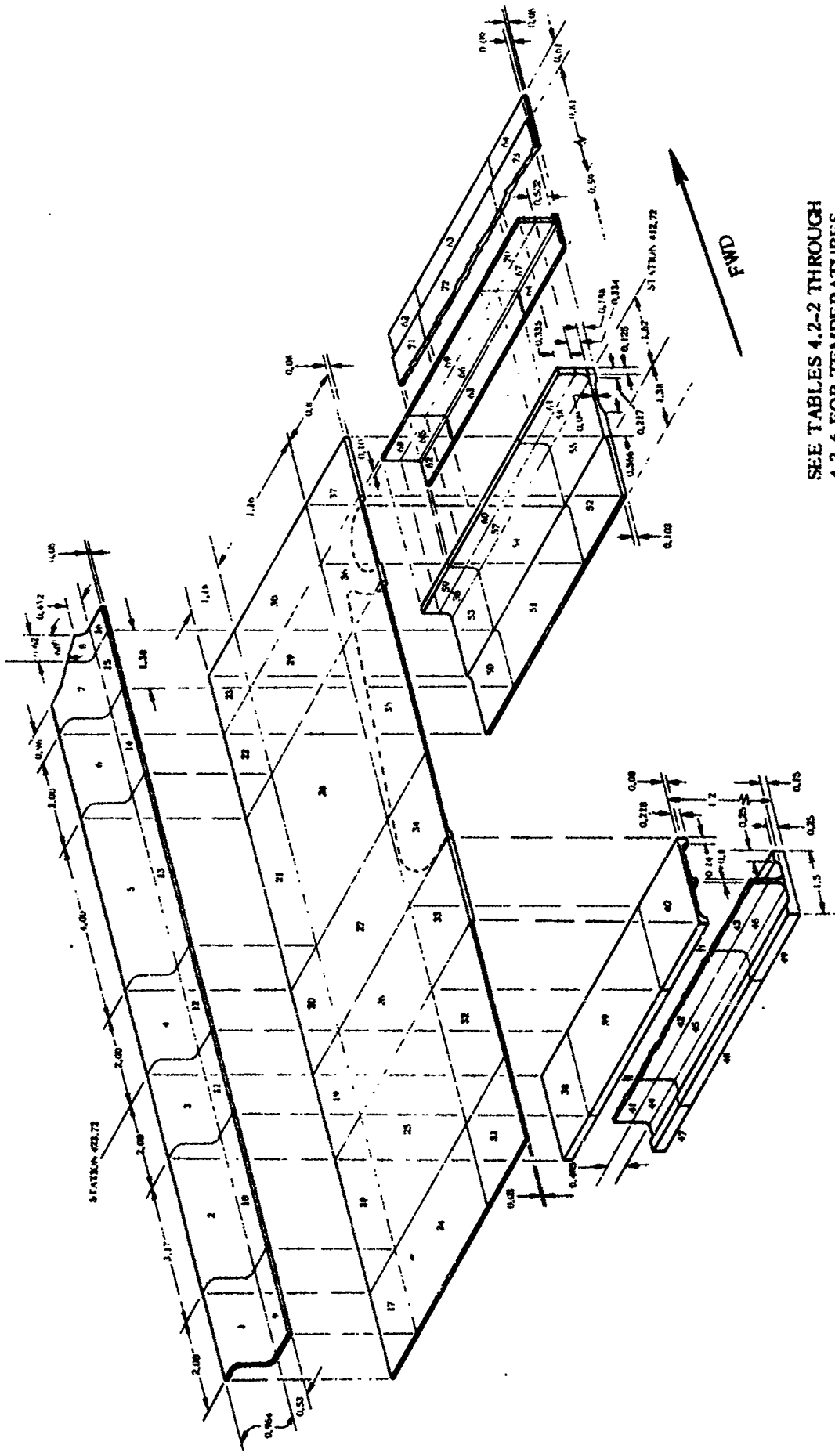

Figure 4.2-4. Station 412.72 Joint (Thermal Model Element Location)

4B38L.T

TABLE 4.2-2. TEMPERATURE HISTORY AT SECTION A-A OF FIGURE 4.2-3

Segment Number (Ref. Figure 4.2-4)	Time From Launch (seconds)				
	0	75	150	170	235
1	72	88	230	230	224
2	70	88	230	231	221
3	61	86	255	277	216
4	52	85	292	319	242
5	34	78	286	320	255
6	-11	54	199	222	172
7	-38	33	140	158	113
8	-57	16	102	116	75
9	72	86	230	230	225
10	70	85	229	230	221
11	60	79	222	243	210
12	51	79	278	303	242
13	32	71	278	309	257
14	-19	43	187	208	170
15	-50	13	115	132	103
16	-73	-6	70	82	51
17	73	83	230	230	225
18	70	82	228	229	221
19	60	70	189	207	205
20	49	72	267	287	243
21	30	64	272	299	258
22	-25	33	177	195	169
23	-59	-5	98	111	98
24	73	94	230	230	220
25	71	93	229	230	214
26	60	74	183	204	197
27	48	92	322	349	233
28	31	87	335	364	248
29	-35	44	186	205	158
30	-62	-1	94	109	90
31	73	96	230	230	218
32	71	95	229	230	212
33	61	75	183	203	195
34	47	95	341	366	230
35	31	91	357	383	246

NOTE:
All temperatures are in °F.

TABLE 4.2-2. TEMPERATURE HISTORY AT SECTION A-A OF FIGURE 4.2-3 (CONTINUED)

Segment Number (Ref. Figure 4.2-4)	Time From Launch (seconds)				
	0	75	150	170	235
36	-37	51	195	213	155
37	-64	0	92	107	86
38	60	67	170	187	199
39	60	69	168	186	195
40	61	70	168	185	193
41	60	65	154	172	194
42	60	67	153	171	191
43	60	67	153	171	190
44	60	63	130	150	187
45	60	64	130	150	185
46	60	64	130	149	184
47	60	62	116	137	182
48	60	62	116	137	181
49	60	62	116	137	181
50	-66	-15	81	93	85
51	-69	-13	79	91	79
52	-70	-12	77	89	76
53	-94	-35	25	33	15
54	-98	-39	18	26	9
55	-99	-40	16	23	6
56	-100	-43	14	22	5
57	-103	-46	8	16	-1
58	-104	-47	6	14	-3
59	-101	-45	11	19	2
60	-104	-47	6	13	-3
61	-105	-48	4	11	-5
62	-265	-260	-252	-251	-251
63	-266	-261	-252	-251	-252
64	-266	-261	-252	-252	-252
65	-137	-97	-50	-46	-54
66	-139	-100	-55	-50	-58
67	-140	-100	-56	-52	-60
68	-110	-63	-7	-1	-11
69	-112	-65	-11	-6	-15
70	-113	-66	-13	-8	-17

NOTE:
All temperatures are in °F.

TABLE 4.2-2. TEMPERATURE HISTORY AT SECTION A-A OF FIGURE 4.2-3 (CONTINUED)

Segment Number (Ref. Figure 4.2-4)	Time From Launch (seconds)				
	0	75	150	170	235
71	-262	-256	-246	-245	-246
72	-262	-256	-247	-246	-247
73	-263	-257	-247	-246	-247

NOTE: All temperatures are in °F.

TABLE 4.2-3. TEMPERATURE HISTORY AT SECTION B-B OF FIGURE 4.2-3

Segment Number (Ref. Figure 4.2-4)	Time From Launch (seconds)			
	0	75	150	235
1	72	88	230	203
2	70	88	230	198
3	61	86	255	190
4	52	85	292	207
5	34	78	286	215
6	-11	54	199	141
7	-38	33	140	88
8	-57	16	102	54
9	72	86	230	203
10	70	85	229	198
11	60	79	222	187
12	51	79	278	208
13	32	71	278	216
14	-19	43	187	139
15	-50	13	115	80
16	-73	-6	70	32
17	73	83	230	203
18	70	82	228	198
19	60	70	189	183
20	49	72	267	208
21	30	64	272	217
22	-25	33	177	138
23	-59	-5	98	76
24	73	94	230	196

NOTE:
All temperatures are in °F.

TABLE 4.2-3. TEMPERATURE HISTORY AT SECTION B-B OF FIGURE 4.2-3 (CONTINUED)

Segment Number (Ref. Figure 4.2-4)	Time From Launch (seconds)			
	0	75	150	235
25	71	93	229	190
26	60	74	183	177
27	48	92	322	198
28	31	87	335	206
29	-35	44	186	128
30	-62	-1	94	68
31	73	96	230	194
32	71	95	229	188
33	61	75	183	175
34	47	95	341	194
35	31	91	357	203
36	-37	51	195	125
37	-64	0	92	65
38	60	67	170	179
39	60	69	168	176
40	61	70	168	175
41	60	65	154	176
42	60	67	153	174
43	60	67	153	173
44	60	63	130	171
45	60	64	130	170
46	60	64	130	169
47	60	62	116	168
48	60	62	116	167
49	60	62	116	167
50	-66	-15	81	64
51	-69	-13	79	58
52	-70	-12	77	56
53	-94	-35	25	-1
54	-98	-39	18	-7
55	-99	-40	16	-9
56	-100	-43	14	-10
57	-103	-46	8	-15
58	-104	-47	6	-17
59	-101	-45	11	-13

NOTE:
All temperatures are in °F.

TABLE 4.2-3. TEMPERATURE HISTORY AT SECTION B-B OF FIGURE 4.2-3 (CONTINUED)

Segment Number (Ref. Figure 4.2-4)	Time From Launch (seconds)			
	0	75	150	235
60	-104	-47	6	-17
61	-105	-48	4	-19
62	-265	-260	-252	-253
63	-266	-261	-252	-254
64	-266	-261	-252	-254
65	-137	-97	-50	-66
66	-139	-100	-55	-69
67	-140	-100	-56	-71
68	-110	-63	-7	-25
69	-112	-65	-11	-29
70	-113	-66	-13	-30
71	-262	-256	-246	-248
72	-262	-256	-247	-249
73	-263	-257	-247	-249

NOTE: All temperatures are in °F.

TABLE 4.2-4. TEMPERATURE HISTORY AT SECTION C-C OF FIGURE 4.2-3

Segment Number (Ref. Figure 4.2-4)	Time From Launch (seconds)				
	0	75	150	170	235
1	72	88	230	230	218
2	70	86	230	230	209
3	61	82	222	236	189
4	52	79	240	259	201
5	34	69	227	250	190
6	-11	37	136	150	111
7	-38	7	72	81	52
8	-57	-16	33	40	16
9	72	85	230	230	219
10	70	84	228	229	209
11	60	76	194	208	183
12	51	74	229	246	201

NOTE:
All temperatures are in °F.

TABLE 4.2-4. TEMPERATURE HISTORY AT SECTION C-C OF FIGURE 4.2-3 (CONTINUED)

Segment Number (Ref. Figure 4.2-4)	Time From Launch (seconds)				
	0	75	150	170	235
13	32	64	221	242	199
14	-19	27	126	139	109
15	-50	-12	51	60	42
16	-73	-38	4	10	-7
17	73	83	230	230	219
18	70	81	227	227	209
19	60	68	166	180	178
20	49	68	220	236	201
21	30	57	216	236	201
22	-25	18	119	130	107
23	-59	-27	38	46	37
24	73	94	230	230	214
25	71	91	229	229	203
26	60	72	161	176	172
27	48	85	265	280	193
28	31	79	269	285	193
29	-35	28	124	134	97
30	-62	-27	32	40	29
31	73	95	230	230	213
32	71	93	229	229	201
33	61	72	160	175	170
34	47	89	280	294	190
35	31	83	287	301	191
36	-37	34	131	141	94
37	-64	-28	29	37	25
38	60	66	150	164	174
39	60	67	148	163	170
40	61	68	148	162	169
41	60	64	137	152	169
42	60	65	136	151	167
43	60	66	136	150	166
44	60	63	117	134	163
45	60	63	117	133	162
46	60	63	117	133	161
47	60	62	105	123	159

NOTE:
All temperatures are in °F.

TABLE 4.2-4. TEMPERATURE HISTORY AT SECTION C-C OF FIGURE 4.2-3 (CONTINUED)

Segment Number (Ref. Figure 4.2-4)	Time From Launch (seconds)				
	0	75	150	170	235
48	60	62	105	123	159
49	60	62	106	122	158
50	-66	-37	23	31	25
51	-69	-37	19	26	19
52	-70	-38	17	24	16
53	-94	-66	-34	-29	-38
54	-98	-70	-40	-36	-44
55	-99	-72	-42	-38	-47
56	-100	-73	-43	-39	-47
57	-103	-77	-48	-45	-52
58	-104	-78	-50	-47	-54
59	-101	-75	-46	-42	-49
60	-104	-78	-50	-47	-54
61	-105	-79	-52	-49	-56
62	-265	-263	-259	-258	-259
63	-266	-264	-260	-259	-259
64	-266	-264	-260	-259	-260
65	-137	-119	-93	-91	-95
66	-139	-121	-97	-95	-99
67	-140	-122	-99	-96	-100
68	-110	-89	-58	-55	-60
69	-112	-91	-63	-60	-64
70	-113	-92	-64	-62	-66
71	-262	-260	-254	-254	-254
72	-262	-260	-255	-255	-255
73	-263	-260	-255	-255	-255

NOTE:
All temperatures are in °F.

TABLE 4.2-5. TEMPERATURE HISTORY AT SECTION D-D OF FIGURE 4.2-3

Segment Number (Ref. Figure 4.2-4)	Time From Launch (seconds)			
	0	75	150	235
1	72	87	230	198
2	70	86	230	188
3	61	82	222	168
4	52	79	240	174
5	34	69	227	168
6	-11	37	136	89
7	-38	7	72	35
8	-57	-16	33	2
9	72	85	230	198
10	70	83	228	188
11	60	76	193	164
12	51	74	229	174
13	32	63	221	169
14	-19	27	126	87
15	-50	-12	51	27
16	-73	-38	4	-19
17	73	83	230	198
18	70	81	227	188
19	60	68	166	161
20	49	68	220	175
21	30	57	216	170
22	-25	18	119	86
23	-59	-27	30	22
24	73	93	230	192
25	71	91	229	181
26	60	72	161	157
27	48	85	265	166
28	31	79	269	161
29	-35	27	124	76
30	-62	-27	32	15
31	73	95	230	189
32	71	93	229	179
33	61	72	160	155
34	47	88	280	163
35	31	83	287	159

NOTE:
All temperatures are in °F.

TABLE 4.2-5. TEMPERATURE HISTORY AT SECTION D-D OF FIGURE 4.2-3 (CONTINUED)

Segment Number (Ref. Figure 4.2-4)	Time From Launch (seconds)			
	0	75	150	235
36	-37	34	131	73
37	-64	-28	29	12
38	60	66	150	158
39	60	67	148	155
40	61	68	148	154
41	60	64	137	156
42	60	65	136	153
43	60	66	136	153
44	60	63	117	151
45	60	63	117	150
46	60	63	117	150
47	60	62	105	149
48	60	62	105	148
49	60	62	105	148
50	-66	-37	23	12
51	-69	-37	19	6
52	-70	-38	17	4
53	-94	-66	-34	-47
54	-98	-70	-41	-53
55	-99	-72	-43	-55
56	-100	-74	-43	-56
57	-103	-77	-49	-61
58	-104	-78	-51	-63
59	-101	-75	-46	-58
60	-104	-78	-50	-62
61	-105	-79	-52	-64
62	-265	-263	-259	-260
63	-266	-264	-260	-260
64	-266	-264	-260	-261
65	-137	-119	-93	-101
66	-139	-121	-97	-105
67	-140	-122	-99	-106
68	-110	-89	-55	-68
69	-112	-92	-63	-72

NOTE:
All temperatures are in °F.

TABLE 4.2-5. TEMPERATURE HISTORY AT SECTION D-D OF FIGURE 4.2-3 (CONTINUED)

Segment Number (Ref. Figure 4.2-4)	Time From Launch (seconds)			
	0	75	150	235
70	-113	-93	-64	-74
71	-262	-260	-254	-255
72	-262	-260	-255	-256
73	-263	-260	-255	-256

NOTE: All temperatures are in °F.

TABLE 4.2-6. TEMPERATURE HISTORY AT SECTION E-E OF FIGURE 4.2-3

Segment Number (Ref. Figure 4.2-4)	Time From Launch (seconds)			
	0	75	150	235
1	72	87	230	192
2	70	85	229	174
3	61	81	191	129
4	52	76	191	120
5	34	64	166	102
6	-11	30	93	39
7	-38	3	47	-3
8	-57	-18	15	-29
9	72	85	230	192
10	70	83	227	174
11	60	73	156	124
12	51	68	168	120
13	32	54	148	103
14	-19	14	74	37
15	-50	-17	24	-10
16	-73	-40	-11	-46
17	73	82	230	192
18	70	80	224	174
19	60	64	123	120
20	49	60	150	120
21	30	45	132	103
22	-25	0	60	36
23	-59	-33	10	-13

NOTE:
All temperatures are in °F.

TABLE 4.2-6. TEMPERATURE HISTORY AT SECTION E-E OF FIGURE 4.2-3 (CONTINUED)

Segment Number (Ref. Figure 4.2-4)	Time From Launch (seconds)			
	0	75	150	235
24	73	93	230	186
25	71	90	228	167
26	60	61	102	116
27	48	52	113	118
28	31	32	96	102
29	-35	-16	35	30
30	-62	-36	0	-18
31	73	95	230	183
32	71	92	228	165
33	61	61	96	115
34	47	50	101	117
35	31	28	83	101
36	-37	-21	26	28
37	-64	-38	-4	-21
38	60	62	109	117
39	60	61	97	115
40	61	60	92	114
41	60	61	100	114
42	60	61	91	112
43	60	60	87	112
44	60	61	87	109
45	60	60	82	109
46	60	60	80	108
47	60	60	79	107
48	60	60	77	106
49	60	60	76	106
50	-66	-42	-1	-21
51	-69	-44	-8	-25
52	-70	-45	-11	-27
53	-94	-67	-44	-69
54	-98	-72	-50	-74
55	-99	-73	-52	-75
56	-100	-75	-52	-76
57	-103	-78	-57	-80
58	-104	-80	-59	-82

NOTE:
All temperatures are in °F.

TABLE 4.2-6. TEMPERATURE HISTORY AT SECTION E-E OF FIGURE 4.2-3 (CONTINUED)

Segment Number (Ref. Figure 4.2-4)	Time From Launch (seconds)			
	0	75	150	235
59	-101	-76	-54	-78
60	-104	-79	-59	-81
61	-105	-81	-61	-83
62	-265	-264	-260	-262
63	-266	-264	-260	-263
64	-266	-264	-261	-263
65	-137	-119	-99	-117
66	-139	-122	-103	-120
67	-140	-123	-105	-121
68	-110	-89	-65	-86
69	-112	-92	-69	-89
70	-113	-93	-71	-91
71	-262	-260	-255	-258
72	-262	-260	-256	-259
73	-263	-260	-256	-259

NOTE:
All temperature are in °F.

4.2.3.2 Temperatures For Unprotected Smooth Areas. Table 4.2-7 presents maximum temperatures predicted for the operational type interstage adapter. The figures shown are for unprotected, undisturbed regions between Stations 425 and 560. All other areas will experience cooler temperatures due to Thermolag protection or proximity to a heat sink.

The areas of the interstage adapter requiring Thermolag protection are shown in Figure 4.2-5.

TABLE 4.2-7. OPERATIONAL INTERSTAGE ADAPTER MAXIMUM TEMPERATURE BETWEEN STATION 425 AND STATION 560

Component	Time from Launch (sec)	Event	Temperature between Frames (°F)	Temperature at Frames (°F)
0.032 SKIN	75	MACH 1	98	78
	150	MAX g	449	243
	170	MAX TEMP	489	276
0.059 STIFFENER	75	MACH 1	89	87
	150	MAX g	391	319
	170	MAX TEMP	440	356
I FRAME (O.D.)	75	MACH 1	-	73
	150	MAX g	-	227
	170	MAX TEMP	-	259
I FRAME (I.D.)	75	MACH 1	-	61
	150	MAX g	-	90
	170	MAX TEMP	-	109

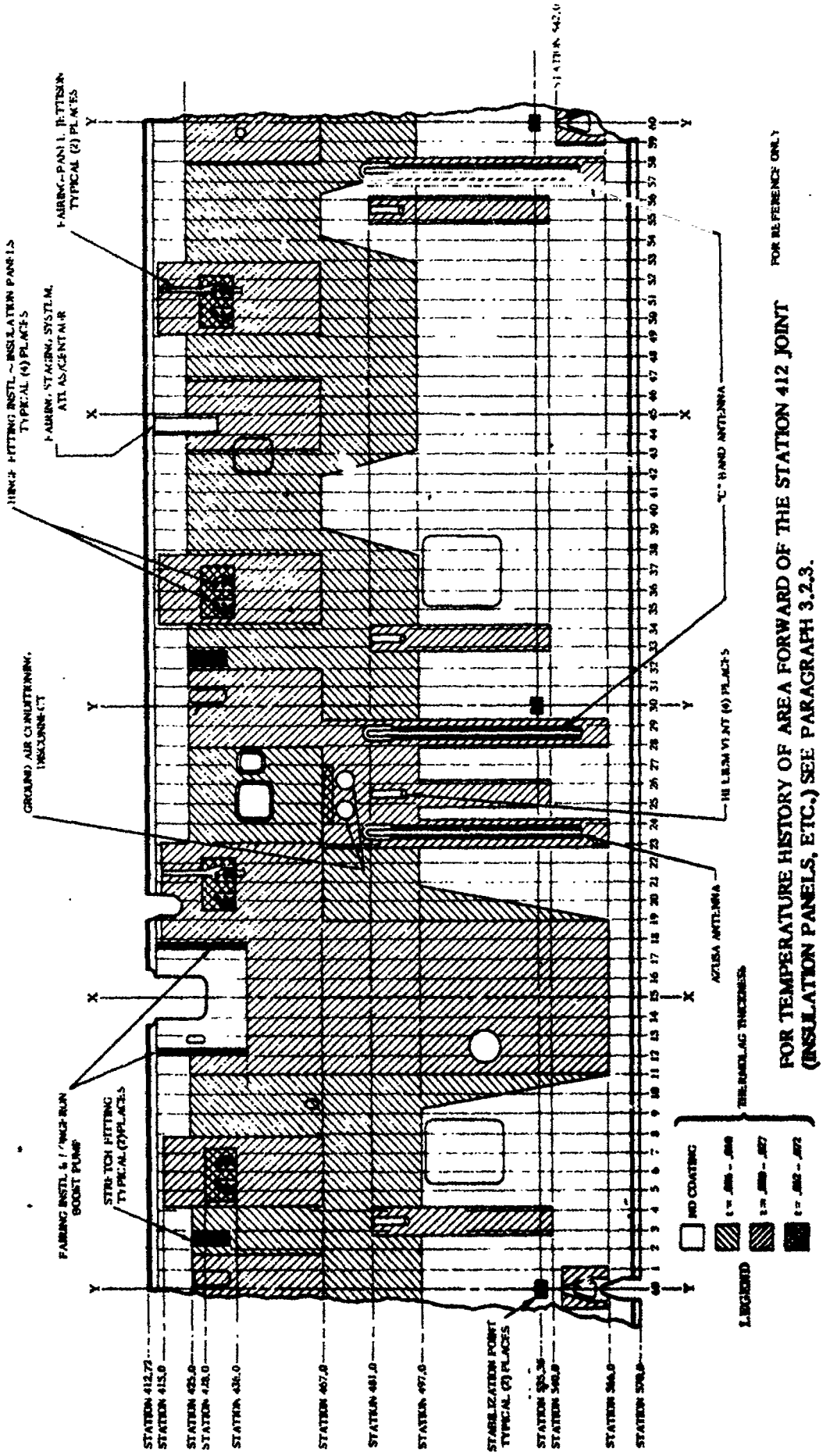

Figure 4.2-5. Operational Interstage Adapter Thermal Insulation Location

4.2.3.3 Station 570 Temperatures. The Station 570 joint is the interface between the interstage adapter and the Atlas liquid oxygen tank. The temperature history of the Station 570 joint and portions of the Atlas tank is given in Paragraph 4.2.3.4.

Figure 4.2-6 shows a cross-section view of the interstage adapter just forward of the Station 570 joint. The section callouts indicate locations where thermal profiles were made. The temperatures at these locations are given in Table 4.2-8.

TABLE 4.2-8. STATION 570 TEMPERATURE DISTRIBUTION-INTERSTAGE ADAPTER

Location	Time (sec)			
	0	60	150	210
1	-[illegible]	-[illegible]	-125	- 60
2	-	-171	-109	- 65
	-	-15[illegible]	- [illegible]	- 32
	-	-[illegible]1	-108	- 65
	-	-17[illegible]	- [illegible]	- 32
	-	- [illegible]	+111	+154
	-	+[illegible]3	+205	+267
	-	[illegible]	+332	+302
	-	-[illegible]4	+[illegible]46	-127
	-	-[illegible]71	-[illegible]	-143
		-[illegible]54	+[illegible]18	+180
	-	-[illegible]2	-10	-[illegible]34
	-	-[illegible]39	-197	+239
14	-[illegible]	-[illegible]53	-[illegible]	-128
15	-[illegible]	-[illegible]70	-[illegible]	+144
16	-[illegible]	-[illegible]88	+116	+180
17	-[illegible]	-[illegible]	+[illegible]1	+214
18	-[illegible]	-[illegible]1[illegible]	+197	+[illegible]238
19	-[illegible]	-[illegible]	+[illegible]37	+129
20	-[illegible]	-[illegible]66	+[illegible]	+144
21	-	-[illegible]90	+117	+180
22	-[illegible]	-[illegible]1	+164	+214
23	-[illegible]51	-[illegible]29	+197	+238

NOTE: ALL TEMPERATURES ARE GIVEN IN °F.

4.2.3.4 Atlas Tank. The temperature histories of various points on the Atlas LO_2 tank skin are presented in Figure 4.2-7 along with the mating rings at the Station 570 joint interface.

The temperatures shown were determined by considering the effects of aerodynamic heating conduction heat transfer into the tank ring, convection heat loss inside the Atlas LO_2 tank, radiation heat loss, and by considering the effects of the flow of hot boundary-layer air flowing in through the front end of the heat shield. Aerodynamic heating on the adapter just forward of the flange was increased by a factor of 1.2 to account for the increase in heating at the base of the wedge shock that forms in front of the heat shield.

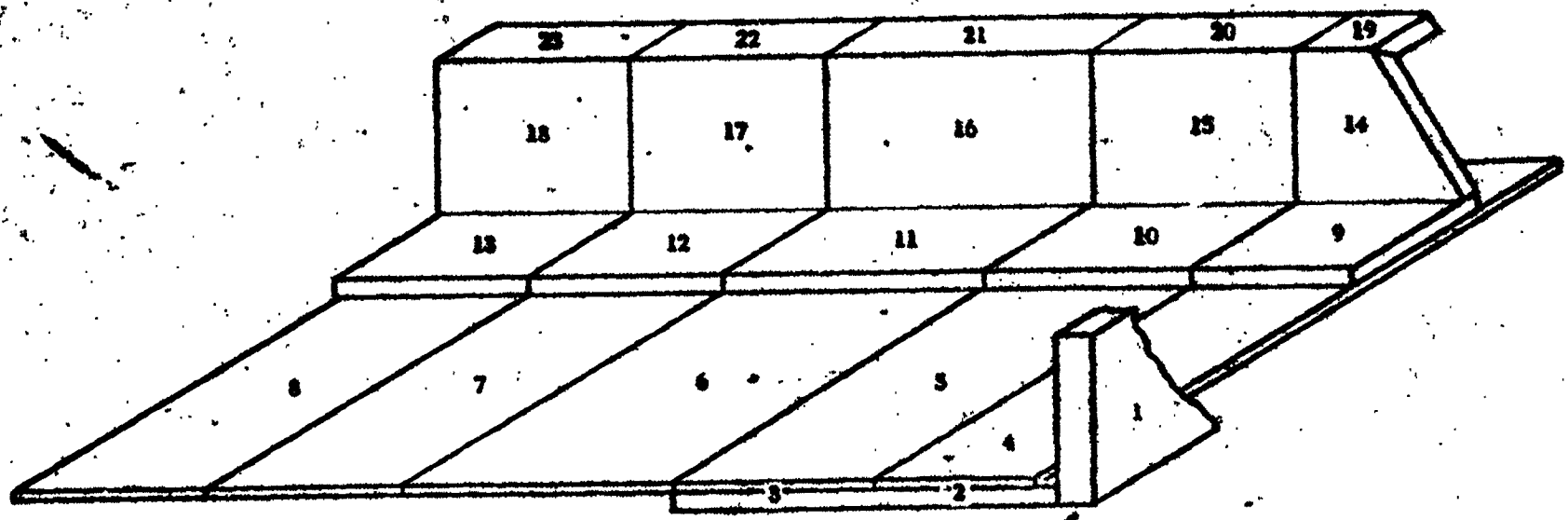

REFERENCE TABLE 4.2-8
FOR DATA POINT TEMPERATURES

Figure 4.2-6. Interstage Adapter - Station 570 Temperature Distribution

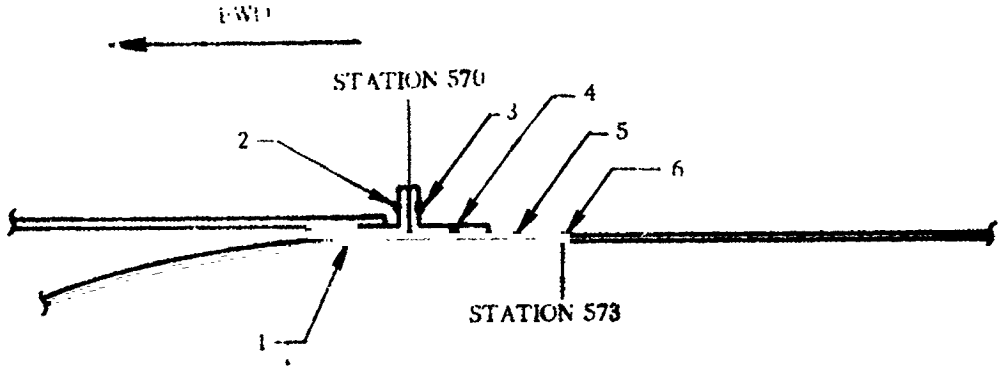

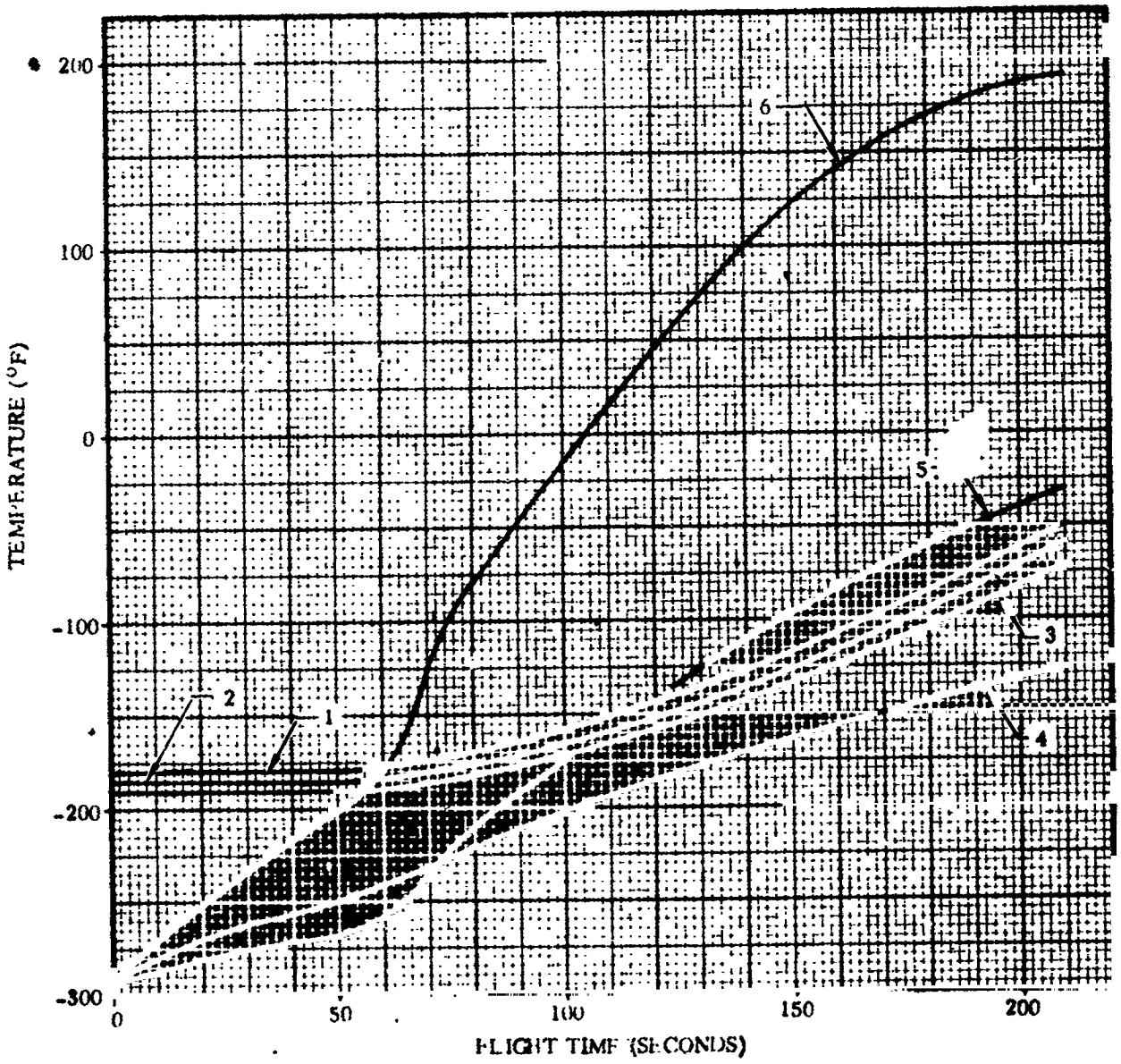

4B41LV

Figure 4.2-7. Station 570 Atlas Tank Ring and Centaur Interstage Adapter Interface - Temperature versus Time

4.2.4 INERTIA LOADS. Inertia loads for the interstage adapter are incorporated in the form of total bending moments and axial loads at Stations 412.72 and 570 respectively.

4.2.4.1 Prelaunch. Effects of vehicle misalignment, initial center of gravity offset, and elastic bending are included:

Bending Moment at Station 412 = 0.805×10^6 in.-lb
Bending Moment at Station 570 = 0.61×10^6 in.-lb

Minimum axial loads associated with the all tanks full prelaunch condition are:

Axial Load (Compression) at Station 412 = 36,820 lb
Axial Load (Compression) at Station 570 = 38,300 lb

Moments and axial loads may be considered to vary linearly over the adapter length.

4.2.4.2 Transonic Flight (Mach Range $0.80 < M < 1.2$). The transonic condition is one of two flight conditions during which peaking longitudinal stresses are imposed on the adapter. Following are the total bending moment and axial load (drag + inertia + ΔP across the adapter):

Bending Moment at Station 412 = 3.15×10^6 in.-lb
Bending Moment at Station 570 = 4.25×10^6 in.-lb

Axial Load at Station 412 = 135,600 lb (Compression)
Axial Load at Station 570 = 140,300 lb (Compression)

Lateral shear forces are obtained from the slope of the bending moment curve ($S = dM/dS$):

Lateral Shear at Station 412 = 8500 lb
Lateral Shear at Station 570 = 7000 lb

4.2.4.3 Maximum Booster Acceleration. Maximum acceleration occurs at booster engine cutoff (BECO). The total bending moments, axial loads, and lateral shears applied to the fore and aft rings of the interstage adapter at Max g are primarily inertia effects and are listed below:

Bending Moment at Station 412 = 0.25×10^6 in.-lb
Bending Moment at Station 570 = 0.46×10^6 in.-lb

Axial Load at Station 412 = 233,000 lb (Compression)
Axial Load at Station 570 = 239,000 lb (Compression)

Lateral Shear at Station 412 = 1670 lb
Lateral Shear at Station 570 = 1000 lb

The above moments and loads may be assumed to vary linearly over the length of the adapter.

4.2.5 STEADY-STATE AIR LOADS. Ground wind loads during prelaunch operations contribute to the total bending moments and axial loads described in Paragraph 4.2.4.1.

Envelopes of maximum crushing and bursting differential pressure at zero angle of attack are presented in Figures 4.2-8 through 4.2-13 for the Mach number range of large differential pressures ($0.80 < M < 1.20$).

Adapter differential pressures behind the major protuberances at the aft end of the Centaur vehicle are also shown in Figures 4.2-8 through 4.2-13. It should be noted that the protuberance effects are shown only for the maximum crushing condition. Protuberance effects for the maximum bursting condition can be obtained by applying the curves for the maximum crushing condition to the maximum bursting "clean area" curves.

Maximum changes in adapter external pressure due to a design angle of attack of six degrees are shown in Figure 4.2-14 and 4.2-15.

For strength analysis purposes, the angle of attack effects shall be applied in the most conservative way:

a. Increase the ΔP on the windward side and decrease the ΔP on the leeward side by the values given in Figures 4.2-14 and 4.2-15 and use a cosine variation in between.

b. Consider the windward side to be that side which causes the most severe loading effect of a. above.

These steady-state differential pressures should be considered simultaneously with the load given in Paragraph 4.2.4.2.

4.2.6 BUFFET AND FLUTTER LOADS. Both empirical and analytical evidence indicate that the combination of stiffness and mass parameters which determine the modal frequencies of the AC-6 adapter are equivalent to those of the AC-2 adapter. For this reason the data obtained from the AC-2 and AC-3 adapter frame vibration was used to determine the AC-6 adapter frame bending moments.

Since there was no flight data on AC-2 stringer deflection, the stringer moments were conservatively calculated from maximum relative frame movement.

The transonic buffet bending moments in the frames and stringers to be used for stress analysis are the following:

B.M. = 2500 in.-lb (frames)

and

B.M. = 140 in.-lb (stringers)

These moments should be superimposed on all other moments to produce maximum stresses.

4.2.7 MISCELLANEOUS LOAD PARAMETERS. No other loads need be considered for the basic structure.

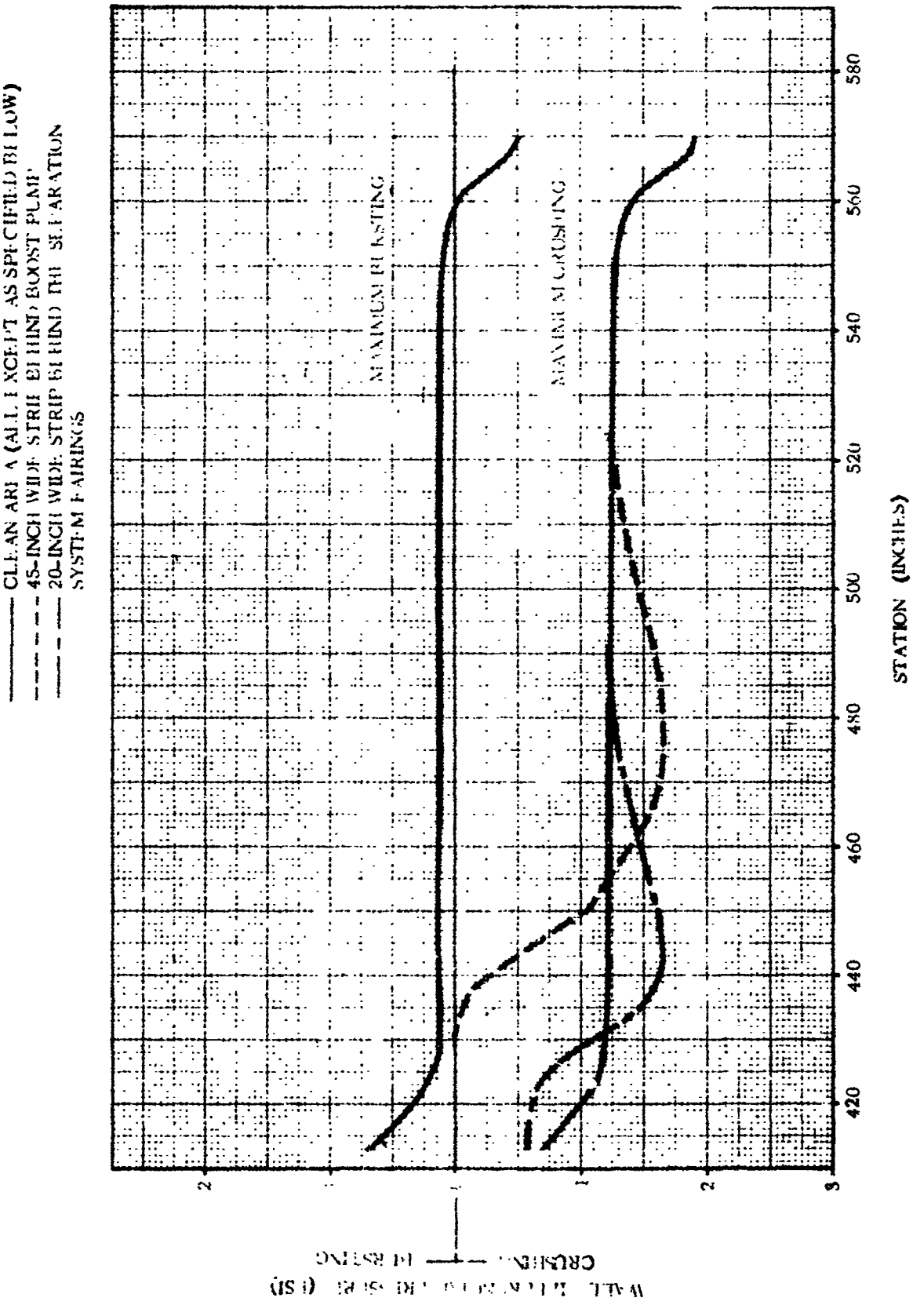

4B29.T

Figure 4.2-8. Operational Interstage Adapter Wall Differential Pressures for $\alpha = 0$, $M_\infty = 0.80$

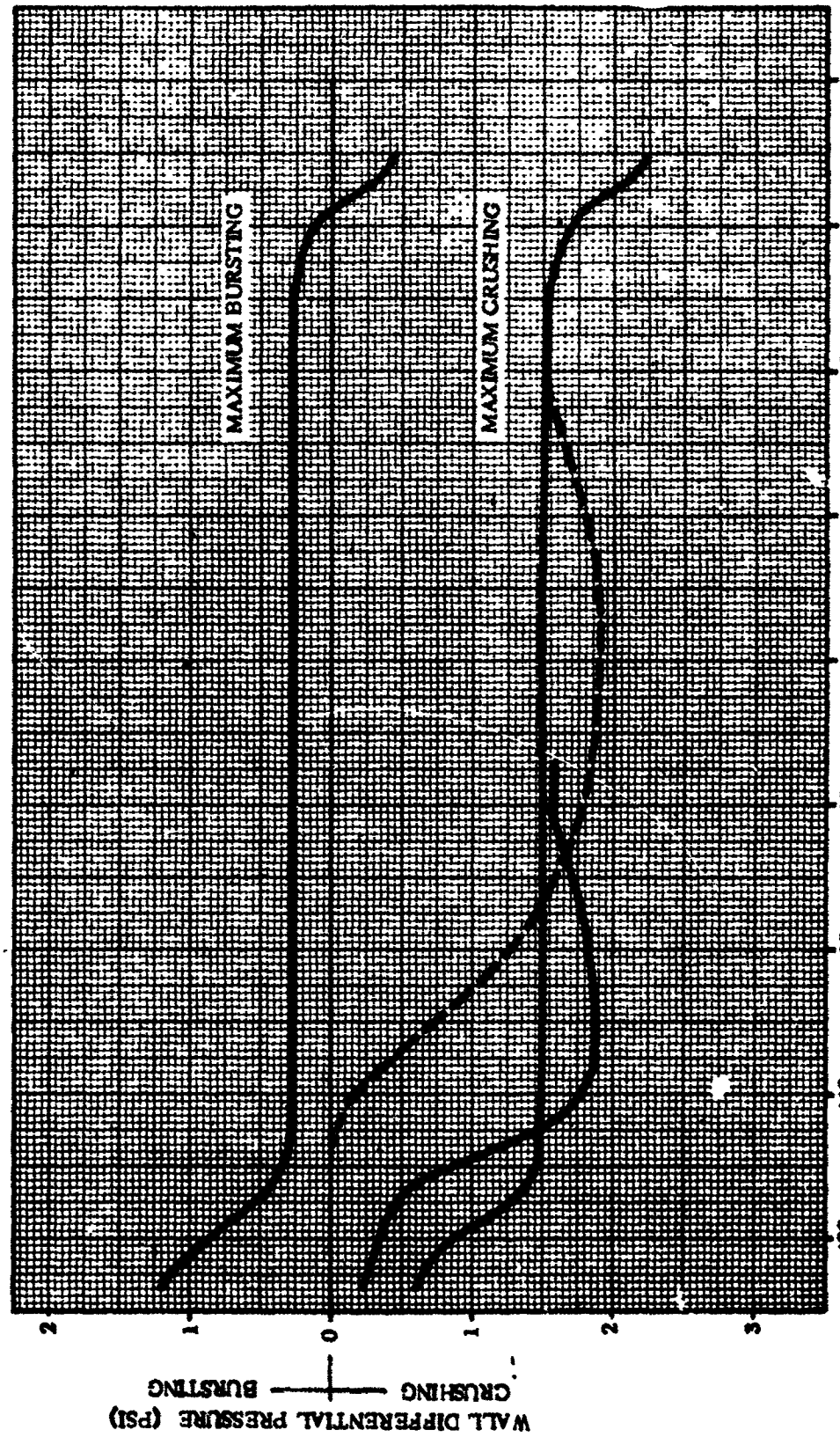

FOR AREAS OF APPLICATION SEE FIGURE 4.2-8

4B3DLT

Figure 4.2-9. Operational Interstage Adapter Wall Differential Pressures for $\alpha = 0$, $M_\infty = 0.90$

FOR AREAS OF APPLICATION SEE FIGURE 4.2-8

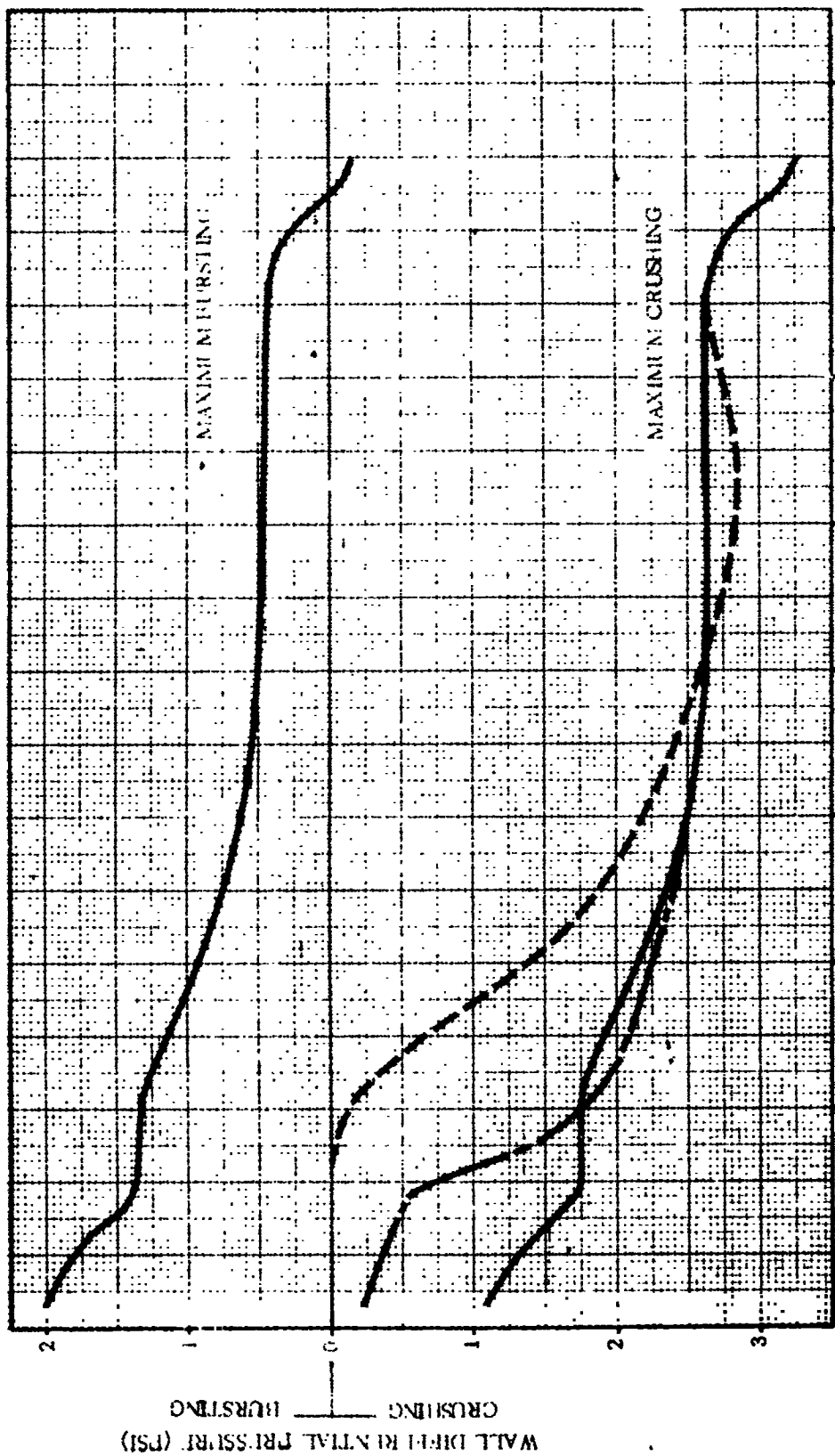

4B31LT

Figure 4.2-10. Operational Interstage Adapter Wall Differential Pressures for $\alpha = 0$, $M_\infty = 1.00$

FOR AREAS OF APPLICATION SEE FIGURE 4.2-8

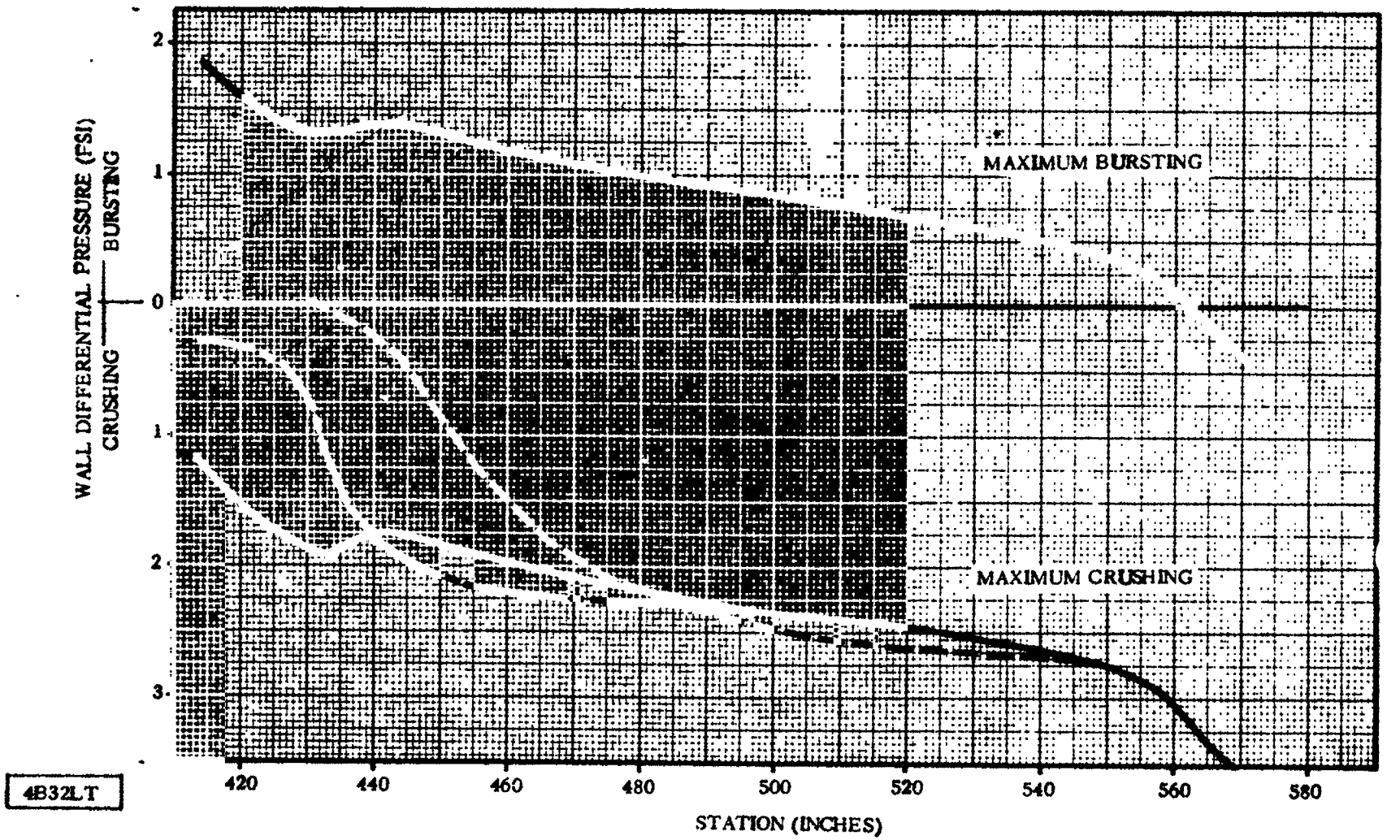

Figure 4.2-11. Operational Interstage Adapter Wall Differential Pressures for $\alpha = 0$, $M_\infty = 1.05$

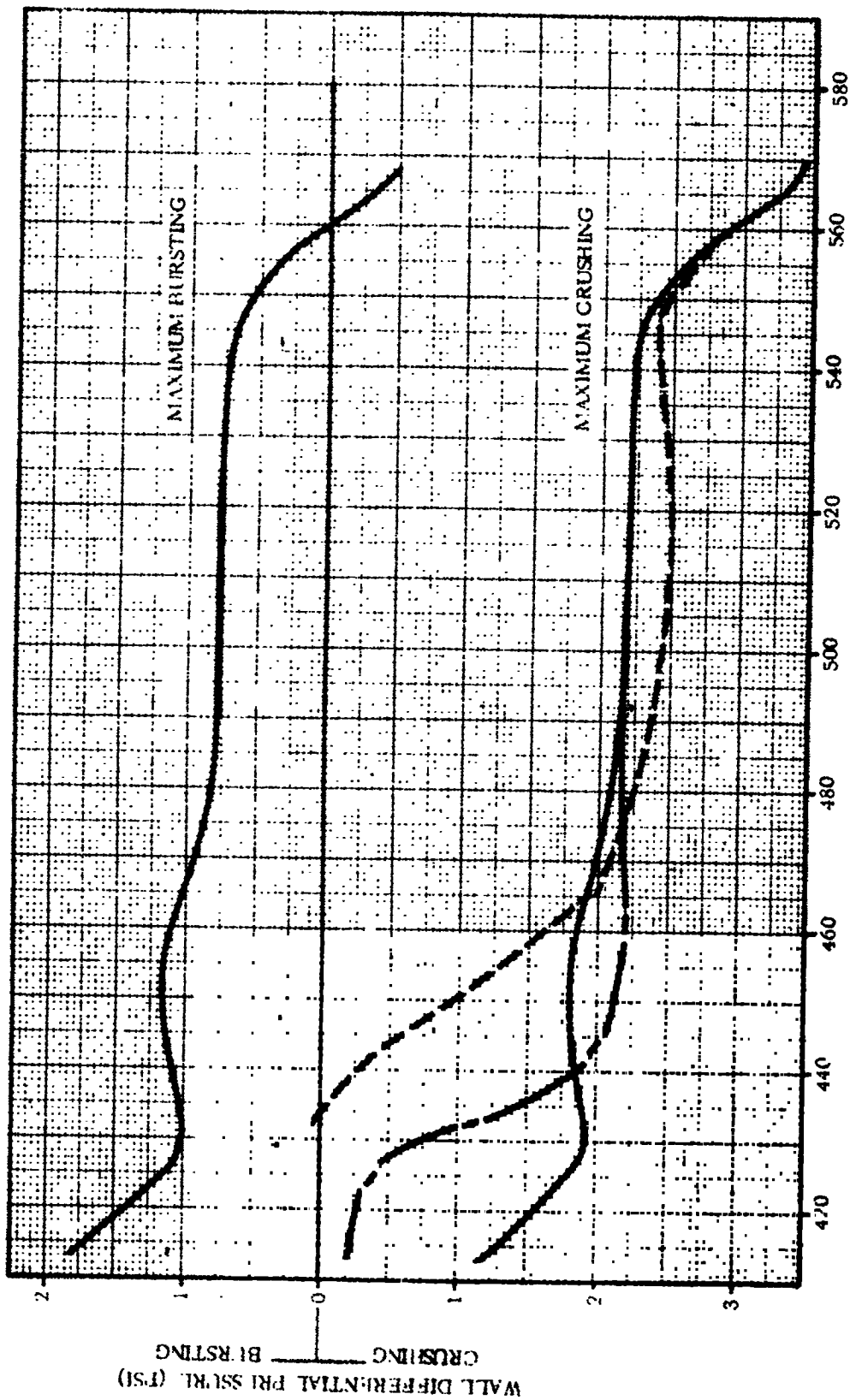

FOR AREAS OF APPLICATION SEE FIGURE 4.2-8

4B33LT

Figure 4.2-12. Operational Interstage Adapter Wall Differential Pressures for $\alpha = 0$, $M_\infty = 1.10$

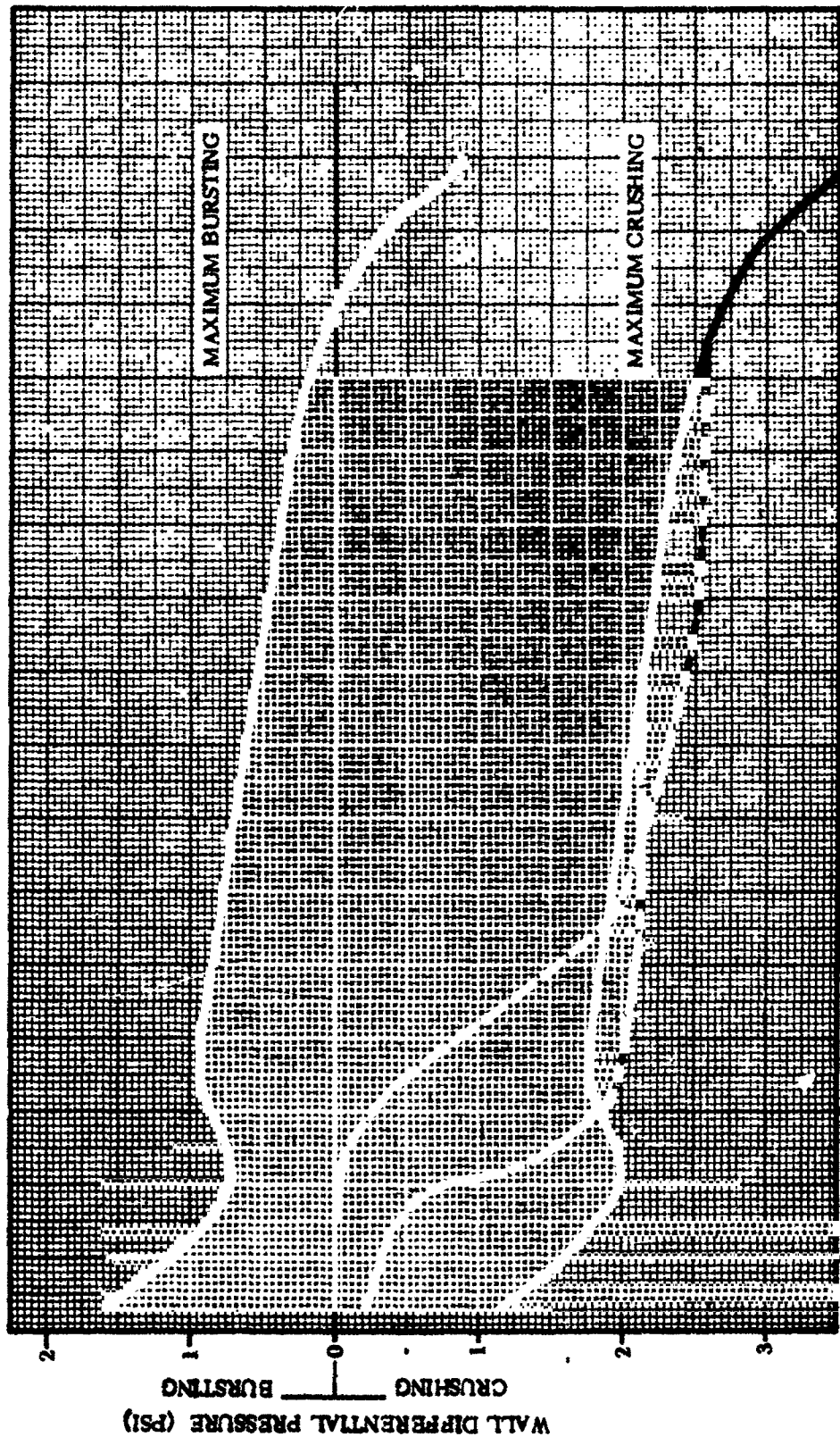

FOR AREAS OF APPLICATION SEE FIGURE 4.2-8

4B34T

Figure 4.2-13. Operational Interstage Adapter Wall Differential Pressures for $\alpha = 0$, $M_\infty = 1.20$

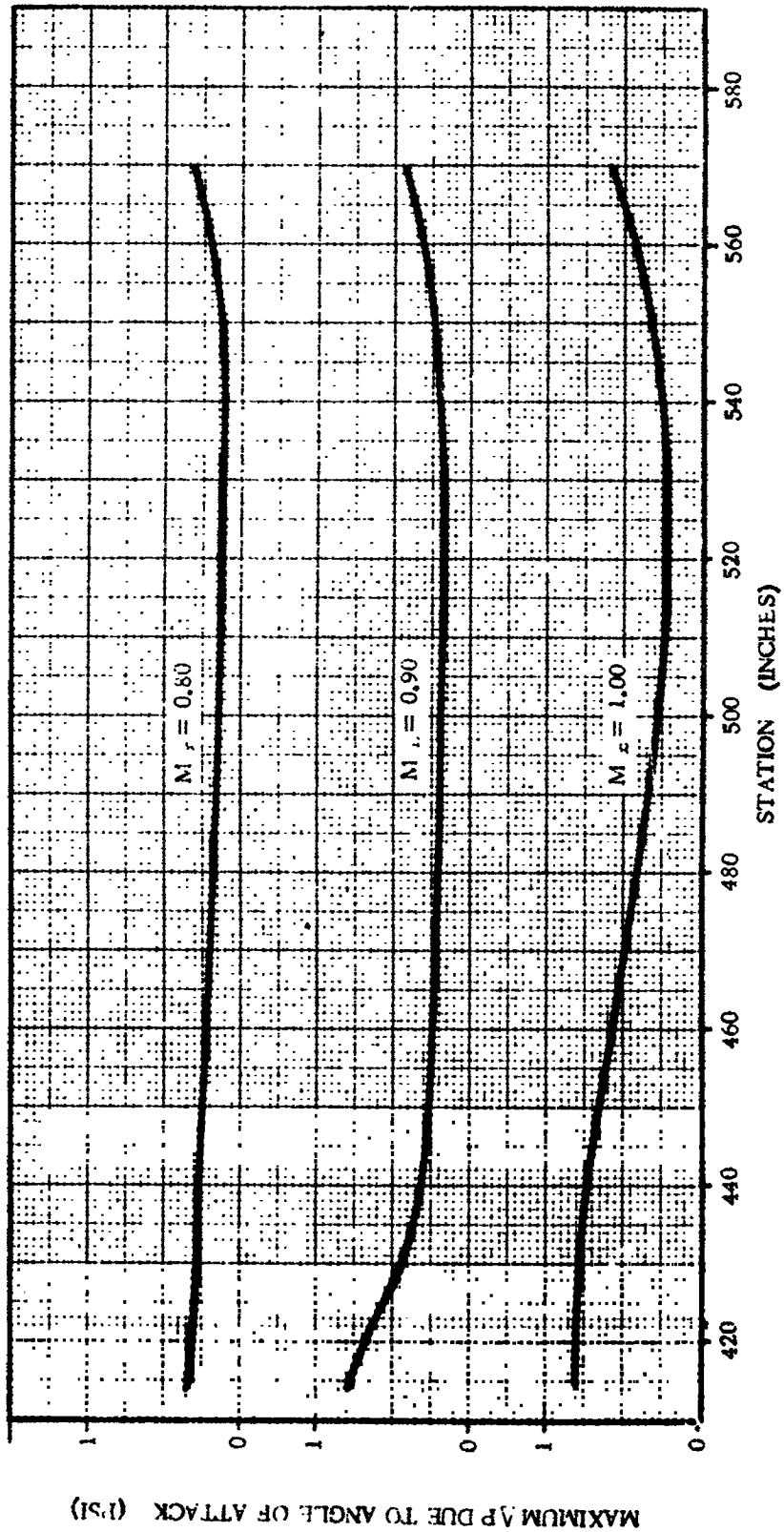

4B35LT

Figure 4.2-14. Operational Interstage Adapter Maximum Change in External Pressure Due to Angle of Attack α = 6 Degrees

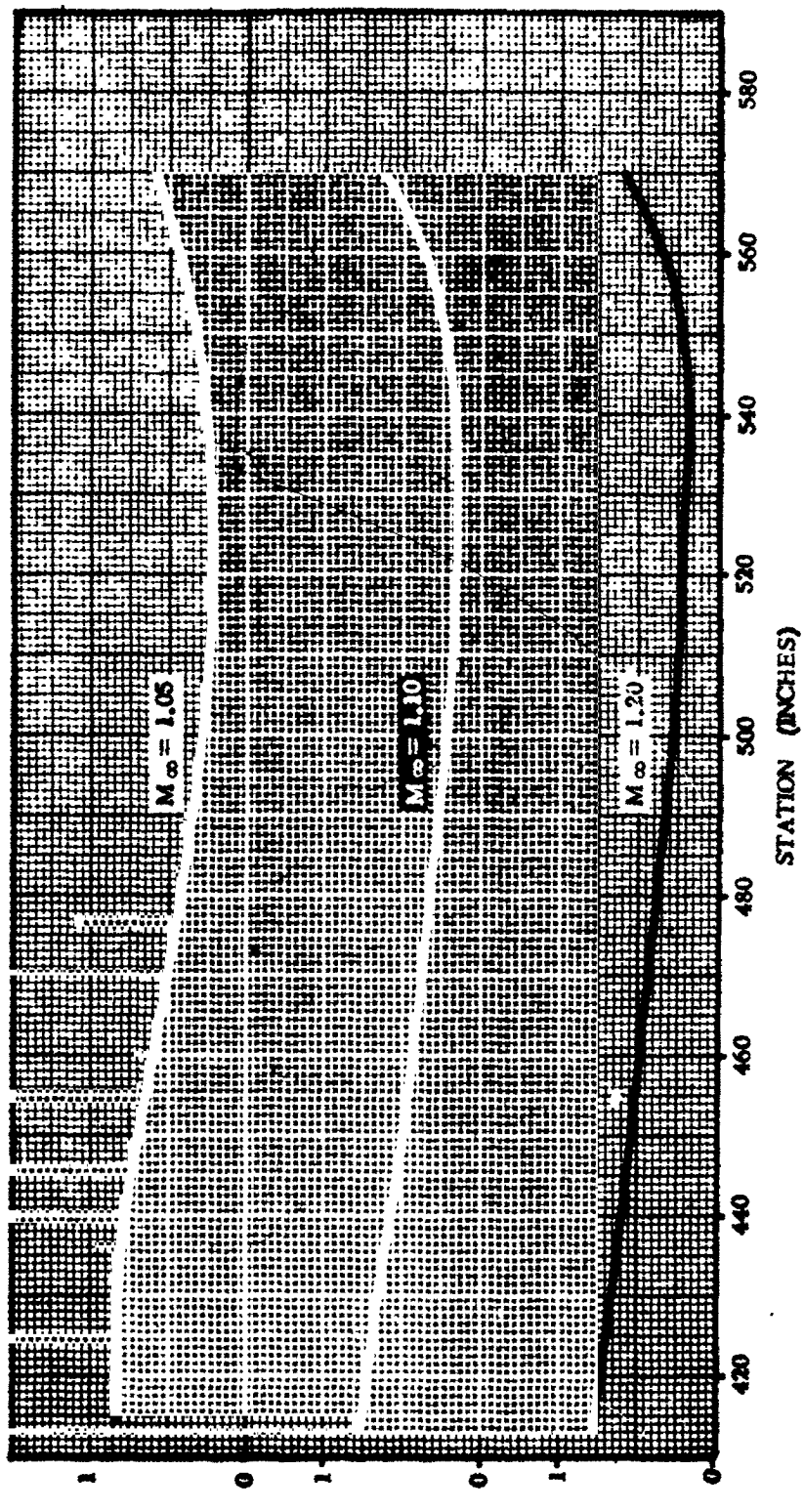

Figure 4.2-15. Operational Interstage Adapter Maximum Change in External Pressure Due to Angle of Attack α = 6 Degrees

THIS PAGE INTENTIONALLY LEFT BLANK.

4.3 HELIUM CHILLDOWN SYSTEM

The purpose of the helium chilldown system is to increase the payload capability over an inflight system by shortening upper stage free-fall time and reduction of in-flight chilldown requirements and attendent overboard propellent losses.

Helium ducts are mounted in the interior of the interstage adapter which extend from the T-4 umbilical panel to the Centaur engines and from the Centaur engines to the four helium vent fins.

The single large helium vent fin which had been used on all previous vehicles is replaced by four smaller vent fins on the operational vehicle. These fins are located at Station 483 (see Figure 4.1-1) and as shown in the configuration sketch (Figure 4.3-1).

4.3.1 CRITICAL CONDITIONS. The helium ducts are considered only for disconnect forces which occur at the Pratt & Whitney interface during Atlas/Centaur separation. Since these duct are essentially made of a plastic or Teflon material, no other loading conditions are applicable.

The helium vent fins are exposed to the airstream, therefore the critical loading occurs during transonic flight when steady-state and fluctuating airloads act simultaneously. Maximum temperatures occur at a later time during flight; however, the airloads have reduced to a negligible magnitude and need not be considered at this time.

4.3.2 WEIGHTS AND CENTER OF GRAVITY DATA. Due to the nature of this hardware (both the ducts and vent fins) inertia loads are of an inconsequential magnitude compared to disconnect forces and aerodynamic loads on the fairing. Weights and C.G. data are not applicable.

4.3.3 THERMAL DATA. Temperature considerations regarding the disconnect forces on the plastic ducts (interface) are further discussed in Paragraph 4.3.7.

Figures 4.3-2 and 4.3-3 present the temperature histories of the internal and external surfaces of the fins at 0 degrees, 45 degrees and 90 degrees from the stagnation line. Figure 4.3-2 is applicable only to the vent that is located in Quadrant II and immediately aft of the GN_2 conditioning ducts. The analysis of this vent took into account the disturbance of its flow field by the presence of the ducts. Figures 4.3-3 gives the temperature histories predicted on the remaining three vent fins, and were obtained from an analysis which assumed that they received free stream swept cylinder heating.

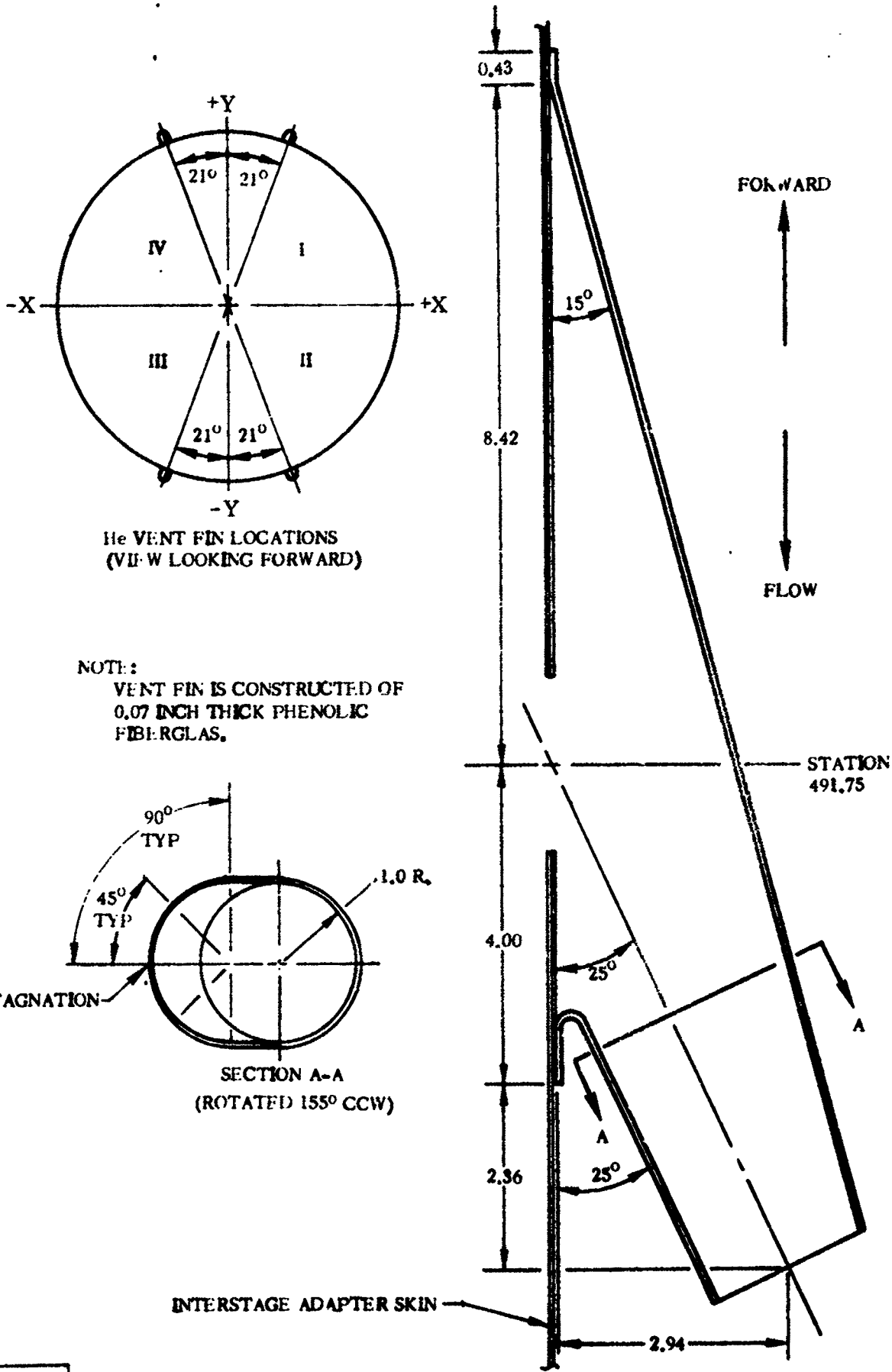

Figure 4.3-1. Helium Vent Fin Configuration

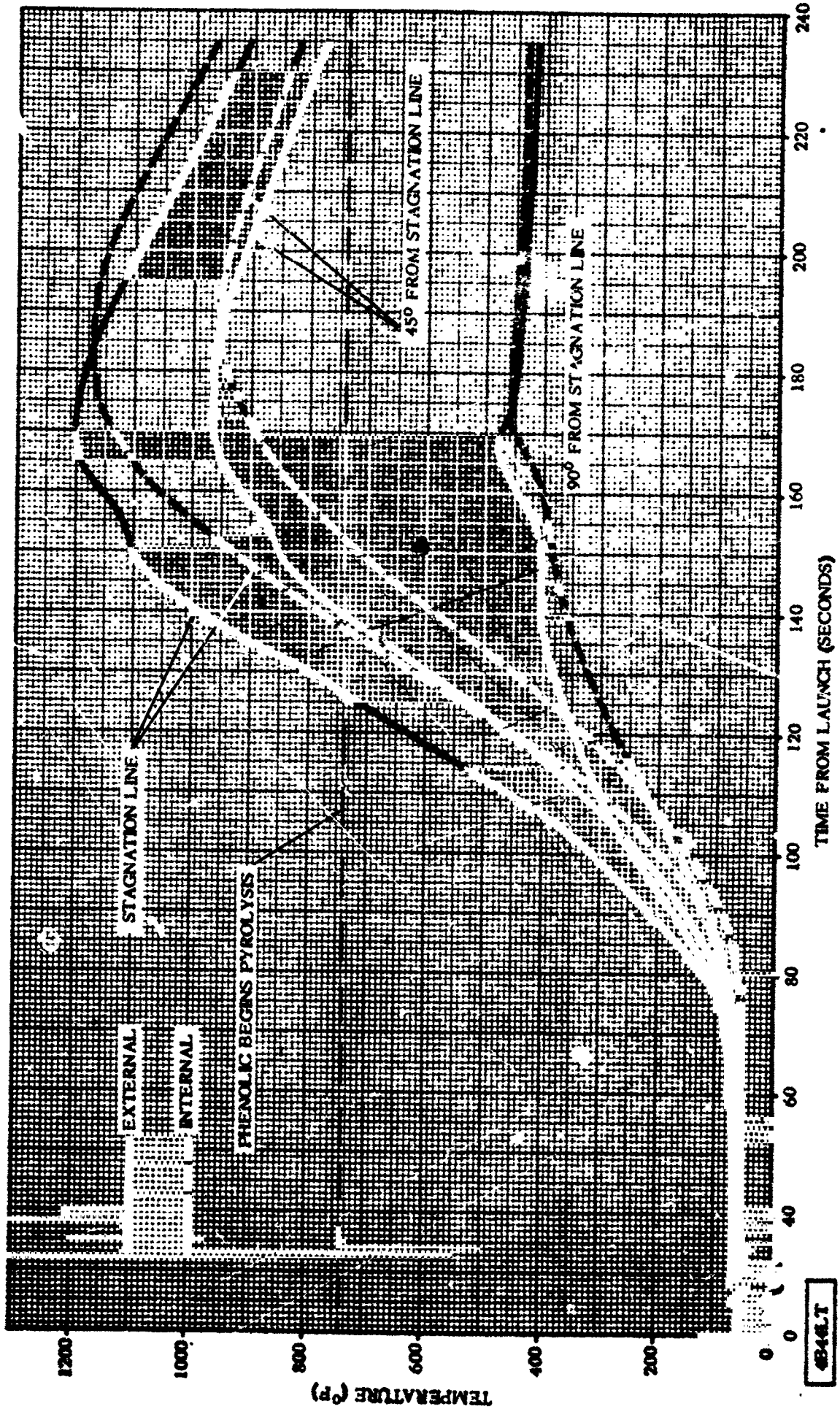

Figure 4.3-2. Quadrant II Helium Vent Fin (Mounted on the Operational Interstage Adapter) - Internal and External Surface Temperature Histories of the Windward Side

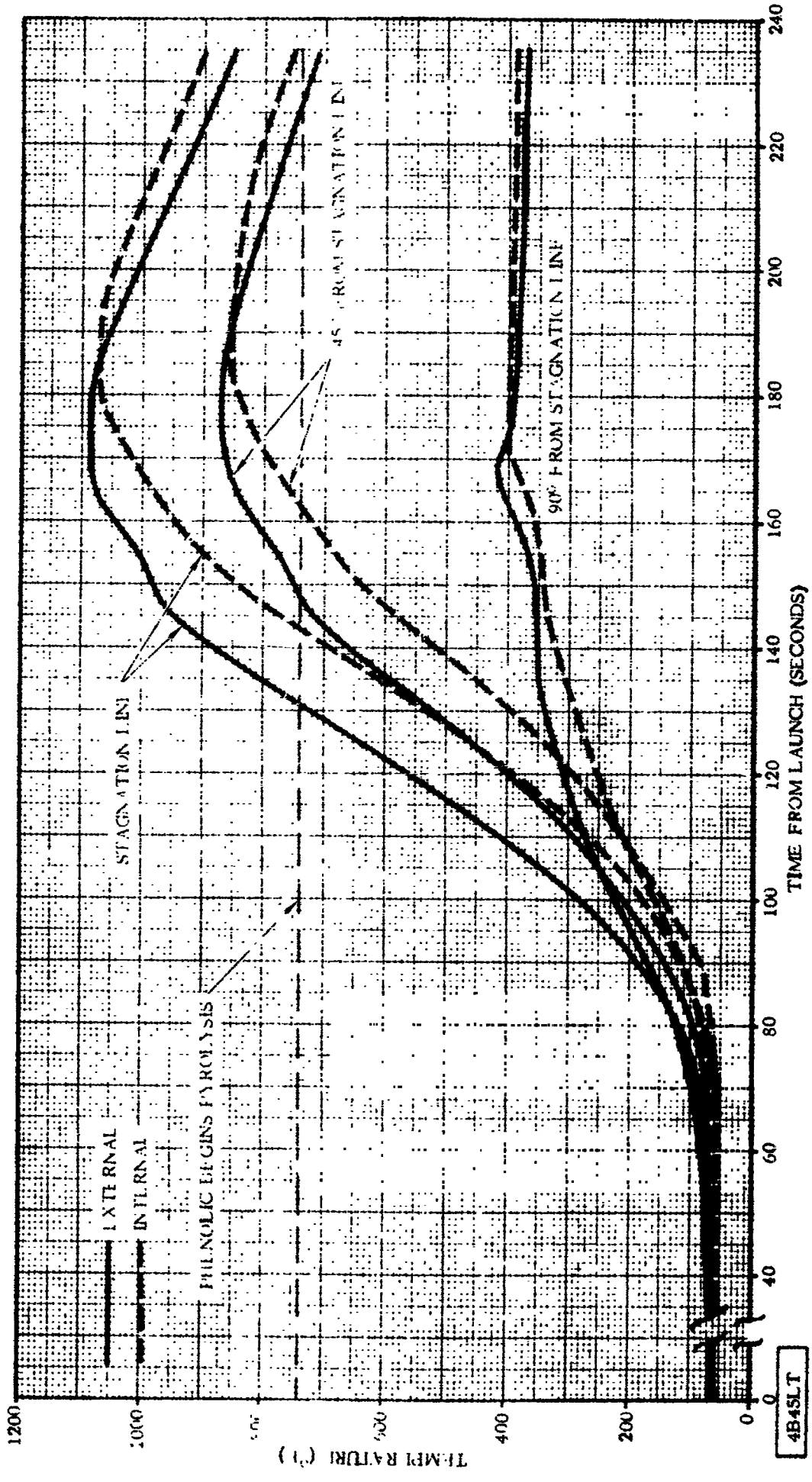

Figure 4.3-3. Quadrants I, III, and IV Helium Vent Fins (Mounted on the Operational Interstage Adapter) – Internal and External Surface Temperature Histories of the Windward Side

Referring to Figures 4.3-2 and 4.3-3, the pyrolyzation temperature of 740°F for phenolic resin is well exceeded throughout the entire wall thickness for a distance of at least 45 degrees on either side of the stagnation line. Even though the resin will char completely, the Refrasil cloth should remain intact since the maximum temperature attained by the fins is well below its melting temperature. The aerodynamic forces acting upon the vent fins at the time of significant resin degradation should be small enough that a failure, other than a change in shape, should not occur.

The heat absorbed by the phenolic pyrolysis reactions is not accounted for in these analyses, which results in somewhat conservative temperature history predictions.

The maximum heating design trajectory described in Reference 1-3 is used for this study which also introduces considerable conservatism.

4.3.4 INERTIA LOADS. Load contribution from inertia effects are not to be considered for this hardware (see Paragraph 4.3.2).

4.3.5 STEADY-STATE AIR LOADS. Steady-state air loads which occur during transonic flight (Mach numbers from 0.85 to 1.30) are given as a maximum differential pressure, a normal force, and a side force as shown in Figure 4.3-4.

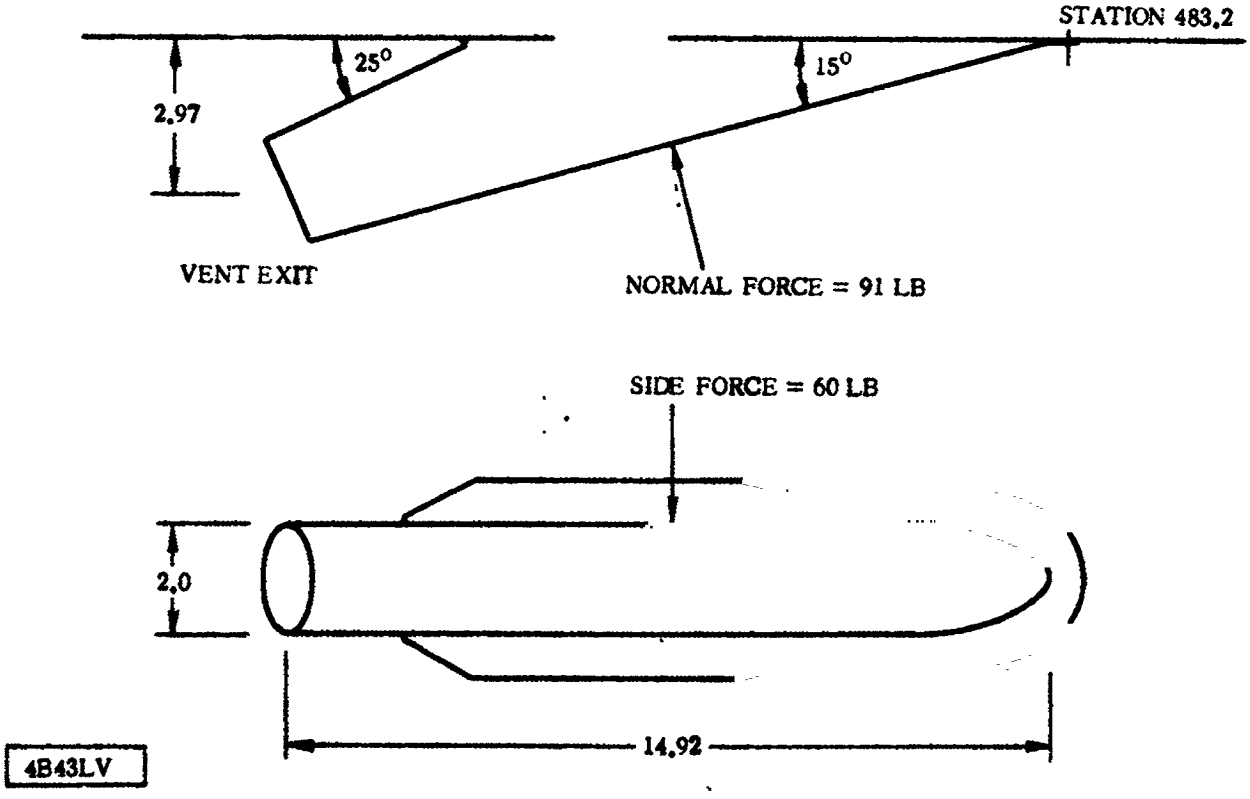

NOTE: (1) APPLY LOADS UNIFORMLY OVER PROJECTED AREAS
(2) MAXIMUM WALL ΔP IS 2.75 PSI CRUSHING

(Reference Figure 4.3-1)

Figure 4.3-4. Helium Chilldown Vent Fin Maximum Steady-State Aerodynamic Loads

4.3.6 BUFFET AND FLUTTER LOADS. As the vehicle ascends through the atmosphere at transonic speeds (Mach numbers 0.85 to 1.30), an additional ΔP results from Chevalier buffeting effects. Due to the dynamic response of the vent fin to this phenomena, an equivalent ΔP of ±1.0 psi should be superimposed upon the steady-state airloads described in Paragraph 4.3.5.

4.3.7 MISCELLANEOUS LOAD PARAMETERS. At Atlas/Centaur separation, the plastic staging ducts experience disconnect forces at the Pratt & Whitney engine chill-down valve interface. These loads are based on two disconnect modes, namely, the primary and backup disconnect systems.

The loads presented in Table 4.3-1 are taken from data obtained in test of the disconnect mechanisms at cryogenic temperatures. Since the temperature is more nearly at 0°F at the lower end (-260°F to -250°F at the upper) during disconnect, these values are conservatively high.

TABLE 4.3-1. HELIUM CHILLDOWN DUCT - LOADS ON THE DISCONNECT MECHANISMS

	Axial (lb)	Shear (lb)	Bending Moment (in.-lb)	Torque (in.-lb)
*Pratt & Whitney Allowable Interface Loads	25	20	300	300
Primary Disconnect	21	6	174	30
Backup Disconnect	21	6	174	30

*Information only

No other loads need be considered for the helium vent fins.

4.4 LIQUID HYDROGEN BOOST PUMP FAIRING

The boost pump fairing has been modified for the operational vehicle by enlarging the cutout on the forward end.

This was done to reduce weight by removing nonfunctional material and does not affect the loads on the fairing. The boost pump fairing skirt has also been modified by the addition of a small shaped charge fairing on the forward ramp. The new fairing does not affect the boost pump fairing wind loads.

The boost pump fairing is physically attached to the interstage adapter immediately aft of Station 412.72 on the X-X axis between Quadrants I and II. See Figure 4.4-1 for configuration of fairing. Reference Figure 4.2-1 for location of cutout in the adapter skin.

4.4.1 CRITICAL CONDITIONS. The interstage adapter liquid hydrogen boost pump fairing experiences most severe loading during the transonic period of flight when steady-state and fluctuating air loads are imposed simultaneously to the fairing. Detrimental temperature effects should not be considered at this time.

Temperature effects should be included after aerodynamic loads have reduced to negligible magnitude.

4.4.2 WEIGHTS AND CENTER OF GRAVITY DATA. Due to the nature of this component, inertia loads are of an inconsequential magnitude compared to the aerodynamic loads, therefore, weights or C.G. data are not applicable.

4.4.3 THERMAL DATA. The predicted temperature history is presented in Figure 4.4-2 for the inner and outer Fiberglas facings. The thermal analysis was performed for a point on the fairing considered to be in an expanded air flow region downstream of a shockwave that is generated by the boost pump fairing.

The following assumptions are made:

a. The exterior surface emissivity was 0.85
b. Forced convection from the interior surfaces of the fairing to liquid oxygen surfaces was considered during chilldown with a heat transfer coefficient equal to 2.0 Btu/hr-ft^2 $^\circ$R (gas temperature - 80° F)
c. No solar heat flux was considered.

4.4.4 INERTIA LOADS. Load contribution from inertia effects are not critical for this component (see Paragraph 4.4.2).

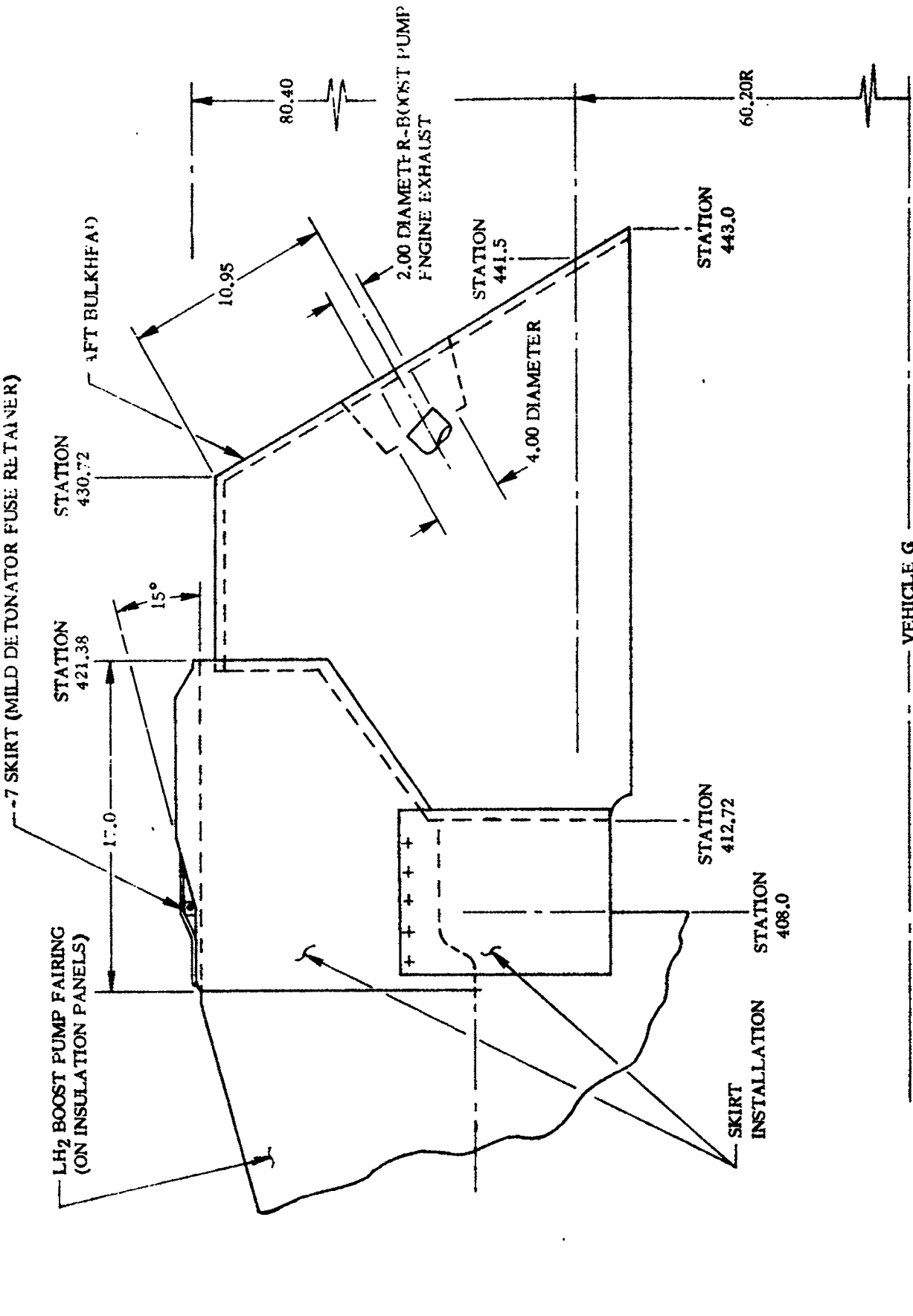

Figure 4.4-1. Interstage Adapter Liquid Hydrogen Boost Pump Fairing Configuration

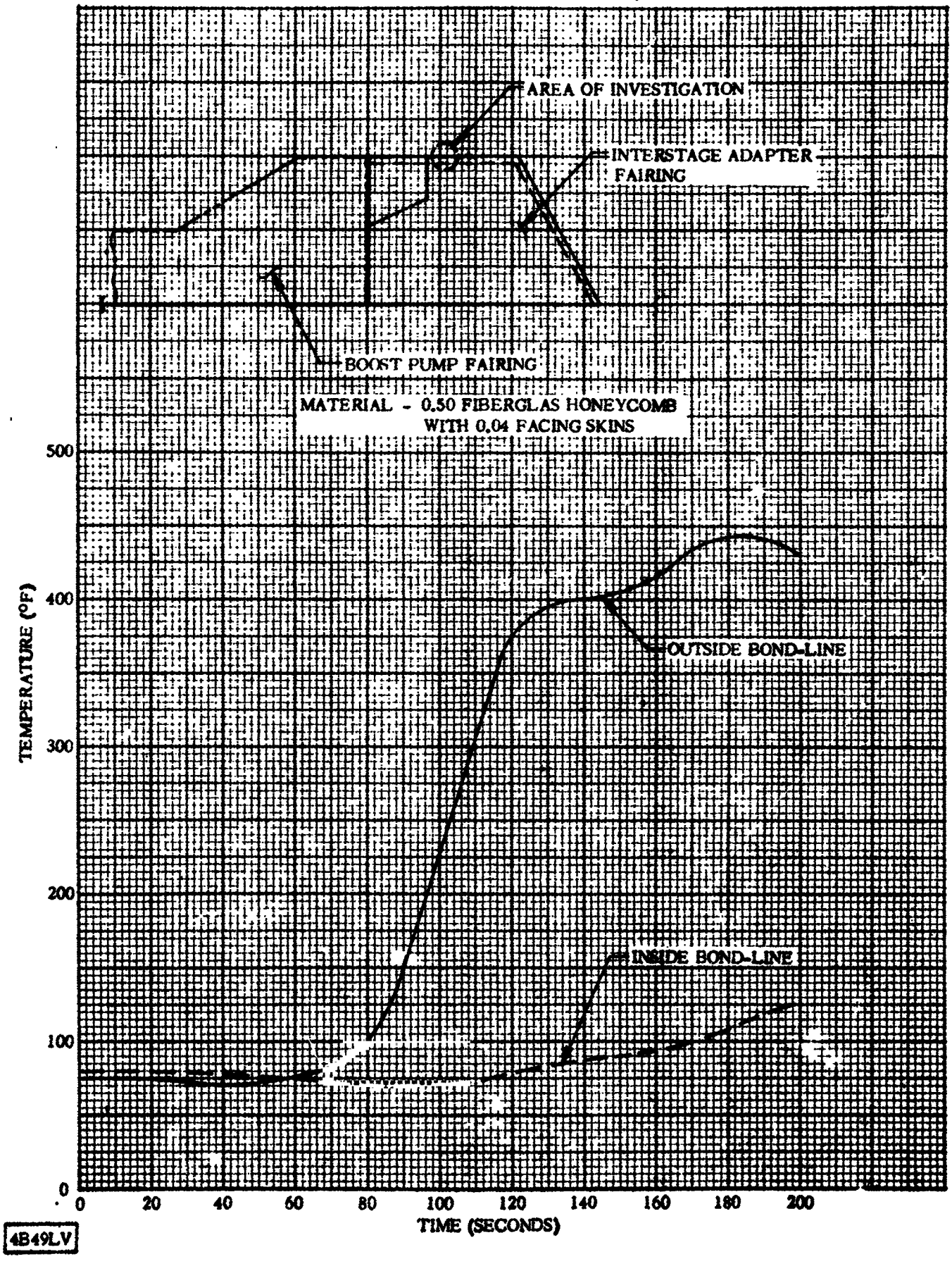

Figure 4.4-2. Interstage Adapter Fairing (Pod 15) Temperature History

4.4.5 STEADY-STATE AIR LOADS. The steady-state wall differential pressure envelope as shown in Figure 4.4-3 represents an average ΔP based on a zero angle of attack (α = 0 degrees). These values are assumed to act uniformly over the surface of the boost pump fairing and bulkhead.

The incremental pressure changes due to six degrees angle of attack as presented in Figure 4.4-4 should be added to the average pressure for the windward wall and subtracted for the lee wall.

For purposes of analysis, determine total side loading from Figures 4.4-3 and 4.4-4:

Windward Side = +1.50 +0.45 = +1.95 psi (Crushing)

Leeward Side = +1.50 -0.45 = +1.05 psi (Crushing)

Therefore, the net side loading, ΔP = +0.90 psi (Crushing)

and, the running side load can be calculated for α = 6 degrees:

0.90 x h (Fairing Height) =

0.90 psi x 20 inches = 18 lb/in.

And the total side loading for α = 6 degrees is:

0.90 x (Fairing Side Area) =

0.90 psi x 400 $in.^2$ = 360 lb

These loads occur during transonic flight (Mach No. 0.85 to 1.30) and must be superimposed with the buffet loads described in Paragraph 4.4.6.

Steady-state aerodynamic loads on the -7 boost pump fairing skirt (mild detonator fuse retainer) are also shown in Figures 4.4-3 and 4.4-4. Drag versus Mach number for the skirt is shown in Figure 4.4-5.

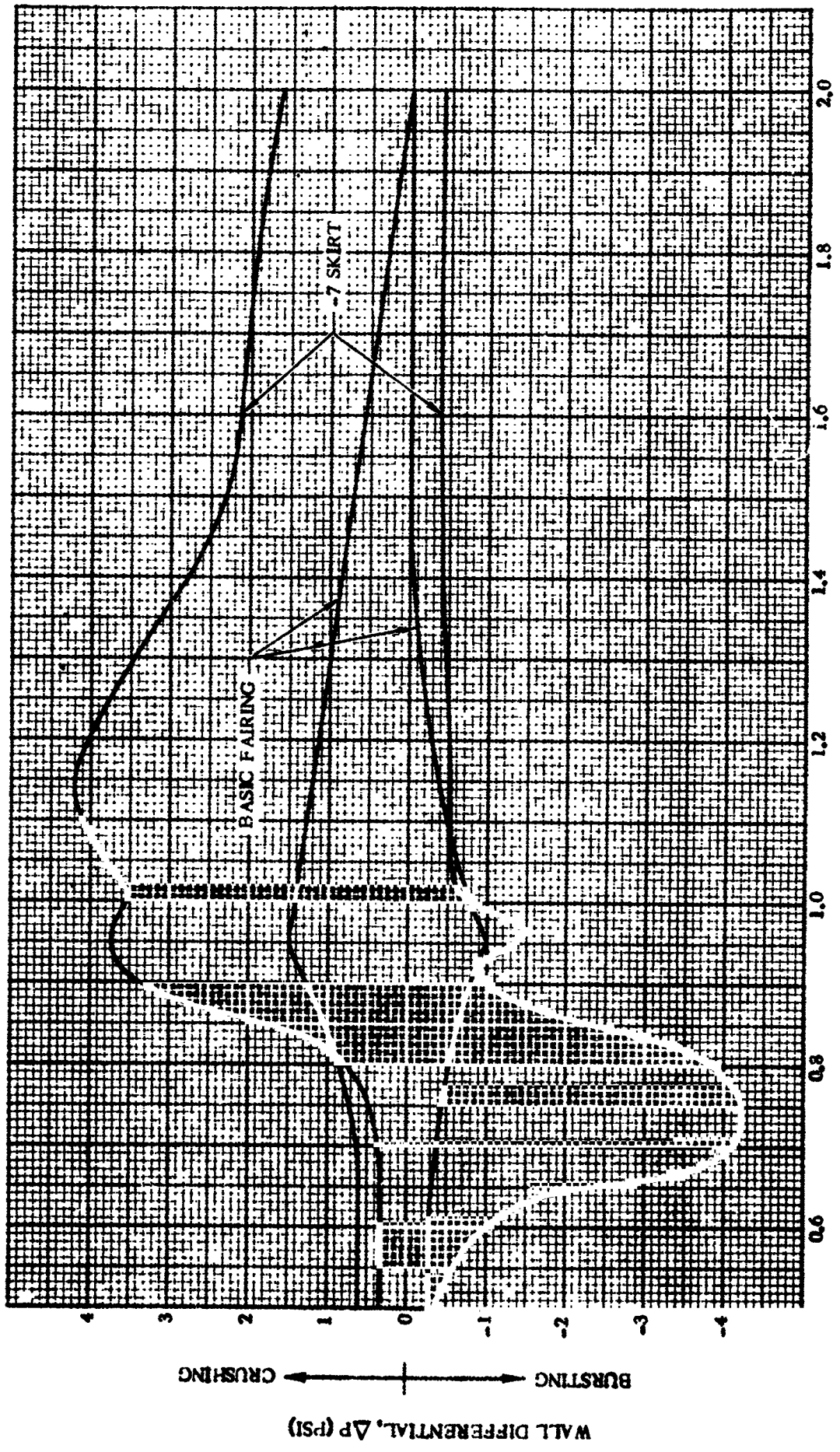

Figure 4.4-3. Interstage Adapter Liquid Hydrogen Boost Pump Fairing, -7 Skirt, and Aft Bulkhead Steady-State Wall Differential Pressure Envelope (α = 0 Degrees)

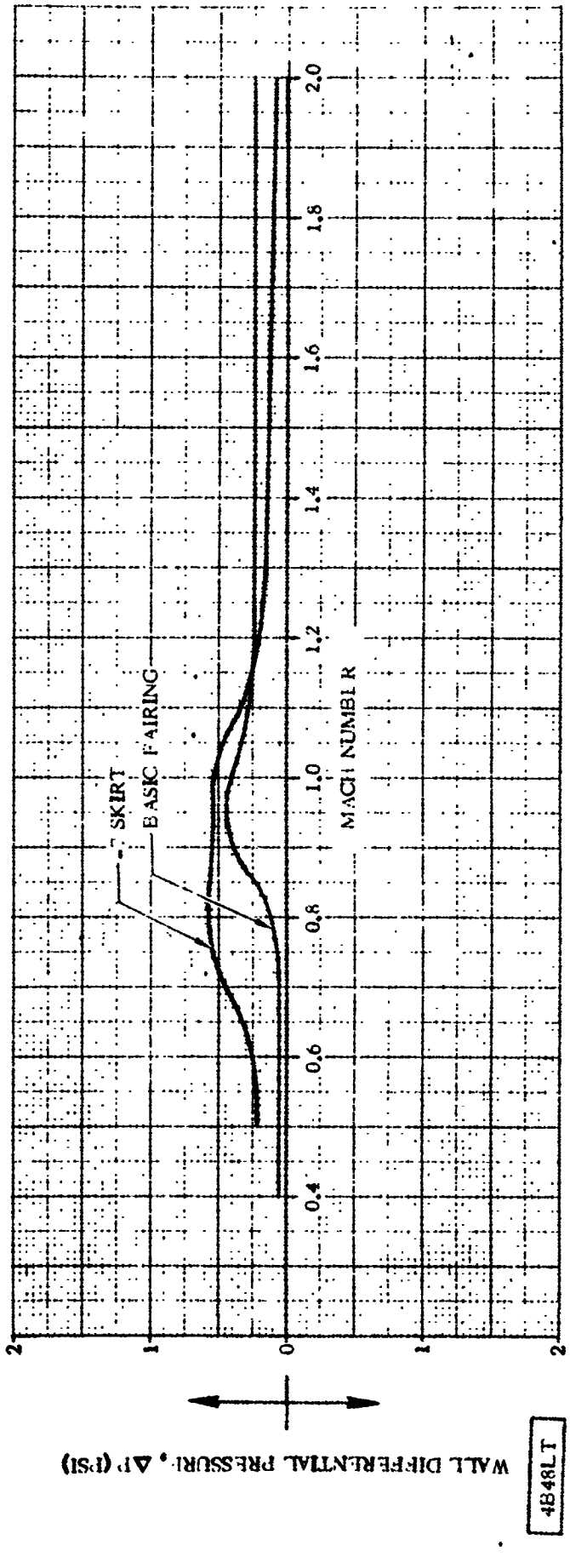

Figure 4.4-4. Interstage Adapter Liquid Hydrogen Boost Pump Fairing and -7 Skirt - Incremental Wall Differential Pressure due to Angle of Attack (α = 6 Degrees)

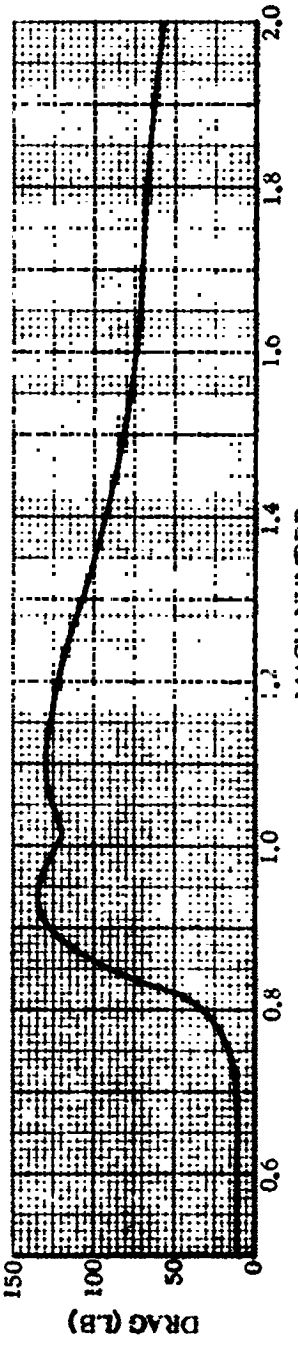

Figure 4.4-5. Aerodynamic Drag on -7 Skirt

4.4.6 BUFFET AND FLUTTER LOADS. Transonic buffet effects can be represented by means of equivalent static pressures as follows (superimpose three loads with those of Paragraph 4.4.5):

AREA	PRESSURE DIFFERENTIAL	
Top and Side	±2.10	Reference Figure 4.4-6
Aft Bulkhead	±1.75	

NOTE: These loads are applicable only in the Mach number range 0.70 - 0.90.

For all other Mach numbers, an equivalent static pressure of ±0.50 psi should be used to account for dynamic effects on both the fairing and the aft bulkhead.

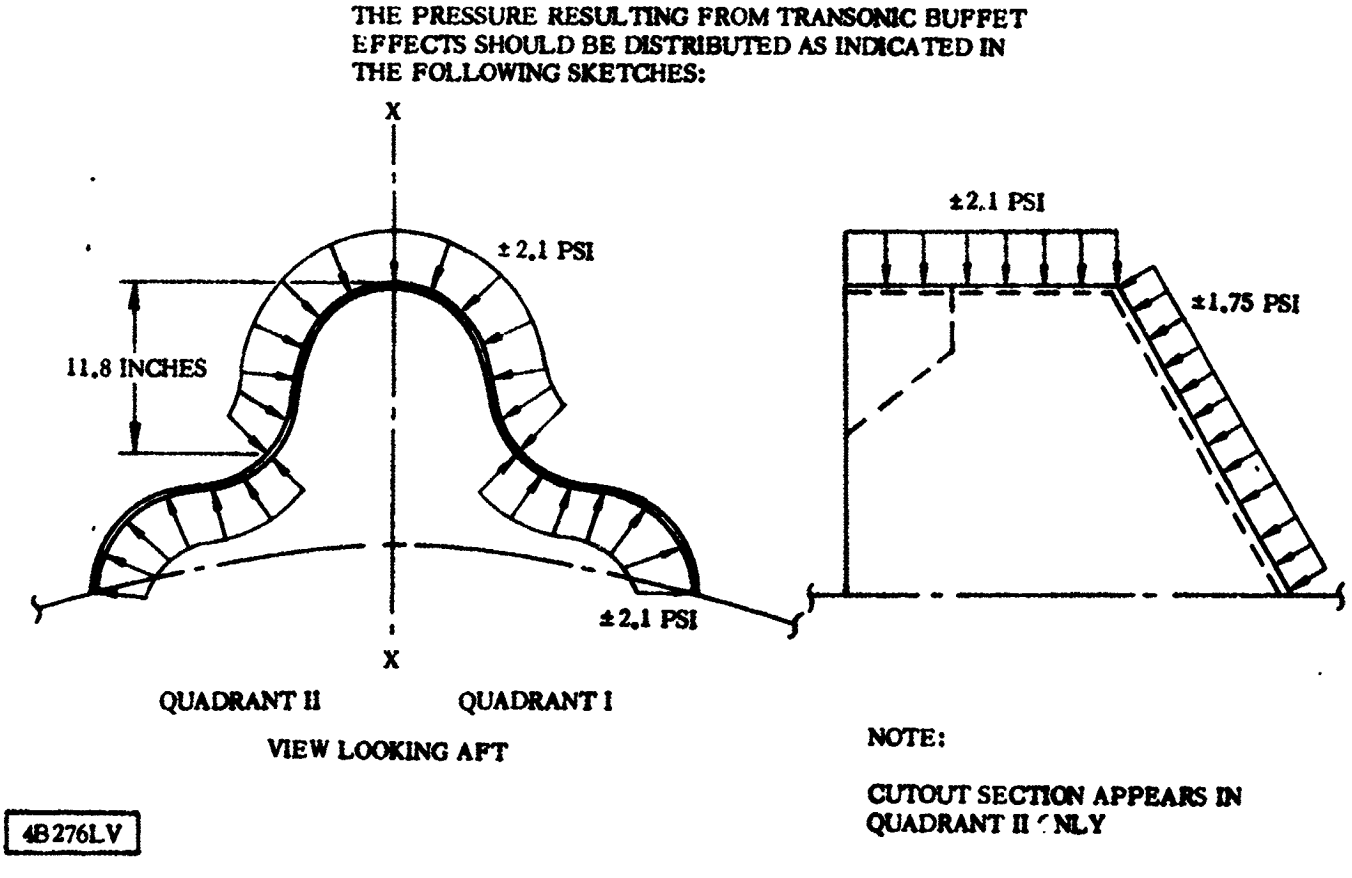

Figure 4.4-6. Liquid Hydrogen Boost Pump Fairing Transonic Buffet Loads

4.4.7 MISCELLANEOUS LOAD PARAMETERS. No other loads need be considered for this component.

THIS PAGE INTENTIONALLY LEFT BLANK.

4.5 SAFE AND ARM FAIRING

The safe and arm fairing protects the safe and arm device from aerodynamic heating. This fairing is associated with the interstage adapter separation system and is located at Station 414 between stringers 44 and 45. See Figure 4.5-1 for safe and arm fairing configuration. Reference Figure 4.2-5 for location on adapter.

4.5.1 CRITICAL CONDITIONS. The fairing is subjected to steady-state and fluctuating air loads simultaneously through the transonic range of flight. Maximum temperatures occur after the aerodynamic loads have essentially diminshed to zero.

4.5.2 WEIGHTS AND CENTER OF GRAVITY DATA. Due to the nature of this component, inertia loads are of an inconsequential magnitude compared to the aerodynamic loads, therefore, weights or C.G. data are not applicable.

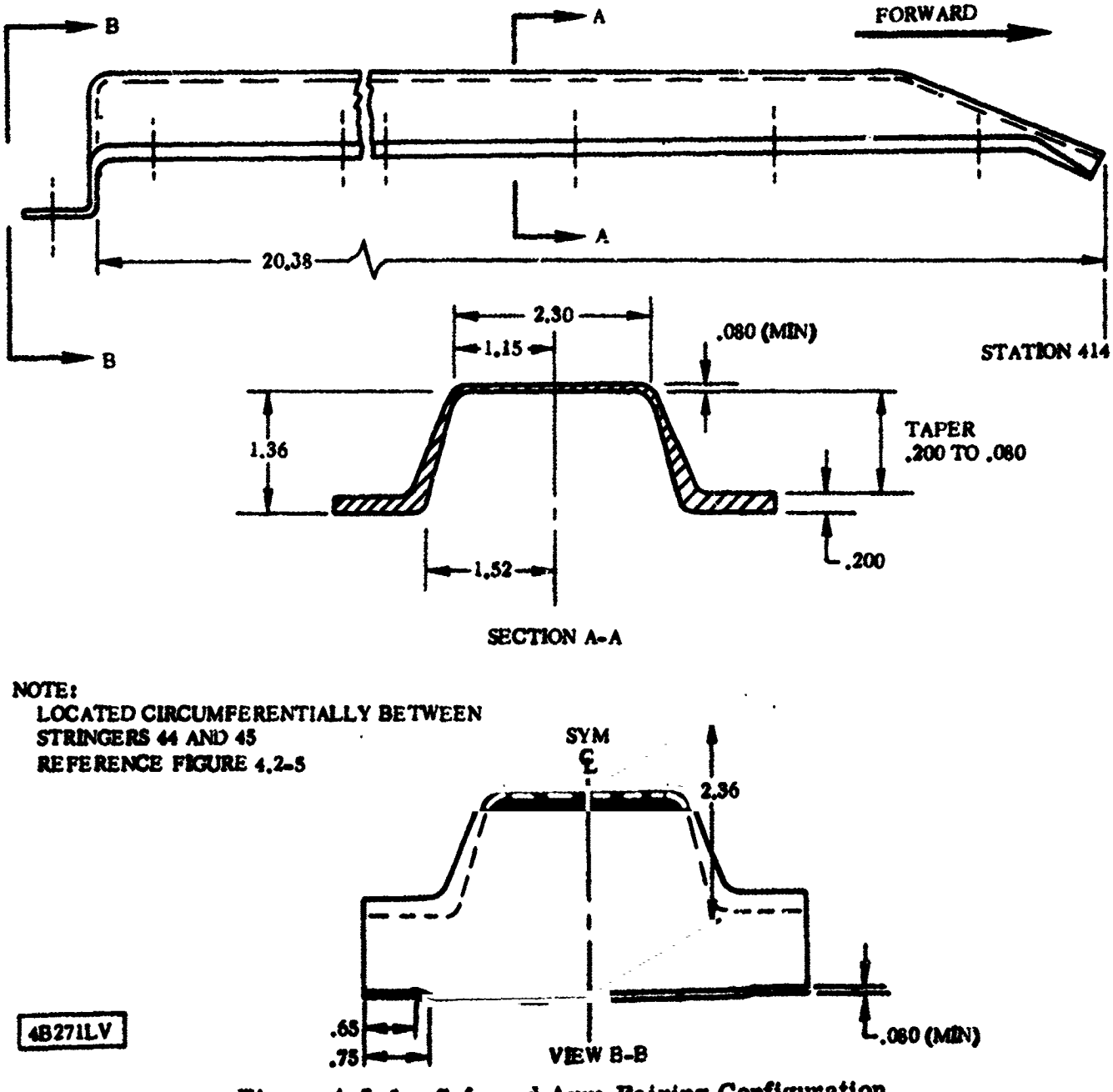

Figure 4.5-1. Safe and Arm Fairing Configuration

4.5.3 THERMAL DATA. The fairing temperature history is shown in Figure 4.5-2. These temperatures are applied to the entire upper surface of the fairing. The thermal analysis is based on the following assumptions:

a. The aerodynamic heating to the upper surface of the fairing was assumed to be 0.4 times undisturbed local flat plate values
b. Maximum heating trajectory DP-35 was used
c. There will be no path of continuity for flow of hot boundary layer air through the fairing.

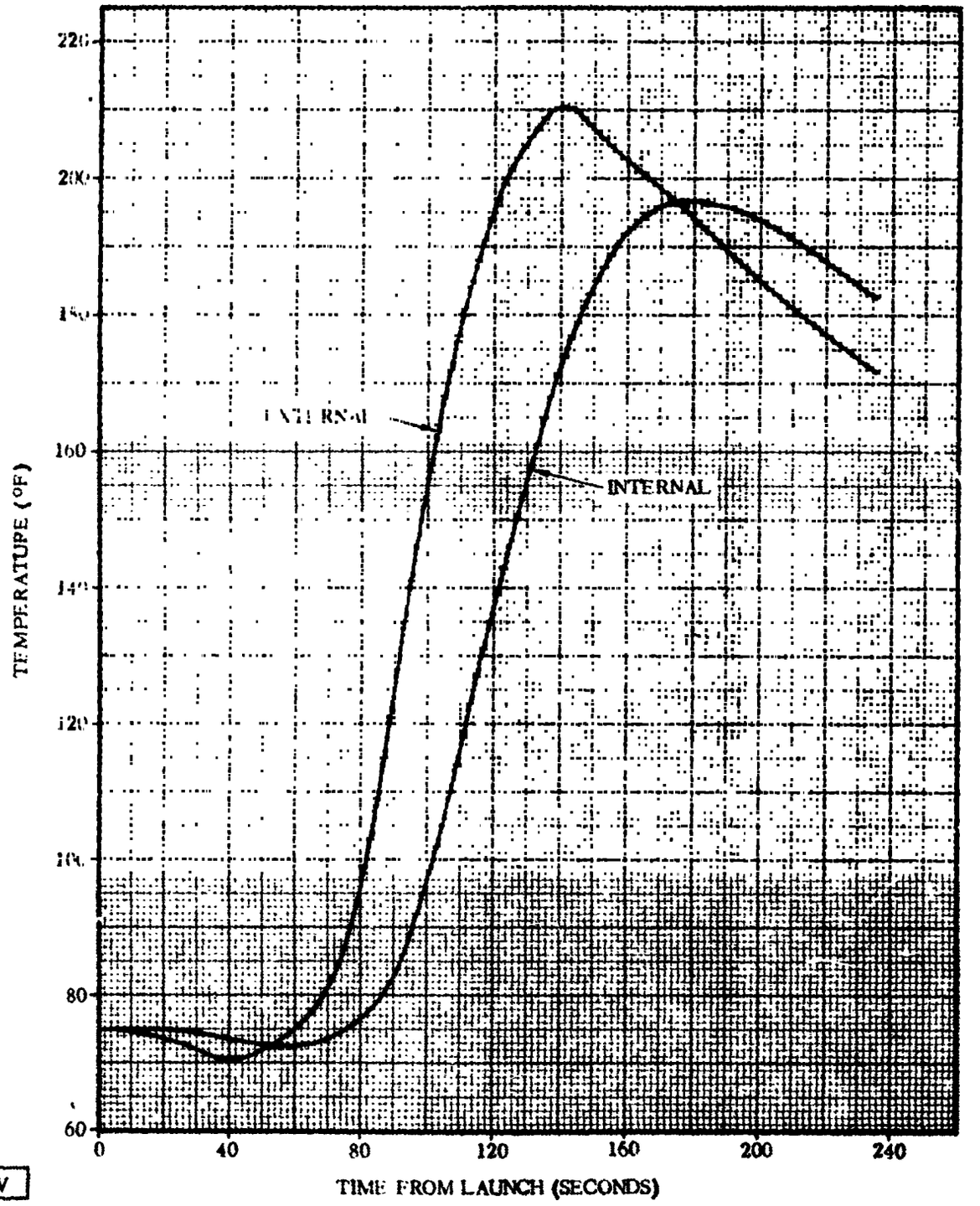

Figure 4.5-2. Safe and Arm Fairing External and Interior Surface Temperature

4.5.4 INERTIA LOADS. Load contribution from inertia effects are not to be considered for this component (see Paragraph 4.5.2).

4.5.5 STEADY-STATE AIR LOADS. The steady-state wall differential pressures are shown in Figure 4.5-3. The axial load and side load due to steady-state aerodynamic loading is shown in Figure 4.5-4.

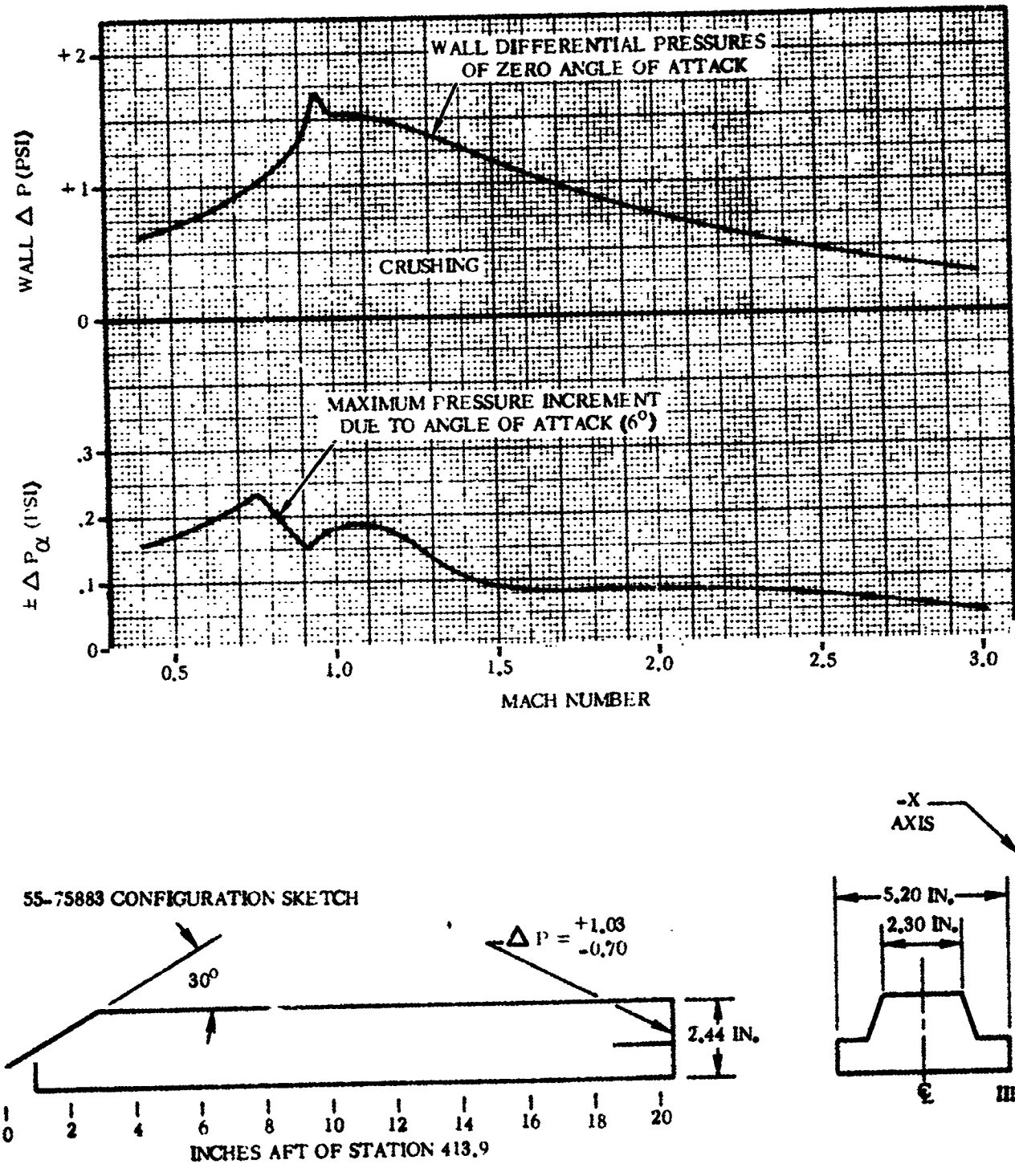

4B50LV

Figure 4.5-3. Safe and Arm Fairing Steady-State Wall Differential Pressures

4.5.6 BUFFET AND FLUTTER LOADS. An equivalent steady-state differential pressure of ±1.0 psi should be imposed on the fairing to account for fluctuating pressures which occur during the transonic portion of flight. This load must be superimposed with the steady-state air loads described in Paragraph 4.5.5.

4.5.7 MISCELLANEOUS LOAD PARAMETERS. No other loads need be considered for this component.

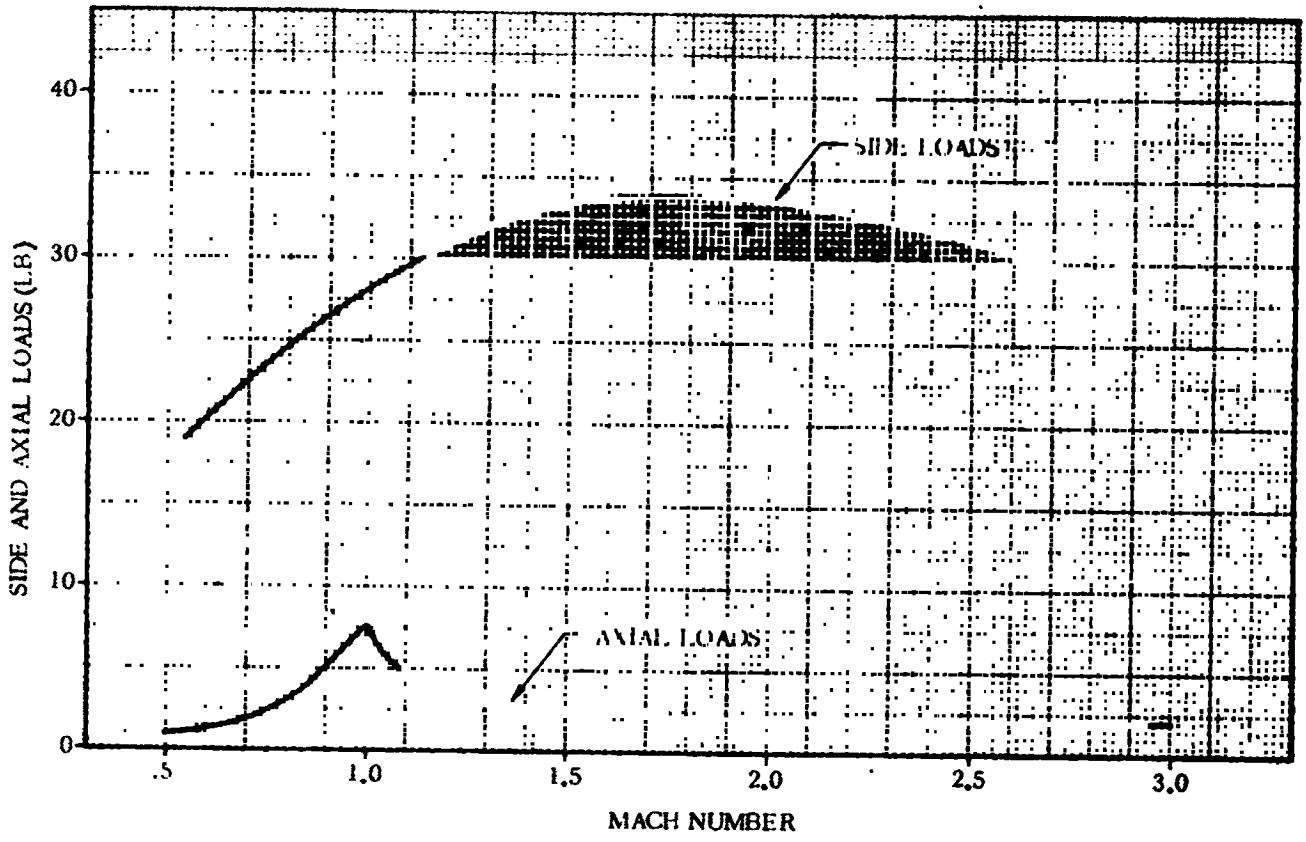

4B51LV

Figure 4.5-4. Safe and Arm Fairing Side and Axial Loads

4.6 STATION 570 HEAT SHIELD

The purpose of the Station 570 heat shield is to promote streamline flow over upstanding legs of the tank and interstage adapter rings. It has a double wedge cross-section and extends circumferentially around the Atlas tank - interstage adapter interface at Station 570. See Figure 4.6-1 for configuration of the Station 570 heat shield.

4.6.1 CRITICAL LOADING CONDITIONS. The environment considered to be most severe regarding the heat shield occurs during transonic flight. Since steady-state and fluctuating pressures must be considered simultaneously, the resulting loads reach a maximum at this time. Detrimental temperature effects, however, should not be considered at this time as maximum heating does not occur until after BECO.

4.6.2 WEIGHTS AND CENTER OF GRAVITY DATA. The safe and arm fairing weight is of an inconsequential magnitude, therefore, weights and C.G. data are not applicable.

4.6.3 THERMAL DATA. The forward ramp on the heat shield was analyzed as a wedge using shock wave theory (Reference 4-4). The aft ramp of the heat shield was analyzed as a flat plate using heating factors from Reference 4-5.

The temperature distribution on the heat shield is shown in Figure 4.6-2. Maximum temperature on the heat shield is 775° F and it occurs after 160 seconds of flight.

Even though the intent of the heat shield is to create a streamline flow over the Station 570 interface joint, it does not completely eliminate boundary layer separation. Re-attachment of the boundary layer occurs on the heat shield. A heating factor of 1.5 was used at the point of boundary layer re-attachment.

4.6.4 INERTIA LOADS. The load contribution from inertia effects are not to be considered for this component (see Paragraph 4.6.2).

4.6.5 STEADY-STATE AIR LOADS. Wall differential pressures on the forward face of the heat shield are given in Figure 4.6-3 for several Mach numbers, the most severe case occurs at M = 1.60. Corresponding axial loads as a function of Mach number are plotted in Figure 4.6-4.

There is a possibility of some unknown amount of air leakage into the underside of the shield at the interstage adapter hat sections where surface mismatches may occur, and there are uncertanties in the flow field aft of Station 570. To account for these unknowns, design wall differential pressures of ± 1.0 psi shall be used for the aft wedge.

The following are the basic assumptions used in the analysis:

a. The maximum dynamic pressure was chosen from trajectories which are conservative for all Surveyor-Centaur flights
b. Angle of attack effects are negligible.

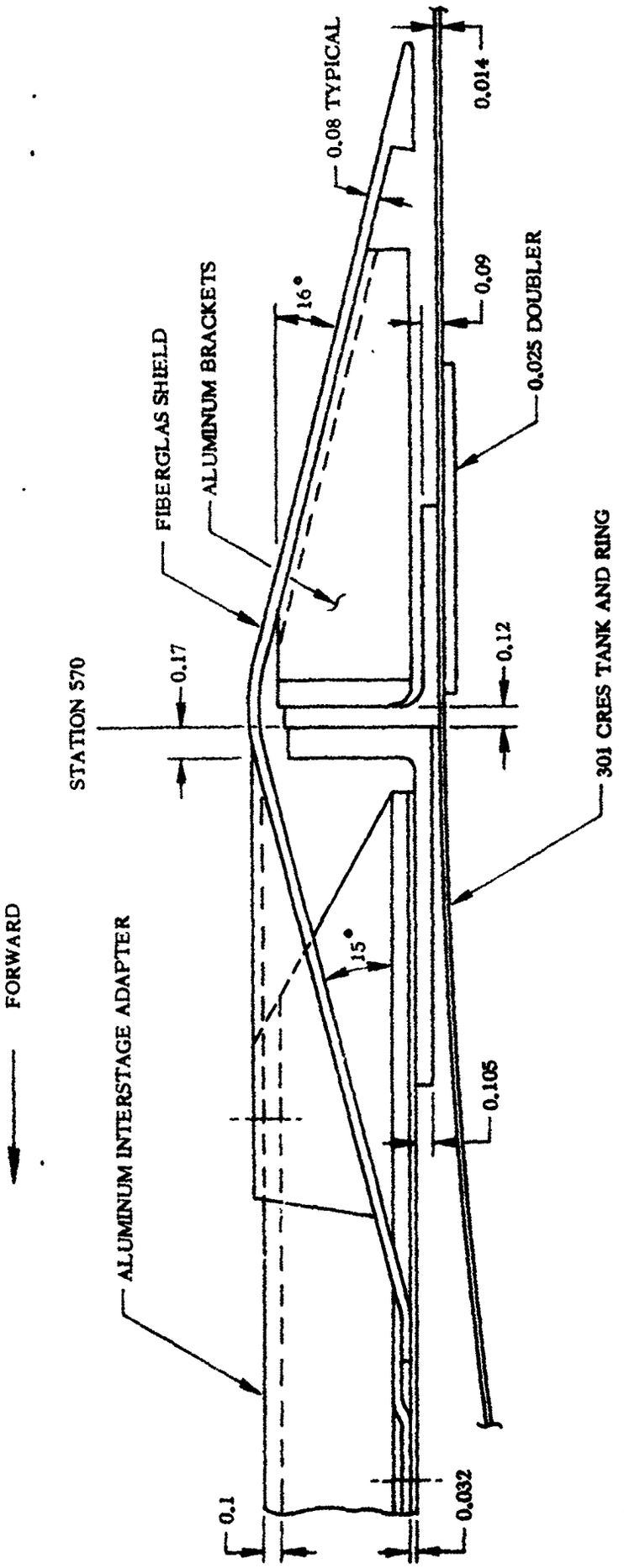

Figure 4.6-1. Heat Shield and Station 570 Interface Configuration

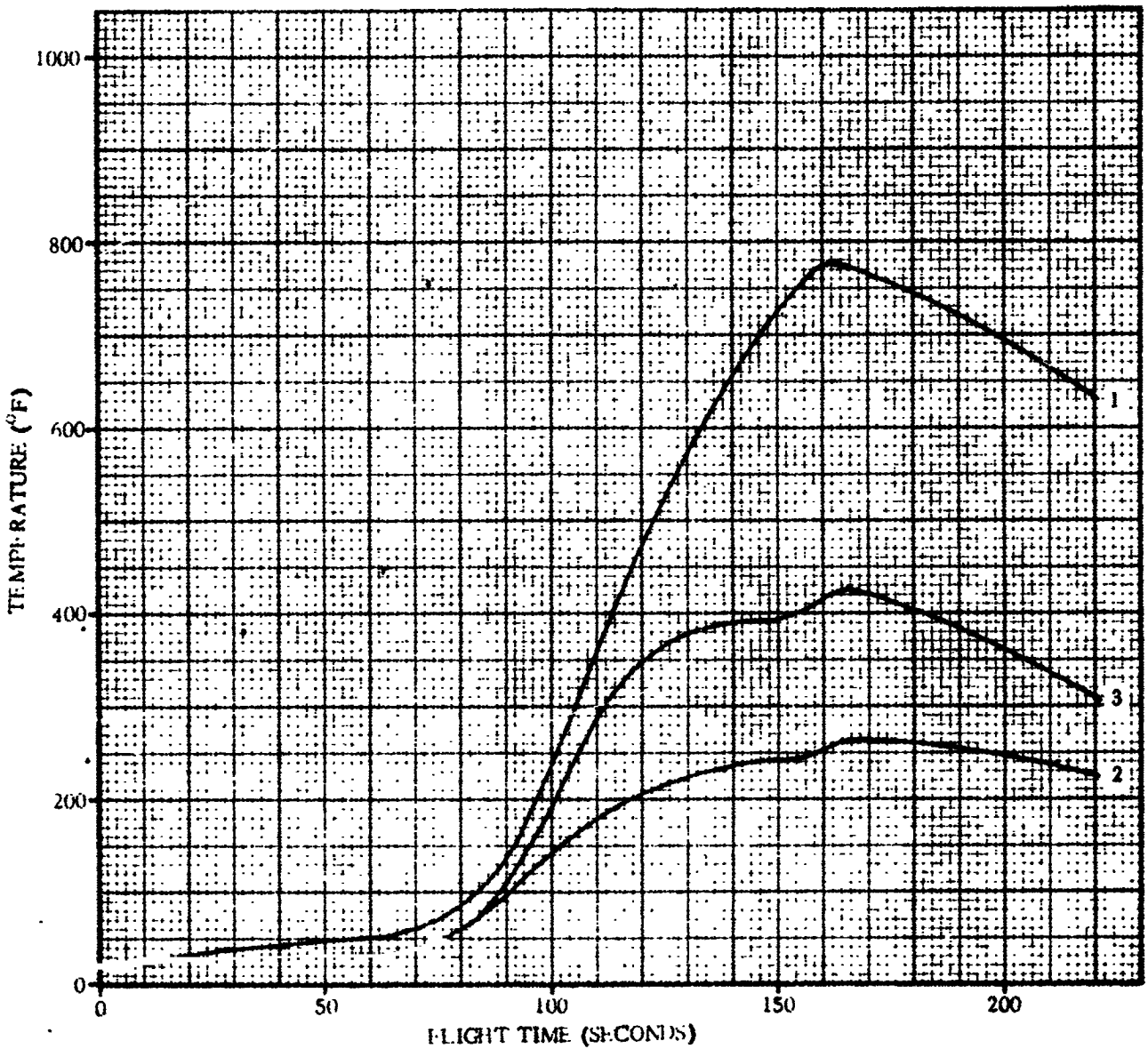

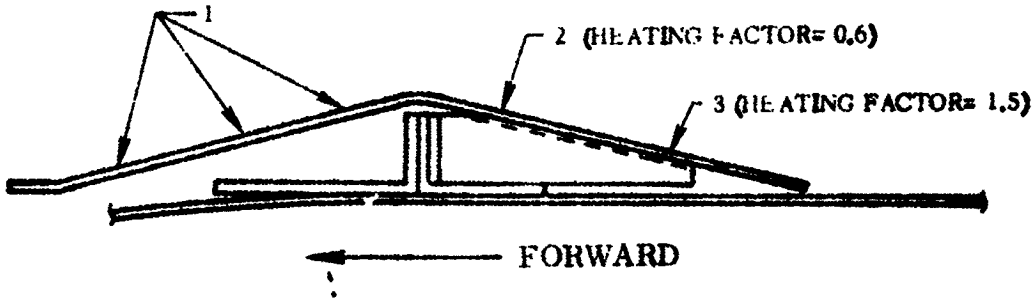

4B272LV

Figure 4.6-2. Station 570 Heat Shield Temperature versus Time Distribution

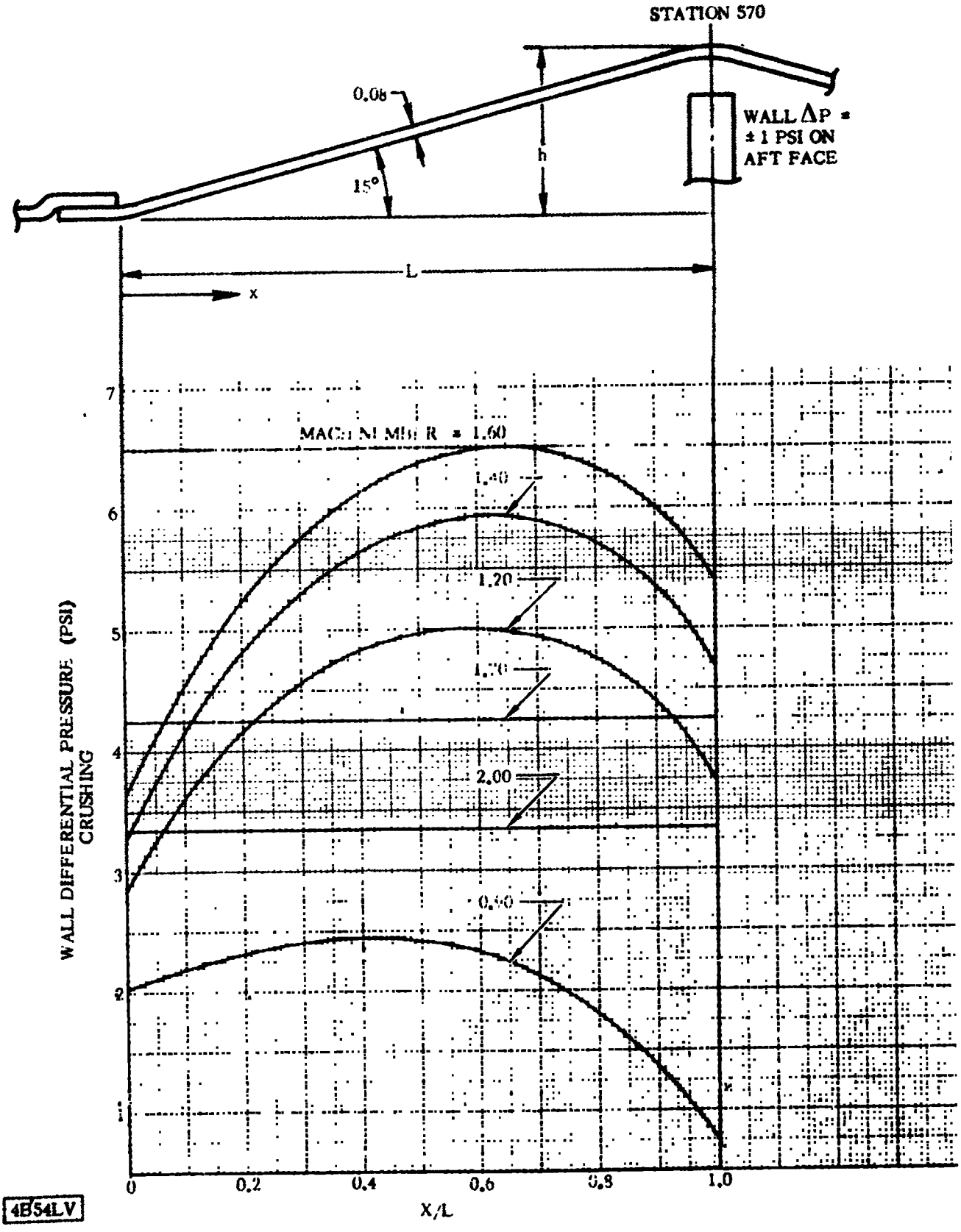

Figure 4.6-3. Station 570 Heat Shield Wall Differential Pressures

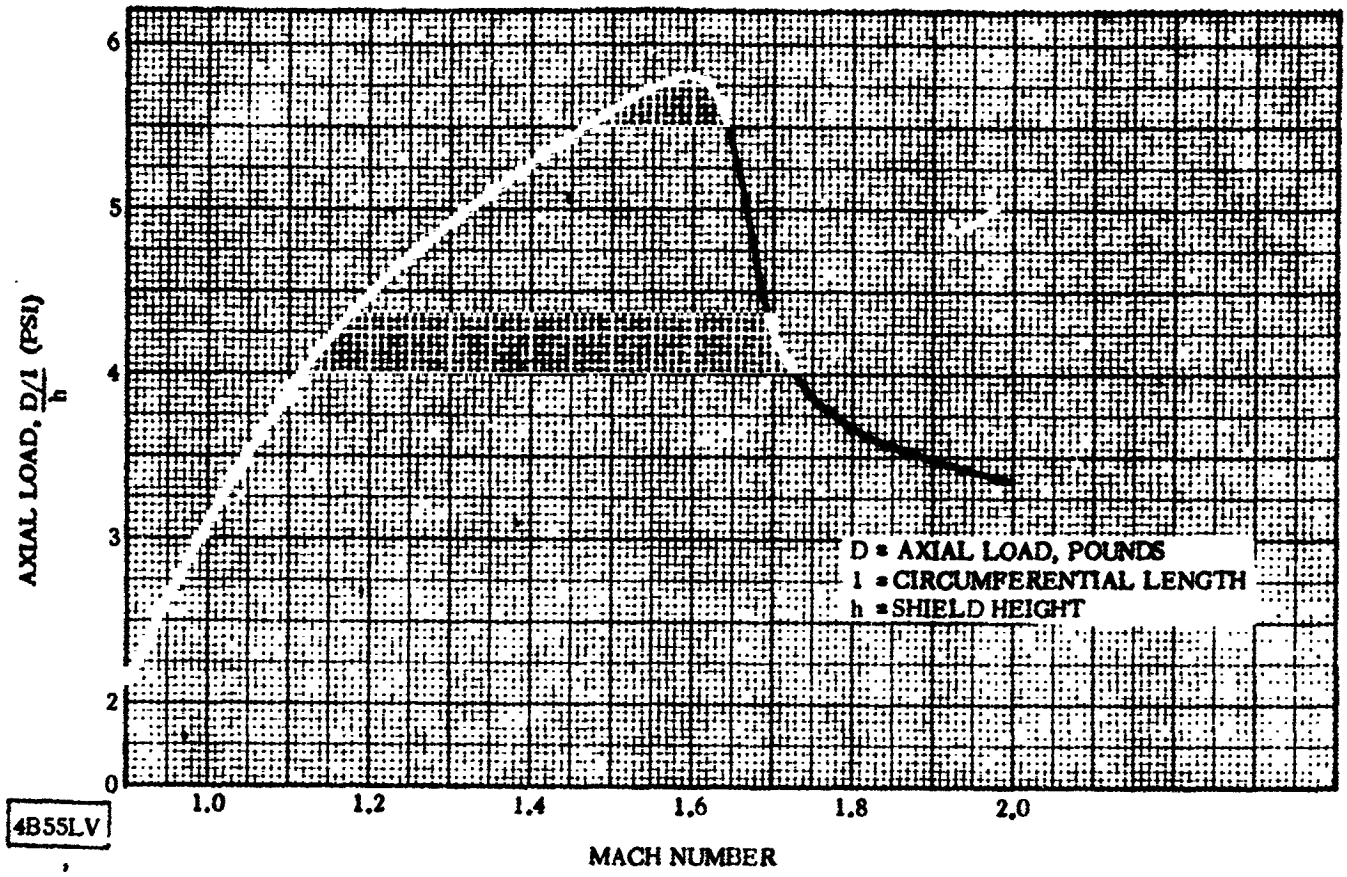

Figure 4.6-4. Station 570 Heat Shield Axial Loads

4.6.6 BUFFET AND FLUTTER LOADS. The following equivalent steady-state loads shall be used to account for fluctuating pressures which occur on the forward and aft ramps of the heat shield. These loads should be superimposed with the steady-state differential pressure (Paragraph 4.6.5) respective to the Mach number in question.

For Mach numbers 0.75 to 1.1:

Up ramp ±1.0 psi, Down ramp ±3.0 psi

For other Mach numbers:

Up ramp and Down ramp ±0.5 psi

4.6.7 MISCELLANEOUS LOAD PARAMETERS. No other loads need be considered for this component.

THIS PAGE INTENTIONALLY LEFT BLANK.

4.7 WIRING TUNNEL CUTOUT FAIRING

The wiring cutout fairing at Station 570 provides a shield for the maze of electrical wiring which extends from the Centaur upper stage down through the wiring tunnel of the Atlas booster. It is circumferentially located on the Y-Y axis between Quadrants I and IV. See Figure 4.7-1 for configuration of fairing.

4.7.1 CRITICAL CONDITIONS. The fairing is subjected to simultaneous loading from steady-state and fluctuating air loads during the transonic range of flight. This condition is considered most critical for the subject fairing; however, a maximum temperature condition occurs at a later time in flight which also must be investigated. Air loads are considered negligible at this time.

4.7.2 WEIGHTS AND CENTER OF GRAVITY DATA. Due to the nature of this component, inertia loads are of an inconsequential magnitude compared to the aerodynamic loads; therefore, weights and C.G. data are of little structural interest.

4.7.3 THERMAL DATA. The physical characteristics of the fairing, along with the regions of interest in this analysis, are shown on Figure 4.7-1. The 15-degree forward facing conical section will receive the largest amount of aerodynamic heating, which is reflected in the temperature histories shown on Figure 4.7-2. These temperature histories, as well as those given for the surfaces parallel to the vehicle axis, are the results of analyses which assume that local flow is undisturbed and fully developed.

The temperatures predicted on this fairing are not high enough to cause significant phenolic resin degradation (pyrolysis); therefore strength reduction from this source is not anticipated.

4.7.4 INERTIA LOADS. Load contribution from inertia effects are not considered critical for this component (see Paragraph 4.7.2).

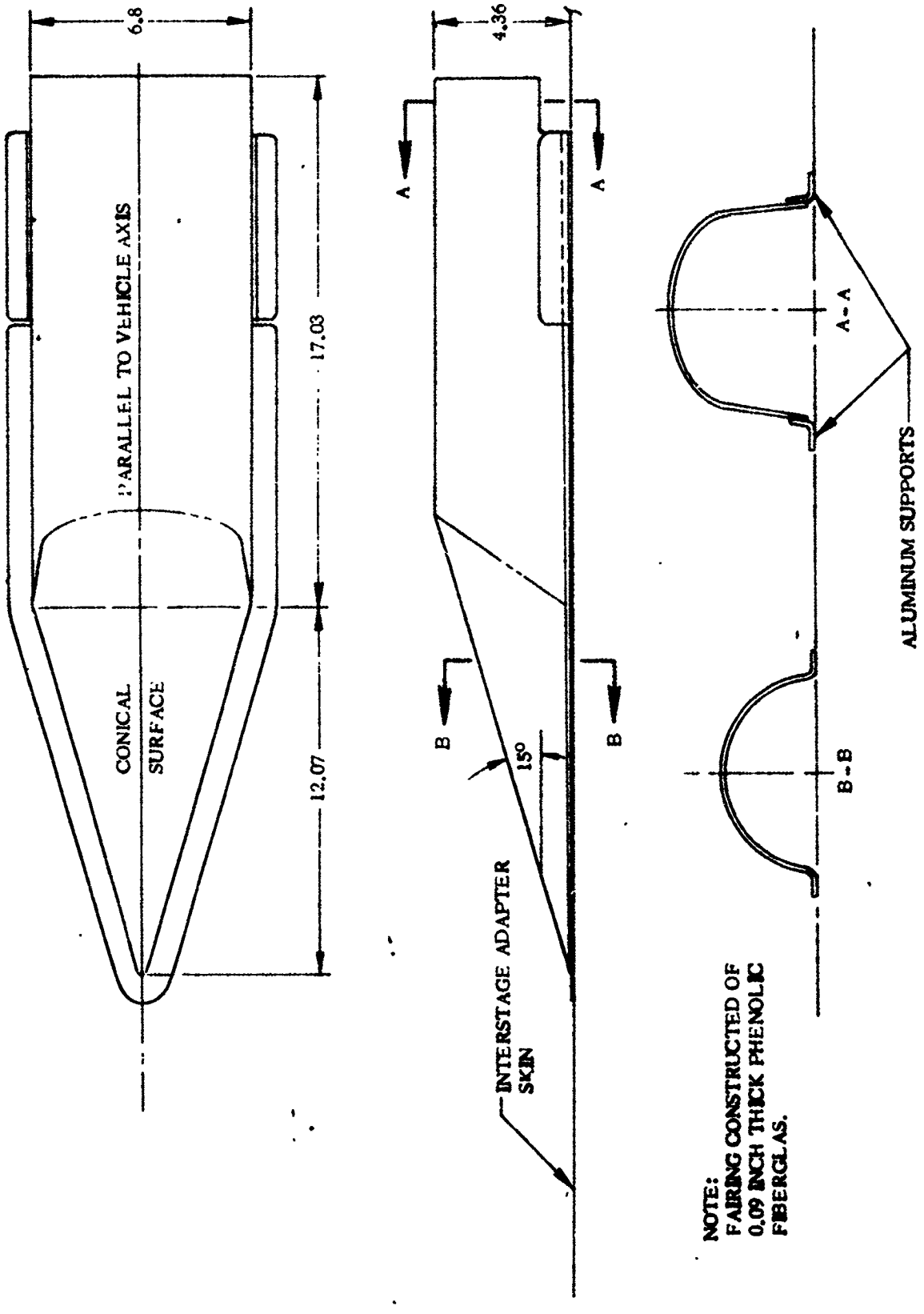

Figure 4.7-1. Wiring Tunnel Cutout Fairing, Station 570 Configuration

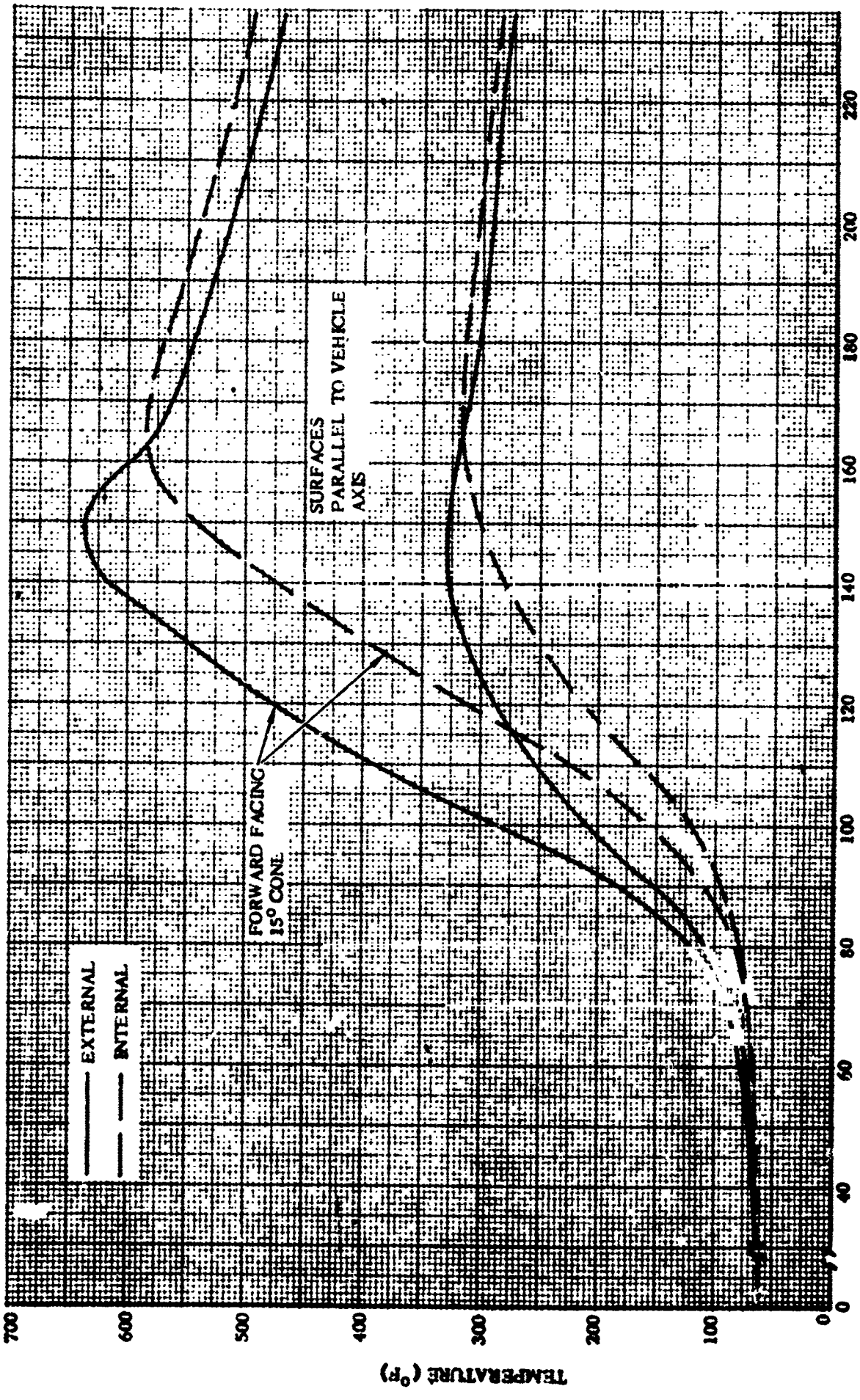

Figure 4.7-2. Wiring Tunnel Cutout Fairing, Station 570 - External and Internal Surface Temperature Histories

4.7.5 STEADY STATE AIR LOADS. As discussed in Paragraph 4.7.1, the steady-state air loads occur during the transonic phase of booster operation.

These steady-state differential pressures on the wiring tunnel cutout fairing are shown in Figures 4.7-3 and 4.7-4. The pressures of Figure 4.7-3 are based on the assumption that the fairing is vented to the interior of the interstage adapter and constitutes the maximum crushing pressure. Figure 4.7-4 pressures are based on the assumption that the fairing vents to the atmosphere and constitutes the maximum bursting (minimum crushing) pressure. The fairing should be designed to withstand both of the above loading conditions.

NOTE: Internal pressure equals interstage adapter internal pressure.

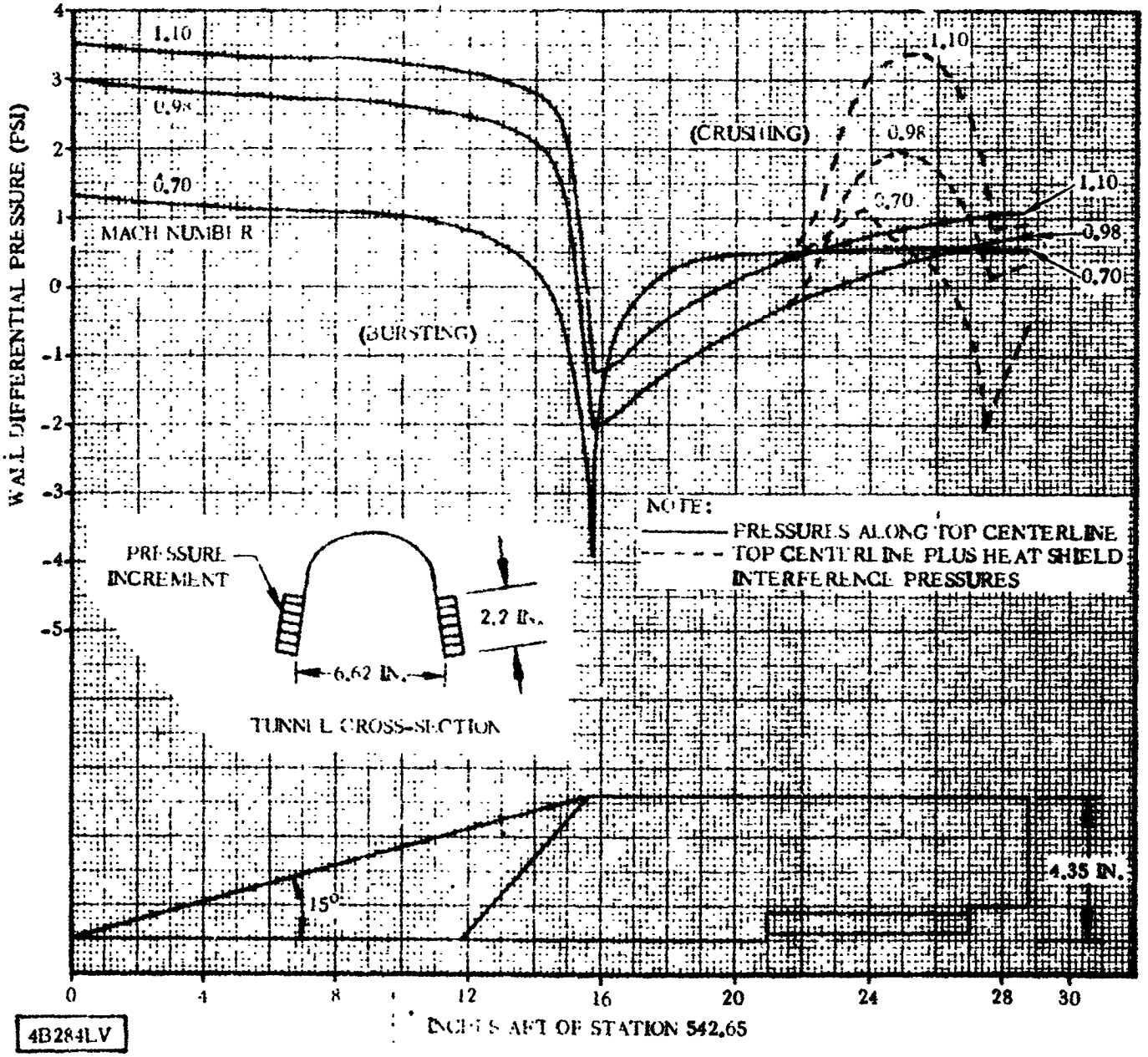

Figure 4.7-3. Wiring Tunnel Cutout Fairing Wall Differential Pressures (Zero Angle of Attack) Maximum Crushing Case

NOTE:
Internal pressure equals
ambient pressure.

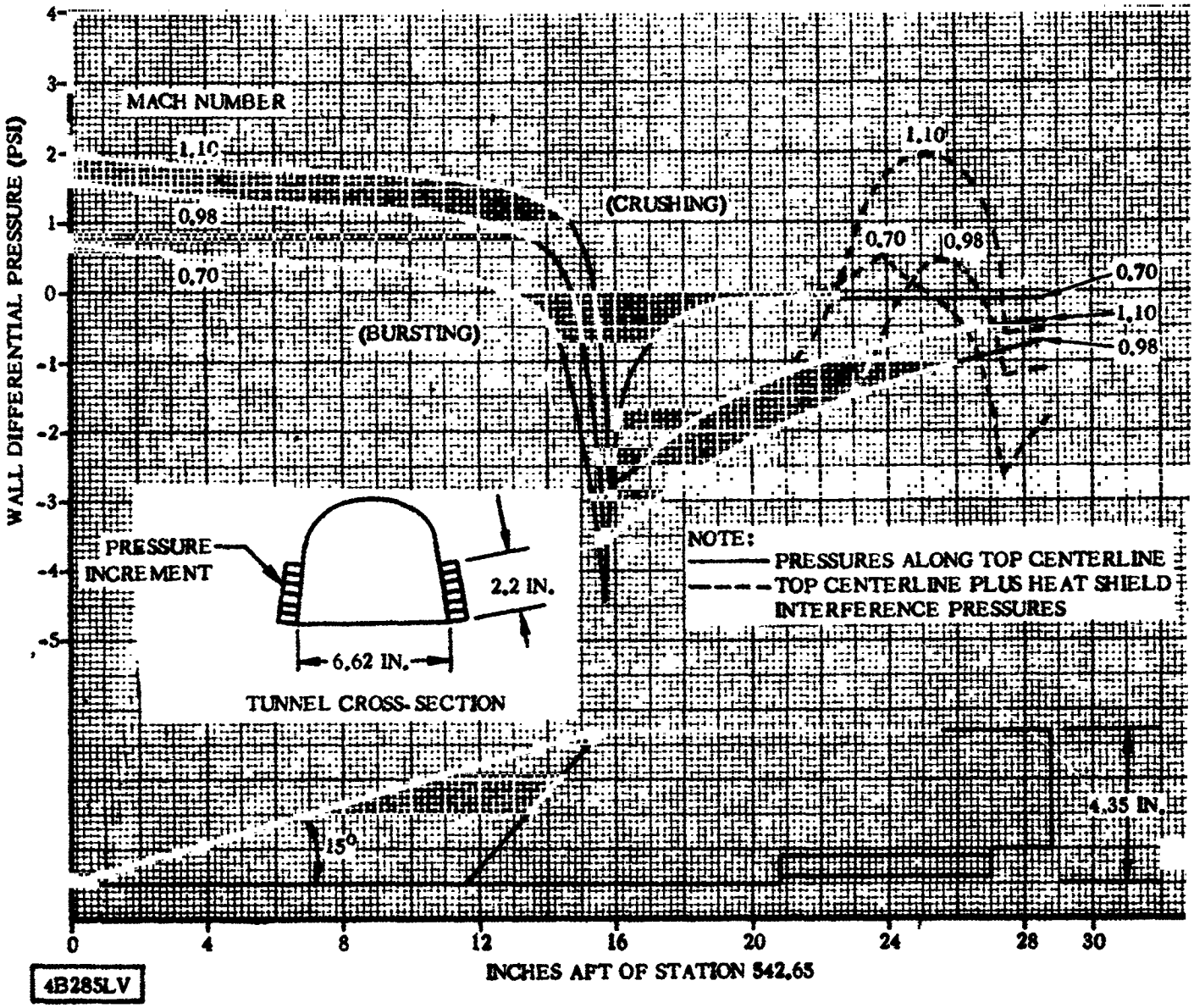

Figure 4.7-4. Wiring Tunnel Cutout Fairing Wall Differential Pressures (Zero Angle of Attack) - Maximum Bursting Case

The solid lines of Figures 4.7-3 and 4.7-4 represent pressures to be applied everywhere except for 2.2-inch strips along the fairing sides. The Station 570 heat shield is attached to the sides of the fairing causing a strip of disturbed air flow. In this region, the pressures represented by dashed lines shall be applied. Maximum axial drag and side loads are presented in Figures 4.7-5 and 4.7-6, respectively. The drag and side loads on the fairing represent only external pressure effects while the wall ΔP includes fairing internal pressure. Thus, these loads are to be used for different purposes in the stress analysis of the structure.

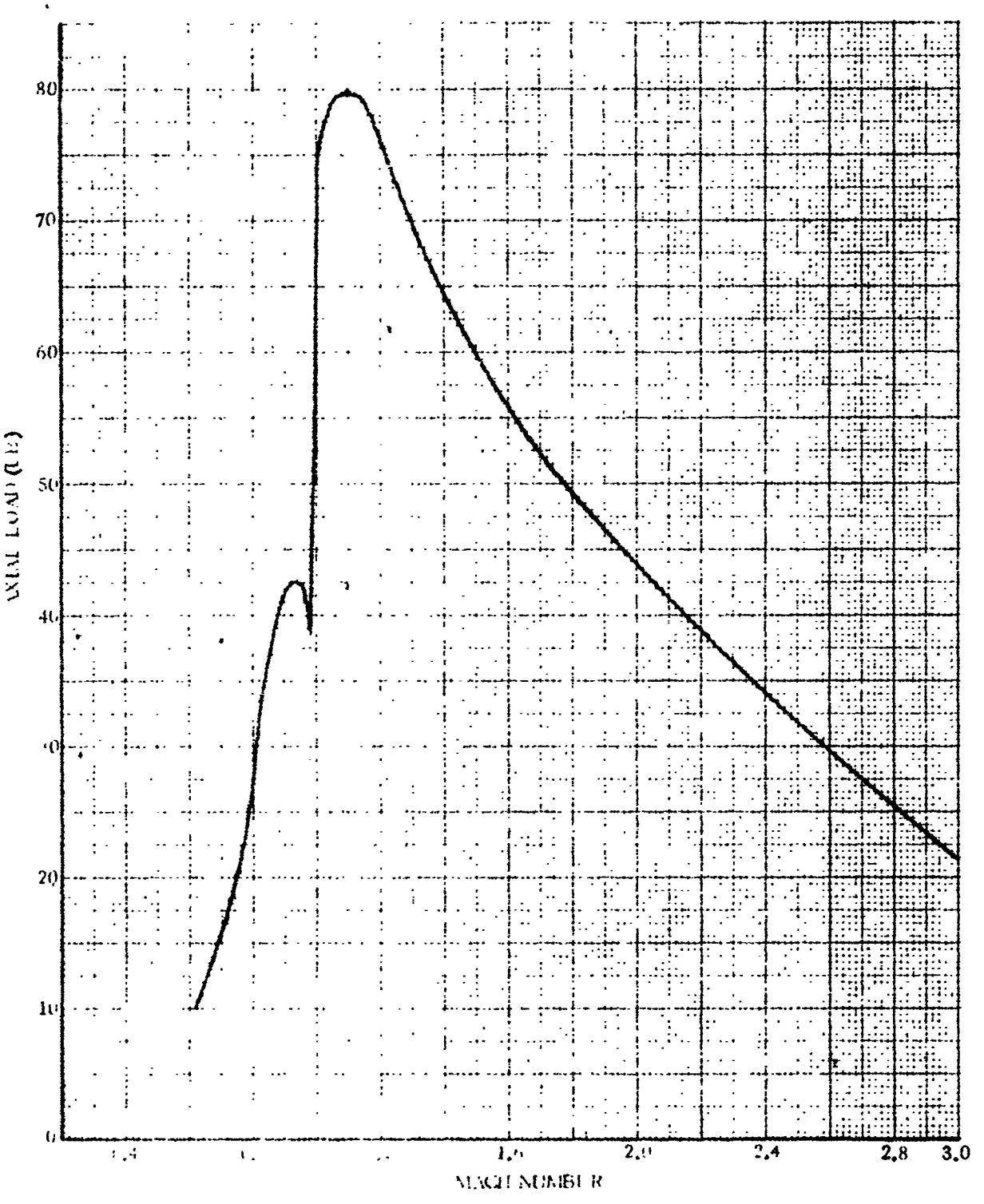

4B2861 V

Figure [illegible] Maximum Axial Loads

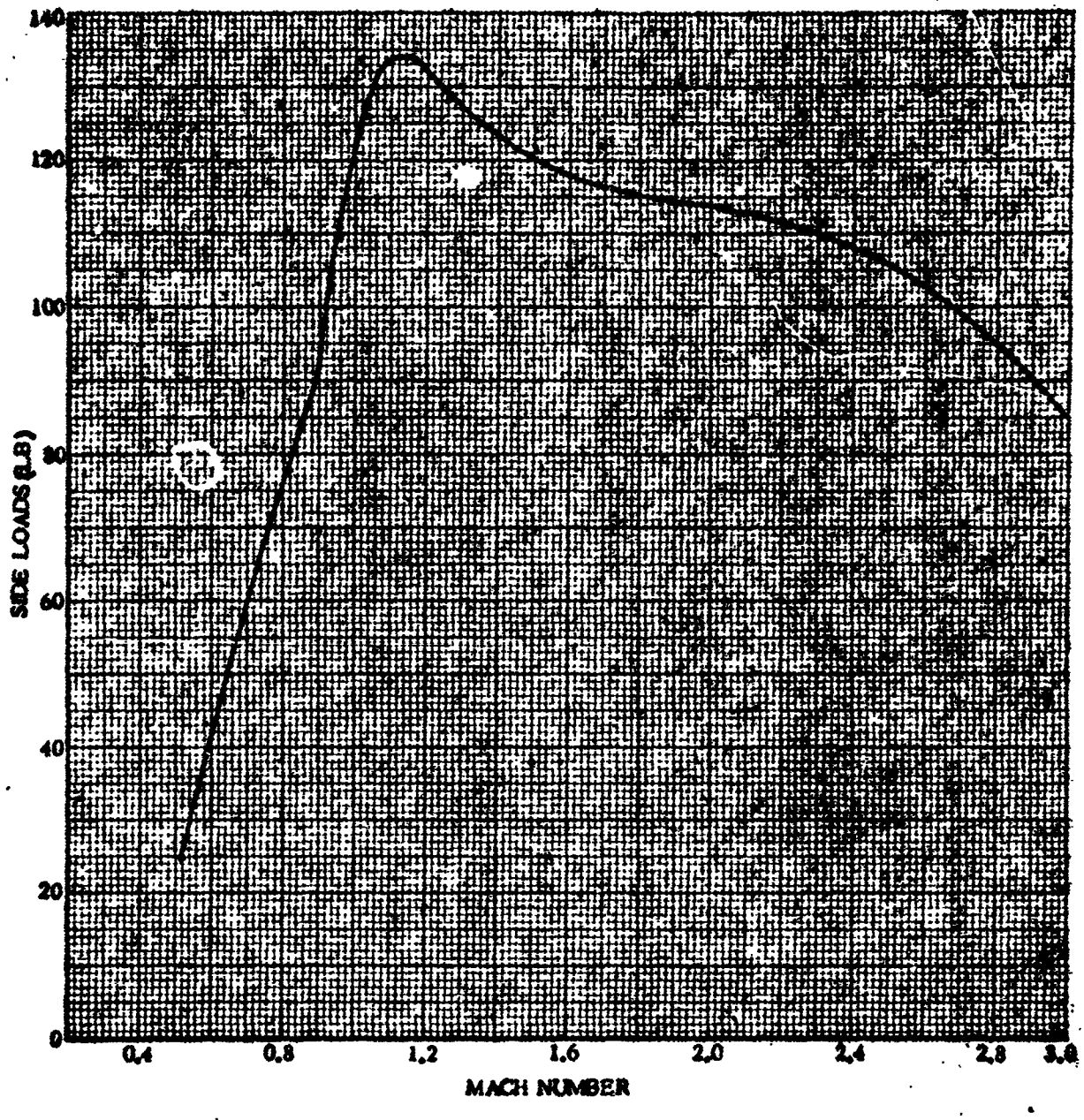

4B287LV

Figure 4.7-6. Wiring Tunnel Cutout Fairing - Maximum Side Loads.

4.7.6 BUFFET AND FLUTTER LOADS. In addition to the steady-state air loads, equivalent steady-state loads as shown in Figure 4.7-7 must be applied to the fairing to account for fluctuating or buffeting effects. These differential pressures occur during transonic flight; therefore, they should be superimposed upon the steady-state loads described in Paragraph 4.7.5.

4.7.7 MISCELLANEOUS LOAD PARAMETERS. No other loads need be considered for this component.

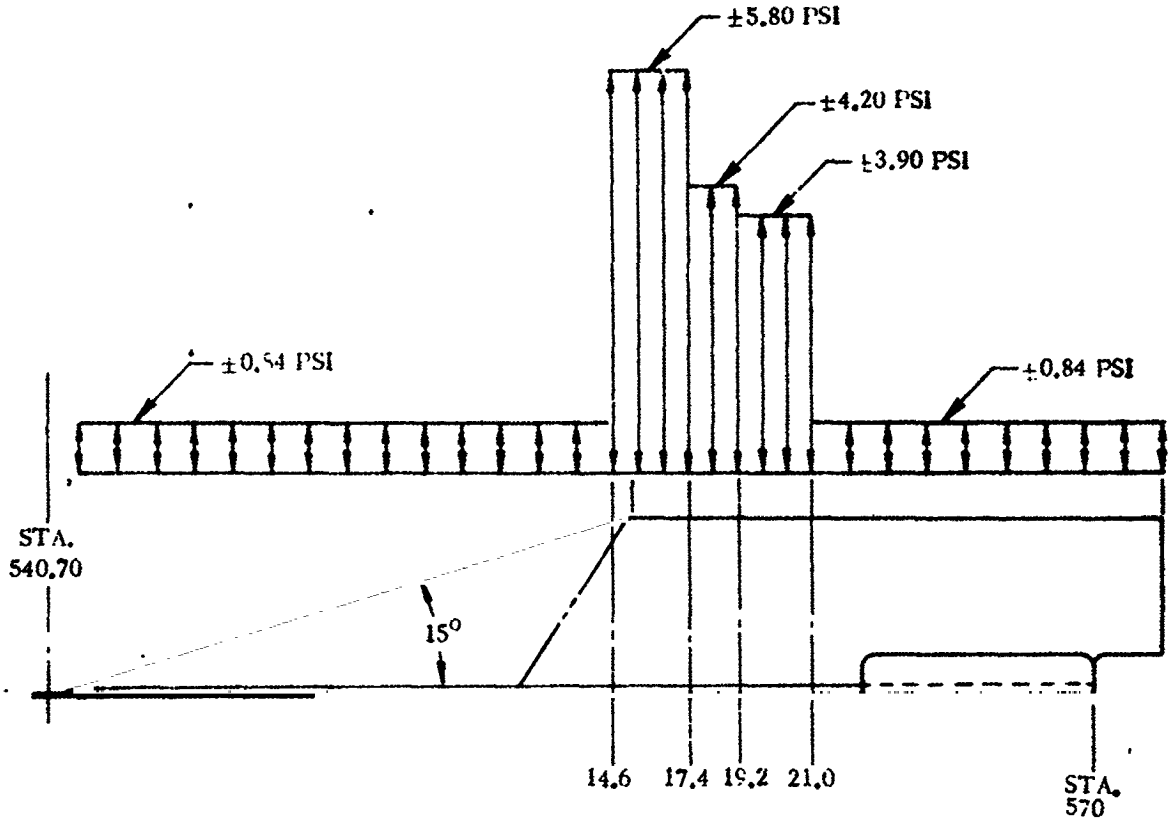

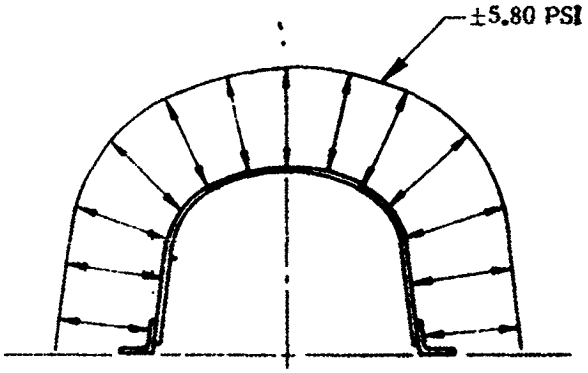

4B293L-V

Figure 4.7-7. Equivalent Peak Static Pressures Due to Fluctuating Pressures on Wiring Tunnel Fairing

4.8 AZUSA AND C-BAND ANTENNA FAIRINGS

The Azusa and C-Band antennas for AC-3 and AC-4 were mounted on a ground plane attached to the interstage adapter. Tests have shown that satisfactory antenna operation can be obtained without the ground plane. The antennas for the operational vehicles are mounted directly to the skin of the interstage adapter.

The Azusa and C-Band antenna fairing originates approximately at Station 482 and terminates approximately at Station 546. The antennas are located circumferentially on the interstage adapter as shown in Figure 4.2-5. See Figure 4.8-1 for the fairing and ramp for detail configuration.

4.8.1 CRITICAL CONDITIONS. The critical loading condition for the subject fairing occurs during transonic flight. At this time, steady-state air loads are combined with buffet loads due to dynamic response of the structure. The maximum heating condition need only be investigated from a thermal standpoint since the aerodynamic loads have essentially diminished to zero.

4.8.2 WEIGHTS AND CENTER OF GRAVITY DATA. Weights and C.G. data for the fairings are not critical (see Paragraph 4.8.4).

4.8.3 THERMAL DATA. The predicted thermal history of the Azusa and C-Band antenna fairings is given in Figures 4.8-2 and 4.8-3. The thermal analysis was based on the DP35 maximum design heating trajectory. A surface emissivity of 0.85 was assumed and the effects of the adapter frames was not considered. The temperatures given are maximums for areas between frames.

4.8.4 INERTIA LOADS. Load contributions from inertia effects are not critical for this component (see Paragraph 4.8.2).

4.8.5 STEADY-STATE AIR LOADS. The steady-state aerodynamic loads are shown in Figure 4.8-4. These loads, which occur during transonic flight ($0.85 \leq M \leq 1.30$), are based on the assumption that the forward half of the fairing vents to the interstage adapter and the aft half vents to the atmosphere. In addition, a uniform pressure increment of ± 0.25 psi will be imposed due to a design 6-degree angle of attack (Reference 1-1).

A maximum side load of 100 pounds, uniformly distributed along the length of the pod, shall be considered at Mach 1.0. The axial drag load versus Mach Number is given in Figure 4.8-5.

4.8.6 BUFFET AND FLUTTER LOADS. The fluctuating pressure loads on the Azusa and C-Band antenna pods, shown in Figure 4.8-6, occur in the transonic region ($0.85 \leq M \leq 1.30$). These fluctuating pressure loads should be added to the applicable steady-state loads in Paragraph 4.8.5 to obtain maximum pressure distributions.

4.8.7 MISCELLANEOUS LOAD PARAMETERS. No other loads need be considered for this component.

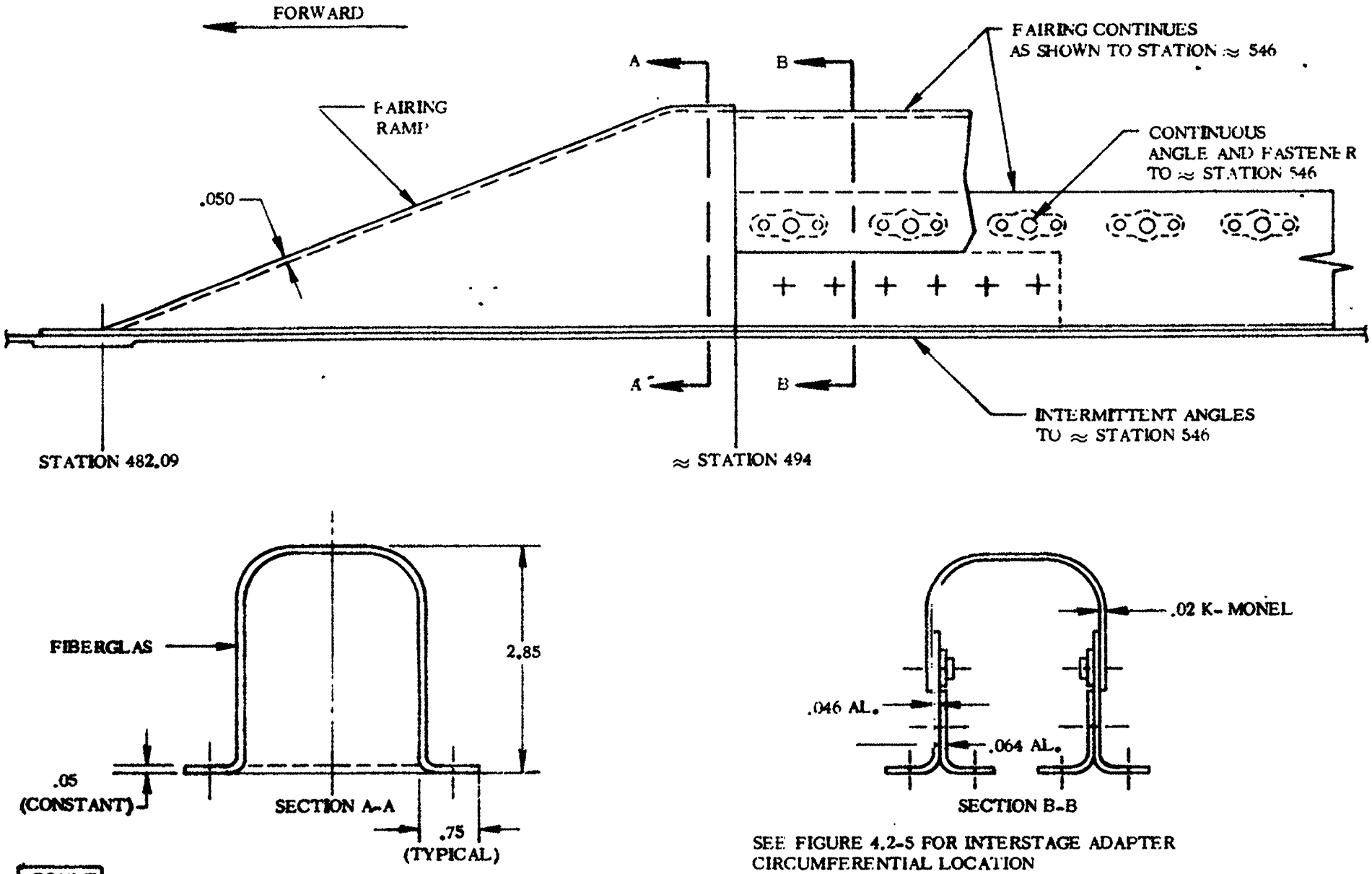

Figure 4.8-1. Azusa and C-Band Antenna - Configuration

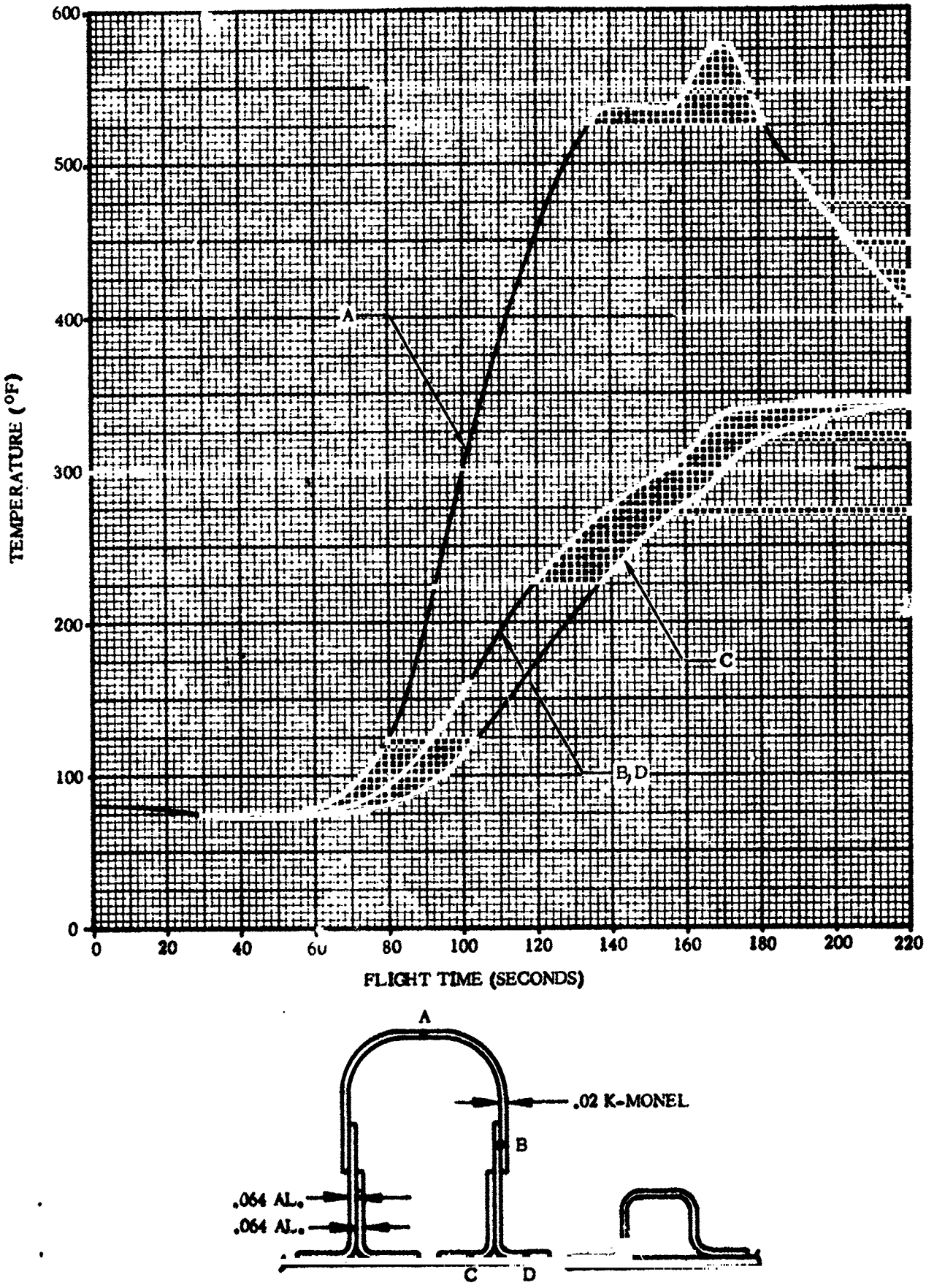

4B64LV

Figure 4.8-2. Azusa and C-Band Antenna - Temperature Histories

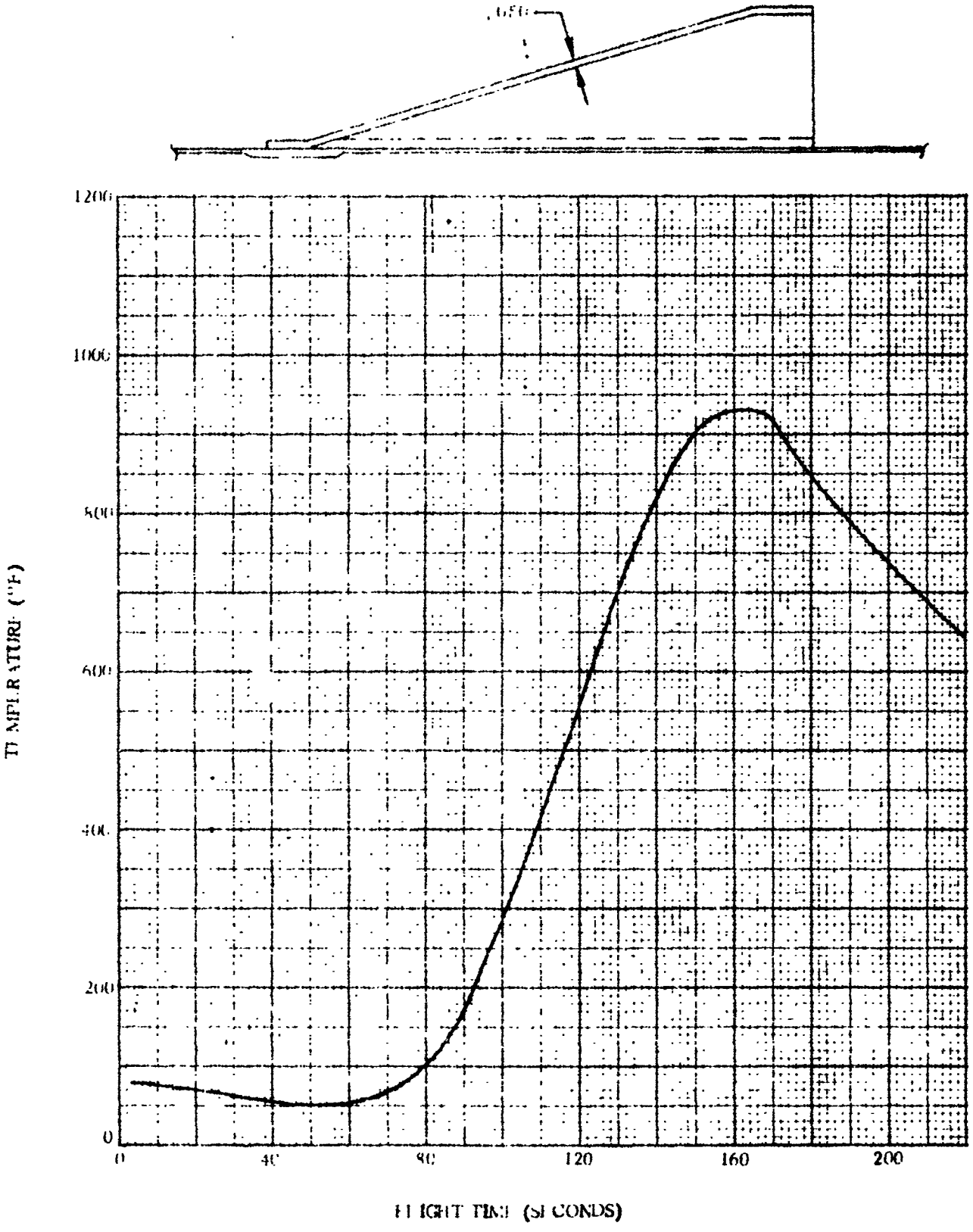

4B65LV

Figure 4.8-3. Azusa and C-Band Antenna Fairing - Temperature Histories

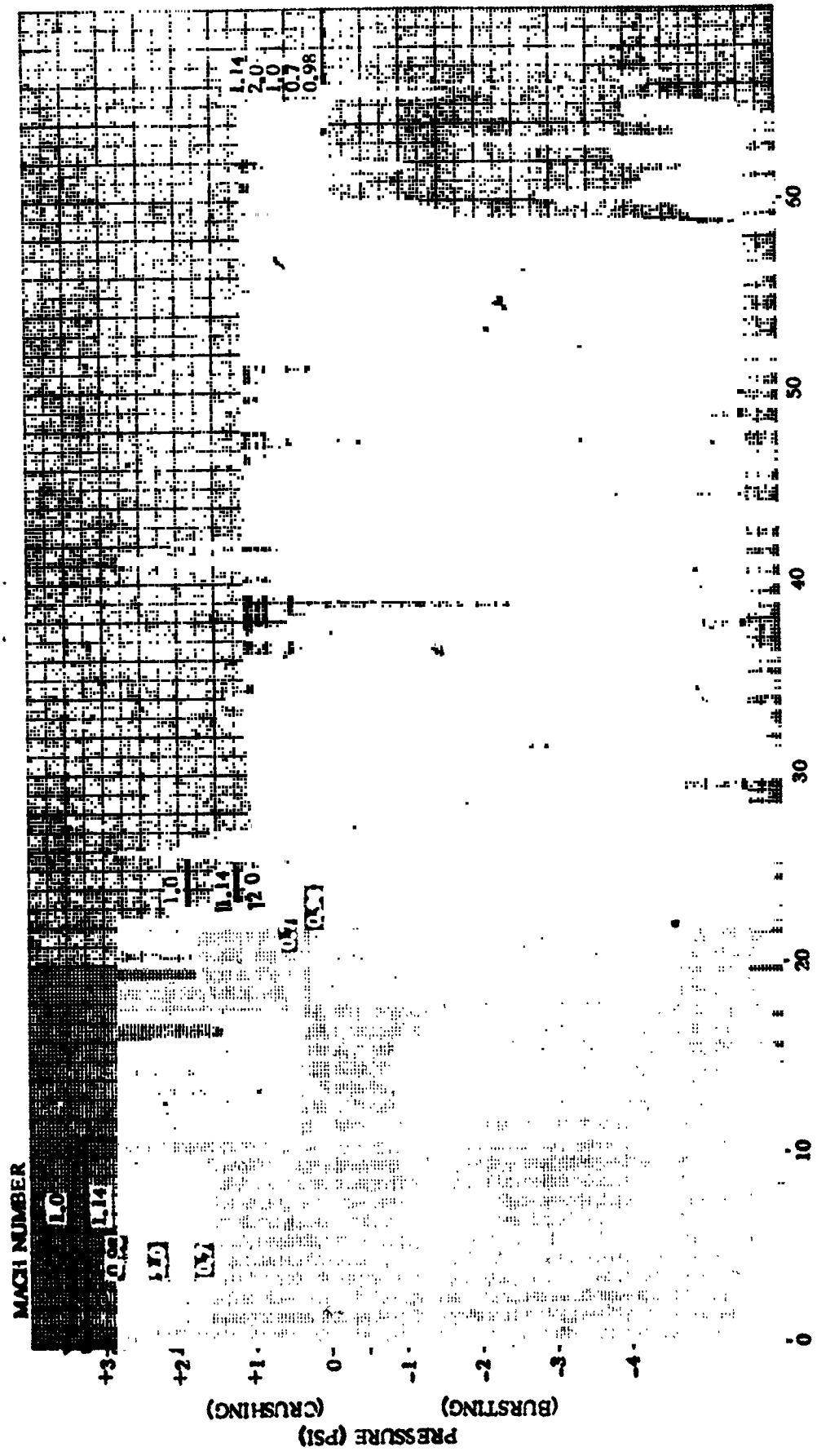

Figure 4.8-4 Ascent and Entry (Zero Angle of Attack) - Steady-State Wall Differential Pressures

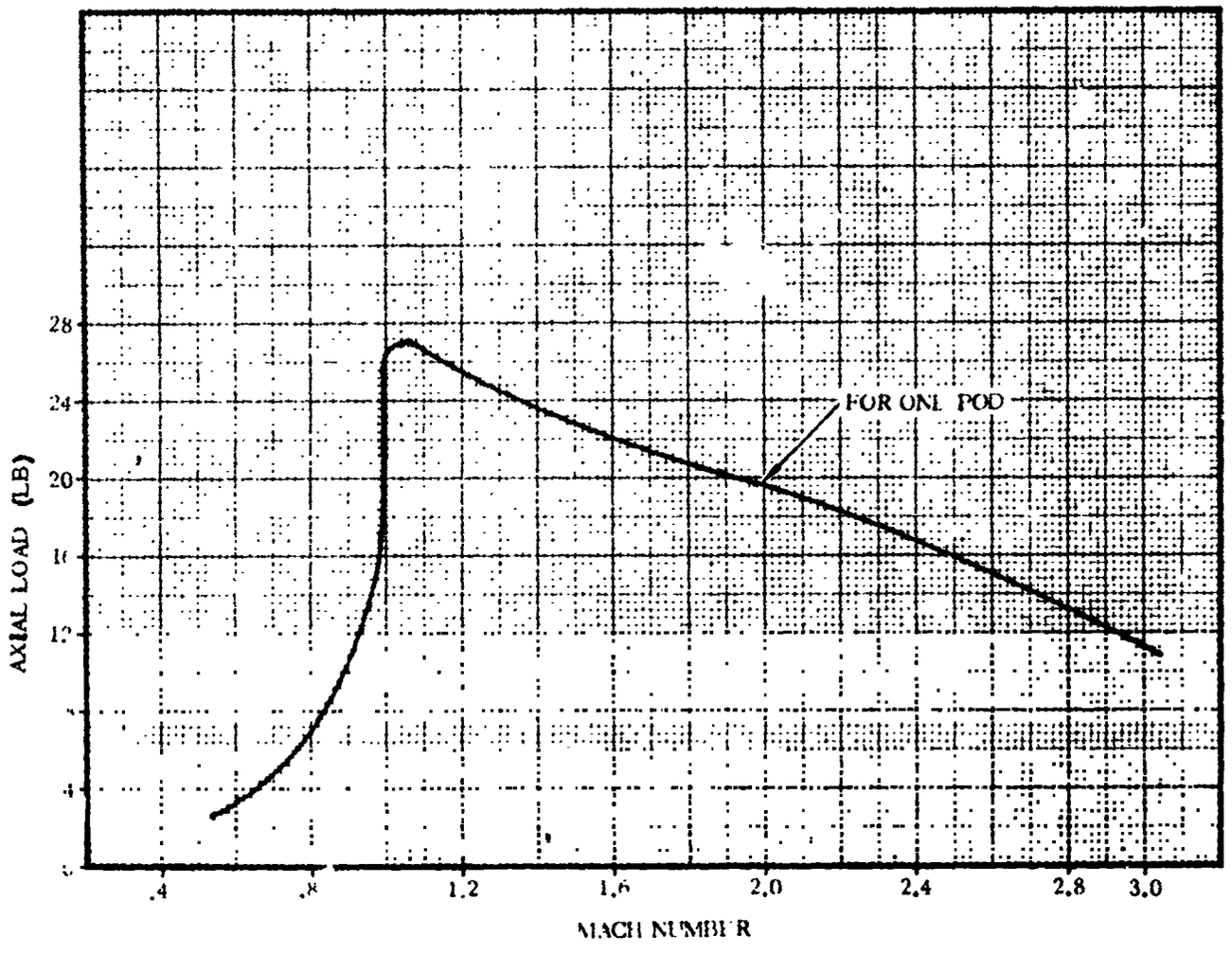

4B62LV

Figure 4.5-5. Azusa and C-Band Antenna - Axial Load versus Mach Number

Figure 4.8-6. Azusa and C-Band Antenna Fairings - Fluctuating Wall Differential Pressure

THIS PAGE INTENTIONALLY LEFT BLANK.

4.9 T-0 AND T-4 UMBILICAL PANEL CHUTES

The T-0 (2-inch rise-off) umbilical panel chute provides a guide for the 2-inch rise-off electrical disconnect, and the T-4 (aft) umbilical panel chute similarly guides the aft umbilical plate during disconnect (Reference Figure 4.1-1 for vehicle location). Both chutes serve to seal the area surrounding the respective panel and electrical disconnect against leakage during prelaunch air conditioning of the interstage adapter. See Figures 4.9-1 and 4.9-2 for the configuration of the T-0 and T-4 umbilical panel chutes respectively.

4.9.1 CRITICAL CONDITIONS. The T-0 and T-4 umbilical panel chutes must be investigated for three loading conditions; namely, launch, Max αq and Max g.

At launch, the chutes are subjected to impact loads as the umbilicals are withdrawn from their respective receptacles.

During transonic flight, the chutes experience a combination of maximum steady-state and fluctuating air loads along with applicable inertia loads.

At BECO (Max g condition), the vehicle attains maximum acceleration; consequently, maximum longitudinal inertia loads are combined with maximum heating simultaneously.

4.9.2 WEIGHTS AND CENTER OF GRAVITY DATA. Structural design weights and C.G.'s for the subject chutes are given in Table 4.9-1.

TABLE 4.9-1. T-0 AND T-4 CHUTES - WEIGHTS AND CENTERS OF GRAVITY

	Weight (lb)	C.G. (in.)		
		z	y	x
T-0 Panel Chute	1.4	442	-58	+18
T-4 Panel Chute	3.1	445	-55	+22

4.9.3 THERMAL DATA. The following temperatures respective to the appropriate time in flight should be used for analysis regarding the umbilical panel chutes.

Flight Time	Temperature (°F)
Transonic	100
BECO (Max g)	550

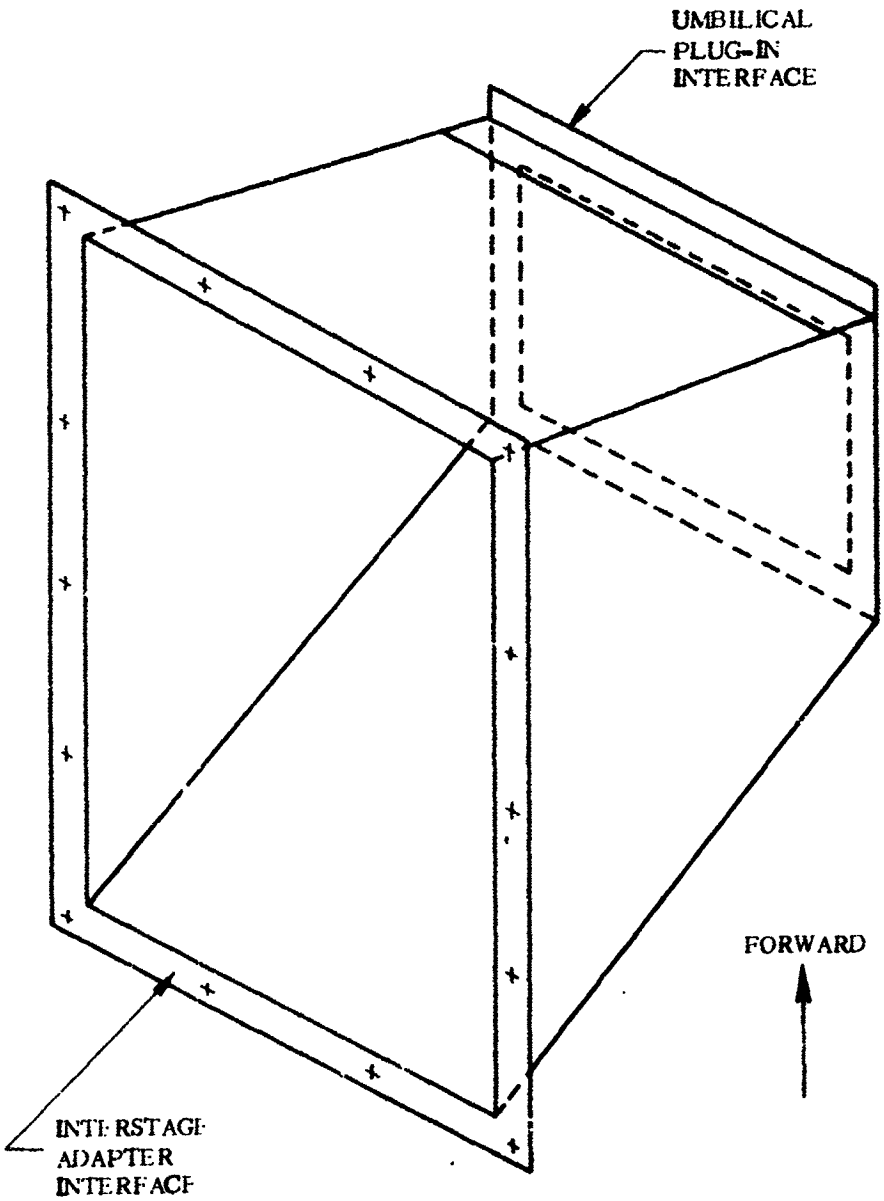

4B277LV

Figure 4.9-1. T-0 Umbilical Panel Chute - Configuration

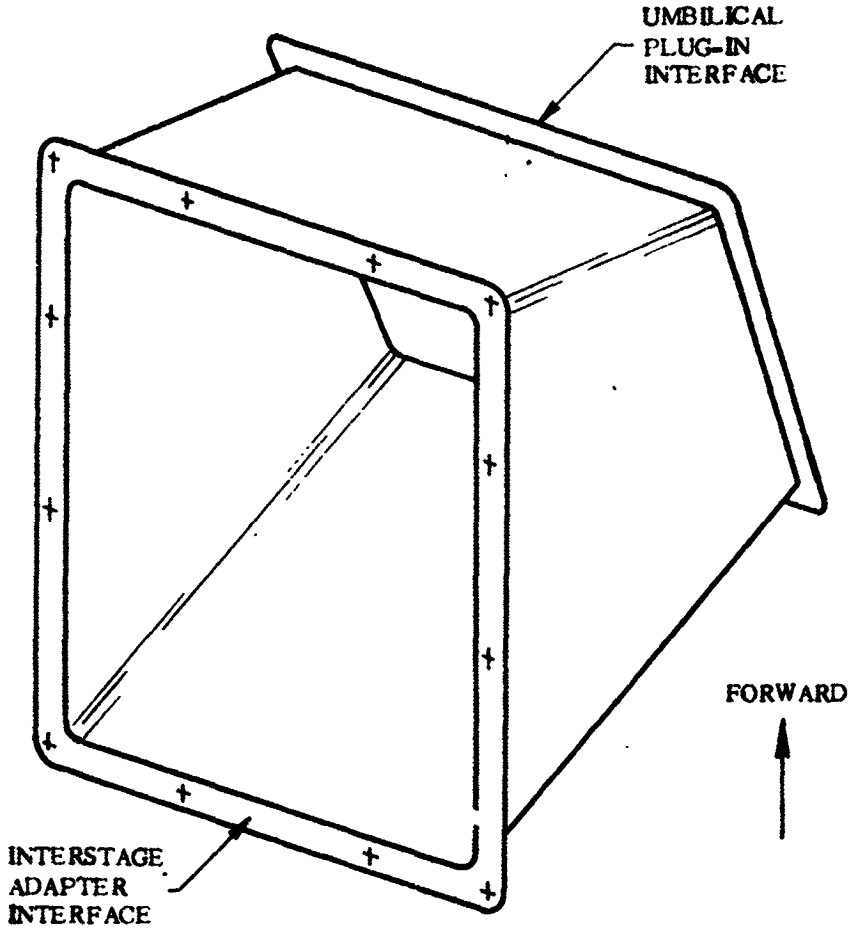

4B278LV

Figure 4.9-2. T-4 Umbilical Panel Chute - Configuration

4.9.4 INERTIA LOADS. During transonic flight, the inertia load factors describe in Table 4.9-2 must be combined with the aerodynamic loads given in Paragraph 4.9.5.

At Max g (BECO), the inertia load factors shown in Table 4.9-3 must be combined with the maximum temperature given in Paragraph 4.9.3.

TABLE 4.9-2. INERTIA LOAD FACTORS DURING TRANSONIC FLIGHT

Condition	Longitudinal Inertia (g's)	Lateral Inertia (g's)
Max Aft Inertia	+8.0	±1.0
Max Fwd Inertia	-4.0	±1.0
Max Lateral Inertia	+2.0	±6.5

TABLE 4.9-3. INERTIA LOAD FACTORS AT MAX g (BECO)

Condition	Longitudinal Inertia (g's)	Lateral Inertia (g's)
Max Longitudinal Inertia	+9.0	±1.0
Max Lateral Inertia	+6.0	±3.5

4.9.5 STEADY-STATE AIR LOADS. During transonic flight ($0.85 \leq M \leq 1.30$) the steady-state air loads are maximized. For analysis of the umbilical panel chutes, a maximum differential pressure of 2.40 psi should be considered; this includes the load contribution resulting from fluctuating pressure effects.

4.9.6 BUFFET AND FLUTTER LOADS. The loads which result from fluctuating pressures also occur during transonic flight and have been incorporated as a maximum design differential pressure within the steady-state criteria described in Paragraph 4.9.5.

4.9.7 MISCELLANEOUS LOAD PARAMETERS. At launch, the T-0 and T-4 umbilicals are withdrawn and the disconnects may impact upon the chutes. In determining the impact loads the following assumptions were used:

a. The chutes were perfectly elastic for very large deformations.

b. A coefficient of restitution equal to 0.707 was used for the disconnect rebound velocity.

c. The disconnects fall vertically from the top of the chute in a 1-g environment.

For the T-0 chute, an impact load of 93 pounds may be applied any place within 1 inch of the vertical sides of the chute.

4.10. INSULATION PANEL - INFLIGHT PURGE SYSTEM

An insulation panel inflight purge system has been incorporated on operational vehicles. The system consists of: a 50-pound helium bottle mounted to the interior of the interstage adapter between Stations 511 and 526; a ground disconnect bracket mounte on the exterior of the adapter at Station 449 (between stringers number 16A and 17); a solenoid operated shutoff valve mounted internally at Station 460 (between stringers number 17 and 18); a staging disconnect and mounting bracket at Station 419 on the exterior of the interstage adapter under the boost pump fairing; and tubing connecting the components.

The purpose of this system is to provide a gaseous helium cavity between the insulation panels and the Centaur LH_2 tank to prevent the panels from freezing to the tank.

See Figures 4.10-1 and 4.10-2 for the configuration of the helium bottle and ground-air disconnect support, respectively.

4.10.1 CRITICAL CONDITIONS. The insulation panel helium purge system consists of several major components all of which experience critical loadings irrespective of their weight, size, location, or function in the system.

The helium bottle is subjected to internal pressure and inertia loads which are considered applicable to all flight conditions.

The ground-air disconnect experiences disconnect forces at launch combined with vibrational or inertia loads from the attached ground hoses.

The solenoid shutoff valve is subjected to inertia loads which are considered consistent throughout flight.

The staging disconnect receives a disconnect force at Atlas/Centaur separation.

The tubing within the system experiences inertia loading which results from the vibrational characteristics of this type of hardware.

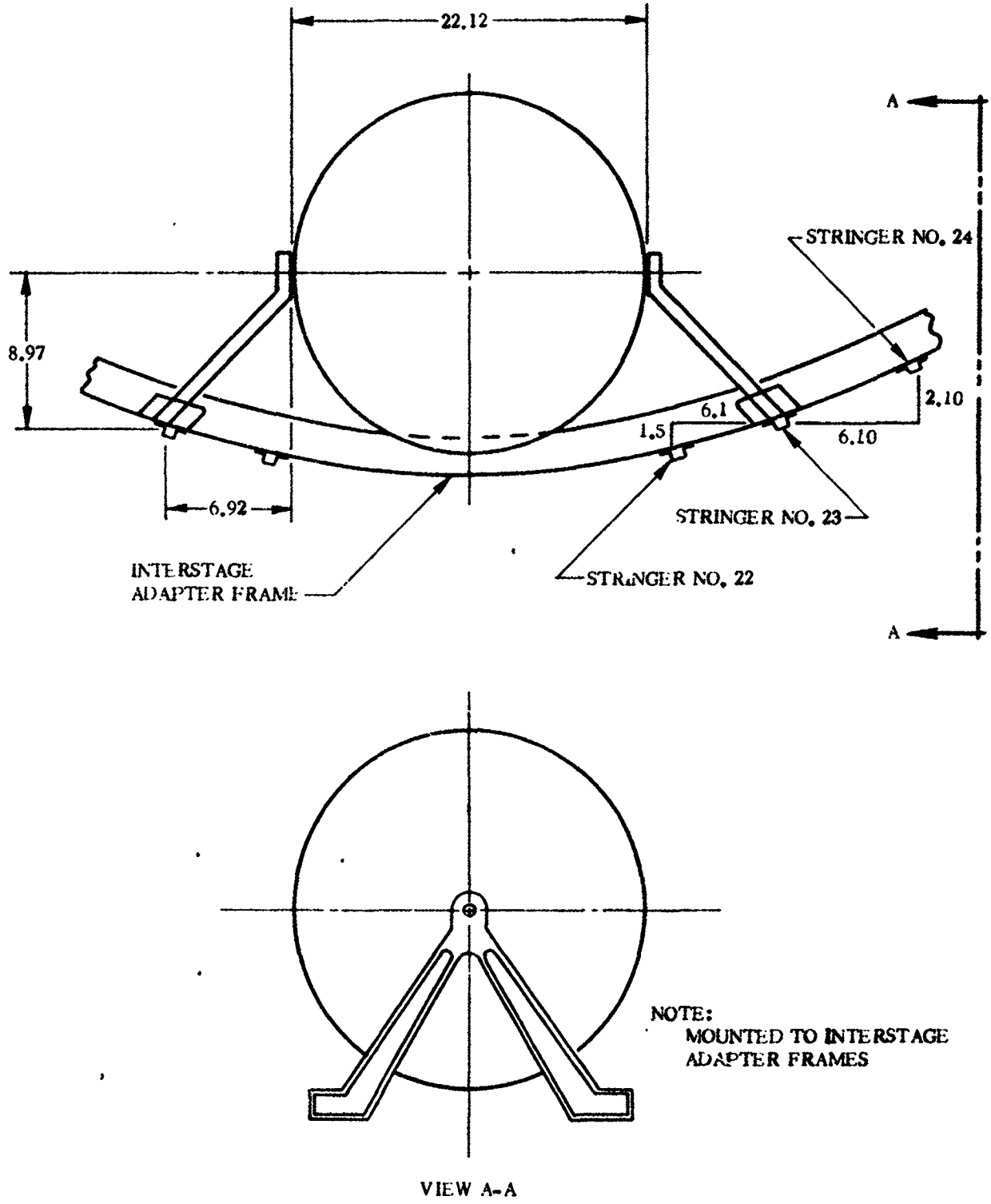

4B279LV

Figure 4.10-1. Helium Bottle Purge System - Configuration

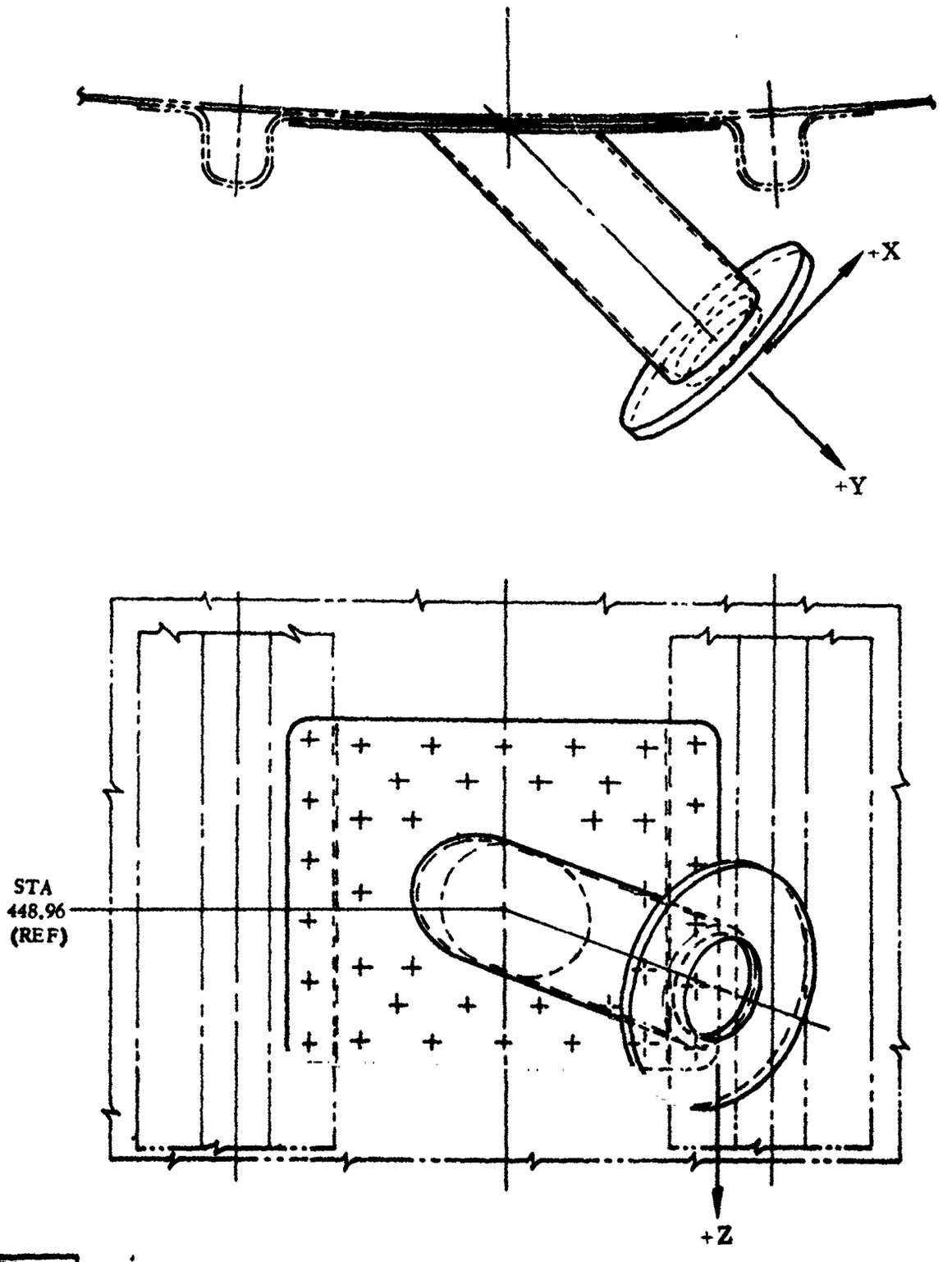

Figure 4.10-2. Ground-Air Disconnect - Support Configuration

4.10.2 WEIGHTS AND CENTER OF GRAVITY DATA. The various weights and C.G.'s for the components within the helium purge system are found in Table 4.10-1.

TABLE 4.10-1. HELIUM PURGE SYSTEM - WEIGHTS AND CENTER OF GRAVITY

Component	Weight (lb)	C.G. (in.)		
		Station	Y	X
Helium Bottle	50	519	0	-48
Solenoid shutoff valve	1.5	460	0	-53

4.10.3 THERMAL DATA. This equipment is mounted within the interstage adapter cavity; therefore, aerodynamic heating is not critical. The temperature of the staging disconnect is assumed to be -50°F at all times.

4.10.4 INERTIA LOADS. The inertia load factors resulting from steady-state acceleration and vibrational characteristics of the hardware are given in Paragraphs 4.10.4.1 through 4.10.4.3.

The maximum load on the tubing installation is due to aerodynamic buffet of the interstage adapter to which the tubing is mounted. The maximum vibrational acceleration is 125 g's in a lateral plane.

4.10.4.1 Helium Bottle Inertia Loads. The inertia load factors for the helium bottle at various flight conditions are listed in Table 4.10-2.

TABLE 4.10-2. HELIUM BOTTLE INERTIA LOAD FACTORS

Condition	Longitudinal (g's)	Lateral (g's)
Launch	+1.4	±16
	+1.4 ±15	± 1
Mach 1	+2.3	±16
	+2.3 ±15	± 1
BECO	+7	± 3
	+7 ±2	± 1

NOTE:
Longitudinal load factors are positive acting aft.
Lateral loads may act in any direction in the X-Y plane.

4.10.4.2 Solenoid Shutoff Valve Inertia Loads. The solenoid shutoff valve is mounted to a sheet metal bracket on the interior of the interstage adapter. The valve and support bracket will be subject to lateral vibration accelerations due to aerodynam buffeting of the adapter and longitudinal acceleration due to vehicle acceleration. Associated load factors are given in Table 4.10-3.

TABLE 4.10-3. SOLENOID SHUTOFF VALVE INERTIA LOAD FACTORS

Longitudinal (g's)	Lateral (g's)
+15, -3	±4.5
Negligible	±125
±20	Negligible

4.10.4.3 Ground-Air Disconnect Inertia Loads. The geometry of the disconnect support and the coordinate system for the loads is shown in Figure 4.10-2. The X and Y axes are in the vehicle X-Y plane and the Z axis is parallel to the vehicle Z axis. Positive forces and moments are in the positive shown directions.

a. Case A: Vertical Hose Vibrational Load at $t \leq 0$.

The maximum vertical acceleration of the hose is 5.5 g. The maximum wind velocity is 46 mph acting horizontally. This combination of forces produces the following loads:

$F_X = -2.6$ lb
$F_Y = 0$
$F_Z = 14.5$ lb
$M_X = 81.5$ in.-lb
$M_Y = 0$
$M_Z = 24.0$ in.-lb

b. Case B: Horizontal Hose Vibrational Load at $t \leq 0$.

The maximum horizontal acceleration of the hose is 4.5 g. The combination of inertia plus drag (46 mph wind velocity) forces yields the following loads:

$F_X = -14.8$ lb
$F_Y = 0$
$F_Z = 0$
$M_X = 0$
$M_Y = 0$
$M_Z = 92.0$ in.-lb

c. Case C: Flight Loads.

In the transonic region, the following load factors shall be applied to the airborne disconnect half and its support:

Longitudinal (g's)	Lateral (g's)
+15, -3	±4.5
Negligible	±125
±20	Negligible

4.10.5 STEADY-STATE AIR LOADS. Since this equipment is mounted within the interstage adapter cavity, direct air impingement loads are not critical.

The ground-air disconnect, however, is exposed to the airstream, but externally just aft of the boost pump fairing at Station 449. The boost pump fairing protects the disconnect installation from aerodynamic heating and wind loading. However this load is negligible compared to the disconnect and inertia loads at the interface.

The staging disconnect is mounted under the boost pump fairing and is thus protected from aerodynamic heating and wind loading.

4.10.6 BUFFET AND FLUTTER LOADS. The loading which results from vibrational characteristics of the tubing is given in Paragraph 4.10.4. See Paragraphs 4.10.4.1 through 4.10.4.3 for load factors on the various components which result from vibration or buffeting of the interstage adapter during flight.

4.10.7 MISCELLANEOUS LOAD PARAMETERS. The individual components are subjected to additional loads as follows:

4.10.7.1 Helium Bottle. The helium bottle maintains an internal operating pressure of 3000 psig which should be superimposed upon other loading conditions imposed on the bottle.

4.10.7.2 Ground-Air Disconnect. The ground-air disconnect experiences lanyard loads and disconnect reactions at launch as follows:

a. The maximum lanyard pull (t - 0) is 110 pounds, applied in the +Y direction within a 15 degree half-angle cone. This load is for the primary lanyard and will not be exceeded by the backup system,

NOTE. This load may be superimposed upon either Case A or B of Paragraph 4.10.4.3.

b. The disconnect reaction ($t > 0$) is equal to a spring force of 150 pounds. Since the spring load is suddenly applied, an impact factor of 2 results in the following loads:

$F_X = 0$
$F_Y = -290$ lb
$F_Z = -77.5$ lb
$M_X = 0$
$M_Y = 0$
$M_Z = 0$

These loads act independent of other loading conditions.

4.10.7.3 Staging Disconnect. The maximum disconnect load is 7.5 pounds applied along the centerline of the disconnect. Because disconnect is initiated by a metal to metal contact, an impact factor of 2 should be applied for stress analysis.

THIS PAGE INTENTIONALLY LEFT BLANK.

4.11 INSULATION PANEL JETTISON HINGES

The insulation panel jettison hinges are mounted on the interstage adapter at Station 437.08. These hinges provide the pivotal points about which the panels rotate at jettison. Two hinges are utilized for each quarter of insulation panel. The configuration of one hinge is shown in Figure 4.11-1. Location of hinges on the interstage adapter is shown in Figure 4.2-5.

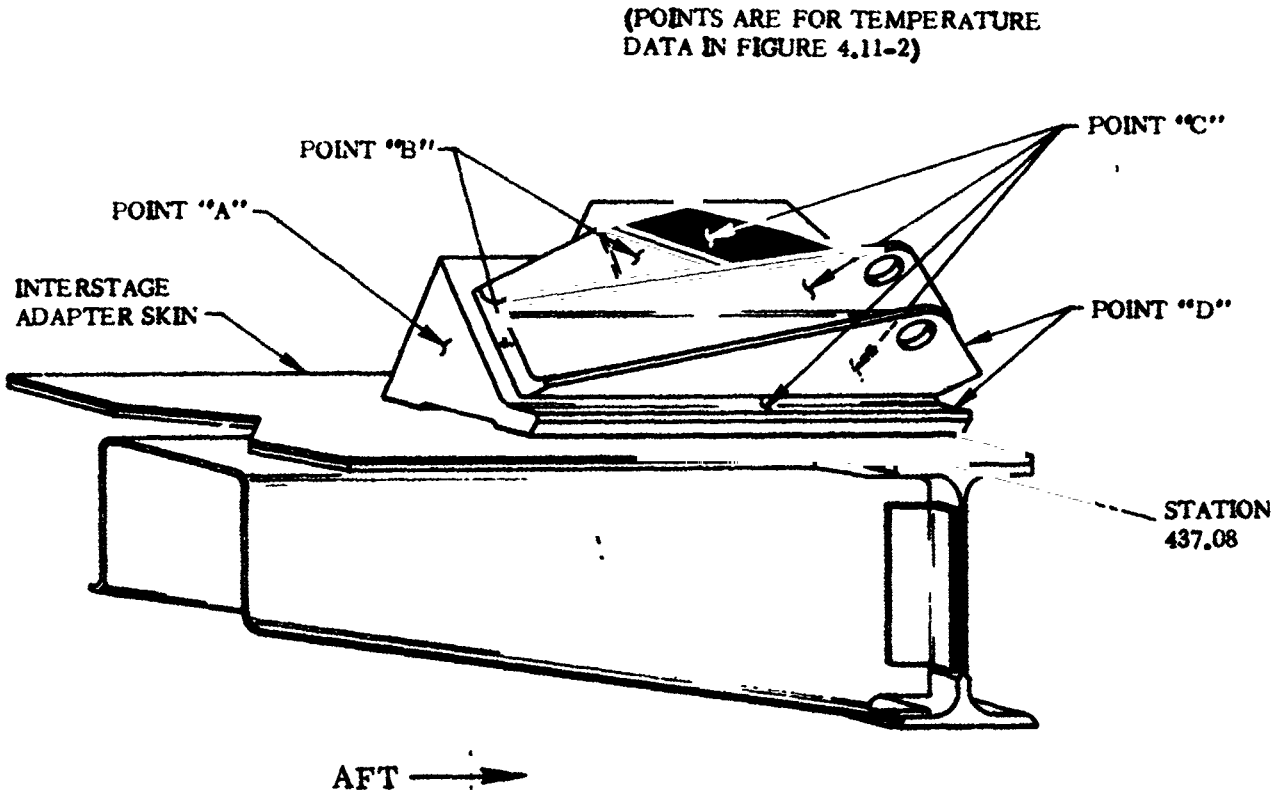

4B273LV

Figure 4.11-1. Insulation Panel Hinge Configuration

4.11.1 CRITICAL CONDITIONS. The critical loading condition for the insulation panel jettison hinges occurs at panel jettison.

4.11.2 WEIGHTS AND CENTER OF GRAVITY. See Paragraph 3.2.2 for insulation panel weights which are used to compute the hinge loads during jettison.

4.11.3 THERMAL Data. [illegible] temperature history for the data points shown in Figure [illegible].

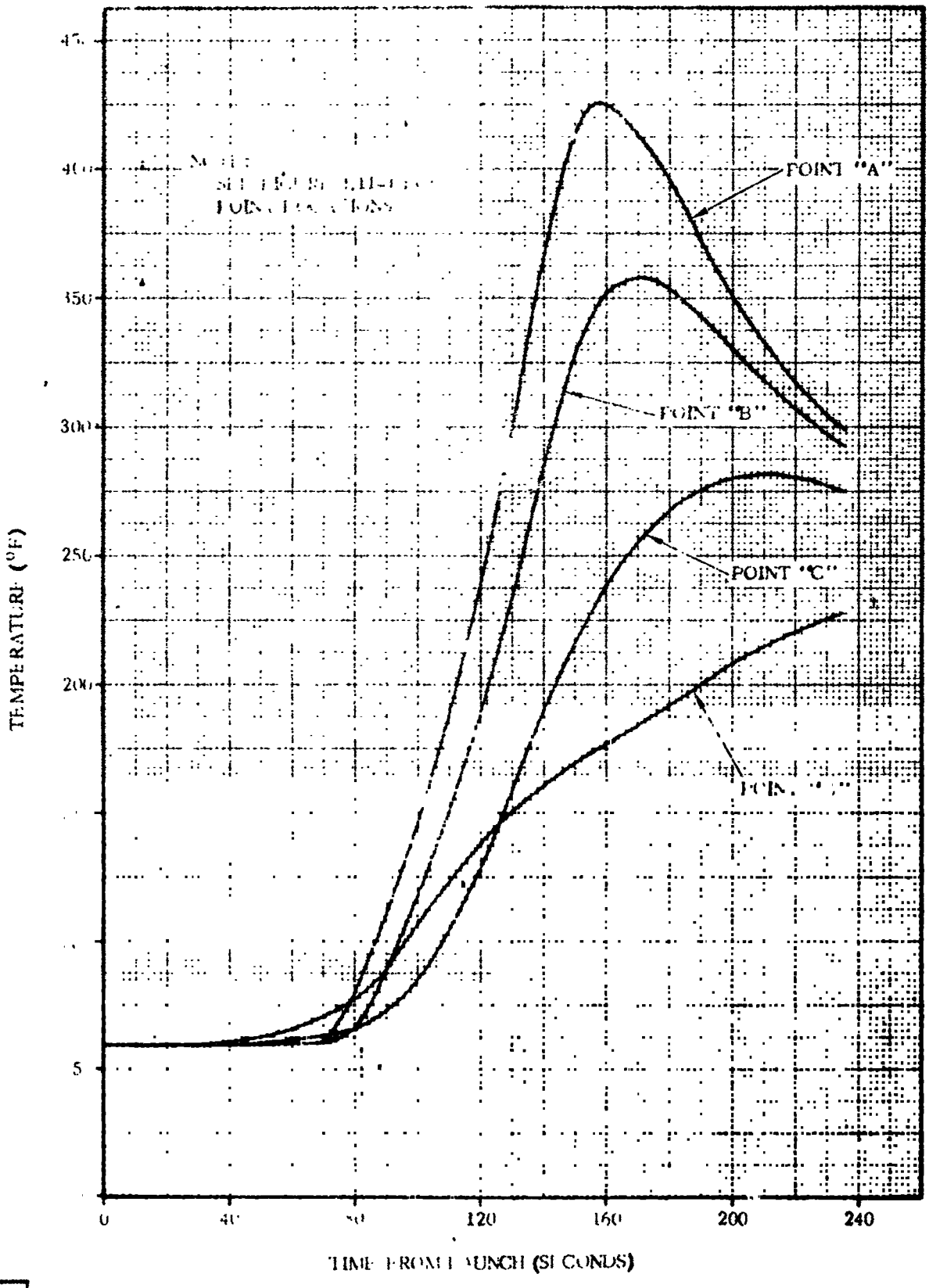

4B274LV

Figure 4.11-2. Insulation Panel Hinge Fittings on the Interstage Adapter - Temperature Histories

4.11.4 INERTIA LOADS. The loads on the hinges due to inertia effects at fairing jettison are included in Table 3.8-1.

4.11.5 STEADY-STATE AIR LOADS. Direct air impingement loads are negligible compared to the jettison loads.

4.11.6 BUFFET AND FLUTTER LOADS. Buffet and flutter loads on the hinges are negligible.

4.11.7 MISCELLANEOUS LOAD PARAMETERS. The loads which occur at insulation panel jettison have already been presented in Subsection 3.8, therefore they will not be repeated here. Reference Subsection 3.8 for critical loads at this time.

THIS PAGE INTENTIONALLY LEFT BLANK.

4.12 AIR CONDITIONING DUCT DOORS

The air conditioning duct doors serve as seal covers to the environmental control receptacles within the interstage adapter. The doors are hinged in order to accept ground air conditioning ducts during prelaunch operations. At launch, the ground lines are removed and as the hinges are spring loaded, the doors automatically close and remain closed during flight by means of a magnetic latch. The configuration of the duct doors is shown in Figure 4.12-1.

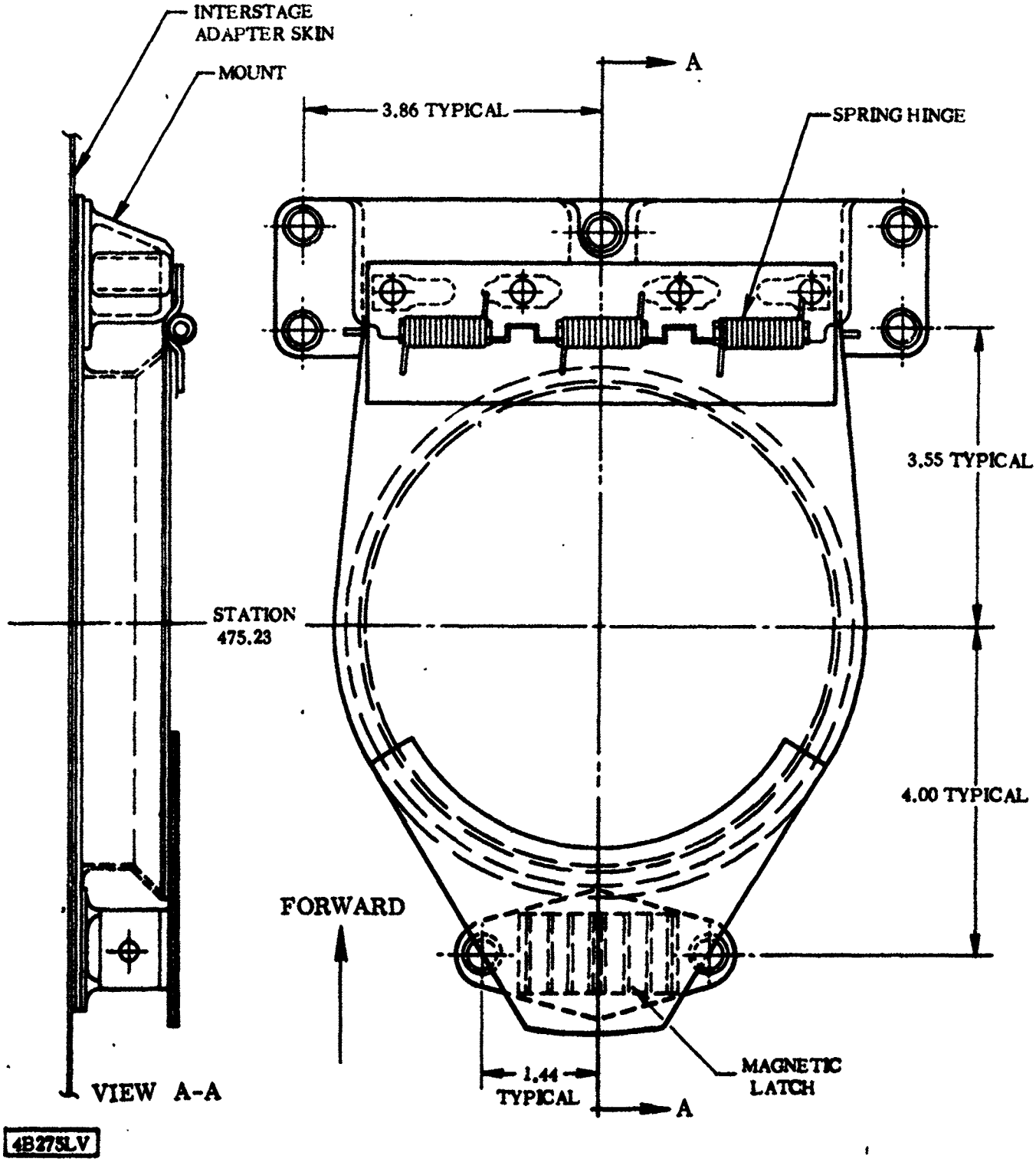

Figure 4.12-1. Air Conditioning Duct Doors (Typical) - Configuration

4.12.1 CRITICAL CONDITIONS. At launch, disconnect forces are developed which are reacted by the interstage adapter, therefore, these loads will be presented in this section simply because of their association with the environmental control receptacles and doors.

The doors are subjected to a maximum loading condition due to a combination of steady-state and fluctuating differential pressures during transonic flight.

4.12.2 WEIGHTS AND CENTER OF GRAVITY DATA. Due to the lightweight nature of the doors, inertia loads are of an inconsequential magnitude compared to the aerodynamic loads; therefore, weights or C.G. data is not critical.

4.12.3 THERMAL DATA. Aerodynamic heating of the duct doors is not critical. See Paragraph 4.2.3.2 for skin temperature associated with undisturbed flow areas on the adapter.

4.12.4 INERTIA LOADS. Load contributions from inertia effects of the doors are not critical (see Paragraph 4.12.2).

4.12.5 STEADY-STATE AIR LOADS. Air impingement loads on the doors are given as a combination of steady-state and fluctuating differential pressures as follows:

Crush pressure = 4.4 psid

Burst pressure = 2.0 psid

These loads may occur at any time during transonic flight ($0.85 \leq M \leq 1.30$).

4.12.6 BUFFET AND FLUTTER LOADS. These loads are included in the equivalent quasi steady-state air loads described in Paragraph 4.12.5.

4.12.7 MISCELLANEOUS LOAD PARAMETERS. Disconnect loads occur at launch which are reacted by the interstage adapter.

Loads resulting from disconnect of the ground heating ducts are presented in Table 4.12-1.

TABLE 4.12-1. GROUND HEATING DUCT TOTAL LOADS AT DISCONNECT

Condition	F_X (lb)	F_Y (lb)	F_Z (lb)	M_X (in.-lb)	M_Y (in.-lb)	M_Z (in.-lb)
Maximum Downward Load	-60	+140	+220	+1710	+1650	+850
Maximum Upward Load	-70	+150	-170	-270	-1600	+920

SIGN CONVENTION

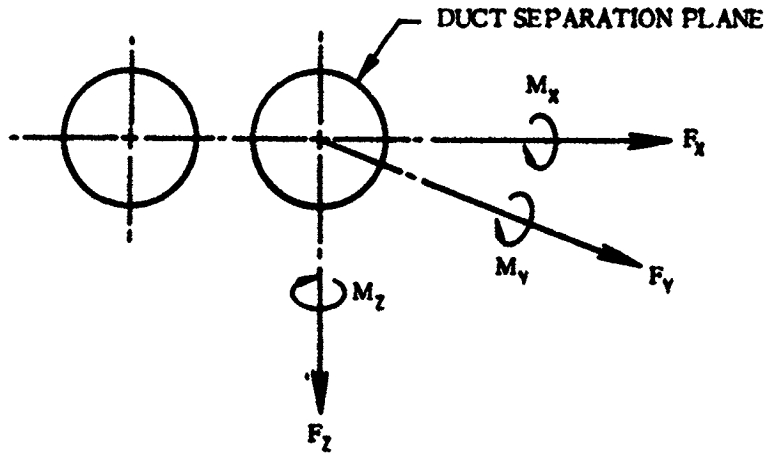

F_X = FORCE TANGENTIAL TO VEHICLE SKIN
F_Y = FORCE IN DIRECTION OF VEHICLE RADIUS
F_Z = FORCE IN LONGITUDINAL DIRECTION
(+) DIRECTION OF FORCES AND MOMENTS ARE AS SHOWN

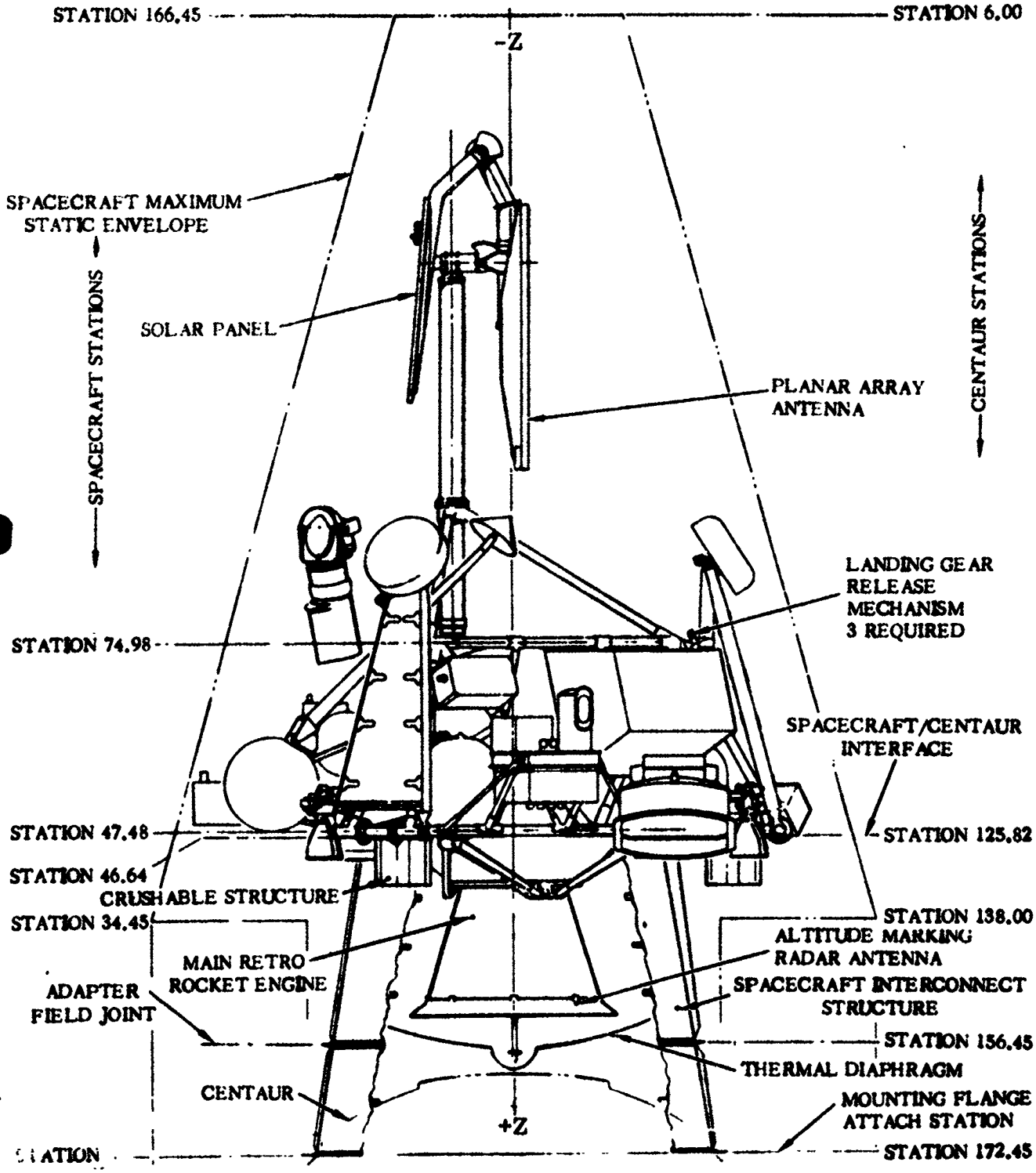

LAUNCH CONFIGURATION

SECTION V

PAYLOAD ADAPTER (SURVEYOR TYPE)

5.1 INTRODUCTION

The Centaur AC-4 (and on) payload adapters (Figure 5.1-1) provide a structural ti between the liquid hydrogen tank forward bulkhead and the payload. The adapter converts a three-point load concentration, imposed by the payload model or spacecraft, to an acceptable load distribution at the mounting ring (Station 172.45). The Surveyor Spacecraft/Centaur interface is shown in Figure 5.1-2.

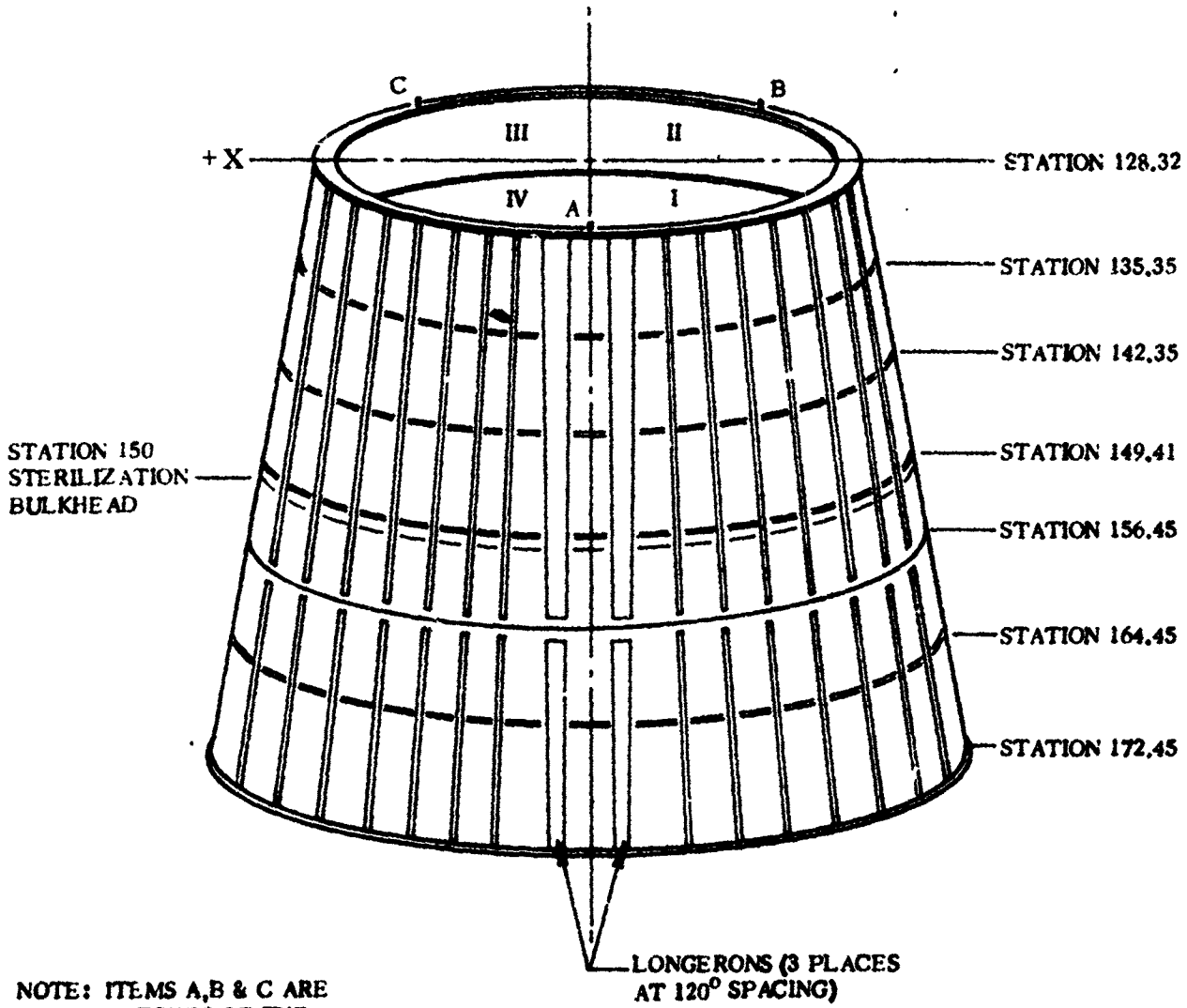

Figure 5.1-1. Payload Adapter

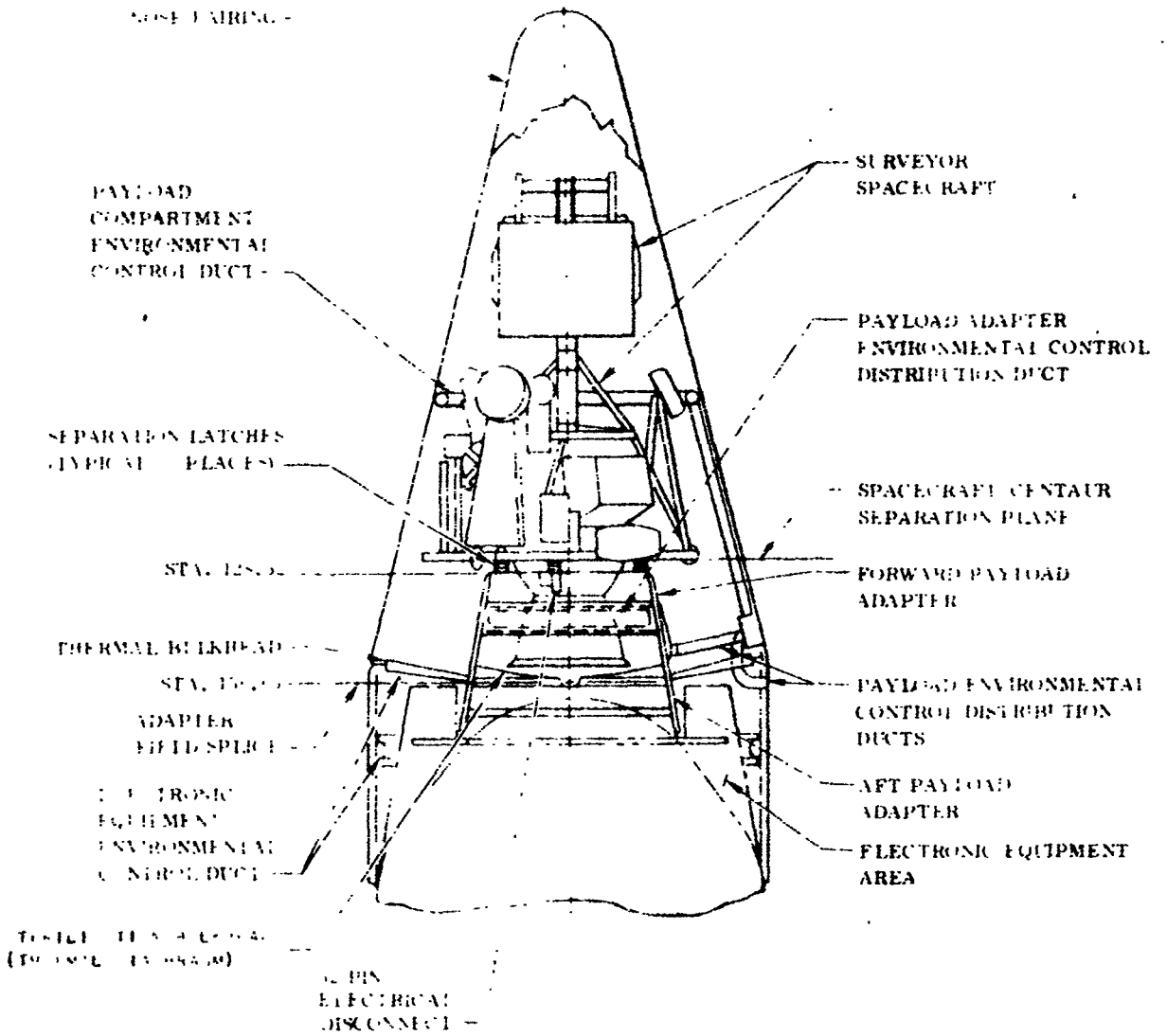

4B211LV

Figure 5.1-2. Surveyor Spacecraft/Centaur Interface General Arrangement

The adapter is a semimonocoque truncated conical shell stiffened by circumferential frames and longitudinal stringers. Three longerons, located at 120-degree intervals around the periphery, react loads introduced at the three payload separation fittings. The adapter further contains a thermal diaphragm to provide a thermal barrier between the payload compartment and the Centaur vehicle.

5.2 PRIMARY ADAPTER STRUCTURE

5.2.1 CRITICAL CONDITIONS. It is necessary to consider three different loading environments in structurally evaluating the payload adapter primary structure:

a. Inertia loads due to dynamic response of the payload.

b. Thermal environment.

c. Differential pressure across adapter wall.

5.2.2 WEIGHTS AND CENTER OF GRAVITY DATA. The payload adapter structure shall be analyzed for a variable payload ranging from 1500 to 2500 pounds. The payload design center of gravity envelope shall be considered as follows:

$\bar{z}$ between Stations 89 and 118
$\bar{y}$ between +2.2 and -1.0
$\bar{x}$ between +2.0 and -2.0
} (Reference 5-3)

The weight of the payload adapter plus miscellaneous equipment (i.e., TLM RF-Systems, Surveyor Destructor, etc.) shall be considered as 135 pounds with a C.G. at Station 147.

5.2.3 THERMAL DATA. Thermal data is of structural concern only to the aft most area of the payload adapter. Maximum relative thermal contraction is seen to occur between Stations 172.45 and 164.45, based on a temperature differential of 133°F. Therefore, only the aft bay of adapter stiffeners need be evaluated for the additive stress due to $\alpha\Delta T$.

Thermal analysis of the Station 172.45 joint assumes perfect contact between the interfaces of dissimilar materials (reference Figure 5.2-1).

The heat transfer through the payload ring is primarily dependent upon the assumed ullage gas temperature during flight; therefore, the temperature distribution for the two times in flight presented in Figure 5.2-2 is considered conservative for structural analysis of the Station 172.57 area.

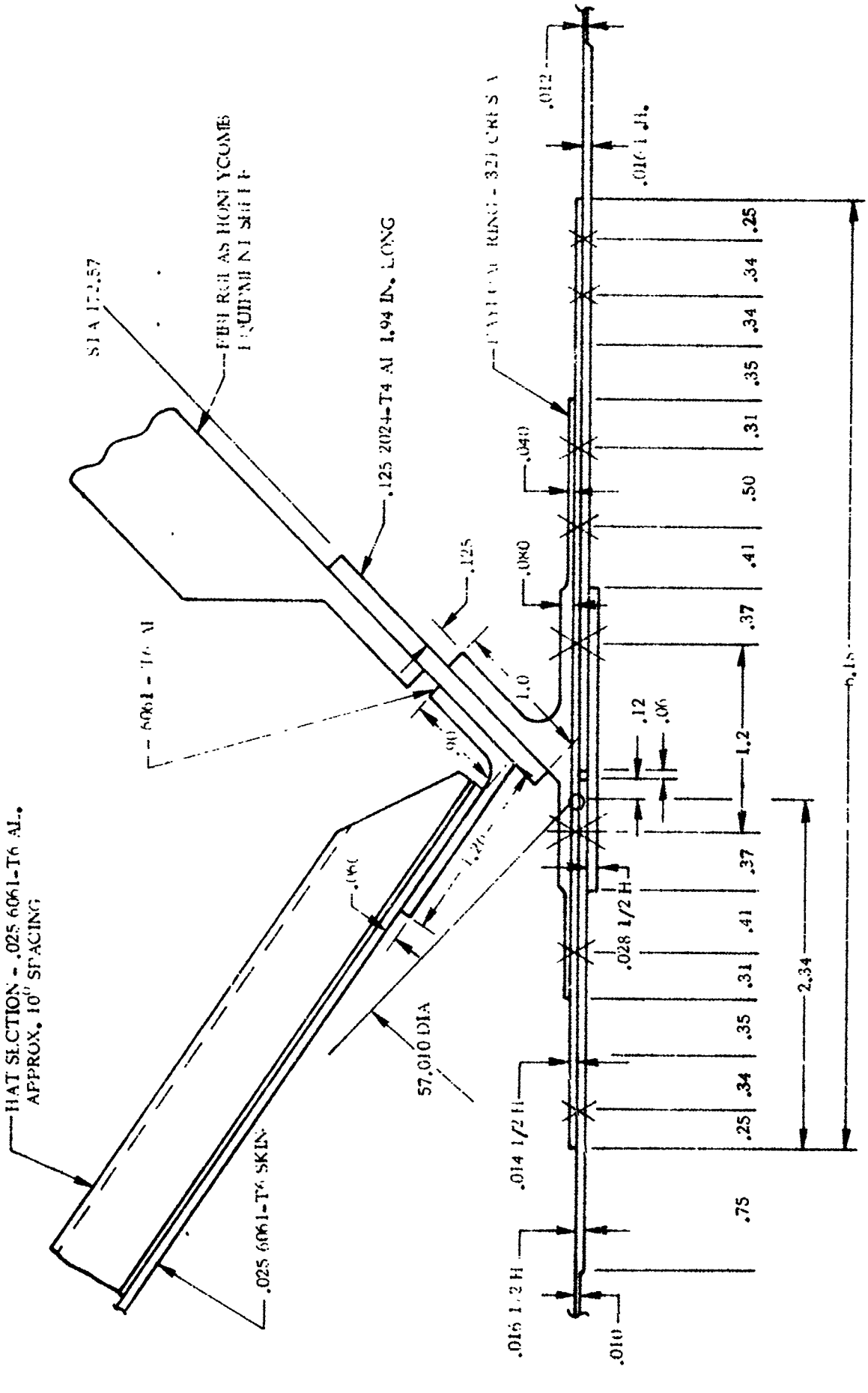

4B212LT

Figure 5.2-1. Station 172.57 Payload Ring Geometry

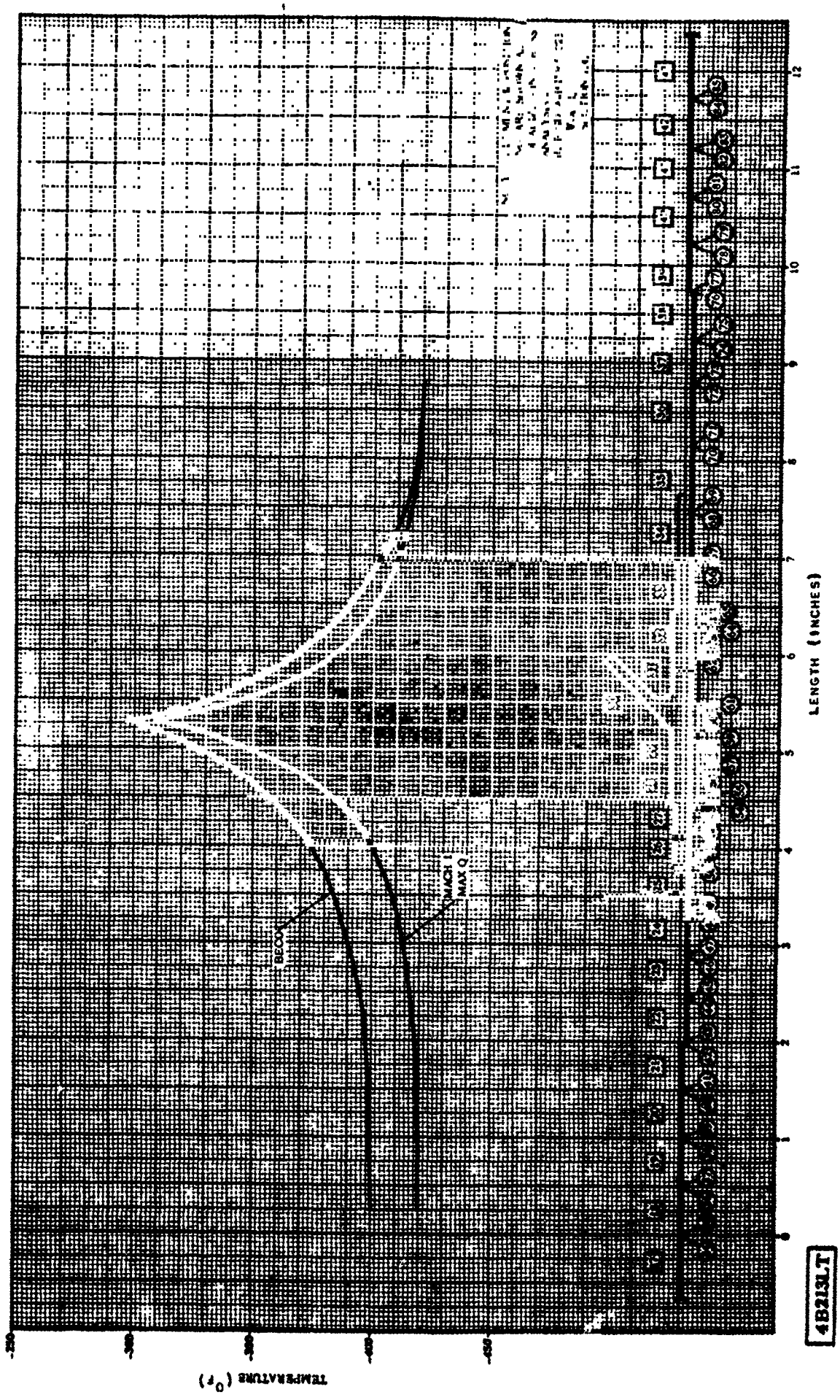

Figure 5.2-2. Station 172.57 Payload Ring Temperature Distribution - Skin Doubler Area

5.2.4 INERTIA LOADS. Table 5.2-1 presents limit load factors for a Surveyor payload with a conservative weight range between 2100 and 2800 pounds. These load factors applied at the C.G. of the payload are used to determine the maximum longitudinal and lateral loads to which the payload adapter will be subjected during all significant phases of flight between Atlas thrust buildup (prelaunch) and Centaur MECO.

TABLE 5.2-1.* SURVEYOR PAYLOAD SUPPORT STRUCTURE DESIGN LOAD FACTORS

LOAD CONDITIONS	MAX LONGITUDINAL (g's)		MAX LATERAL (g's)	
	LONGITUDINAL	LATERAL	LONGITUDINAL	LATERAL
(1) PRELAUNCH	+1.0 ±0.1	±0.02	+1.0	±0.12
(2) ATLAS THRUST BUILDUP	+1.0 ±1.3	±0.52	+1.0 ±0.6	±1.22
(3) LAUNCH	+1.3 +1.2	+1.25	+1.3 ±0.5	±1.95
(4) POST LAUNCH LONG. OSC	+1.3 +1.0	+0.25	+1.3 +0.3	±0.95
(5) t = 30 SEC	+1.5 ±0.7	±0.50	+1.5	±1.20
(6) MACH 1 - MAX Q	+2.4 ±0.7	±1.02	+2.4	±1.72
(7) BECO	+5.8 ±0.45	±0.10	+5.8 ±0.1	±0.45
(8) CENTAUR 1ST THRUST BUILDUP	+0.87 ±1.2	±0.60	+0.87 ±0.5	±1.30
(9) CENTAUR 2ND THRUST BUILDUP	+2.3 ±1.7	±0.60	+2.3 +1.0	±1.30
(10) CENTAUR MAX ACCELERATION	+4.0 ±0.7	±0.10	+4.0	±0.80
(11) MECO	+0.05 ±1.7	±0.50	+0.05 ±1.2	±1.00

*Reference 5-1

5.2.5 STEADY-STATE AIR LOADS. During the transonic portion of flight ($0.8 \leq M \leq 1.3$), differential pressures are developed across the walls of the payload adapter. The design differential pressures which introduce critical loads into the payload adapter are the following:

a. A 0.4 psid pressure, acting aft on the sterilization bulkhead (Station 150).

b. A 0.4 psid pressure, imposed between Stations 149.41 and 156.45, acting inboard.

c. A 0.2 psid pressure, imposed between Stations 156.45 and 172.45, acting outboard.

5.2.6 BUFFET AND FLUTTER LOADS. No consideration need be given for buffet and flutter loads as the payload adapter and payload are shrouded during the transonic portion of flight.

5.2.7 MISCELLANEOUS LOAD PARAMETERS. No other loads or loading parameters need be considered.

5.3 STERILIZATION BULKHEAD (THERMAL DIAPHRAGM)

5.3.1 CRITICAL CONDITIONS. The sterilization bulkhead is located within the payload adapter and attached to the inside periphery of the adapter at Station 150. Its primary purpose is to provide a thermal barrier between the Centaur vehicle and the payload and is designed by differential pressure requirements. Configuration is shown in Figure 5.3-1. Reference Figure 5.1-2 for bulkhead location.

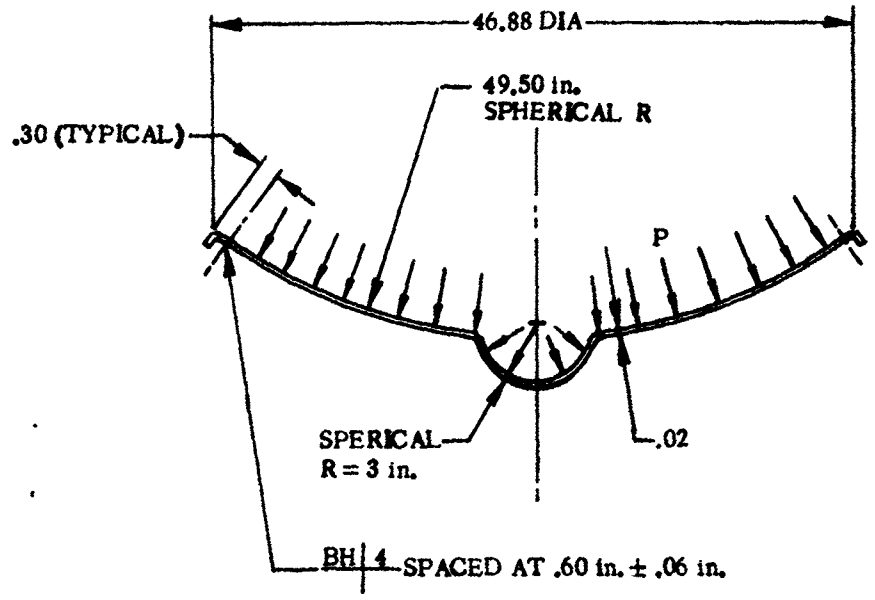

Figure 5.3-1. Sterilization Bulkhead

5.3.2 WEIGHTS AND CENTER OF GRAVITY DATA. Weight and C.G. of this component are of little structural interest due to very small inertia loads resulting.

5.3.3 THERMAL DATA. Thermal data of this component is of minor structural interest except to note that the sterilization bulkhead or inner thermal bulkhead simply serves as a thermal barrier between the spacecraft engine compartment and the LH_2 tank forward bulkhead.

5.3.4 INERTIA LOADS. The sterilization bulkhead does not receive critical loads due to inertia.

5.3.5 STEADY-STATE AIR LOADS. Design differential pressure occurring across the sterilization bulkhead is considered to be 0.4 psid (acting aft) during transonic flight ($0.85 \leq M \leq 1.3$). The pressure differential causes the diaphragm to develop membrane loads which are in turn reacted by hoop compression and bending in the supporting ring and in addition, by the vertical component induced into the payload ring.

5.3.6 BUFFET AND FLUTTER. The sterilization bulkhead does not receive critical loading due to buffet or fluctuating pressures.

5.3.7 MISCELLANEOUS LOAD PARAMETERS. No other loads or loading parameters need be considered.

THIS PAGE INTENTIONALLY LEFT BLANK.

5.4 SEPARATION LATCHES

5.4.1 CRITICAL CONDITIONS. The separation latch system (Figure 5.4-1) is designed for a maximum pretension load of 3000 pounds plus reverse longitudinal loads induced at MECO (reference Table 5.2-1, Condition 11). Refer to applicable section of the final AC-6 stress report (Reference 5-2) for internal loads and detail stress analysis of this component.

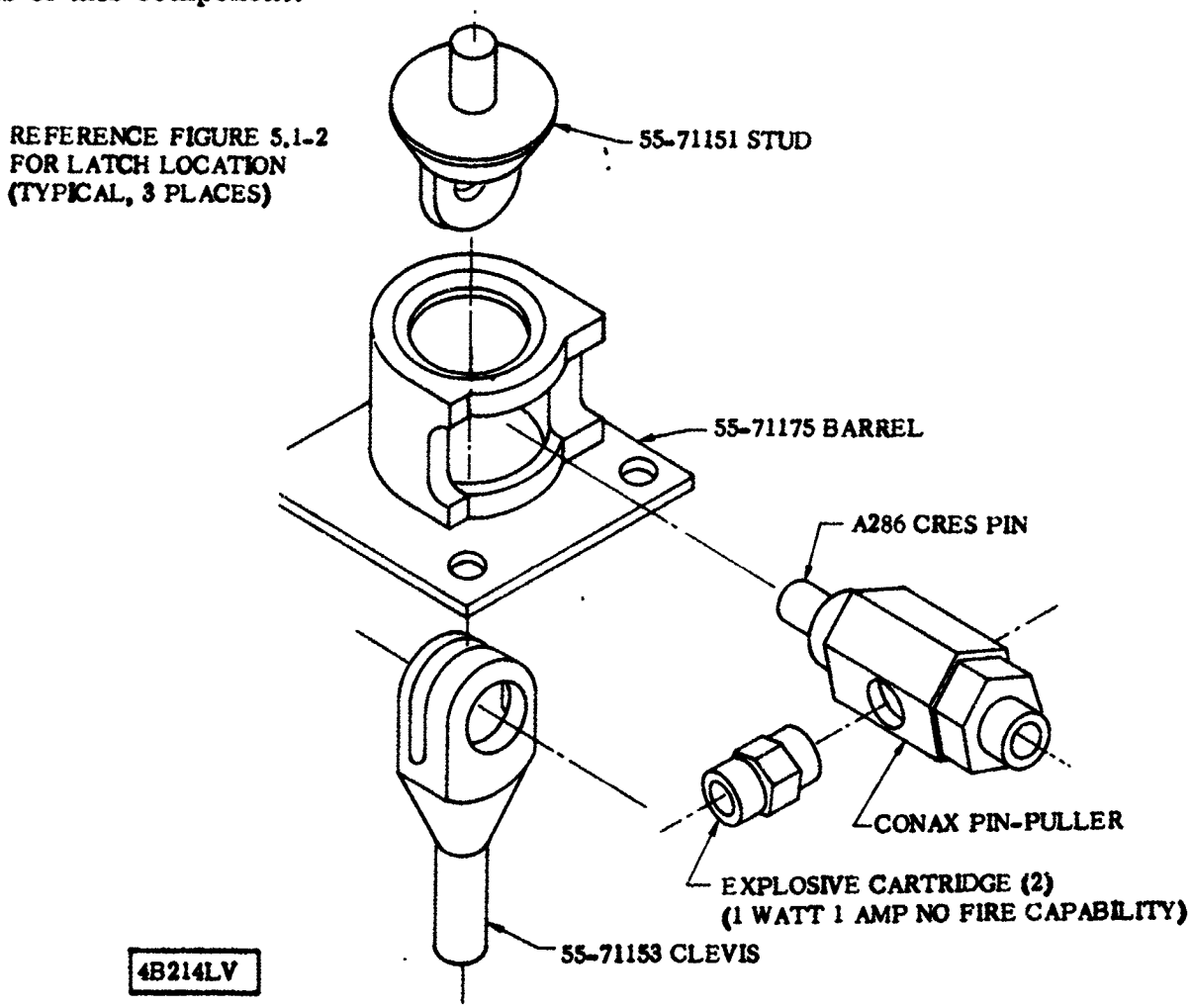

Figure 5.4-1. Payload Separation Latch System

5.4.2 WEIGHTS AND CENTER OF GRAVITY DATA. (Not critical)

5.4.3 THERMAL DATA. (Not critical)

5.4.4 INERTIA LOADS. (Not critical)

5.4.5 STEADY-STATE AIR LOADS. (Not critical)

5.4.6 BUFFET AND FLUTTER LOADS. (Not critical)

5.4.7 MISCELLANEOUS LOAD PARAMETERS. No other loads or loading parameters need be considered.

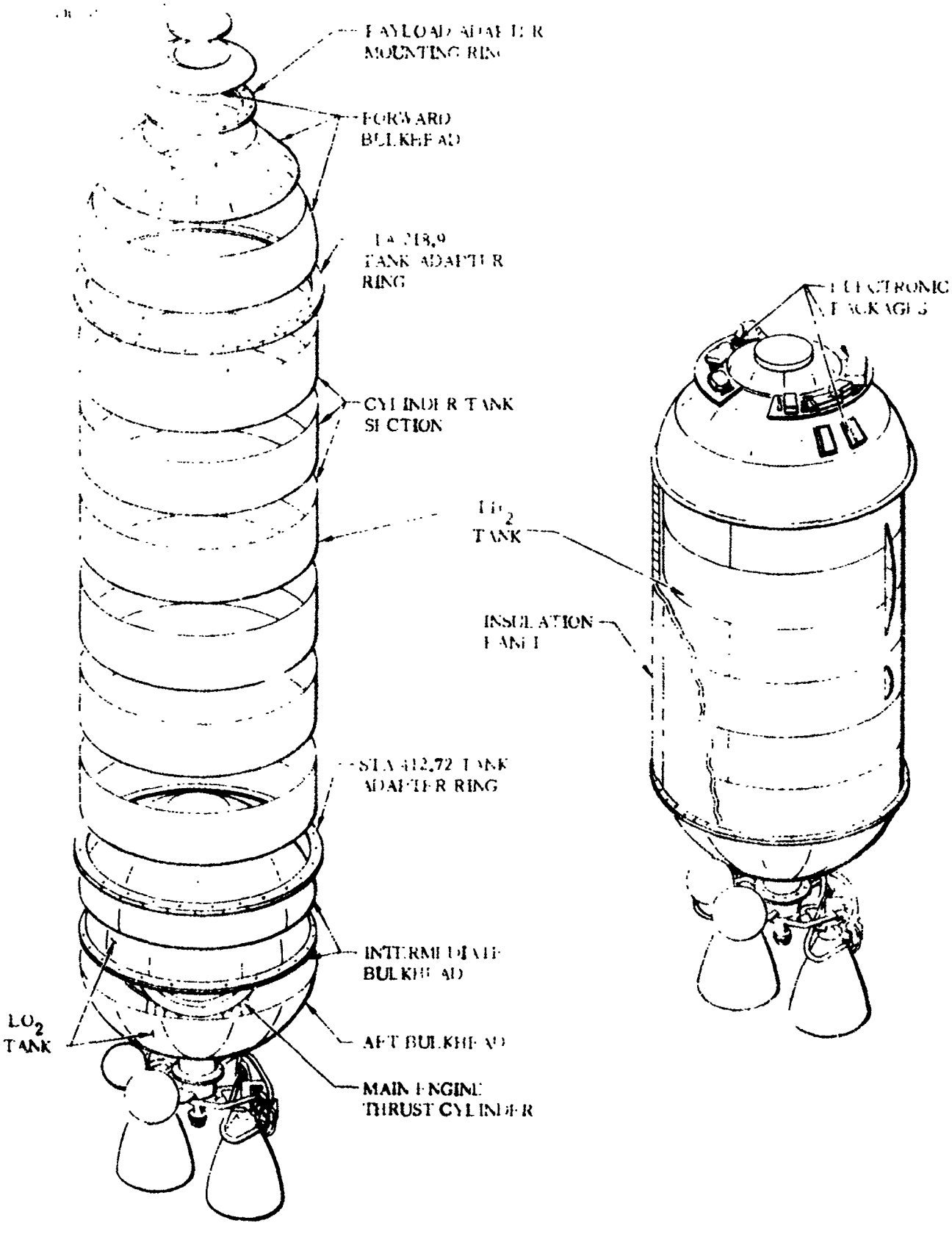
PAYLOAD ADAPTER MOUNTING RING
FORWARD BULKHEAD
STA 218.9 TANK ADAPTER RING
CYLINDER TANK SECTION
LH_2 TANK
INSULATION PANEL
STA 412.72 TANK ADAPTER RING
INTERMEDIATE BULKHEAD
LO_2 TANK
AFT BULKHEAD
MAIN ENGINE THRUST CYLINDER
ELECTRONIC PACKAGES

SECTION VI

PROPELLANT TANKS

6.1 INTRODUCTION

The data presented in this section is only that required to analyze the basic tank structure. All bolt-on's and bracket weldments are covered in Sections VII and VIII.

6.2 BASIC TANK STRUCTURE

The function of the propellant tanks is twofold - to serve as the container for fuel and oxidizer, and to provide the primary vehicle structure. The propellant tanks are of monocoque construction and derive structural stability from internal pressure. The over-all configuration of the propellant tanks is shown in Figure 6.2-1.

6.2.1 CRITICAL CONDITIONS. The propellant tanks are loaded by a combination of the following:

a. Internal pressure (hydrostatic plus ullage pressure).

b. Inertia loads from structural weight times vehicle acceleration.

c. Bending moment due to air loads, C.G. offset, lateral inertia, and propellant sloshing.

d. Aerodynamic drag from nose fairing and insulation panels.

e. Nose fairing and interstage adapter internal pressure.

Only loads data of a general nature which is applicable to several portions of the tank structure is presented in Subsection 6.2. Loads on specific portions of the structure are presented in other sections of this report.

6.2.2 WEIGHTS AND CENTER OF GRAVITY DATA. The upper stage propellant level stations and C.G. locations are presented in Figure 6.2-2. This data represents current nominal values for the AC-6 (operational) vehicle flying the direct ascent Surveyor mission. Any changes to this data for future vehicles are expected to be minimal.

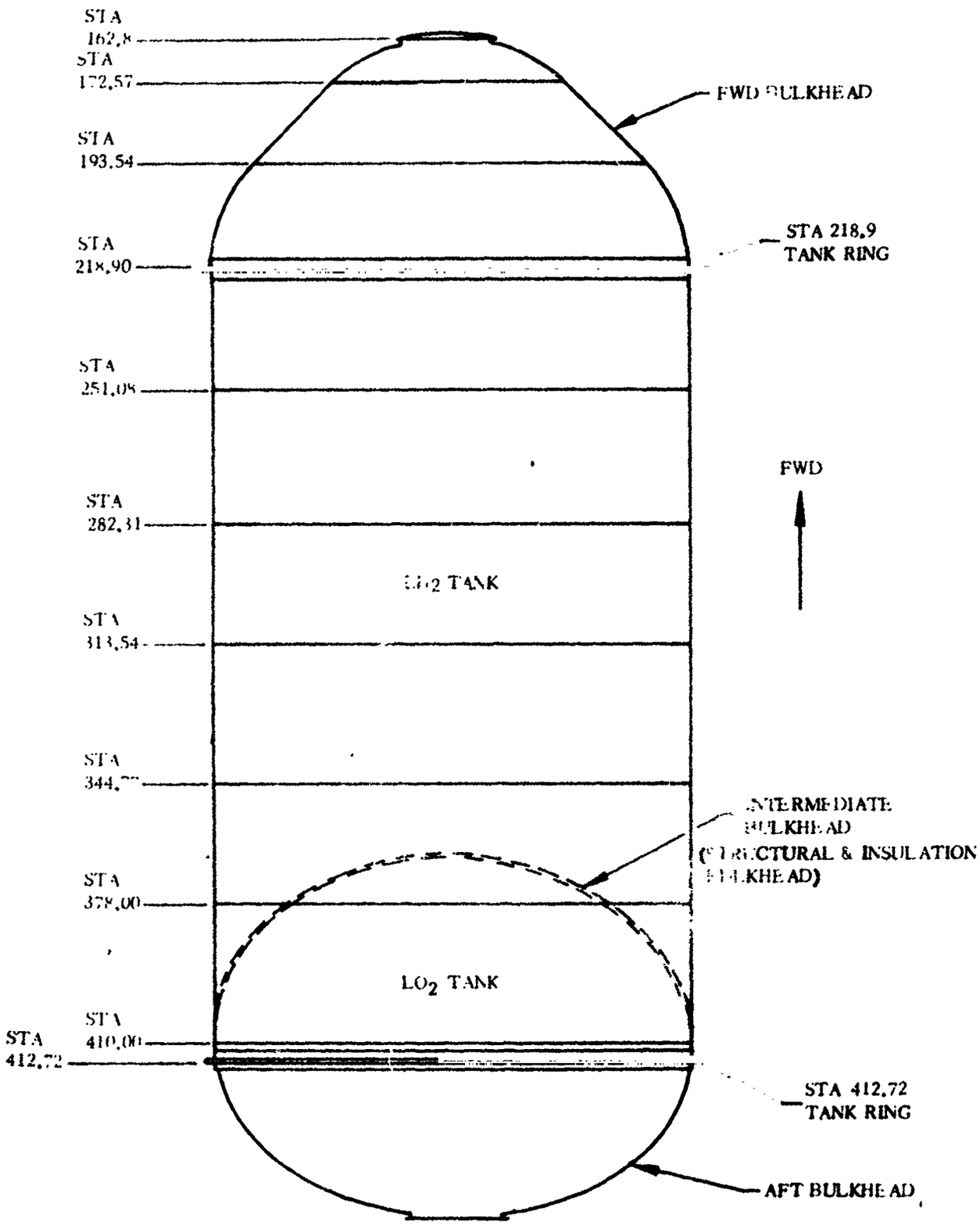

4B1171.V

Figure 6.2-1. Basic Propellant Tank Configuration

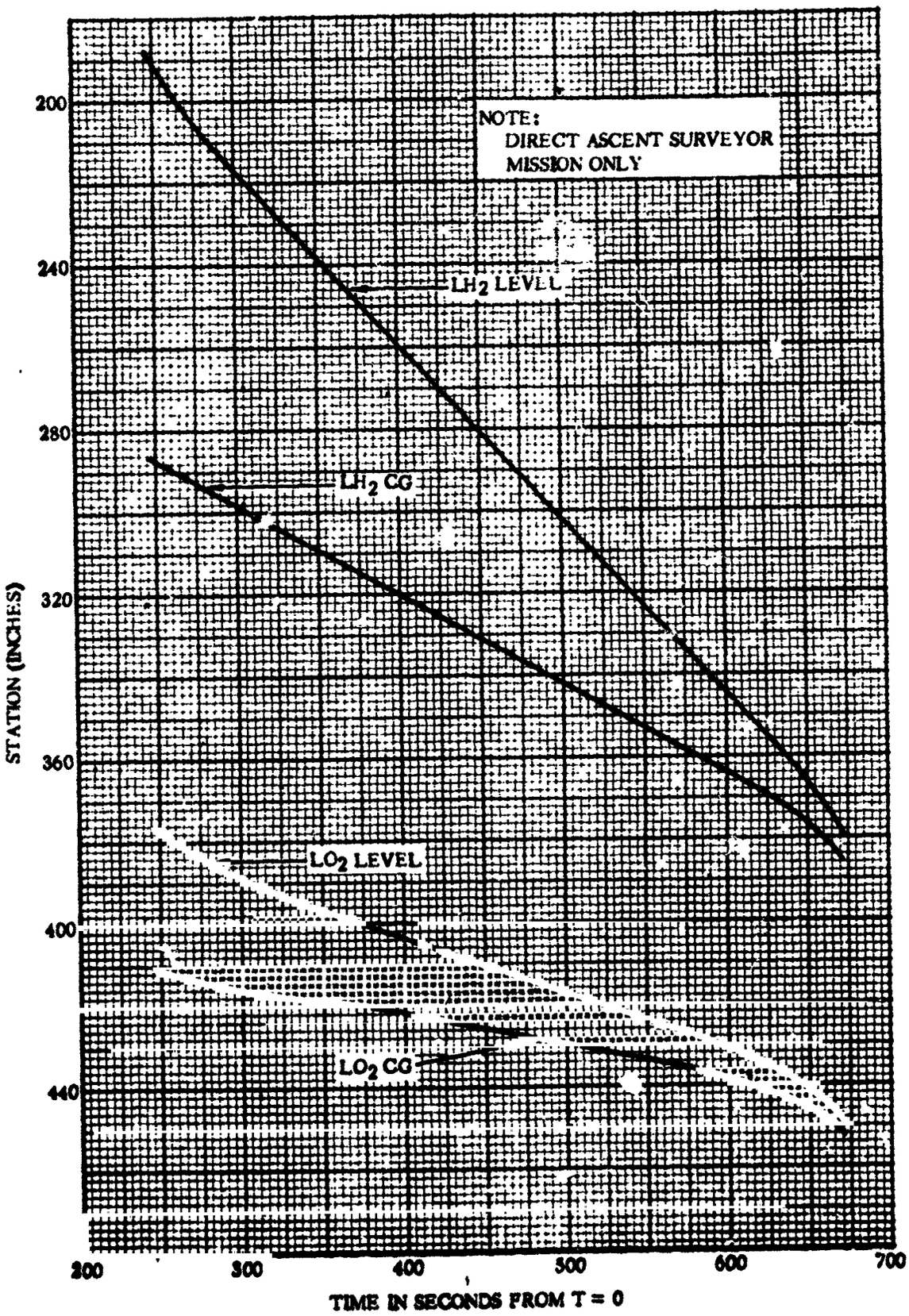

4B118LV

Figure 6.2-2. AC-6 (Operational) Vehicle Propellant Levels and Center of Gravity Locations versus Time

6.2.3 THERMAL DATA All portions of the propellant tanks which are wetted by the contents shall be assumed to be at the following temperatures:

LO_2 Tank	-297° F
LH_2 Tank	-423° F

A specific thermal analysis of each major tank skin discontinuity is presented in the respective report section dealing with the discontinuity joint.

6.2.4 INERTIA LOADS. The steady-state acceleration of the vehicle is presented in Figures 1.3-1, 1.3-2 and 1.3-3. Maximum steady-state acceleration at BECO equals 5.7 ±0.1 g's. Bending moment on the vehicle at BECO, as presented in Figure 6.2-3, acts simultaneously with maximum vehicle acceleration.

6.2.5 STEADY-STATE AIR LOADS. The propellant tanks are not subjected to direct aerodynamic impingement. The steady-state differential pressure across the tank wall is the difference between absolute internal pressure and absolute external pressure. The internal tank pressure is presented in Paragraph 6.2.7. The nose fairing internal pressure (the external pressure on the forward bulkhead) is presented in Table 6.2-1. The interstage adapter internal pressure (the external pressure on the aft bulkhead) is presented in Table 6.2-2. Local ambient pressure is presented in Table 6.2-3.

The data in Table 6.2-1 is currently valid only for the AC-6 vehicle. Revisions to this data will be published upon finalization of AC-7 and On pitch programs.

TABLE 6.2-1. AC-6 NOSE FAIRING INTERNAL PRESSURE

Time*	Pressure Limits**	Time*	Pressure Limits**
30	12.51 to 11.15	68	4.03 to 2.21
40	10.64 to 8.71	70	3.84 to 2.03
42	10.21 to 8.15	72	3.64 to 1.83
44	9.76 to 7.51	74	3.43 to 1.62
46	9.31 to 6.62	76	3.21 to 1.44
48	8.84 to 3.85	78	2.99 to 1.24
50	8.32 to 2.80	80	2.77 to 1.07
52	7.13 to 2.92	82	2.55 to 0.92
54	5.20 to 2.90	84	2.31 to 0.78
56	4.58 to 2.89	86	2.08 to 0.67
58	4.37 to 2.89	88	1.86 to 0.57
60	4.34 to 2.85	90	1.65 to 0.49
62	4.28 to 2.74	100	0.90 to 0.22
64	4.25 to 2.57	110	0.48 to 0.09
66	4.17 to 2.39	120	0.24 to 0.04

*Times are in seconds from 2-inch motion.
**Pressures are in psia.

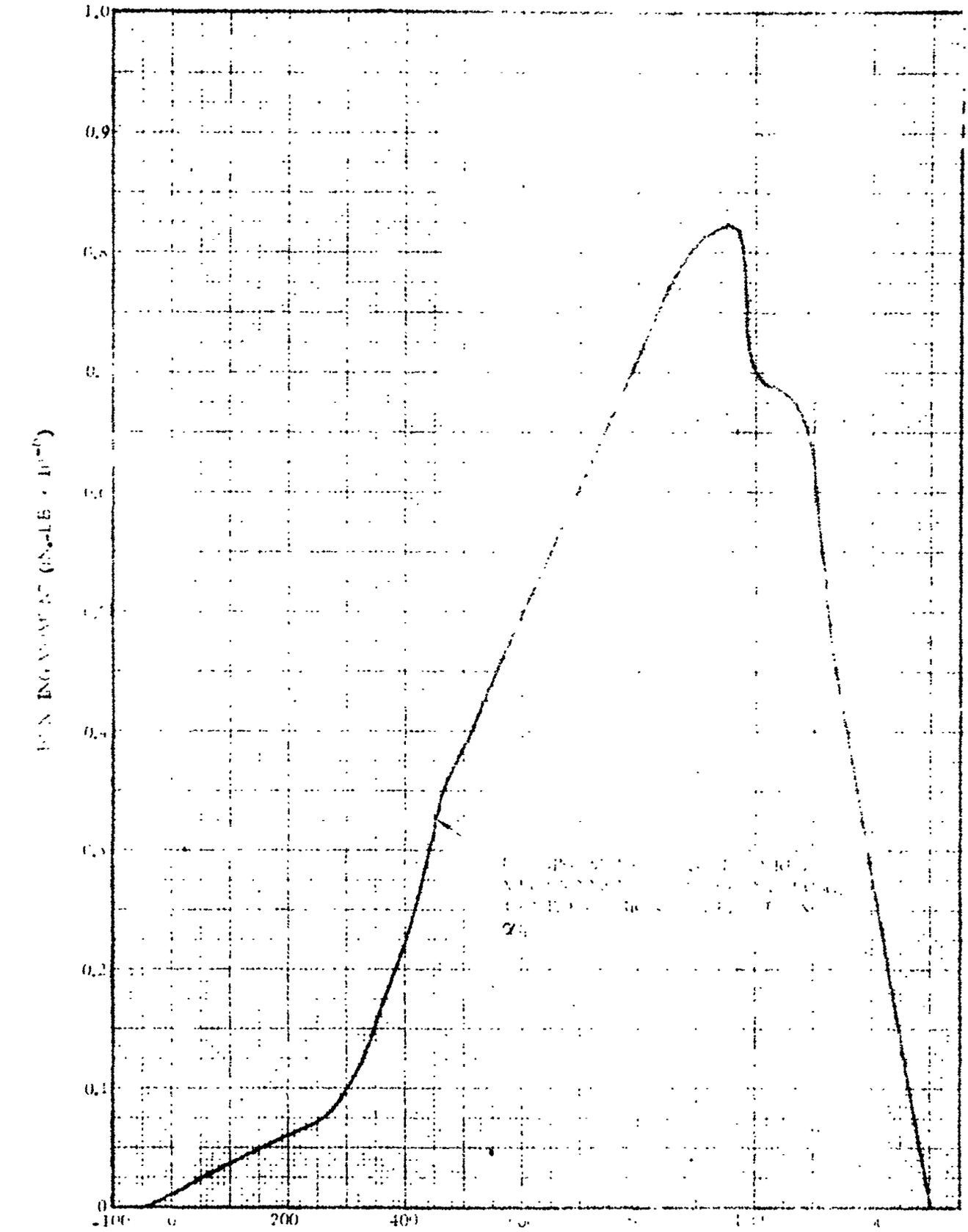

Figure 6.2-3. Bending Moment Versus Station for Engine Out

TABLE 6.2-2. INTERSTAGE ADAPTER INTERNAL PRESSURE

Time*	Pressure Limits**	Time*	Pressure Limits**
40	10.74 to 8.98	72	3.04 to 0.67
44	9.73 to 7.91	76	2.54 to 0.29
48	8.74 to 6.71	80	2.03 to 0.02
52	7.59 to 5.42	84	1.57 to 0.0
56	6.47 to 3.82	88	1.24 to 0.0
60	5.26 to 2.83	92	0.94 to 0.0
64	4.16 to 1.93	96	0.70 to 0.0
68	3.67 to 1.26	100	0.53 to 0.0

*Times are in seconds from 2-inch motion
**Pressures are in psia

TABLE 6.2-3. AMBIENT PRESSURE LIMITS

Time*	Pressure Limits**	Time*	Pressure Limits**
40	10.83 to 9.69	72	3.63 to 2.63
44	9.87 to 8.81	76	2.95 to 2.02
48	8.99 to 7.88	80	2.20 to 1.49
52	7.97 to 6.93	84	1.70 to 1.05
56	7.04 to 5.98	88	1.30 to 0.75
60	6.16 to 5.05	92	0.96 to 0.52
64	5.17 to 4.19	96	0.71 to 0.34
68	4.44 to 3.38	100	0.53 to 0.23

*Times are in seconds from 2-inch motion
**Pressures are in psia

6.2.6 BUFFET AND FLUTTER LOADS. The basic tank structure is not directly subjected to buffet or flutter loads except at local attach points with external structure. The reactions on each tank attach point may be computed from the buffet or flutter loads presented for the respective attached component.

6.2.7 MISCELLANEOUS LOAD PARAMETERS. Figures 6.2-4 through 6.2-8 present the propellant tank pressure profiles. The data presented in these figures are applicable only to AC-6 and AC-7 vehicles. Revisions to this data will be published later providing applicable data for AC-8 through AC-15 vehicles.

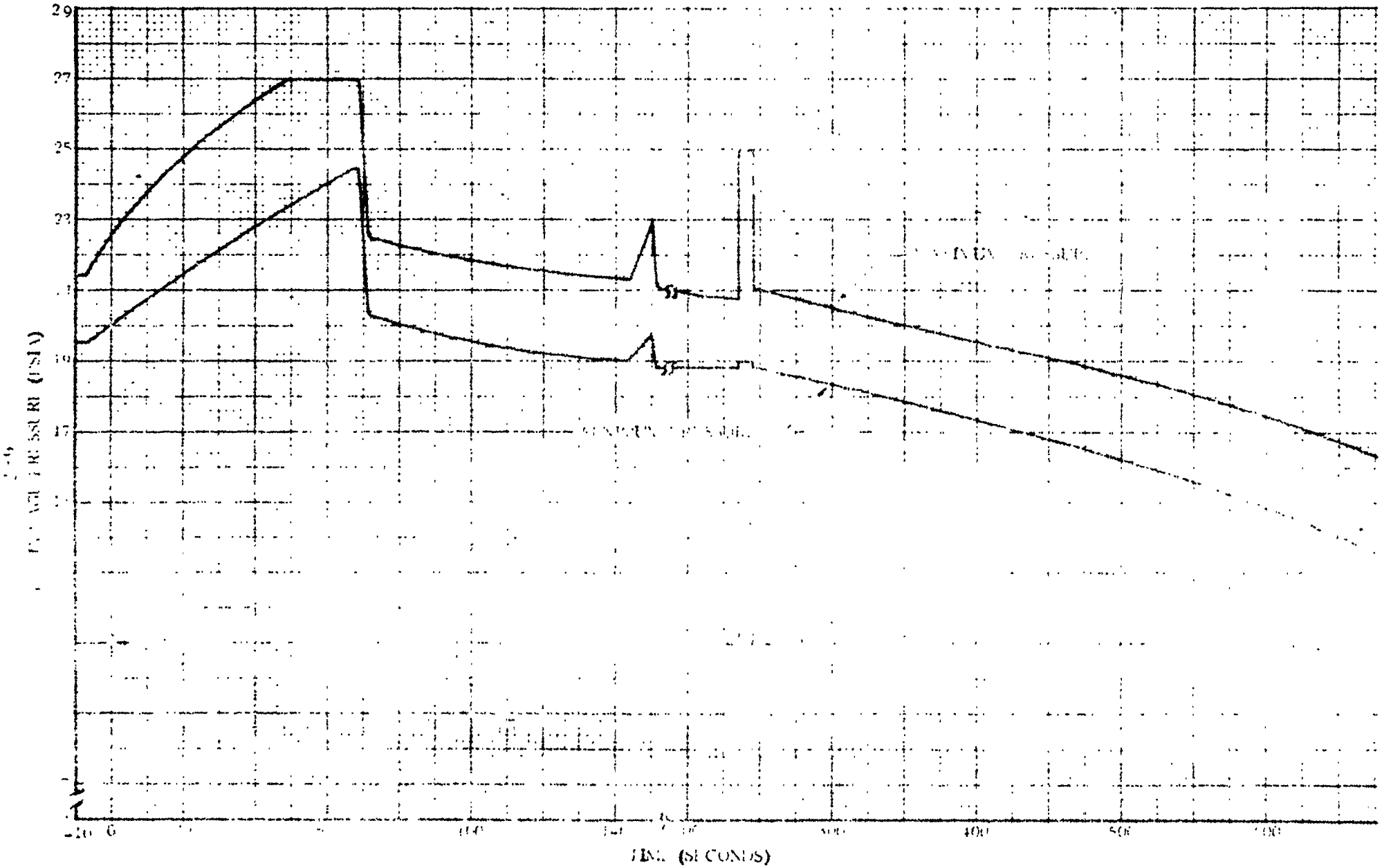

4B120LT

Figure 6.2-4. Liquid Hydrogen Tank Ullage Pressure - AC-6 and AC-7

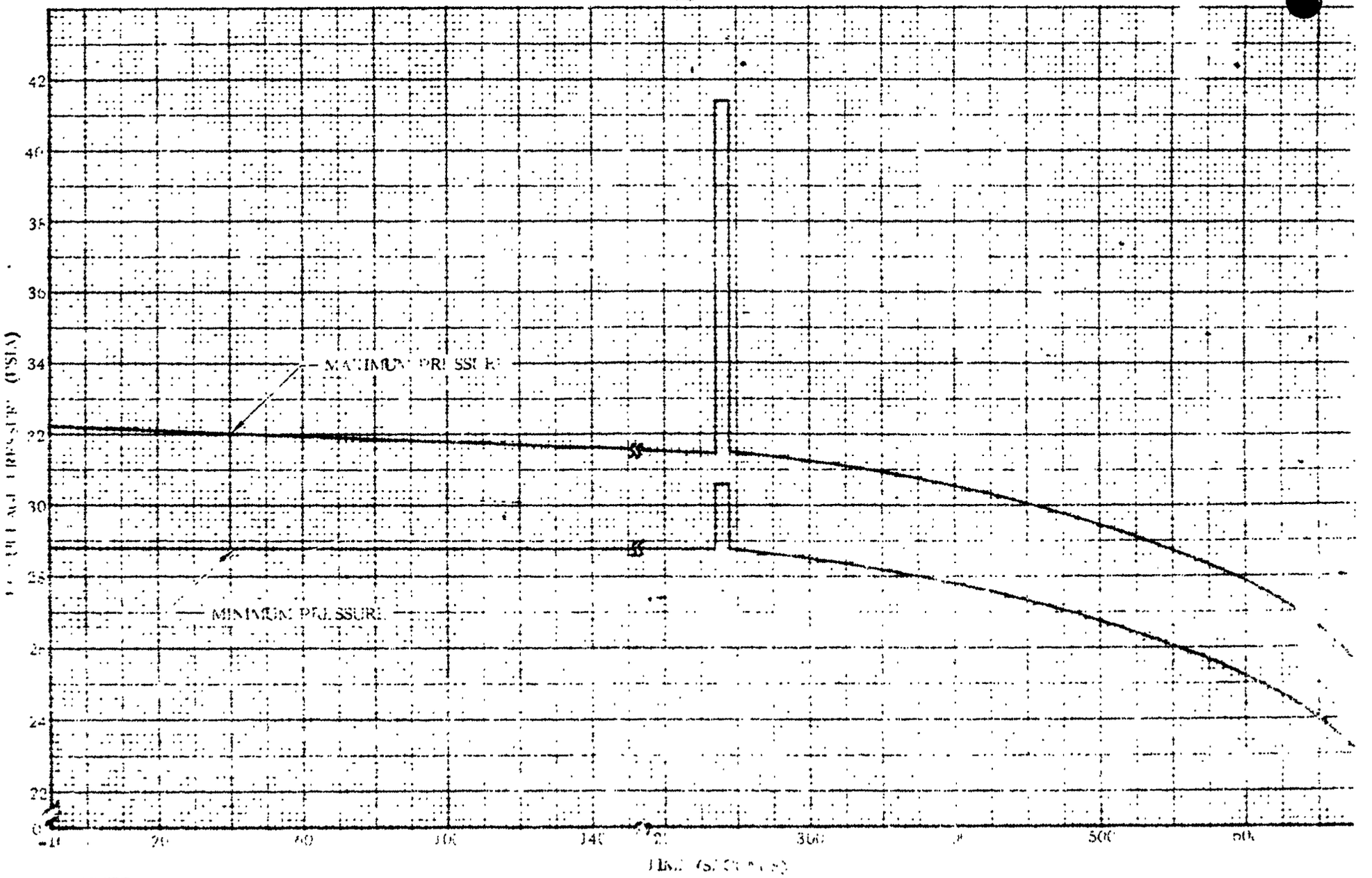

45150.7

Figure 6.2-3 Liquid Oxygen Tank Ullage Pressure - AC-6 and AC-7

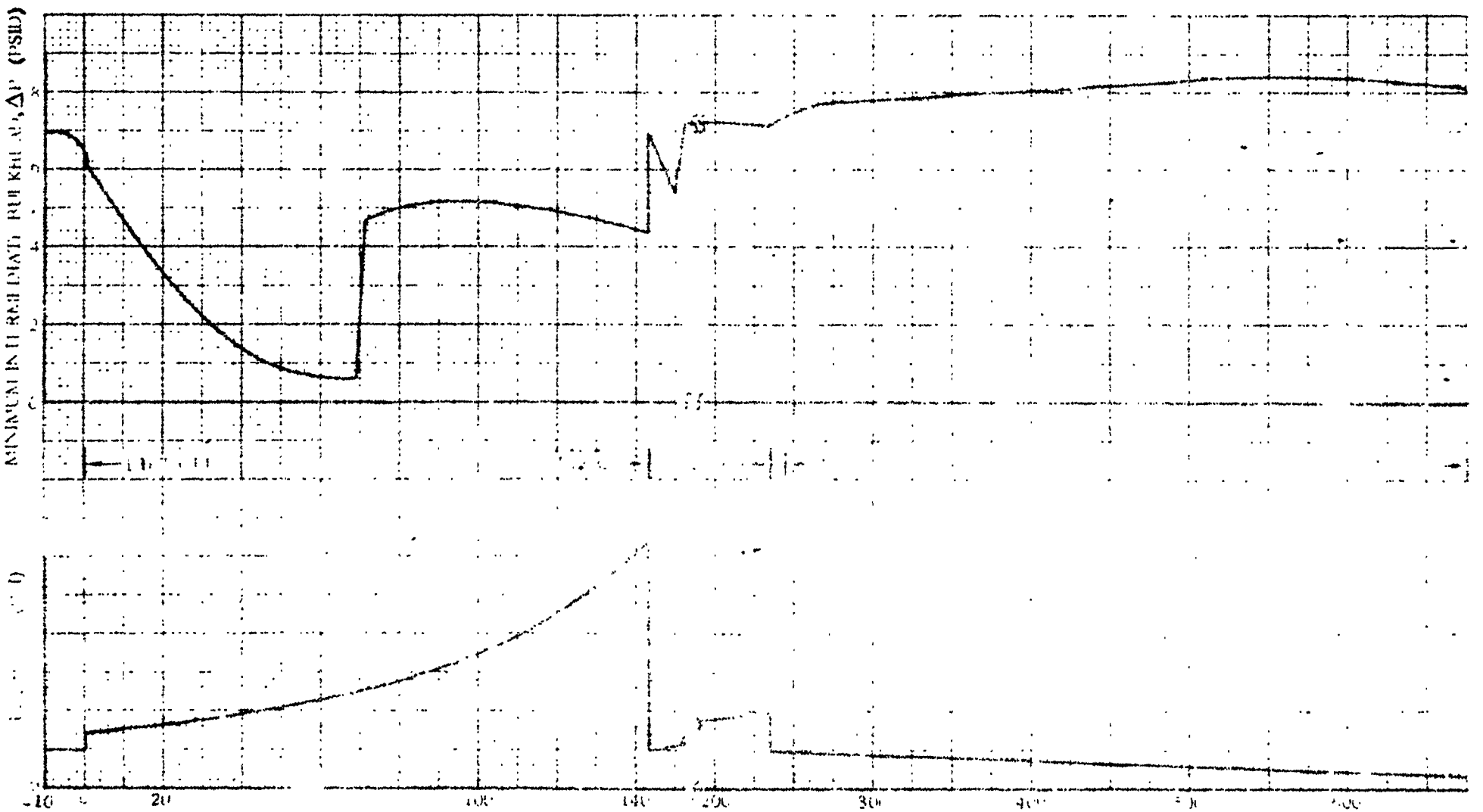

4F122LT

Figure 6.2-6. Intermediate Bulkhead Minimum Differential Pressure - AC-6 and AC-7

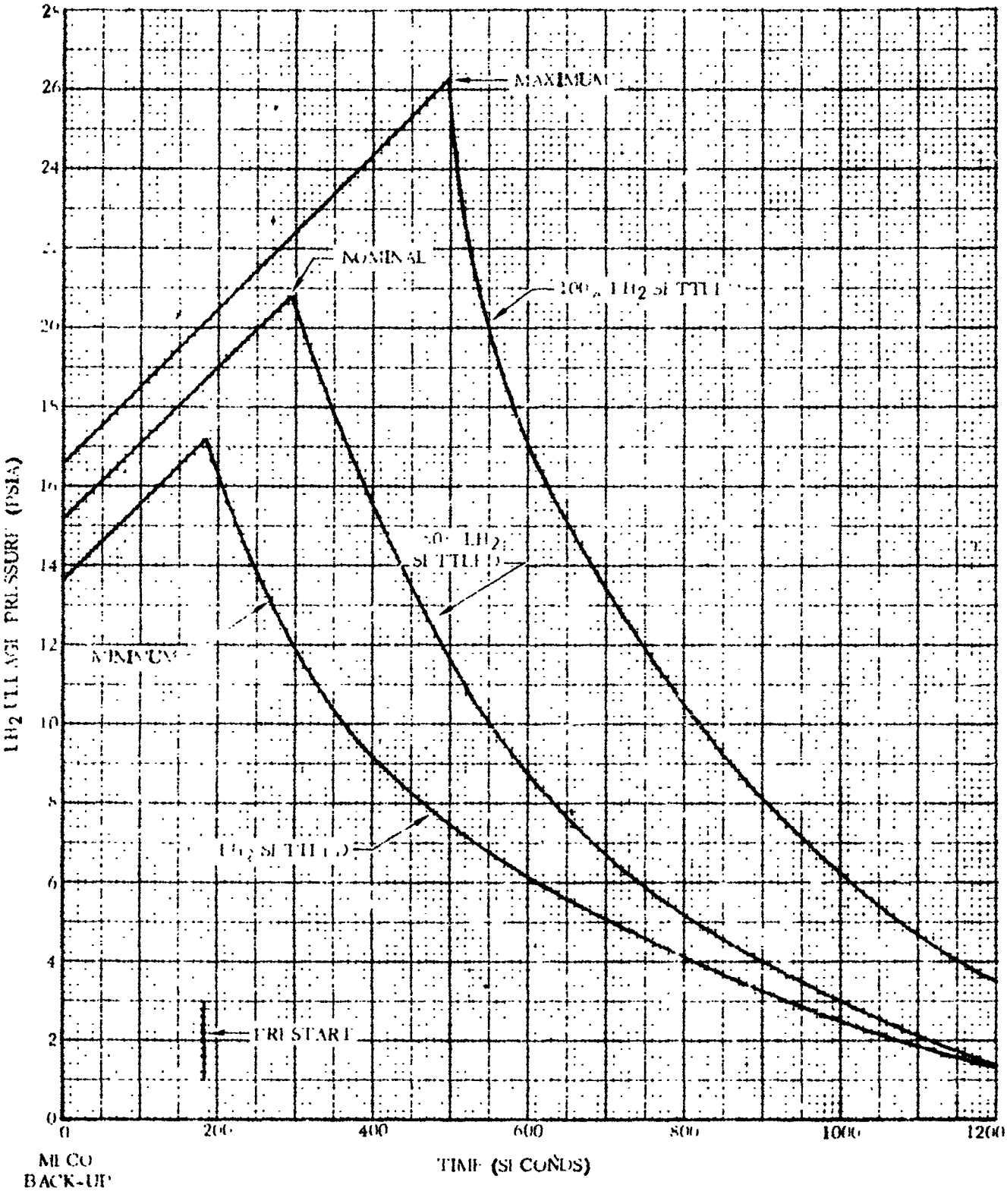

4B1231V

Figure 6.2-7. Liquid Hydrogen Tank Ullage Pressure Post MECO Coast - AC-6 and AC-7

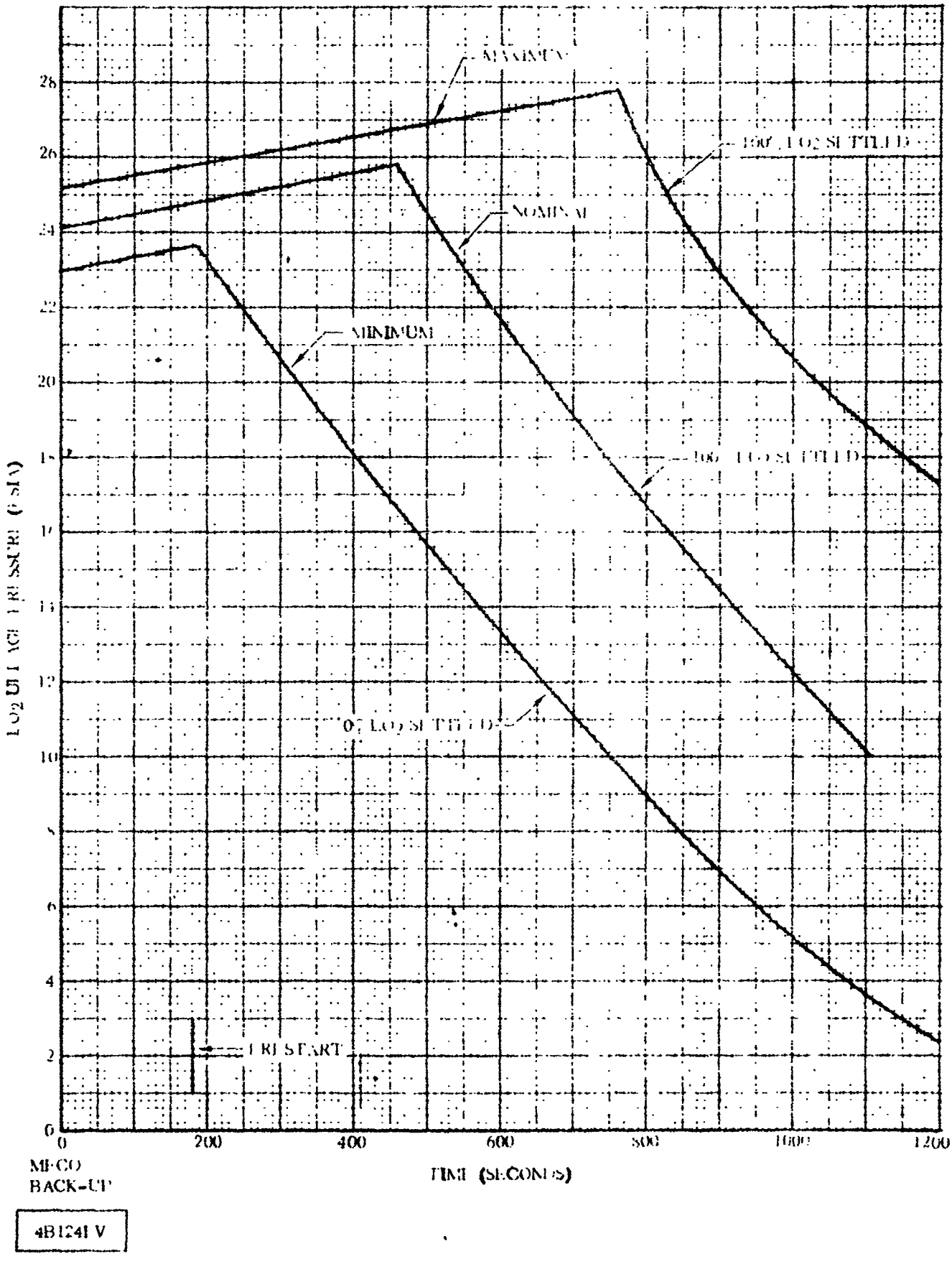

Figure 6.2-8. Liquid Oxygen Tank Ullage Pressure Post MECO Coast - AC-6 and AC-7

THIS PAGE INTENTIONALLY LEFT BLANK.

6.3 STATION 218.9 JOINT

The Station 218.9 joint reacts all aerodynamic and inertia loads on the nose fairing. The configuration of the joint is presented in Figure 6.3-1.

6.3.1 CRITICAL CONDITIONS. The critical loads on the Station 218.9 joint occur during the first 100 seconds of flight when air loads are high, and at BECO (maximum vehicle acceleration).

6.3.2 WEIGHTS AND CENTER OF GRAVITY DATA. Nose fairing weights and C.G.'s are presented in Paragraph 2.2.2.

6.3.3 THERMAL DATA. The data presented herein reflects the most severe thermal environment for any of the operational vehicles. Maximum temperatures for various times during flight are given in Table 6.3-1 which are associated with the points described in Figure 6.3-2. Points (32), (33) and (34) may be construed as the typical temperature gradient through the outer surface of the skirt which exists along its entire length.

The temperatures in Table 6.3-1 are based on the use of a 0.03 inch layer of Thermolag T-230 and correspond to the maximum heating trajectory for a parking orbit (DP35).

(Additional analysis was performed which considered a direct ascent trajectory SD35A based on the use of an 0.018-inch layer of Thermolag T-230. For this application, Table 6.3-1 remains unchanged with the exception of Points (30) and (31). The maximum temperatures at these points decrease 27° and 11° respectively.)

6.3.4 INERTIA LOADS. The inertia contribution to Station 218.9 joint loads during the first 100 seconds of flight is included in the data presented in Table 6.3-2.

At BECO, the longitudinal inertia load = +5.7 ± 0.1 g's. This acts simultaneously with the bending moment at Station 218.9 presented in Figure 6.3-3.

6.3.5 STEADY-STATE AIR LOADS. Drag and nose fairing internal pressure contributions are included in the axial loads data presented in Table 6.3-2. The bending moment due to angle of attack is included in the plot shown in Figure 6.3-3. Since the time of maximum bending moment is not well defined, it shall be assumed to occur between 56 and 76 seconds.

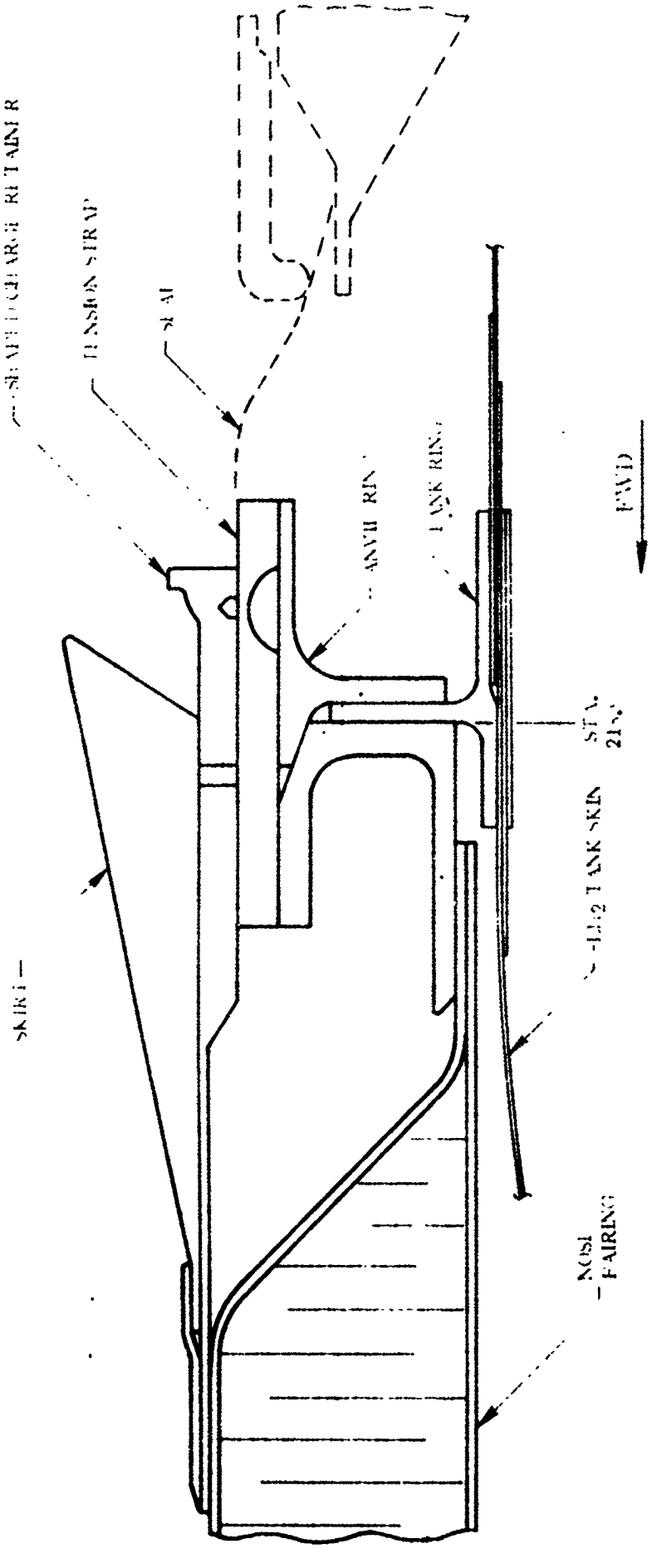

Figure 6.3-1. Station 218.9 Joint Configuration

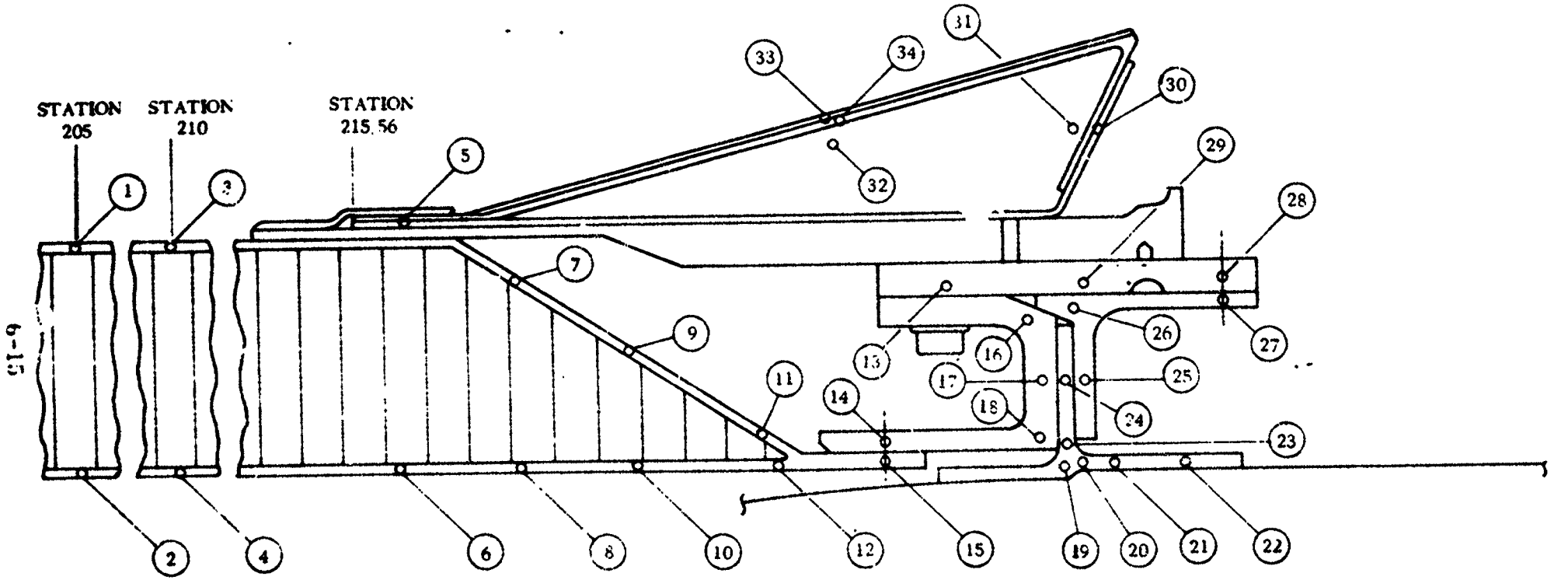

NOTE: SEE TABLE 6.3-1 FOR TEMPERATURES AT VARIOUS FLIGHT TIMES.

4B126L.T

Figure 6.3-2. Station 218.9 Joint Temperature Profile

TABLE 6.3-1, NOSE FAIRING STATION 265 TO STATION 220.5 - TEMPERATURE PROFILES

Zone (Ref. Figure 6.3-2)	Condition			
	Prelaunch (T + 0 sec)	Transonic (T + 60 sec)	Maximum g (T + 150 sec)	(T + 210 sec)
1	57	76	390	340
2	20	20	19	24
3	19	75	390	340
4	20	20	19	24
5	31	68	357	301
6	-226	-225	-221	-220
7	-262	262	-251	-242
8	-317	-317	-317	-315
9	-293	-293	-293	-292
10	-387	-387	-388	-388
11	-334	-335	-347	-355
12	-394	-395	-396	-397
13	-368	-368	-363	-361
14	-372	-373	-371	-369
15	-383	-384	-385	-381
16	-370	-370	-366	-364
17	-371	-371	-367	-365
18	-373	-373	-370	-368
19	-394	-395	-393	-392
20	-417	-411	-411	-411
21	-416	-417	-415	-419
22	-414	-415	-420	-420
23	-375	-375	-372	-370
24	-370	-370	-366	-364
25	-370	-369	-364	-363
26	-369	-368	-362	-361
27	-368	-364	-351	-356
28	-350	-350	-350	-350
29	-368	-368	-362	-361
30	50	58	175	170
31	42	50	129	142
32	42	52	155	180
33	50	60	230	230
34	50	57	227	227

Note:
All temperatures are in ° F

TABLE 6.3-2. STATION 218.9 JOINT - AXIAL LOADS (AXIAL COMPRESSION)

Time (sec)	Maximum Load (lb)	Minimum Load (lb)
10	15,800	6,000
44	20,500	7,200
48	54,100	9,900
52	59,200	27,000
56	59,400	35,600
60	58,400	34,600
64	56,400	26,900
68	49,000	21,900
72	42,100	18,600
76	36,100	15,500
80	32,100	13,200
84	29,200	11,100
88	26,500	9,500
92	23,800	8,400
96	21,200	7,600
100	18,900	7,000

NOTE:
The loads presented above include the effects of inertia, drag, and differential pressure across the nose fairing. Bending moment on the Station 218.9 joint is presented in Figure 6.3-3.

6.3.6 BUFFET AND FLUTTER LOADS. The Station 218.9 joint is subjected to a reaction from buffet loads acting on the nose fairing. A discussion of buffet loads on the nose fairing is found in Paragraph 2.2.6.

6.3.7 MISCELLANEOUS LOAD PARAMETERS. During nose fairing jettison, the Station 218.9 tank ring is subjected to dynamic loads. These loads are discussed in Paragraph 2.9.7. No other loads are considered critical.

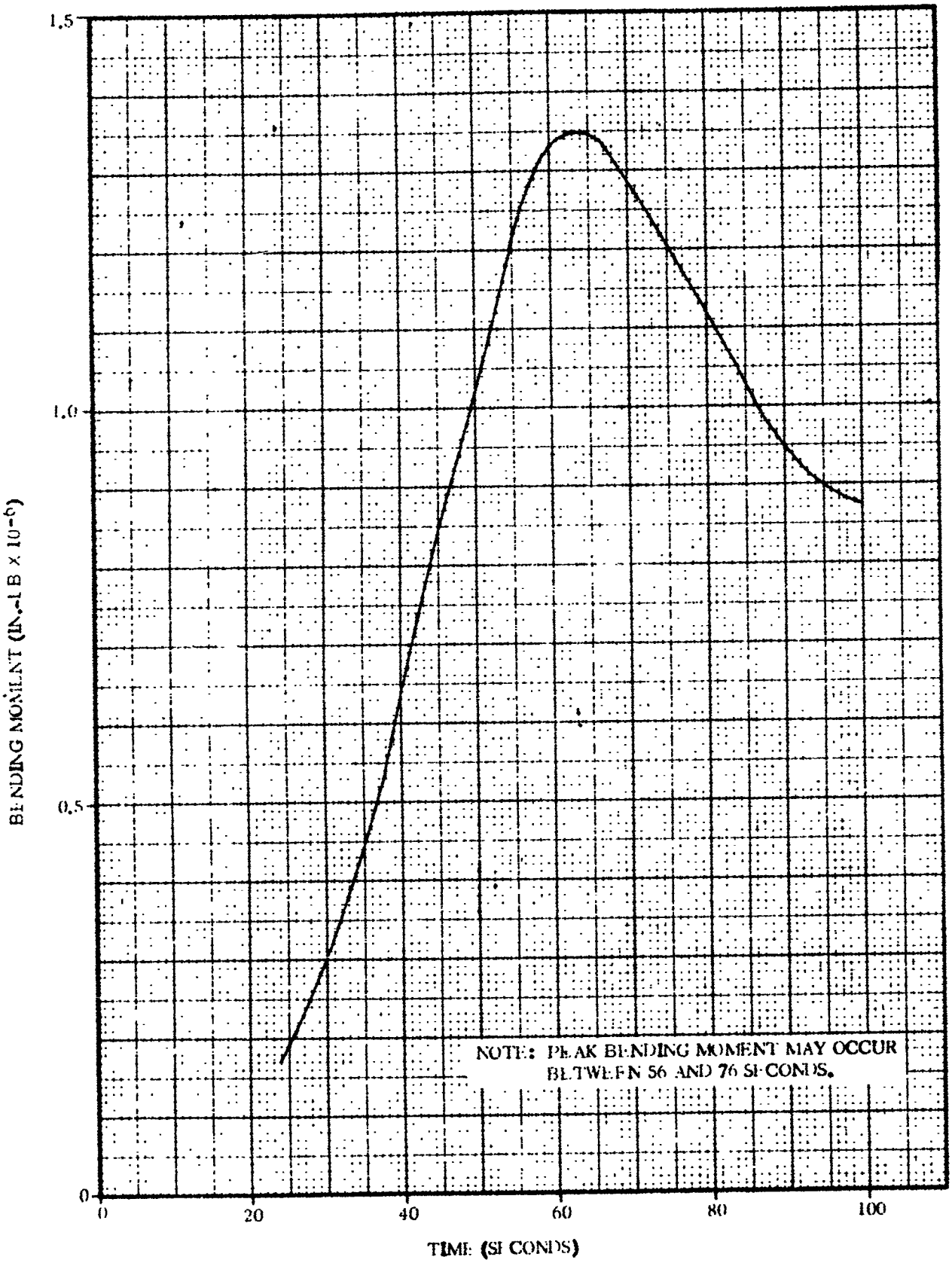

4B127LV

Figure 6.3-3. Station 218.9 Joint and Cylindrical Tank Skin aft of Station 218.9 - Bending Moment versus Time

6.4 FORWARD BULKHEAD - FORWARD OF STATION 218.9.

The forward bulkhead (Figure 6.4-1) reacts inertia loads from the payload and electronic equipment mounted to the equipment shelves. The section of the forward bulkhead under consideration is that immediately forward of the Station 218.9 tank ring. See Figure 6.3-1 for Station 218.9 joint configuration.

6.4.1 CRITICAL CONDITIONS. The forward bulkhead is subjected to a combination of inertia loads and ΔP across the tank skin. The most critical loads occur during the first 100 seconds of flight.

6.4.2 WEIGHTS AND CENTER OF GRAVITY DATA. The following weights and C.G. locations shall be used for structural design and analysis.

a. Weight of all structure forward of Station 218.9 (including payload) which imposes inertia loads on the forward bulkhead:

Maximum Weight	3990 lb
Minimum Weight	2890 lb

b. C.G. location of the above assumed lumped mass (except the payload) shall be taken at Station 175 ± 2 in.

The weight and C.G. location of the payload and payload adapter are presented in Paragraph 5.1.2.

6.4.3 THERMAL DATA. The portion of the tank skin wetted by the liquid hydrogen is at a temperature of -423° F.

6.4.4 INERTIA LOADS. Bending moment in the forward bulkhead immediately forward of Station 218.9 is presented in Figure 6.4-2. This is entirely due to inertia, and does not add to the bending moment at the Station 218.9 joint.

The axial load in the forward bulkhead due to inertia is presented in Table 6.4-1. The effect of ΔP across the forward bulkhead must be included in the analysis of the tank structure. See Paragraph 6.4.5 for a discussion of ΔP across the forward bulkhead.

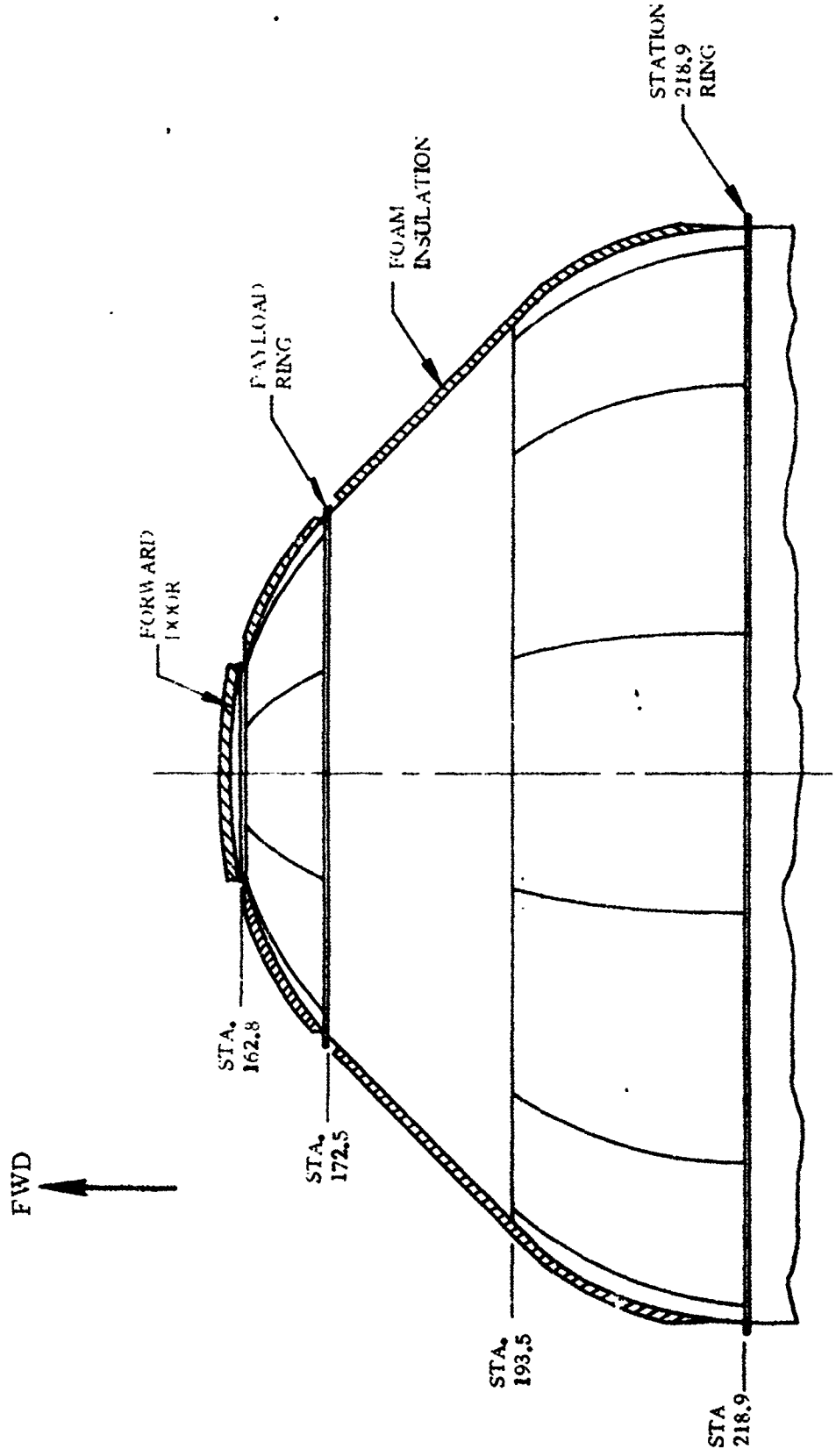

Figure 6.4-1. Forward Bulkhead Configuration

4B128LT

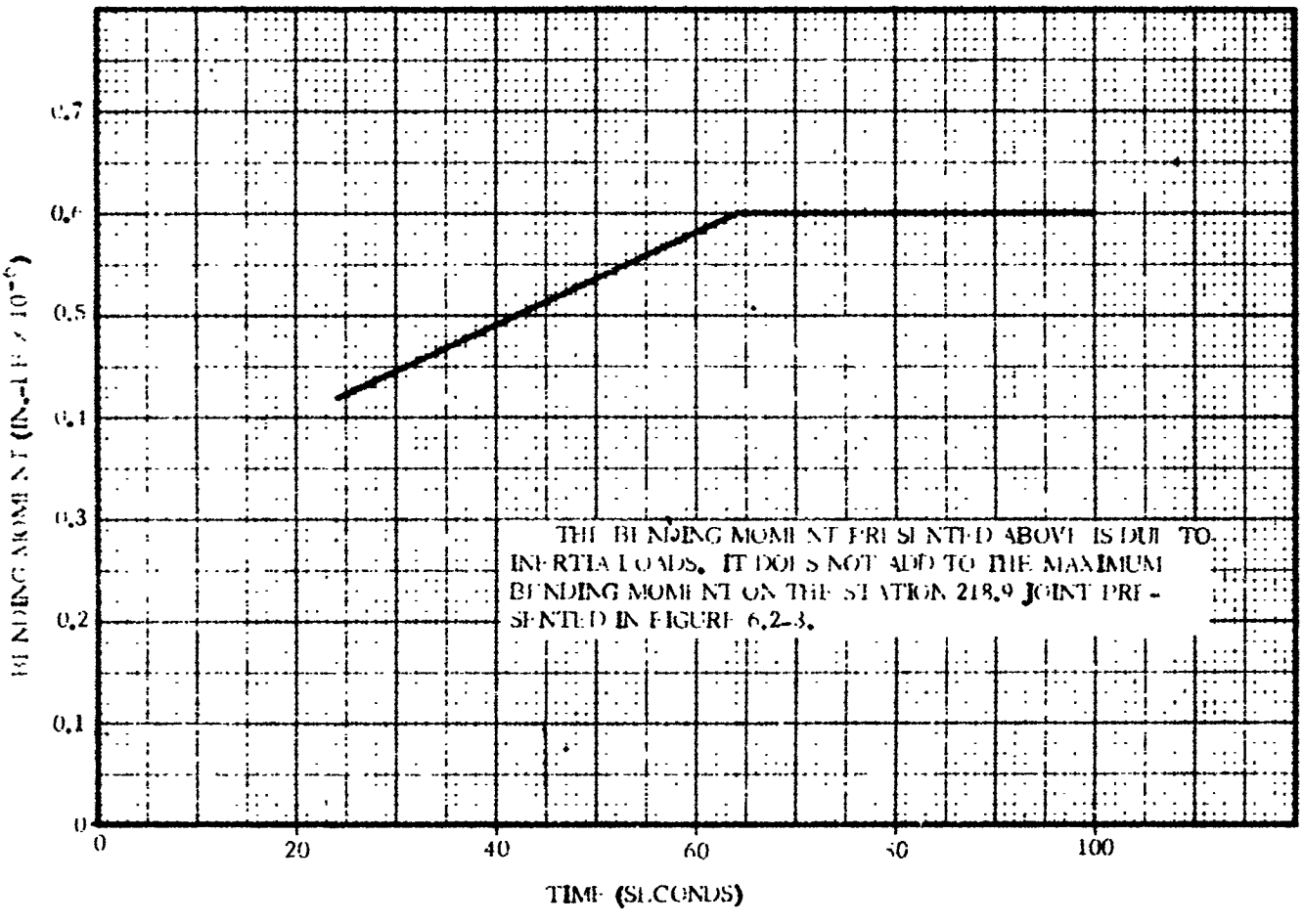

4B129LV

Figure 6.4-2. Forward Bulkhead, Forward of Station 218.9 - Bending Moment versus Time

TABLE 6.4-1. FORWARD BULKHEAD MAXIMUM AXIAL INERTIA LOADS - FORWARD OF STATION 218.9

Time (sec)	Maximum Axial Compression (lb)
40	6,800
44	7,000
48	7,300
52	7,400
56	7,500
60	7,700
64	8,000
68	8,300
72	8,700
76	9,200
80	9,700
84	10,400
88	11,000
92	11,600
96	12,200
100	12,800

Note:
For a discussion of loads due to differential pressure across the forward bulkhead, see Paragraph 6.4.5.

6.4.5 STEADY-STATE AIR LOADS. The forward bulkhead is subjected to a burst pressure due to the difference between LH_2 tank ullage pressure and nose fairing internal pressure. The LH_2 tank ullage pressure is presented in Figure 6.2-4, and the nose fairing internal pressure is presented in Table 6.2-1. The loads due to differential pressure are applied simultaneously with the inertia loads presented in Paragraph 6.4.4.

6.4.6 BUFFET AND FLUTTER LOADS. The forward bulkhead does not receive critical loading due to buffet or fluctuating pressures.

6.4.7 MISCELLANEOUS LOAD PARAMETERS. No other loads on the forward bulkhead are critical.

6.5 CYLINDRICAL TANK - AFT OF STATION 218.9

The loads presented in this subsection are for the cylindrical tank skin immediately aft of the Station 218.9 tank ring. The general configuration of the Station 218.9 joint and tank skin buildup is shown in Figure 6.3-1.

6.5.1 CRITICAL CONDITIONS. The forward portion of the cylindrical tank reacts a combination of aerodynamic and inertia loads from both the nose fairing and inertia loads from the forward bulkhead. Critical times during flight are the first 100 seconds of flight, and BECO.

6.5.2 WEIGHTS AND CENTER OF GRAVITY DATA. The following weights and C.G. locations shall be used for structural design and analysis.

a. Maximum weight forward of Station 218.9 = 5570 lb

b. Minimum weight forward of Station 218.9 = 4430 lb

See Paragraph 2.2.2 for nose fairing C.G. and Paragraph 6.4.2 for forward bulkhead C G.

6.5.3 THERMAL DATA. The portion of the tank skin wetted by the liquid hydrogen is at a temperature of -423° F.

6.5.4 INERTIA LOADS. The inertia contribution to axial loads is included in the data presented in Table 6.5-1. The inertia contribution to bending moment is included in the data presented in Figure 6.3-3. It should be noted that the maximum bending moment on the cylindrical tank aft of Station 218.9 is the same as that for the Station 218.9 joint. The bending moment due to inertia loads on the payload and forward bulkhead does not add to bending moment from the nose fairing.

6.5.5 STEADY-STATE AIR LOADS. The axial loads due to aerodynamic drag are included in the data presented in Table 6.5-1. Fuel tank ullage pressure must be included in the axial loads analysis (see Figure 6.2-4).

The bending moment due to angle of attack is included in the data shown in Figure 6.3-3.

6.5.6 BUFFET AND FLUTTER. The forward portion of the cylindrical tank does not receive critical loads due to buffet or fluctuating pressures

6.5.7 MISCELLANEOUS LOAD PARAMETERS. No other loads on the forward portion of the cylindrical tank are critical.

TABLE 6.5-1. STATION 218.9 CYLINDRICAL TANK - MAXIMUM AXIAL LOADS

Time (sec)	Maximum Axial Compression (lb)
40	11,500
44	13,000
48	15,500
52	20,900
56	31,000
60	36,900
64	36,800
68	36,600
72	35,500
76	34,700
80	34,200
84	33,500
88	32,700
92	31,700
96	30,700
100	29,700

NOTE:
The loads presented above include only the effects of inertia and drag. LH_2 ullage pressure and bending moment must be included in the stress analysis of the joint and tank skin.

6.6 STATION 412.72 JOINT

The Station 412.72 joint is the interface between the Centaur upper stage aft tank ring and the forward mating ring of the interstage adapter. However, a circumferential linear shaped charge at Station 413.38 provides a separation plane between the Atlas and Centaur in flight. The configuration of the Station 412.72 joint is shown in Figure 6.6-1.

6.6.1 CRITICAL CONDITIONS. The Station 412.72 joint receives critical loads during the first 100 seconds of flight when air loads are maximum, and at BECO (maximum vehicle acceleration) when axial inertia loads are maximum. The loading on the joint is a combination of inertia loads from the entire Centaur stage, aerodynamic loads, and differential pressure across the interstage adapter.

6.6.2 WEIGHTS AND CENTER OF GRAVITY DATA. The following weights shall be used for structural design and analysis.

a. Maximum weight above Station 412.72 joint 40,700 lb

b. Minimum weight above Station 412.72 joint 37,800 lb

6.6.3 THERMAL DATA. The thermal environment of the Station 412.72 joint is presented in Paragraphs 3.2.3 and 4.1.3.

6.6.4 INERTIA LOADS. The inertia plus drag contribution to Station 412.72 joint axial loads is included in the data presented in Table 6.6-1.

At BECO the longitudinal inertia load -5.7 ± 0.1 g's. This acts simultaneously with the bending moment presented in Figure 6.2-3.

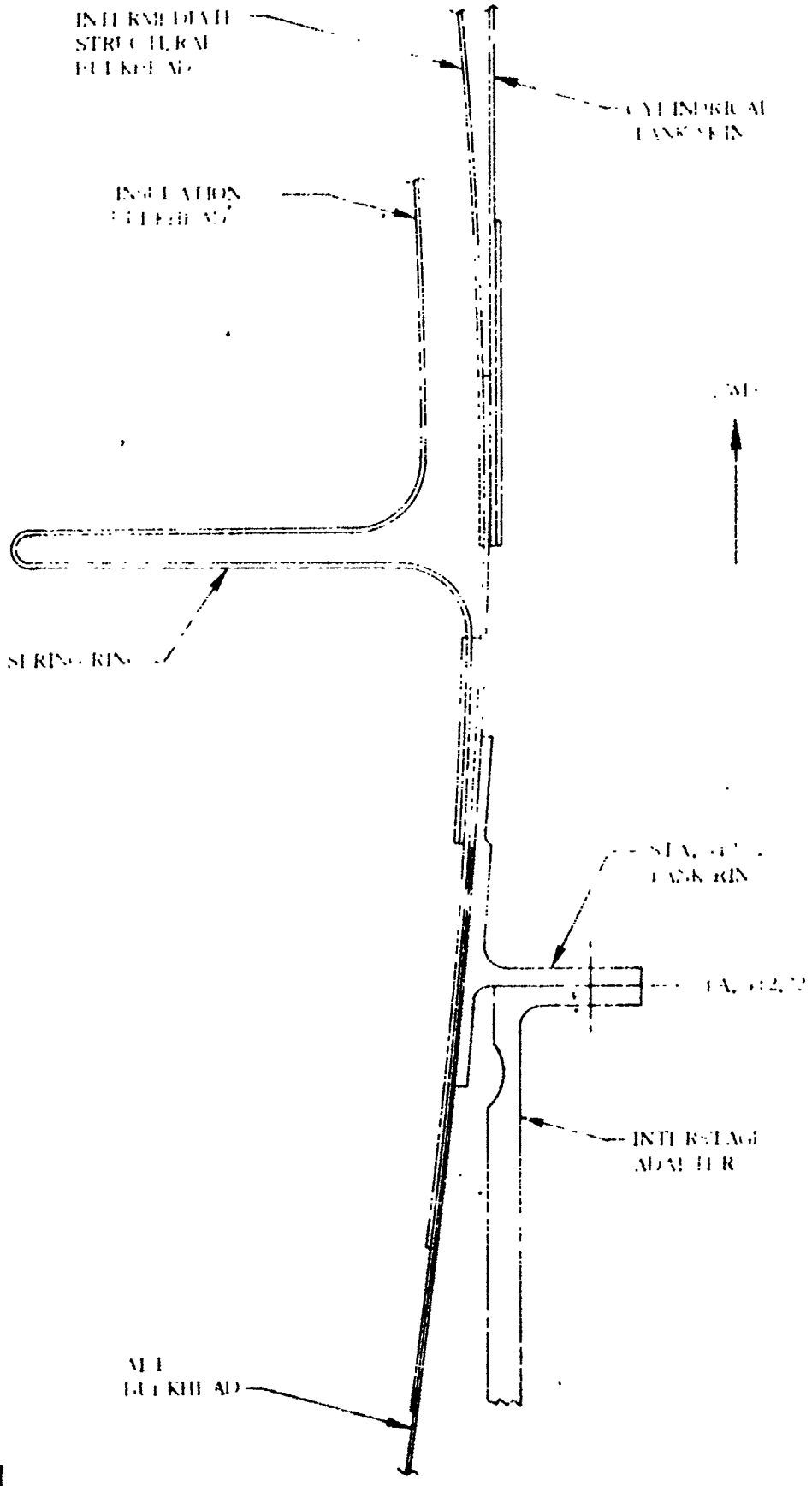

Figure 6.6-1. Station 412.72 Joint Configuration

TABLE 6.6-1. STATION 412.72 JOINT AXIAL LOADS

Time (sec)	Axial Compression (lb)	
	Maximum	Minimum
40	80,500	64,600
44	86,500	68,000
48	94,400	72,400
52	100,100	78,200
56	124,800	86,300
60	133,200	98,300
64	133,700	106,800
68	133,900	106,100
72	133,900	106,400
76	134,500	106,900
80	135,300	107,300
84	137,000	107,500
88	138,500	107,900
92	140,500	109,100
96	143,200	111,500
100	146,800	114,800

NOTE:
The loads presented above include the effects of inertia, drag, and differential pressure across the interstage adapter. Bending moment on the 412.72 joint is presented in Figure 6.6-2.

6.6.5 STEADY-STATE AIR LOADS. Drag and interstage adapter internal pressure contributions to axial load are included in the data presented in Table 6.6-1. Effects of angle of attack are included in the bending moment data presented in Figure 6.6-2. Since the exact time of maximum bending moment is not well defined, it shall be assumed to occur between 56 and 76 seconds.

6.6.6 BUFFET AND FLUTTER LOADS. The Station 412.72 joint does not receive critical loading due to buffet or fluctuating pressures.

6.6.7 MISCELLANEOUS LOAD PARAMETERS. No other loads at the Station 412.72 joint are considered critical.

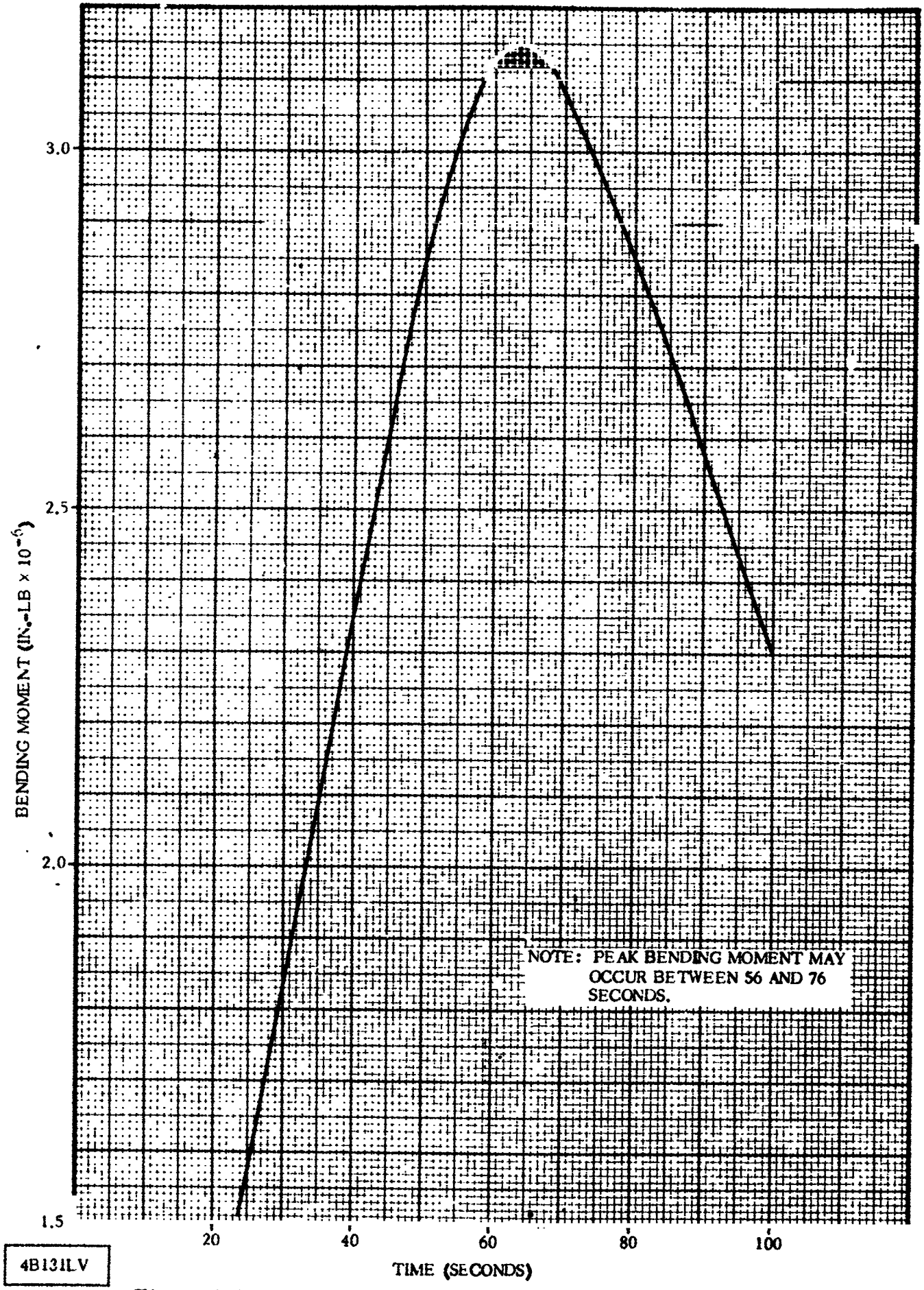

Figure 6.6-2. Station 412.72 - Bending Moment versus Time

6.7 CYLINDRICAL TANK SECTION FORWARD OF STATION 412.72

The loads presented in this subsection are for the cylindrical tank immediately forward of the Station 412.72 tank ring. The configuration of this portion of the tank is shown in Figure 6.6-1.

6.7.1 CRITICAL CONDITIONS. The aft portion of the cylindrical tank reacts aerodynamic and inertia loads which are applied forward of the Station 412.82 ring. The critical loading conditions occur during the first 100 seconds of flight, and at BECO.

6.7.2 WEIGHTS AND CENTER OF GRAVITY DATA. For structural design and analysis purposes, the maximum weight which imposes inertia loads on the cylindrical tank forward of Station 412.72 7730 lb.

6.7.3 THERMAL DATA. The portion of the tank skin wetted by liquid hydrogen is at a temperature of -423° F.

6.7.4 INERTIA LOADS. The inertia contribution to axial load is included in the data presented in Table 6.7-1. Fuel tank ullage pressure must be included in the analysis of the structure (see Figure 6.2-4). The inertia contribution to bending moment is included in the data presented in Figure 6.6-2.

The maximum axial acceleration of the vehicle at BECO + 5.7 ± 0.1 g's. This acts simultaneously with the BECO bending moment presented in Figure 6.2-3.

6.7.5 STEADY-STATE AIR LOADS. Drag contribution to axial loads is included in the loads presented in Table 6.7-1. The aerodynamic contribution to bending moment is included in the data presented in Figure 6.6-2.

6.7.6 BUFFET AND FLUTTER LOADS. The aft end of the cylindrical tank does not receive critical loading due to buffet or fluctuating pressures.

6.7.7 MISCELLANEOUS LOAD PARAMETERS. No other loads at the aft end of the cylindrical tank are considered critical.

TABLE 6.7-1. CYLINDRICAL TANK FORWARD OF STATION 412.72 - MAXIMUM AXIAL LOADS

Time (sec)	Maximum Axial Compression (lb)
40	16,200
44	18,100
48	21,100
52	27,400
56	38,500
60	44,700
64	44,600
68	44,500
72	43,600
76	42,900
80	42,300
84	41,500
88	40,900
92	39,800
96	38,700
100	37,800
These loads include inertia and drag contribution only. For LH_2 tank ullage pressure, see Figure 6.2-4.	

6.8 AFT BULKHEAD - AFT OF STATION 412.72

The aft bulkhead reacts the inertia loads of the liquid oxygen mass plus aft bulkhead structure, and transmits the load into the Station 412.72 tank ring. The configuration of the aft bulkhead is shown in Figure 6.8-1.

6.8.1 CRITICAL CONDITIONS. A combination of inertia loads and differential pressure across the tank skin causes critical loading on the aft bulkhead. The critical times during flight are during the first 100 seconds of flight and at BECO.

6.8.2 WEIGHTS AND CENTER OF GRAVITY DATA. For structural design and analysis, the maximum weight which imposes inertia loads on the aft bulkhead, aft of Station 412.72 28,100 pounds. This includes the weight of the liquid oxygen and engines.

6.8.3 THERMAL DATA. The portion of the tank skin wetted by liquid oxygen is at a temperature of -297 F.

6.8.4 INERTIA LOADS. The maximum axial inertia loads on the aft bulkhead aft of Station 412.72 are presented in Table 6.8-1. The effects of LO_2 tank ullage pressure and interstage adapter internal pressure must be included in the aft bulkhead stability analysis. LO_2 tank ullage pressure is presented in Figure 6.2-5, and interstage adapter internal pressure is presented in Table 6.2-2. Bending moment effects are minimal during the first 100 seconds of flight.

TABLE 6.8-1. AFT BULKHEAD MAXIMUM AXIAL INERTIA LOADS - AFT OF STATION 412.72

Time (sec)	Maximum Axial Compression (lb)
40	48,000
44	49,600
48	51,200
52	52,400
56	52,700
60	54,000
64	56,300
68	58,700
72	61,200
76	64,600
80	68,500
84	72,900
88	77,200
92	81,500
96	85,700
100	90,300

NOTE: For a discussion of loads due to differential pressure across the aft bulkhead, see Paragraph 6.8.5.

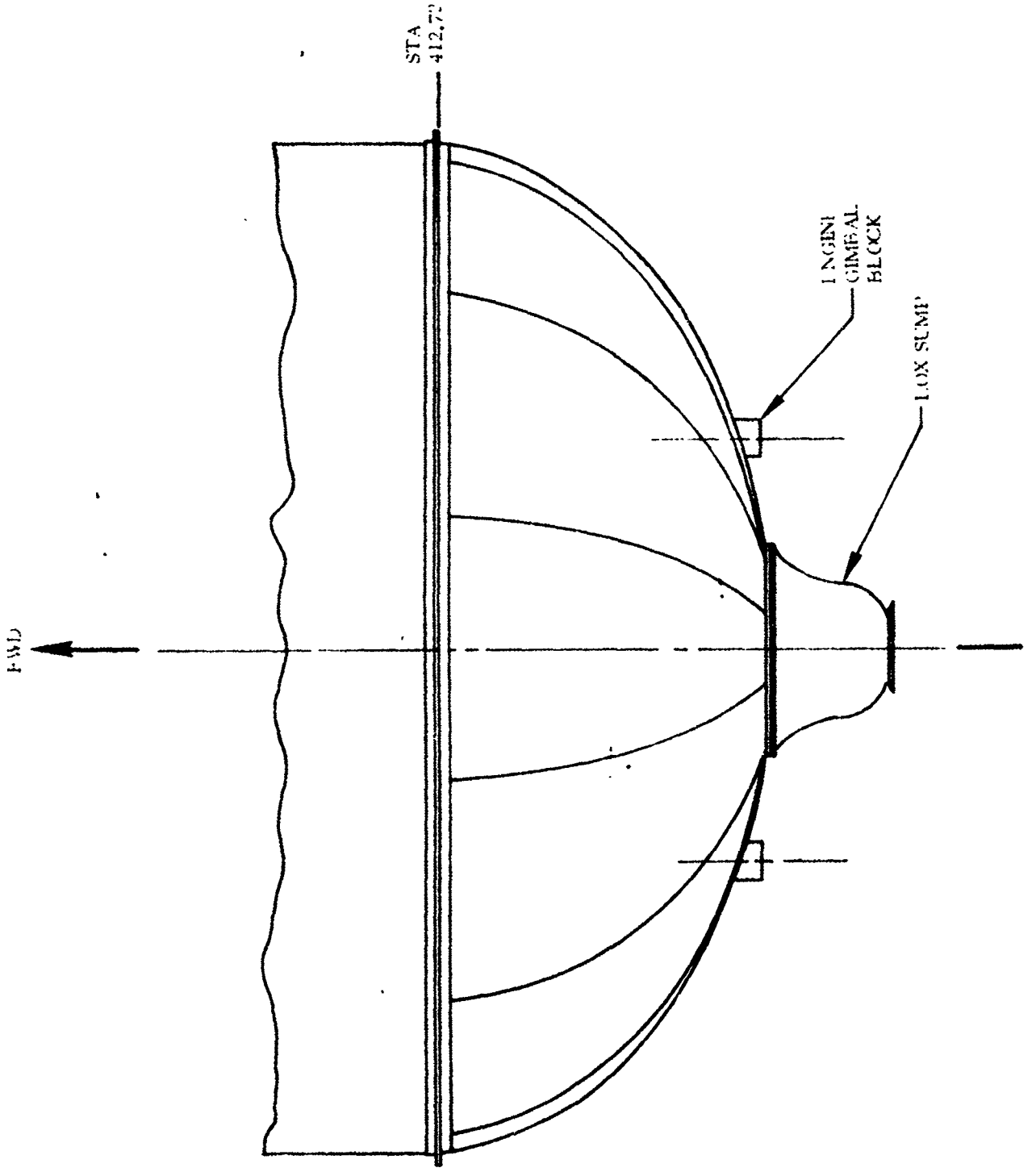

Figure 6.5-1. Aft Bulkhead Configuration

4B132LT

At BECO, the maximum vehicle acceleration +5.7 ±0.1 g's. The bending moment on the aft bulkhead is considered negligible at this time.

6.8.5 STEADY-STATE AIR LOADS. The effects of interstage adapter internal pressure must be included in the analysis of the aft bulkhead. See Table 6.2-2 for limits of interstage adapter internal pressure.

6.8.6 BUFFET AND FLUTTER LOADS. The aft bulkhead does not receive critical loading due to buffet or fluctuating pressures.

6.8.7 MISCELLANEOUS LOAD PARAMETERS. No other loads on the aft bulkhead are considered critical.

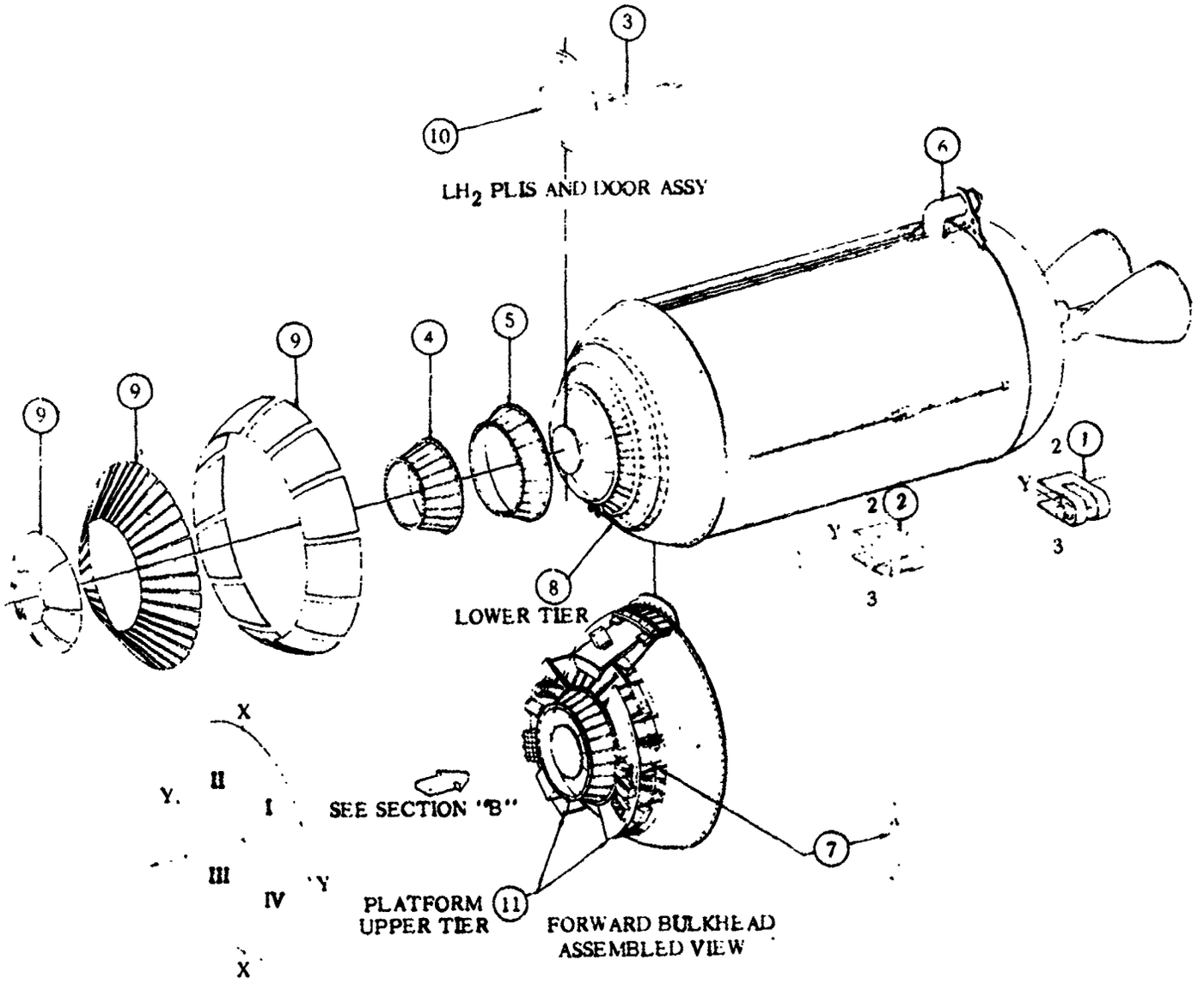

1 ANTENNA - C-BAND

2 ANTENNA - AZUSA

3 LH_2 PLIS ASSY

4 PAYLOAD ADAPTER - FWD*

5 PAYLOAD ADAPTER - AFT*

6 FUEL ELBOW SUMP ASSY

7 FWD EQUIP PLATFORM STRUTS

8 FWD EQUIP RAIL ASSY

9 FWD BHD INSULATION

10 FWD DOOR ASSY

11 FWD ELECT EQUIP PLATFORM

*REFERENCE SECTION V

SECTION VII

LIQUID HYDROGEN TANK BOLT-ONS AND WELDMENTS

7.1 INTRODUCTION

The data presented in this section is applicable to major components bolted or welded to the basic liquid hydrogen (LH_2) tank structure. The loads on the basic tank are presented in Section VI of this report.

7.2 DUAL VENT VALVE AND STANDPIPE

The fuel tank dual vent valve and duct installation is located between Quadrants III and IV on the X-X axis at Station 177.52 as shown in Figure 7.2-1.

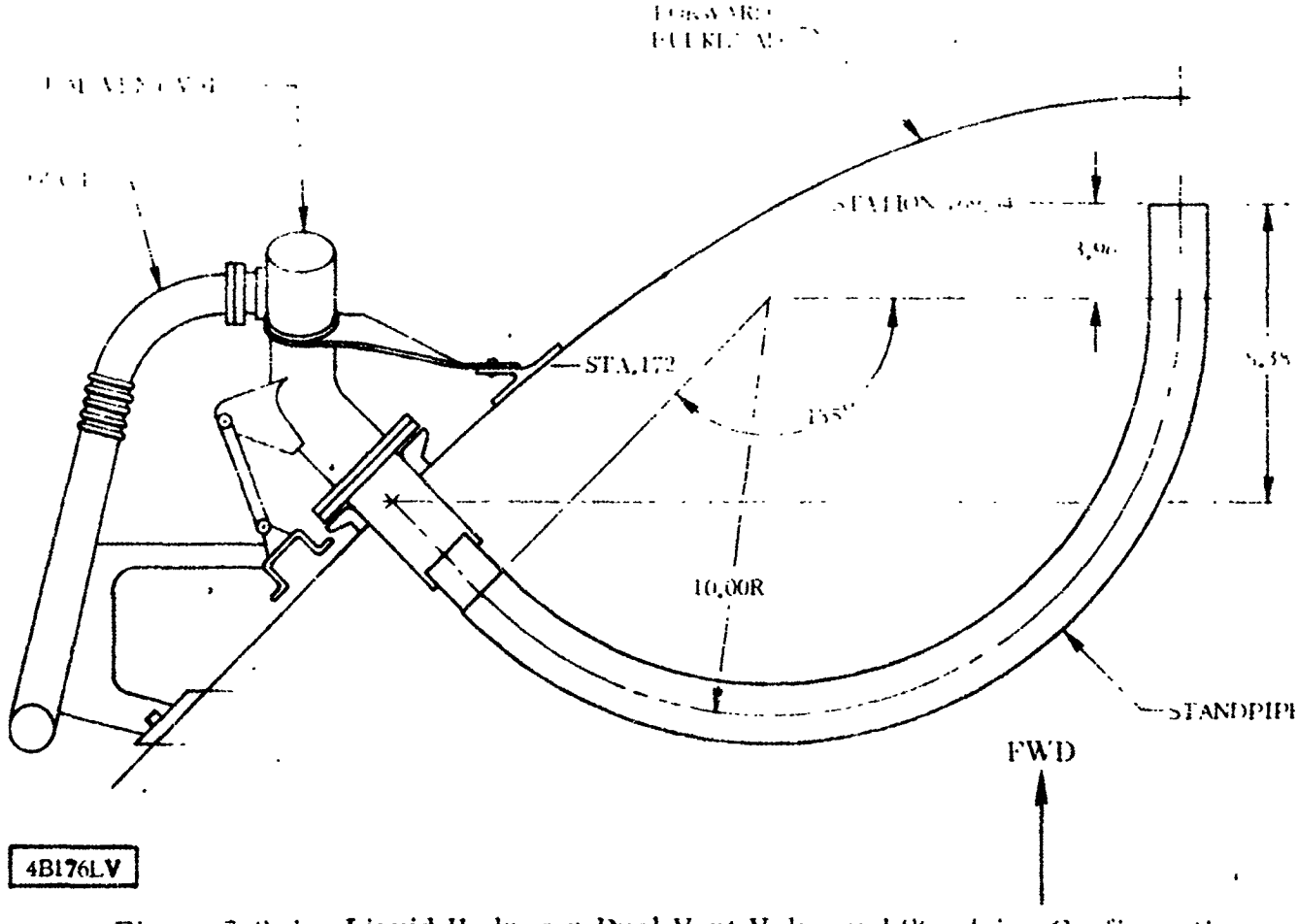

Figure 7.2-1. Liquid Hydrogen Dual Vent Valve and Standpipe Configuration

The dual vent valve is a liquid hydrogen boiloff component for controlling the ullage pressure in the fuel tank.

7.2.1 CRITICAL CONDITIONS. The critical loading conditions on the dual boiloff valve and standpipe are the inertia loads at Centaur main engine start (MES) and during Centaur firing and burnout, and the disconnect load on the duct when the nose fairing is jettisoned.

7.2.2 WEIGHTS AND CENTER OF GRAVITY DATA. The weights and C.G. locations for design and analysis are presented in Figures 7.2-2 and 7.2-3.

Part	Weight
①	0.255 LB
② · ③	0.916 LB
④	2.06 LB
NOTE: ② · ③ combined because ③ is small	

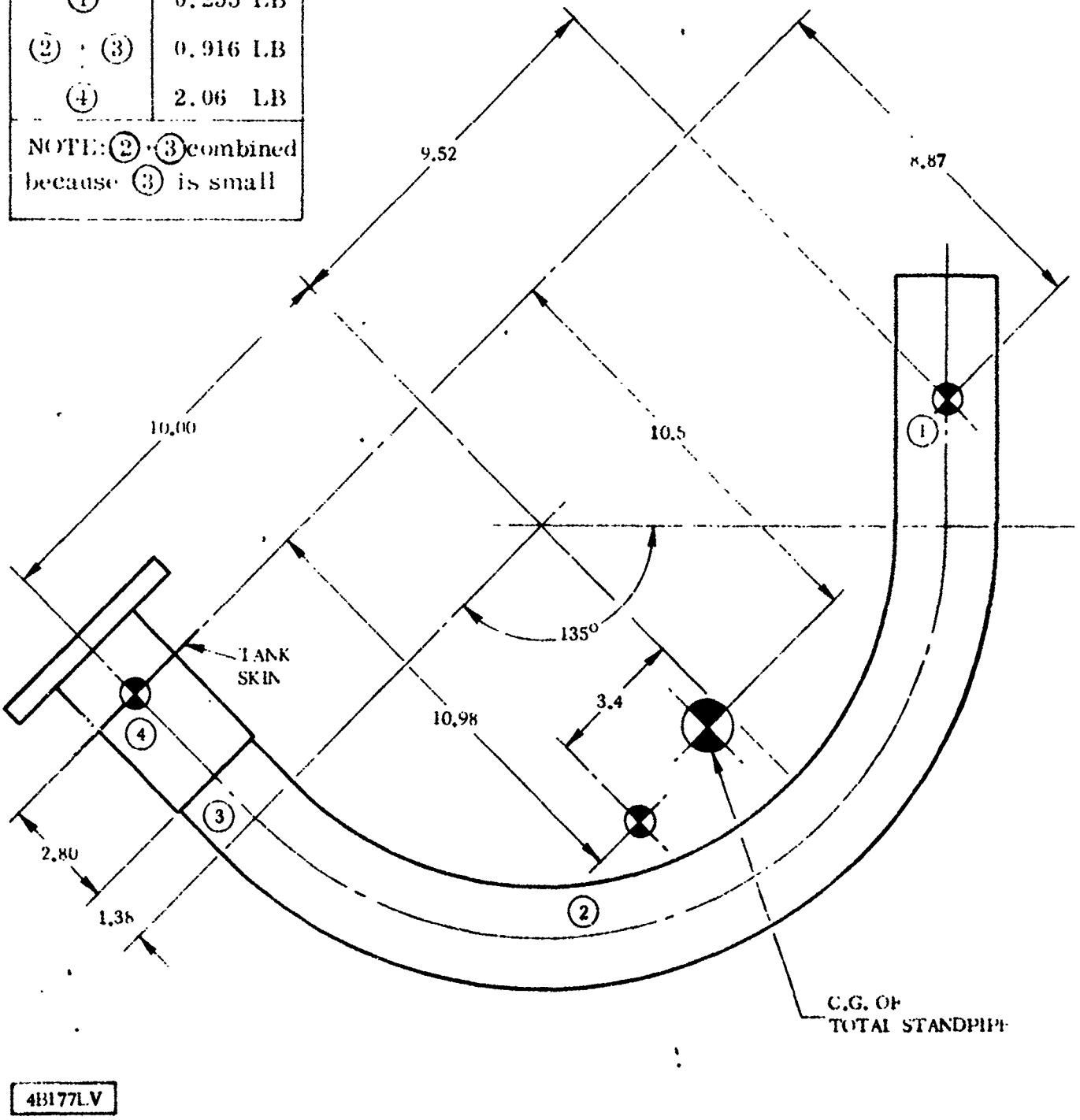

4B177LV

Figure 7.2-2. Standpipe Weight and Center of Gravity

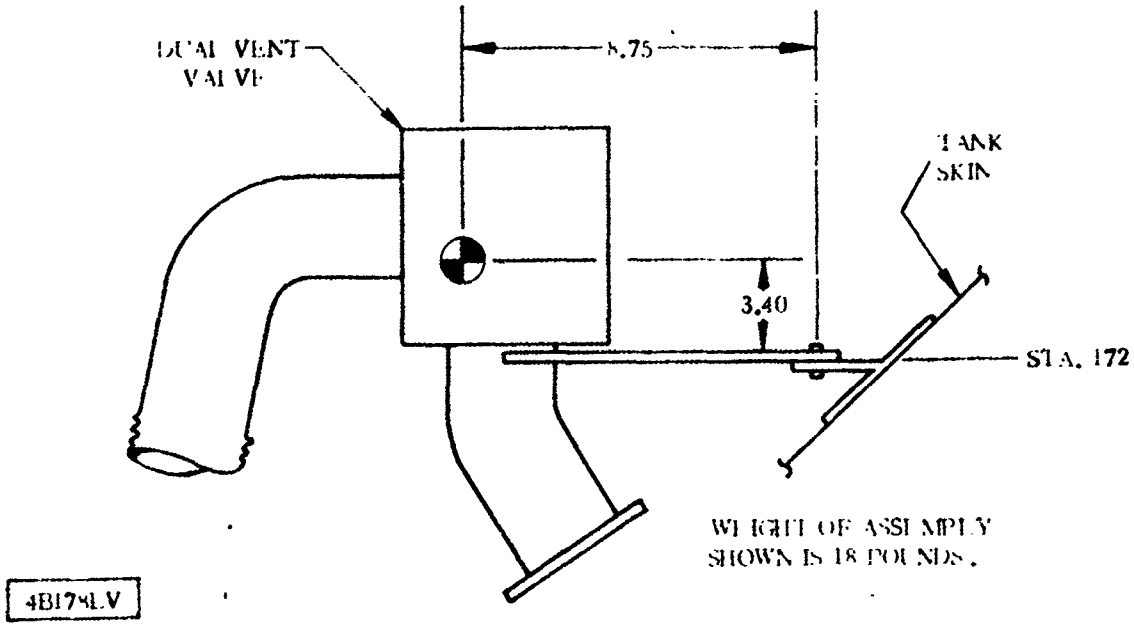

Figure 7.2-3. Dual Vent Valve Assembly Weight and Center of Gravity

7.2.3 THERMAL DATA. The dual vent valve and standpipe shall be analyzed using a temperature of -423 F.

7.2.4 INERTIA LOADS. Inertia load factors which act on the LH_2 dual vent valve and standpipe are listed in Table 7.2-1.

TABLE 7.2-1. LIQUID HYDROGEN DUAL VENT VALVE AND STANDPIPE INERTIA LOADS

Loading Condition	Dual Vent Valve		Standpipe	
	Longitudinal* g's	Associated Lateral g's	Longitudinal* g's	Associated Lateral g's
Centaur Firing and Burnout	+ 7.0	±6.0	+ 7.0	±18.0
Centaur Firing and Burnout	+12.0	±1.0	+25.0	± 1.0
Centaur Start	- 5.0	±1.0	- 5.0	± 1.0
Sustainer Flight	+ 3.5	±1.0	———	———
Sustainer Flight	+ 2.0	±1.8	———	———

* + Longitudinal load acts aft

7.2.5 STEADY-STATE AIR LOADS. The LH_2 dual vent valve and standpipe do not receive critical loads due to aerodynamic forces.

7.2.6 BUFFET AND FLUTTER LOADS. The LH_2 dual vent valve and standpipe do not receive critical loads due to fluctuating pressures.

7.2.7 MISCELLANEOUS LOAD PARAMETERS. Since the dual vent valve and standpipe are connected to the ullage volume of the LH_2 tank, they are subjected to an internal pressure equal to the LH_2 tank ullage pressure. This reaches a maximum of 27 psia. See Figure 6.2-4 for ullage pressure versus time.

When the nose fairing is jettisoned, the maximum load at the separation interface 190 pounds (tension).

7.3 LIQUID HYDROGEN FILL AND DRAIN VALVE OUTLET

The liquid hydrogen fill and drain valve outlet is located in Quadrant II at Station 384.00 as shown in Figure 7.3-1.

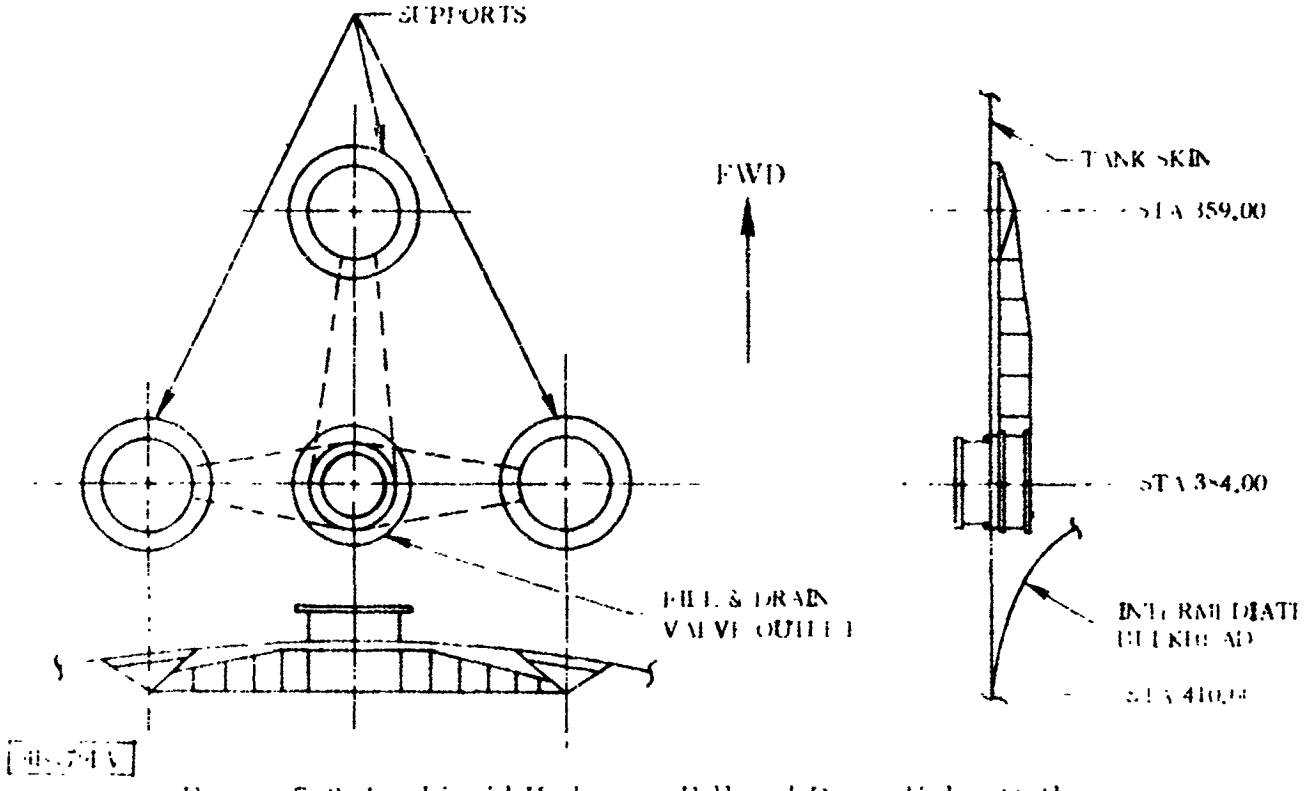

Figure 7.3-1. Liquid Hydrogen Fill and Drain Valve Outlet

7.3.1 CRITICAL CONDITIONS. The critical loading condition for the LH_2 fill and drain valve outlet is the umbilical disconnect load at launch. The ground portion of the valve is pulled downward and outward by a lanyard which breaks the two bolts at the GSE Airborne interface. The backup disconnect system, a static lanyard activated by missile rise, imposes the most severe loads on the airborne structure.

7.3.2 WEIGHTS AND CENTER OF GRAVITY DATA. The weight of the LH_2 fill and drain valve installation is small compared to disconnect loads at launch.

7.3.3 THERMAL DATA. The operating temperature of the LH_2 fill and drain valve outlet is -423 F.

7.3.4 INERTIA LOADS. Inertia loads on the LH_2 fill and drain valve outlet are not critical.

7.3.5 STEADY-STATE AIR LOADS. The LH_2 fill and drain valve outlet does not receive critical loads due to aerodynamic forces.

7.3.6 BUFFET AND FLUTTER LOADS. The LH_2 fill and drain valve outlet does not receive critical loads due to buffet or fluctuating pressures.

7.3.7 MISCELLANEOUS LOAD PARAMETERS. The fuel ullage and head pressure must be considered when performing the stress analysis of the airborne structure. See Subsection 6.2 for ullage pressure and fuel level station.

Two loading conditions are considered during fill and drain valve disconnect. The loads associated with each condition are presented in Table 7.3-1, using the sign convention illustrated in Figure 7.3-2. These loads represent the total loading on the airborne structure, and all dynamic effects are included.

TABLE 7.3-1. LIQUID HYDROGEN FILL AND DRAIN VALVE DISCONNECT LOADS

Loading Condition	M_z (in.-lb)	M_r (in.-lb)	M_θ (in.-lb)	P_z (lb)	P_T (lb)	P_R (lb)
Disconnect with no misalignment	0	13,660	0	1050	0	650
Disconnect with maximum misalignment	6500	11,300	2470	910	530	650

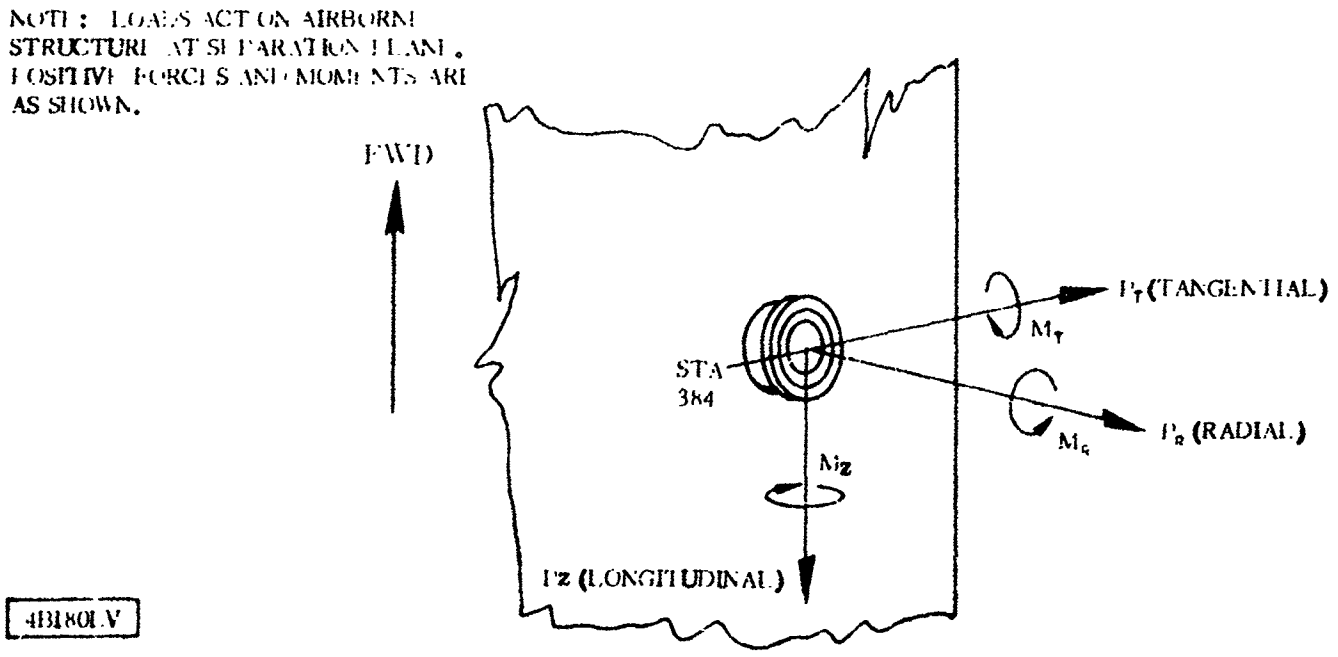

Figure 7.3-2. Liquid Hydrogen Fill and Drain Outlet Sign Convention

7.4 LIQUID HYDROGEN BOOST PUMP AND SUMP

The LH_2 boost pump and sump elbow are located on the X-X axis between Quadrants I and II as shown in Figure 7.4-1. The boost pump is a low NPSH pump used to provide liquid hydrogen at the proper pressure to the Centaur engine turbopumps.

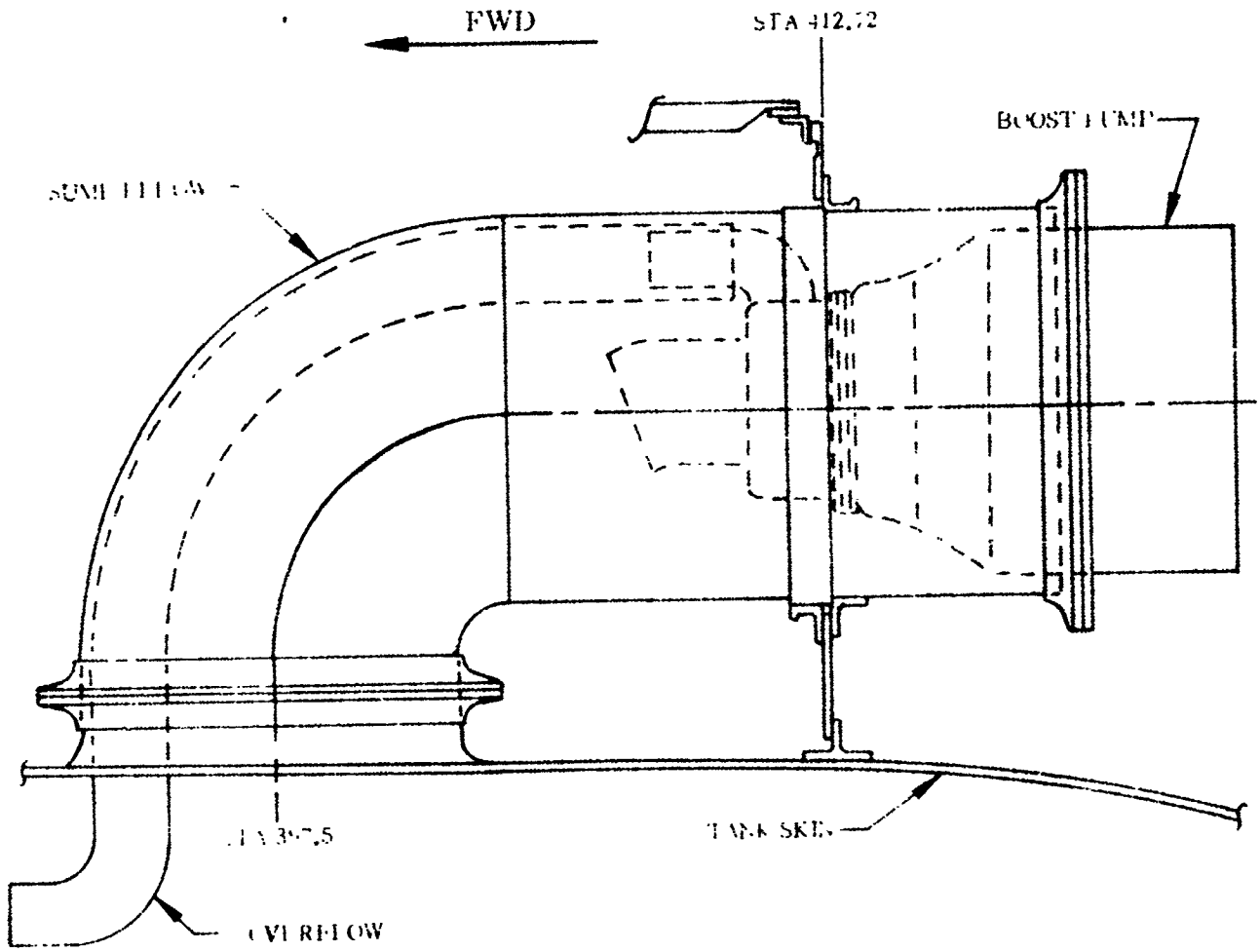

Figure 7.4-1. Liquid Hydrogen Boost Pump and Sump

7.4.1 CRITICAL CONDITIONS. The critical loading conditions of the LH_2 boost pump are the inertia loads at BECO, MES, and MECO, combined with the internal pressure at each respective time.

7.4.2 WEIGHTS AND CENTER OF GRAVITY DATA. The following weights and C.G. locations shall be used for design and analysis. The sump elbow weighs 16 pounds and the boost pump and drive weigh 60 pounds. The C.G. location is shown in Figure 7.1.2.

7.4.3 THERMAL DATA. The temperature of the boost pump inlet versus time is shown in Figure 7.4-3.

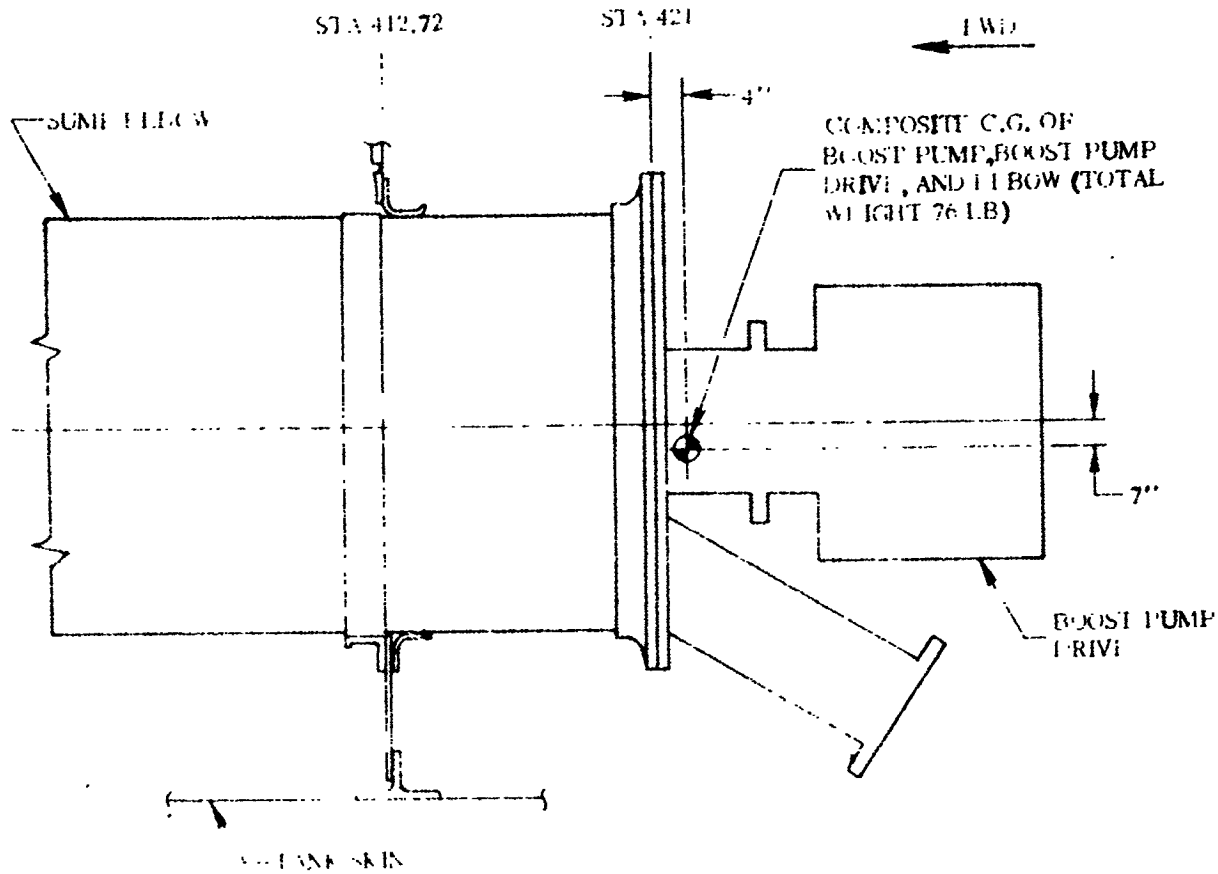

4BI-21 V

Figure 7.4-2. Boost Pump and Sump Center of Gravity Location

7.4.4 INERTIA LOADS. Inertia loads on the boost pump and sump listed in Table 7.4-1.

TABLE 7.4-1. BOOST PUMP AND SUMP INERTIA LOADS

Condition	Longitudinal g's	Lateral g's	Vibration g's
BECO	±5.9	±0.5	±2.0
Centaur Thrust Buildup	±1.2	±0.5	±6.0
Centaur Burnout	±7.0	±0.5	±6.0

7.4.5 STEADY-STATE AIR LOADS. The LH_2 boost pump and sump do not receive critical loads due to aerodynamic forces.

7.4.6 BUFFET AND FLUTTER LOADS. The LH_2 boost pump and sump do not receive critical loads due to buffet or fluctuating pressures.

7.4.7 MISCELLANEOUS LOAD PARAMETERS. The internal pressure of the boost pump inlet is plotted versus time in Figure 7.4-4. The pressure acts simultaneously with the applicable inertia load factors presented in Paragraph 7.4.4.

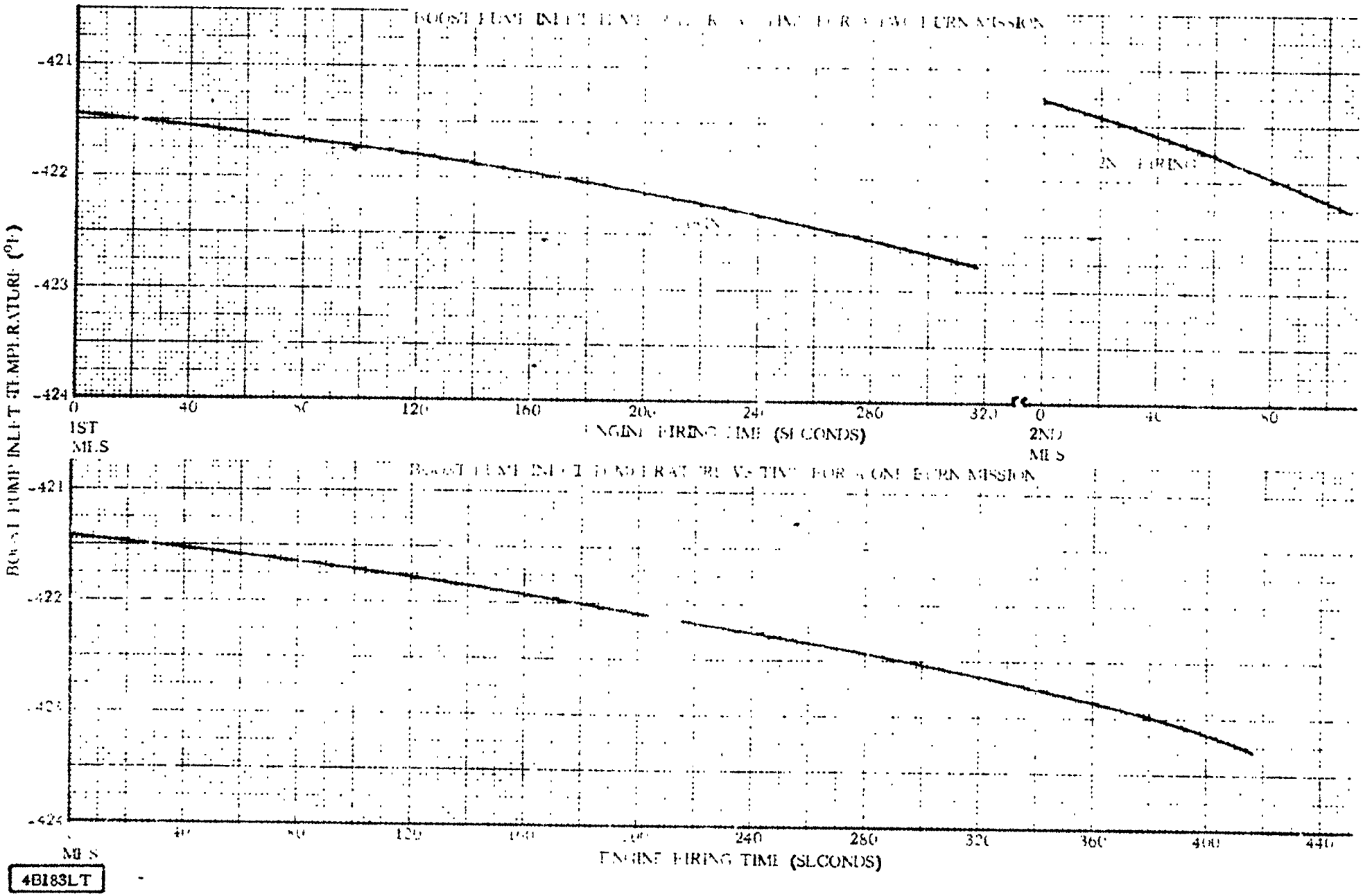
-421
-422
-423
-424
0
40
80
120
160
200
240
280
320
0
40
80
1ST
MLS
2ND
MLS
ENGINE FIRING TIME (SECONDS)
-421
-422
-423
-424
0
40
80
120
160
200
240
280
320
360
400
440
MLS
ENGINE FIRING TIME (SECONDS)
4B183LT

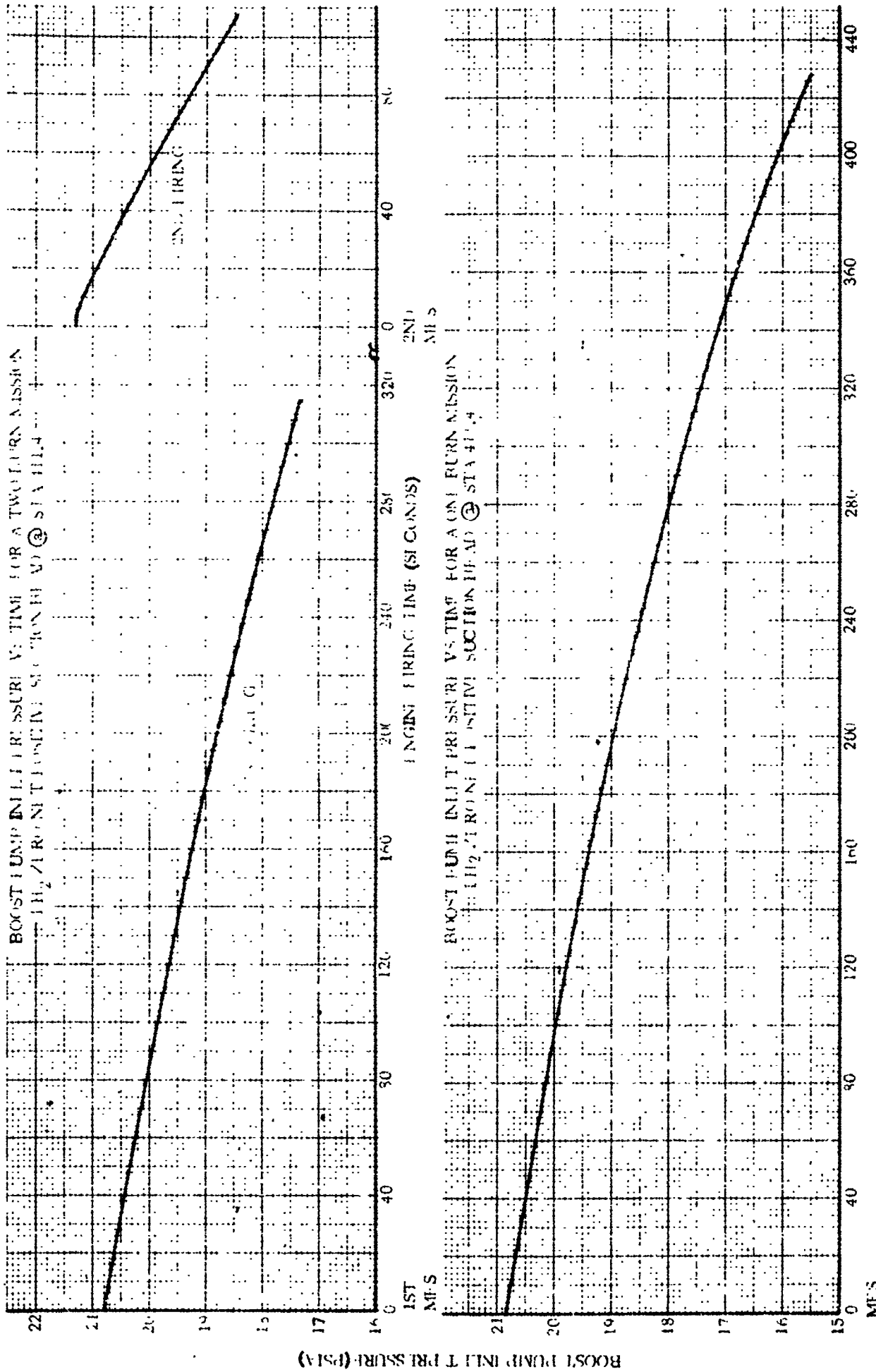

Figure 7.4-4. Boost Pump Inlet Pressure versus Time

7.5 COMMAND DESTRUCT UNIT - SUPPORT STRUCTURE

The command destruct unit is located on the Y-Y axis between Quadrants I and IV near the aft end of the LH_2 tank. The configuration is illustrated in Figure 7.5-1.

7.5.1 CRITICAL CONDITIONS. The critical condition for design of the command destruct unit support structure is the inertia forces due to longitudinal and lateral acceleration and vibration during flight.

7.5.2 WEIGHTS AND CENTER OF GRAVITY DATA. Structural design weight of the command destruct unit is 5.0 pounds. The C.G. of the unit is at Station 404.64 inches from the vehicle centerline on the Y-Y axis.

7.5.3 THERMAL DATA. The command destruct unit supports attach to the LH_2 tank skin which is at a temperature of -420°F.

7.5.4 INERTIA LOADS. Inertia load factors for the command destruct unit support structure are listed in Table 7.5-1.

TABLE 7.5-1. COMMAND DESTRUCT UNIT SUPPORT STRUCTURE - INERTIA LOAD FACTORS

Condition	Longitudinal* (g's)	Lateral (g's)
Maximum Longitudinal Inertia	-12.0	±1.0
Maximum Lateral Inertia	-7.0	±12.0

* - Longitudinal load acts aft.

7.5.5 STEADY-STATE AIR LOADS. The command destruct unit does not receive critical loads due to aerodynamic forces.

7.5.6 BUFFET AND FLUTTER LOADS. The command destruct unit does not receive critical loads due to buffet or fluctuating pressure.

7.5.7 MISCELLANEOUS LOAD PARAMETERS. No other critical loads are applied to the command destruct unit.

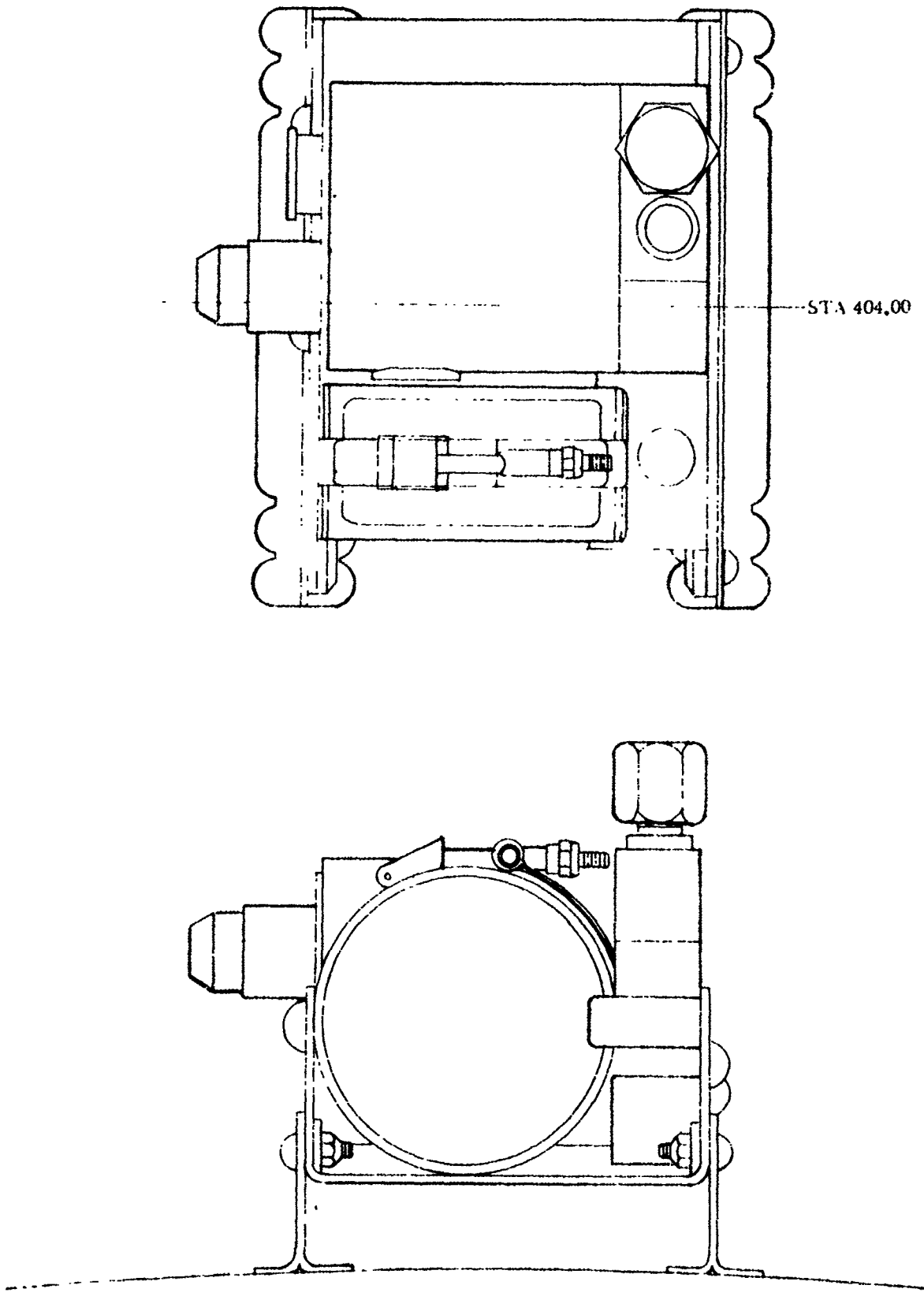

4B185LV

Figure 7.5-1. Command Destruct Unit Configuration

7.6 FORWARD BULKHEAD PACKAGES

Figures 7.6-1 and 7.6-2 show the packages and their arrangement on the forward bulkhead. The upper tier equipment shelf is located at Station 172. The lower tier equipment is mounted on two rails that run circumferentially around the vehicle at Stations 178 and 189.

7.6.1 CRITICAL CONDITIONS. The critical loading conditions on the forward bulkhead packages are the inertia loads during Atlas Launch, Max q, Max g, and Centaur MES and MECO.

7.6.2 WEIGHT AND CENTER OF GRAVITY DATA. The weight and C.G. data for the major items on the upper and lower equipment shelves is given in Tables 7.6-1 and 7.6-2 respectively.

7.6.3 THERMAL DATA. For the purpose of stress analysis the temperature of the packages shall be considered to be 60° F.

The struts that support the upper platform become very cold due to the fuel boiloff through the LH$_2$ vent. The strut nearest the vent can reach a temperature of -360° F in an extreme venting case.

7.6.4 INERTIA LOADS. The inertia load factors in Table 7.6-3 shall be used for the analysis of all packages on the forward bulkhead. The package supports shall be analyzed using Tables 7.6-3 and 7.6-4. All of the package supports on the upper tier and the C-band transponder, NASA Strain Gage and Range Safety Power Control supports on the lower tier, shall be analyzed using Table 7.6-3. The remainder of the package supports on the lower tier shall be analyzed using Table 7.6-4, except for the Inverter and Telemetry Packages No. 1, 2, and 3 which have applicable load factors shown in Table 7.6-5.

7.6.5 STEADY-STATE AIR LOADS. The forward bulkhead packages do not receive critical loads due to aerodynamic forces.

7.6.6 BUFFET AND FLUTTER LOADS. The forward bulkhead packages do not receive critical loads due to buffet or fluctuating pressures.

7.6.7 MISCELLANEOUS LOAD PARAMETERS. No other critical loads are applied to the forward bulkhead packages.

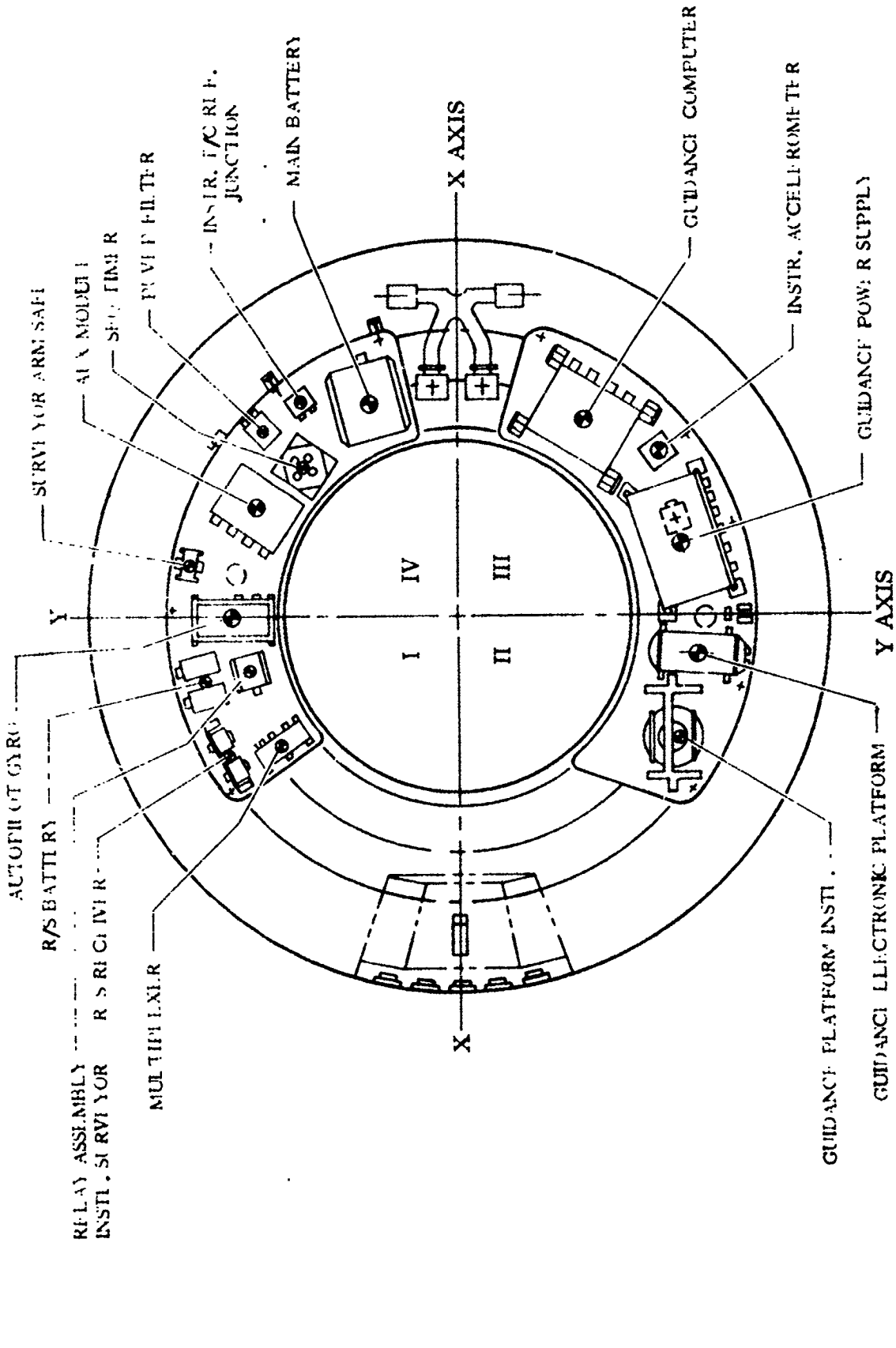

4B186LT

Figure 7.6-1. Upper Tier Equipment for AC-6 - View Looking Aft

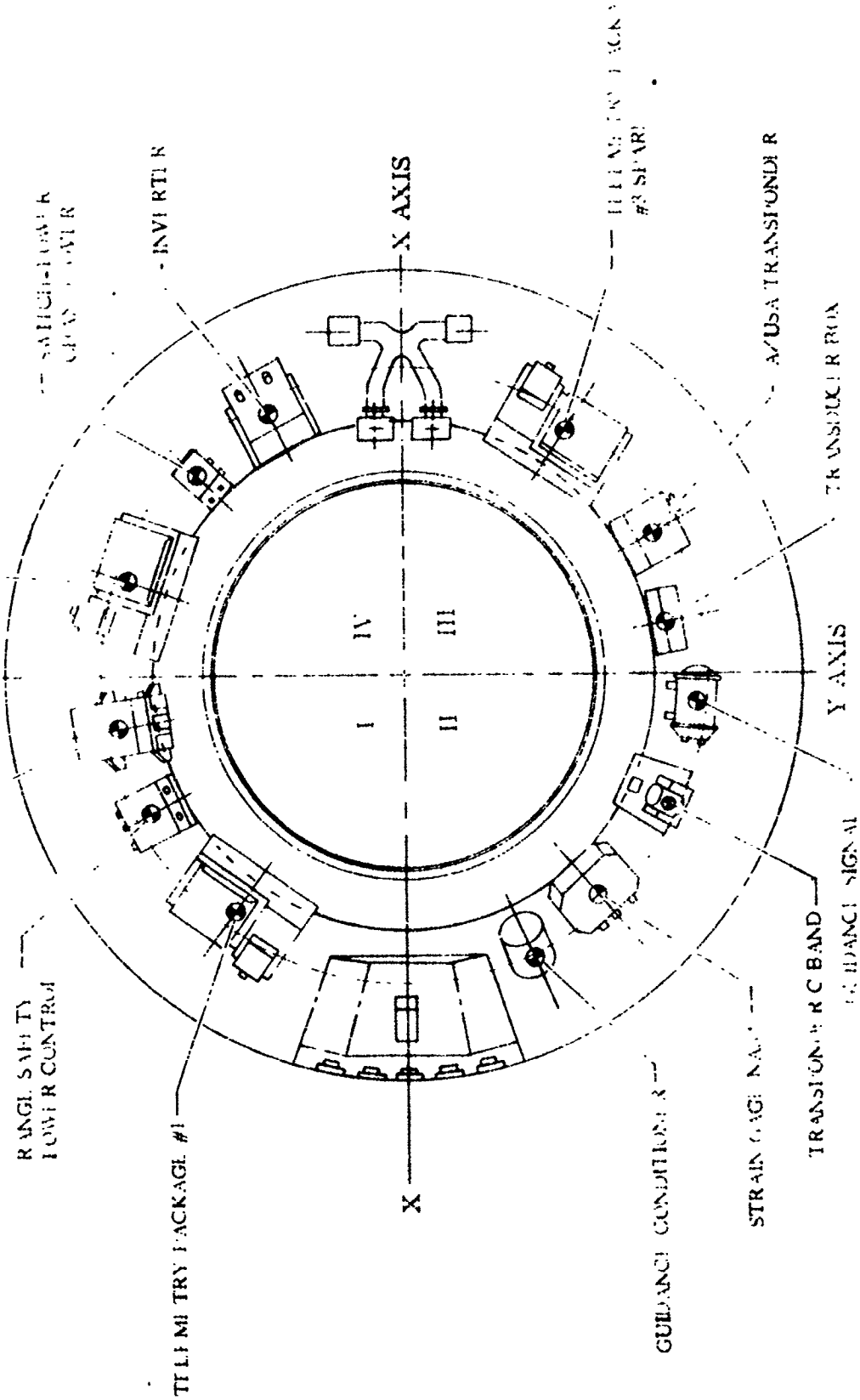

Figure 7.6-2. Lower Tier Equipment for AC-6 - View Looking Aft

4B187L1

TABLE 7.6-1. UPPER TIER EQUIPMENT WEIGHTS AND CENTERS OF GRAVITY

Item	Weight (lb)	z (in.)	y (in.)	x (in.)
Autopilot Gyro	18.92	168	38	0
Surveyor Arm Safe	3.03	172	45	-7
Aux Module Timer	20.0	168	33	-18
PUVEP Filter	5.4	173	34	-30
Seq Timer	10.5	168	26	-26
Instr T/C Reference Junction	1.9	170	26	-36
Main Battery	67.0	168	15	-35
Guidance Computer	65.02	167	-20	-32
Instr Accelerometer	4.36	171	-33	-27
Guidance Power Supply	60.85	167	-37	-12
Guidance Electronic Platform	18.87	168	-39	6
Guidance Platform Installation	35.78	164	-35	19
Multiplexer	5.36	170	21	30
Range Safety Receiver (2)	18.92	168	38	22
Relay Assembly Installation Surveyor	6.63	170	33	9
Range Safety Battery (2)	15.08	170	42	10

TABLE 7.6-2. LOWER TIER EQUIPMENT WEIGHTS AND CENTERS OF GRAVITY

Item	Weight (lb)	z (in.)	y (in.)	x (in.)
Amplifier - Autopilot Servo	17.49	179	45	8
Range Safety Power Control	9.81	183	38	20
Telemetry Package Number 1	45.13	181	27	38
Guidance Conditioner	10.96	180	-20	47
Strain Gage - NASA	16.96	181	-31	33
Transponder C-Band	6.7	181	-42	19
Guidance Signal	10.97	182	-44	4
Transducer Box	4.74	180	-41	-8
Azusa Transponder	19.28	180	-39	-22
Telemetry Package Number 3 Spare	45.0	181	-26	-39
Inverter	40.82	179	20	-41
Switch - Power Changeover	14.0	181	33	-32
Telemetry Package Number 2	45.15	181	44	-16

TABLE 7.6-3. ELECTRICAL/ELECTRONIC PACKAGES INERTIA LOAD FACTORS

Condition	Weight (lb)	Maximum Longitudinal (g's)		Maximum Lateral (g's)	
		N_x	N_{LAT}	N_z	N_{LAT}
Launch	0-29	+7.1 or -1.6	±1.0	±1.1	±6.3
	35	+6.1 or -3.6	±1.0	±1.4	±5.3
	50	+5.6 or -2.8	±1.0	±1.1	±4.5
	135	+4.2 or -1.4	±1.0	±1.4	±3.2
Max q	0-20	+8.0 or -1.0	1.0	±2.3	±7.0
	35	+7.3 or -2.7	±1.0	±2.3	±6.0
	50	+6.5 or -1.9	±1.0	±2.3	±5.2
	135	+5.2 or -0.6	±1.0	±2.3	±3.9
SECO	0-20	+8.9	±1.0	±5.9	±3.3
	35	+8.1	1.0	±5.9	±2.8
	50	+8.0	±1.0	±5.9	±2.4
	135	+7.1	±1.0	±5.9	±1.8
Centaur MES	0-20	+7.2 or -1.8	±1.0	±1.2	±6.5
	35	+6.2 or -3.8	±1.0	±1.2	±5.5
	50	+5.1 or -3.0	±1.0	±1.2	±4.7
	135	+4.0 or -1.6	±1.0	±1.2	±3.3
Centaur MECO	0-20	+12.5	±1.0	±6.5	±6.0
	35	+11.5	±1.0	±6.5	±5.0
	50	+10.7	±1.0	±6.5	±4.2
	135	+9.4	±1.0	±6.5	±2.8

TABLE 7.6-4. ELECTRICAL/ELECTRONIC PACKAGE INERTIA LOAD FACTORS* - POST 55-00200E ENVIRONMENTAL LEVELS**

N_z Longitudinal Steady-State (g's)	N_x Lateral Steady-State (g's)	N_y Vibration (g's)
+15.0 - 3.0	±4.5 —	±15.0 —

*N_z, N_x, and N_y are to be applied independently.

**Reference 1-1

TABLE 7.6-5. INVERTER AND TELEMETRY PACKAGES 1, 2, AND 3 INERTIA LOAD FACTORS* - POST 55-00200E ENVIRONMENTAL LEVELS**

N_z Longitudinal Steady-State (g's)	N_x Lateral Steady-State (g's)	N_y Vibration (g's)
+15.0 - 3.0	±4.5 —	±11.4 —

*N_z, N_x, and N_y are to be applied independently.

**Reference 1-1

7.7 FORWARD UMBILICAL PANEL

The forward umbilical panel is located on the X-X axis between Quadrants I and II and shown in Figure 7.7-1. This panel holds four electrical umbilical lines prior to disconnect.

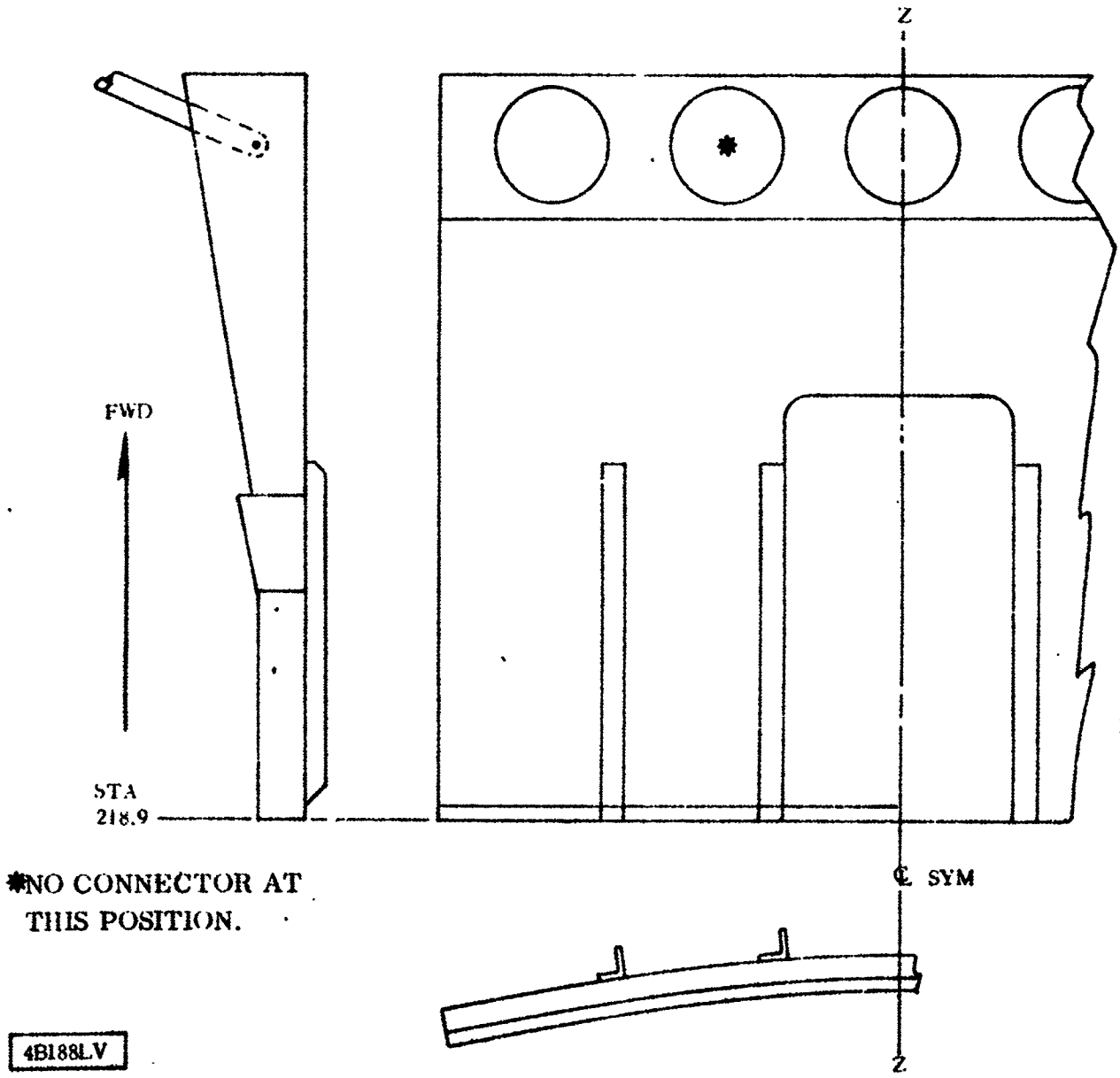

Figure 7.7-1. Forward Umbilical Panel

7.7.1 CRITICAL CONDITIONS. The critical loading conditions of the forward umbilical panel occur at disconnect and during transonic flight. The umbilical disconnect loads are applied in combination with inertia loads due to vibration of the vehicle at launch.

The loads during transonic flight consist of a combination of aerodynamic plus inertia loads.

7.7.2 WEIGHT AND CENTER OF GRAVITY DATA. The weight of the panel and attachments is 31.2 pounds and the weight of the receptacles and cables is 24.0 pounds. The C.G location of the total structure is shown in Figure 7.7-2.

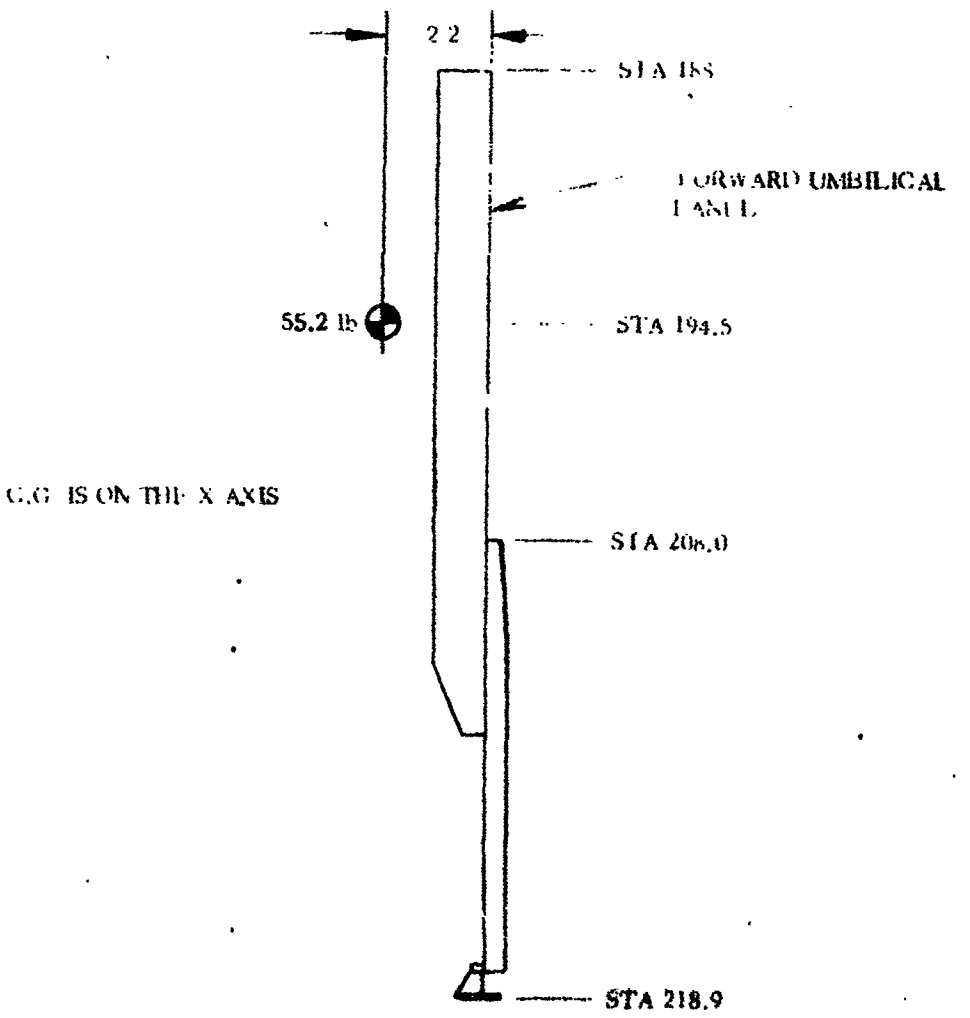

Figure 7.7-2. Forward Umbilical Panel - Center of Gravity Location

7.7.3 THERMAL DATA. A temperature history of the forward umbilical panel is presented in Figures 7.7-3 and 7.7-4.

NOTE:
REFERENCE FIGURE 7.7-4 FOR TEMPERATURE HISTORIES OF DATA POINTS.

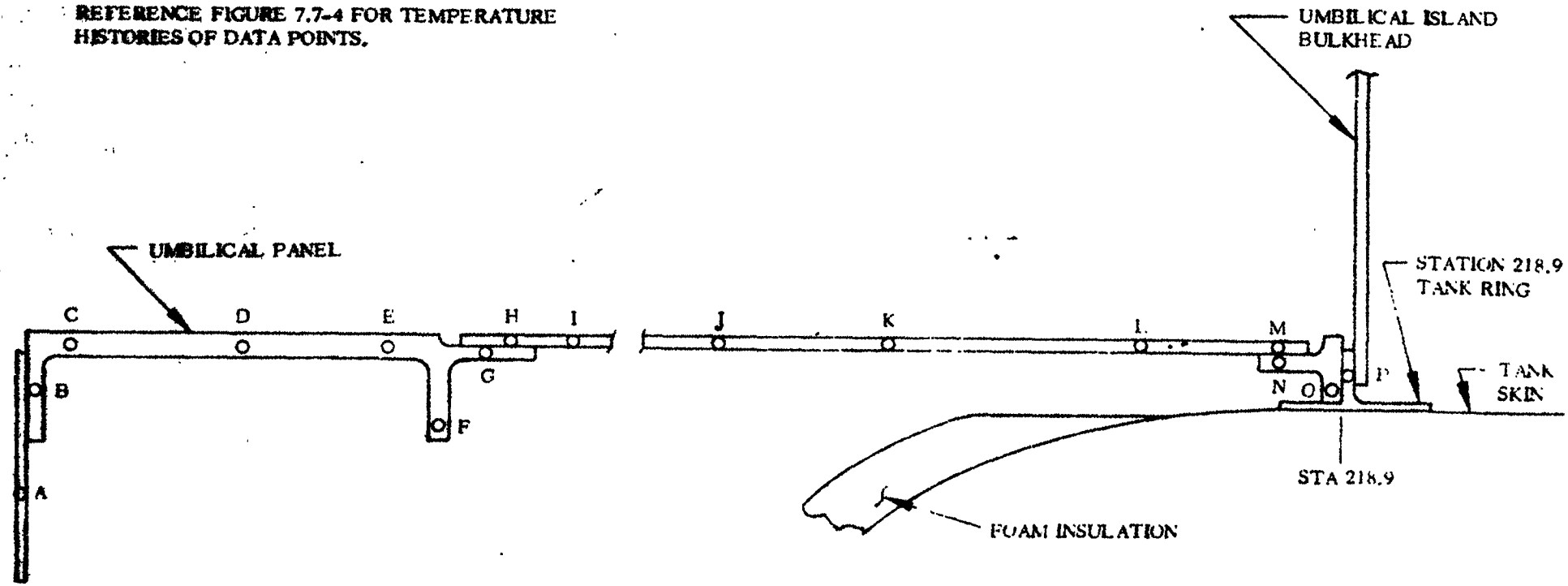

Figure 7.7-3. Forward Umbilical Panel - Temperature Distribution

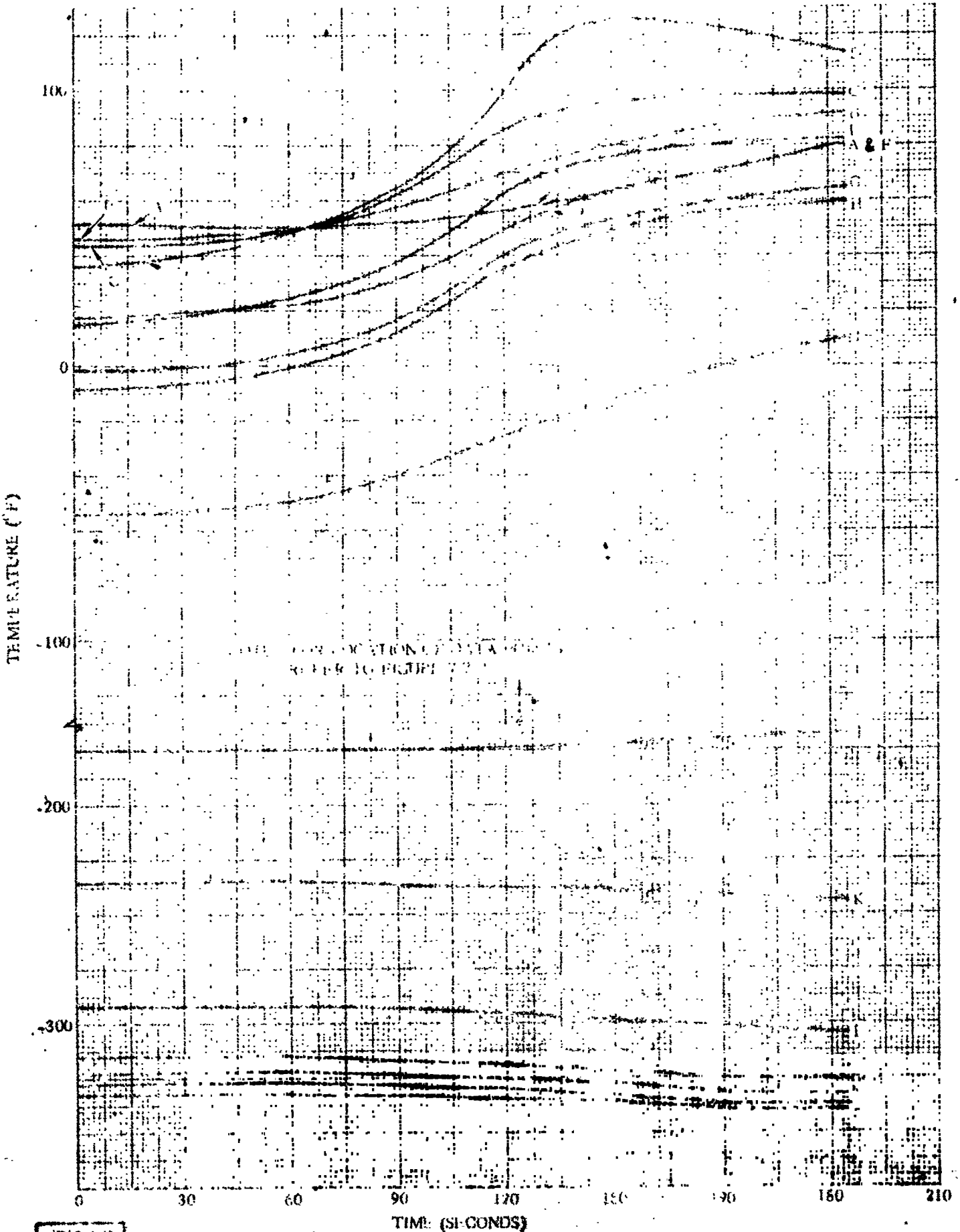

Figure 7.7-4. Forward Umbilical Panel Temperature History

7.7.4 INERTIA LOADS. Load factors for the umbilical panel at launch and during flight are presented in Table 7.7-1.

TABLE 7.7-1. FORWARD UMBILICAL ISLAND INERTIA LOADS

Condition	Max Longitudinal Inertia (g's)		Max Lateral Inertia (g's)	
	Longitudinal	Associated Lateral	Associated Longitudinal	Lateral
*Launch	-1.4 +4.2	±0.3	+1.4	±4.5
Mach 1	+2.0 +4.2	±0.2† +2.4‡	+2.0	±6.0† ±8.4‡
Max q	+2.3 +4.2	±0.3† ±0.9‡	+2.3	±2.5† ±3.9‡
BECO	+8.0	±1.0	+5.8 ±0.1	±2.4
Centaur MES	+1.0 ±4.2	±0.5	+1.0	±4.5
Centaur MECO	+6.5 ±4.2	±0.5	+6.5	±4.5

*Disconnect loads shall be superimposed for this condition.
†Tangential
‡Radial

7.7.5 STEADY-STATE AIR LOADS. The maximum differential crush and burst pressures are plotted against Mach number in Figure 7.7-5.

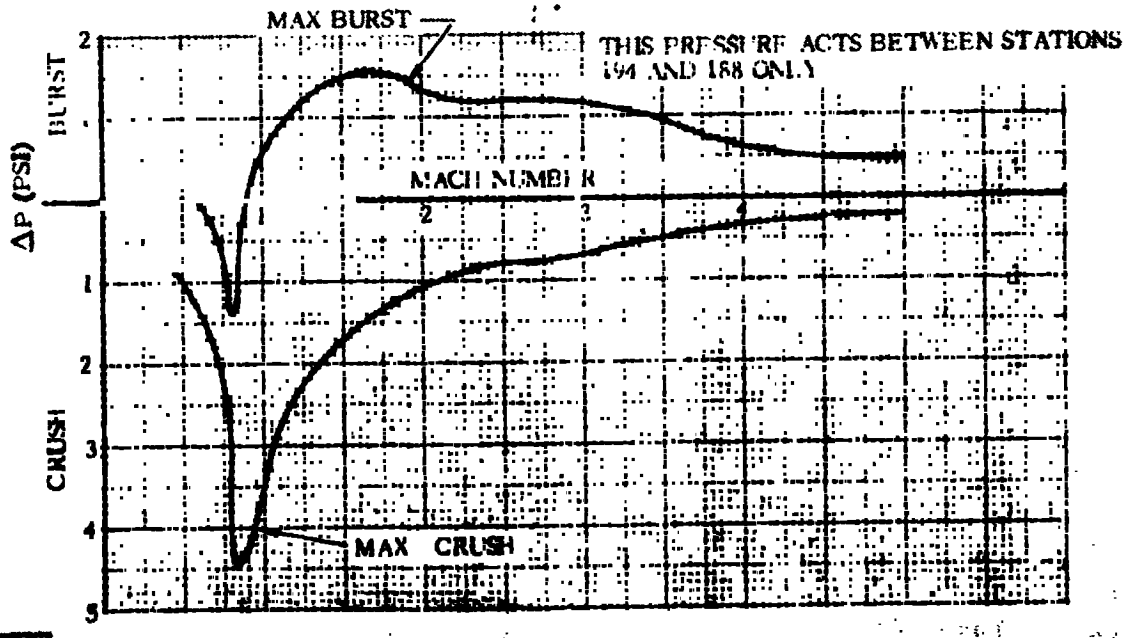

4B192LV

Figure 7.7-5. Forward Umbilical Island Differential Pressure

7.7.6 BUFFET AND FLUTTER LOADS. The forward umbilical panel does not receive critical loads due to buffet or fluctuating pressure.

7.7.7 MISCELLANEOUS LOAD PARAMETERS. Disconnect loads are shown in Figure 7.7-6. These act simulataneously with inertia loads at launch presented in Table 7.7-1.

SIGN CONVENTION - LOADS APPLIED TO EACH CONNECTOR* AT AIRBORNE - GSE INTERFACE

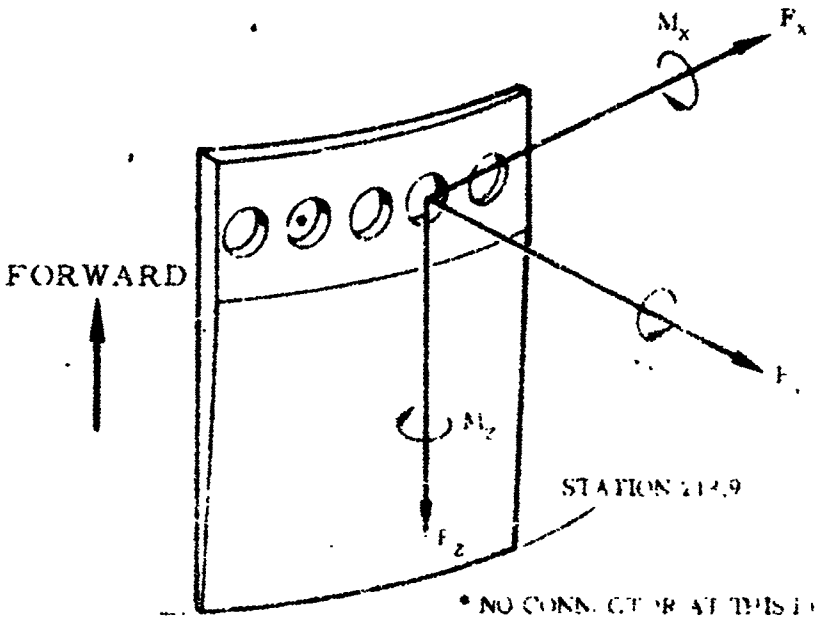

* NO CONNECTOR AT THIS LOCATION

POSITIVE FORCES AND MOMENTS ARE AS SHOWN

F_x = FORCE TANGENTIAL TO MISSILE SKIN

F_y = FORCE NORMAL TO MISSILE SKIN

F_z = FORCE IN LONGITUDINAL DIRECTION

LOAD ON EACH CONNECTOR

	LOADS JUST PRIOR TO DISCONNECT	MAXIMUM DISCONNECT LOADS
F_x	10 LB	±10 LB
F_y	+20 LB **	-390 LB ***
F_z	+50 LB	+50 LB
M_x	+140 IN.-LB	+140 IN.-LB
M_y	± 50 IN.-LB	± 50 IN.-LB
M_z	60 IN.-LB	± 60 IN.-LB

** THIS INCLUDES WEIGHT AND WIND ONLY. A LANYARD LOAD OF 45 LB PER PLUG ALSO ACTS IN THE $+F_y$ DIRECTION AND SHOULD BE ADDED TO IT.

*** THIS LOAD IS SUDDENLY APPLIED, THEREFORE IT SHOULD BE MULTIPLIED BY AN IMPACT FACTOR OF 2.0 PROVIDING THE UMBILICAL ISLAND AND SUPPORT STRUCTURE REMAIN ELASTIC. SHOULD THE STRUCTURE YIELD, THE IMPACT FACTOR IS REDUCED AND NOTED IN APPLICABLE STRESS ANALYSIS.

4B193LV

Figure 7.7-6. Forward Umbilical Island - Disconnect Loads

7.8 GROUND PLANE AND ANTENNA

The ground plane attaches to the forward umbilical panel at Station 188 and is centered on the X-X axis. It is also supported by two struts which extend out from the forward bulkhead as shown in Figure 7.8.1.

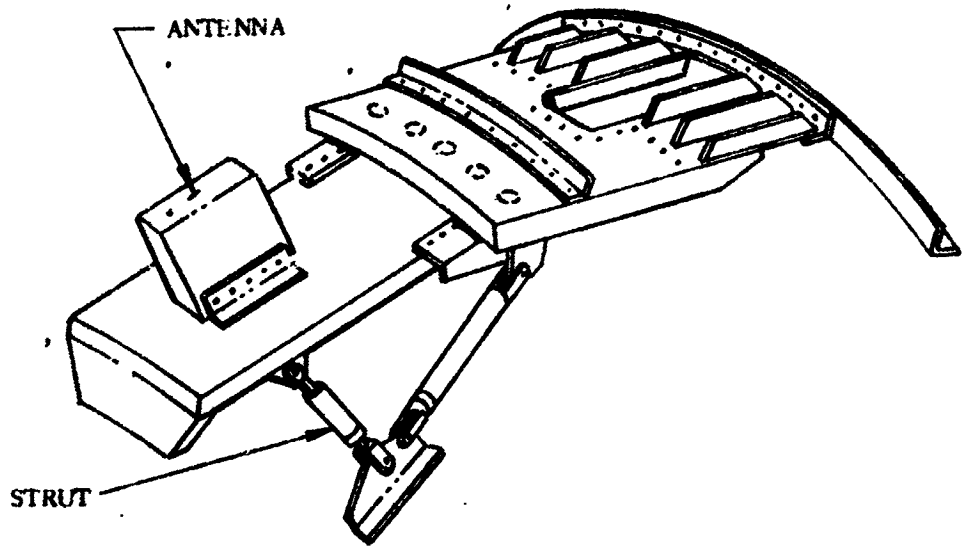

4B194LV

Figure 7.8-1. Ground Plane and Antenna

7.8.1 CRITICAL CONDITIONS. The critical loading conditions for the ground plane and antenna occur at BECO and Centaur MECO. The only significant loads applied are inertia loads.

7.8.2 WEIGHTS AND CENTER OF GRAVITY DATA. The total weight of the ground plane, antenna and strut is 11.3 pounds. The location of the C.G. is shown in Figure 7.8-2.

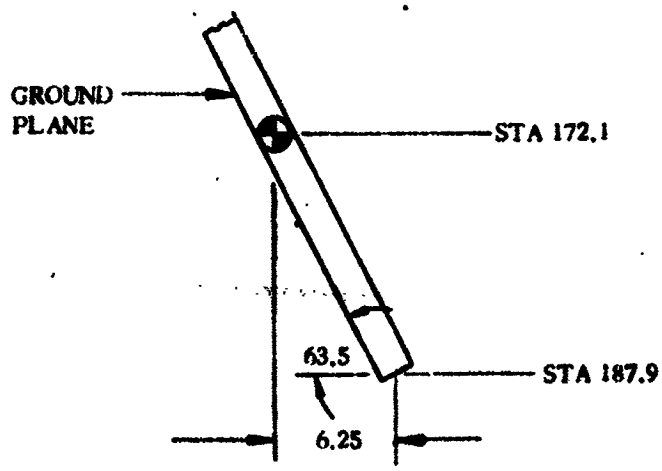

4B195LV

C.G. LOCATION

Figure 7.8-2. Ground Plane and Antenna Center of Gravity Location

7.8.3 THERMAL DATA. Temperatures are not critical for the ground plane and antenna.

7.8.4 INERTIA LOADS. Inertia loads for the ground plane and antenna are presented in Table 7.8-1.

TABLE 7.8-1. GROUND PLANE AND ANTENNA - INERTIA LOAD FACTORS

Condition	Nominal Time (Sec) (Approx)	Maximum Longitudinal (g's)		Maximum Lateral (g's)	
		Longitudinal	Associated Lateral	Associated Longitudinal	Lateral
Prelaunch	0	+1.0 +6.9	0	+1.0	±6.0
Thrust Buildup	0	+1.0 -6.0	±0.12	1.0	-6.0
Launch	0	+1.4 ±6.0	±0.4	+1.4	-6.3
Mach 1	40-65	+2.0 -5.0	±0.5	+2.0 ±0.54	±6.5
Max q	70-85	+2.3 -6.0	±1.0	+2.3 ±0.21	±7.0
Max Slosh	120.	-1.0 +3.0	±0.3	1.0	±3.3
BECO	+18	-5.8 +3.0	±0.3	-5.8	±3.3
Sustainer Flight	200	+1.5 -1.5	0	1.0	±2.0
Sustainer Cutoff	250	2.0 +1.0	±0.3	2.0	±1.8
Centaur 1st MES	-	+1.2 -6.0	±0.5	+1.2	-6.5
Centaur Flight	-	+3.0 -6.0	±0.5	+3.0	±6.5
Centaur 2nd MECO	-	+6.3 -6.0	0	6.0	±6.0

7.8.5 STEADY-STATE AIR LOADS. The ground plane and antenna do not receive critical loads due to aerodynamic forces.

7.8.6 BUFFET AND FLUTTER LOADS. The ground plane and antenna do not receive critical loads due to buffet or fluctuating pressure.

7.8.7 MISCELLANEOUS LOAD PARAMETERS. No other critical loads are applied to the ground plane and antenna.

7.9 FORWARD UMBILICAL ISLAND BULKHEAD

The forward umbilical island bulkhead is located on the X-X axis between Quadrants I and II at Station 218.9. This bulkhead supports the cabling that extend along the side of Centaur and is shown in Figure 7.9-1.

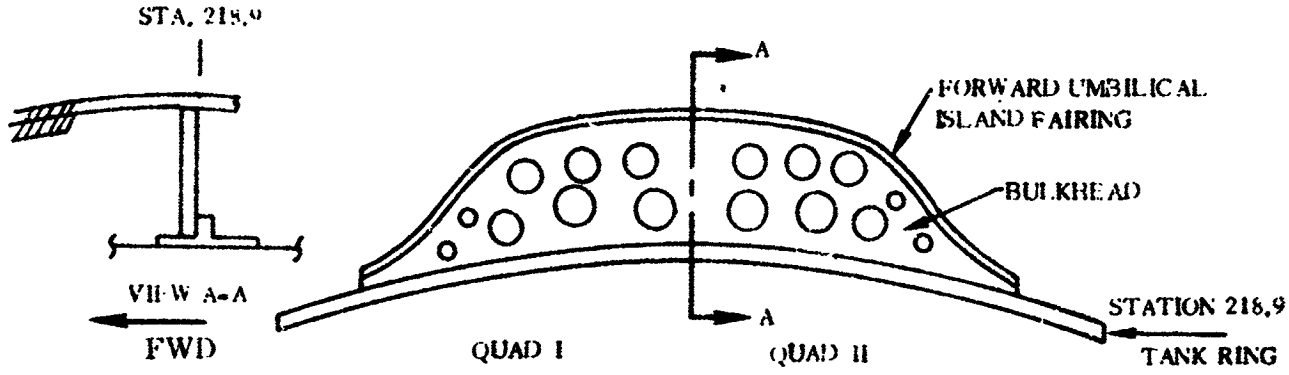

Figure 7.9-1. Forward Umbilical Island Bulkhead

7.9.1 CRITICAL CONDITIONS. The critical loading condition on the forward umbilical island bulkhead occurs during transonic flight when differential pressure across the bulkhead is a maximum. Buffet loads along with the respective plug and receptacle inertia loads act simultaneously with maximum steady-state differential pressure to create the maximum loading condition.

7.9.2 WEIGHTS AND CENTER OF GRAVITY DATA. The weight of the forward umbilical island bulkhead is small and does not impose critical loads on the structure, however the concentration of disconnect plugs, receptacle and associated cable weights must be considered for analysis of the bulkhead itself

A typical plug and receptacle combination at the forward umbilical island bulkhead interface weighs approximately 0.5 pounds. The length of cable, which is assumed reacted at the bulkhead, is estimated at approximately 1.0 pounds. Therefore, for purposes of analysis, the following weight criterion is applicable.

	Weight per each cutout in Bulkhead (pounds)
Plug and Receptacle Combination	0.5
Length of Cable	1.0
Total	1.5

The center of gravity of each weight concentration is placed directly at the midpoint of the bulkhead and at the centerline of each of the bulkhead cutouts.

7.9.3 THERMAL DATA. Temperatures are not critical for the forward umbilical island bulkhead.

7.9.4 INERTIA LOADS. The inertia loads applicable to the plugs, receptacles, and cables which are attached to the umbilical island bulkhead are presented in Table 7.10-1.

7.9.5 STEADY-STATE AIR LOADS. The steady state differential pressure across the forward umbilical island bulkhead is plotted versus Mach number in Figure 7.9-2. This acts simultaneously with buffet loads as presented in Paragraph 7.9.6.

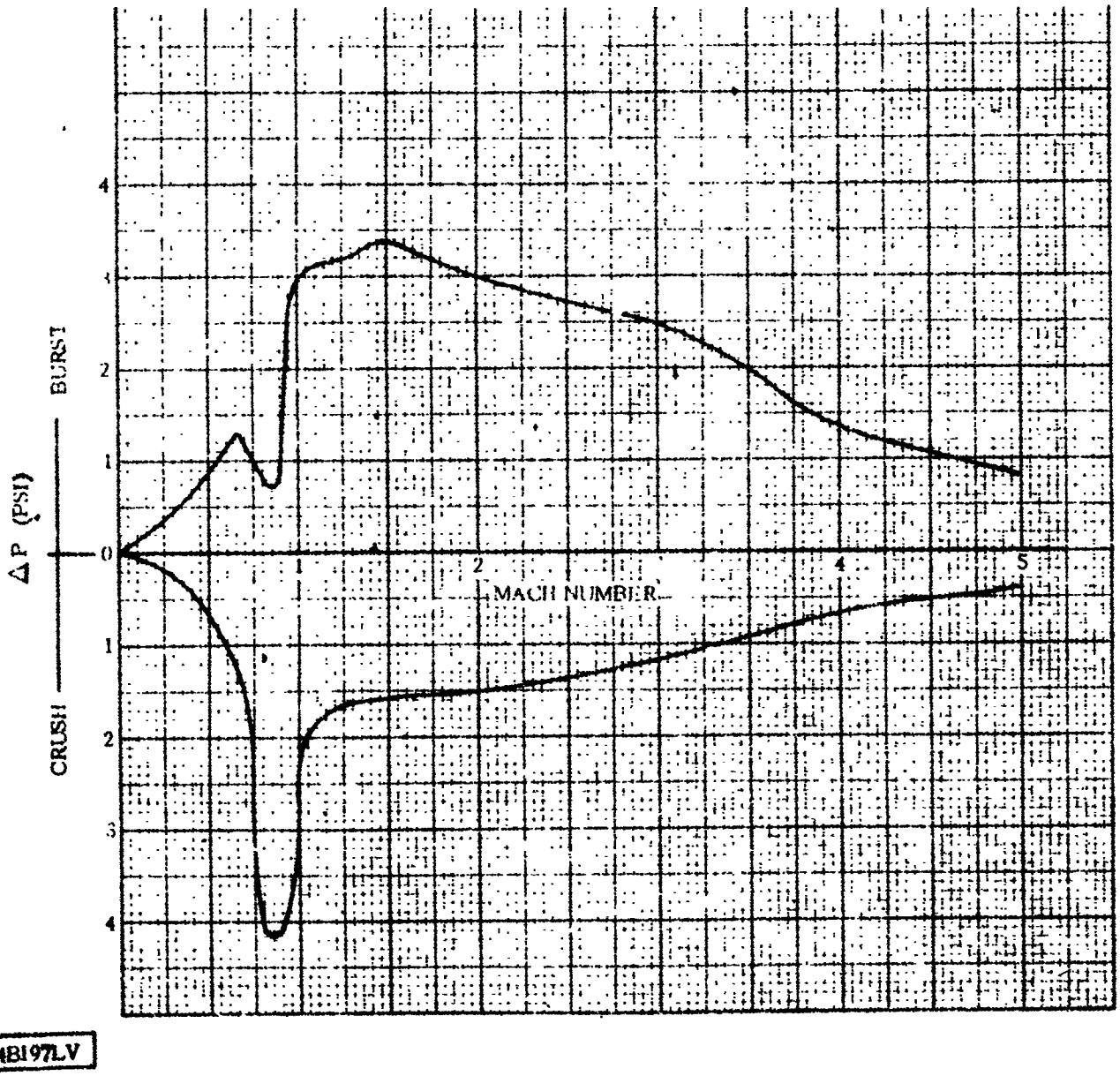

Figure 7.9-2. Forward Umbilical Island Bulkhead - Differential Pressure

7.9.6 BUFFET AND FLUTTER LOADS. For design and stress analysis of the forward umbilical island bulkhead, an equivalent static pressure is used to represent buffet loads. Equivalent static pressures are presented in Table 7.9-1. Data presented in Table 7.9-1 and Figure 7.9-2 shall be combined for the applicable Mach range.

TABLE 7.9-1. FORWARD UMBILICAL ISLAND BULKHEAD - EQUIVALENT STATIC PRESSURE

Mach Number	Equivalent Static Pressure
0-0.75	±0.50 psi
0.75-0.85	±2.40 psi
0.85 and higher	±0.50 psi

7.9.7 MISCELLANEOUS LOAD PARAMETERS. No other loads need be considered in the design of the forward umbilical island bulkhead.

THIS PAGE INTENTIONALLY LEFT BLANK.

7.10 FORWARD UMBILICAL ISLAND FAIRING

The forward umbilical island fairing provides a smooth aerodynamic ramp in front of the wiring tunnel which runs along the X-X axis between Quadrants I and II. The configuration of the fairing is shown in Figure 7.10-1.

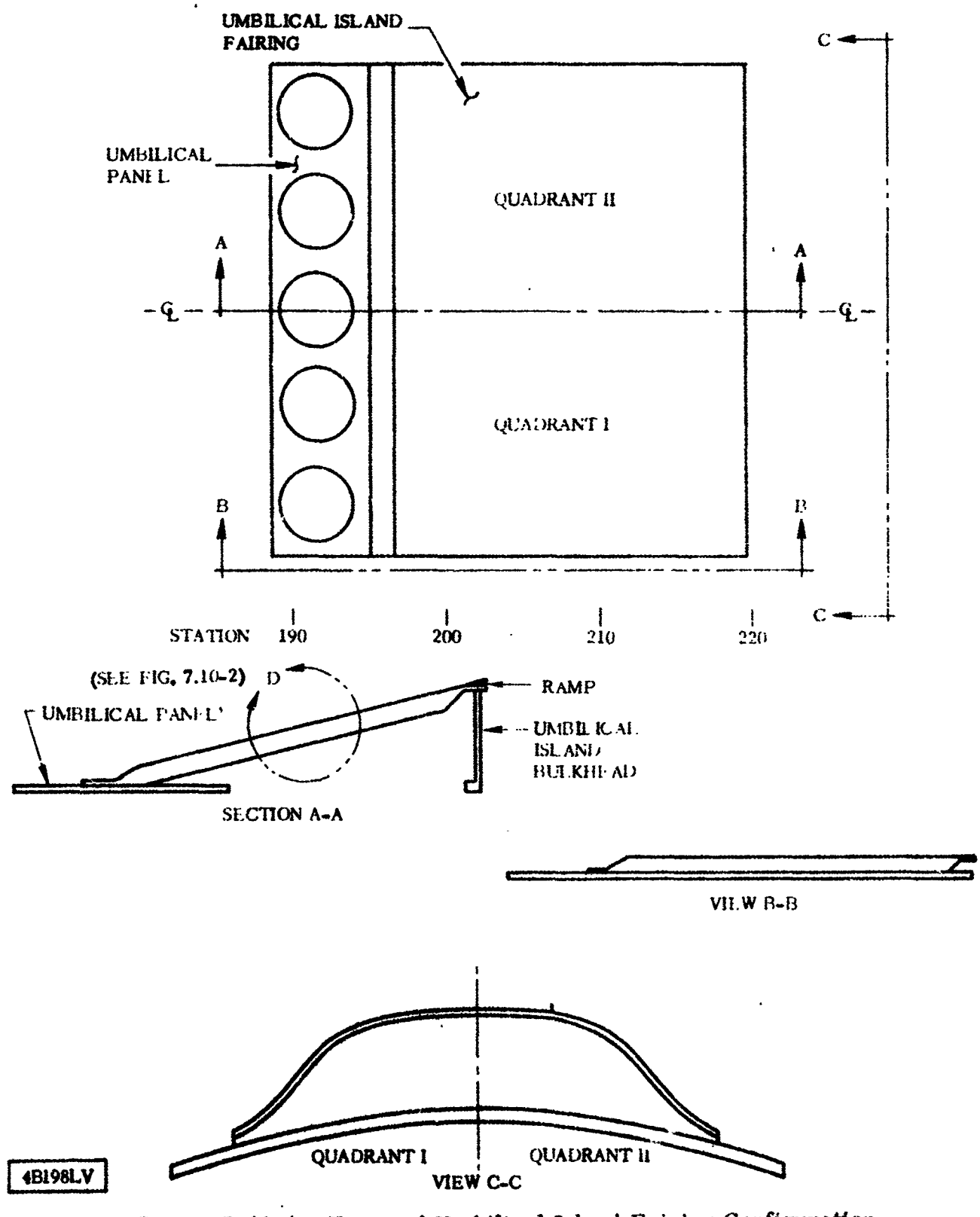

Figure 7.10-1. Forward Umbilical Island Fairing Configuration

7.10.1 CRITICAL CONDITIONS. Critical loads on the forward umbilical island fairing are those due to steady-state air loads, buffet, and inertia. Maximum air loads occur during transonic flight, while inertia loads are highest at BECO and Centaur MECO. Maximum temperatures on the fairing coincide with high inertia loads at BECO.

7.10.2 WEIGHT AND CENTER OF GRAVITY DATA. The umbilical island fairing weighs 14.5 pounds. The C.G. is on the X-X axis at Station 208 on the inside surface of the fairing.

7.10.3 THERMAL DATA. Temperature histories for several data points on the forward umbilical island fairing, as shown in Figure 7.10-2, are plotted in Figure 7.10-3.

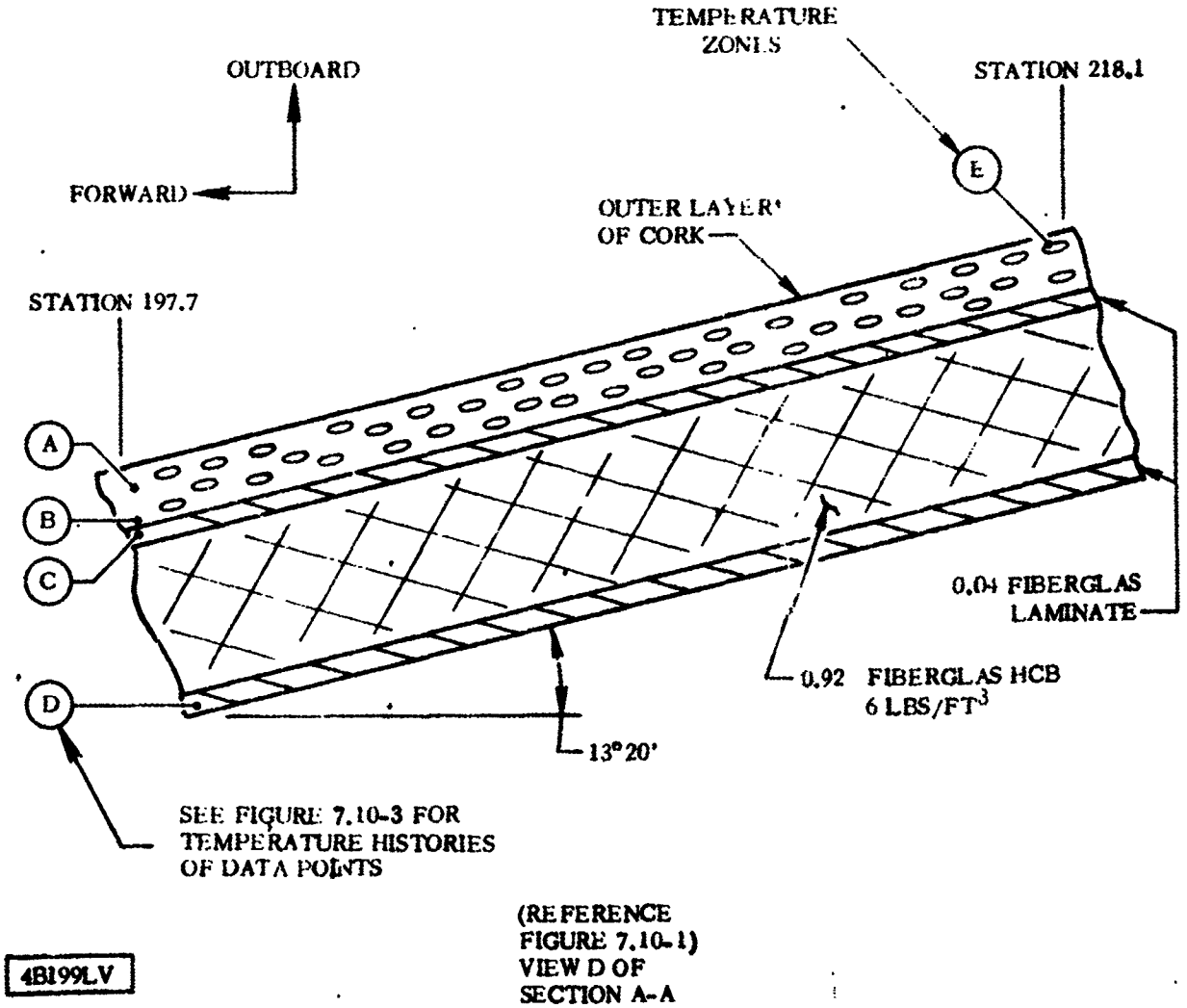

Figure 7.10-2. Forward Umbilical Island Fairing - Temperature Profile at Point of Maximum Heating on Fairing.

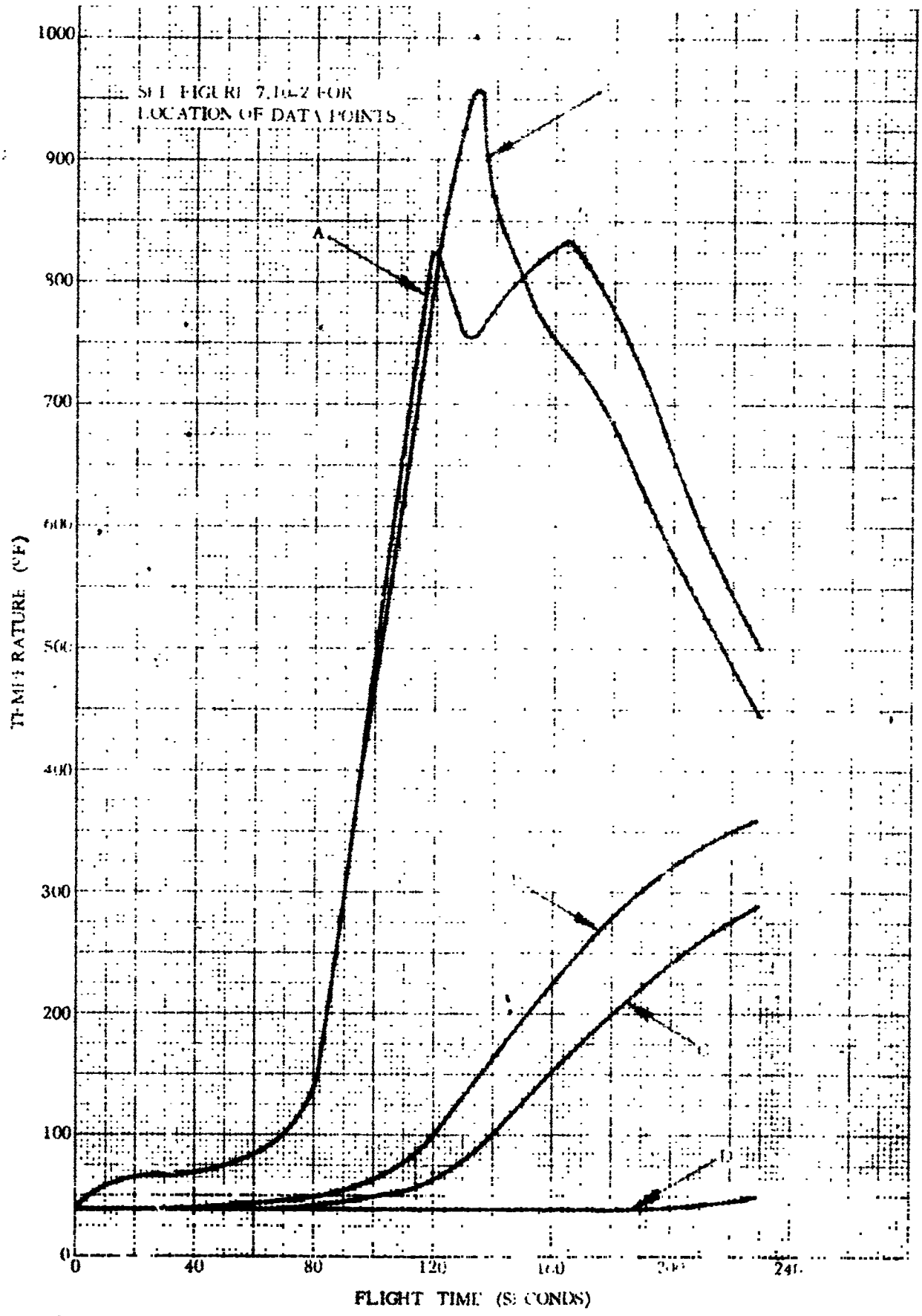

4B200LV

Figure 7.10-3. Forward Umbilical Island Fairing Temperature Histories

7.10.4 INERTIA LOADS. The inertia loads for the umbilical island fairing are presented in Table 7.10-1.

TABLE 7.10-1. FORWARD UMBILICAL ISLAND FAIRING - INERTIA LOAD FACTORS

Condition	Maximum Longitudinal Inertia (g's)		Maximum Lateral Inertia (g's)	
	Longitudinal	Associated Lateral	Associated Longitudinal	Lateral
Prelaunch	-1.0 ±0.1	±0.02	1.0	±0.12
Thrust Buildup	-1.0 ±4.2	±0.12	±1.0	±4.32
Launch	-1.4 ±4.2	±0.3	±1.1	±4.5
Mach 1	-2.0 ±4.2	±0.2†	-2.6	±6.0†
		±1.4‡		±7.4‡
Max q	-2.3 ±4.2	±0.3†	2.3	±2.5†
		±0.9‡		±3.6‡
Max Slosh	6.1	±0.5	±1.0	±2.4
BECO	-8.0	±1.0	-5.5 ±0.1	±2.4
Sustainer Flight	-2.6	0.5	-1.5	±1.6
Sustainer Cutoff	-3.1	±0.5	-2.0	±1.4
Centaur 1st MES	+1.0 ±4.2	±0.5	-1.0	±4.5
Centaur Flight	+5.1	±0.5	-4.0	±1.6
Centaur 2nd MECO	-6.5 ±4.2	±0.5	-6.1	±4.5

†Tangential
‡Radial

7.10.5 STEADY-STATE AIR LOADS. Steady-state differential pressure on the fairing is shown in Figures 7.10-4 and 7.10-5. Side loads on the fairing are presented in Figure 7.10-6. Drag loads are given in Figures 7.10-7 and 7.10-8 and should be applied at the centroid of the fairing cross-sectional area. It should be noted that the fairing axial load should be combined with the radial component of wall differential pressures in determining loads on umbilical island attachments.

It is recommended that the loads information presented in Figures 7.10-4 through 7.10-8 be combined in the most conservative manner in the stress analysis. For example, radial bursting load and fairing drag load add in producing moment about the umbilical panel base (Station 218.9). Maximum drag load should be used with the radial component of bursting load in this case, and minimum drag should be used with the radial crushing load to obtain maximum moment about Station 218.9 in the opposite direction.

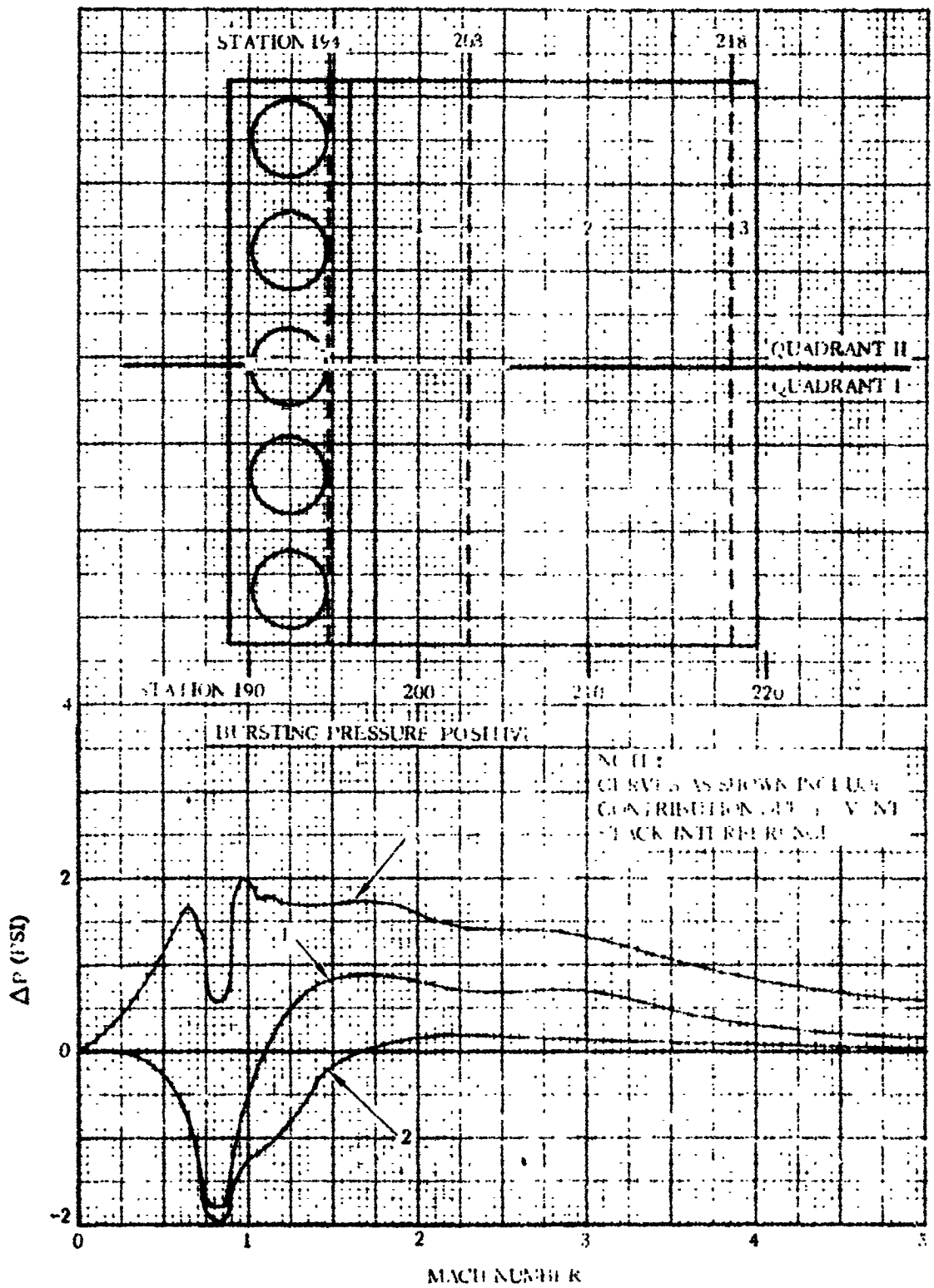

4B201LV

Figure 7.10-4. Forward Umbilical Island Fairing Bursting Wall Differential Pressure

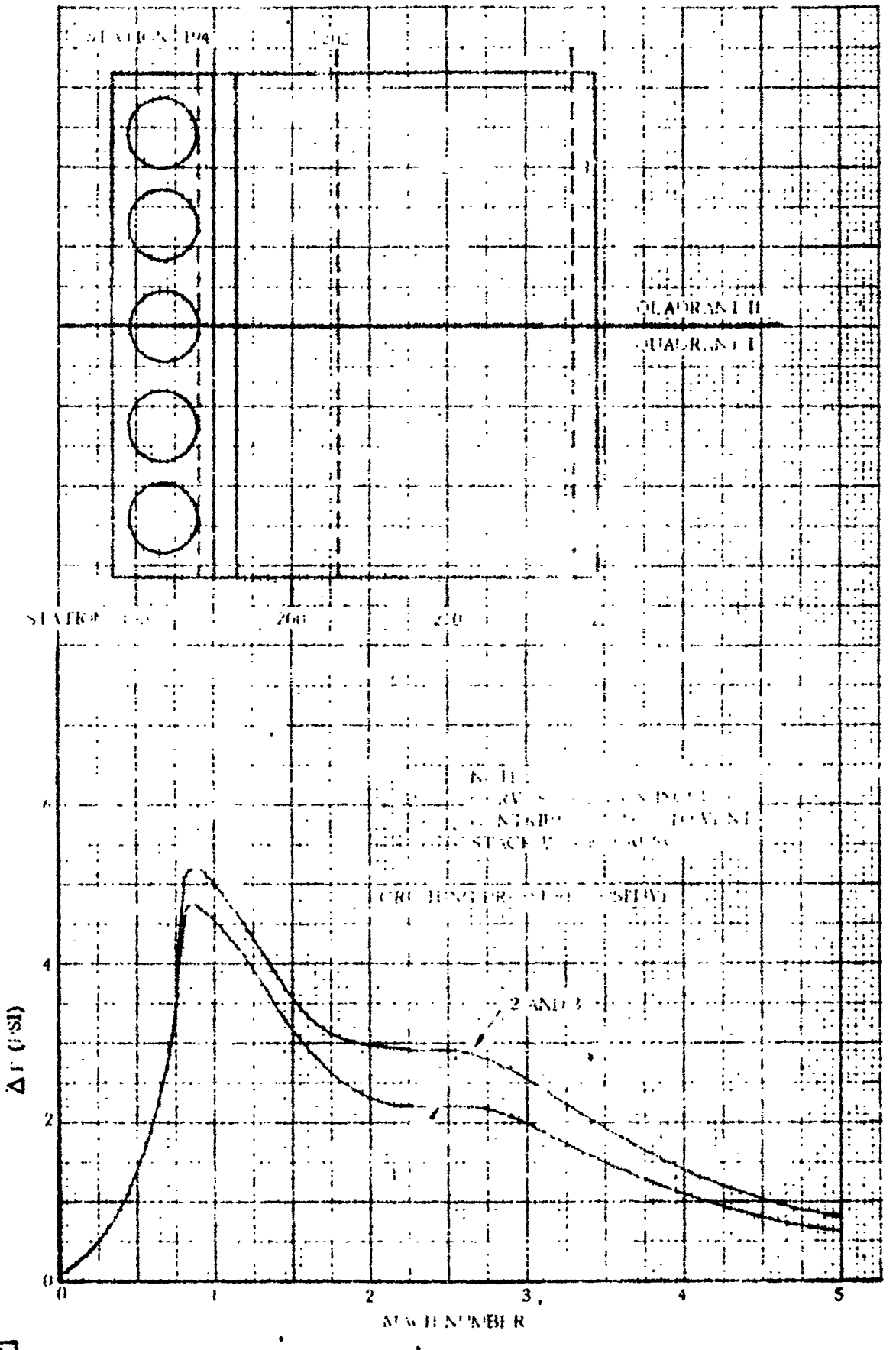

4B2021.V

Figure 7.10-5. Forward Umbilical Island Fairing Crushing Wall Differential Pressure

NOTE:

TO OBTAIN MAXIMUM LOCAL [illegible] MULTIPLY [illegible] LOCAL SIDE LOAD BY LOCAL FAIRING [illegible] TO FIGURE 7.10-4 [illegible] VALUES [illegible] ABOARD SIDE OF THE FAIRING AND [illegible] PRESSURE ON THE LEE SIDE. THIS SIDE LOAD [illegible] CHANGE THE MAGNITUDE OF THE BURSTING OR CRUSHING LOAD, [illegible] MOVES THE CENTER OF PRESSURE.

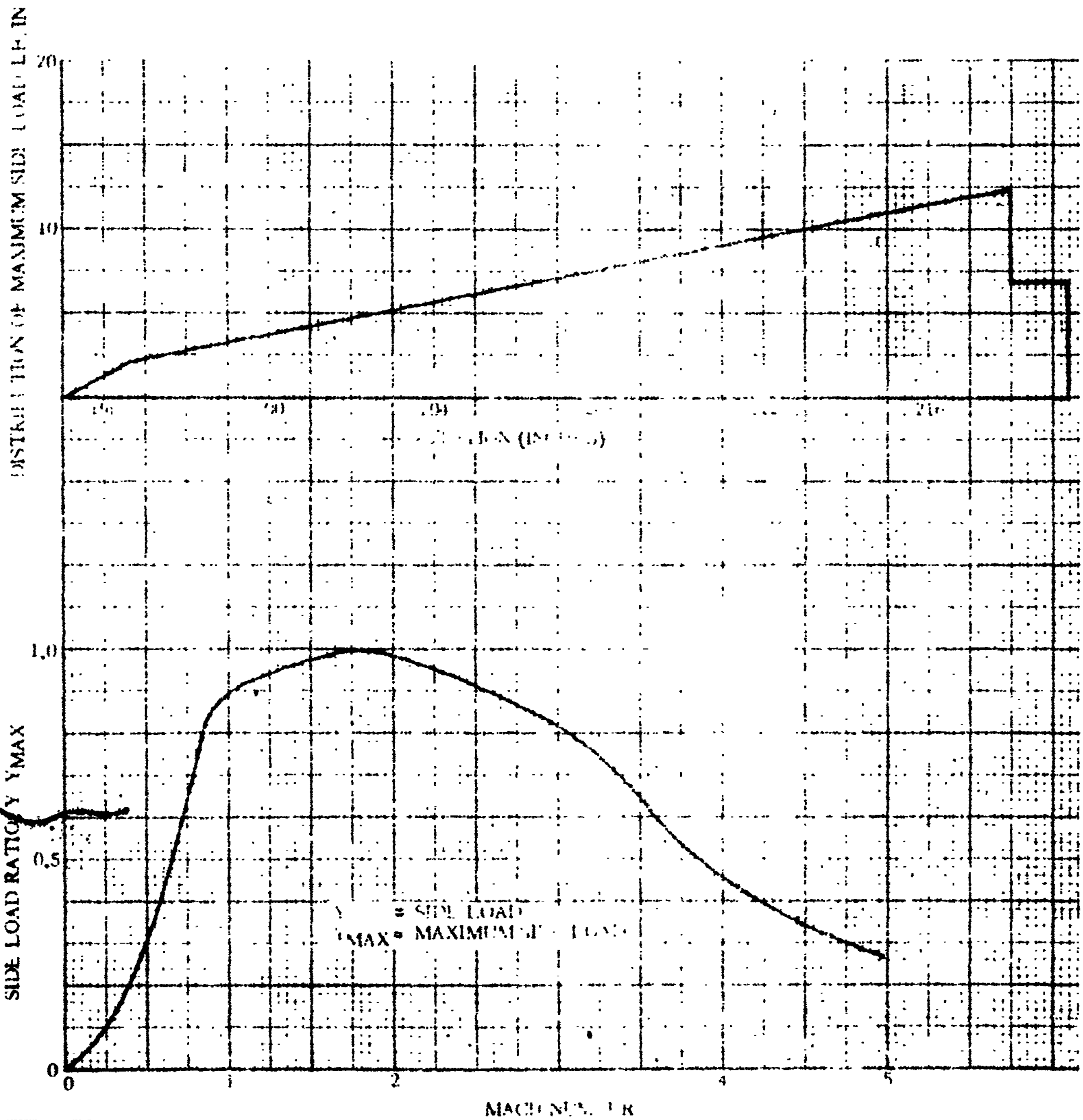

4B203LV

Figure 7.10-6. Forward Umbilical Island Fairing Distribution of Aerodynamic Side Load

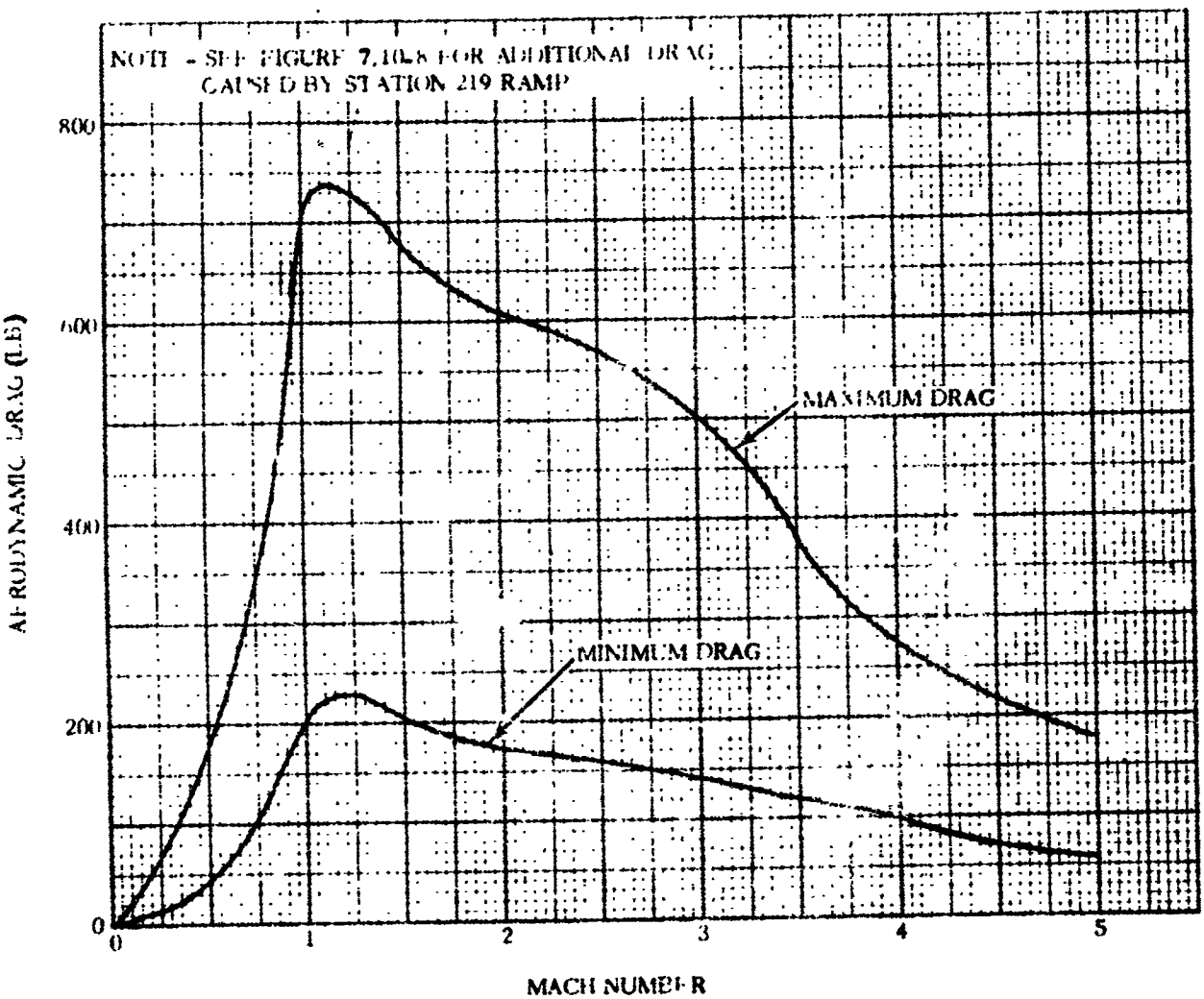

4B2041.V

Figure 7.10-7. Forward Umbilical Island Fairing Variation of Aerodynamic Drag with Mach Number (Not including Station 219 Ramp)

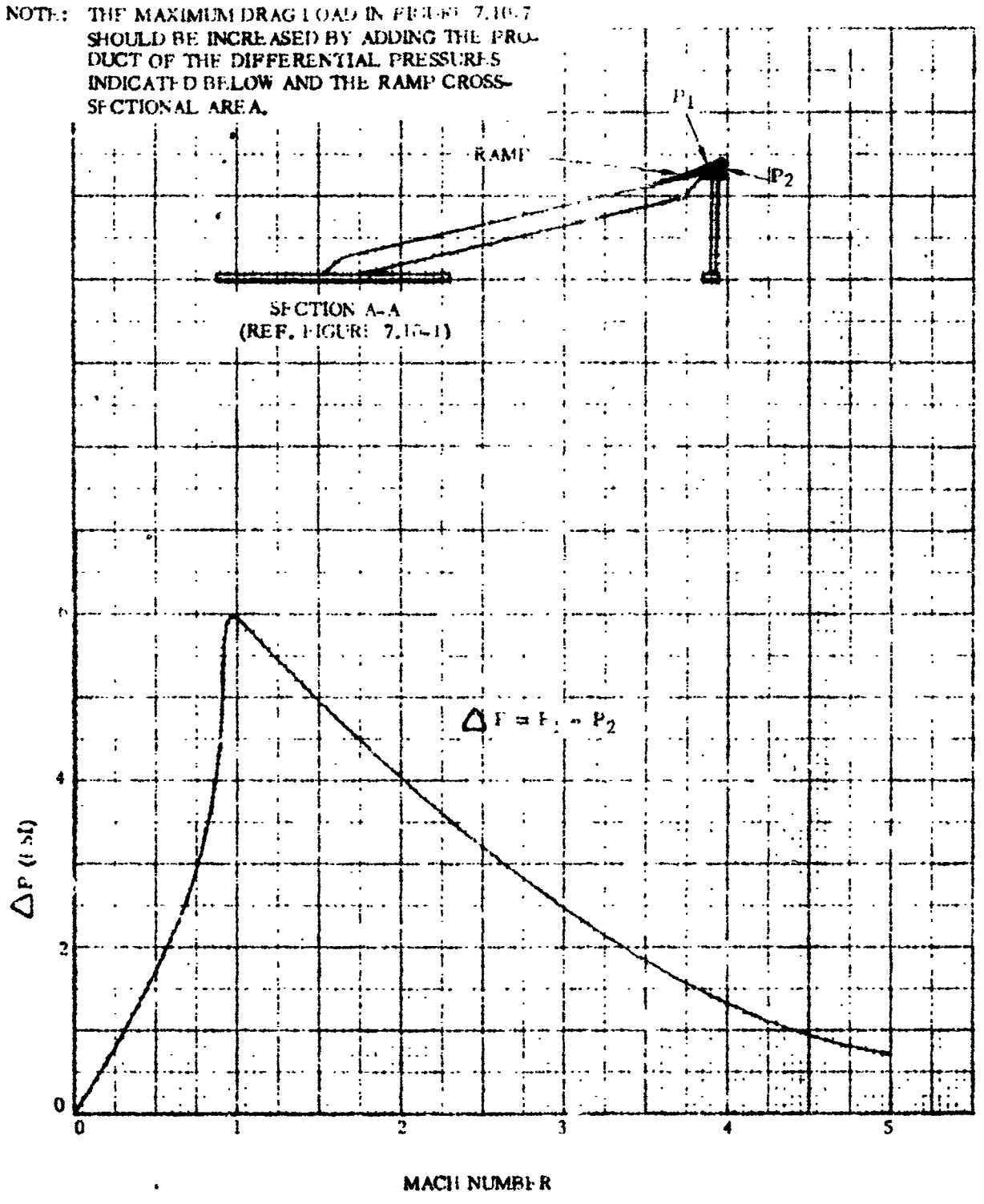

4B205L.V

Figure 7.10-8. Forward Umbilical Island Fairing Differential Pressure across the Ramp Located at Station 219

7.10.6 BUFFET AND FLUTTER LOADS. An equivalent static pressure is used to represent the buffet loads. The buffet loads vary with Mach number and are listed in Table 7.10-2.

TABLE 7.10-2. FORWARD UMBILICAL ISLAND FAIRING - EQUIVALENT STATIC PRESSURE

Mach Number	Equivalent Static Pressure
0-0.75	±0.50 psi
0.75-0.85	±1.1 psi
0.85 and higher	±0.50 psi

7.10.7 MISSCELLANEOUS LOAD PARAMETERS. No other critical loads are applied to the forward umbilical island fairing.

7.11 CHRISTMAS TREE FUEL SENSOR

The Christmas Tree fuel sensor installation consists of a network of aluminum struts within the LH_2 tank which support instruments for measuring fuel location during a two-burn mission. The location of the struts is shown in Figure 7.11-1. The joint at the end of each strut consists of a bolted clevis as shown in Figure 7.11-2.

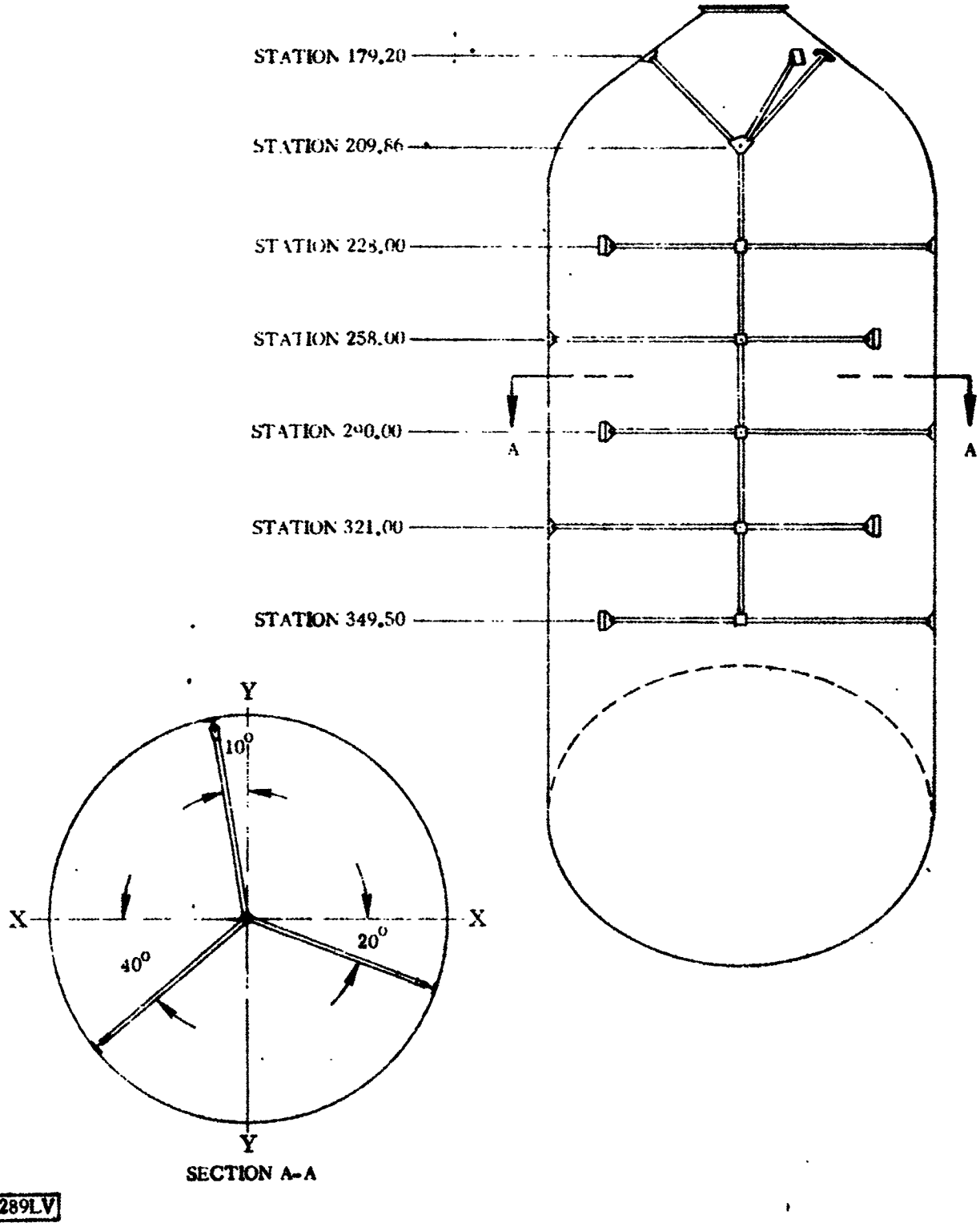

Figure 7.11-1. Christmas Tree Fuel Sensor Strut Configuration

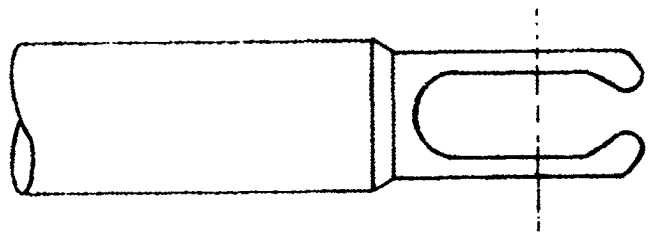

4B2961 V

Figure 7.11-2. Christmas Tree Strut Clevis Configuration

7.11.1 CRITICAL CONDITIONS. The only critical loading condition imposed on the Christmas Tree installation is inertia loads, mainly caused by vibration of the structure. All other loads on the structure are negligible.

7.11.2 WEIGHTS AND CENTER OF GRAVITY DATA. The weights presented in Table 7.11-1 shall be used for structural design and analysis.

TABLE 7.11-1. CHRISTMAS TREE COMPONENT WEIGHTS

Item	Weight (lb)
Total Christmas Tree Structure	12.15
Total Sensors plus Harnesses	6.50
Total Harness Clamps	3.06
Vertical Strut	1.84
Top Strut (each)	0.40
Heaviest Horizontal Strut	0.64 or 0.1067 lb/in.
55-11976-3 Vapor Sensor	0.13
55-01278-101 Temperature Transducer	0.01
Harness per Horizontal Strut	0.002 lb/in.

7.11.3 THERMAL DATA. The temperature of the structure is at -423° F when wetted by the liquid hydrogen.

7.11.4 INERTIA LOADS. The inertia loads for the Christmas Tree as a complete unit are presented in Table 7.11-2. The inertia loads on each strut are given in Table 7.11-3.

TABLE 7.11-2. CHRISTMAS TREE AS A COMPLETE UNIT - INERTIA LOAD FACTORS

Time of Flight	Longitudinal (g's)	Associated Lateral (g's)
Launch	1.5 ±24.0	±1.0
	1.5	±25.0
Transonic - Max q	2.3 ±21.0	±1.0
	2.3	±25.0
BECO	5.5 ±12.0	±1.0
Centaur 2nd MES	3.0 ±13.0	±1.0
MECO	9.0 ±12.9	±1.0
	9.0	±13.0

TABLE 7.11-3. CHRISTMAS TREE STRUTS AND ATTACHMENTS - INERTIA LOAD FACTORS

Time of Flight	Longitudinal (g's)	Associated Lateral (g's)
Launch	1.5 ±27.0	±1
	1.5	± 27.0
Transonic - Max q	2.3 ±27.0	±1
	2.3	±27.0
MECO	9.0 ± 12.0	±1.0
	9.0	±13.0

NOTE:
All vibratory (±) inertia loads act normal to the strut and parabolically distributed to zero at the ends.

7.11.5 STEADY-STATE AIR LOADS. The Christmas Tree fuel sensor installation does not receive critical loads due to aerodynamic forces.

7.11.6 BUFFET AND FLUTTER LOADS. The Christmas Tree fuel sensor installation does not receive critical loads due to buffet or fluctuating pressures.

7.11.7 MISCELLANEOUS LOAD PARAMETERS. No other loads on the Christmas Tree fuel sensor installation are critical.

7.12 LIQUID HYDROGEN ZERO - G BAFFLE

The zero-g baffle is a device used on two-burn mission vehicles (only) to damp out sloshing in the LH_2 tank during the coast phase of fight. The baffle consists of a ring attached to the cylindrical portion of the LH_2 tank at Station 333.30. The configuration of the Baffle is shown in Figure 7.12-1.

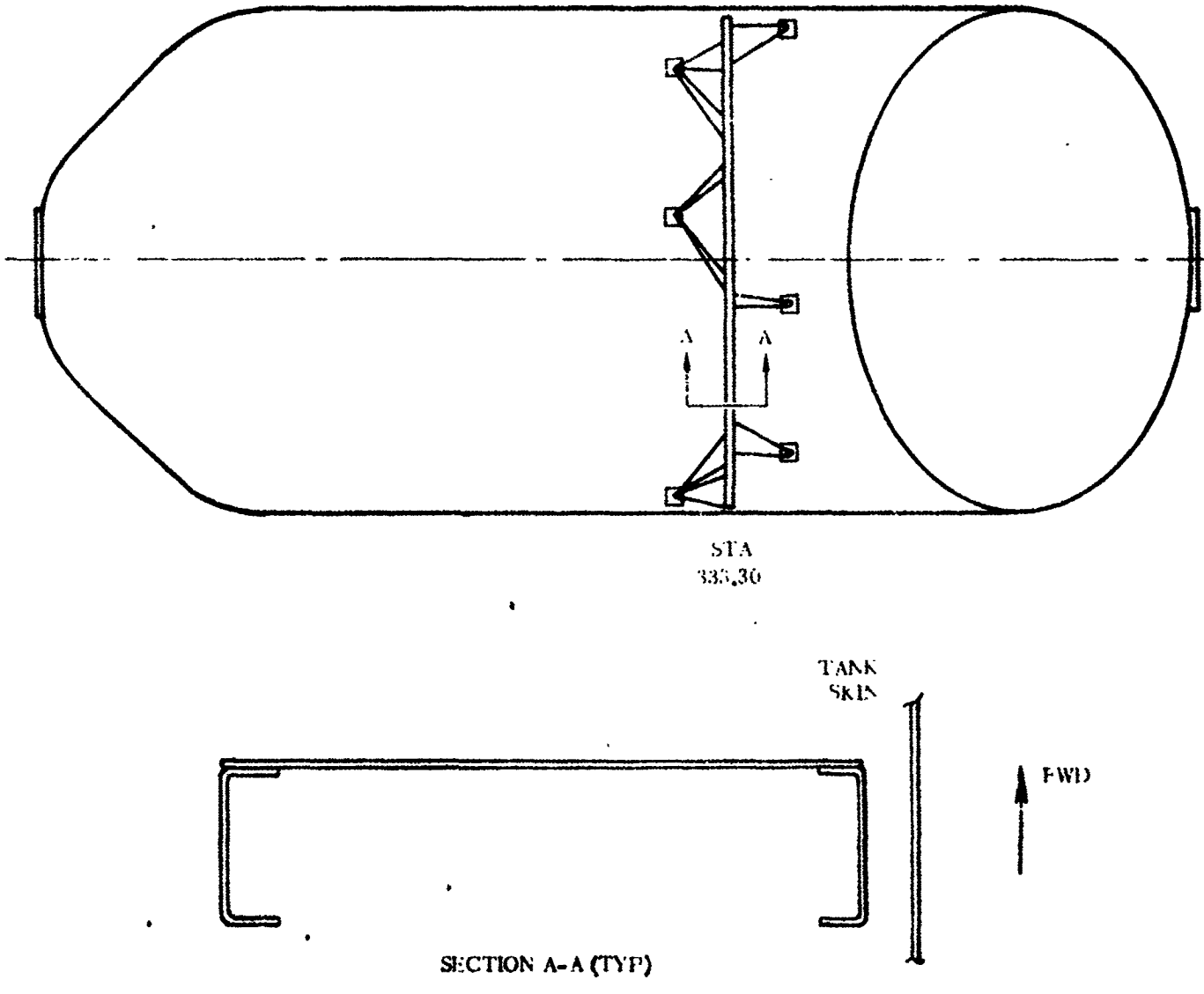

4B29ILV

Figure 7.12-1. Liquid Hydrogen Zero-g Baffle Configuration

7.12.1 CRITICAL CONDITIONS. The critical loads on the zero-g baffle are due to vibratory and steady-state inertia, combined with differential pressure due to fuel sloshing. In addition, a localized pressure on the baffle exists due to flow from the volute bleed line impinging on the structure.

7.12.2 WEIGHT AND CENTER OF GRAVITY DATA. The structural design weight of the entire baffle = 15.0 pounds. The C.G. is located on the Z-axis of the vehicle.

7.12.3 THERMAL DATA. The baffle and support structure is at a temperature of -423°F while immersed in the liquid hydrogen.

7.12.4 INERTIA LOADS. Inertia loads on the baffle are presented in Table 7.12-1 for all critical times during flight.

TABLE 7.12-1. LIQUID HYDROGEN ZERO-G BAFFLE INERTIA LOAD FACTORS

Event	Steady-State Inertia (G's)		Vibratory Inertia (G's)	
	Longitudinal	Lateral	Longitudinal	Lateral
Launch	+1.0	±0.1	±10.0	±2.0
Launch	+1.3	±0.3	±10.0	±2.0
Max q	2.3	±1.0	±10.0	±2.0
BECO	+3 → ±0.1	±0.3	±10.0	±2.0
Boost Phase Start	+1.5	±0.3	±10.0	±2.0
Centaur First MES	+0.9 ±0.5	±0.1	±10.0	±2.0
First MECO	+3.0 ±0.5	±0.5	±10.0	±2.0
Coast	0	0	0	0
Centaur Second MES	+3.0 ±0.5	±0.5	±10.0	±2.0
Second MECO	+7.0	±0.5	±10.0	±2.0

NOTE: These inertia loads act simultaneously with pressure loads presented in Table 7.12-2

7.12.5 STEADY-STATE AIR LOADS. The liquid hydrogen zero-g baffle does not receive critical loads due to aerodynamic forces.

7.12.6 BUFFET AND FLUTTER LOADS. The liquid hydrogen zero-g baffle does not receive critical loads due to buffet or fluctuating pressures.

7.12.7 MISCELLANEOUS LOADING PARAMETERS. In addition to the inertia loads presented in Paragraph 7.12.4, a differential pressure exists across the baffle due to fuel sloshing and flow from the volute bleed line. These differential pressures are presented in Table 7.12-2, with the method of load application shown in Figure 7.12-2.

TABLE 7.12-2. LIQUID HYDROGEN ZERO-G BAFFLE LOADS DUE TO FUEL SLOSHING AND VOLUTE BLEED LINE FLOW

Time	$(P_s)_{MAX}$ (psf)	P_{VB} (psf)	P_{SP} (psf)
Thrust Buildup	0	0	0.025
Launch	0	0	0.025
Mach 1, Max q	0	0	0.025
BECO	0	0	0.025
Boost Pump Start	0	1.6	0.025
Centaur First MES	6.0	0.85	0.37
First MECO	6.0	11.8	0.37
Coast	0.05	1.6	0.025
Centaur Second MES	6.0	0.85	0.37
Second MECO	0	0	0

NOTES: (1) These pressures act simultaneously with the inertia loads presented in Table 7.12-1.
(2) See Figure 7.12-2 for method of load application.

P_s = Pressure due to slosh
P_{VB} = Pressure due to flow from volute bleed
P_{SP} = Pressure due to fluid circumferential flow
(P_{SP} acts on anti-swirl plates)

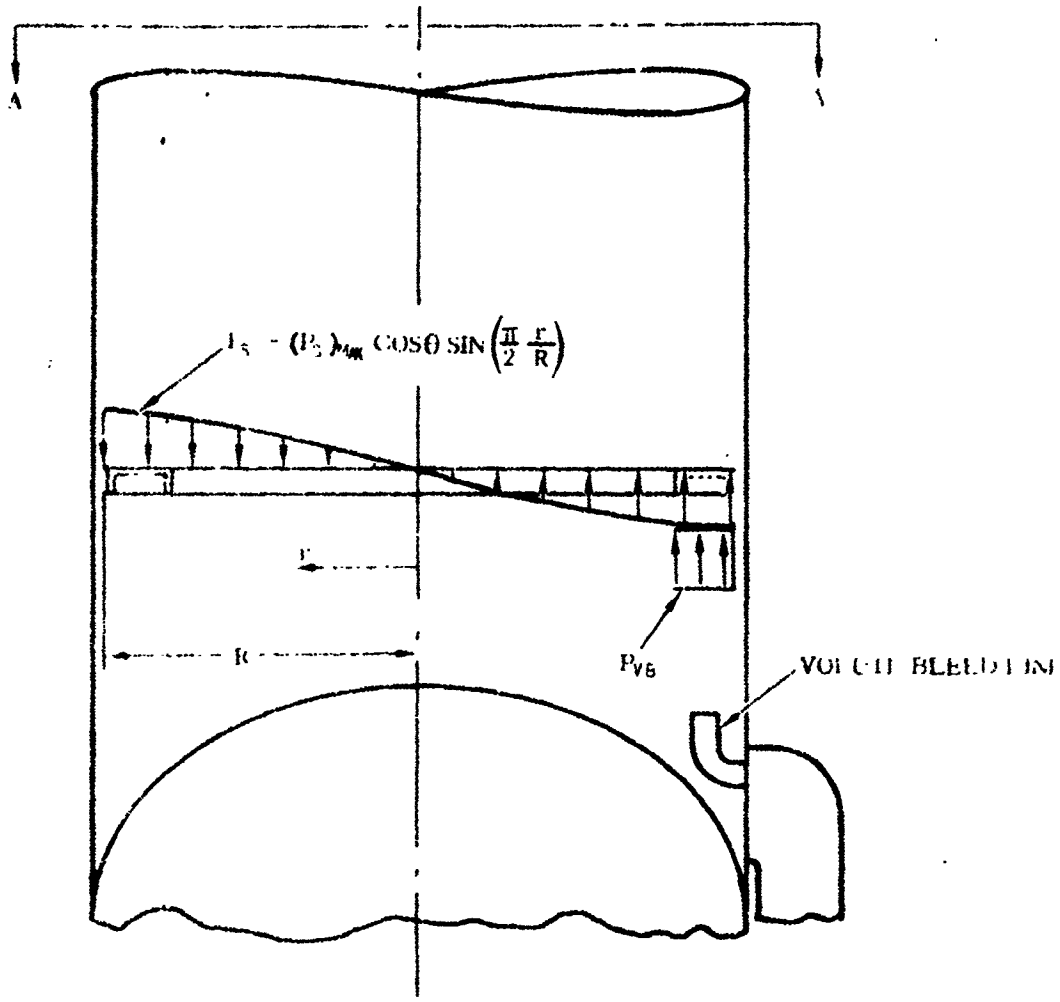

NOTES:

1. $(P_S)_{MAX}$ is the value given in Table 7.12-2
2. P_{VB} acts on the shaded portion of the baffle as shown in View A-A (uniformly distributed at the value given in Table 7.12-2)

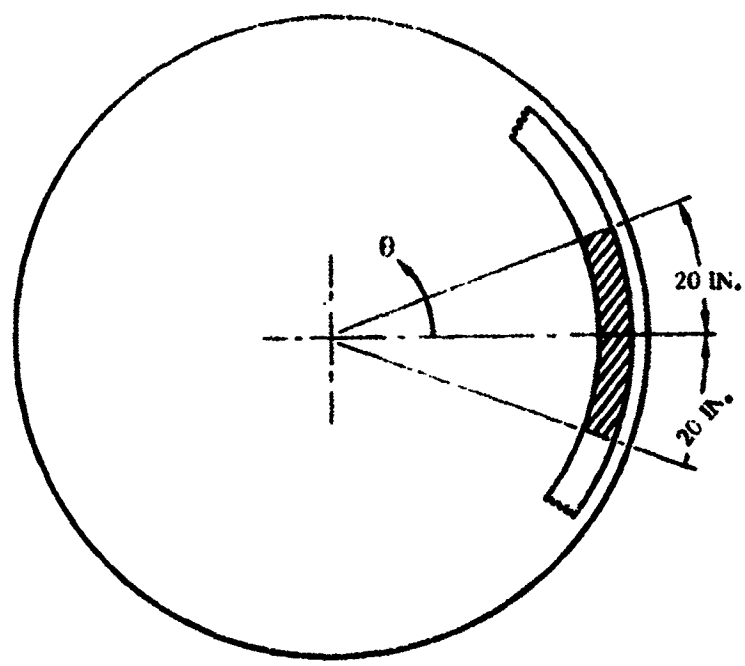

VIEW A-A

4B292LV

Figure 7.12-2. Liquid Hydrogen Zero-g Baffle Loads Due to Fuel Sloshing and Volute Bleed Line Flow

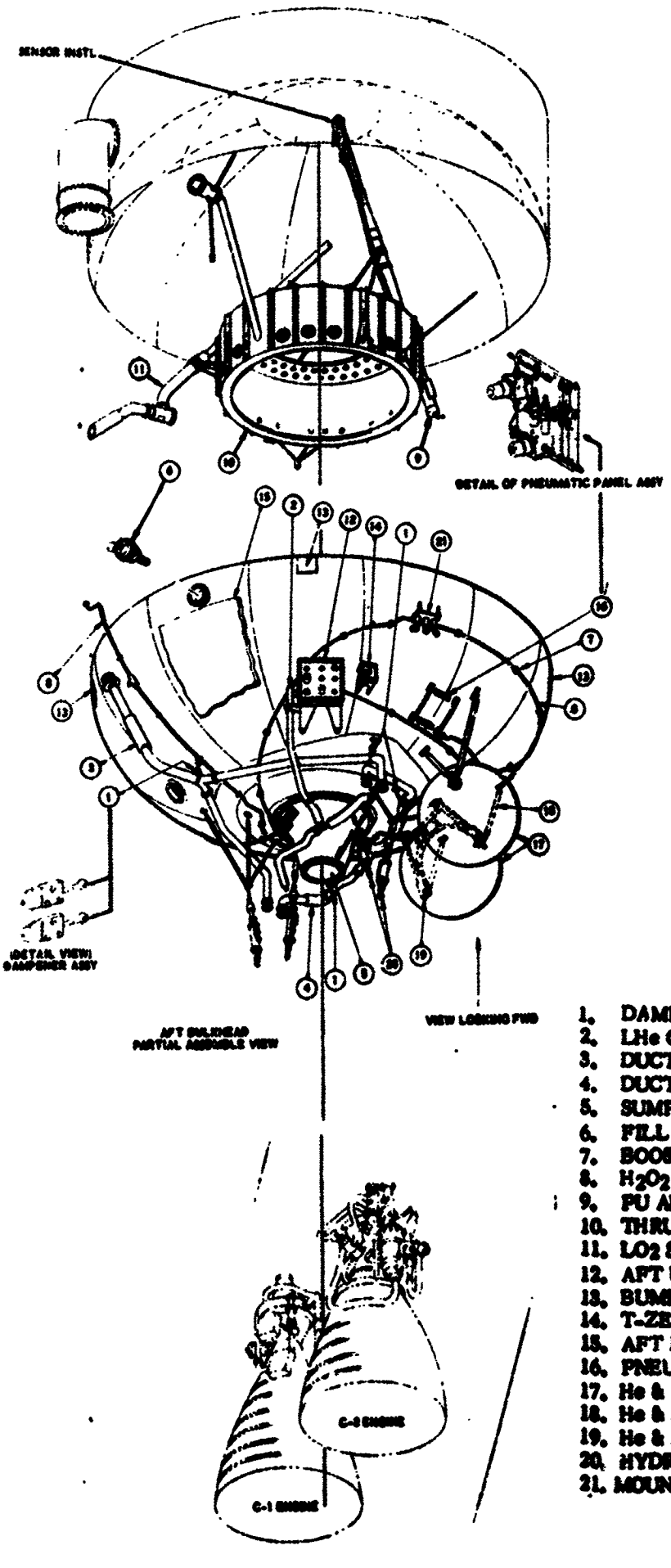

1. DAMPENER ASSY - FUEL & OXIDIZER LINES
2. LHe CHILLDOWN LINES
3. DUCT ASSY - INSULATED, FUEL
4. DUCT ASSY - INSULATED, OXIDIZER
5. SUMP - OXIDIZER
6. FILL & DRAIN VALVE - AIRBORNE
7. BOOST PUMP H_2O_2 SYS SPACER ASSY
8. H_2O_2 HEATED TUBE ASSY
9. PU AND PLIS ASSY
10. THRUST CYLINDER
11. LO_2 STANDPIPE ASSY
12. AFT UMBILICAL PANEL & SUPPORTS
13. BUMPER ASSY
14. T-ZERO PANEL
15. AFT RADIATION SHIELDS
16. PNEUMATIC PANEL ASSY
17. He & H_2O_2 BOTTLES
18. He & H_2O_2 BOTTLE STRUTS
19. He & H_2O_2 BOTTLE STRUTS
20. HYDRAULIC ACTUATOR PACKAGE
21. MOUNT - ENGINE ATTITUDE CONTROL

SECTION VIII

LIQUID OXYGEN TANK BOLT-ONS AND WELDMENTS

8.1 INTRODUCTION

The data presented in this section is applicable to major components bolted or welded to the basic liquid oxygen tank structure. The loads on the basic tank are presented in Section VI.

8.2 LIQUID OXYGEN BOOST PUMP AND SUMP

The liquid oxygen (LO_2) sump is located on the Z-Z Axis between Stations 468 and 454. The boost pump is attached aft of Station 468 with the pump shaft running into sump as shown in Figure 8.2-1.

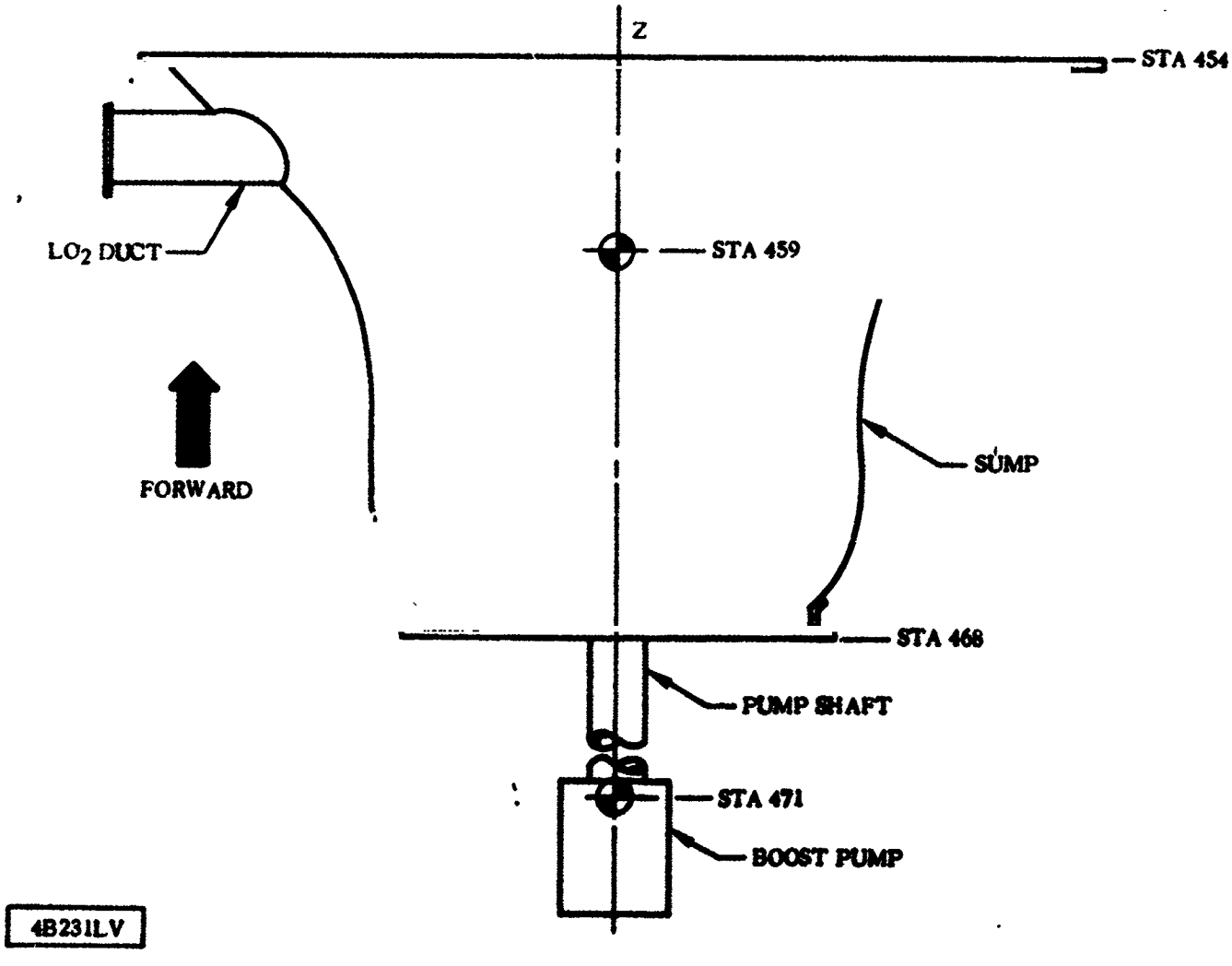

Figure 8.2-1. Liquid Oxygen Boost Pump and Sump

The sump serves as a cold reservoir for the oxygen boost pump, which in turn provides a constant supply of liquid oxygen to the two main engines through the liquid oxygen duct.

8.2.1 CRITICAL CONDITIONS. The critical loading condition on the LO_2 boost pump is a combination of pressure, Max g, and vibration loads.

8.2.2 WEIGHT AND CENTER OF GRAVITY DATA. The weight of the sump bell is 20.5 pounds and its center of gravity (C.G.) is at Station 459 on the Z-Z Axis. The boost pump weighs 51.2 pounds and its C.G. is at Station 471, also on the Z-Z axis (see Figure 8.2-1).

8.2.3 THERMAL DATA. The temperature at the boost pump inlet is plotted against Centaur engine firing time in Figure 8.2-2 for both one- and two-burn missions.

8.2.4 INERTIA LOADS. Inertia load factors for the LO_2 boost pump and sump are listed in Table 8.2-1.

TABLE 8.2-1. LIQUID OXYGEN BOOST PUMP AND SUMP INERTIA LOAD FACTORS

Longitudinal* (g's)	Lateral (g's)
±12	± 1.0
+ 7	±12.0
* +g load acts aft	

8.2.5 STEADY-STATE AIR LOADS. The LO_2 boost pump and sump do not receive critical loads due to aerodynamic forces.

8.2.6 BUFFET AND FLUTTER LOADS. The LO_2 boost pump and sump do not receive critical loads due to buffet or fluctuating pressure.

8.2.7 MISCELLANEOUS LOAD PARAMETERS. The boost pump inlet pressure is plotted against Centaur engine firing time in Figure 8.2-3 for both a one-burn and a two-burn mission.

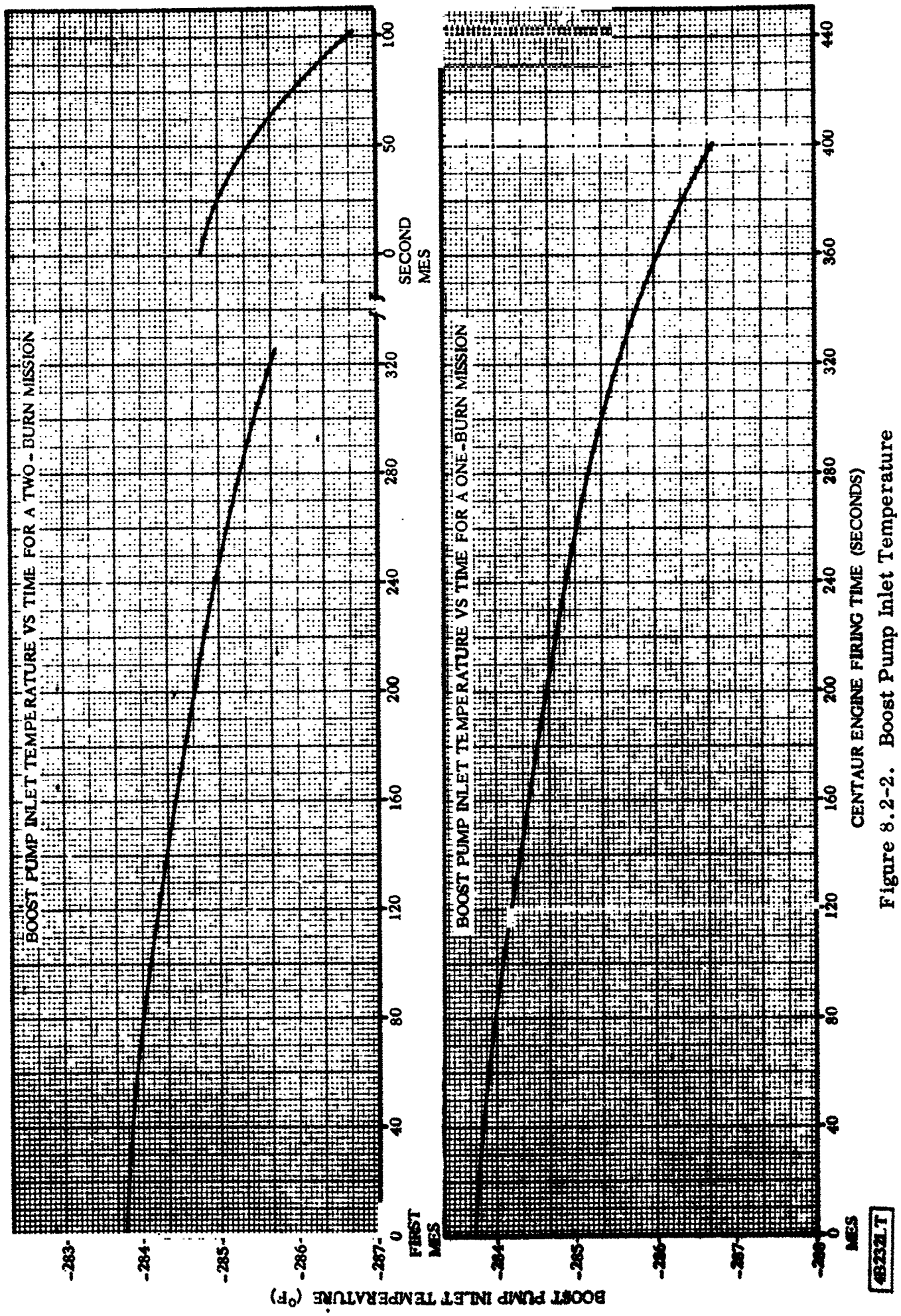

Figure 8.2-2. Boost Pump Inlet Temperature

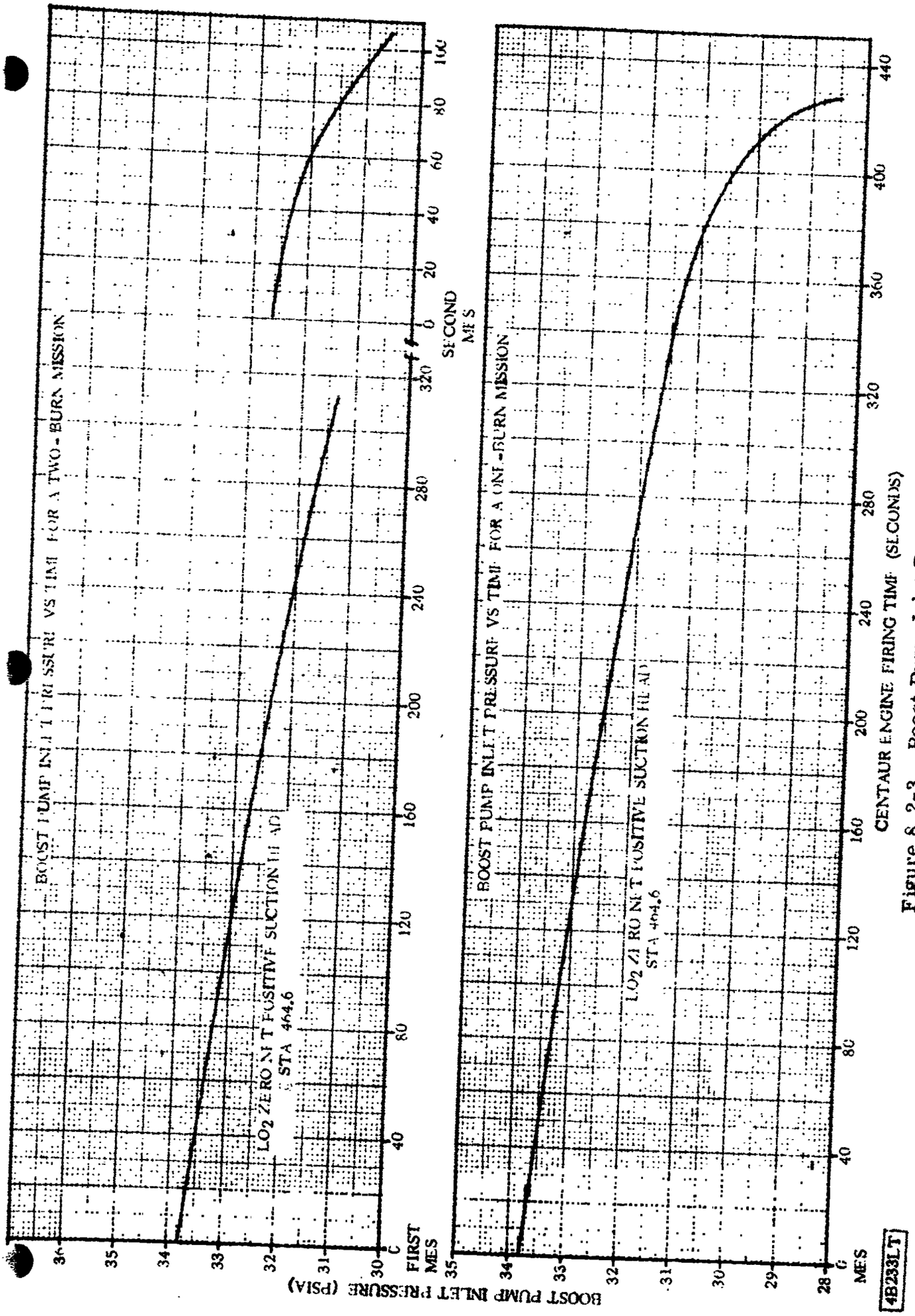

Figure 8.2-3. Boost Pump Inlet Pressure

8.3 THRUST CYLINDER MEMBRANE

The thrust cylinder membrane is located on top of the thrust barrel in the LO_2 tank at Station 443 as shown in Figure 8.3-1. The purpose of the membrane is to keep the thrust barrel from going out of round due to applied thrust loads.

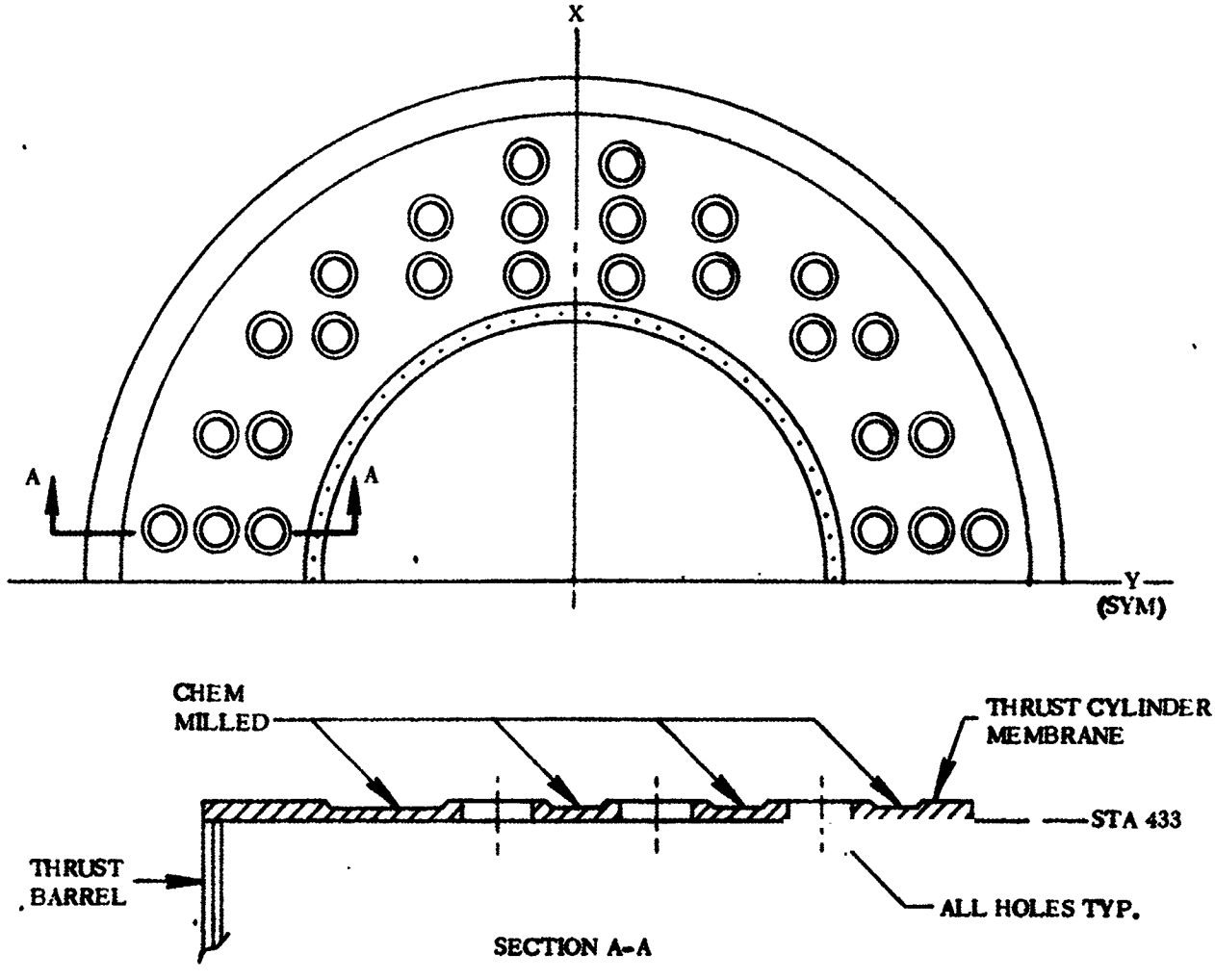

4B234LV

Figure 8.3-1. Thrust Cylinder Membrane Configuration

8.3.1 CRITICAL CONDITIONS. The critical loading condition for the thrust cylinder membrane is a combination of a differential pressure across the membrane due to LO_2 sloshing, and tension in the plane of the membrane caused by the engine thrust loads. The maximum membrane tension due to thrust loads occurs during Centaur engines thrust buildup.

8.3.2 WEIGHT AND CENTER OF GRAVITY DATA. Loads due to the weight of the thrust cylinder membrane are not critical.

8.3.3 THERMAL DATA. Since the thrust cylinder membrane is located in the LO_2 tank, it experiences a temperature of -297°F.

8.3.4 INERTIA LOADS. Loads on the thrust cylinder membrane due to inertia are not critical.

8.3.5 STEADY-STATE AIR LOADS. The thrust cylinder membrane does not receive critical loads due to aerodynamic forces.

8.3.6 BUFFET AND FLUTTER LOADS. The thrust cylinder membrane does not receive critical loads due to buffet or fluctuating pressure.

8.3.7 MISCELLANEOUS LOAD PARAMETERS. A differential pressure across the membrane of 0.015 psi must be combined with the maximum tension due to engine thrust loads when the membrane is submerged in liquid oxygen. After the LO_2 level has dropped below the membrane, the differential pressure across it is increased to 0.033 psi because of lack of fluid damping.

8.4 ENGINE GIMBAL BLOCKS

The main engine system of the Centaur stage has two Pratt and Whitney RL10A liquid oxygen - liquid hydrogen engines. These are fixed thrust, single chamber, regeneratively cooled, gimbal mounted engines. The main engines provide the major portion of the propulsion thrust required after burnout and separation from the Atlas first stage.

Three different engine systems are structurally considered for the Centaur vehicle: the 15,000 pound thrust RL10A-3-1 engine on AC-6, AC-7, and AC-11; the 15,000 pound thrust RL10A-3CM-1 engine on AC-8 and AC-10; and the 17,500 pound thrust RL10A-3-3 engine on AC-9 and AC-12 through AC-15. The -3CM-1 and -3-1 engines are very similar physically and have identical thrust ratings. The -3-3 engine differs only slightly physically. The greater thrust of the -3-3 is attained through minor internal modifications. Thrust characteristics of the engines are listed in Table 8.4-1.

TABLE 8.4-1. ENGINE THRUST CHARACTERISTICS

Engine Parameters	Units	RL10A-3-1 and RL10A-3CM-1	RL10A-3-3
Steady-State Thrust (Vacuum)	lb	15,000	17,500
Thrust Tolerance	%	±2	±2
Thrust Overshoot	%	+15	+15
Angular Thrust Misalignment	deg	±0.5	±0.5
Linear Thrust Misalignment	in.	±0.125	±0.125

Each of the two Centaur engines is supported at its forward end by a gimbal block which connects the engine to the aft bulkhead. The engine is fastened to the gimbal block by four bolts and the gimbal block is fastened to the aft bulkhead by four bolts. The gimbal block transfers longitudinal loads, lateral loads, and torsion about the longitudinal axis from the engine to the aft bulkhead and thrust cylinder. The engine configuration is shown in Figure 8.4-1.

The symbols listed below are those used in Figure 8.4-1 and in the tabular material that follows.

Symbols	Description
α	Angular acceleration of engine
C.G.	Engine center of gravity
C.P.	Engine center of percussion

Symbols	Description
F	Force on gimbal block at gimbal pivot axis
I	Moment of inertia of engine about pivot
M	Mass of engine
N	Dynamic load factor
P	Force on engine at pitch actuator pickup
$\tilde{r}$	Distance from gimbal pivot to center of gravity of engine
S	Yaw actuator support strut force on gimbal block
T	Engine thrust
T_o	Torsion on gimbal block about z-axis
W	Weight of engine
Y	Force on engine at yaw actuator pickup
x	Component along X-axis
y	Component along Y-axis
x-z	In the X-Z plane
y-z	In the Y-Z plane

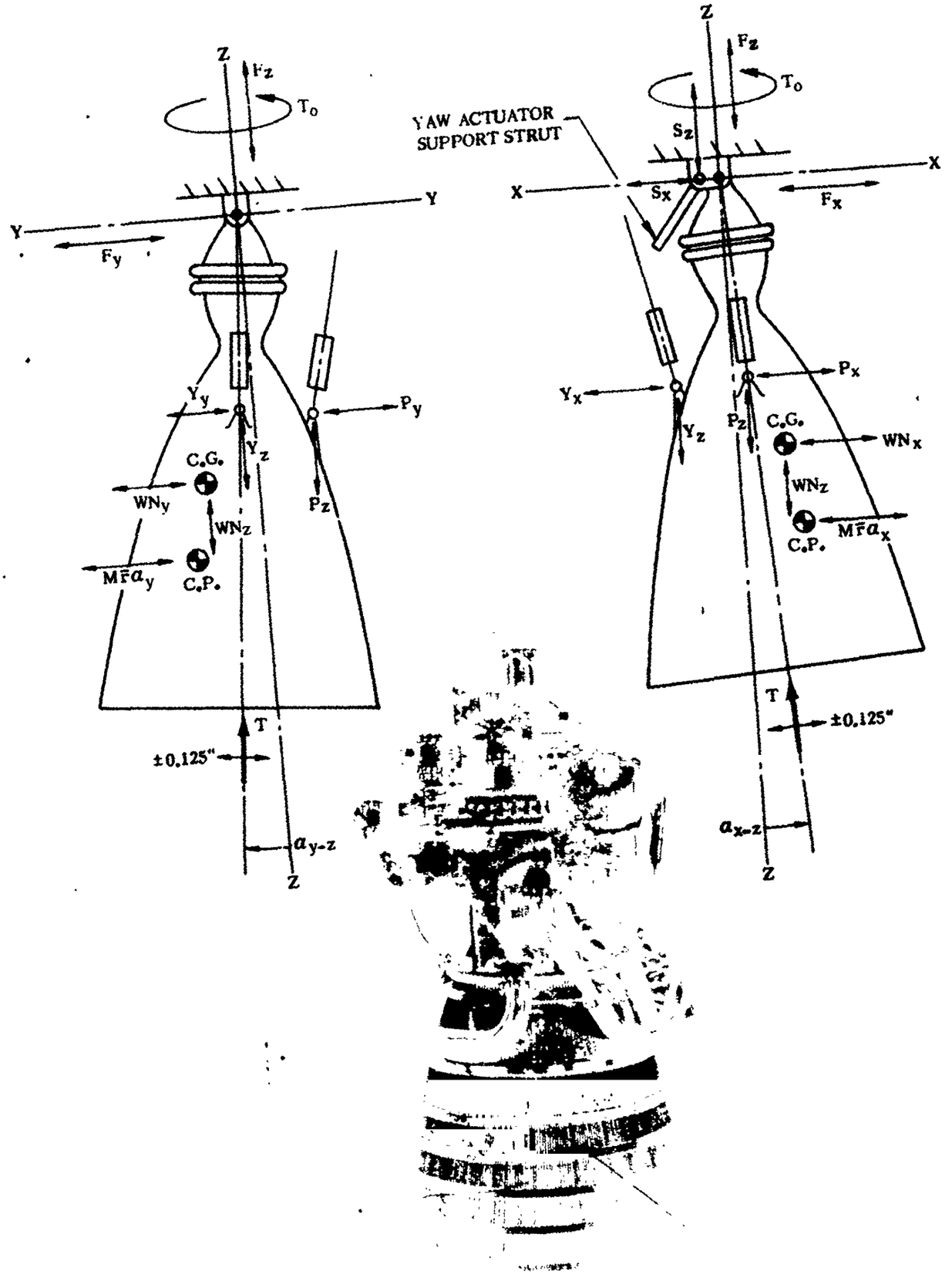

4B27LV

Figure 8.4-1. Engine Configuration

8.4.1 CRITICAL CONDITIONS. The loads presented are those acting on the gimbal block at the gimbal pivot axes. $+F_z$ acts in the aft direction, causing tension in the gimbal block. Three loading conditions are considered: thrust buildup, steady-state thrust, and thrust decay. All known possible loading variables were incorporated in all possible combinations to determine the maximum loads for each condition. The loads corresponding to each maximum are also presented to represent a complete loading condition on the gimbal block pivot axis.

The loads acting on the interface between the gimbal block and the tank must include the load in the yaw actuator support strut which is bolted to the gimbal block. The strut design loads are presented in Subsection 8.5. The nine gimbal positions are noted in Figure 8.4-2 and in Table 8.4-2. For a given engine gimbal position, the gimbal block loads and the strut load should be combined to attain maximum loading.

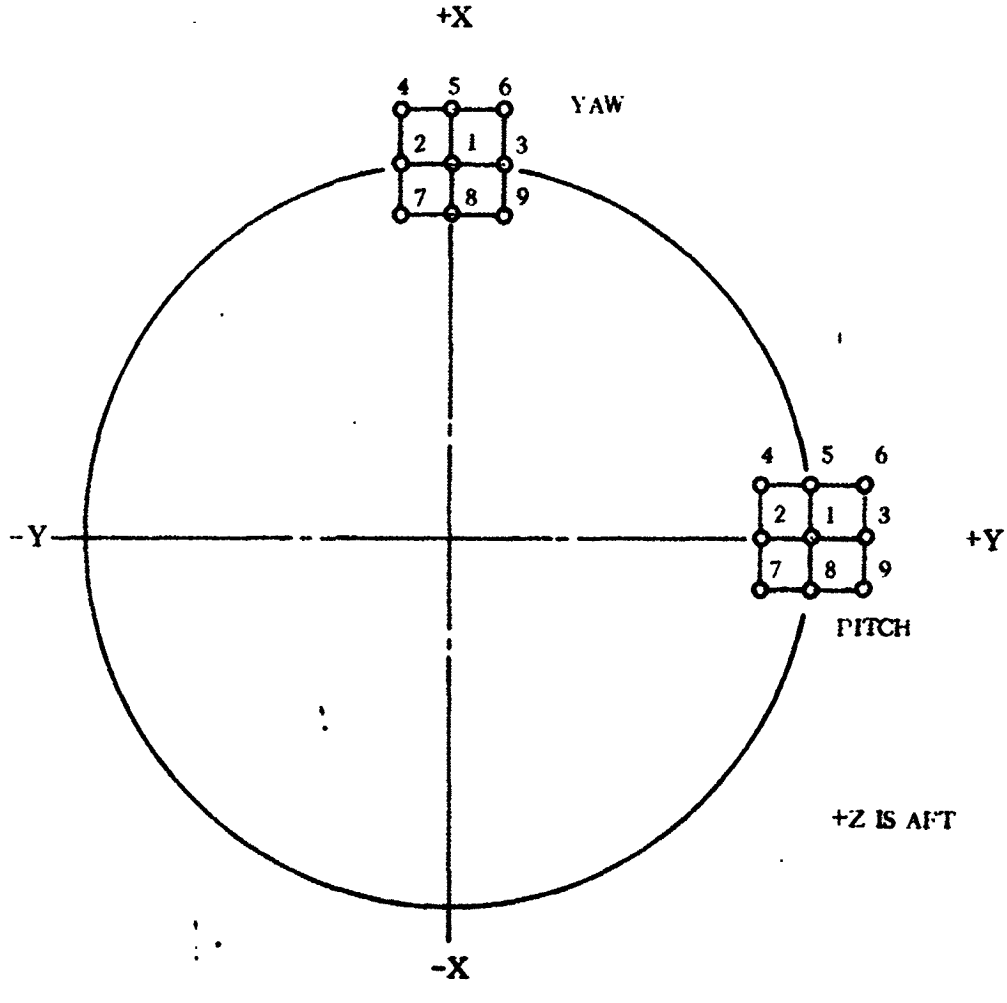

4B28LV

Figure 8.4-2. Engine Gimbal - Pitch and Yaw Positions

TABLE 8.4-2. ENGINE GIMBAL POSITIONS

Position*	Pitch (Degrees)	Yaw (Degrees)
1	0	0
2	-4	0
3	+4	0
4	-4	+4
5	0	+4
6	+4	+4
7	-4	-4
8	0	-4
9	+4	-4

*Reference Figure 6.4-2 for position locations.

8.4.2 WEIGHT AND CENTER OF GRAVITY DATA. The weights and mass moments of inertia about the gimbal point for the Centaur engines are listed in Table 8.4-3.

TABLE 8.4-3. ENGINE WEIGHTS, CENTERS OF GRAVITY, AND MOMENTS OF INERTIA ABOUT THE GIMBAL POINT

	Units	RL10A-3-1 and RL10A-3CM-1 (15K)	RL10A-3-3 (17.5K)
Weight	lb	350	365
C.G.*	in.	23.9*	24.6*
I_{xx}	slug-ft^2	66.4	70.2
I_{yy}	slug-ft^2	65.1	68.6

Note: *Located from gimbal point.

8.4.3 THERMAL DATA. The engine gimbal blocks are bolted to the LO_2 tank which is at -297°F throughout vehicle flight.

8.4.4 INERTIA LOADS. The Centaur engine inertia load factors for three critical loading conditions are shown in Table 8.4-4.

8.4.5 STEADY-STATE AIR LOADS. The engine gimbal blocks are not subjected to critical loads due to aerodynamic forces.

8.4.6 BUFFET AND FLUTTER LOADS. The engine gimbal blocks are not subjected to critical loads due to buffet or fluctuating pressure.

TABLE 8.4-4. ENGINE INERTIA LOAD FACTORS

	N_x (g's)	N_y (g's)	N_z (g's)
Thrust Buildup Condition			
Max N_x	±1.1	±1.1	+10, -2.3
Max N_y	±1.1	±1.1	+10, -2.3
Max N_z	+0.1	±0.1	+11, -3.3
Steady-State Thrust Condition			
Max N_x	+1.0	0	0
Max N_y	0	±1.0	0
Max N_z	0	0	±1.0
Thrust Decay Condition			
Max N_x	±1.1	±1.1	+7.7, -2.2
Max N_y	±1.1	±1.1	+7.7, -2.2
Max N_z	± 0.1	+0.1	+8.7, -3.2

8.4.7 MISCELLANEOUS LOAD PARAMETERS. The total loads acting on the gimbal blocks are due to a combination of engine thrust, inertia, engine gimbaling, and actuator loads. Total loads on the gimbal blocks have been calculated for thrust buildup, steady-state thrust, and thrust decay. These loads are summarized in the following paragraphs for both the 15K and 17.5K thrust engines.

8.4.7.1 Gimbal Block Loads on the RL10A-3-1 and RL10A-3CM-1, 15K Engines. Yaw actuator strut loads, Paragraph 8.4.7.3, must be added to the loads in Tables 8.4-5 through 8.4-9.

During thrust buildup, the thrust may exceed the steady-state thrust rating by 15 percent. This condition exerts the highest value of longitudinal load on the gimbal block.

TABLE 8.4-5. MAXIMUM LONGITUDINAL (Z-DIRECTIONAL) INERTIA LOADING CONDITION - THRUST BUILDUP

	Gimbal Position	N_x (lb)	N_y (lb)	N_z (lb)	T_o (in.-lb)
Max N_x	6	+1837	±2272	-21,347	±3943
Max N_y	3	± 310	±2272	-21,383	±3491
Max N_z	1	± 312	± 774	-21,423	±3814
Max T	4	± 648	±1484	-15,423	±4356

TABLE 8.4-6. MAXIMUM LATERAL (X- OR Y-DIRECTIONAL) INERTIA LOADING CONDITION - THRUST BUILDUP

	Gimbal Position	N_x (lb)	N_y (lb)	N_z (lb)	T_o (in.-lb)
Max N_x	6	±1946	±2320	-20,985	±4014
Max N_y	3	± 436	±2321	-21,021	±3558
Max N_z	1	± 433	± 835	-21,061	±3841
Max T_o	4	± 525	±1619	-15,061	±4371

Steady-state thrust is the normal operating condition of the Centaur engines. This condition exerts the highest lateral loads on the gimbal block.

TABLE 8.4-7. MAXIMUM Z-DIRECTIONAL INERTIA LOADING CONDITION - STEADY- STATE THRUST

	Gimbal Position	N_x (lb)	N_y (lb)	N_z (lb)	T_o (in.-lb)
Max N_x	6	±2253	±2332	-20,742	±7524
Max N_y	3	± 729	±2334	-20,799	±7240
Max N_z	1	± 733	± 813	-20,822	±8022
Max T_o	4	±2211	± 764	-19,967	±9062

TABLE 8.4-8. MAXIMUM X-DIRECTIONAL INERTIA LOADING CONDITION - STEADY-STATE THRUST

	Gimbal Position	N_x (lb)	N_y (lb)	N_z (lb)	T_o (in.-lb)
Max N_x	6	±2361	±2268	-20,380	±7593
Max N_y	3	± 855	±2270	-20,437	±7305
Max N_z	1	± 855	± 766	-20,460	±8046
Max T_o	4	±2334	± 735	-20,328	±9069

TABLE 8.4-9. MAXIMUM Y-DIRECTIONAL INERTIA LOADING CONDITION - STEADY-STATE THRUST

	Gimbal Position	N_x (lb)	N_y (lb)	N_z (lb)	T_o (in.-lb)
Max N_x	6	±2243	±2380	-20,380	±7528
Max N_y	9	± 868	±2382	-20,328	±6845
Max N_z	1	± 740	± 874	-20,460	±8023
Max T_o	4	±2221	± 629	-20,328	±9068

The thrust decay case imposes maximum longitudinal vibratory accelerations upon the aft bulkhead but does not produce critical gimbal block loads.

8.4.7.2 Gimbal Block Loads for the RL10A-3-3, 17.5K Engine. Yaw actuator strut loads, Paragraph 8.4.7.3, must be added to the loads of Tables 8.4-10 through 8.4-14.

During thrust buildup, the thrust overshoot of the 17.5K engine is 15 percent as with the 15K engine. This condition again produces maximum longitudinal gimbal block loads.

TABLE 8.4-10. MAXIMUM LONGITUDINAL Z-DIRECTIONAL INERTIA LOADING CONDITION - THRUST BUILDUP

	Gimbal Position	N_x (lb)	N_y (lb)	N_z (lb)	T_O (in.-lb)
Max N_x	6	±2050	±2490	-24,206	±4211
Max N_y	3	± 324	±2495	-24,265	±3603
Max N_z	1	± 325	± 792	-24,303	±3917
Max T_O	4	± 834	±1699	-18,282	±4429

TABLE 8.4-11. MAXIMUM LATERAL X- OR Y-DIRECTIONAL INERTIA LOADING CONDITION - THRUST BUILDUP

	Gimbal Position	N_x (lb)	N_y (lb)	N_z (lb)	T_O (in.-lb)
Max N_x	6	±2154	±2533	-23,846	±4234
Max N_y	3	± 449	±2543	-23,905	±3652
Max N_z	1	± 445	± 853	-23,943	±3935
Max T_O	4	± 712	±1833	-17,922	±4439

Steady-state thrust, the normal operating condition of the Centaur engines, imposes the highest lateral loads on the gimbal block.

TABLE 8.4-12. MAXIMUM Z-DIRECTIONAL INERTIA LOADING CONDITION - STEADY-STATE THRUST

	Gimbal Position	N_x (lb)	N_y (lb)	N_z (lb)	T_o (in.-lb)
Max N_x	6	±2451	±2531	-23,296	±7779
Max N_y	6	±2451	±2531	-23,296	±7595
Max N_z	1	± 750	± 831	-23,375	±8149
Max T	4	±2409	± 928	-22,514	±9148

TABLE 8.4-13. MAXIMUM X-DIRECTIONAL INERTIA LOADING CONDITION - STEADY-STATE THRUST

	Gimbal Position	N_x (lb)	N_y (lb)	N_z (lb)	T_o (in.-lb)
Max N_x	6	±2554	±2466	-22,931	±7809
Max N_y	6	±2554	±2466	-22,931	±7625
Max N_z	1	± 871	± 783	-23,010	±8162
Max T	4	±2530	± 898	-22,879	±9148

TABLE 8.4-14. MAXIMUM Y-DIRECTIONAL INERTIA LOADING CONDITION - STEADY-STATE THRUST

	Gimbal Position	N_x (lb)	N_y (lb)	N_z (lb)	T_o (in.-lb)
Max N_x	6	±2441	±2573	-22,931	±7774
Max N_y	3	± 754	±2574	-22,973	±7384
Max N_z	1	± 757	± 891	-23,010	±8153
Max T	4	±2419	± 793	-22,879	±9157

The thrust decay case imposes maximum longitudinal vibratory accelerations on the aft bulkhead but does not produce critical gimbal block loads.

8.4.7.3 Yaw Actuator Strut Loads. One leg of the yaw actuator support tripod is bolted to the gimbal block. The loads on the gimbal block from the strut should be added to the gimbal block loads of Paragraphs 8.4.7.1 and 8.4.7.2. The strut loads are the same for both the 15K and 17.5K engine and are presented in Tables 8.4-15 and 8.4-16.

TABLE 8.4-15. YAW ACTUATOR STRUT LOADS - THRUST BUILDUP CASE

Engine Position	Pitch Angle (degrees)	Yaw Angle (degrees)	S_x (lb)	S_z (lb)
1	0	0	±200	±128
2	-4	0	±197	±125
3	+4	0	±200	±128
4	-4	+4	±104	± 67
5	0	+4	±107	± 68
6	+4	+4	±107	± 68
7	-4	-4	±288	±183
8	0	-4	±292	±186
9	+4	-4	±292	±186

TABLE 8.4-16. YAW ACTUATOR STRUT LOADS - STEADY-STATE THRUST CASE

Engine Position	Pitch Angle (degrees)	Yaw Angle (degrees)	S_x (lb)	S_z (lb)
1	0	0	±519	±332
2	-4	0	±511	±327
3	+4	0	±519	±332
4	-4	+4	±269	±172
5	0	+4	±278	±178
6	+4	+4	±278	±178
7	-4	-4	±748	±478
8	0	-4	±757	±484
9	+4	-4	±756	±484

The thrust decay case does not yield critical loads.

8.5 ENGINE ACTUATORS

Thrust-vector control of the two P&W RL10A main engines, for pitch, yaw, and roll control during Centaur stage flight, is provided by electrohydraulic actuators which gimbal the thrust chambers. The actuators are in turn driven by signals from the servoamplifier package mounted on the lower electrical equipment tier. The actuators consist of three major components: the actuator cylinder, a servovalve, and a feedback transducer. Pitch and yaw/roll actuators are shown in Figure 8.5-1. A schematic of the actuator hydraulic system supply is shown in Figure 8.5-2.

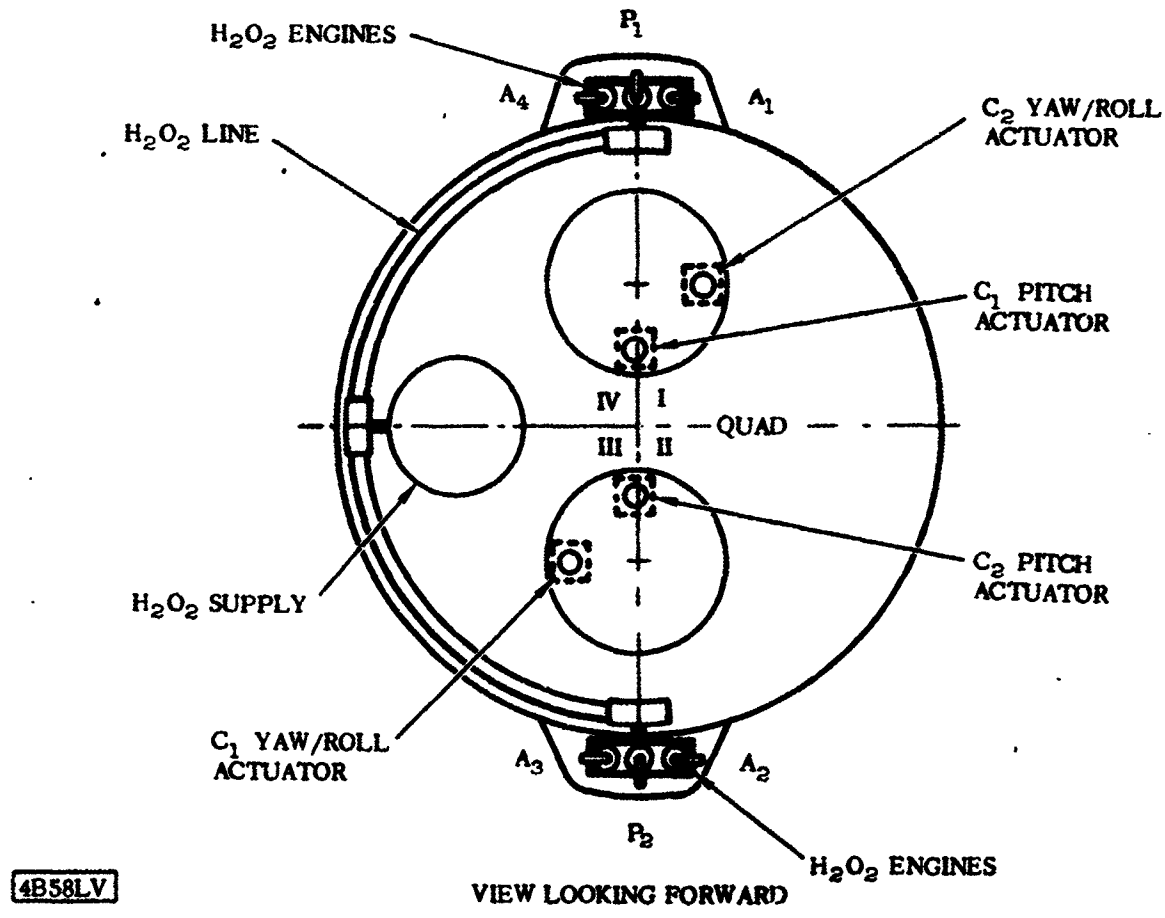

Figure 8.5-1. Electrohydraulic Main Engine Actuators - Location

8.5.1 CRITICAL CONDITIONS. The critical loads on the engine actuators occur during Centaur engine firing. Consideration was made of the possible limiting condition where the engine are forced against the actuator stops at the maximum angular velocity of the engines. This condition could exist only if maximum demand is made on the vehicle control system.

8.5.2 WEIGHTS AND CENTER OF GRAVITY DATA. Loads due to the weight of the actuators are not critical.

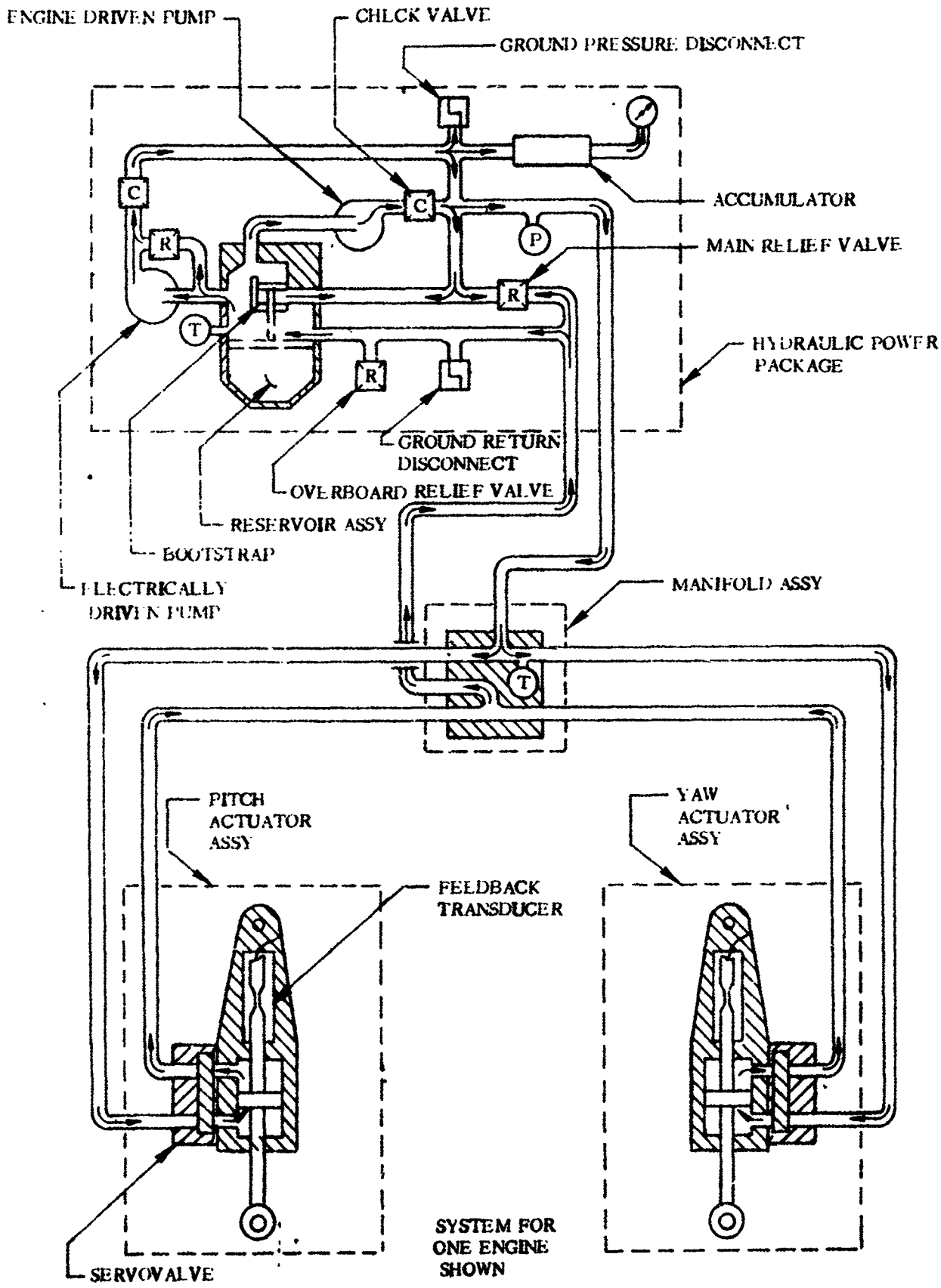

4B2351_V

Figure 8.5-2. Hydraulic System Schematic

8.5.3 THERMAL DATA. A temperature versus time study was conducted for the hydraulic system for a two-burn mission. The system was divided into segments as shown in Figure 8.5-3. Attachment temperatures are shown in Figure 8.5-4. Temperature distributions in the actuator ends are shown in Figure 8.5-5. Yaw actuator and actuator piston temperatures are given in Figures 8.5-6 and 8.5-7. Maximum and minimum temperatures of the hydraulic lines are shown in Figures 8.5-8, 8.5-9, and 8.5-10. The reservoir oil temperature predicted extremes are given in Figure 8.5-11, and maximum and minimum predicted manifold oil temperatures are presented in Figure 8.5-12.

The main pump temperature history is shown in Figure 8.5-12. Temperature histories of the manifold skin and oil are shown in Figures 8.5-13 and 8.5-14.

8.5.4 INERTIA LOADS. Inertia loads on the engine actuators are not critical.

8.5.5 STEADY-STATE AIR LOADS. The engine actuators do not receive critical loads due to aerodynamic forces.

8.5.6 BUFFET AND FLUTTER LOADS. The engine actuators do not receive critical loads due to buffet or fluctuating pressure.

8.5.7 MISCELLANEOUS LOAD PARAMETERS. Actuator loads are caused by thrust misalignment, thrust buildup transients, and engine gimbaling. An offset of ±0.125 inches in any direction is assumed to exist between the thrust vector and the engine centerline. The Pratt & Whitney engine specifications list a maximum thrust of 1.15 times the steady-state thrust for both the 15K and 17.5K engines during thrust buildup. Actuator gimbal loads have been investigated for the nine possible engine positions described in Paragraph 8.4.1 of this report. The positions include a neutral setting along with a maximum excursion of ±4 degrees in either the pitch (Y-Y axis) or yaw (X-X axis) direction, or in both pitch and yaw directions simultaneously. The actuator design loads resulting from the above conditions are listed in Table 8.5-1.

TABLE 8.5-1. ENGINE ACTUATOR DESIGN LOADS

Condition	Load on Pitch Actuator (lb)	Load on Yaw Actuator (lb)
Thrust Buildup	2000	1000
Steady-State Thrust and Thrust Decay	2600	2600

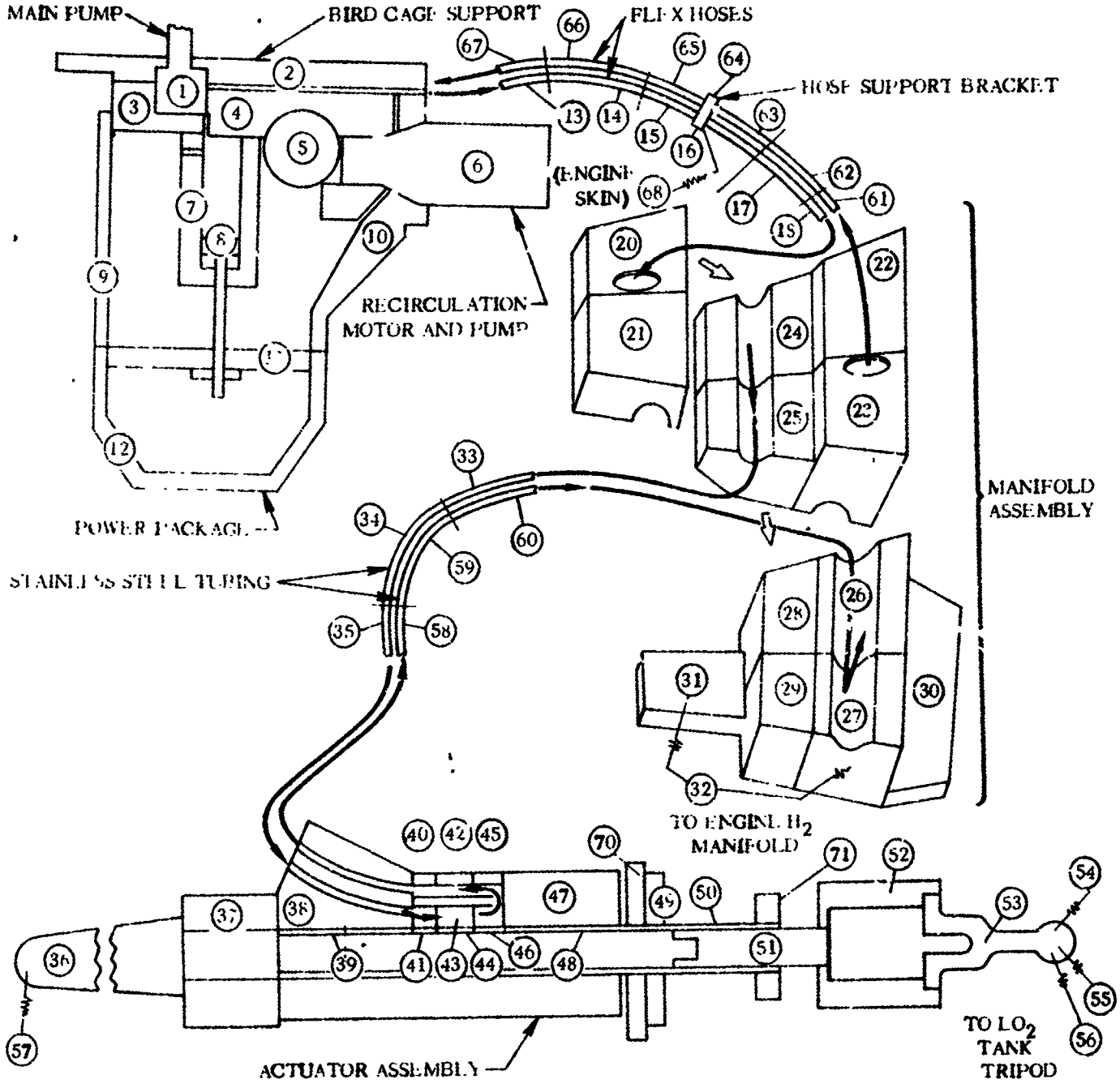

NOTE: IN ADDITION TO THE ABOVE NOTED SOLID SEGMENTS THE FOLLOWING FLUID SEGMENTS WERE ALSO USED:

LOCATION		FLUID SEGMENT NO.
ACTUATOR ASSEMBLY	(RETURN LINE)	1, 2, 3, 4
STAINLESS STEEL TUBING	(RETURN LINE)	5, 6, 7
MANIFOLD ASSEMBLY	(RETURN LINE)	8, 9
FLEX HOSE LINE	(RETURN LINE)	10, 11, 12
POWER PACKAGE		13, 14, 15, 16, 17, 18
FLEX HOSE LINE	(PRESSURE LINE)	19, 20, 21
MANIFOLD ASSEMBLY	(PRESSURE LINE)	22, 23
STAINLESS STEEL TUBING	(PRESSURE LINE)	24, 25, 26
ACTUATOR ASSEMBLY	(PRESSURE LINE)	27, 28

4B236LV

Figure 8.5-3. Hydraulic System Segmentation for Thermal Analysis

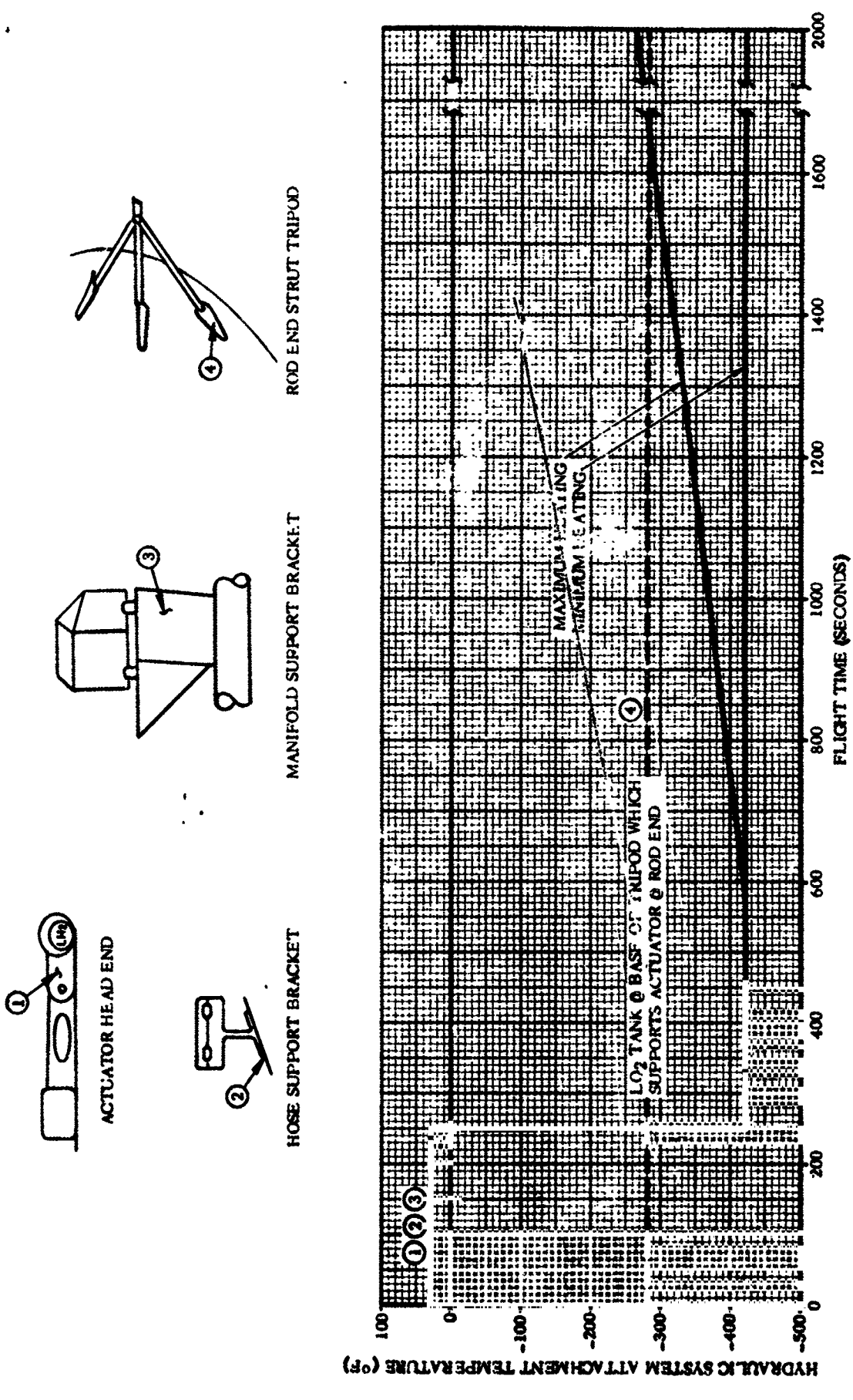

Figure 8-5-4. Hydraulic System Attachment Temperatures versus Flight Time

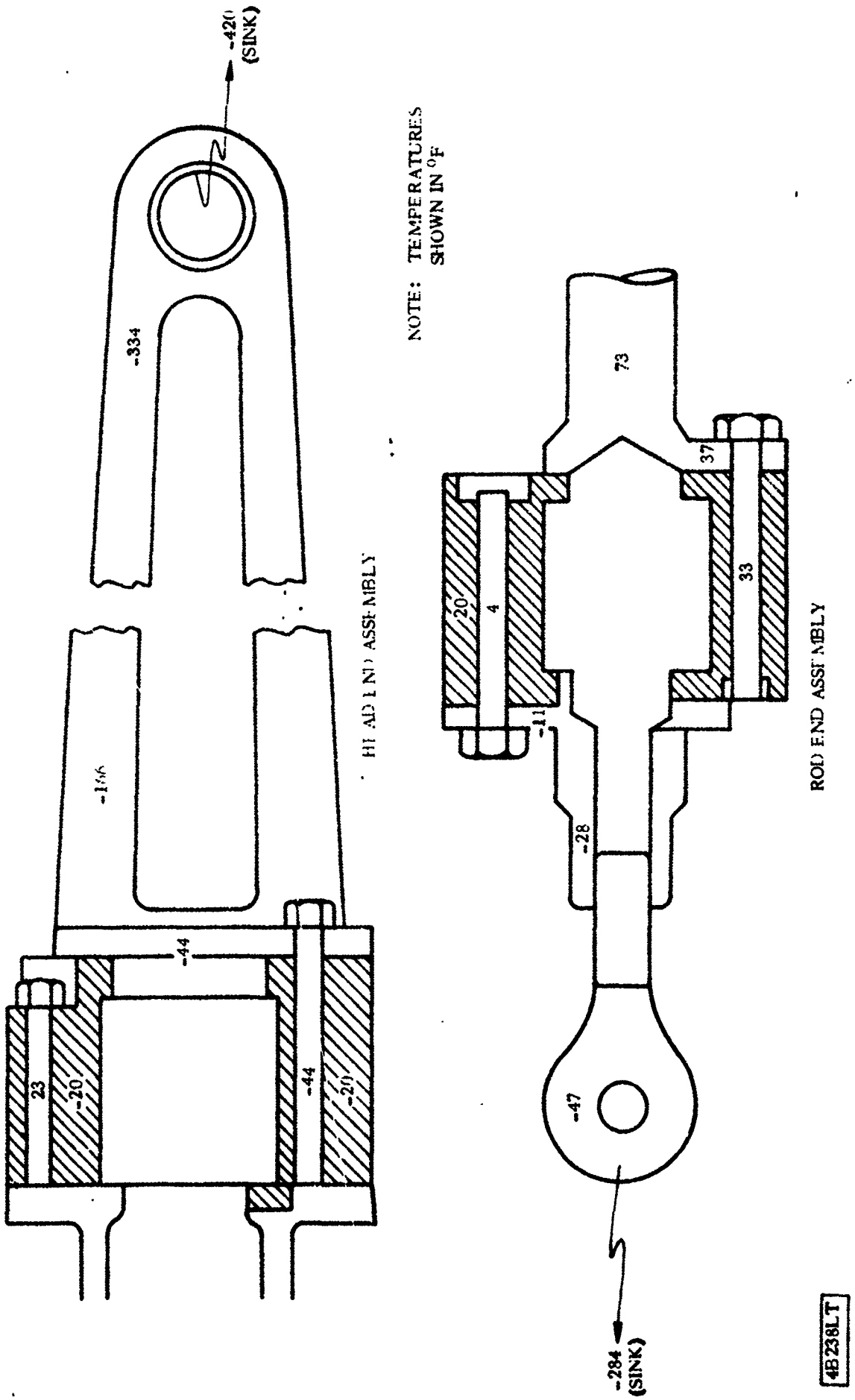

Figure 8.5-5. Actuator Temperature Distributions

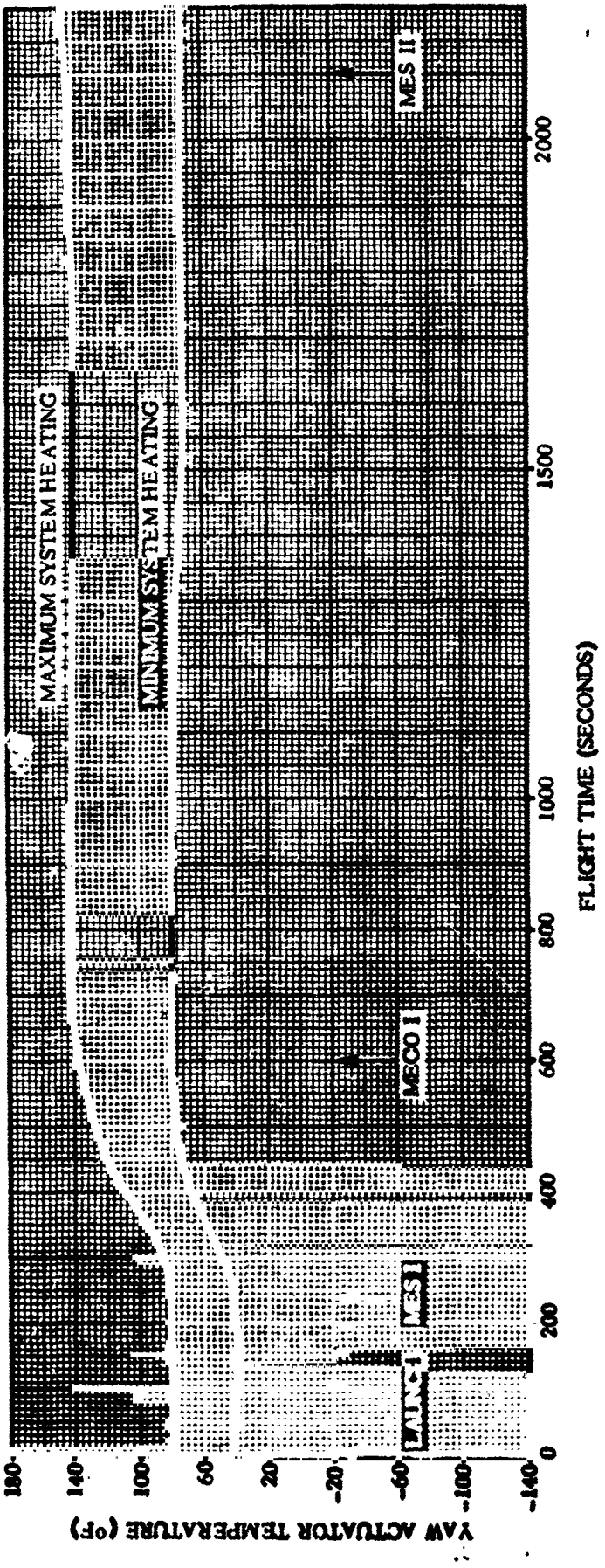

Figure 8.5-6. Yaw Actuator Temperature versus Flight Time

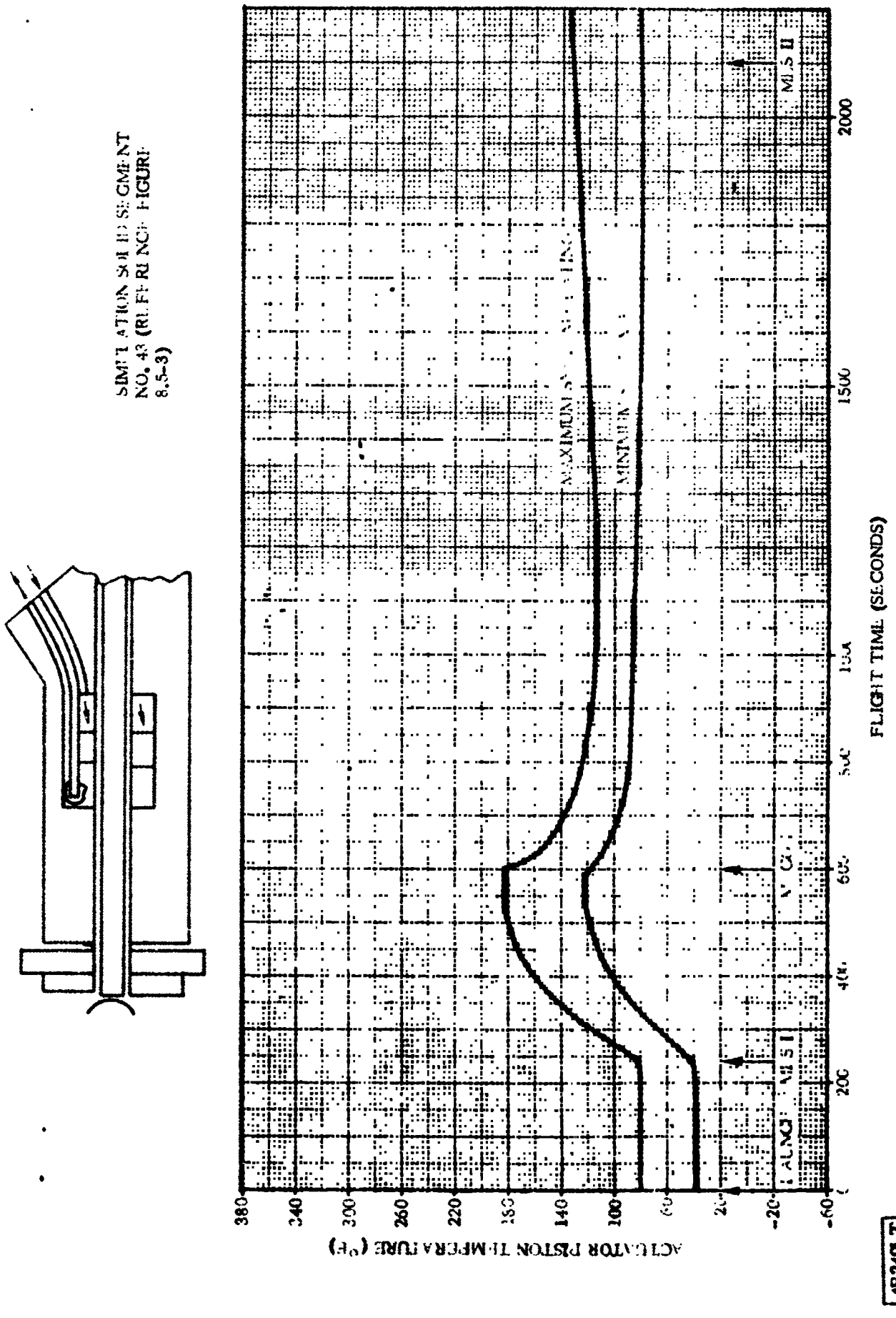

Figure 8.5-7. Actuator Piston Temperature versus Flight Time

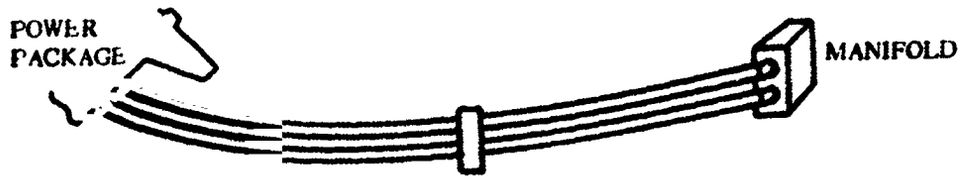

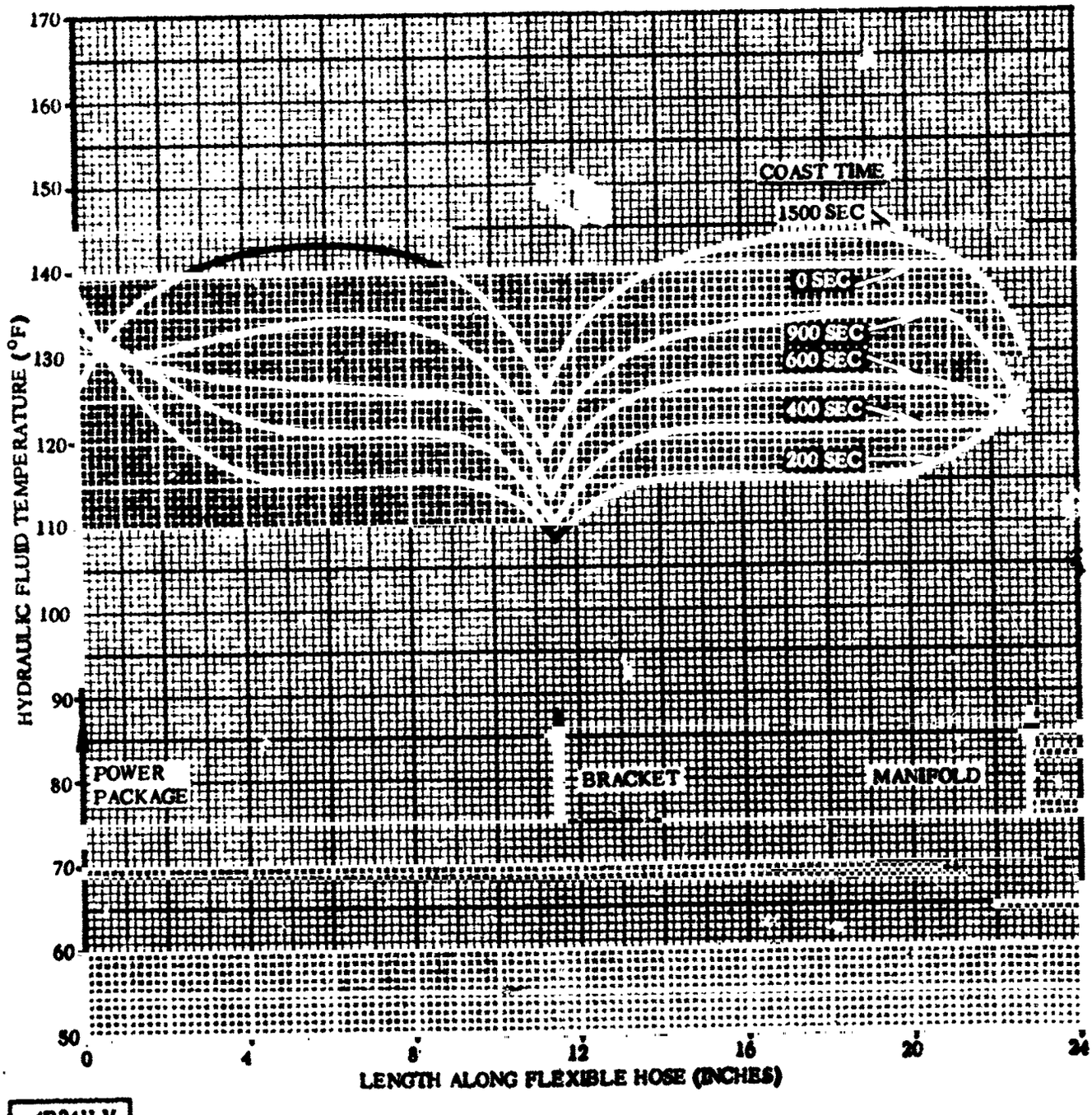

4B241LV

Figure 8.5-8. Flexible Hose Maximum Hydraulic Fluid Temperature during Coast

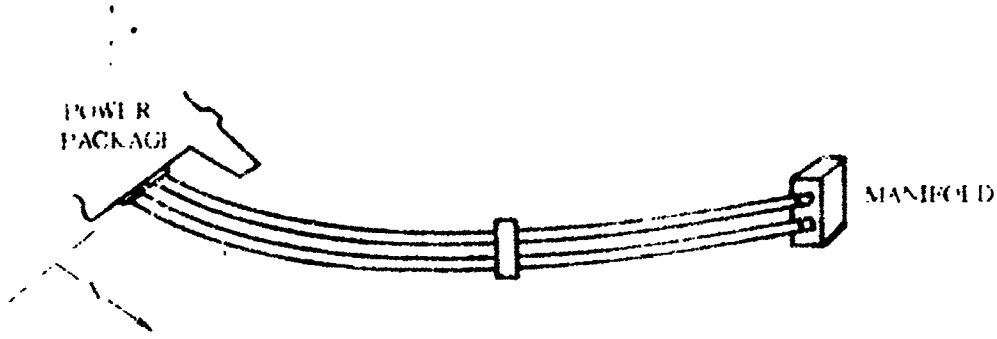

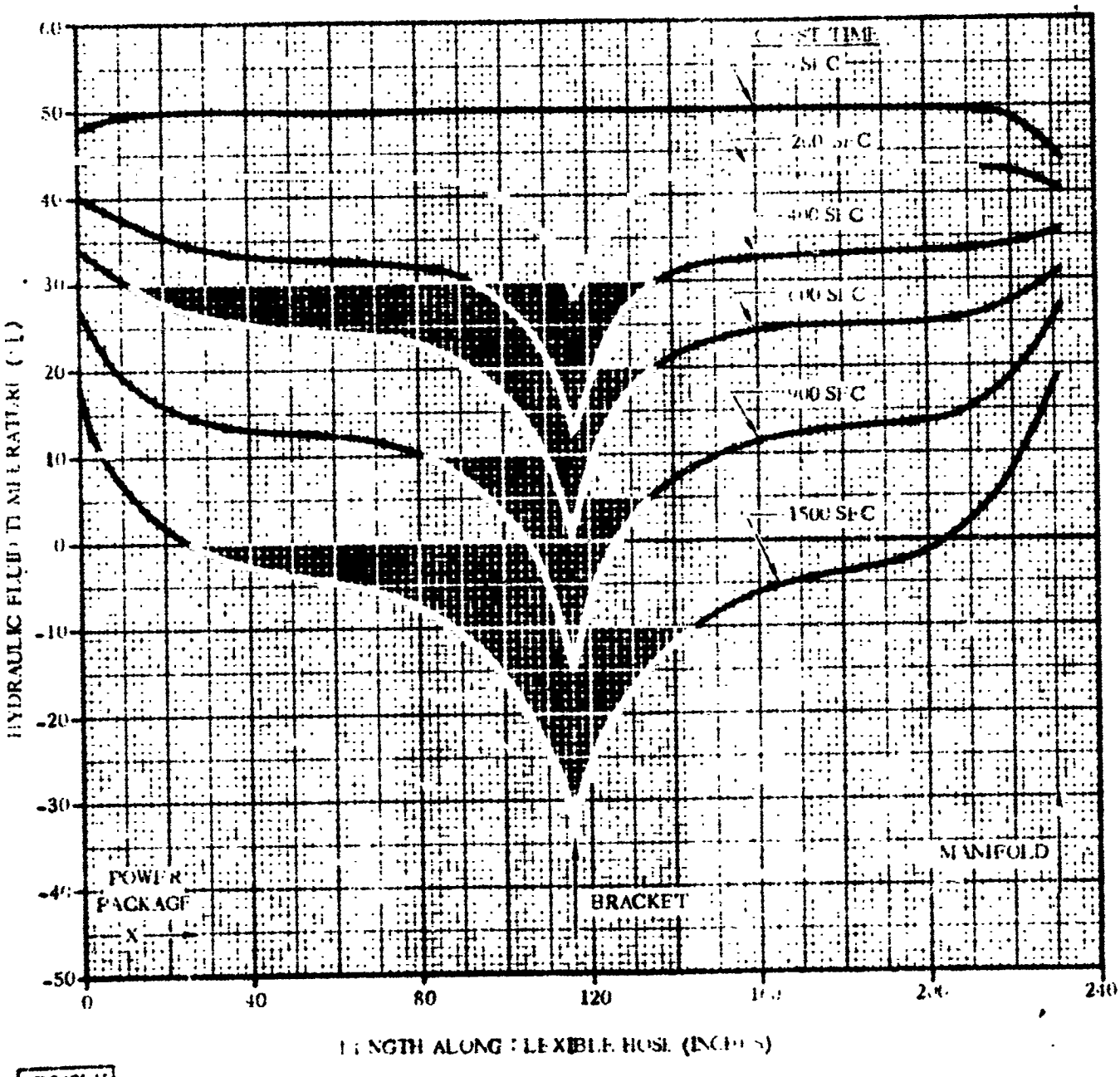

Figure 8.5-9. Flexible Hose Minimum Hydraulic Fluid Temperature during Coast

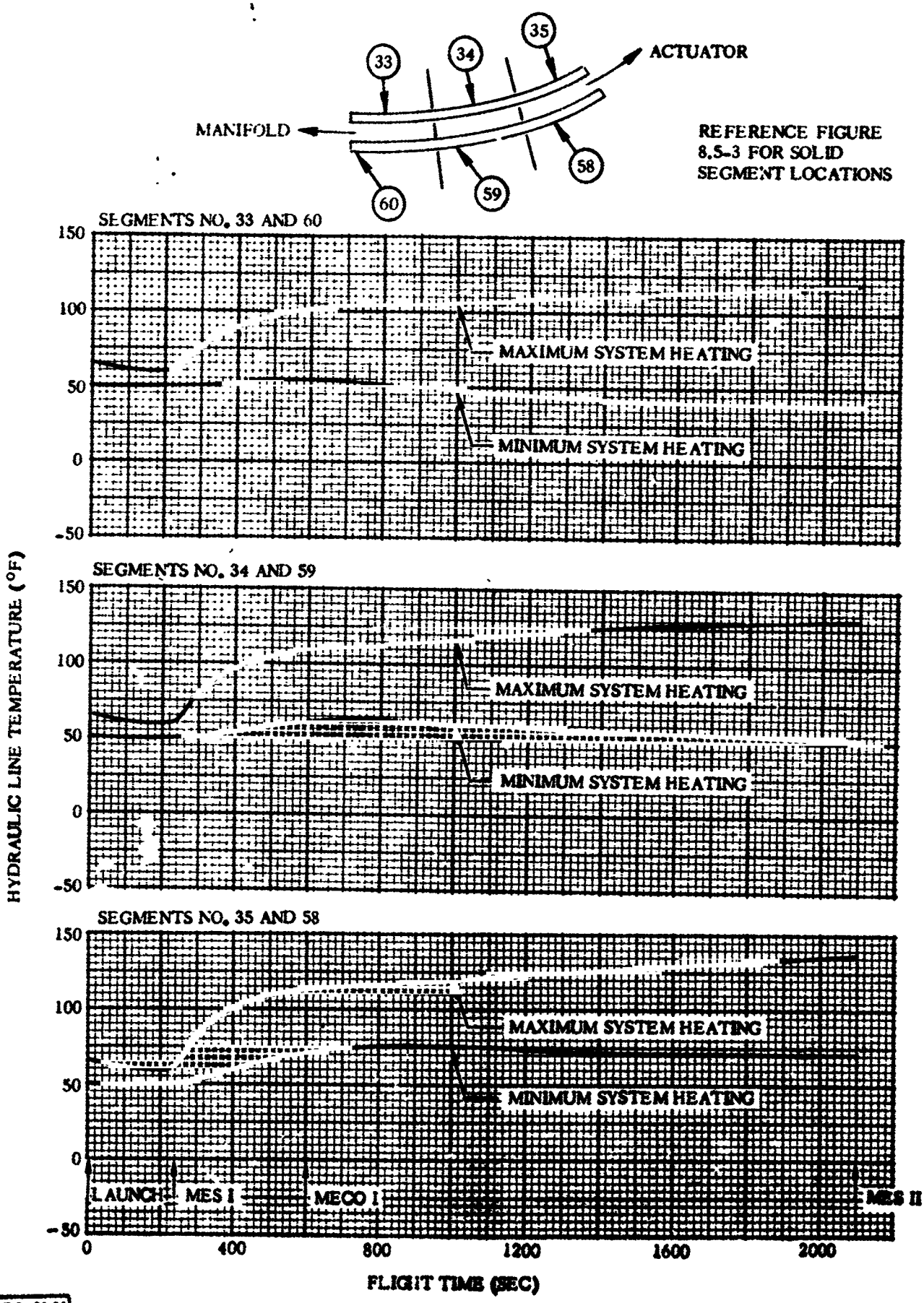

4B243LV

Figure 8.5-10. Stainless Steel Hydraulic Line Temperature versus Flight Time

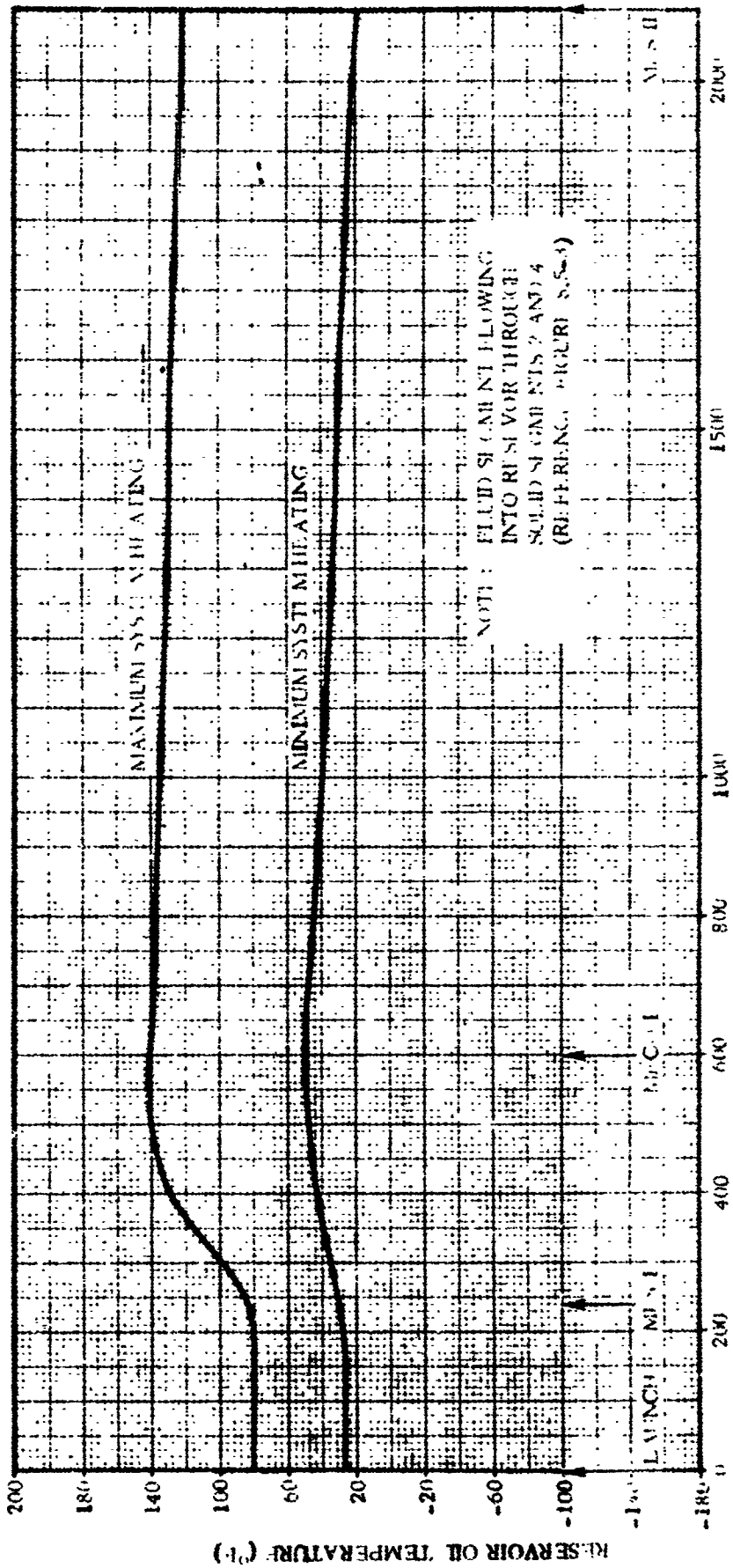

4B244LT

Figure 8.5.11. Reservoir Oil Temperature versus Flight Time

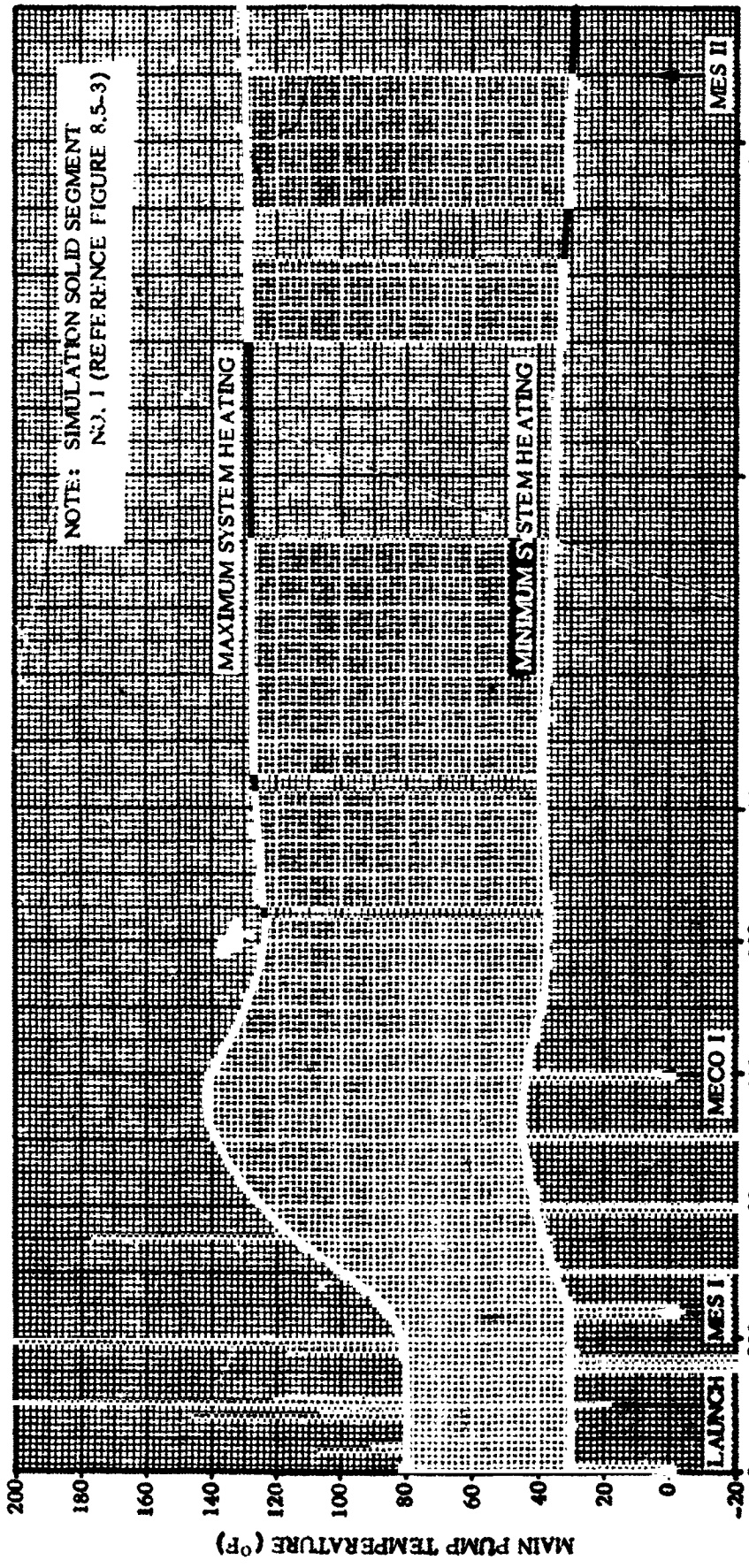

4824SLT

Figure 8.5-12. Main Pump Temperature versus Flight Time

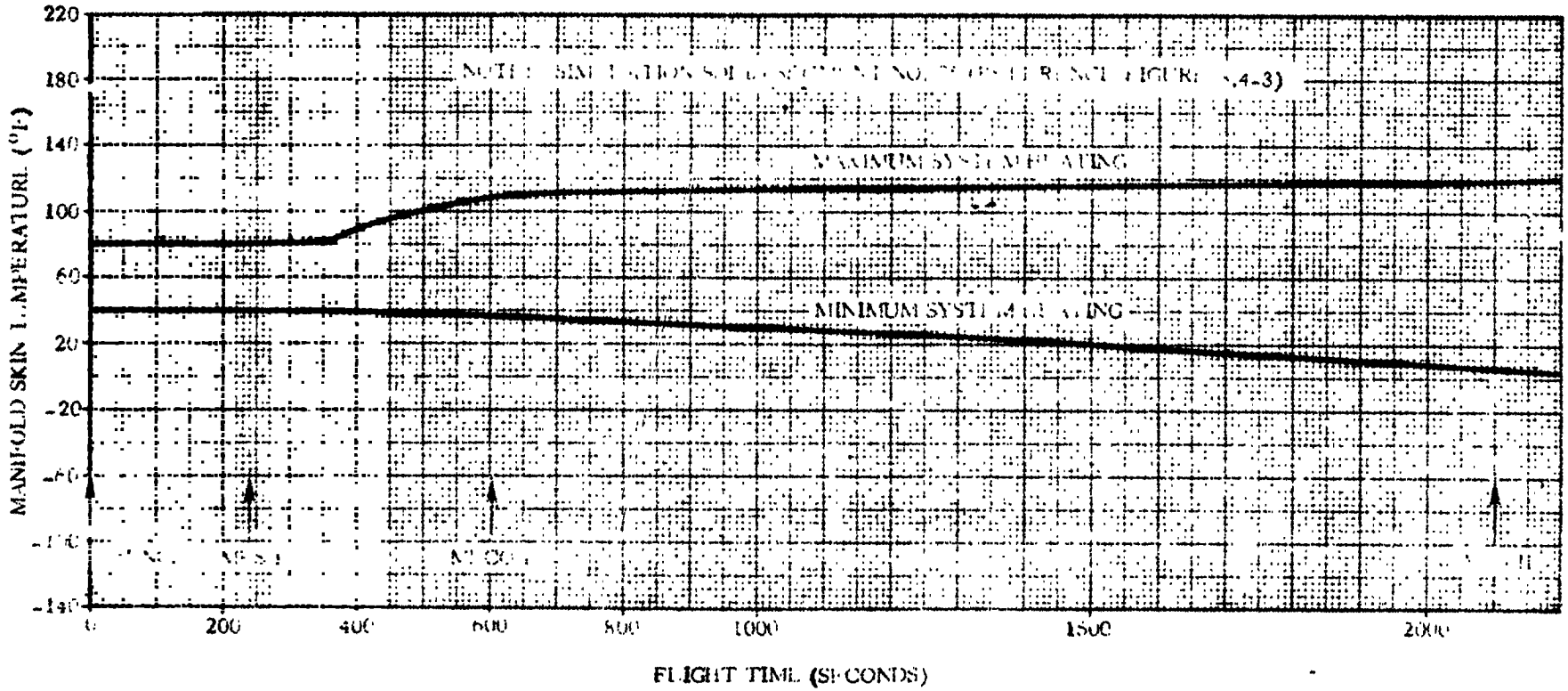

Figure 8.5-13. Manifold Skin Temperature versus Flight Time

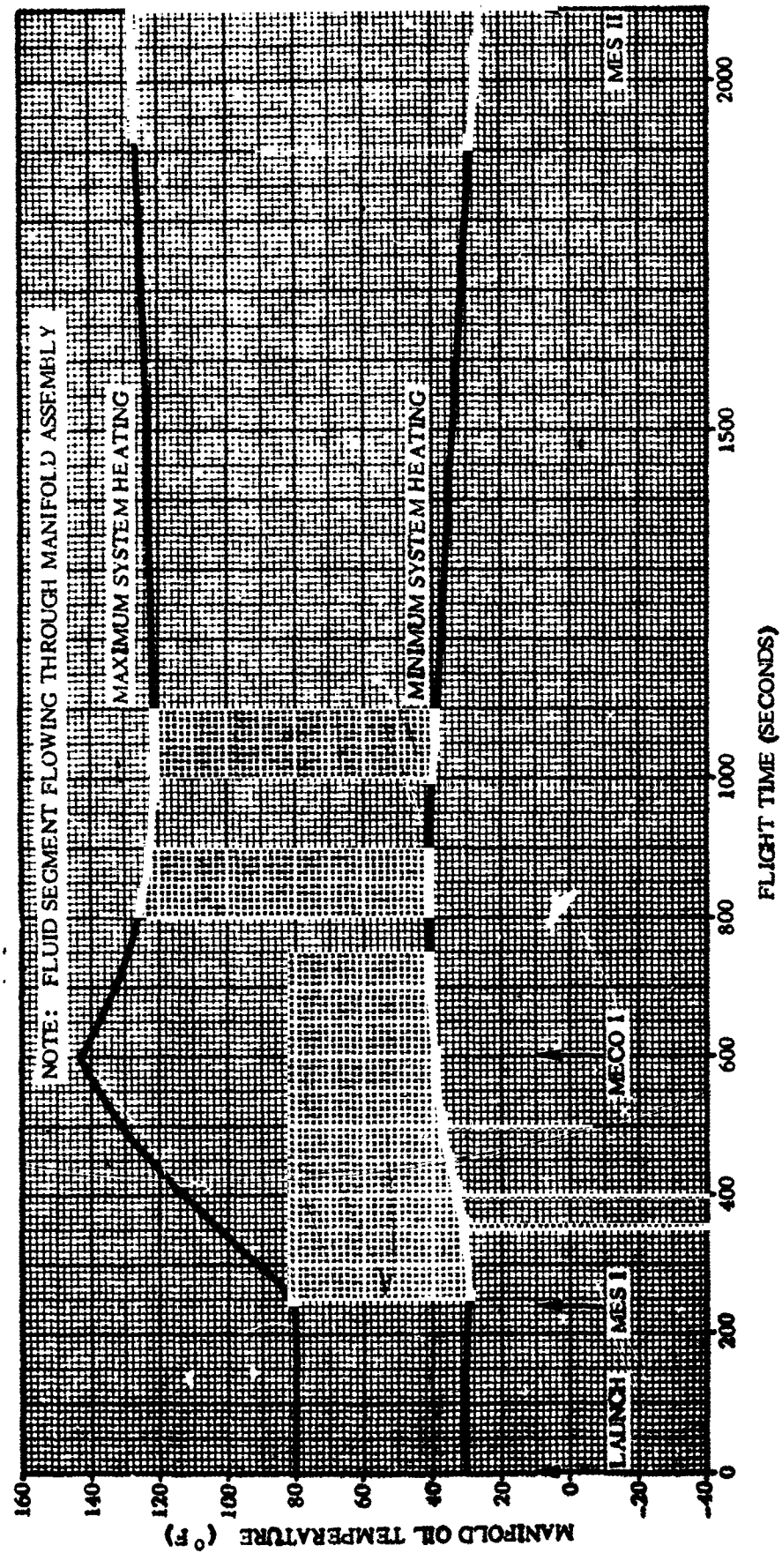

Figure 8.5-14. Mainfold Oil Temperature versus Flight Time

THIS PAGE INTENTIONALLY LEFT BLANK.

8.6 HYDROGEN PEROXIDE AND HELIUM BOTTLES

The hydrogen peroxide and helium bottles are mounted on the aft bulkhead as shown in Figure 8.6-1. The H_2O_2 bottle is on the X-X axis in Quadrants II and IV. There is only on He bottle for AC-6 and it is mounted in Quadrant III as shown in Figure 8.6-1. Later vehicles may require more than one helium bottle, and this section of the report will be suitably revised to include loads for other bottle arrangements.

The helium bottle is the storage vessel for the helium gas used in the ullage pressurization system. The hydrogen peroxide bottle is used to store liquid hydrogen peroxide for use in the monopropellant attitude control engines.

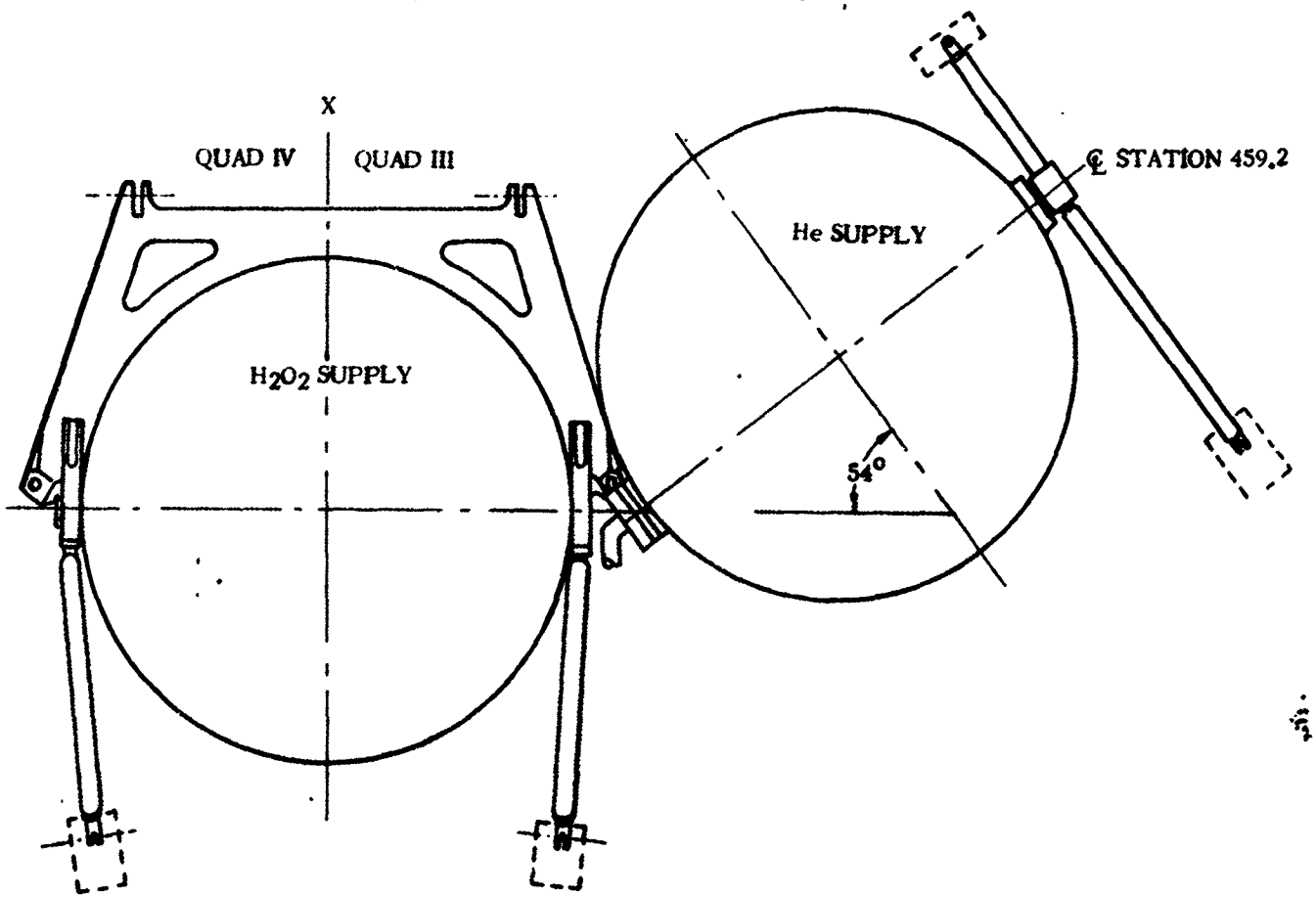

4B248LV

Figure 8.6-1. Hydrogen Peroxide and Helium Bottles

8.6.1 CRITICAL CONDITIONS. The critical loading conditions on the hydrogen peroxide and helium bottle support structures are cuased by the inertia loads at Max q, BECO, Centaur MES and MECO. The critical inertia loads are a combination of the steady-state and vibratory inertia loads.

8.6.2 WEIGHT AND CENTER OF GRAVITY DATA. Weights and C.G's for the bottles, bottle contents, and bottle supports are listed in Table 8.6-1. The bottle content weights listed are representative of a two-burn mission and will not be exceeded for any mission. The C.G. of each bottle and its contents is assumed to be at the geometric center of the bottle.

TABLE 8.6-1. HYDROGEN PEROXIDE AND HELIUM BOTTLE STRUCTURAL DESIGN WEIGHTS (MAXIMUM)

	Units	Hydrogen Peroxide	Helium
Bottle Dry Weight	lb	27	50
Bottle Contents Weight*			
Full	lb	250	7
Liftoff	lb	240	
MECO (Final)	lb	160	
Bottle Support Weight	lb	13	5
Bottle and Contents C.G.			
z	Station	459	459
y	in.	0	-24
x	in.	-38	-32

*These weights are representative of a two-burn mission and are higher than those of a one-burn mission

8.6.3 THERMAL DATA. The operating temperature of the bottles is room temperature, although when the bottles are charged they may reach a temperature of 165°F. Sufficient time exists between charging the bottles and launch for them to cool to ambient temperature.

8.6.4 INERTIA LOADS. The steady-state inertia loads are given in Table 8.6-2 and the vibratory inertia loads in Figure 8.6-2.

8.6.5 STEADY-STATE AIR LOADS. The engine area bottles do not receive critical loads due to aerodynamic forces.

TABLE 8.6-2. ENGINE AREA BOTTLES STEADY-STATE INERTIA LOAD FACTORS*

Condition	Longitudinal Load ** (g's)	Lateral Load (g's)
Max αq	+2.3	±1.0
Max q	+5.8 ±0.1	±0.3
Centaur First MES	+1.2	±0.5
Centaur First MECO	+3.2	±0.5
Centaur Second MES	+3.5	±0.5
Centaur Second MECO	+4.5	±0.5

NOTES: * These steady-state loads must be combined with vibratory inertia loads presented in Figure 8.6-2.
** (+)Longitudinal load acts aft.

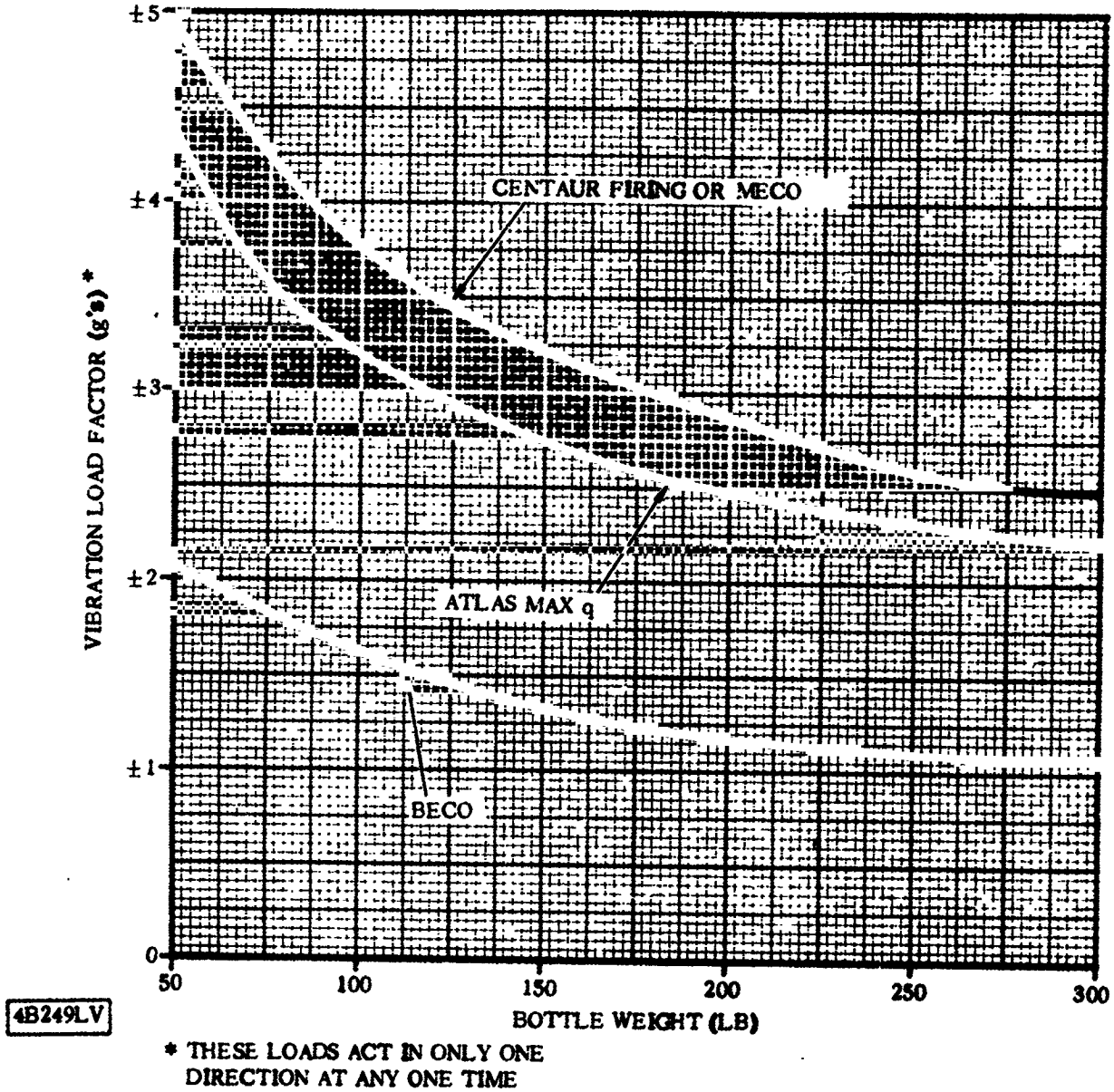

Figure 8.6-2. Engine Area Bottles Vibratory Inertia Load Factors

8.6.6 BUFFET AND FLUTTER LOADS. The engine area bottles do not receive critical loads due to duffet or fluctuating pressure.

8.6.7 MISCELLANEOUS LOAD PARAMETERS. No other critical loads are applied to the bottles.

THIS PAGE INTENTIONALLY LEFT BLANK

8.7 T-4 AFT UMBILICAL PANEL

The T-4 aft umbilical panel is located on the aft bulkhead at Station 445. It is 28°40′ from the Y-Y axis in Quadrant II. The panel supports the airborne portion of the disconnects as shown in Figure 8.7-1. The location of the connectors on the face of the panel is shown in Figure 8.7-2. The latch and ejection mechanism is shown in Figure 8.7-3.

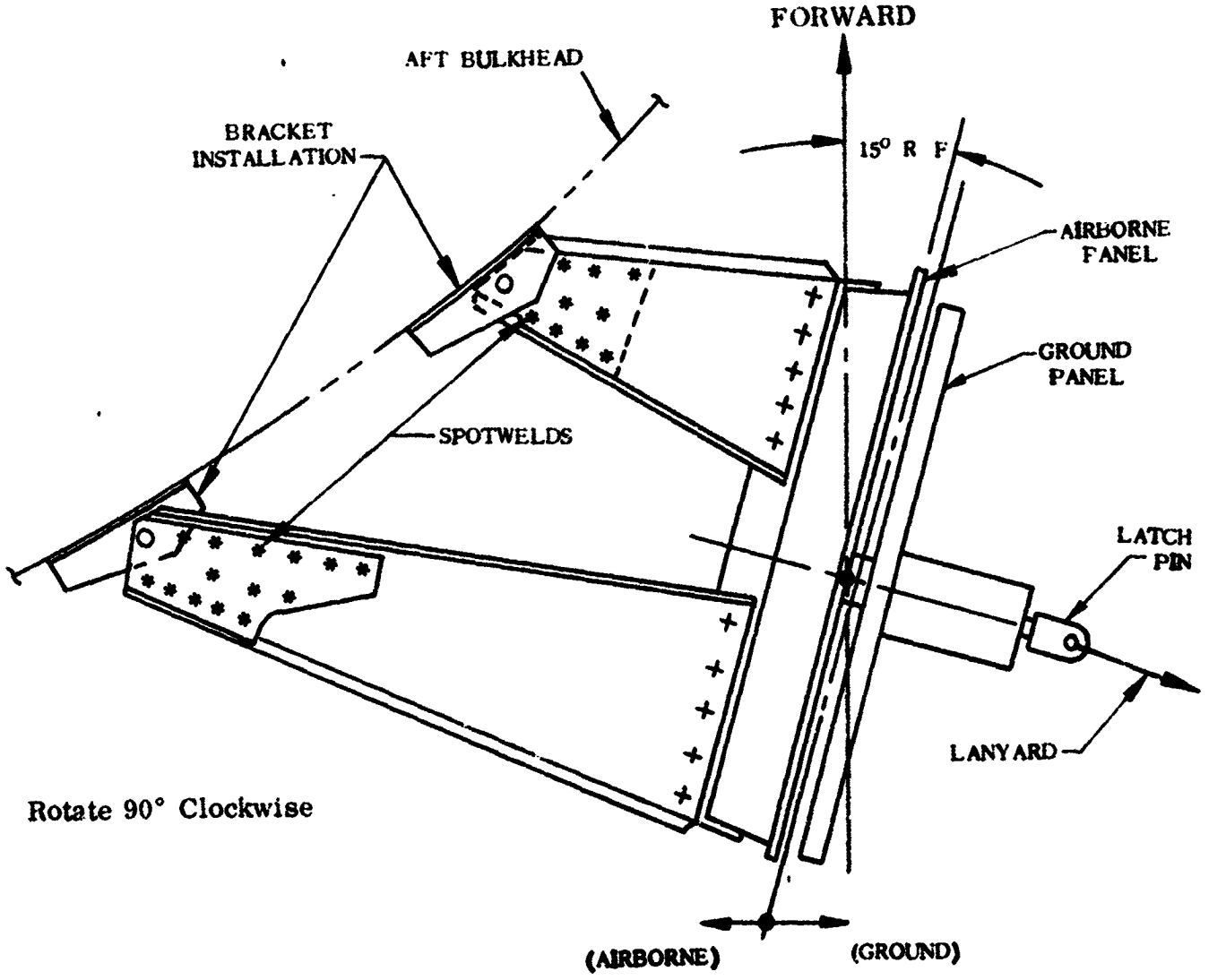

4B250LT

Figure 8.7-1. T-4 Aft Umbilical Panel Configuration

8.7.1 CRITICAL CONDITIONS. The critical loading conditions for the T-4 aft umbilical panel occur during umbilical disconnect and during transonic flight. At the instant of disconnect, ejection loads plus dead weight and wind combine to produce a critical loading condition on the airborne structure. Other critical times during the disconnect sequence are at maximum lanyard tension and just as the guide pins are sliding free of the airborne panel (maximum friction).

During flight, inertia loads plus aerodynamic loads produce critical loads on the structure.

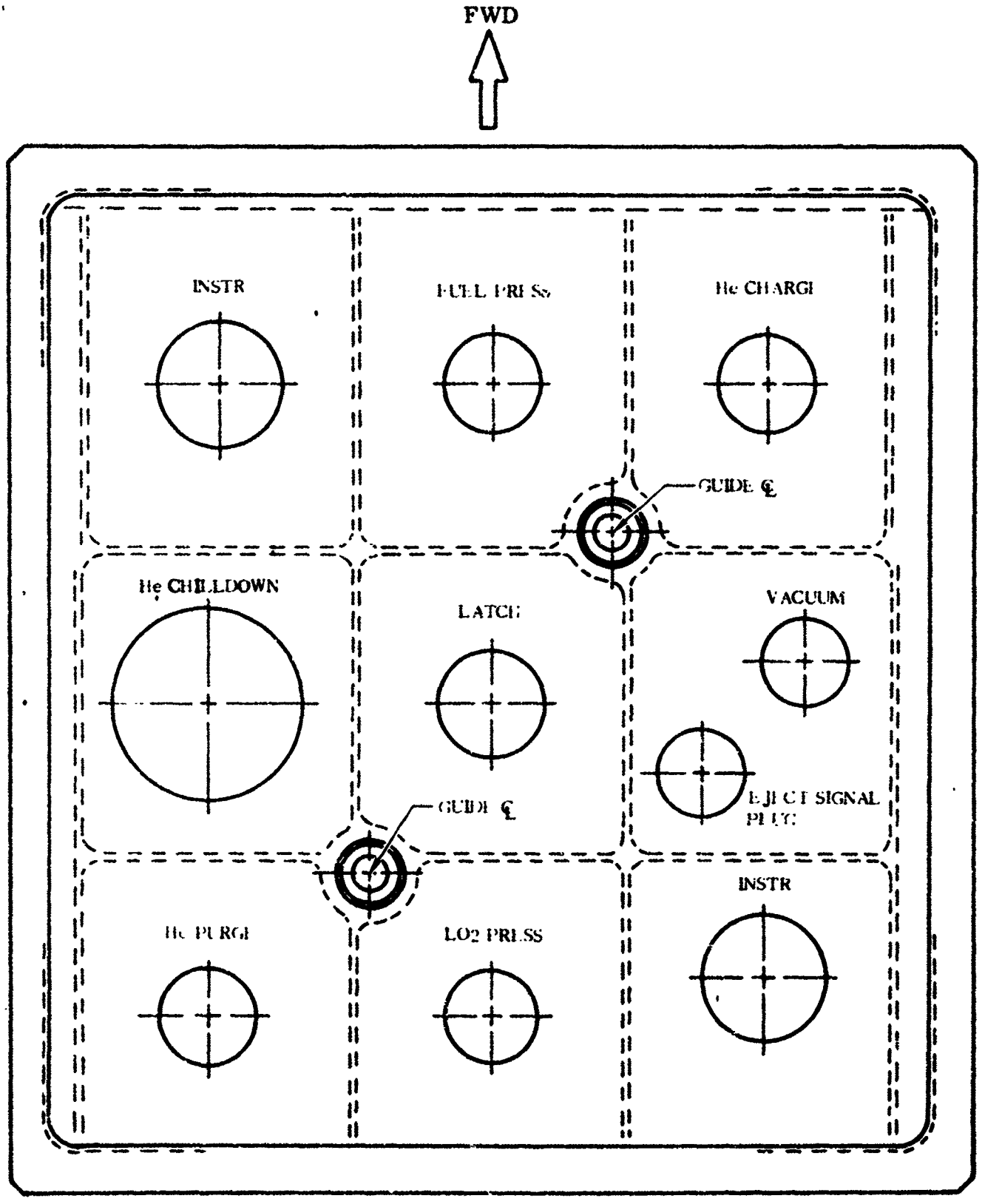

4B251LV

Figure 8.7-2. T-4 Airborne Panel (Looking Inboard) - Orientation of Disconnects

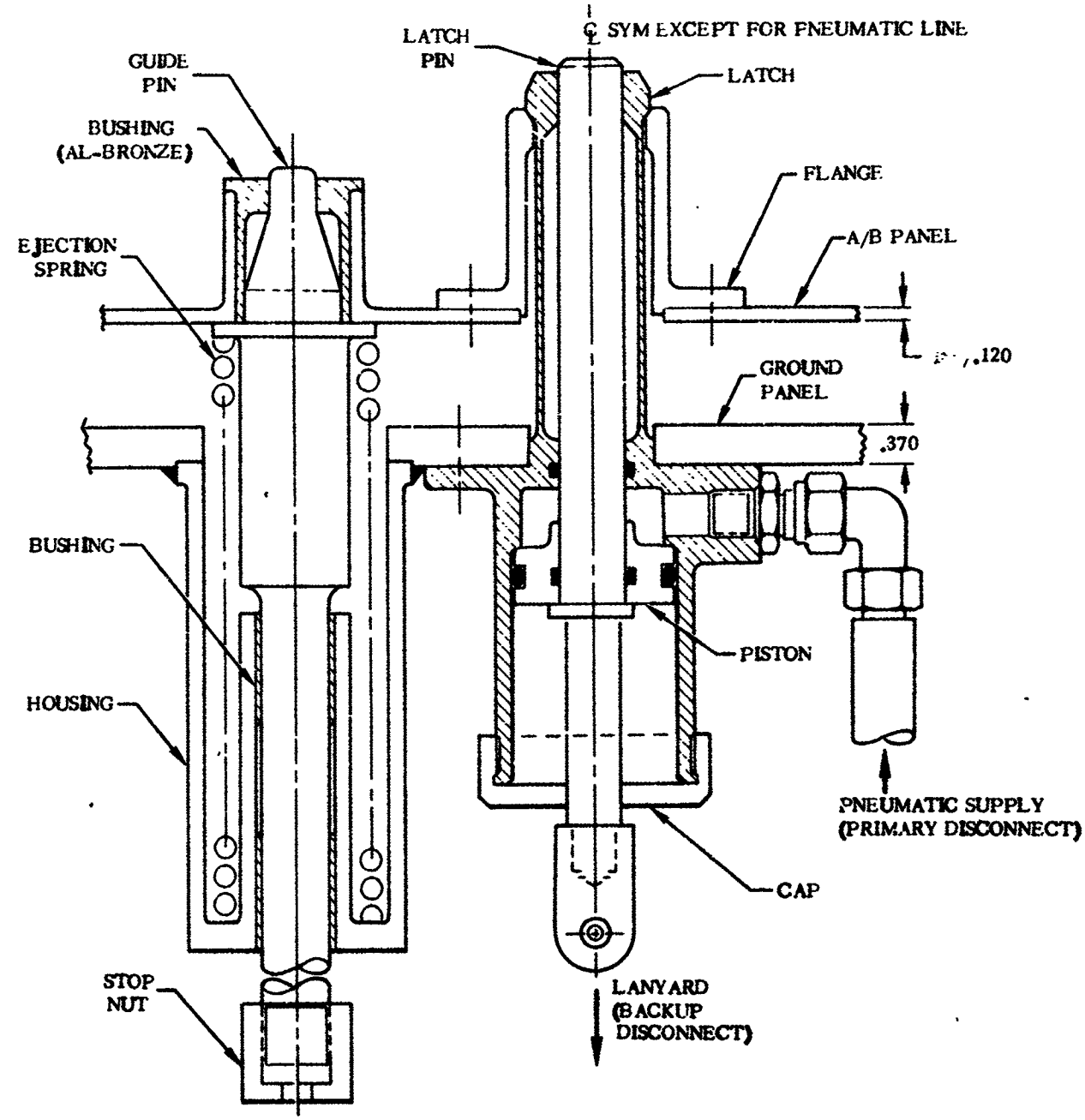

Figure 8.7-3. T-4 Aft Umbilical Panel Latch and Ejection Mechanism

8.7.2 WEIGHT AND CENTER OF GRAVITY DATA. The weight and C.G. shown in Figure 8.7-4 includes all tubes, wires, and connectors that are fastened to the umbilical panel, as well as the panel itself.

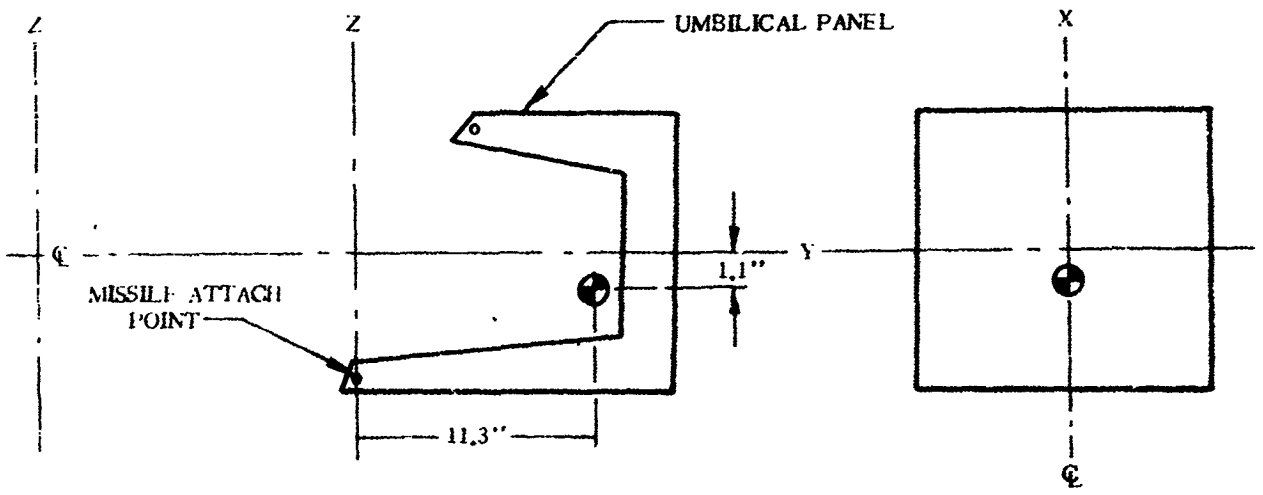

TOTAL WEIGHT = 15.5 LB

4B2531 V

Figure 8.7-4. T-4 Umbilical Panel Weight and Center of Gravity - Location

8.7.3 THERMAL DATA. The temperature of the brackets at the tank is -293° F and that of the GSE/airborne interface is assumed to be 70° F during launch. The temperature history of the umbilical panel during flight is presented in Figure 8.7-5.

8.7.4 INERTIA LOADS. The T-4 aft umbilical panel inertia load factors during critical times of flight are presented in Table 8.7-1.

8.7.5 STEADY-STATE AIR LOADS. The maximum steady-state crush pressure on the T-4 aft umbilical panel is plotted against Mach number in Figure 8.7-6.

8.7.6 BUFFET AND FLUTTER LOADS. The T-4 aft umbilical panel is subjected to a ±0.54 psi steady-state equivalent buffeting load. This load should be combined with the steady-state air loads presented in Paragraph 8.7.5.

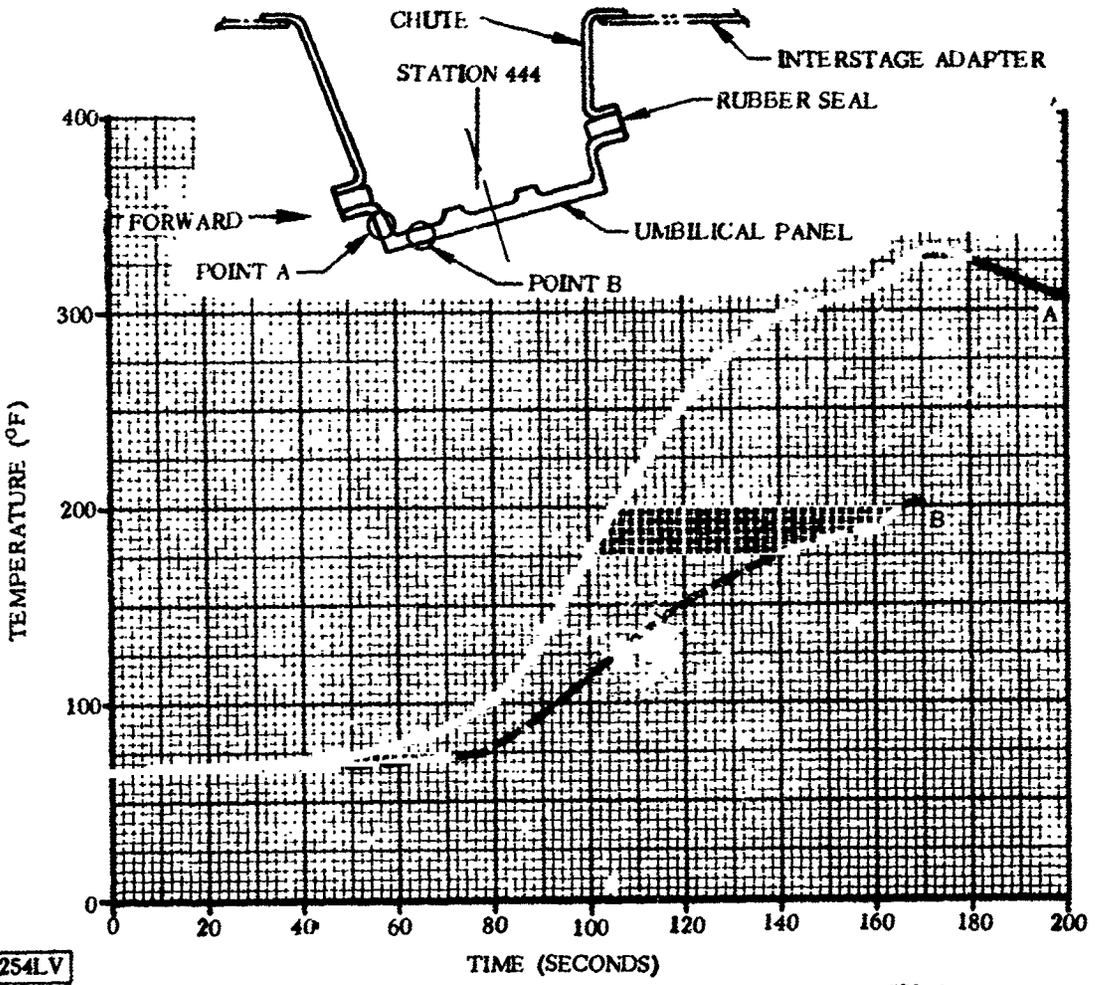

Figure 8.7-5. T-4 Aft Umbilical Panel Temperature History

TABLE 8.7-1. T-4 AFT UMBILICAL PANEL COMBINED STEADY-STATE ACCELERATION AND VIBRATION LOAD FACTORS DURING FLIGHT

Loading Condition	Load Factors	
	Longitudinal (g's)	Lateral (g's)
Launch*	+ 7.0	± 3.0
Launch*	- 5.0	± 3.0
Launch*	+ 1.0	± 6.0
Mach 1	+ 2.0	± 6.5
Mach 1	+ 8.0	± 1.0
Mach 1	- 4.0	± 1.0
Max q	+ 8.3	± 1.0
Max q	- 3.7	± 1.0
Max q	+ 2.3	± 6.5
Centaur MES	+12.0	± 1.0
Centaur MES	-10.8	± 1.0
Centaur MECO	+ 7.0	±12.0

*These loads are not combined with disconnect loads.

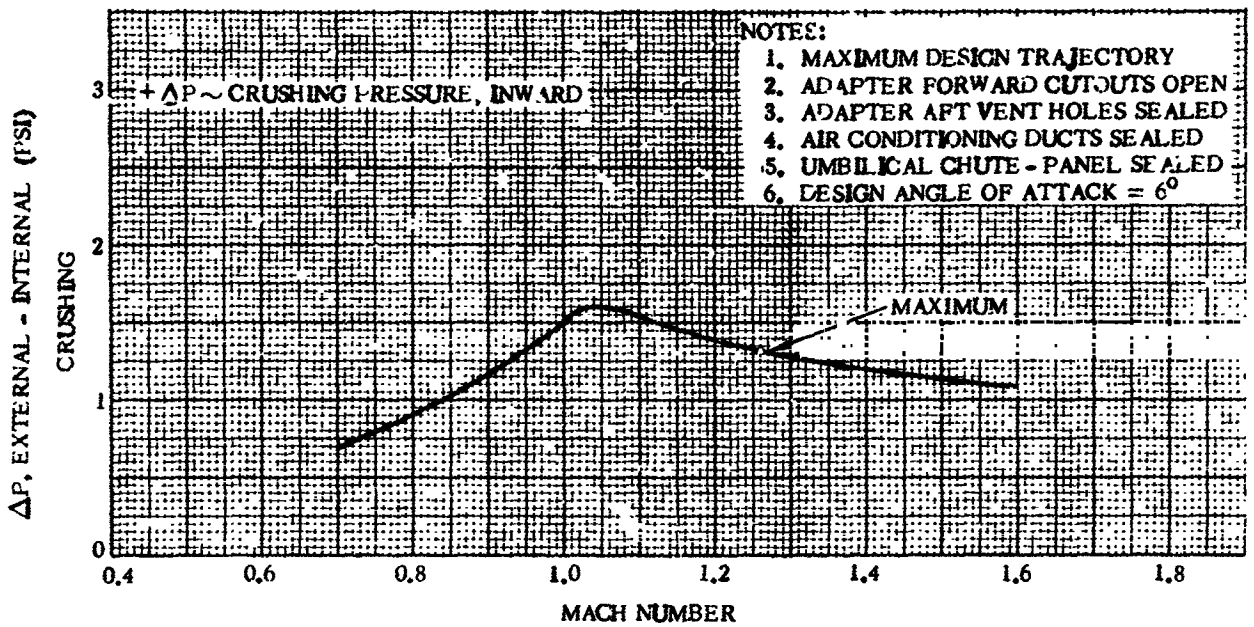

Figure 8.7-6. T-4 Aft Umbilical Panel Steady-State Aerodynamic Loads

8.7.7 MISCELLANEOUS LOAD PARAMETERS. Other critical loads on the T-4 aft umbilical panel are disconnect and impact loads.

8.7.7.1 Disconnect Loads. Figure 8.7-7 presents loads for the most critical conditions during disconnect, namely:

a. Latch pin release

b. Spring ejection

c. Guide pin movement.

These loads are imposed on the airborne structure at the GSE/airborne interface.

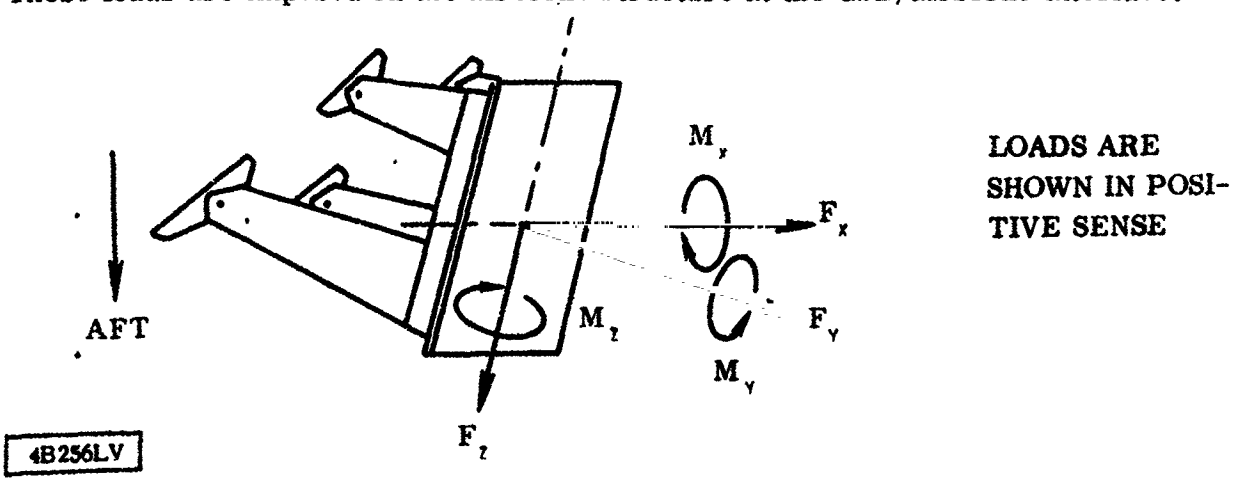

Figure 8.7-7. T-4 Aft Umbilical Panel Disconnect Load Sense

The 170-pound force of the liquid helium disconnect (Table 8.7-2) is due to maximum pressure in the line; and the other forces are spring loads. All ejection loads are considered to be suddenly applied and should be multiplied by an impact factor of 2.0 for stress analysis of the structure.

TABLE 8.7-2. T-4 AFT UMBILICAL PANEL FORCES AND MOMENTS

Load Condition	Force (lb)			Moment (in.-lb)		
	F_X	F_Y	F_Z	M_X	M_Y	M_Z
Latch Pin Release (maximum layard pull)	±110	+340	+100	+625	±125	±835
Spring Ejection (beginning of ground panel motion)	± 25	*-860	+ 70	+415	±125	±255
Guide Pin Movement (end of guided motion)	± 25	+250	+ 70	+690	±125	±360

*The -860 lb load is the sum of the individual ejection loads acting at the airborne/GSE interface, as itemized below:

2 Instrumentation	(40 lb each)	=	80 lb
4 Pneumatic	(50 lb each)	=	200 lb
1 Vacuum	(0 lb)	=	0
1 Liquid Helium	(170 lb)	=	170 lb
2 Springs	(205 lb each)	=	410 lb
	Total	=	860 lb

8.7.7.2 Impact Loads. Three impact loads which occur on the GSE portion of the T-4 aft umbilical panel are:

a. Maximum lanyard tension = 360 lb

b. Load on guide pin stop nut = 4450 lb per pin

c. Load on latch housing due to piston bottoming out = 2500 lb
An internal pressure of 400 psig is present in the latch housing at this time.
Maximum internal pressure after latch impact = 1500 psig.

THIS PAGE INTENTIONALLY LEFT BLANK.

8.8 T-0 UMBILICAL PANEL

The T-0 umbilical panel is located in Quadrant II, at Station 437, 16°25′ from the Y-Y axis. The panel supports the airborne portion of the T-0 umbilical disconnect. Figure 8.8-1 shows the airborne panel configuration.

8.8.1 CRITICAL CONDITIONS. The T-0 umbilical panel is subjected to critical loads at umbilical disconnect and during transonic flight. The panel is subjected to two critical loading conditions at T-0 disconnect. These are when the lanyard pull is a maximum (backup disconnect), and during a normal (primary) disconnect sequence when ejection spring loads are critical.

During flight, inertia and aerodynamic loads combine to create a critical loading condition on the structure.

8.8.2 WEIGHT AND CENTER OF GRAVITY DATA. The weight of the T-0 panel, receptacle and cable is 3.8 lb. The C.G. location is shown in Figure 8.8-2.

8.8.3 THERMAL DATA. The tank brackets are a temperature of -293°F while the GSE/airborne interface is assumed to be at 70°F.

8.8.4 INERTIA LOADS. The inertia loads for the T-0 umbilical panel are given in Table 8.8-1.

TABLE 8.8-1. T-0 UMBILICAL PANEL COMBINED STEADY-STAT ACCEL-ERATION AND VIBRATION LOAD FACTORS DURING FLIGHT

Loading Condition	Load Factors	
	Longitudinal (g's)	Lateral (g's)
Launch *	+ 7.0	±3.0
Launch *	- 5.0	±3.0
Launch *	+ 1.0	±6.0
Mach 1	+ 2.0	±6.5
Mach 1	+ 8.0	±1.0
Mach 1	- 4.0	±1.0
Max q	+ 8.3	±1.0
Max q	- 3.7	±1.0
Max q	+ 2.3	±6.5
Centaur MES	+12.0	±1.0
Centaur MES	-10.8	±1.0
Centaur MECO	+ 7.0	±12.0

*These loads are not to be combined with disconnect loads.

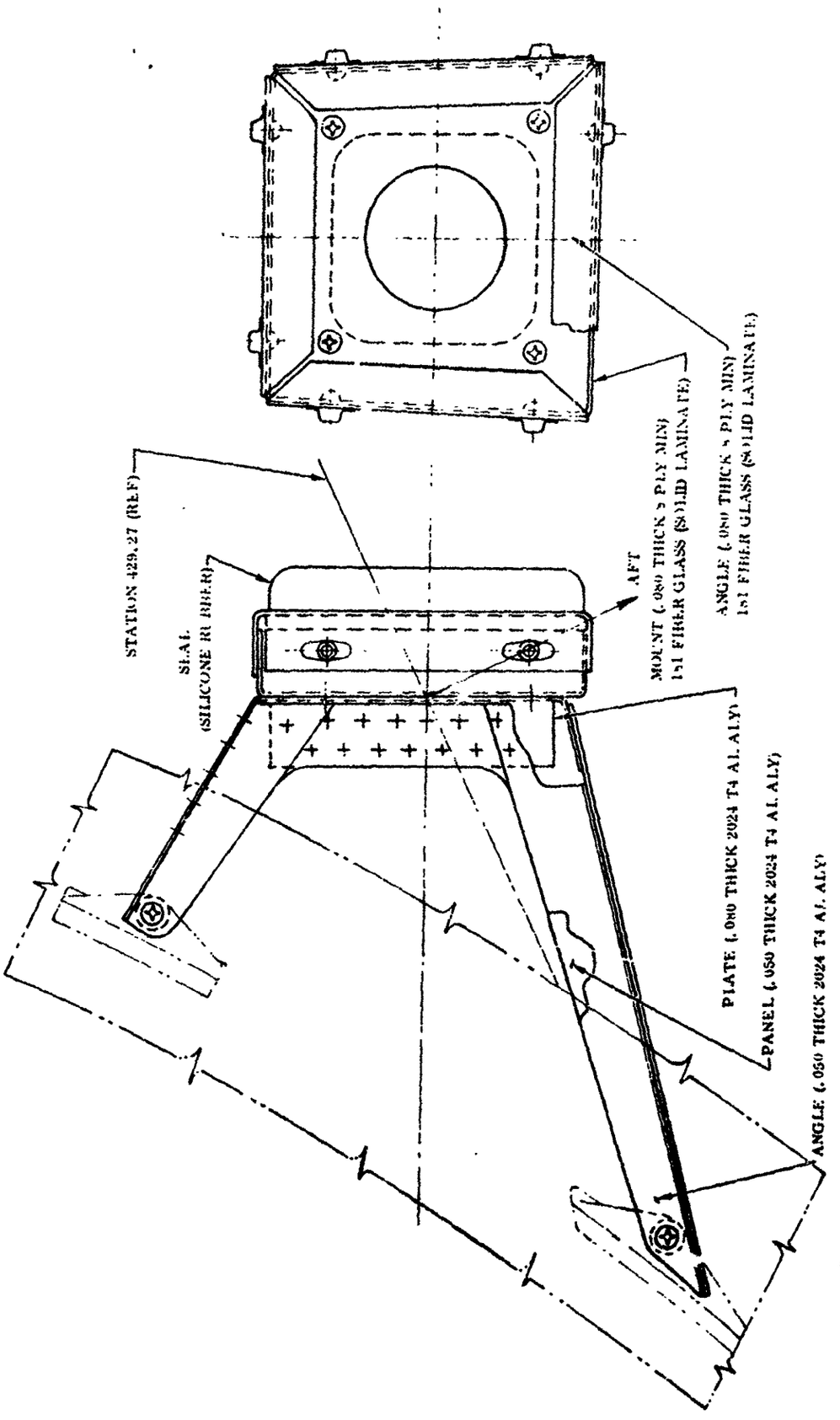

Figure 8.8-1. T-0 Umbilical Panel Configuration

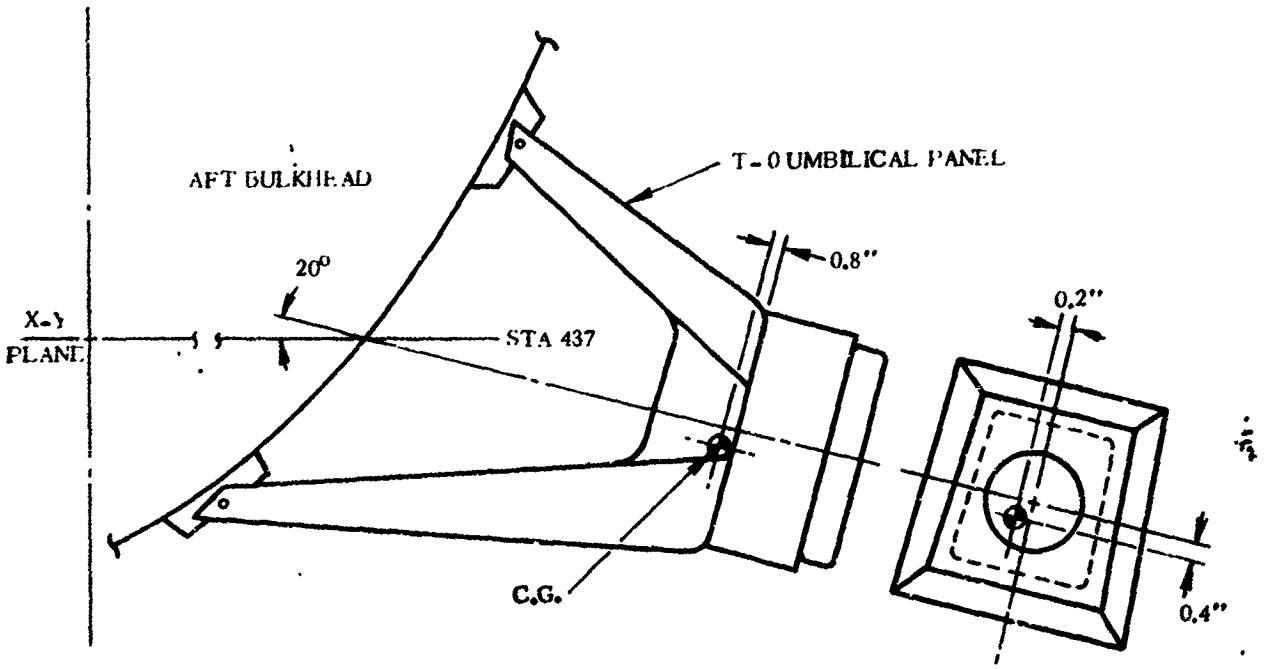

4B258LV

Figure 8.8-2. T-0 Umbilical Panel Center of Gravity Location

8.8.5 STEADY-STATE AIR LOADS. The steady-state air loads for the T-0 umbilical panel is platted against Mach number in Figure 8.8-3. These loads act in combination with buffet loads presented in Paragraph 8.8.6.

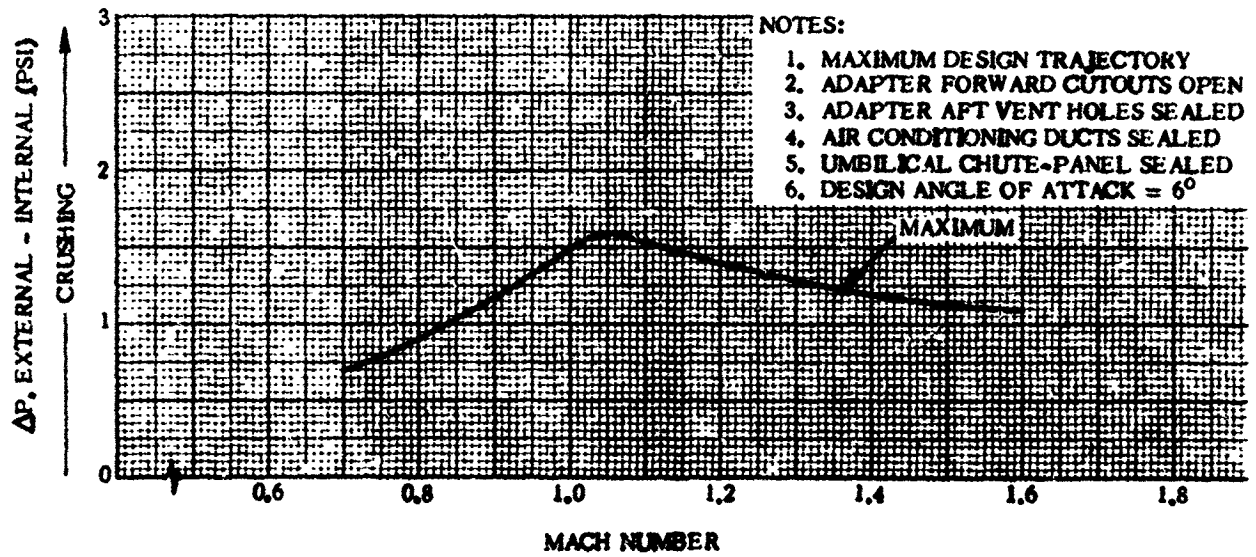

[illegible]259LV

Figure 8.8-3. T-0 Umbilical Panel - Steady-State Aerodynamic Loads

8.8.6 BUFFET AND FLUTTER LOADS. The buffet load on the T-0 umbilical panel must be added to the steady-state air load presented in Paragraph 8.8.5. The equivalent static pressure which represents buffet loading is ±0.54 psi.

8.8.7 MISCELLANEOUS LOAD PARAMETERS. The critical loads on the T-0 umbilical panel disconnect are presented in Figure 8.8-4 and Table 8.8-2. These loads include wind, dead weight, and lanyard misalignment effects.

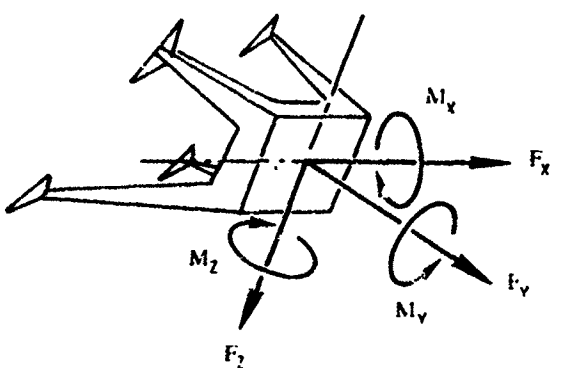

LOADS ARE SHOWN IN POSITIVE SENSE

4B250LV

Figure 8.8-4. T-0 Umbilical Panel Loads at Disconnect

TABLE 8.8-2. T-0 UMBILICAL PANEL FORCES AND MOMENTS

Condition	Force (lb)			Moment (in.-lb)		
	F_X	F_Y	F_Z	M_X	M_Y	M_Z
Primary Disconnect	± 5	-275*	+15	+115	±30	± 40
Backup Disconnect	±35	+125	+30	+145	±30	±135

*This ejection spring load is applied suddenly, and should be multiplied by an impact factor of 2.0 for stress analysis of the structure.

8.9 PROPELLANT DUCTING

The primary function of this component is to transfer liquid oxygen and fuel from the pumps to the engines. The ducting configuration is shown in Figure 8.9-1.

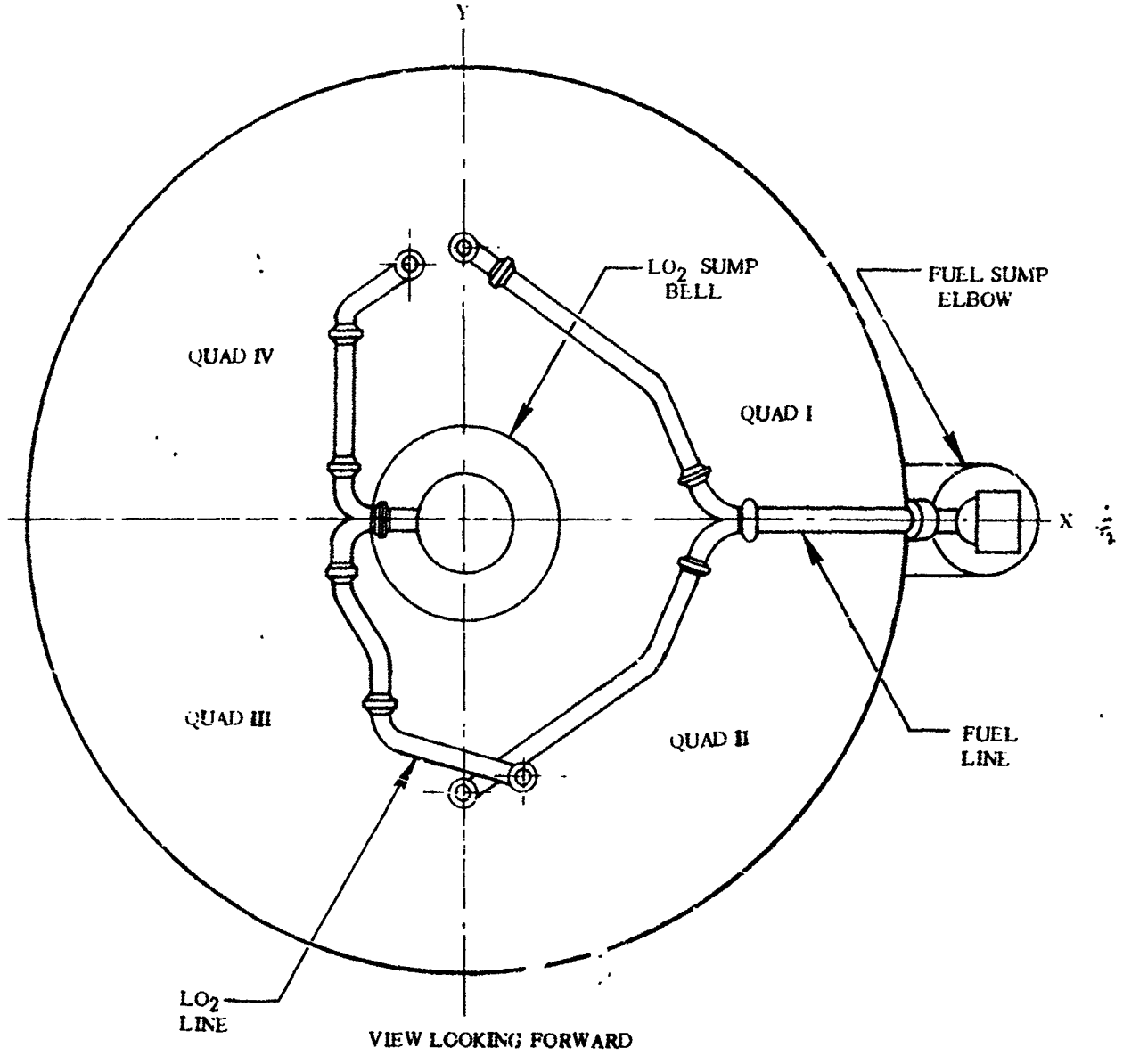

4B261LV

Figure 8.9-1. Propellant Ducting Configuration - Main Engines

8.9.1 CRITICAL CONDITIONS. The critical loading conditions on the ducting occur during Centaur thrust buildup and Centaur MECO when the inertia loads are the greatest. Internal pressure acts simultaneously with maximum inertia loads.

8.9.2 WEIGHT AND CENTER OF GRAVITY DATA. The weight of the empty propellant ducts are as follows:

LO_2 Duct = 18 lb
Fuel Duct = 20 lb

A C.G. is not applicable for this installation due to the length, number of supports, and complex geometry of the ducting.

8.9.3 THERMAL DATA. The temperatures for the propellant ducts are:

Fuel Duct = -423°F
LO_2 Duct = -297°F

8.9.4 INERTIA LOADS. The inertia loads for the propellant ducting are given in Table 8.9-1.

TABLE 8.9-1. PROPELLANT DUCTING INERTIA LOAD FACTORS

Condition	Longitudinal* (g's)	Lateral Vibration (g's)
MECO	+ 12	±1.0
MECO	+ 7	± 6
TBU	-3.2	±1.0
* + longitudinal load acts aft		

8.9.5 STEADY-STATE AIR LOADS. The propellant ducts are not subjected to critical loads due to aerodynamic forces.

8.9.6 BUFFET AND FLUTTER LOADS. The propellant ducts are not subjected to critical loads due to buffet or fluctuating pressure.

8.9.7 MISCELLANEOUS LOAD PARAMETERS. Propellant duct internal pressure is presented in Table 8.9-2. The LO_2 and LH_2 line pressures are the same for both the 15K and 17.5K engines.

TABLE 8.9-2. PROPELLANT DUCT MAXIMUM STEADY-STATE OPERATING & TRANSIENT PRESSURES

Condition	Pressure (psia)	
	LO_2	Fuel
Maximum S.S. Operating Pressure	125	50
Transient (proof) Pressure	200	200

8.10 LIQUID OXYGEN VENT VALVE AND STANDPIPE

The LO_2 vent valve and standpipe are located in Quadrant I, 30 degrees from the X-X axis as shown in Figure 8.10-1.

The vent valve controls the ullage pressure in the liquid oxygen tank by venting the gaseous oxygen through the standpipe and vent duct into the atmosphere.

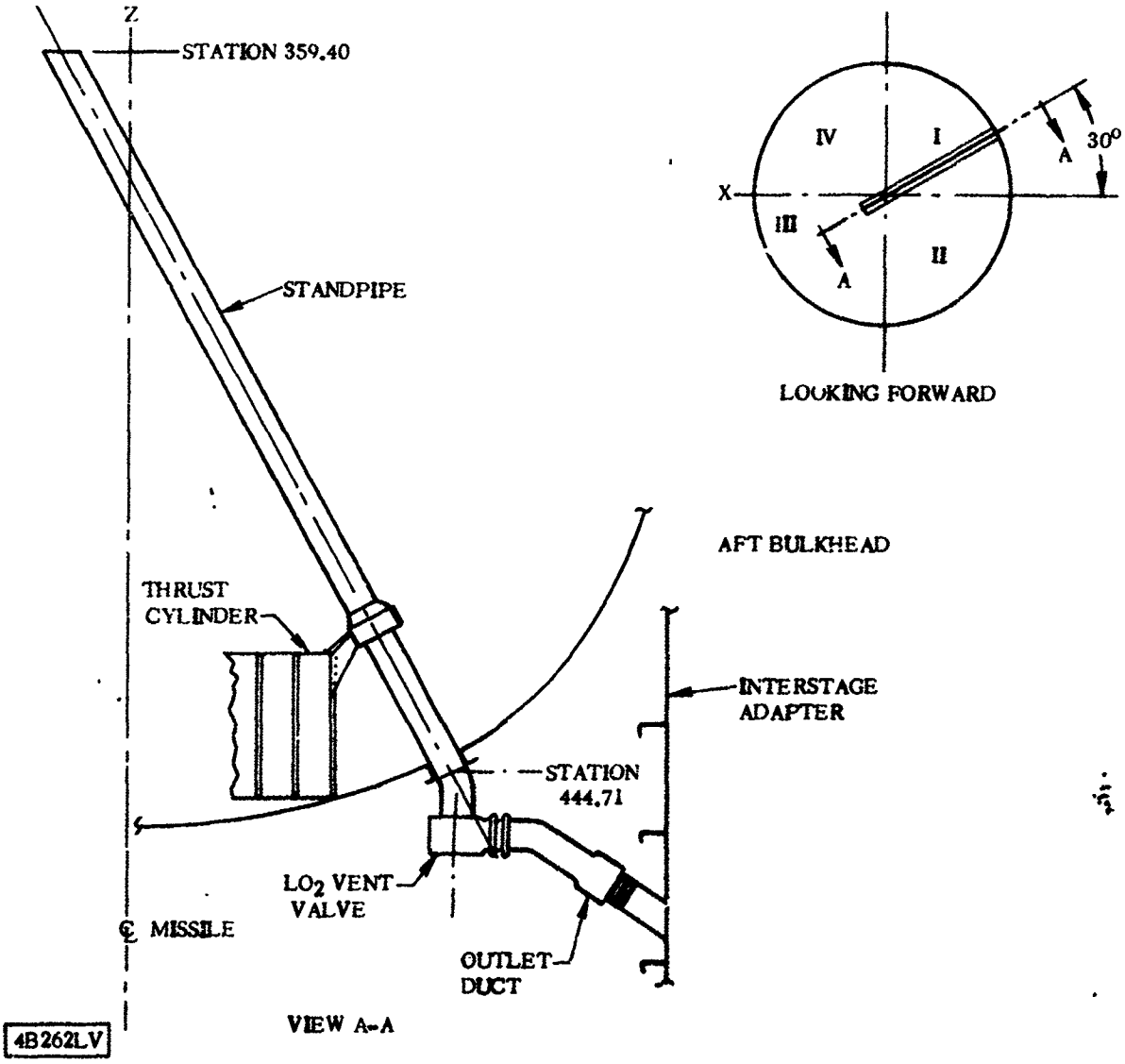

Figure 8.10-1. Liquid Oxygen Vent Valve and Standpipe Configuration

8.10.1 CRITICAL CONDITIONS. There are two critical loading conditions for the LO_2 standpipe. The first one occurs at BECO when the maximum slosh load acts with the Max g inertia loads. The second critical condition for the standpipe arises from the inertia loads at Centaur MECO.

The critical loading conditions for the vent valve are the inertia loads at Centaur MES and MECO.

8.10.2 WEIGHTS AND CENTER OF GRAVITY DATA. The structural design weight of the vent valve and associated equipment outside the tank is 10.5 lb. The total weight of the standpipe and miscellaneous attached hardware inside the tank is 8.3 lb. The C.G.'s of both items are located as shown in Figure 8.10-2.

8.10.3 THERMAL DATA. The temperature of the LO_2 vent valve and standpipe is -297°F.

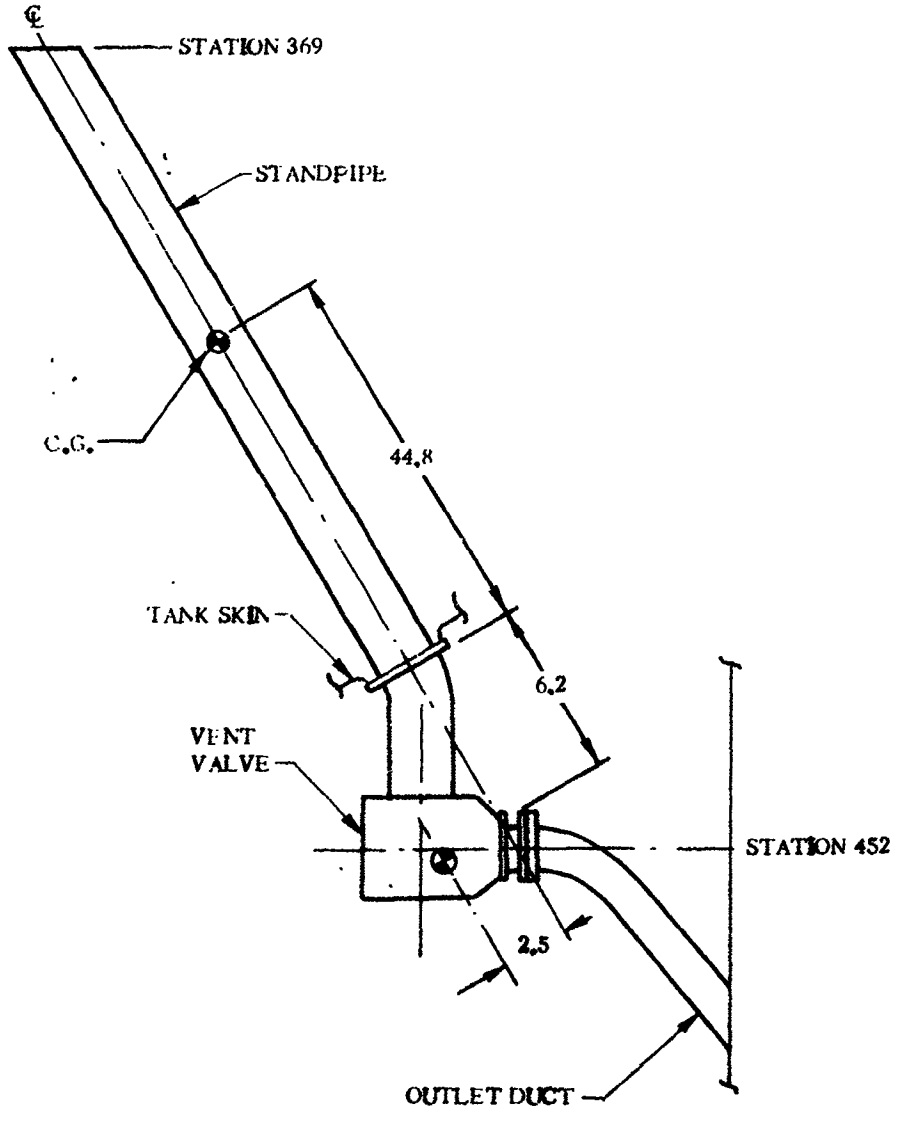

4B263LV

Figure 8.10-2. Liquid Oxygen Vent Valve and Standpipe - Center of Gravity Location

8.10.4 INERTIA LOADS. The inertia load factors for the LO_2 standpipe and vent valve are found in Tables 8.10-1 and 8.10-2, respectively.

TABLE 8.10-1. LIQUID OXYGEN STANDPIPE INERTIA LOAD FACTORS

Condition	Steady-State Acceleration (g's)		Vibration (g's)
	Longitudinal	Lateral	Normal to Standpipe
BECO	+5.9	±0.3	negligible
MECO	+7.0	±0.5	±24

TABLE 8.10-2. LIQUID OXYGEN VENT VALVE AND DUCTING INERTIA LOAD FACTORS

Condition	Load Factors	
	Longitudinal (g's)	Lateral (g's)
MES	+16.0	± 1.0
MES	-10.8	± 1.0
MECO	+ 7.0	±16.0
MECO	—	±30.0*

*Acting in any direction on the outlet duct only (Reference Figure 8.10-2).

8.10.5 STEADY-STATE AIR LOADS. The LO_2 vent valve and standpipe do not receive critical loads due to aerodynamic forces.

8.10.6 BUFFET AND FLUTTER LOADS. The LO_2 vent valve and standpipe do not receive critical loads due to buffet or fluctuating pressure.

8.10.7 MISCELLANEOUS LOAD PARAMETERS. During the first 70 seconds of flight, the LO_2 standpipe experiences slosh loads reaching values as high as 50 pounds, acting normal to its length. The slosh loads are considered uniformly distributed along the length of the standpipe.

THIS PAGE INTENTIONALLY LEFT BLANK.

8.11 WIRING TUNNEL AFT BULKHEAD

The wiring tunnel aft bulkhead is located on the X-X axis between Quadrants I and II. The bulkhead supports the liquid hydrogen (LH_2) sump elbow at Station 412 and the connectors and fittings for the wiring and tubing in the wiring tunnel. Figure 8.11-1 shows the tunnel aft bulkhead configuration. The hole arrangement shown does not represent a particular bulkhead configuration but is typical for vehicles AC-6 through AC-15.

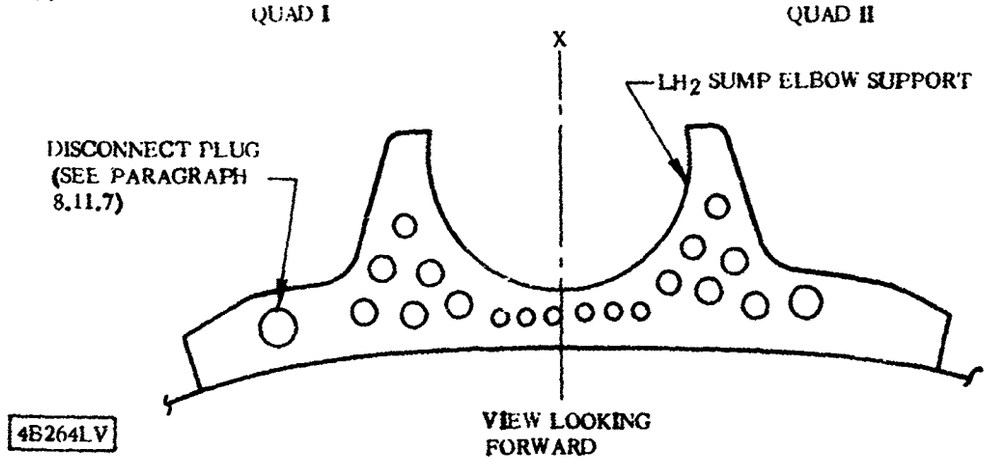

Figure 8.11-1. Wiring Tunnel Aft Bulkhead Configuration

8.11.1 CRITICAL CONDITIONS. The critical loading condition on the wiring tunnel aft bulkhead is a combination differential pressure, the loads imposed from the boost pump fairing and skirt, the LH_2 sump elbow imposed loads and the disconnect force at Atlas/Centaur separation.

8.11.2 WEIGHT AND CENTER OF GRAVITY DATA. The weight of the aft wiring tunnel bulkhead does not impose critical loads on the structure. The plugs, receptacles and wiring which are supported by the bulkhead conservatively consist of 2.0 pounds (total) per bulkhead cutout. This weight is negligible compared to the disconnect force described in Paragraph 8.11.7.

8.11.3 THERMAL DATA. The minimum temperature of the wiring tunnel aft bulkhead is -280° F.

8.11.4 INERTIA LOADS. Inertia loads on the aft wiring tunnel bulkhead are not critical. At BECO, the plugs, receptacles and supported wiring length receive a maximum axial acceleration of 5.9 g's (acting aft), however, the bulkhead is subjected to more critical loadings during transonic flight and at Atlas/Centaur separation. Reference Paragraphs 8.11.5 and 8.11.7.

8.11.5 STEADY-STATE AIR LOADS. See Figure 8.11-2 for air loads on wiring tunnel aft bulkhead. The air loads shown on the bulkhead include the effect of fluctuating pressures.

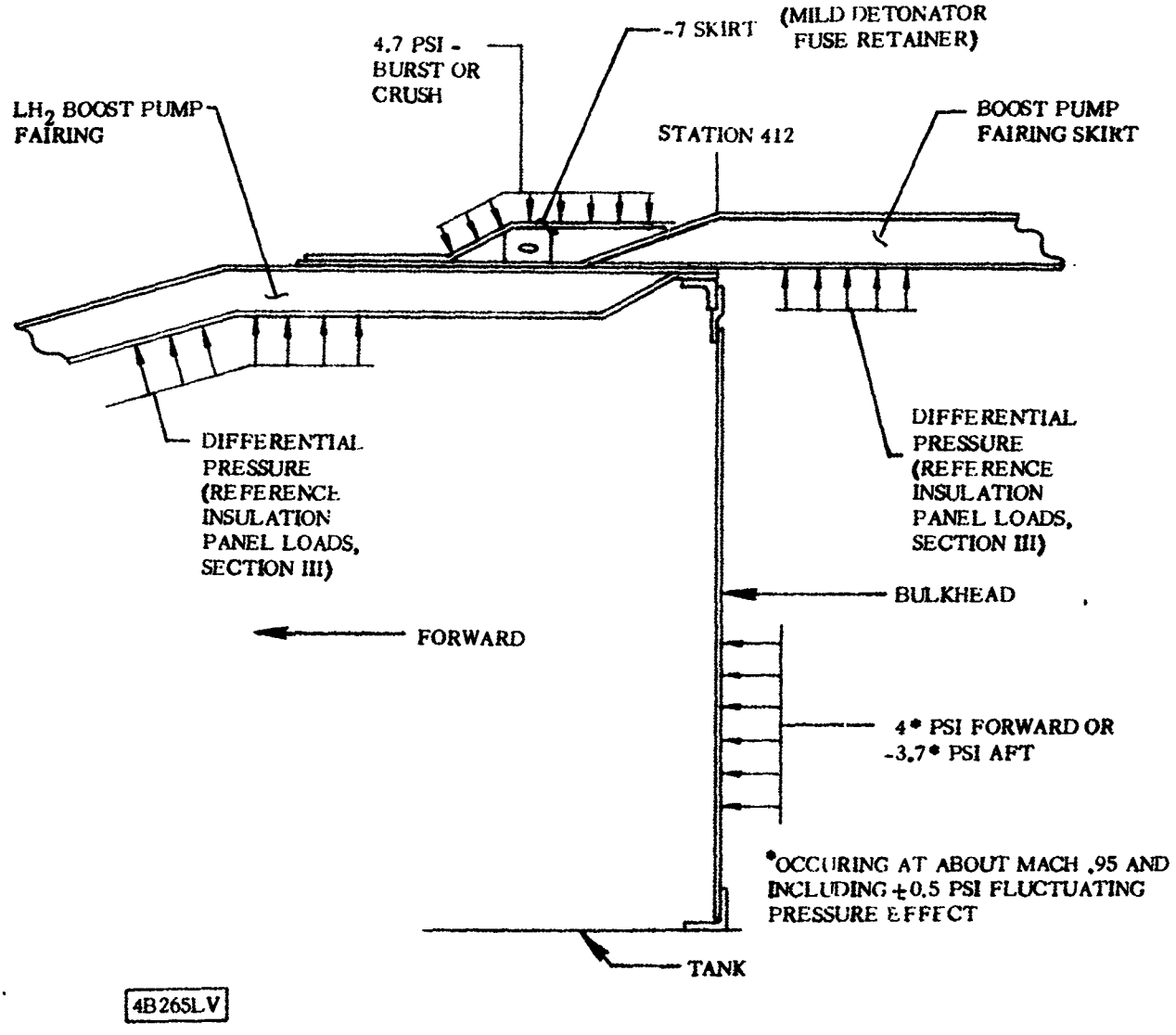

Figure 8.11-2. Wiring Tunnel Aft Bulkhead - Differential Pressures

8.11.6 BUFFET AND FLUTTER LOADS. The effects of fluctuating pressure are included in the loads presented in Figure 8.11-2.

8.11.7 MISCELLANEOUS LOAD PARAMETERS. At Atlas/Centaur separation, the disconnect plug and receptacle electrically demate and release a system of springs which push the two halves apart. The maximum design load for the plug and receptacle combination is 300 pounds. (Acting forward-on the wiring tunnel bulkhead).

8.12 LIQUID OXYGEN FILL AND DRAIN LINE

The LO_2 fill and drain line is located in Quadrant II with the disconnect interface located at Station 418 as shown in Figure 8.12-1.

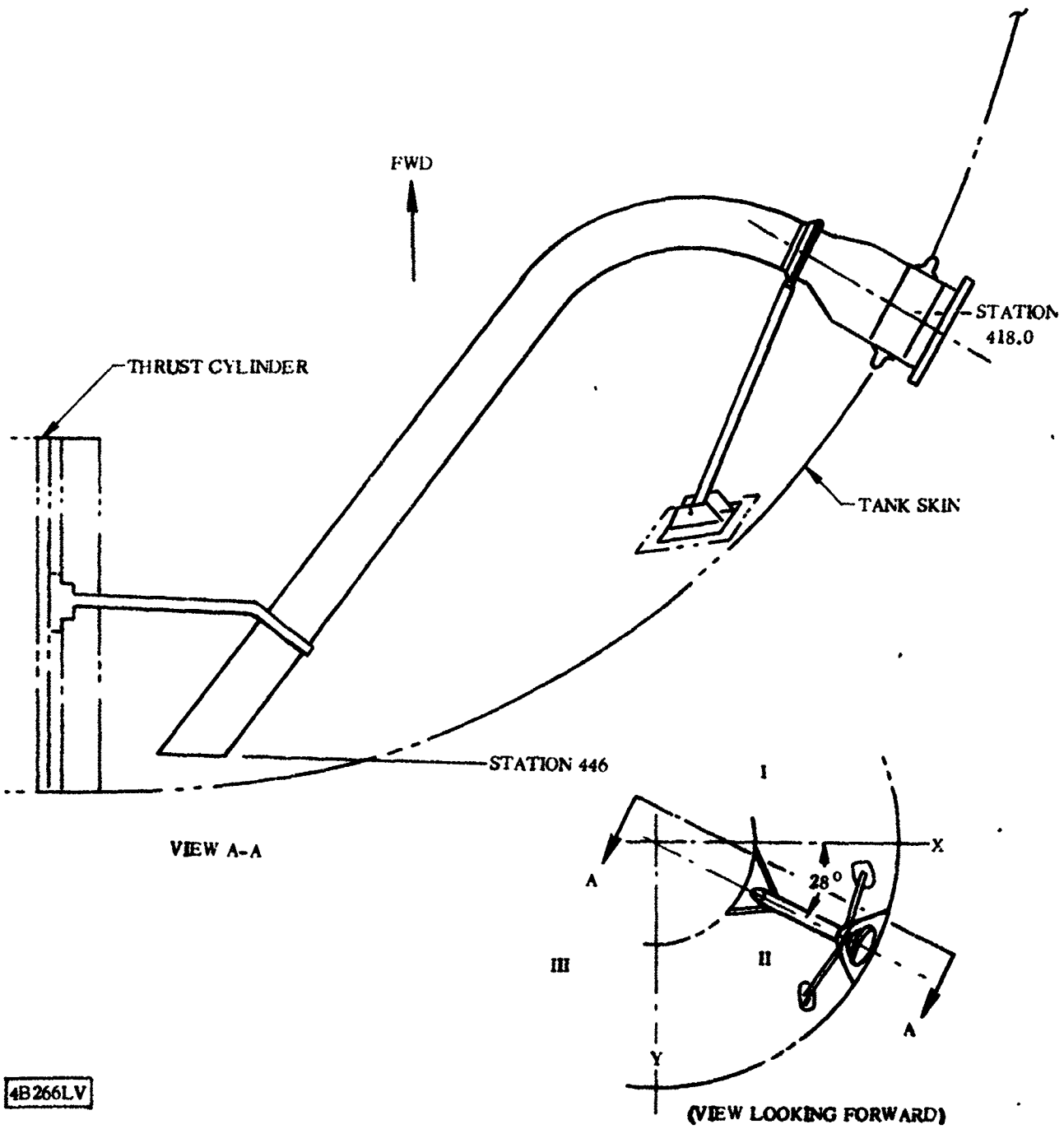

Figure 8.12-1. Liquid Oxygen Fill and Drain Line Configuration

8.12.1 CRITICAL CONDITIONS. The critical loading condition of the LO_2 fill and drain line is at disconnect, when a combination of disconnect loads and pressures are acting on the structure.

8.12.2 WEIGHT AND CENTER OF GRAVITY DATA. The weight of the LO_2 fill and drain line does not impose critical loads on the structure.

8.12.3 THERMAL DATA. The temperature of the LO_2 fill and drain line is -297°F.

8.12.4 INERTIA LOADS. Inertia loads do not add to the critical loading condition due to the time of ground disconnect for the fill and drain valve.

8.12.5 STEADY-STATE AIR LOADS. The LO_2 fill and drain line does not receive critical loads due to aerodynamic forces.

8.12.6 BUFFET AND FLUTTER LOADS. The LO_2 fill and drain line does not receive critical loads due to buffet or fluctuating pressure.

8.12.7 MISCELLANEOUS LOAD PARAMETERS. Pressure and disconnect loads must be considered in the analysis.

8.12.7.1 Pressure. Liquid oxygen ullage and head pressure act on the LO_2 fill and drain line. The ullage pressure is given in Section VI of this report.

8.12.7.2 Disconnect Loads. Consideration is made of the effects of impact, missile drift, and possible boom and vehicle misalignment. It is further assumed that the static line disconnect is in operation, since it results in higher loads then the primary bolt breaker. Loading conditions and associated loads are presented in Table 8.12-1. The disconnect load sign convention is shown in Figure 8.12-2.

TABLE 8.12-1. LIQUID OXYGEN FILL AND DRAIN VALVE DISCONNECT LOADS

Loading Condition	M_Z (in.-lb)	M_T (in.-lb)	M_R (in.-lb)	P_Z (lb)	P_T (lb)	P_R (lb)
Disconnect with no misalignment	0	13,000	0	1050	0	1300
Disconnect with maximum misalignment	6500	11,300	2470	910	530	1300

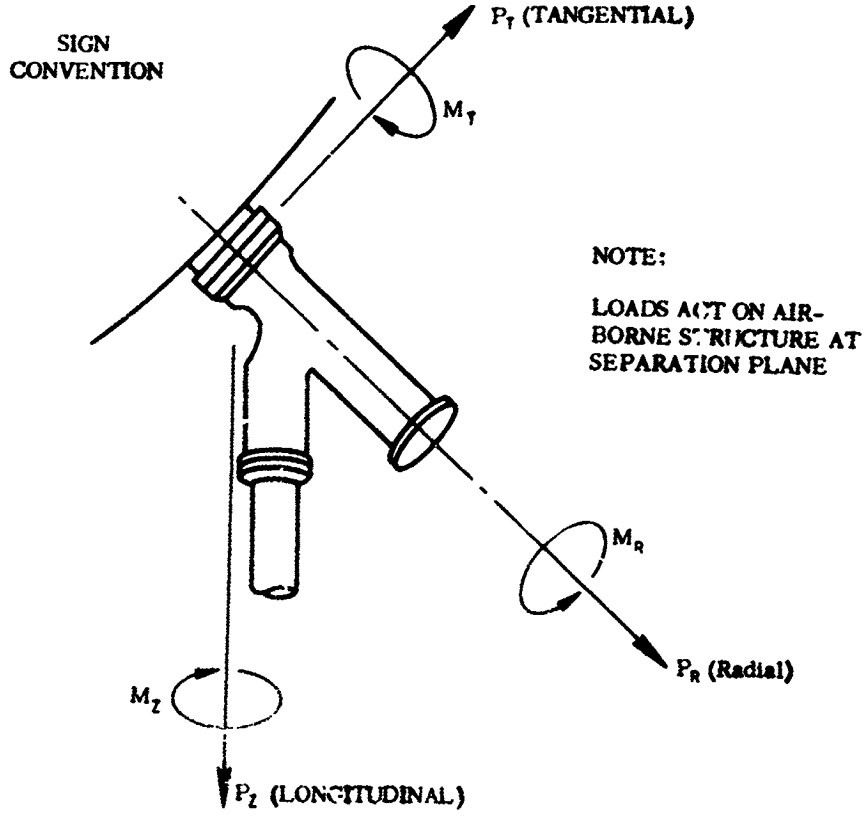

4B267LV

Figure 8.12-2. Liquid Oxygen Fill and Drain Valve Disconnect Load Sign Convention

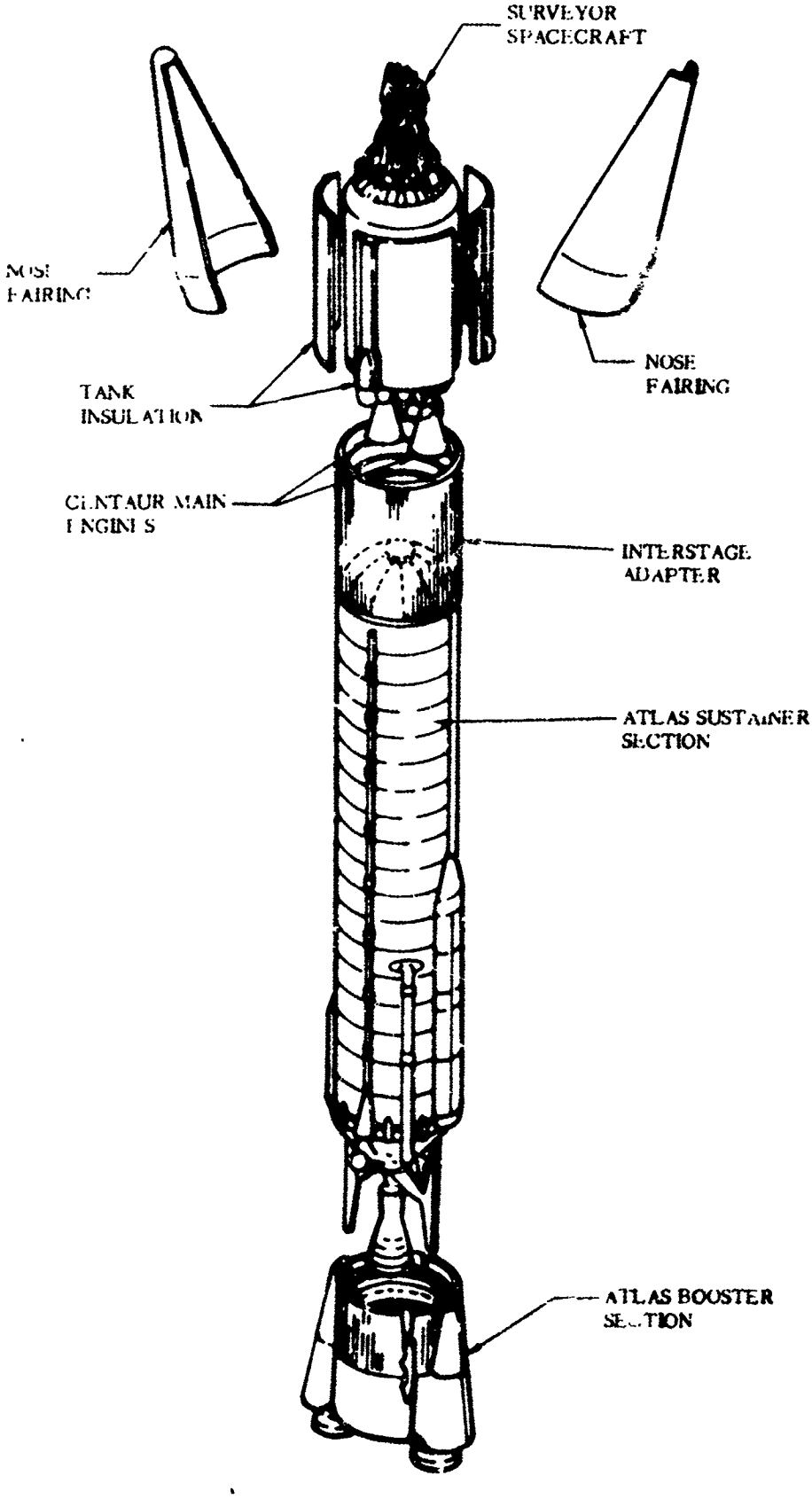
SURVEYOR
SPACECRAFT
NOSE
FAIRING
NOSE
FAIRING
TANK
INSULATION
CENTAUR MAIN
ENGINES
INTERSTAGE
ADAPTER
ATLAS SUSTAINER
SECTION
ATLAS BOOSTER
SECTION

SECTION IX

ATLAS BOOSTER VEHICLE

9.1 INTRODUCTION

The Atlas booster vehicle structure consists of two sections: the tank section and the booster section (see Figure 9.1-1). The tank section consists of a pressurized stainless steel cylinder which is divided into fuel and oxidizer containers by an intermediate bulkhead. The Centaur vehicle is mated to the Atlas by means of the interstage adapter, which in turn is attached to the forward end of the liquid oxygen tank at Station 570. The jettisonable booster section, secured to a thrust ring at the aft end of the tank, consists of a main thrust cylinder, two forward nacelle door assemblies (attached to opposite sides of the thrust cylinder), an aft engine fairing assembly, and a fire-shield assembly.

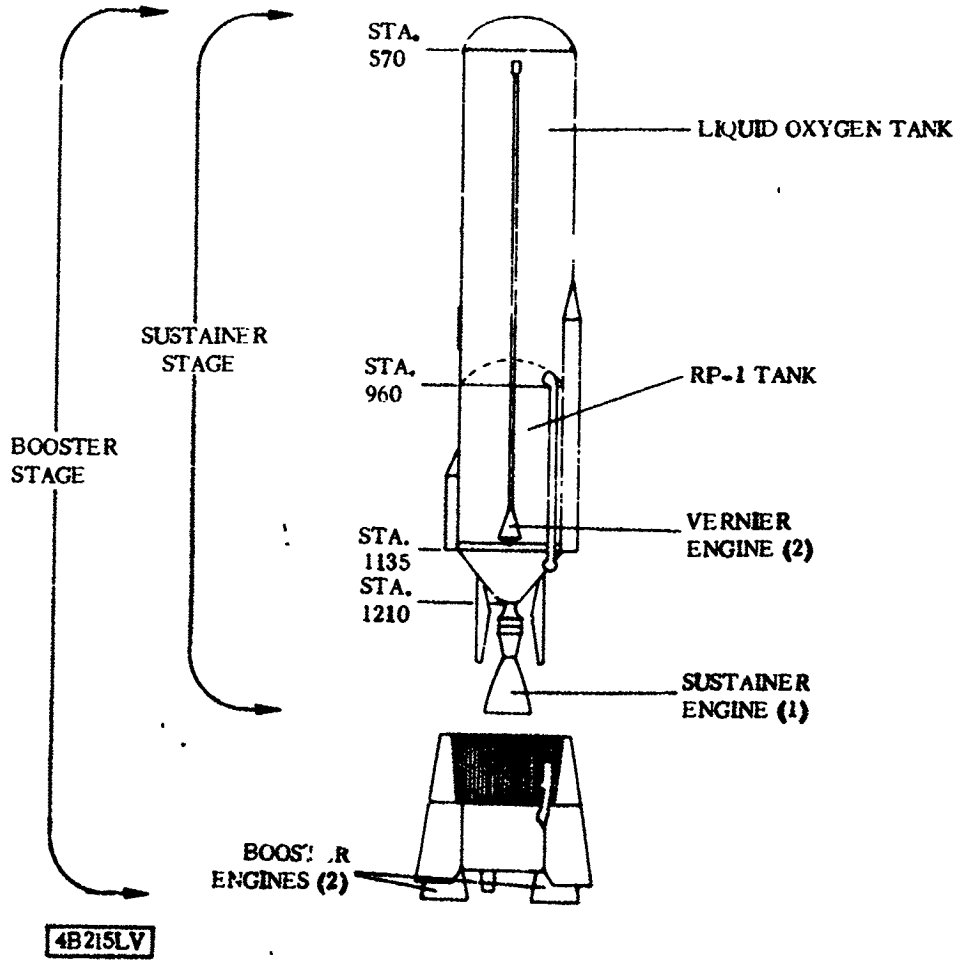

Figure 9.1-1. Atlas Booster Vehicle

THIS PAGE INTENTIONALLY LEFT BLANK.

9.2 STATION 570 JOINT

The Station 570 joint is the interface between the Atlas booster vehicle and the interstage adapter. The joint configuration is shown in Figure 9.2-1.

9.2.1 CRITICAL CONDITIONS. The Station 570 joint is subjected to a combination of axial loads and bending moments. The axial loads are due to aerodynamic drag, inertia loads, and differential pressure across the interstage adapter. The bending moments during the first 100 seconds of flight are primarily due to vehicle angle of attack. At booster engine cutoff (BECO), the air loads are small, and the principal bending moment contribution is vehicle center of gravity (C.G.) offset.

9.2.2 WEIGHTS AND CENTER OF GRAVITY DATA. The following weights shall be used for design and analysis of the Station 570 joint:

Maximum weight forward of the Station 570 joint = 41,100 lb

Minimum weight forward of the Station 570 joint = 39,050 lb

9.2.3 THERMAL DATA. Thermal environment of the Station 570 joint is presented in Paragraph 4.1.3.

9.2.4 INERTIA LOADS. The inertia contribution to axial loads during the first 100 seconds of flight is included in the data presented in Table 9.2-1. At BECO, the longitudinal inertia load = +5.7 ±0.1 g's. This acts simultaneously with the bending moment at Station presented in Figure 6.2-3.

TABLE 9.2-1. STATION 570 JOINT - MAXIMUM AND MINIMUM AXIAL LOADS

Time (sec)	Maximum Axial Load (lb)	Minimum Axial Load (lb)
40	81,900	67,200
44	88,000	70,800
48	96,500	75,400
52	108,700	81,700
56	128,000	90,200
60	137,300	102,500
64	137,800	112,000
68	137,900	111,200
72	138,000	111,600
76	138,000	112,100
80	139,200	112,400
84	140,400	112,600
88	141,700	112,500
92	143,400	113,600
96	145,900	115,800
100	149,300	119,000

NOTE: These loads include contributions of inertia, drag, and interstage adapter internal pressure.

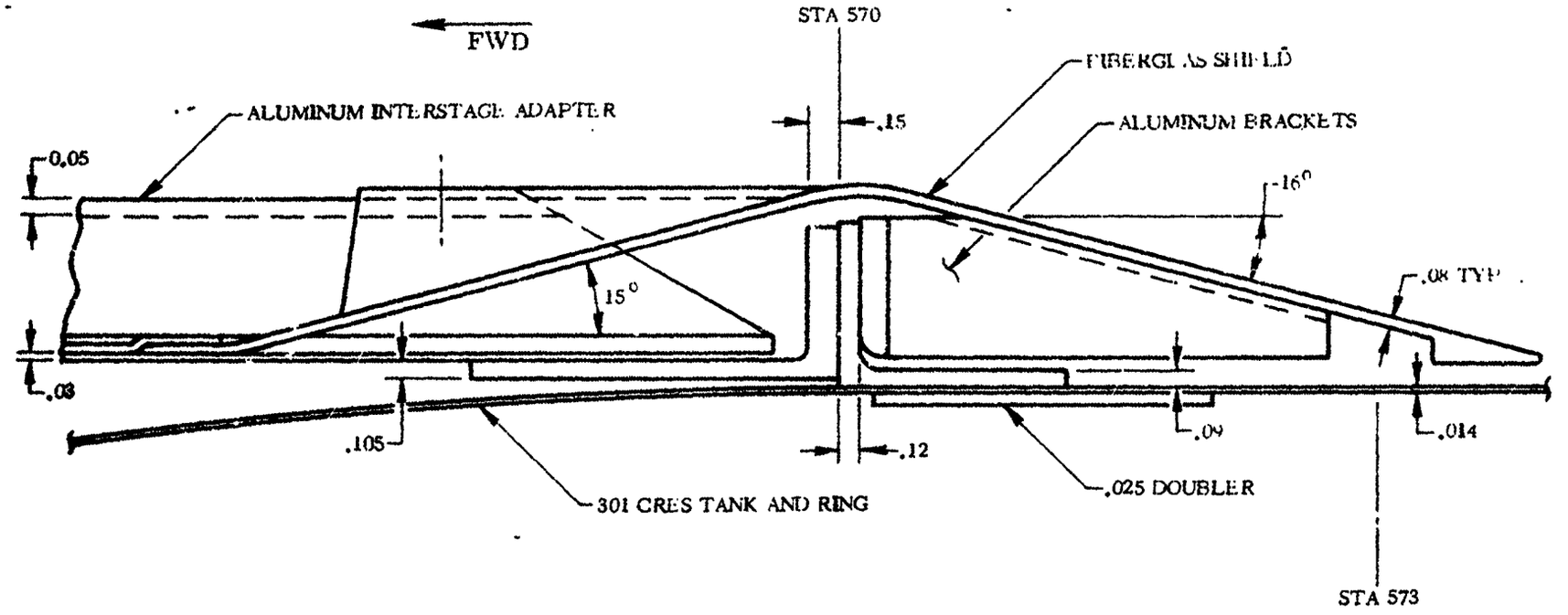

Figure 9.2-1. Station 570 Joint

9.2.5 STEADY-STATE AIR LOADS. Drag and interstage adapter internal pressure contributions are included in the axial loads data presented in Table 9.2-1. The bending moment due to angle of attack is included in the plot shown in Figure 9.2-2. The time of maximum bending moment is not well defined and is therefore assumed to occur between 56 and 76 seconds.

9.2.6 BUFFET AND FLUTTER LOADS. The Station 570 joint does not receive critical loads due to buffet or fluctuating pressure.

9.2.7 MISCELLANEOUS LOAD PARAMETERS. No other critical loads are imposed on the Station 570 joint.

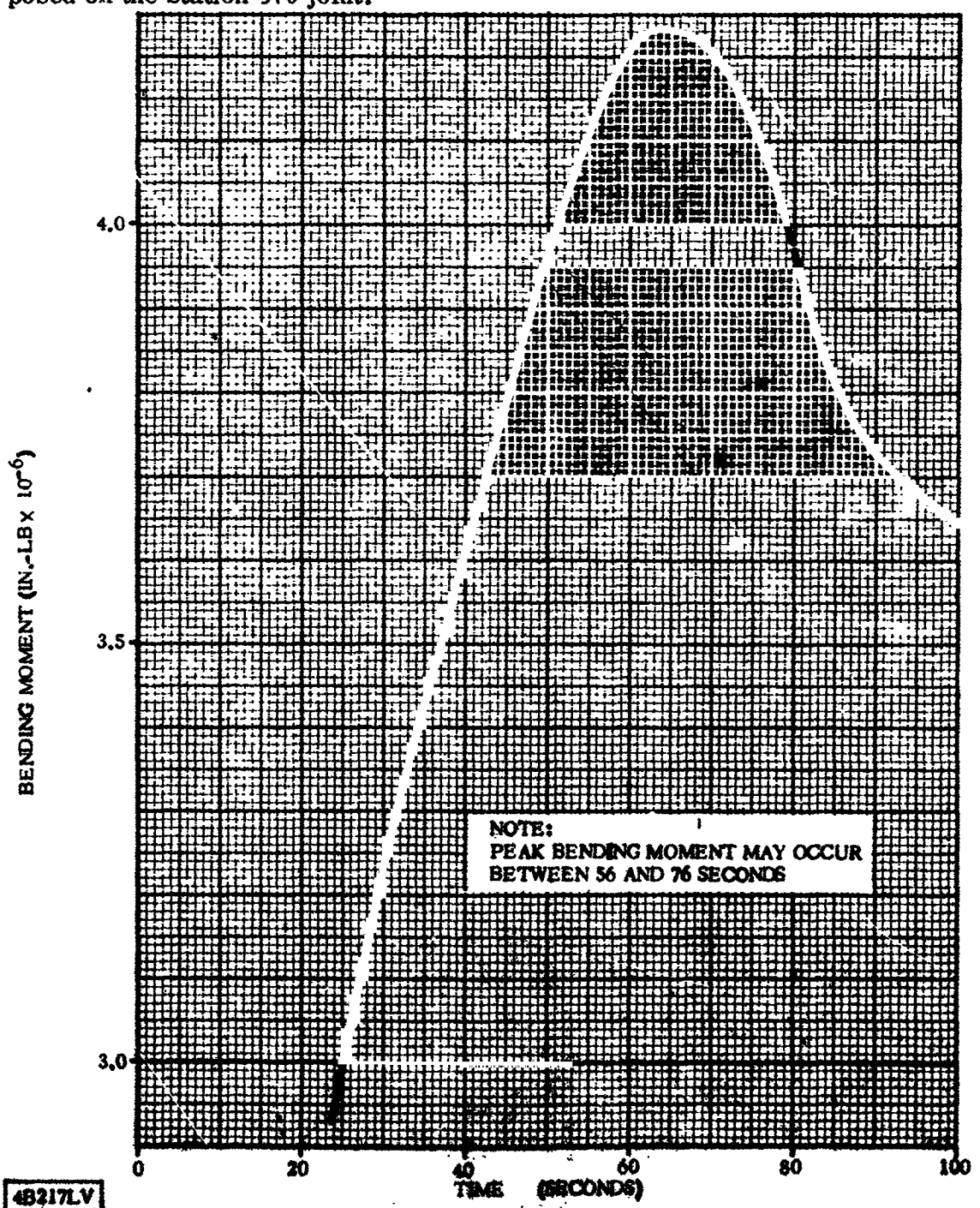

Figure 9.2-2. Station 570 Joint - Bending Moment versus Time

THIS PAGE INTENTIONALLY LEFT BLANK.

9.3 PROPELLANT TANKS

The data presented in the subsection is only that required for minimal stress analysis of the Atlas basic tank skins and flight readiness certification. The critical vehicle stations analyzed are: Stations 570 (immediately aft of the interstage adapter interface), 770, 812, and 960. See Figure 9.3-1 for basic tank configuration.

9.3.1 CRITICAL CONDITIONS. The critical loading conditions for the Atlas propellant tanks occur during the first 100 seconds of flight and at BECO. During the first 100 seconds of flight, axial loads due to inertia and aerodynamic drag act in combination with maximum bending moments. At BECO, axial inertia loads are highest, and they act in combination with a smaller value of bending moment.

9.3.2 WEIGHT AND CENTER OF GRAVITY DATA. The weights listed in Table 9.3-1 shall be considered for stress analysis and flight certification of Centaur boosters.

TABLE 9.3-1. FLIGHT CERTIFICATION ATLAS BOOSTER STRUCTURAL ANALYSIS WEIGHTS

Station	Weight Forward of Station (lb)	
	Maximum	Minimum
570 (Aft)	41,300	39,200
770	41,920	39,820
812	42,040	39,940
960 (Fwd)	42,740	40,640

The propellant levels versus time are plotted in Figure 9.3-2 for both Atlas tanks. The propellant station levels at launch are presented in Table 9.3-2.

TABLE 9.3-2. ATLAS BOOSTER VEHICLE PROPELLANT LEVELS AT LAUNCH

Condition	Station	Tolerance
Tanking		
Liquid Oxygen	542.5	±0.8
Fuel	932.3	±0.7
Thrust Buildup (Ignition)		
Liquid Oxygen	546.8	±1.2
Fuel	935.3	±0.8
Transient Launch (2-Inch Motion)		
Liquid Oxygen	553.6	±3.2
Fuel	939.1	±1.9

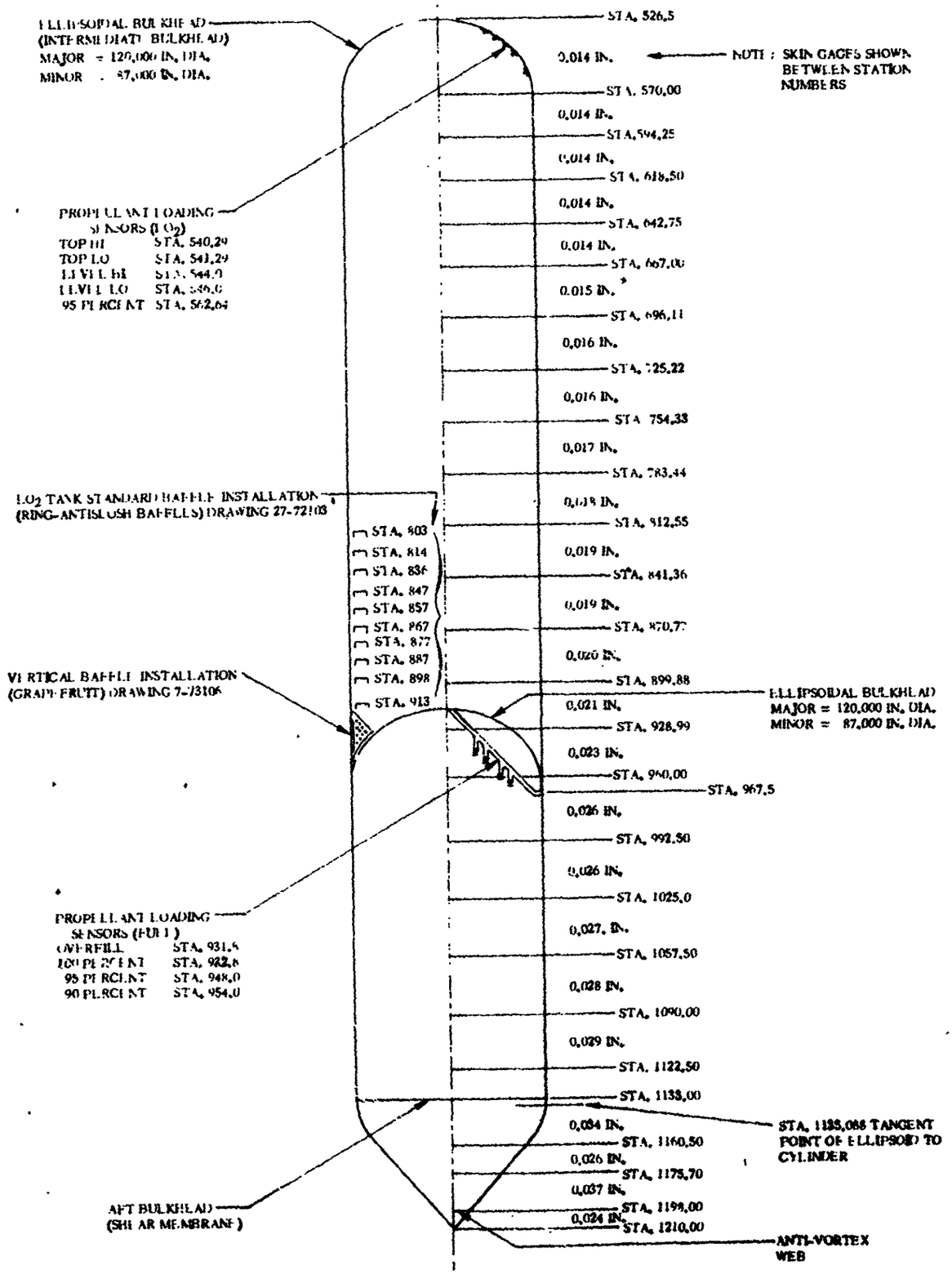

4B116LV

Figure 9.3-1. Atlas Vehicle Propellant Tank Configuration

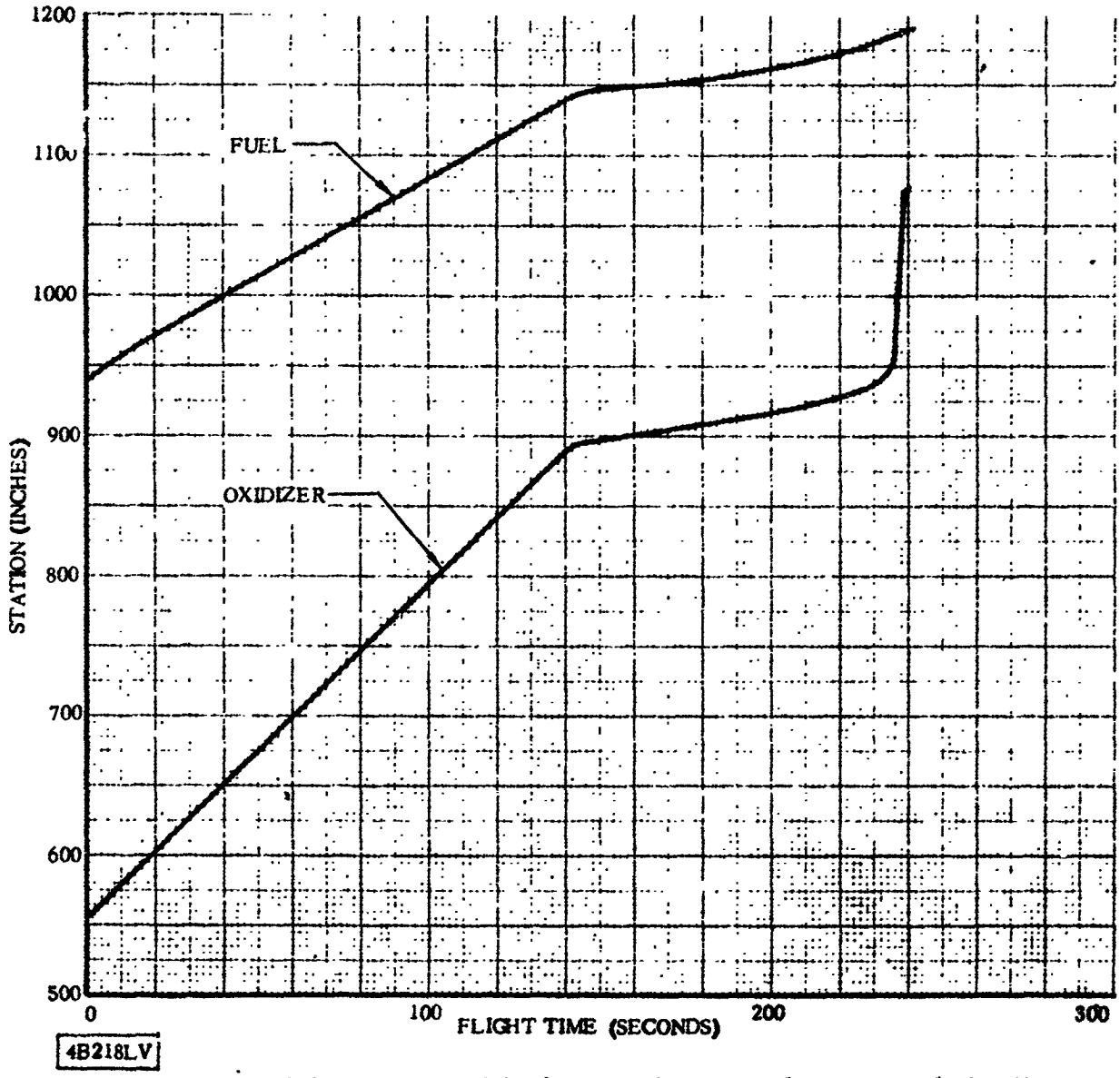

Figure 9.3-2. Atlas Booster Vehicle Propellant Levels versus Flight Time

9.3.3 THERMAL DATA. The portion of the Atlas LO_2 tank that is wetted by the LO_2 contents is at a temperature of -297° F. The forward portion of the tank skin is subjected to aerodynamic heating. The maximum LO_2 tank skin temperatures are predicted in Figure 9.3-3.

9.3.4 INERTIA LOADS. At launch, the propellants are subjected to transient accelerations due to the response of the vehicle to thrust buildup. The inertia loads on the propellants due to the thrust transients plus steady-state acceleration are presented below.

During the first five seconds of launch, the longitudinal oscillatory transient acceleration factors are:

Liquid oxygen	1.65 g's
Fuel	0.7 to 2.2 g's

Page 9 - 10 Not Utilized

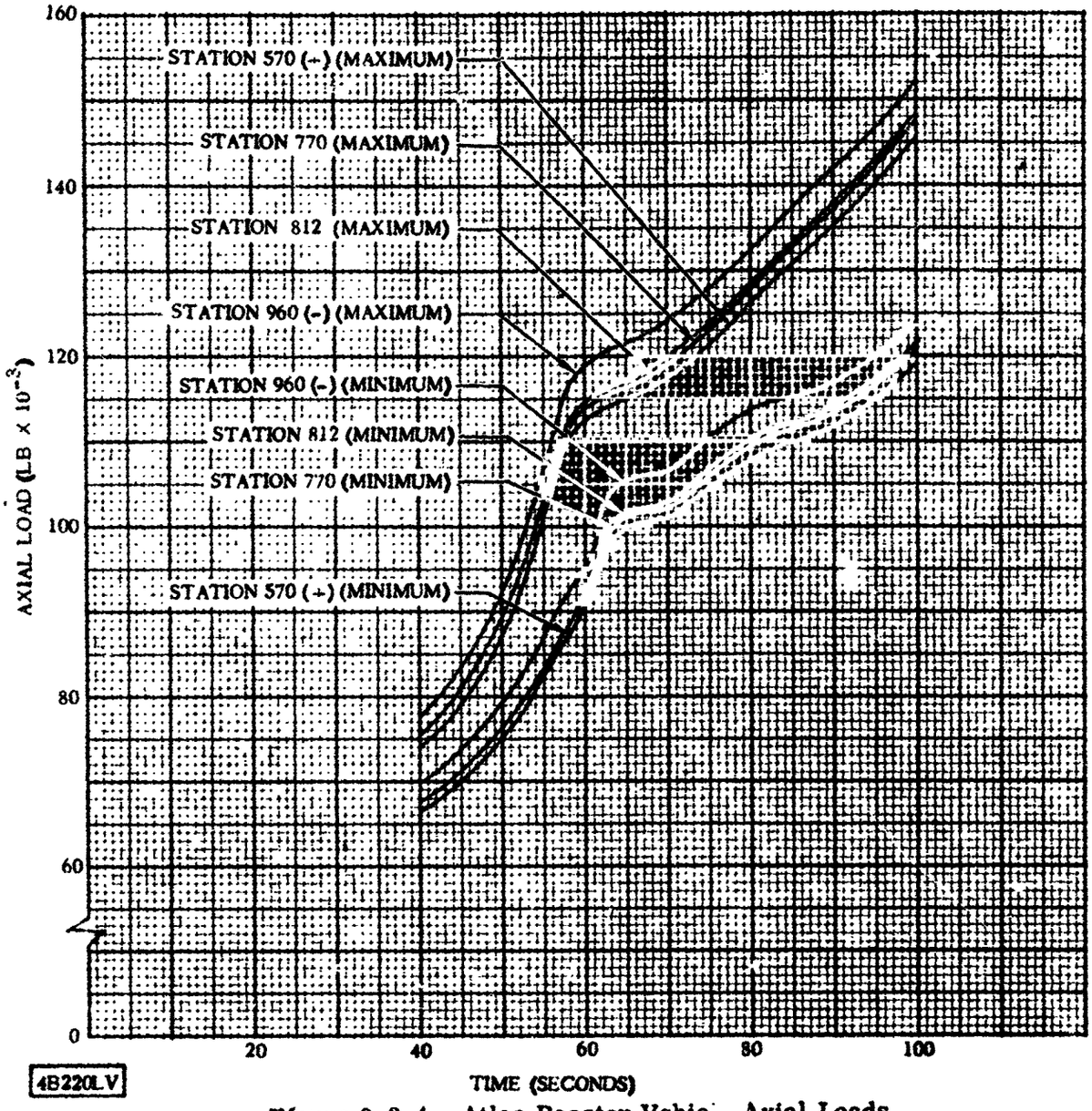

Figure 9.3-4. Atlas Booster Vehic Axial Loads

TABLE 9.3-3. AXIAL ACCELERATION VERSUS TIME (110 ≥ t ≥ BECO)

Time (sec)	High Limit $\frac{T-D}{W}$ (g's)	Low Limit $\frac{T-D}{W}$ (g's)
110	3.55	3.29
120	4.07	3.75
126	4.47	4.10
132	4.94	4.50
138	5.50	4.98
BECO	(Reference Paragraph 9.3.4)	

9.3.5 STEADY-STATE AIR LOADS. The aerodynamic drag contribution to axial loads on the Atlas propellant tanks is included in the data presented in Figure 9.3-4 These axial loads are intended only for the stress analysis of the vehicle, and they represent an extreme condition for all flights. Reference 9-1 presents methods by which actual flight loads are predicted immediately prior to flight.

The ground wind loads on the free-standing vehicle prior to launch cause a critical loading condition. In order that the structural integrity of the vehicle not be jeopardized during the tanking and standby sequences of the countdown, the maximum ground wind speed to which the vehicle shall be allowed to be exposed is presented in Reference 9-2.

9.3.6 BUFFET AND FLUTTER LOADS. The basic Atlas propellant tank structure does not receive critical loads due to buffet or fluctuating pressure

9.3.7 MISCELLANEOUS LOAD PARAMETERS. No other loads on the basic Atlas propellant tanks are critical.

SECTION X

BIBLIOGRAPHY

Supplementary documentation used as reference material for this report is tabulated herein. The first digit of each reference number indicates the section of the report where the data is generally applicable.

1-1 Structural Design Criteria, Centaur Operational Vehicles, AC-6 Through AC-15, GD/C-BTD65-036, 1 April 1965.

1-2 Centaur Unified Test Plan, AY62-0047, Sections 8.6 through 8.15.

1-3 Vehicle Design Trajectory Data, Atlas/Centaur/Surveyor, GD/A63-1096A, 15 April 1964.

1-4 Pratt and Whitney Engine Model Specification No. 2272, 28 April 1961.

1-5 Structural Design Criteria Centaur Ground Support Equipment (GSE) 55-00210D, 3 April 1964.

2-1 Aerodynamic Heating Analysis of the Centaur/Surveyor Nose Cone and Attached Fairings for Vehicles AC-4 and On, CTM-181, 11 February 1964.

2-2 Nose Fairing Thermal Support for the AC-5 Design Review, CTL-64-348, 17 December 1964.

2-3 Steady-State Wind Loads on Centaur Vehicle and Components during Erection, CA-AM-60, 5 September 1963.

2-4 Aerodynamic Loads and Pressures for Design of the Surveyor/Centaur Payload Shroud, AE62-0034, 24 January 1962.

2-5 Preliminary Surveyor Nose Fairing Buffet Loads, SD-64-39-CEN, 18 February 1964.

2-6 Thermal Study of the 1) Nose Fairing Shoulder Cover and the 2) Nose Fairing Hinge Pod for the AC-3 and AC-4 Missions, CTL-64-126, 6 May 1964.

2-7 Transonic Buffet Loads on AC-3 and On Nose Fairing Cover Fairing (Station 146.75), SD-64-289-CEN, 18 December 1964.

2-8 Temperature Distribution at Station 219 for AC-6 and On, CTL-64-353, 10 March 1965.

2-9 Predicted Maximum In-Flight Differential Pressure History Across Surveyor Nose Fairing Thermal Bulkhead, AC-6 and On, CTL-65-113, 2 April 1965.

2-10 AC-6 Nose Fairing Upper Cavity and Thermal Bulkhead Loads during Jettison, CTL-65-108, 14 April 1965.

2-11 Temperature Distribution at Station 219 for AC-6 and On, CTL-64-353, Addendum 2, 23 March 1965.

2-12 Weights and C.G.s for AC-6 and On Components, CW65-48, 26 February 1965.

2-13 Fluctuating Pressures on 55-71210 Skirt Installation, SD-65-97-CEN 26 March 1965.

2-14 Centaur Monthly Configuration, Performance, and Weight Status Report, GD/C 63-0495-23, 21 April 1965. (Confidential)

2-15 Distributions and Total Vehicle Aerodynamic Coefficients for the Atlas/Centaur/Surveyor Vehicle, GD/A-BTD64-072, 23 November 1964.

2-16 AC-4 and AC-5 Umbilical Loads, ACS-64-239, 15 December 1964.

2-17 Thermolag T-230 Application Requirements for the Nose Fairing - AC-6 and On, CTM-248, March 1965.

2-18 Design Limits of Nose Fairing Internal Pressure - AC-6, CA-AM-115, 1 March 1965.

2-19 Steady-State Aerodynamic Loads on AC-4 Surveyor Nose Fairing Latch Covers, CA-AM-109, 6 October 1964.

2-20 Surface Temperature Histories of the Nose Fairing Tension Straps, FLSC Detonator and Insulation Panel Longitudinal Joint Fairings at Station 219, AC-6 and On, CTL-65-135, 27 April 1965.

2-21 Temperature Survey of the Nose Fairing Hinge Assembly for AC-4, CTL-64-293, 22 October 1964.

2-22 Explosive Bolt Fairings for AC-4 and On, CTL-64-299, 10 November 1964.

2-23 The Use of Conolon 525-T2 as Thermal Insulation on the Leading Edge of the GN_2 Vent Stack for the AC-2 and Operational Surveyor Flights, CTM-158 Addendum I, 24 March 1965.

2-24 Aerodynamic Loads on AC-3 Surveyor Nose Fairing Skirt, CA-AM-78, Addendum I, 4 February 1964.

2-25 Aerodynamic Loads on AC-6 Nose Fairing Skirt Installation, CA-AM-117, 31 March 1965.

2-26 AC-6 Nose Fairing Jettison Final Root-Sum-Square Total Loads, SD-65-114-CEN, 15 April 1965.

2-27 Aerodynamic Loads on AC-3 Surveyor Nose Fairing Hinge Pods, CA-AM-79, 10 February 1964.

2-28 Buffet Loads, AC-3 Nose Fairing Skirt (55-72153) and AC-3 Nose Fairing Hinge Pod (55-72152), SD-64-23-CEN, 30 January 1964.

2-29 Fluctuating Pressures on Air Conditioning Duct Door (Station 156.25) for AC-5 and On, SD-64-279-CEN, 11 December 1964.

2-30 Electronic Cooling Duct Door, AC-2 Nose Fairing, SD-63-160-CEN, 12 August 1963.

2-31 Maximum Steady-State Aerodynamic Loads for the Surveyor Centaur Hydrogen Fuel Vent Stack, CA-AM-72, 3 December 1963.

2-32 Fluctuating Pressures on Air Conditioning Duct Doors, SD-63-194-CEN, 26 September 1963.

2-33 AC-4 and On Thermal Bulkhead (55-71166, Revision U), SD-64-239, 9 October 1964.

2-34 Maximum Forward Vertical RSS Total Load at 0.075 Seconds after the Start of Nose Fairing Jettison, SD-65-138-CEN, 27 May 1965.

3-1 Thermal Analysis of the LO_2 Tank Joint and Insulation Panel at Station 412 for the AC-6 and On Mission, CTL-64-127, Addendum I, 9 March 1965.

3-2 Buffet Loads AC-4 and On, Forward Wiring Tunnel, SD-64-211-CEN, 8 September 1964.

3-3 Predicted In-Flight Insulation Panel Internal Pressure Histories for Maximum Burst Conditions, Single Vent Configuration, Revision 1, CTM-194, 5 May 1964.

3-4 Steady-State Aerodynamic Load Analysis for Insulation Panels and Protuberances on Centaur with Surveyor Nose Fairing, Addendums I and II, CA-AM-77, 30 January 1964.

3-5 Thermolag T-230 Requirements on the AC-6 Insulation Panels, CTL-65-026, 19 January 1965.

3-6 Aerodynamic Heating Analysis of the Lightweight Insulation Panels and Associated Fairings for Vehicles AC-4 and On, CTM-175, 14 January 1964.

3-7 Insulation Panel Hinge Arm Temperatures, CTL-65-024, 18 January 1965.

3-8 Aerodynamic Coefficients for the Surveyor Centaur Insulation Panels during Jettison (Panels Attached to the Vehicle), CA-AM-90, 10 April 1964.

3-9 Thermal Study of the LO_2 Fill and Drain Fairing for AC-4 and On, Addendum I, CTL-64-294, 27 November 1964.

3-10 Steady-State Aerodynamic Loads on LOX Fill and Drain Outlet Deflector Fairing for Vehicles AC-6 and On, Addendum I, CA-AM-106, 11 November 1964.

3-11 Fluctuating Pressures on 55-74321 Fairing Installation - LO_2 Fill and Drain, and 55-75017 Door Installation - Air Conditioning Duct, Interstage Adapter, SD-64-232-CEN, 6 October 1964.

3-12 Thermolag T-230 Insulation Requirements on the AC-4 Insulation Panels, CTL-64-174, 12 June 1964.

3-13 Temperature Histories of the Insulation Panel Severance System Fairings (55-74357) and the Boost Pump Fairing Skirt (55-74363) for AC-6 and On, CTL-65-110, 2 April 1965.

3-14 Aerodynamic Loads, AC-6 Insulation Panel Severance System Fairings, CA-AM-118, 1 April 1965.

3-15 Steady-State Aerodynamic Loads on AC-6 Boost Pump Fairing Skirt (Mild Detonator Fuse Retainer), CA-AM-119, 7 April 1965.

3-16 Buffet Loads: AC-3 and On Insulation Panels and Fairings, SD-64-13-CEN, 17 January 1964.

3-17 Aerodynamic Loads on AC-3 Nose Fairing Skirt, Nose Fairing Hinge (Vent) Pod, and Insulation Panel Hinge Pods, CA-AM-77, Addendum 2, 27 May 1964.

3-18 Limits of Differential Pressure Across the Surveyor Centaur Wiring Tunnel Aft Bulkhead, CA-AM-65, 8 November 1963.

4-1 Aerodynamic Heating Analysis of the Atlas/Centaur Interface at Station 570 for AC-6 and On, CTM-258, 14 April 1965.

4-2 Thermal Analysis of the AC-6 and On Helium Vent Fins, CTL-65-105, 2 April 1965.

4-3 Disconnect Loads at the PW/A Engine Chilldown Interface, ACS-64-307, 19 November 1964.

4-4 Variable - Boundary Transient Heat Conduction Program, R. F. O'Neill, AY63-0065, 17 June 1963.

4-5 Test Report for Phase III of the Aerodynamic Heating Test at the NASA Langley Unitary Plan Wind Tunnel, P. S. Yip, ZT-7-027, 2 July 1959.

4-6 Temperature Histories of the Station 570 Wiring Tunnel Fairing - AC-6 and On, CTL-65-115, 6 April 1965.

4-7 AC-6 and On Interstage Adapter Thermolag T-230 Requirements, CTL-64-233, 3 September 1964.

4-8 Thermal Analysis of the AC-6 Interstage Adapter, CTL-64-087, 31 March 1964.

4-9 AC-6 and On Interstage Adapter Venting Requirements, CTM-184, 12 June 1964.

4-10 Thermal Analysis of the 55-74017 Interstage Adapter Fairing for AC-4 and On, CTL-64-096, 7 April 1964.

4-11 Steady-State Wall Differential Pressure Envelope for the Surveyor/Centaur Interstage Adapter LH_2 Boost Pump (Aft) Fairing and Bulkhead, CA-AM-70, 26 November 1963.

4-12 Station 570 Heat Shield Design Loads and Environment AC-4 and On, ACS-64-54, 27 February 1964.

4-13 Steady-State Aerodynamic Loads on 55-75048, Wiring Tunnel (AC-6 Station 542.65), CA-AM-102, 24 June 1964.

4-14 Aerodynamic Heating Analysis of the Azusa and C-Band Antenna for AC-5, AC-6 and On, CTL-65-003, 8 January 1965.

4-15 Steady-State Aerodynamic Loads on AC-5 and AC-6 Azusa and C-Band Installations, Station 486.85, CA-AM-104 (Revision 1), 5 February 1965.

4-16 Temperature Histories of the Interstage Adapter and Insulation Panel Separation Systems Detonators and Fairings, AC-6 and On, CTM-234, 19 January 1965.

4-17 Aerothermodynamic Analysis of the Insulation Panel Hinge Fittings, AC-6 and On, CTL-65-119, 12 April 1965.

4-18 Steady-State Aerodynamic Loads on AC-6 Safe & Arm Fairing, CA-AM-116, 4 March 1965.

4-19 Station 412 LOX Tank Joint and Interstage Adapter Ring Analysis for AC-6 and On, CTL-64-253, 16 September 1964.

4-20 Buffet Loads, AC-3 Interstage Adapter Boost Pump Fairing (55-74017), SD-64-36-CEN, 13 February 1964.

4-21 Buffet Loads AC-6 Station 570.00 Wiring Tunnel Fairing, SD-64-213-CEN, 9 September 1964.

4-22 Design Loads for the 570 Ring Heat Shield, AC-4, SD-64-72-CEN, 27 March 1964.

4-23 Dynamic Loads, AC-3 C-Band Antennas on the Interstage Adapter, SD-64-48-CEN, 6 March 1964.

4-24 Inertia and Fluctuating Pressure Loads on Ground Plane and Azusa Antenna on Interstage Adapter, AC-3 and On, SD-63-234-CEN, 15 November 1963.

4-25 Steady-State Aerodynamic Loads on AC-5 and AC-6 Azusa and C-Band Antenna Installations, CA-AM-104, Revision 1, 5 February 1965.

4-26 Exit Pressure Coefficients and Maximum Steady Aerodynamic Loads for the AC-6 Centaur Helium Chilldown Ducts, CA-AM-97, 21 May 1964.

4-27 Aerodynamic Loads on a Proposed Configuration for AC-3 Heat Shield Located at Station 570, CA-AM-82, 18 February 1964.

4-28 Wall Differential Pressures for the Surveyor Centaur/Atlas Interstage Adapter, CA-AM-63, 4 November 1963.

4-29 Temperature Histories of the Interstage Adapter and Insulation Panel Separation Systems Detonators and Fairings, AC-6 and On, CTM-234, Addendum 1, 21 May 1965.

5-1 Revised Limit Load Factors for the Surveyor Payload Support Structure and Surveyor Payload Models, SD-65-21-CEN, 10 February 1965.

5-2 ΔP Across Payload Adapter (AC-4 Vehicle), CTA-64-111, 3 August 1964.

5-3 Interface Control Drawing - Centaur/Surveyor, GD/C Contractor Drawing 55-00050, Sheet 1 of 7.

6-1 Thermodynamic Analysis of Centaur Tank Blowdown of Propellant Residuals through the RL-10 Engines during the Retrothrust, CTM-185, 25 February 1964.

6-2 Hydrogen Tank Heating Rates Prior to Lightweight Insulation Panel Jettison for a Parking Orbit and Direct Ascent Mission, CTM-180, 15 May 1964.

6-3 Temperature History of Centaur Unwetted Tank Skin, CTM-102, 23 February 1963.

6-4 Temperature Distribution at Station 219 for AC-6 and On, CTL-64-353, 29 December 1964.

6-5 Thermal Analysis of the Station 219 Ring Area of the Nose Fairing for AC-4 and On, CTM-200, 13 August 1964.

6-6 Station 412 LOX Tank Joint and Interstage Adapter Ring Analysis for AC-6 and On, CTL-64-253, 16 September 1964.

6-7 Thermal Analysis of the LO_2 Tank Joint and Insulation Panel at Station 412 for the AC-6 and On Missions, CTL-64-217, 8 May 1964.

6-8 Predicted AC-6 Propellant Tank Pressure Profiles and Blowdown Mode Thrusts and Flow Rates, CTM-254, 30 March 1965.

6-9 AC-6 and AC-7 Bending Moment and Drag at BECO, SD-65-119-CEN, 20 May 1965.

7-1 LH_2 Overboard Vent Duct Disconnect Severity Test, Evaluation Test Report No. 55A3777, 28 October 1964.

7-2 Boost Pump Inlet Pressure and Temperature History for an AC-6 and AC-8 Type Mission, CTL-64-270, 29 September 1964.

7-3 Thermal Analysis of Centaur Electronic Equipment Platform Strut, 55-72246, CTL-64-305, 4 November 1964.

7-4 Specifications for Environmental Design & Test Requirements for Project Centaur Equipment, 55-00200E.

7-5 Revised Load Factors and Vibration Test Requirements for the "Christmas Tree" Fuel Sensor, SD-65-111-CEN, 13 April 1965.

7-6 Thermal Analysis of the Forward Umbilical Island Fairing For AC-3 and On, CTL-63-202, 4 February 1964.

7-7 Steady-State Aerodynamic Loads for the AC-6 Forward Umbilical Island Fairing, CA-AM-112, 23 October 1964.

7-8 Fluctuating Pressure Loads on the Redesigned AC-6 Forward Umbilical Island Fairing, SD-64-272-CEN, 7 December 1964.

7-9 Design Inertia Factors: AC-3 and On Forward Umbilical Island, Forward Umbilical Island with Proposed Ground Plane Antenna (SK 55-72399), and Forward Umbilical Island Fairing (55-72392), SD-63-233-CEN, 12 November 1963.

7-10 Inertial Load Factors For 55-72391 Support Installation LH_2 Level Sensor (AC-4 and On), SD-63-123-CEN, 20 June 1963.

7-11 Limit Load Factor and Qualification Test Recommendations for General Equipment, SD-65-67-CEN, 20 February 1965.

8-1 Hydraulic System Temperature during a Velocity Oriented Two-Burn Mission, CTM-229, 6 January 1965.

8-2 Pre-Launch Temperatures on VAF 55-02020-B-MH-001, Helium Chilldown Disconnect for AC-6 and On, CTL-64-144, 28 May 1964.

8-3 Inertia Load Factors for Centaur LO_2 Boiloff Valve and Tube End, SD-63-167-CEN, 20 August 1963.

8-4 Insulation Panel Helium Purge Disconnect Redesign; AC-6 and On, CTL-65-005, 7 January 1965.

8-5 Buffet Loads AC-3 and On Insulation Panels and Fairings, SD-64-13-CEN, 17 January 1964.

8-6 AC-6 Engine Actuator Loads and Engine Gimbal Block Loads, ACS64-44, 18 February 1964.

8-7 Inertial Design Load Factors for the Centaur LOX Boost Pump and Sump, SD-64-87-CEN, 17 April 1964.

8-8 Design Load Factors for Advanced Propellant Utilization Probe (LOX) (AC-5 and On), SD-64-18-CEN, 24 January 1964.

8-9 Inertial Load Factors for the Attitude Engine Instl. CTS-0009, and Ullage Engine Instl. CTS-0010 (AC-6), SD-63-162-CEN, 13 August, 1963.

8-10 LOX Boil-Off Standpipe Design Loads - AC-7, SD-63-120-CEN, 10 June 1963.

8-11 Maximum Wall Differential Pressures Imposed on the Aft Umbilical Panel for AC-4 and On, CA-AM-80, 12 February 1964.

9-1 Flight Wind Restriction Procedure - Atlas/Centaur Flights AC-6 through AC-
GD/C-BTD65-068, 15 May 1965.

9-2 Ground-Wind Restrictions Procedure for Atlas/Centaur/Surveyor AC-6 and AC
GD/C-BTD65-061, 1 June 1965.